Identification and functional characterization of a subset of goldfish (*Carassius auratus*) leukocyte immune-type receptors (CaLITRs) expressed by myeloid cell-types

by

Jiahui Wang

A thesis submitted in partial fulfillment of the requirements for the degree of

Doctor of Philosophy

in

Physiology, Cell, and Developmental Biology

Department of Biological Sciences

University of Alberta

ABSTRACT

Originally discovered in the channel catfish, *Ictalurus punctatus* leukocyte immune-type receptors (IpLITRs) are members of the immunoglobulin superfamily (IgSF) and several of their transcripts are known to be expressed in a variety of catfish innate and adaptive immune cells. Phylogenetically, IpLITRs have a unique "chimeric" composition of Ig-like domains that are distantly related to mammalian immunoregulatory receptors of the Fc receptor (FcR) family and leukocyte receptor complex (LRC). Using heterologous overexpression systems, our lab has shown that select IpLITRs likely use dynamic tyrosine-based signaling mechanisms to control various innate immune effector responses. Although LITRs have been studied for almost two decades, their immunoregulatory roles in teleost immunity remain poorly understood. The goldfish, with its published genome, well-characterized primary myeloid cells such as primary kidney macrophages (PKMs) and neutrophils (PKNs), and large molecular toolkit, represent an ideal model system for studying the native functions of LITRs in teleost immune cells.

The overall aim of my thesis was to set up the goldfish as a new model system for investigating the native immunoregulatory roles of LITRs in teleost immunity. I have identified and cloned a total of seventeen *calitr* transcripts. The mRNAs of several CaLITRs were found to be present in an assortment of goldfish tissues and isolated PKMs and PKNs. Sequence analyses of these receptors have shown that they have diverse configurations of Ig-like domains and cytoplasmic tails (CYTs) containing various tyrosine-based signaling motifs such as immunoreceptor tyrosine-based activation motifs (ITAMs), immunoreceptor tyrosine-based switch motifs (ITSMs), and immunoreceptor tyrosine-based inhibition motifs (ITIMs). Additionally, I have also identified several putative CaLITR ectodomain and CYT splice forms. These results indicate that alternative splicing may play a significant role in diversifying the

ligand binding and/or signaling potentials of CaLITRs. Overall, the identification and cloning of the various *calitr* sequences open up new avenues for exploring how these sequences may contribute to the regulation of the goldfish immune system.

Using a comparative genomics approach, I further examined the possible evolutionary connections between teleost LITRs and various vertebrate immunoregulatory receptor types. My results show that teleost *litrs* generally exist in large genomic clusters, which are linked to *vangl2*, *arhgef11*, and slam family genes, features that are also shared by amphibian and mammalian Fc receptor-like molecules (*fcrls*). Moreover, detailed phylogenetic comparisons between the individual Ig-like domains of LITRs and mammalian FCRLs show that these receptors share related Ig-like domains indicative of their common ancestry. These data support that LITRs are likely to be distant homologs of vertebrate FCRLs.

Using qPCR, I investigated the transcriptional activities of several *calitrs* from distinct goldfish chromosomes. My findings demonstrate that these *calitrs* are differentially expressed during PKM development and in activated goldfish leukocyte cultures. Specifically, I showed that *calitr1* exhibited transcriptional kinetics similar to several goldfish proinflammatory markers in mitogen-simulated goldfish leukocytes, while the expression of the other *calitrs* examined (*calitr2*, *calitr3*, and *calitr4*) remained unchanged under the same conditions. Furthermore, immunosuppressive drugs, including dimethyl sulfoxide (DMSO), and to a much less extent, cyclosporin A (CsA), were shown to downregulate the mRNA expressions of several goldfish proinflammatory genes and *calitr1*, with minimal to no effects observed on the expression of the other *calitrs* examined. Altogether, these results suggest that the select *calitrs* from distinct goldfish chromosomes are likely under the influence of different cis- and trans-regulatory elements.

To further study the native roles of CaLITRs in goldfish myeloid cells, I developed and characterized several CaLITR pAbs specific for CaLITR3, a predicted stimulatory receptor-type with a transmembrane domain (TM) containing a positively charged histidine. I demonstrate that the anti-CaL3.D1 pAb stains various hematopoietic cell types within the goldfish kidney, as well as in PKNs and PKMs. Moreover, cross-linking of the anti-CaL3.D1-pAb on PKN membranes induces phosphorylation of p38 and ERK1/2, critical components of the MAPK pathway involved in controlling a wide variety of innate immune effector responses such as NETosis, respiratory burst, and cytokine release. These findings support the stimulatory potential of CaLITR3 proteins as activators of fish granulocytes and pave the way for a more in-depth examination of the immunoregulatory functions of CaLITRs in goldfish myeloid cells.

PREFACE

This thesis is the original work of Jiahui Wang. All experiments conducted adhered to the guidelines established by the Canadian Council of Animal Care guidelines and the University of Alberta Animal Care and Use Committee (AUP#00000069).

Chapter II herein is published in part as Wang, J., Gurupalli, H. V., & Stafford, J. L. (2023). Teleost leukocyte immune-type receptors. *Developmental & Comparative Immunology*, 104768. Chapter IV herein is published in part as Wang, J., Belosevic, M., & Stafford, J. L. (2020). Identification of goldfish (Carassius auratus L.) leukocyte immune-type receptors shows alternative splicing as a potential mechanism for receptor diversification. *Molecular Immunology*, *125*, 83-94. Chapter V herein is published in part as Wang, J., Belosevic, M., & Stafford, J. L. (2021). Identification of distinct LRC-and Fc receptor complex-like chromosomal regions in fish supports that teleost leukocyte immune-type receptors are distant relatives of mammalian Fc receptor-like molecules. *Immunogenetics*, *73*(1), 93-109. Chapter VI herein is published in part as Wang, J., Soliman, A. M., Norlin, J., Barreda, D. R., & Stafford, J. L. (2023). Expression analysis of Carassius auratus-leukocyte-immune-type receptors (CaLITRs) during goldfish kidney macrophage development and in activated kidney leukocyte cultures. *Immunogenetics*, *75*(2), 171-189. Chapter VII herein is published in part as Wang, J., Amoah, S., & Stafford, J. L. (2024). A leukocyte immune-type receptor specific polyclonal antibody recognizes goldfish kidney leukocytes and activates the MAPK pathway in isolated goldfish kidney neutrophil-like cells. *Developmental & Comparative Immunology*, 105228.

I collected and analyzed all data and was responsible for manuscript writing. Dr. James L. Stafford contributed philosophical, conceptual and technical guidance and edited this thesis. I supervised five undergraduate students: Maham Qamer (Biology 499), Hussain Al-Rikabi

(Biology 499), Muna Mohamed (Biology 399), Jeff Norlin (Biology 498), and Jade Raychaudhuri (Biology 399).

ACKNOWLEDGEMENTS

First, I would like to thank Dr. Miodrag Belosevic for taking me in as an MSc student and providing financial support throughout my PhD program! Thank you for believing in me and giving me the courage to complete my PhD! Next, I would like to express my deepest gratitude to my supervisor, Dr. James L. Stafford, for his excellent mentorship! Thank you for editing my manuscripts and offering words of encouragement whenever my experiments failed. Your guidance has made me a critical thinker and problem solver. I will forever cherish the time spent with you in the lab!

I would like to thank Dr. Patrick Hanington and Dr. Daniel Barreda for agreeing to be on my PhD defense committee. Dan, thank you for providing useful suggestions for one of my manuscripts and allowing me to use your lab instruments. Patrick, thank you for your insightful advice throughout my graduate program. To Dr. Robert Ingham and Dr. Jeffery Yoder, thank you for being a part of my PhD defense. To Dr. John Chang, thank you for being a part of my PhD candidacy exam committee. To Dr. Aja Rieger, thank you for making me not afraid of flow cytometry and for teaching me to use the Sony MA900, Attune NxT, and ImageStream flow cytometers.

I would not have made it to this point without the support from all of my wonderful lab mates. Thank you all for creating such a comfortable lab environment for learning! Hussain, thank you for enduring the hardships with me. I still have nightmares about CaLITRs not being expressed on AD293 cells… Also, thank you for training me to become a Ping Pong master. Nora, thank you for your mental support during my most depressing times. You are an amazing friend! Thank you also for maintaining the lab, and ensuring everything runs smoothly. You are the glue that's keeping the lab intact. Sunanda, thank you for playing Ping Pong with me during my experiment breaks and for helping me out with all kinds of experiments throughout my PhD. You are a strong and independent person, and I am sure you will be able to succeed in your PhD. Najia, your laid-back vibes have truly enriched our lab environment! Kareem, thank you for teaching me the history of the Roman Empire! I really enjoyed our history conversations. Kendra, thank you for inviting me to your house to pet your cat and for writing such kind and warm messages on my birthday cards! Samuel, thank you for practicing Ping Pong with me and for your help with my experiments. I really appreciated your kind words and your psychological counseling! Aoxue, although we have only recently met, I think that you are a very smart and capable person. Jeff, I had a lot of fun talking to you about Skyrim! Rikus, thank you for helping me out with my flow cytometry problems! Myron, I really enjoyed our LITR discussions! Harry, your presence brought so much joy to the lab. Yemaya, thanks for organizing the bubble tea trips. Hima, I had a lot of fun discovering the LITRs with you. Jiasong, thank you for teaching me about the goldfish system.

To my other colleagues, Mirza and RJ, I cannot thank you enough for all your help during my most difficult days. I was very fortunate to have met you guys. Amro and Farah, I had a lot of fun collaborating with you two on different goldfish projects! To Dr. Jacob Hambrook, I appreciate all your help with the generation of LITR recombinant proteins! I would also like to thank all my other friends: Enezi, Matt, Aradana, Doaa, Won Yong, Diyor, Reema, and Emmanuel. It was a pleasure to have met all of you.

To Carol, Tad, Sarah, Lauresha, and Ricardo, thank you so much for keeping the goldfish healthy and assisting me with carp bleeding.

Finally, I want to extend my heartfelt thanks to my partner, Wanwei, and my cat, Pebble, for being by my side during the writing of this thesis. I am also deeply grateful to my loving parents, my little sister, and my dog (Puzzle) for their continuous support throughout my life.

TABLE OF CONTENTS

CHAPTER III

MATERIALS AND METHODS

CHAPTER IV

IDENTIFICATION OF GOLDFISH (CARASSIUS AURATUS L.) LEUKOCYTE IMMUNE-TYPE RECEPTORS SHOWS ALTERNATIVE SPLICING AS A POTENTIAL MECHANISM FOR RECEPTOR DIVERSIFICATION

CHAPTER V

IDENTIFICATION OF DISTINCT LRC- AND FC RECEPTOR COMPLEX-LIKE CHROMOSOMAL REGIONS IN FISH SUPPORTS THAT TELEOST LEUKOCYTE IMMUNE-TYPE RECEPTORS ARE DISTANT RELATIVES OF MAMMALIAN FC RECEPTOR-LIKE MOLECULES

LIST OF TABLES

LIST OF FIGURES

LIST OF ABBREVIATIONS

- CYTs — cytoplasmic tails
- ITAMs — immunoreceptor tyrosine-based activation motifs
- TMs — transmembrane domains
- ITIMs — immunoreceptor tyrosine-based inhibitory motifs
- SFKs — Src family protein kinases
- Syk — spleen tyrosine kinase
- SHP — Src homology 2 domain-containing protein tyrosine phosphatase
- IgSF — immunoglobulin superfamily
- Chrs — chromosomes
- FcR — Fc receptor
- Ig — immunoglobulin
- KIRs — killer Ig-like receptors
- LRC — leukocyte receptor complex
- LITRs — Leukocyte immune-type receptors
- Ip — *Ictalurus punctatus*
- FCRLs — Fc receptor-like molecules
- RBL — rat basophilic leukemia
- HEK — human embryonic kidney
- SH2 — Src homology 2
- Nck — non-catalytic region of tyrosine kinase adaptor protein
- Csk — C-terminal Src kinase
- mAbs — monoclonal antibodies
- CTL — cytotoxic T cell line
- CCV — channel catfish virus
- MHC — major histocompatibility complex
- ADCC — antibody-dependent cellular cytotoxicity
- HSCs — hematopoietic stem cells
- APCs — professional antigen-presenting cells
- TNF-α — tumor necrosis factor alpha
- IFNγ — interferon-gamma
- LPS — lipopolysaccharide
- iNOS — inducible nitrate oxide synthase enzyme
- NO — nitric oxide
- IL — interleukin
- Mincle — macrophage-inducible C-type lectin
- CRs — complement receptors
- Fc — fragment crystallizable region
- Vav — vav guanine nucleotide exchange factor
- PLCγ — phospholipase C-gamma
- PI3K — phosphatidylinositol 3-kinase
- Rac1 — Ras-related C3 botulinum toxin substrate 1

- Cdc42 cell division cycle 42
- Arp2/3 Actin Related Protein 2/3 complex
- PIP2 phosphatidylinositol 4,5-biphosphate
- DAG diacylglycerol
- IP3 inositol triphosphate
- PKC protein kinase C
- NOX nicotinamide adenine dinucleotide phosphate (NADPH) oxidase
- PIP3 phosphatidylinositol (3,4,5)-triphosphate
- WASp Wiskott-Aldrich Syndrome protein
- MPO myeloperoxidase
- NE elastase
- NETs neutrophil extracellular traps
- ROS reactive oxygen species
- PAD4 peptidyl arginine deiminase
- h hours
- min minutes
- BCRs B cell receptors
- NCCs non-specific cytotoxic cells
- NCCRP-1 NCC receptor protein-1
- MAC membrane attack complex
- C1q complement component 1q
- MBLs mannose-binding lectins
- APPs Acute phase proteins
- CRP C-reactive protein
- IFNs interferons
- TGFs transforming growth factors
- PRRs pattern recognition receptors
- PAMPs pathogen-associated molecular patterns
- TLRs toll-like receptors
- RLRs RIG-I-like receptors
- CLRs C-type lectin receptors
- NLRs Nod-like receptors
- DAMPs damage-associated molecular patterns
- ATP adenosine triphosphate
- HSPs heat shock proteins
- HAMPs homeostasis-altering molecular processes
- LRRs leucine-rich-repeats
- MyD88 myeloid differentiation primary response 88
- TRIF TIR-domain-containing adaptor-inducing beta interferon
- TIR toll/IL-1 receptor domain
- MDA5 melanoma differentiation-associated protein 5
- LGP2 laboratory of genetics and physiology
- CTD carboxy-terminal domain
- CARDs caspase activation and recruitment domains

- MAVS mitochondrial antiviral-signaling proteins
- IRF3 interferon regulatory factor 3
- IRF7 interferon regulatory factor 7
- NFκb nuclear factor κb
- dsRNA double-stranded RNA
- SVCV spring viremia of carp virus
- DAP12 DNAX activating protein 12
- FcRγ Fc common gamma chain
- PTPs protein tyrosine phosphatases
- SHIP SH2-containing Inositol 5'-Phosphatase
- ITSM Immunoreceptor tyrosine-based switch motif
- SAP SLAM-associated protein
- EAT Ewing sarcoma associated transcript
- ERT EAT-2-related transducer
- ITAMi inhibitory ITAM
- Fab fragment antigen binding
- ITIMa activating ITIM
- TLT1 TREM-like transcript-1
- SIRPα signal regulatory protein α
- (JAK)-STAT Janus kinase/signal transducers and activators of transcription
- pIgR polymeric immunoglobulin receptor
- FcRn neonatal Fc receptor
- TRIM21 tripartite motif containing 21
- DC-SIGN dendritic cell-specific ICAM-grabbing non-integrin
- Treg regulatory T cells
- ER endoplasmic reticulum
- Mb million base pairs
- LILRs leukocyte immunoglobulin-like receptors
- OSCAR osteoclast-associated receptor
- LAIR-1 leukocyte-associated immunoglobulin-like receptor-1
- HLA human leukocyte antigen
- B2M beta-2-microglobulin domain
- CNS central nervous system
- WGD whole-genome duplication
- mya million years ago
- VSGDs vertebrate-specific WGDs
- TSGD teleost-specific WGD
- NITRs novel immune-type receptors
- NILTs novel immunoglobulin-like transcripts
- DICPs diverse immunoglobulin domain-containing proteins
- PIGRLs polymeric immunoglobulin receptor-like proteins
- RFLP restriction fragment length polymorphism
- HA-tag hemagglutinin tag
- DYKDDDDK-tag FLAG-tag

- IpFcRγ-L IpFcRγ-like
- ERK1/2 extracellular signal-regulated kinase 1/2
- Akt protein kinase B
- MAPK mitogen-activated protein kinase
- JNKs c-Jun N-terminal kinases
- GSK-3β glycogen synthase kinase 3-beta
- RSK1 ribosomal S6 kinases
- CREB cAMP-response element binding protein
- MSK stress-activated protein kinase
- PMA phorbol myristate acetate
- CytoD cytochalasin D
- PDK1 phosphoinositide-dependent kinase
- LAK lymphokine-activated killer
- Grb2 growth factor receptor-bound 2
- Gabs Grb2-associated binders
- MAFs macrophage activating factors
- rgCSF-1 macrophage colony stimulatory factor 1
- RNAi RNA interference
- CSF-1R CSF-1 receptor
- sCSF-1R CSF-1R
- G-CSFR granulocyte colony-stimulating factor
- MS222 methanesulfonate
- MLR mixed leukocyte reaction
- WCLs whole cell lysates
- RT-PCR Reverse transcription polymerase chain reaction
- SMART Simple Modular Architecture Research Tool
- NJ neighbor joining
- *ef1a* elongation factor 1 alpha
- PE phycoerythrin
- CHIRs chicken Ig-like receptors
- q quantitative
- ORFs complete open reading frames
- S2 second half of the signal peptide
- bp base pairs
- XFLs xenopus FCRL-like molecules
- Dscam Down syndrome cell adhesion molecule
- RAGE receptor for advanced glycation end products
- CAECAM1 Carcinoembryonic antigen-related cell adhesion molecule 1
- *ttyh1* tweety family member 1
- *leng8* leukocyte receptor cluster member 8
- *leng9* leukocyte receptor cluster member 9
- *pirs* paired immunoglobulin-like receptors
- *silrs* *Silurana tropicalis* immunoglobulin-like receptor
- A1BGs alpha-1B-glycoproteins

- PGK phosphoglycerate kinase
- GFP green fluorescent protein
- Mb megabase pair
- RDs regulatory domains
- HPCs hematopoietic progenitor cells
- DMSO Dimethyl Sulfoxide
- CsA Cyclosporin A
- *cmyb* c-myeloblastosis
- *tcrα* T-cell receptor alpha chain
- *igm* B cell marker
- *runx1* runt-related transcription factor 1
- sp1 specificity protein 1
- NFATc1 nuclear factor of activated T-cells 1
- HSV-1 Herpes simplex virus-1
- TFBS transcription factor binding sites
- GR glucocorticoid receptor
- C/EBP CCAAT enhancing binding protein
- TFIID transcription factor II D
- GATA-1 GATA binding factor 1
- ER estrogen receptor
- FOXP3 forkhead box p3
- MULT murine UL-16-binding protein-like transcript
- MIC-A MHC class 1 polypeptide-related sequence A
- MMCs melanomacrophage clusters
- GCSFR granulocyte colony stimulating factor receptor
- TECs renal tubular epithelial cells
- FISH fluorescent in situ hybridization
- RACE rapid amplification of cDNA ends
- ATAC-seq Assay for Transposase Accessible Chromatin Sequencing
- ChIP-seq chromatin immunoprecipitation sequencing
- EMSA electrophoretic mobility shift assays
- DHR dihydrorhodamine
- NBT nitroblue tetrazolium
- TMB 3,3’,5,5’-tetramethylbenzidine
- AlphaScreen Amplified Luminescent Proximity Homogenous Assay Screen
- BLAST Basic Local Alignment Search Tool
- HKDM head kidney-derived macrophages
- CCM cell-conditioned medium
- S seconds

CHAPTER I

INTRODUCTION

1.1 Overview

Immunoregulatory receptors control activation and suppression of immune cell effector responses to ensure the elimination of microbes while minimizing inflammation-associated tissue damage (Barrow & Trowsdale, 2006; Billadeau & Leibson, 2002). Generally, activating immunoregulatory receptor-types have cytoplasmic tails (CYTs) containing immunoreceptor tyrosine-based activation motifs (ITAMs) that are defined by the motif; D/ExxYxxL/Ix(6-12)YxxL/I (D and E denote aspartic acid and glutamic acid, respectively; Y represents a tyrosine residue; L represents leucine; I represents isoleucine; x represents any other residues except D, E, Y, L, and I) (Underhill & Goodridge, 2007). Some activating receptor-types may also have positively charged transmembrane domains (TMs) that enable them to associate with several intracellular ITAM-bearing adaptor signaling proteins (Underhill & Goodridge, 2007). Conversely, inhibitory receptor-types have long CYTs containing one or more immunoreceptor tyrosine-based inhibitory motifs (ITIMs) that are defined by the consensus sequence; S/I/V/LxYxxI/V/L (S and V represent serine and valine residues, respectively) (Barrow & Trowsdale, 2006). During ligand-induced receptor crosslinking, tyrosine residues within the ITAMs are phosphorylated by Src family protein kinases (SFKs) causing recruitment of spleen tyrosine kinase (Syk), which is an important proximal kinase required to trigger immune cell effectors responses via distinct stimulatory signaling pathways (Underhill & Goodridge, 2007). Alternatively, phosphorylated tyrosine residues within the ITIMs of inhibitory receptor-types

recruit phosphatases such as Src homology 2 domain-containing protein tyrosine phosphatase (SHP)-1/2 that dephosphorylate tyrosine residues within activating signaling intermediates to reduce or block immune cell effector responses (Barrow & Trowsdale, 2006).

In mammals, many immunoregulatory receptor-types that control innate immune cell responses belong to the immunoglobulin superfamily (IgSF), where they exist in dense gene clusters on distinct chromosomes (Chrs) throughout the genome (Rostamzadeh et al., 2018; Trowsdale et al., 2015). For example, Fc receptor (FcR) family genes (e.g. CD64, CD32, and CD16) are located on human Chr 1 (Bruhns & Jönsson, 2015). FcRs recognize the Fc region of several immunoglobulin (Ig) classes and participate in various immune reactions such as phagocytosis and antibody-dependent cellular cytotoxicity (ADCC) (Bruhns & Jönsson, 2015). In comparison, activating and inhibitory receptors such as the killer Ig-like receptors (KIRs)) are encoded within the leukocyte receptor complex (LRC) on human Chr 19 (Trowsdale et al., 2015). KIRs interact with classical and non-classical MHC class 1 molecules and play a crucial role in viral and tumor immunosurveillance (Thielens et al., 2012). Overall, mechanistic insights into mammalian immunoregulatory receptor functions have unveiled that complex networks of immunoregulatory receptors cooperate in the sensing of self/non-self ligands and regulation of a diverse range of innate immune responses.

Several immunoregulatory receptor families have been identified in the genomes of distinct vertebrates including birds, amphibians, fish, and sharks, but very little is known about their immunoregulatory roles (Cannon et al., 2006; Dennis Jr et al., 2000; Guselnikov et al., 2010; Montgomery et al., 2011). Studies designed to understand the functional roles of these non-mammalian immunoregulatory receptors may aid in the identification of conserved and divergent features of immunoregulatory receptor functional mechanisms across vertebrates.

Leukocyte immune-type receptors (LITRs) belong to a diverse family of teleost immunoregulatory receptors that were originally identified from an expressed sequence tag cDNA library constructed from stimulated channel catfish cytotoxic lymphocytes (Stafford, Bengten, et al., 2006). *Ictalurus punctatus* (Ip)-LITRs are members of the IgSF, and they are expressed in various channel catfish immune cell lines including macrophages, B cells, cytotoxic T cells, and NK cells (Stafford, Bengten, et al., 2006). Sequence examination of several IpLITR cDNAs revealed that they contain variable number of extracellular C2-set Ig-like domains and a wide variety of tyrosine-based signaling motifs in their CYTs (Stafford, Bengten, et al., 2006; Stafford et al., 2007). Phylogenetic analyses also showed that the membrane proximal and distal Ig-like domains of IpLITRs are distantly related to the Ig-like domains of mammalian LRC-encoded receptors (e.g. KIRs and LILRs) and FCR family receptors (e.g. FcRs and Fc receptor-like molecules (FCRLs)), respectively (Stafford, Bengten, et al., 2006). Several IpLITRs (IpLITR2.6b and IpLITR1.1b) have been biochemically and functionally characterized by ligating the cDNAs of these receptors into mammalian expression vectors. These vectors were then transfected into various mammalian cell lines (e.g. rat basophilic leukemia (RBL)-2H3 and human embryonic kidney (HEK) epithelial cells) to be overexpressed as N-terminal epitope-tagged recombinant transmembrane proteins. Overall, this strategy has yielded important insights into the immunomodulatory potentials of LITRs and revealed conserved and unique mechanisms of LITR-mediated control of innate immune effector responses (Fei et al., 2016). For example, IpLITR1.1b used a novel SHP-1-independent mechanism to abrogate cellular killing of MHC class 1 deficient B cell targets when overexpressed in mouse lymphokine activated killer cells (Montgomery et al., 2012). Additional experiments also revealed that the proximal and distal CYT segments of IpLITR1.1b independently regulated phagocytosis and differentially recruited

several Src homology 2 (SH2) domain-containing effector molecules (Zwozdesky et al., 2017). Moreover, fluorescent microscopy experiments showed that the non-catalytic region of tyrosine kinase adaptor protein (Nck) and Syk localized with IpLITR1.1b during IpLITR1.1b-mediated phagocytosis, indicated that IpLITR1.1b uses diverse signaling mechanisms to regulate phagocytosis (Lillico et al., 2020). Recently, a new receptor crosstalk model was established by Fei et al., (2020). This new model demonstrated that LITRs could cooperate to regulate each other's signaling activities (Fei et al., 2020). Specifically, IpLITR1.1b's inhibitory action on IpLITR2.6b-mediated phagocytosis was shown to require the prior activation of IpLITR2.6b. This result is consistent with findings in mammalian receptor systems whereby the activation of an inhibitory immunoregulatory receptor often requires previous stimulatory stimuli (Srivastava et al., 2003). Furthermore, these experiments also demonstrated that the proximal and distal CYT segments of IpLITR1.1b recruited the inhibitory molecules C-terminal Src kinase (Csk) and SHP-2, respectively (Fei et al., 2020). Recruitment of these molecules was shown to be required for sustaining IpLITR1.1b-mediated inhibition of phagocytosis and signaling transduction. Altogether, this new receptor crosstalk model has revealed important mechanistic insights into receptor crosstalk-mediated regulation of innate immune responses and shown that LITRs use novel intra- and inter-cytoplasmic signaling mechanisms to modulate immunoregulatory receptor functions.

Although LITRs have been studied for almost two decades, their functional roles in teleost immunity remain largely uncharacterized. Nonetheless, the handful of studies carried out thus far have significantly improved our understanding of the immunoregulatory roles of LITRs in teleost immune cells (Wang et al., 2023). These investigations have been made feasible by the development of IpLITR-specific monoclonal antibodies (mAbs) and the use of channel catfish

immune cell lines (Wang et al., 2023). For example, the Ab CC41, an IpLITR-reactive mAb, was shown to stain multiple channel catfish cell lines such as the TS32.15 cytotoxic T cell line (CTL) and 15 other NK-like catfish cell lines (Shen et al., 2002; Taylor et al., 2016). Subsequent immunoprecipitation experiments showed that CC41 recognized a variety of putative inhibitory and activating IpLITR-types in TS32.15 CTLs (Taylor et al., 2016). Furthermore, researchers showed that channel catfish virus (CCV)-infected fish exhibited a significantly elevated proportion of $CC41^+$ cells in their PBLs compared to mock-infected counterparts. Additional experiments revealed that $CC41^+$ isolated cells displayed robust cytotoxicity against CCV-infected syngeneic G14D γδ T cells. Moreover, pre-treatment of a mixed leukocyte culture with CC41 diminished the capacity of this cell population to lyse CCV-G14D targets. Overall, this suggests that CC41-reactive IpLITRs play a role in regulating cell-mediated immunity against viral infections. Similarly, another investigation showed that $CC41^+$ PBLs proliferated in response to *Edwardsiella ictalurid*-infected channel catfish macrophages, supporting the potential involvement of select IpLITRs in anti-bacterial defenses (Blackmon et al., 2020). In a more recent study, given that CC41 primarily recognizes putative inhibitory IpLITR types, while another IpLITR mAb, 125.2, mainly identifies putative activating IpLITR types, researchers explored potential cross-talk signaling events between IpLITRs with presumed opposing functions (Crider et al., 2023). This investigation utilized the channel catfish 42TA macrophage cell line, which expresses both 125.2- and CC41-reactive LITRs. Consistent with the ability of the 125.2 mAb to interact with putative activating IpLITR forms, 125.2-coated microbeads induced 42TA macrophage cells to perform phagocytosis. However, pre-treatment of 42TA macrophages with CC41-coated beads significantly reduced the phagocytic capacity of these cells. Hence, these findings supported the results from our heterologous expression studies

(Crider et al., 2023) and reinforced that IpLITRs can regulate phagocytosis through crosstalk mechanisms in channel catfish immune cells. Altogether, the development of IpLITR-specific mAbs has played a pivotal role in advancing our knowledge of the immunomodulatory functions of LITRs in catfish immune cells.

Overall, our initial phylogenetic analyses of the Ig-like domains of IpLITRs suggested that they might be evolutionary equivalents of the vertebrate FcR family and LRC-encoded receptors. However, it is unknown whether LITRs share similar exon-intron organization or conserved synteny with these receptors. Moreover, the ligands of LITRs remain unidentified, posing challenges in establishing their orthology with either the vertebrate FcR family or LRC-encoded receptors. While the heterologous overexpression studies have yielded detailed mechanistic insights into the immunoregulatory potentials of IpLITRs, their actual roles in teleost immunity have largely been unexplored. The goldfish (*Carassius auratus* L.), with its well-established primary myeloid cell culture system, including primary kidney macrophages and neutrophils, and a variety of established immune functional assays (i.e., degranulation, respiratory burst, and phagocytosis assays), represents an ideal model system for further investigation of the native roles of LITRs in teleost myeloid cells.

1.2 Objectives

The overall aim of my thesis was to establish the goldfish as a new model system for studying the native functions of LITRs. The specific objectives of my thesis were as follows: i) identification of *Carassius auratus* (Ca)-LITRs and examination of their genetic organization and transcript expression in various goldfish tissues, primary PKM, and PKN cultures; ii) examination of the syntenic relationships between LITRs and immunoregulatory receptors found in other vertebrates; iii) analysis of transcript expression of *calitrs* during PKM development and

in activated goldfish kidney leukocyte cultures, and; iv) development of new Ab-based tools for investigating the native functions of CaLITRs in goldfish primary myeloid cells.

1.3 Thesis outline

Chapter II provides a thorough review of the literature essential for understanding the various topics covered in this thesis. It begins with an overview of the vertebrate innate immunity and immunoregulatory receptors. Following this, I will summarize the IpLITR findings obtained from the heterologous expression studies and the use of IpLITR-specific mAbs. Finally, the advantages of the goldfish model system will be discussed, along with an iteration of the main objectives of this thesis. Chapter III details the specific protocols, methods, and reagents used for collecting the data presented in this thesis. Chapter IV describes the initial discovery of several *calitr* transcripts and their sequence variants. Further sequence analyses showed that these genes share similar exon-intron organizations as their mammalian LRC counterparts. Additionally, this study suggests that alternative splicing may play a significant role in diversifying the ligand binding and/or cytoplasmic signaling capabilities of CaLITRs. In Chapter V, I used a comparative genomics approach to comprehensively investigate the possible syntenic relationships between teleost *litrs* and various vertebrate receptors of the FcR family and LRC. My findings support that teleost LITRs are likely to be distant relatives of the vertebrate FCRLs. In Chapter VI, I examined the transcriptional activities of several *calitrs* from distinct goldfish Chrs. These data revealed that these *calitrs* are differentially expressed during PKM development and in activated goldfish leukocyte cultures. Therefore, these data support that select *calitrs* from distinct goldfish genomic regions may be under the influence of different cis- and/or trans-regulatory elements. Chapter VII details the development and characterization of several CaLITR3-specific pAbs. This study showed that the anti-CaL3.D1 pAb stained

various leukocytes within the goldfish kidney, as well as isolated goldfish PKNs and PKMs. Additionally, cross-linking of anti-CaL3.D1-pAb-reactive membrane proteins activated the MAPK signaling pathway in goldfish PKNs, supporting that stimulatory CaLITR-types may regulate innate immune effector functions in goldfish myeloid cells. Chapter VIII summarizes the main findings of this thesis. It also outlines future directions for further exploration of the native immunoregulatory roles of LITRs in goldfish myeloid cells, as well as possible approaches for the identification of LITR ligands. The references are also listed.

CHAPTER II

LITERATURE REVIEW

2.1 Overview of the vertebrate innate immunity

To counter infectious agents, vertebrates have evolved two major branches of immune defense strategies: innate immunity and adaptive immunity. Innate immunity constitutes the 'inborn' arm, responsible for generating a rapid response against a broad spectrum of pathogens (Marshall et al., 2018). In contrast, adaptive immunity is triggered later during infection, displaying high specificity towards particular pathogens, and establishing a long-lasting memory that enables targeted defense upon re-exposure (Marshall et al., 2018).

The vertebrate innate immune system comprises physical and chemical barriers, highly conserved and sophisticated networks of innate immune cells equipped with their pathogen recognition molecules, and potent anti-microbial soluble immune factors (Riera Romo et al., 2016). Despite the categorical distinction between innate and adaptive immunity, these two systems are intricately intertwined, and their collaboration is essential for the successful defense of the vertebrate host (Smith et al., 2019). For instance, when innate phagocytes like dendritic cells sense microbial threats, they can engulf these microbes and present the antigenic peptides bound by major histocompatibility complex (MHC) molecules to naive T-helper cells of the adaptive immune system. Following stimulation by dendritic cells, activated T helper cells then prompt select B cells to secrete their antigen-specific cell-surface receptors, known as Abs. These soluble proteins are capable of recognizing and eliminating microbial threats through various mechanisms such as neutralization, complement activation, and ADCC (Smith et al., 2019). Simultaneously, the adaptive immune cells can also influence their innate immune counterparts

by secreting immunomodulatory proteins to either positively or negatively regulate their functional activities (Smith et al., 2019).

In this review, I will begin by outlining the fundamental components of vertebrate innate immunity before discussing the specifics of innate immunoregulatory receptors. I will predominately address the innate components of both teleost fish and mammals, as they are essential for understanding the data chapters covered in this thesis.

2.1.1 Biochemical 'shields' of the innate immunity

All vertebrates rely on a form of outer covering or integument to shield themselves from the external environment and potential microbial threats. While the shapes and sizes of these integuments can differ considerably depending on the diverse lifestyles of different vertebrates, they exhibit similar overall structures, cellular and humoral compositions, and functions (Riera Romo et al., 2016).

Using mammals as an example, the first barriers preventing pathogens from invading the body are the physical and chemical barriers of the innate immune system. Physical barriers include structures like the skin, mucus membranes lining the gastrointestinal and urogenital tracts, and respiratory system (Zhang et al., 2022). For example, dead keratinocytes from the epidermis form a protective layer that blocks microbes from penetrating deeper into the skin tissues (Zhang et al., 2022). Furthermore, goblet cells produce and secrete mucins (glycoproteins) to coat the intestinal epithelium with thick mucus lining to control microbiome homeostasis (Zhang & Wu, 2020). Similar to how steel provides additional flexibility and strength to a high-rise building, the physical barriers are bolstered by chemical defenses. For instance, a diverse array of antimicrobial peptides, such as cathelicidin and β-defensins, are

secreted by the sebaceous and sweat glands, along with acidic free fatty acids from the skin, creating an environment hostile to microbial colonization (Zhang et al., 2022). Another example is the stomach acid. The low pH of the stomach acid not only helps in the digestion of food particles but also aid in the destruction of pathogenic microbes (Smith, 2003).

In contrast to the keratinized skin of mammals, the skin of teleost fish is often covered with bony scales and thick mucus (Cain & Swan, 2010). Besides its roles in osmoregulation, ion regulation, and reducing drag, the teleost skin serves as a major barrier to pathogen invasion in the aquatic environment. Specifically, the viscous nature of the mucus creates an impenetrable barrier to pathogen attachment. Additionally, fish regularly regenerate and slough off this mucus layer, further impeding the establishment of harmful microbes (Ángeles Esteban, 2012). Similar to mammalian skin epithelium, the teleost skin contains a complex cocktail of antimicrobial compounds such as lysozymes, proteases, cathelicidins, and defensins (Ángeles Esteban, 2012). Since fish guts and gills are also intimately connected to the external environment, they are likewise covered with mucus (Ángeles Esteban, 2012). Moreover, in all jawed vertebrates, microbiota on mucosal surfaces also help maintain the integrity of these delicate areas by competitively inhibiting the colonization of pathogens and secreting antimicrobial products (Takiishi et al., 2017).

2.1.2 Cellular innate immunity

If exogenous invaders manage to overcome the physical and chemical barriers, they will encounter the second line of immune defense. This defense line consists of diverse types of innate immune cell types and soluble proteins (Riera Romo et al., 2016) that are evolutionarily conserved. Various lineages of innate immune cells, such as macrophages, neutrophils, NK cells, and many others, perform specialized functions and collaborate to detect and respond to both

external and internal threats, thus providing a coordinated defense against infections (Riera Romo et al., 2016).

In the next sections, I will introduce several innate immune cell types that play integral roles in cellular innate immunity.

2.1.2.1 Macrophages

Macrophages are a heterogeneous population of cells belonging to the myeloid lineage (Wynn et al., 2013). Like all other blood cells, they are derived from hematopoietic stem cells (HSCs) in the bone marrow (Wynn et al., 2013). However, they are also known to originate from other sources such as the yolk sac and fetal liver (Wynn et al., 2013). These cells undergo several differentiation stages, ultimately becoming circulating monocytes with a round morphology and kidney-shaped nuclei (Lawrence & Natoli, 2011). These monocytes can then differentiate into macrophages, which have irregular shapes and more rounded nuclei (Wynn et al., 2013). Functionally, macrophages are immune cells that are highly efficient at engulfing and digesting pathogens (Aderem & Underhill, 1999). Additionally, they serve as ‘janitors’, actively scanning their surroundings for damaged cells undergoing apoptosis and/or necrosis (Mosser & Edwards, 2008). These clearance processes are critical, as inefficient removal of damaged or apoptotic cells can often lead to the development of autoimmune diseases or other physiological defects (Ma et al., 2023). Along with dendritic cells, and B cells, macrophages are professional antigen-presenting cells (APCs) (Mellman et al., 1998). Following the engulfment of microbes, these cells process microbial peptides and present them to naïve T helper cells located in lymph nodes, priming them for the activation of the adaptive immune system (Mellman et al., 1998). Two functionally distinct macrophage types are present in both teleost fish and mammals (Grayfer et al., 2018). The classically activated/M1 macrophages represent the proinflammatory type. When

these cells are stimulated by proinflammatory cytokines (i.e., tumor necrosis factor alpha (TNF-α) and interferon-gamma (IFNγ) or microbial components like lipopolysaccharide (LPS)), they upregulate the expression levels of the inducible nitrate oxide synthase enzyme (iNOS/NOS2) (Grayfer et al., 2018). This enzyme mediates the conversion of L-arginine to L-citrulline to produce nitric oxide (NO), a powerful antimicrobial agent (Grayfer & Belosevic, 2012). Conversely, the alternative/M2 macrophages represent the anti-inflammatory type. These cells can be polarized by pro-healing/anti-inflammatory cytokines such as interleukin(IL)-4 and IL-13 (Grayfer et al., 2018). The arginase enzyme in M2 macrophages converts L-arginine to L-ornithine and urea. L-ornithine serves as a substrate to produce proline and polyamines, which facilitate cellular proliferation and collagen production for wound healing (Grayfer et al., 2018).

As briefly mentioned, a prominent function of macrophages is phagocytosis (Gregory & Devitt, 2004). Phagocytosis refers to the receptor-mediated cellular process of sensing and engulfment of particles larger than or equal to 0.5 μm, such as microbes and apoptotic cells (Uribe-Querol & Rosales, 2020). This is an incredibly intricate process requiring the coordinated action of various molecules, which are precisely controlled and organized both in terms of their physical locations within the cell and the timing of their activities.

Diverse families of receptors are known to control phagocytosis by recognizing the phagocytic substrates and initiating complex signaling pathways (Fu & Harrison, 2021). These receptors cooperate in sensing phagocytic particles, and the decision for phagocytes to engulf them depends on the nature of the cell type as well as the specific sets of phagocytic receptors engaged. Phagocytic receptors can be categorized into opsonic or non-opsonic receptors (Uribe-Querol & Rosales, 2020). Opsonins are soluble molecules synthesized by the host (i.e., Abs) to mark targets for enhanced destruction by phagocytes (Uribe-Querol & Rosales, 2020). Non-

opsonic receptors can directly interact with distinct molecular patterns on particles for engulfment, with examples including Dectin-1, macrophage-inducible C-type lectin (Mincle), and scavenger receptors (Uribe-Querol & Rosales, 2020). In contrast, opsonic receptors indirectly recognize opsonin-particle complexes (Uribe-Querol & Rosales, 2020). These receptors include FcRs and complement receptors (CRs).

Once particles are sensed by phagocytic receptors, intricate signaling pathways are initiated, leading to the dynamic remodeling of the actin cytoskeleton and membrane lipids (Levin et al., 2015). This causes pseudopod extension around the target, forming a phagocytic cup (Levin et al., 2015). Subsequently, the membrane at the distal ends of the pseudopods close to form a phagosome containing the internalized target (Levin et al., 2015). The early phagosome then undergoes membrane fusion and fission events by associating with endosomes and lysosomes to ultimately form a phagolysosome (Levin et al., 2015). This compartment is characterized by low pH, and it is essential for the degradation of the internalized particle and the processing of microbial peptides for antigen presentation (Levin et al., 2015).

While a large number of phagocytic receptors are known to control phagocytosis, the mechanistic basis of this process is best understood in FcγR and CR-mediated phagocytosis (Uribe-Querol & Rosales, 2020). FcγRs are opsonic receptors that specifically bind the fragment crystallizable region (Fc) region of IgGs. FcRs will be discussed in more detail in the dedicated section on the FcR family receptors in this review. Upon Ab recognition by select cell surface FcγRs, this induces phosphorylation of the ITAMs within the CYT of these receptors (Uribe-Querol & Rosales, 2020). The Activation of ITAMs then sets off a sequence of highly ordered membrane remodeling events and subsequent activation of complex kinase-mediated signaling cascades (Uribe-Querol & Rosales, 2020).

Specifically, the phosphorylated ITAM can recruit Syk. Activation of Syk in turn stimulates various downstream molecules such as vav guanine nucleotide exchange factor (Vav), phospholipase C-gamma (PLCγ), and phosphatidylinositol 3-kinase (PI3K) (Rosales & Uribe-Querol, 2017). Vav is responsible for activating several small GTPases (i.e., Ras-related C3 botulinum toxin substrate 1 (Rac1), Rac2, and cell division cycle 42 (Cdc42)), which, when bound to GTP, participate in activating the Actin Related Protein 2/3 complex (Arp2/3) that is ultimately required for initiating actin polymerization (Rosales & Uribe-Querol, 2017). Furthermore, PLCγ cleaves the membrane lipid phosphatidylinositol 4,5-biphosphate (PIP2) into diacylglycerol (DAG) and inositol triphosphate (IP3) (Rosales & Uribe-Querol, 2017). DAG activates protein kinase C (PKC), which induces the activation of nicotinamide adenine dinucleotide phosphate (NADPH) oxidase (NOX) for ROS production, while IP3 binds to the IP3 receptor (calcium channel) on the ER membrane, triggering calcium release and calcium-mediated signaling pathways (Rosales & Uribe-Querol, 2017). Additionally, PI3K converts PIP2 into phosphatidylinositol (3,4,5)-triphosphate (PIP3), facilitating the recruitment of various molecules such as PLCγ and myosin, a motor protein implicated in sealing the phagocytic cup (Rosales & Uribe-Querol, 2017).

Regarding membrane lipid remodeling, during the formation of the phagocytic cup, PIP2, located in the inner leaflet of the plasma membrane, begins to accumulate around the phagocytic cup (Levin et al., 2015). This accumulation leads to an interaction of PIP2 with Wiskott-Aldrich Syndrome protein (WASp) (an actin nucleation promoting factor), thereby activating Arp2/3 to promote F-actin polymerization for pseudopod extension around the phagocytic target (Levin et al., 2015). As the pseudopods extend around the phagocytic target, the PIP2 concentration directly beneath the phagocytic cup starts to decline and becomes

undetectable shortly following phagosome closure (Levin et al., 2015). The disappearance of PIP2 is closely associated with actin disassembly, a vital step for phagosome formation known to be mediated by PI3K (Levin et al., 2015). Specifically, following the recruitment of PI3K by Syk, PI3K converts PIP2 into PIP3, leading to a decrease in PIP2 concentration and an increase in PIP3 concentration around the phagocytic cup (Levin et al., 2015). Additionally, PIP3 recruits PLCγ, further contributing to the disappearance of PIP2 (Levin et al., 2015). For more information on FcγR-mediated phagocytosis, refer to these excellent reviews (Levin et al., 2015; Mao & Finnemann, 2015; Rosales & Uribe-Querol, 2017; Uribe-Querol & Rosales, 2020).

2.1.2.2 Neutrophils

Mammalian neutrophils are myeloid cells derived from HSCs in the bone marrow (Rosales, 2018). During differentiation, they progress through several stages, starting with a round nucleus that gradually changes to a kidney shape, known as band neutrophils, and ultimately becoming mature neutrophils with multi-lobed nuclei (Rosales, 2018). These mature cells are granulated and have diameters ranging from 12-15 μm (Rosales, 2018). Functionally, neutrophils are ‘emergency responders’ of the innate immune system. Upon sensing inflammatory stimuli, these cells quickly migrate to the infection site following chemokine gradients (i.e., CXCL8) (Burn et al., 2021). Like macrophages, they are recognized as ‘professional’ phagocytes due to their superior phagocytic capabilities compared to other ‘amateur’ phagocytes (i.e., epithelial, and endothelial cells) (Sihombing et al., 2021). Apart from phagocytosis, neutrophils possess numerous other anti-microbial defense mechanisms (Burn et al., 2021). Both teleost and mammalian neutrophils, for instance, contain intracellular granules packed with powerful anti-microbial agents such as myeloperoxidase (MPO), elastase (NE), and acid hydrolases (Havixbeck & Barreda, 2015). Upon activation, neutrophils promptly release

these toxic molecules through degranulation to aid in pathogen eradication and the breakdown of extracellular matrixes for transendothelial migration (Havixbeck & Barreda, 2015). Additionally, both teleost and mammalian neutrophils are well-known for their ability to release neutrophil extracellular traps (NETs) (the process is termed NETosis), a phylogenetically conserved defense strategy (Brinkmann et al., 2004). NETs are characterized by decondensed chromatin that are released by neutrophils in response to a wide variety of stimuli such as LPS, zymosan, and mitogens (Chen et al., 2021). Although the mechanism of NETosis is better characterized in mammals than in teleost fish, this process is known to be induced through both NOX-dependent and independent mechanisms in both groups (Pijanowski et al., 2013). In the case of NOX-dependent mechanism, the release of NETs is dependent on the formation of reactive oxygen species (ROS) (Schoen et al., 2022). For example, following stimulation by select pathogens, PKC and NOX are activated (Schoen et al., 2022). The activated NOX then catalyze the formation of ROS, which subsequently activates the MPO, NE, and peptidyl arginine deiminase (PAD4) enzymes (Schoen et al., 2022). These activities cause MPO and NE to translocate to the nucleus, leading to chromatin unfolding. Additionally, the activation of PAD4 results in the citrullination of histone proteins, causing further unwrapping of the chromatin. The combined actions of MPO and NE ultimately lead to the rupture of the nuclear membrane and the expulsion of NETs, which are adorned with potent antimicrobial compounds like histones to entrap and kill pathogens (Schoen et al., 2022). As the neutrophils disintegrate during NOX-dependent NETosis, this form of cell death is referred to as suicidal NETosis, a process that typically takes hours (h) (2-4 h) to complete (de Buhr & von Kockritz-Blickwede, 2016).

Alternatively, NETosis can also occur independently of NOX activity (de Buhr & von Kockritz-Blickwede, 2016). For instance, when neutrophils are stimulated by activated platelets,

calcium signaling is triggered, which directly activates the PAD4 enzyme. This results in the release of NETs through vesicle release. Consequently, neutrophils remain intact and can still perform other functions like phagocytosis (de Buhr & von Kockritz-Blickwede, 2016). This form of NETosis is known as vital NETosis and typically takes a much shorter time (5-60 minutes (min)) to complete compared to suicidal NETosis (Favor et al., 2021).

Another major neutrophil-mediated innate immune effector response is the synthesis of ROS (Havixbeck & Barreda, 2015). Various factors can induce ROS production in neutrophils. For example, when select receptors (i.e., integrins and FcRs) on neutrophils are activated, this drives the assembly of NOX (Chen et al., 2021). Two events then follow: activation of Rac2 and phosphorylation of intracellular components of NOX ($p37^{phox}$, $p40^{phox}$, and $p67^{phox}$) (Nguyen et al., 2017). These molecules then move to the cell membrane to interact with the membrane components of NOX ($cytb_{558}$) to form the NOX complex. The fully assembled NOX is now capable of transferring electrons from the cytosol to oxygen, generating ROS. The ROS can either be pumped outside to directly target the infectious agents or into the phagolysosome following neutrophil phagocytosis (Nguyen et al., 2017). Interestingly, some factors are known to directly activate ROS production in neutrophils, whereas others function as priming agents (Nguyen et al., 2017). Prior stimulation by these priming agents can lead to enhanced neutrophil reaction to other stimuli, but they do not directly activate neutrophil functions.

2.1.2.3 Natural killer cells (NK cells)

NK cells originate from an NK-T-cell progenitor during hematopoiesis (Rahman & Bordoni, 2023). They are characterized as large granular lymphocytes that do not express both T cell receptors and B cell receptors (BCRs) (Rahman & Bordoni, 2023). NK cells are important players in the elimination of cancerous and virally infected cells (Caligiuri, 2008). These cells

continuously monitor non-self and/or altered self-patterns on the surface of abnormal cells. Once recognized, NK cells establish physical contact with these cells and induce apoptosis either by releasing cytotoxic granular contents containing granzymes and perforin or through a Fas/FasL-based mechanism (Caligiuri, 2008).

NK-like cells have also been described in teleost fish, such as the channel catfish and common carp (Suzumura et al., 1994). In the channel catfish, non-specific cytotoxic cells (NCCs) are among the best-characterized cytotoxic cells (Shen et al., 2002). Predominately located in the kidney, these cells share similar ultrastructural features and functional properties with mammalian NK cells (Shen et al., 2002). They can lyse a variety of mammalian NK cell targets and specific fish parasites (Evans & Jaso-Friedmann, 1992; Graves et al., 1984). Additionally, they can be labeled by the 5C6 mAb, which recognizes a type 3 transmembrane receptor known as NCC receptor protein-1 (NCCRP-1) (Evans et al., 1988; Jaso-Friedmann et al., 1997) on the surface of NCCs. Ligation of this receptor can trigger signaling in NCCs (Evans et al., 1996). Furthermore, 56C has also been shown to be capable of blocking the cytotoxicity of NCCs (Evans et al., 1988).

Besides NCCs, another population of cytotoxic cells functionally distinct from NCCs has been identified (Stuge et al., 1995). These are known simply as NK-like cells. Unlike NCCs, these cells are primarily found in the peripheral blood and preferentially lyse allogeneic channel catfish cell lines (Hogan et al., 1999). In contrast to NCCs, 5C6 does not inhibit the cytotoxicity of these NK-like cells (Stuge et al., 1995). However, the calcium chelator, EDTA, effectively inhibits their cytotoxicity, suggesting that these cells utilize a calcium-dependent perforin/granzyme-mediated mechanism for inducing target cell lysis (Hogan et al., 1999).

2.1.3 Humoral arm of innate immunity

Soluble innate immune proteins play a crucial role in immune defense and maintaining physiological homeostasis. These soluble factors encompass a wide variety of proteins that include, but are not limited to, molecules of the complement system, acute phase proteins, natural Abs, cytokines, and chemokines (Mantovani & Garlanda, 2023). Furthermore, many of these molecules are found across vertebrates and have conserved functions (Uribe et al., 2011).

2.1.3.1 Complement system

The complement system is composed of a large collection of serum proteins that serve to detect and generate complex inflammatory responses to combat pathogenic microbes (Sarma & Ward, 2011). Members of the complement system are generally activated through protease-mediated cleavage or function as proteases themselves (Sarma & Ward, 2011). These proteins interact with one another to trigger a series of reaction cascades in the bloodstream and contribute to the clearance of microbes using various mechanisms (Sarma & Ward, 2011). For example, complement molecules can act as opsonins, marking pathogens for destruction by macrophages (Sarma & Ward, 2011). Additionally, these molecules can directly lyse microbial intruders by forming pores (membrane attack complex (MAC)) on their surface or by acting as anaphylactic toxins to recruit and activate immune cells (Sarma & Ward, 2011). The complement system is evolutionarily conserved in vertebrates, and both teleost and mammalian complement systems can be activated via three distinct pathways: the classical pathway, the alternative pathway, and the lectin pathway (Li & Zhang, 2022). Although the initial recognition molecules for complement activation are different between the three complement pathways, they share a similar overall sequence of events.

In the classical pathway, Abs like IgM (CH3 domain) and IgG (CH2 domain) serve as platforms for the binding of complement component 1q (C1q) (Li & Zhang, 2022).

Subsequently, C1q, along with its associated serine proteases, cleaves other complement proteins, including C4 and C2 (Li & Zhang, 2022). The cleavage products of C4 and C2 then assemble to form a C3 convertase, which cleaves C3 into C3a and C3b. C3a acts as a chemoattractant for immune cells, whereas C3b functions to opsonize pathogens for elimination by phagocytes. Furthermore, C3b interacts with C4b and C2b to generate a C5 convertase. The C5 convertase then cleaves C5 into C5a, a chemoattract, and C5b. C5b, along with C6, C7, C8, and C9, combines to form the MAC (Li & Zhang, 2022). In contrast, in the lectin pathway, ficolins and mannose-binding lectins (MBLs) provide the platform for complement activation (Holland & Lambris, 2002). The alternative pathway is initiated when C3 spontaneously hydrolyzes in the vicinity of microbes (Li & Zhang, 2022).

2.1.3.2 Acute phase proteins (APPs)

APPs are synthesized in the liver and characterized by a rapid and sharp increase or decrease in their plasma concentration by at least 25% during the acute phase (~ the first seven days) of inflammation (Mantovani & Garlanda, 2023). Primarily synthesized and secreted by the liver, APPs include various classes of serum proteins, such as C-reactive protein (CRP), haptoglobin, alpha-2-macroglobulin, and fibrinogen, with the purpose of limiting pathogen spread and promoting tissue healing (Gabay & Kushner, 1999). For example, CRP recognizes phosphocholine molecules on microbes and serves as a platform for complement activation (Mold et al., 1999). Haptoglobin, along with hemopexin, binds to free heme in the blood to control oxidative damage and sequester iron, an essential nutrient for microbial growth (Gabay & Kushner, 1999). Alpha-2-macroglobulin participates in neutralizing proteases released by pathogens and tissue injury (Vandooren & Itoh, 2021). Fibrinogen, in addition to its role in coagulation, functions to contain bacterial dissemination and act as an antimicrobial factor (Ko &

Flick, 2016). For a comprehensive review of teleost APPs, see this publication (Bayne & Gerwick, 2001).

2.1.3.3 Chemokines

Chemokines comprise a large family of small, secreted proteins (8-10 kDa) that share structural similarities (Hughes & Nibbs, 2018). These proteins interact with membrane-derived chemokine G-protein-coupled heptahelical chemokine receptors and act as chemical signals for immune cells, enabling intercellular communications. This interaction facilitates diverse functions such as pathogen defense and migration of immune cells (Hughes & Nibbs, 2018). In general, chemokines are responsible for recruiting immune cells to the site of inflammation (Hughes & Nibbs, 2018). In humans, chemokines are categorized into four subfamilies according to the arrangement of the two N-terminal cysteine residues: CXC, CC, XC, and CX_3C (where C represents a cysteine residue, and X denotes any residues except cysteine) (Hughes & Nibbs, 2018). The first teleost chemokine, CK-1 (a CC-type chemokine) was discovered in rainbow trout in 1998. Since then, due to advances in genome sequencing technologies, many other chemokines have been uncovered in other teleost species (Xu & Liu, 2024). While the CC and CXC chemokine types are known to be shared by mammals and teleost fish, some (CX-type) are unique to the teleost group (Xu & Liu, 2024). Mammalian and teleost chemokines have been shown to perform a wide variety of functions, including regulating immune cell trafficking (Chen et al., 2013; Krumbholz et al., 2007), exhibiting direct antimicrobial activities (Munoz-Atienza et al., 2019; Yung & Murphy, 2012), and regulating blood vessel formation (Bonapace et al., 2014; Lu et al., 2012).

2.1.3.4 Cytokines

In addition to chemokines, which are part of the cytokine family, a wide variety of other low molecular weight cytokine molecules (generally under 30 kDa) also regulate immune cell functions in both mammals and teleost fish (Zou & Secombes, 2016). Cytokines are loosely categorized and generally function by binding to specific receptors on their target cells (Zou & Secombes, 2016). They are secreted by a diverse range of innate and adaptive cells and can be classified into several categories, including ILs, interferons (IFNs), transforming growth factors (TGFs), and TNFs (Sakai et al., 2020). Additionally, many of these proteins either function as proinflammatory or anti-inflammatory cytokines. Pro-inflammatory cytokines enhance the inflammatory activities of immune cells, whereas anti-inflammatory cytokines work to reduce inflammation (Grayfer & Belosevic, 2012). As an example, upon stimulation, macrophages produce and secrete proinflammatory cytokines like IL-6, IL-1β, and TNF to induce fever and prompt the liver to secrete acute phase proteins (Gabay & Kushner, 1999; Grayfer & Belosevic, 2012). Following pathogen clearance, anti-inflammatory cytokines like IL-10 and TGF-β contribute to the termination of immune responses while mitigating tissue damage (Grayfer & Belosevic, 2012). For a comprehensive review of teleost and mammalian cytokines, refer to Zhou and Secombes (2016).

2.1.4 Innate immune sensing receptors

Unlike adaptive immunity, which can generate random configurations of Ig-based sensors/receptors (Abs) that subsequently undergo further mutations and selection processes to produce pathogen-specific recognition molecules, receptors of the innate immune system are derived from germ-line encoded genes and remain relatively static during inflammation. Consequently, the innate immunity system compensates for this inflexible nature with a diverse assortment of both extracellular and intracellular receptors (Li & Wu, 2021). For instance,

pattern recognition receptors (PRRs) have evolved to recognize evolutionarily conserved molecular signatures (i.e., LPS and peptidoglycan) on microbes, formally termed pathogen-associated molecular patterns (PAMPs) (Liao & Su, 2021). These receptors are either located on the membrane of an innate immune cell to deal with extracellular pathogens or are situated intracellularly to combat intracellular pathogens, such as viruses (Liao & Su, 2021). Example PRRs include toll-like receptors (TLRs), RIG-I-like receptors (RLRs), C-type lectin receptors (CLRs), and Nod-like receptors (NLRs). In addition to sensing PAMPs, many PRRs detect damage-associated molecular patterns (DAMPs) released from compromised cells, such as self-DNA and RNA, adenosine triphosphate (ATP), histones, and heat shock proteins (HSPs) (Gong et al., 2020). This broadens the recognition capabilities of innate immune cells, enabling them not just to perceive pathogens but also to discern the consequences of pathogen attack or tissue injury. Besides PAMP- and DAMP-sensing receptors, a distinct innate sensing mechanism has been recently identified: the ability of innate immune proteins to detect homeostasis-altering molecular processes (HAMPs) (Liston & Masters, 2017). This discovery stemmed from the observation that several intracellular sensing molecules (i.e., pyrin inflammasome) interact with a diverse range of ligands, a characteristic not in line with traditional PRRs (Liston & Masters, 2017). Rather than directly sensing DAMPs and PAMPs, these proteins are proposed to function as indirect sensors of disruptions in homeostatic processes caused by infection or tissue injury (Liston & Masters, 2017).

In the sections below, I will briefly introduce several PRR families and discuss the roles they play in mammalian and teleost immunity.

2.1.4.1 TLRs

Among the PRR families, TLRs represent the most extensively studied innate immune receptor family (Mahapatra et al., 2023). Originally discovered in drosophila (Lemaitre, 2004; Lemaitre et al., 1996), these receptors are composed of leucine-rich-repeats (LRRs), which can fold into a horseshoe-like shape and form dimers with either identical TLR-types or with different TLR-types, thereby creating a wide variety of ligand-binding interfaces (Duan et al., 2022). TLRs are expressed in various immune and non-immune cell types like macrophages, dendritic cells, and epithelial cells (Fitzgerald & Kagan, 2020). Members of the TLR family possess the ability to recognize a broad spectrum of PAMPs (Mahapatra et al., 2023) such as unmethylated CpG DNA, flagellin, and LPS, as well as DAMPs (Yu & Feng, 2018). While certain TLRs are localized on the cell surface, others are located within endosomes (Mahapatra et al., 2023). Engagement of TLRs by ligands typically lead to increased transcription and production of pro-inflammatory cytokines and chemokines through either the myeloid differentiation primary response 88 (MyD88)-dependent pathway, the TIR-domain-containing adaptor-inducing beta interferon (TRIF)-dependent pathway, or both (Duan et al., 2022).

Several TLRs have been discovered in teleost fish (Mahapatra et al., 2023). These proteins include mammalian TLR orthologs (i.e., TLR1, TLR2, TLR3, and TLR5) as well as teleost-specific versions (i.e., TLR14 and TLR19) (Matsuo et al., 2008). Like their mammalian counterparts, teleost TLRs are type 1 transmembrane proteins composed of N-terminal LRRs, TM domains that anchor them in the membrane, and a cytoplasmic toll/IL-1 receptor domain (TIR) that associate with TIR domain-containing adaptors to initiate downstream signaling cascades (Liao & Su, 2021). Teleost TLRs are known to engage a wide array of ligands of microbial origins (Mahapatra et al., 2023). For instance, the TLR5 of rainbow trout binds to bacterial flagellin (Tsujita et al., 2004), TLR9 (Lee et al., 2015) detects unmethylated CpG DNA

motifs from bacterial or viral genomes, and TLR19 senses double-stranded RNA (dsRNA) from viruses ((Ji et al., 2018).

2.1.4.2 RLRs

RLRs are evolutionarily conserved cytoplasmic RNA sensors in vertebrates (Chen et al., 2017). This group has three members: RIG-I, melanoma differentiation-associated protein 5 (MDA5), and laboratory of genetics and physiology (LGP2) (Chen et al., 2017). All RLRs possess a central helicase domain and a carboxy-terminal domain (CTD), essential for binding to viral RNAs (Rehwinkel & Gack, 2020). Except for LGP2, RIG-I and MDA5 also have two caspase activation and recruitment domains (CARDs), enabling them to interact with mitochondrial antiviral-signaling proteins (MAVS) bearing CARDs to trigger anti-viral defense signaling pathways (Rehwinkel & Gack, 2020). Using RIG-I as an example, when RIG-I recognizes short viral RNAs, it exposes and oligomerizes their CARDs, allowing them to interact with MAVS anchored on the surface of mitochondria (Rehwinkel & Gack, 2020). MAVS then activates a series of downstream signaling cascades, leading to the activation of several transcription factors, including interferon regulatory factor 3 (IRF3), interferon regulatory factor 7 (IRF7), and nuclear factor κb (NFκb) (Rehwinkel & Gack, 2020). Collectively, these transcription factors induce the transcription of type 1 IFN genes as well as other proinflammatory genes.

RIG-I, MDA5, and LGP2 have also been identified in a variety of teleost fish species (Chen et al., 2017). Like mammals, recombinant proteins of MDA5 and LGP2 have been shown to interact with poly (I:C), a synthetic double-stranded RNA (dsRNA). However, there is no experimental evidence supporting the RNA-binding capability of teleost RIG-I so far (Chen et al., 2017). Interestingly, the transcripts of zebrafish RIG-I variants, RIG-Ia and RIG-Ib, were

shown to upregulate in ZF4 cells (a zebrafish fibroblast cell line) upon exposure to both the spring viremia of carp virus (SVCV) and *Edwardsiella tarda* (a gram-negative bacterium) (Zou et al., 2015). Additionally, luciferase and immunoprecipitation assays supported the interaction of RIG-Ib with MAVS to induce the transcription of IFN response. Furthermore, studies have shown that teleost MDA5 and LGP2 regulate anti-viral defenses in various teleost species (Chen et al., 2017). Overall, this suggests that teleost RLRs share conserved functions with their mammalian counterparts as crucial regulators of anti-viral and bacterial defenses.

2.2 Vertebrate immunoregulatory receptors

Besides the PRR families mentioned above, innate immune cells also utilize complex sets of immunoregulatory receptor-types to sense an array of external insults and internal abnormalities. These receptors play a crucial role in initiating or ceasing immune cell effector responses, which help to effectively eliminate pathogens and facilitate the healing of tissues. In vertebrates, many immunoregulatory receptor-types belong to the IgSF (Takai, 2005b). These receptors generally feature a ligand-recognition region made up of one or more extracellular Ig-like domains, hydrophobic TMs that anchor them within the phospholipid bilayers of a cell, and intracellular CYT regions containing one or more tyrosine-based signaling motifs, enabling them to regulate the activation and/or inhibition of potent innate immune functions. Functionally, immunoregulatory receptors can be classified into either activating receptors or inhibitory receptors (Barrow & Trowsdale, 2006). Activating receptors generally use ITAM to positively regulate immune responses (Barrow & Trowsdale, 2006). Conversely, inhibitory receptors typically rely on the ITIM to suppress ITAM-based signaling pathways (Barrow & Trowsdale, 2006). One common theme among these receptors is that the activating and inhibitory receptors often have highly homologous extracellular domains, allowing them to engage similar ligands

(Takai, 2005b). Thus, they are also referred to as paired receptors. Additionally, inhibitory receptors generally exhibit higher affinity toward their targets than their activating counterparts (Kuroki et al., 2012). This characteristic aids in establishing the threshold for immune activation, thereby preventing inadvertent triggering of the powerful antimicrobial arsenal of the immune system.

In the following sections, I will introduce several tyrosine-based motifs commonly used by immunoregulatory receptors for regulating immune system functions.

2.2.1 ITAM-based signaling pathways

Originally discovered by Reth in 1989 (Reth, 1989), the ITAM motif is defined by the consensus amino acid sequence D/ExxYxxL/Ix(6-12)YxxL/I (Kane et al., 2014; Sims et al., 2012). Typically, this motif is found in the CYTs of activating receptors. However, activating receptors bearing TMs containing positively charged residues (i.e., lysine and arginine) can also form non-covalent associations with various adaptor molecules containing ITAMs, such as DNAX activating protein 12 (DAP12) and Fc common gamma chain (FcRγ) (Call & Wucherpfennig, 2007). When activating receptors bearing ITAMs are engaged by their ligands, this induces phosphorylation of the tyrosine residues of ITAMs by SFKs (i.e., Fyn and Lyn). The phosphorylated tyrosine residues of ITAM then serve as docking sites for the tandem SH2 domains of Syk. Consequently, phosphorylated Syk activates various downstream signaling cascades to initiate a wide variety of immune effector functions (Barrow & Trowsdale, 2006).

2.2.2 ITIM-based signaling pathways

In contrast to activating receptors, inhibitory receptors generally feature long CYTs containing one or more ITIM motifs (Coxon et al., 2017). The ITIM motif is defined by the

consensus sequence S/I/V/LxYxxI/V/L (Kane et al., 2014). Co-engagement of activating and inhibitory receptors by shared ligands induces phosphorylation of the ITIM motif (Coxon et al., 2017). Subsequently, the phosphorylated ITIM serves as a platform for the recruitment of several protein tyrosine phosphatases (PTPs) such as SHP-1, SHP-2, and SH2-containing Inositol 5'-Phosphatase (SHIP). As a result, activated PTPs can dephosphorylate intermediates of the ITAM-mediated signaling pathways, thereby attenuating the overall immune response (Coxon et al., 2017).

2.2.3 Immunoreceptor tyrosine-based switch motif (ITSM)

In addition to ITAM and ITIM motifs, another commonly observed tyrosine-based motif in immunoregulatory receptors is the ITSM. The ITSM is characterized by the consensus amino acid sequence TxYxxV/I (where T represents threonine) (Eissmann et al., 2005). This motif is predominantly found in the signaling lymphocyte activation molecule (SLAM) family receptors, most of which bind to self-ligands (Dong & Veillette, 2010). When SLAM receptors bearing ITSM motifs bind to their ligands, these motifs become phosphorylated, enabling them to specifically recruit SLAM-associated protein (SAP) adaptors, including SAP and its relatives, Ewing sarcoma-associated transcript (EAT)-2 and EAT-2-related transducer (ERT) (Ma et al., 2007). The SAP adaptors are primarily expressed at high levels in various adaptive immune cells such as NK and T cells (Ma et al., 2007). The recruitment of SAP adaptors to SLAM receptors is recognized to trigger stimulating signaling pathways through two proposed mechanisms (Ostrakhovitch & Li, 2006): 1) SAP adaptors can block PTPs like SHP-1, SHIP-1, and Csk from binding to SLAM receptors, and 2) SAP adaptors can interact with SFKs (i.e., Fyn) and other activating intermediates (i.e., PLC-γ) to engage activating signaling pathways. However, in the

absence of SAP adaptors, ITSM motifs associate with PTPs such as SHP-2 to negatively regulate immune responses, akin to ITIMs (Ma et al., 2007).

2.2.4 Functional plasticity of tyrosine-based signaling motifs

Classically, ITAM-bearing and ITIM-bearing immunoregulatory receptors are known to control the activation and inhibition of immune functions, respectively (Barrow & Trowsdale, 2006). However, we now understand that activation of ITAM-bearing receptors may result in functional inhibition, and engagement of ITIM-bearing receptors can sometimes lead to immune activation (Blank et al., 2009). This phenomenon is referred to as functional plasticity.

A well-recognized inhibitory-ITAM(ITAMi)-bearing receptor is FcαR (Pasquier et al., 2005). Since FcαR has a short CYT, it associates with its ITAM-bearing adaptor, FcRγ, to trigger immunostimulatory signals upon receptor binding by IgA-complexes (Bakema & van Egmond, 2011). Sustained aggregation of FcαR results in strong phosphorylation of the ITAM motif, leading to the recruitment of Syk and the initiation of activating signaling pathways (Bakema & van Egmond, 2011). However, engagement of FcαR by low avidity or weakly binding ligands, such as IgA Fab (fragment antigen binding), results in weak/partial phosphorylation of the ITAM motif on FcRγ. Instead of recruiting Syk, this partial ITAM phosphorylation preferentially recruits SHP-1, leading to an overall downregulation of the immune response (Blank et al., 2009). It has been proposed that the dual functionality of FcαR helps maintain physiological homeostasis by establishing an activation threshold for immune responses, thereby preventing the development of autoimmune diseases (Blank et al., 2009). In addition to FcαR, several other ITAM-containing immunoregulatory receptors have been reported to exhibit inhibitory functions. For further information, refer to this manuscript (Blank et al., 2009).

ITIM-bearing receptors, typically associated with inhibitory functions, have also been reported to play stimulatory roles (Kane et al., 2014). These stimulatory ITIMs are known as activating ITIMs (ITIMas). For example, TREM-like transcript-1 (TLT1) is a platelet receptor having a CYT containing tandem ITIM motifs. Following receptor activation, the classical ITIM motif of TLT1 recruits SHP-2, a PTP that normally inhibits immune functions (Barrow et al., 2004). However, the co-engagement of TLT1 and FcεR (an activating receptor) results in an overall enhancement of FcεR-dependent calcium signaling (Barrow et al., 2004). This augmentation of FcεR-dependent calcium response is dependent on SHP-2, as mutation of the tyrosine residue in the classical ITIM of TLT1 abolishes this response. Another example is the signal regulatory protein α (SIRPα), which has a CYT containing four ITIMs (Alblas et al., 2005). When these motifs are phosphorylated, they recruit SHP-1 and SHP-2, which are known to inhibit LPS-mediated TNFα production in human monocytes (Alblas et al., 2005). However, ligation of SIRPα on rat macrophages has also been shown to trigger stimulatory signaling pathways such as NO production, activation of the Janus kinase/signal transducers and activators of transcription (JAK)-STAT signaling, and activation of NOX (Alblas et al., 2005).

Overall, these findings highlight the functional plasticity of immunoregulatory receptors. This characteristic likely provides these receptors with greater dynamic control over immune responses, enabling them to elicit immune reactions appropriate to the cellular or inflammatory context.

In the upcoming sections, I will be describing the functional roles of FcR family proteins and LRC-encoded receptors, protein families that play diverse immunoregulatory roles in vertebrates.

2.2.5 FcR family receptors

2.2.5.1 FcRs

The FcR family members include FcRs and their distant relatives, FCRLs (Davis et al., 2002). The FcR genes are located within a gene complex (a chromosomal region containing many linked homologous genes) on human Chr 1q21-23 (Davis et al., 2002). These genes encode cell-surface receptors with several extracellular Ig-like domains for binding to Fc regions of Abs (Daëron, 1997). FcRs are classified based on the Ab class that they recognize (Daëron, 1997). For instance, FcRs that interact with IgM, IgA, IgG, and IgE, are named FcμR, FcαR, FcγR, and IgεR, respectively. While FcRs all share the ability to interact with the Fc region of Abs, they are not necessarily related phylogenetically. For instance, the Ig-like domains of FcμR are more closely related to those of polymeric immunoglobulin receptor (pIgR) and Fcα/μR than to the classical FcRs, including FcγRs and FcεR (Kubagawa et al., 2009). pIgRs are responsible for binding and transporting polymeric IgM and IgA from the basolateral membrane of mucosal epithelial cells to the apical surface to maintain microbiome homeostasis (Turula & Wobus, 2018). In contrast, Fcα/μR has been shown to endocytose IgM-coated microbes and IgA immune complexes (Shibuya et al., 2000; Yoo et al., 2011). Unlike the classical FcR genes located on human Chr 1, the FcαR gene is situated in a distinct gene complex on human Chr 19q13, known as the LRC (Breedveld & van Egmond, 2019). Additionally, the Ig-like domains of FcαR share closer homology with LRC-encoded receptors than with the classical FcRs (i.e., FcγRs and FcεR). Besides the FcRs of the IgSF, non-IgSF Fc-binding proteins, including neonatal Fc receptor (FcRn), tripartite motif containing 21 (TRIM21), dendritic cell-specific ICAM-grabbing non-integrin (DC-SIGN), and CD23, have also been reported to bind to Abs via the Fc region (Ben Mkaddem et al., 2019; Dickson et al., 2018).

Classical FcRs are primarily expressed on the membrane of myeloid cells and are well-known to regulate a diverse range of immune functions such as phagocytosis, endocytosis, antigen presentation, and ADCC (Daëron, 1997). These receptors are typically categorized into activating and inhibitory FcR-types (Daëron, 1997). Activating FcR-types feature two or three Ig-like domains, a positively charged TM, and short CYTs. As a result, they rely on association with ITAM-containing adaptor molecules like FcRγ to transmit stimulatory signals. Alternatively, activating FcRs can utilize CYTs containing ITAMs to positively regulate immune responses (Daëron, 1997). Conversely, inhibitory FcR-types use an ITIM-containing CYT to attenuate immune functions (Daëron, 1997). Interestingly, among teleost fish, only one bona-fide FcR has been identified in the channel catfish, IpFcRI. This receptor shares phylogenetic and structural similarities with human classical FcRs and has been shown to bind channel catfish IgM (Stafford, Wilson, et al., 2006).

2.2.5.2 FCRLs

The FCRL genes are closely linked to the classical FcR genes and are co-localized in the FcR gene cluster on human Chr 1q21-23 (Li et al., 2014). FCRL proteins generally contain two or more extracellular Ig-like domains that are distantly related to those of the classical FcRs (Li et al., 2014). Like classical FcRs, several FCRL molecules have been reported to bind various Ab classes, including IgM, IgG, and IgA (Li et al., 2014). However, they are also known to interact with MHC and MHC-like molecules (Campbell et al., 2010; Schreeder et al., 2010). In contrast to classical FcRs, FCRLs are exclusively expressed in lymphocytes such as B cells, NK, and T cells, with several FCRLs proposed to play roles in regulating mucosal immune defenses (Tolnay, 2022).

Specifically, human FCRL3 is expressed in a variety of lymphocytes, such as memory B cells, regulatory T cells (Treg), and NK cells, and it is known to recognize only the secretory version of IgA (dimeric IgA with the secretory component of pIgR) (Agarwal et al., 2020). Upon exposure to SIgA, FCRL3-expressing Treg cells undergo reprogramming to become more like Th17 cells and release a cocktail of inflammatory cytokines, including IL-17, IL-26, and IFN-γ (Agarwal et al., 2020). Since SIgA is normally present in the mucus layer of mucosal tissues, its presence in tissues likely signals a mucosal breach (Agarwal et al., 2020). Therefore, FCRL3 has been postulated to function as a sensor of mucosal tissue integrity (Agarwal et al., 2020).

Unlike FCRL3, FCRL4 has a specific affinity for dimeric IgA and is primarily expressed in memory B cells (Ehrhardt et al., 2005). Given that FCRL4-expressing memory B cells prefer to recognize commensal microbes (Liu et al., 2018), and FCRL4 functions as an inhibitory receptor containing multiple ITIM motifs (Ehrhardt et al., 2003), it has been hypothesized that FCRL4 contributes to the maintenance of mucosal tolerance to commensal microbes (Tolnay, 2022).

In contrast to classical FcRs that recognize Abs via the Fc region, FCRL5 interacts with both the Fc and Fab regions of IgG molecules (Franco et al., 2013). Additionally, FCRL5 exhibits a higher affinity for deamidated IgGs (Alabi et al., 2017). Deamidation is a chemical modification in which asparagine residues on proteins are converted into aspartate residues, serving as a molecular indicator of the proteins' age (Robinson & Robinson, 2001a, 2001b). Therefore, it has been proposed that FCRL5 acts as a sensor of aged IgGs and may be used by immune cells to regulate chronic immune complex-mediated responses (Tolnay, 2022).

Another unique feature of FCRLs is that these receptors generally have long CYTs containing one or more tyrosine-based motifs (Tolnay, 2022). Unlike classical FcRs, which

function either as activating or inhibitory receptors, the majority of FCRLs (i.e., FCRL2, FCRL3, and FCRL5) have CYTs containing both ITAM-like and ITIM motifs, suggestive of their potential ability to regulate both the activation and/or inhibition of immune responses (Tolnay, 2022). Indeed, several studies support the dual functionality of these receptors (Tolnay, 2022). For instance, co-aggregation of FCRL3 and FCRL5 with BCRs has been shown to negatively regulate BCR-mediated signaling pathways (Li et al., 2013). However, FCRL3 has also been found to augment TLR9-mediated B cell activation (Li et al., 2013). While human FCR5 normally represses BCR-mediated signaling, it is known to cooperate with CD21 (a CR), to promote B cell activation (Franco et al., 2018). Additionally, phosphorylation of the ITAM-like and ITIM motifs of mouse FCRL5 recruits Lyn and SHP-1, respectively, enabling the receptor to both enhance and dampen BCR-mediated signaling (Zhu et al., 2013). Lastly, although FCRL4 contains only ITIM motifs, it has been shown to dampen B cell activity while also enhancing TLR9-mediated signaling (Sohn et al., 2011).

Together, these observations demonstrate the complex immunoregulatory capabilities of FCRLs and indicate that FCRLs modulate immune responses based on the composition of immune complexes. This ensures the elicitation of immune responses that are appropriate for the specific context.

Several intracellular FCRLs, including FCRLA and FCRLB, have also been discovered in humans and mice (Santiago et al., 2011; Wilson et al., 2010). The human FCRLA has been shown to be expressed in the endoplasmic reticulum (ER) of B cells and is uniquely capable of binding to various Ab classes, including IgM, IgG, and IgA, within the ER lumen (Santiago et al., 2011). Similarly, mouse FCRLA also has an intracellular localization and can interact with IgM and IgG (Wilson et al., 2010). Due to the intracellular localization of FCRLA and its ability

to bind to intracellular Abs, it has been speculated that FCRLA may primarily function as an ER chaperon for the assembly of Abs before their secretion (Santiago et al., 2011). However, no concrete evidence has yet been shown to support its role as an Ab-quality-control protein.

2.2.6 LRC-encoded receptors

Like the FcR family genes, the LRC genes are organized as a large gene complex on human Chr 19q, spanning 1 million base pairs (Mb) and encompassing 45 sequences, most of which encode receptors with phylogenetically related Ig-like domains (Martin et al., 2002). Examples of LRC-encoded receptors include KIRs, leukocyte immunoglobulin-like receptors (LILRs), osteoclast-associated receptor (OSCAR), leukocyte-associated immunoglobulin-like receptor-1 (LAIR-1), and NKp36 (Martin et al., 2002). These receptors recognize a wide range of exogenous and endogenous ligands and collectively participate in maintaining the balance of the immune system (Martin et al., 2002).

2.2.6.1 Killer Ig-like receptors (KIRs)

Early research on NK cells revealed that a lymphoma cell line that lost MHC class 1 molecules was more susceptible to NK cell killing, whereas the original MHC I+ cells were spared from NK-cell-mediated lysis (Kärre et al., 1986). This led to the hypothesis that certain receptors on the surface of NK cells could detect the absence of self-molecules on the membranes of their target cells, enabling them to distinguish self from non-self (i.e., healthy cells from diseased cells) (Ljunggren & Kärre, 1990). This concept is known as the ‘missing self’ hypothesis. Following these observations, KIRs were eventually identified as a key group of NK cell receptors responsible for mediating self-non-self-recognition in humans (Pende et al., 2019).

KIRs are specific to primates (Martin et al., 2002) and are categorized based on the number of Ig-like domains they possess and whether they contain activating or inhibitory motifs (Pende et al., 2019). For instance, KIR2DL receptors have two Ig-like domains and long CYTs with inhibitory motifs. In contrast, KIR3DS receptors have three Ig-like domains and short CYTs with activating functions. The KIR gene family is extremely diverse in both gene content and alleles (Middleton & Gonzelez, 2010). For instance, approximately 1000 alleles of human KIRs are known (Pende et al., 2019). The polymorphism of KIR is attributed to its ability to interact with human leukocyte antigen (HLA) class 1 molecules, which also exhibit extensive polymorphism (Middleton & Gonzelez, 2010). Mechanistically, several KIR receptors are known to interact with the polymorphic α1 and α2 domains of HLA class 1 molecules (Boyington & Sun, 2002). Furthermore, different KIRs show specificity towards select HLA-class 1 allotypes (protein products of HLA alleles) (Boyington & Sun, 2002). For example, KIR2DL2 specifically interacts with the HLA-Cw3 allotype, while KIR2DL1 specifically recognizes HLA-Cw4 (Fan et al., 2001). The structural basis of the KIR allotype discrimination has been elucidated for a few KIRs due to the availability of KIR-HLA complex crystal structures (Fan et al., 2001; Moradi et al., 2015). In addition to their ability to discriminate between HLA-class 1 allotypes, crystallographic structures of select KIRs have revealed that they can interact with the C-terminal end of the self-peptide bound to HLA-class 1 molecules (Hilton & Parham, 2017). This interaction allows them to detect subtle changes in HLA-bound peptides, which has been implicated in the sensing and elimination of viral infections (Hilton & Parham, 2017). Besides HLA class 1 molecules, several KIRs have also been shown to recognize non-classical HLA proteins, including HLA-G and HLA-F, as well as CpG oligodeoxynucleotides (ODNs) (Pende et al., 2019).

Functionally, KIRs can be classified into activating and inhibitory KIRs. Activating KIRs are characterized by having TMs containing positively charged lysine residues and CYTs devoid of signaling motifs (Debska-Zielkowska et al., 2021). Upon ligand recognition, these receptors associate with DAP12 to initiate ITAM-based stimulatory pathways (Debska-Zielkowska et al., 2021). In contrast, inhibitory KIRs have long CYTs containing one or more ITIMs (Debska-Zielkowska et al., 2021). This enables them to recruit PTPs, such as SHP-1 and SHP-2, to dampen immune responses. Thus, the decision for NK cells to kill or spare their targets relies on integrated signals they receive from activating and inhibitory KIRs. Among KIRs, KIR2DL4 is unique in that it has a positively charged TM and a CYT containing an ITIM motif (Faure & Long, 2002). Additionally, experiments have shown that this receptor has both activating and inhibitory potentials (Faure & Long, 2002).

2.2.6.2 Leukocyte Ig-like receptors (LILRs)

Human LILRs share a close phylogenetic relationship with KIRs, and their homologs are found across vertebrates (Martin et al., 2002). In contrast to KIRs, which are limited in expression to NK cells and T cells, LILRs exhibit a wider expression profile and are present in various innate and adaptive immune cells, as well as in non-immune cell types (Hudson & Allen, 2016). Similar to KIRs, select LILRs are known to interact with HLA class 1 molecules (Redondo-Garcia et al., 2023). However, they adopt different HLA class 1 binding mechanisms from KIRs (Radwan et al., 2020). Unlike KIRs, which typically recognize the highly polymorphic α1 and α2 domains of HLA class 1 molecules, several LILRs specifically engage with the non-polymorphic α3 domain and the conserved beta-2-microglobulin domain (B2M) of HLA class 1 proteins via their distal D1 and D2 Ig-like domains (Radwan et al., 2020). This unique binding mode likely explains the ability of LILRs to broadly recognize both classical and

non-classical HLA class 1 molecules. Detailed examination of the crystallographic structures of LILR-HLA-complexes reveals that LILRs can be divided into two groups based on the similarity of their amino acid residues to those known to facilitate the interaction between LILRB1 and HLA-A2 (Willcox et al., 2003). Specifically, group 1 LILRs (i.e., LILRA1, LILRB1 and LILRB2) share approximately 70% amino acid similarity with LILRB1 and have conserved B2M domain contact residues (≥10/13 B2M-domain-contact residues are conserved), enabling them to bind to a wide range of HLA class 1 ligands, including HLA-A, HLA-B, HLA-C, HLA-E, HLA-F, and HLA-G (Willcox et al., 2003). In contrast, group 2 LILRs exhibit less than 60% amino acid similarity to their group 1 counterparts and do not share conserved B2M domain contact sites (≤ 4/13 residues are conserved) (Shiroishi et al., 2006; Willcox et al., 2003). Consequently, group 2 LILRs (i.e., LILRA4, LILRA5, and LILRB3) are proposed to recognize non-HLA class 1 ligands (Shiroishi et al., 2006). In addition to HLA class 1 ligands, LILRs are known to bind to a wide variety of non-HLA-based targets, including angiopoietin-like proteins (Zheng et al., 2012), S100A (a DAMP) (Arnold et al., 2013), central nervous system (CNS)-derived ligands (Takeda & Nakamura, 2017), truncated Abs (Hirayasu et al., 2016; Yamazaki et al., 2020), PAMPs (Burshtyn & Morcos, 2016), CD1 (Li et al., 2012; Li et al., 2009), and β-amyloid (Kim et al., 2013). These observations indicate that LILRs play diverse regulatory roles in immunity and other physiological systems.

LILRs are also functionally classified into activating (LILRAs), inhibitory (LILRBs), and secreted members (Redondo-Garcia et al., 2023). Activating LILRs have positively charged TMs containing arginine residues and short CYTs (Redondo-Garcia et al., 2023). Upon ligand engagement, these receptors associate with negatively charged FcεRIγ containing ITAMs to transduce activating signals. In contrast, inhibitory LILRBs have long CYTs with ITIMs

(Redondo-Garcia et al., 2023). Upon phosphorylation of ITIMs, these motifs recruit SHP-1/SHP-2 to attenuate ITAM-mediated signaling pathways.

In the following sections, I will provide a brief overview of teleost immunity and their immunoregulatory receptor repertoires. Afterward, I will discuss the discovery of LITRs and their functional characterizations using heterologous overexpression systems, before reviewing the available information on immunoregulatory functions of LITRs using teleost model systems.

2.3 Teleost immunity

Ray-finned fishes constitute approximately half of all extant vertebrate species and exhibit incredible diversity in their lifestyles and morphologies (Volff, 2005). Within this group, teleost fish account for 99.8%. Despite having both innate and adaptive immune systems, teleost fish predominately rely on innate immunity to fight off pathogens as their adaptive immunity is relatively less efficient (Uribe et al., 2011). This deficiency is evidenced by the absence of Ab isotype switching, delayed antibody response (Magnadottir, 2010), lower Ab affinity maturation, and less diverse Ab repertoires (Pasquier, 1982; Tort et al., 2003; Yu et al., 2020). One explanation for the limited adaptive immunity in teleosts is their status as basal vertebrates, resulting in a less sophisticated adaptive immunity compared to the ones found in higher vertebrates (Uribe et al., 2011). Additionally, due to their poikilothermic nature and the diminished efficacy of their adaptive immunity observed at lower ambient temperatures (Le Morvan et al., 1998), teleost fish tend to favour the relatively more stable innate immunity for immune defenses.

Another unifying feature of teleost fish is that their immune genes are generally present in multiple copies compared to other jawed vertebrates (Glasauer & Neuhauss, 2014). This

phenomenon stems from a teleost whole-genome duplication (WGD) event that occurred roughly 320-350 million years ago (mya) (Glasauer & Neuhauss, 2014). Specifically, while all jawed vertebrates are believed to have undergone two rounds of WGDs (termed vertebrate-specific WGDs (VSGDs)), all teleost fish have experienced three rounds of WGDs (termed teleost-specific WGD (TSGD)), with select teleost fish groups proposed to have undergone further WGD events (Glasauer & Neuhauss, 2014). The TSGD is believed to enhance the potential for teleost speciation and the diversification of their physiological systems, including the immune system (Grimholt, 2018; Opazo et al., 2013), by providing redundant genes for evolutionary selection pressures to act upon.

The most common fate of paralogs following WGD events is postulated to be non-functionalization, where one copy of the duplicated genes becomes non-functional due to reduced selection pressure to maintain the extra copy (Glasauer & Neuhauss, 2014). However, paralogs are also believed to diversify their functions through sub-functionalization and neo-functionalization (Glasauer & Neuhauss, 2014). Sub-functionalization refers to the process where the original functions of the gene before duplication are subdivided between its paralogs (Glasauer & Neuhauss, 2014). Neo-functionalization occurs when one paralog acquires a new function distinct from the ancestral gene, as the genome duplication event frees one paralog from the evolutionary selection pressures required to maintain the original function (Glasauer & Neuhauss, 2014).

Interestingly, a study on teleost fish provides direct evidence to support that WGD can enhance the resistance of a teleost species to infections (Bell et al., 2020). Specifically, researchers examined the parasite load and diversity of TLRs in two different Corydoras catfish species, *C. maculifer* and *C. araguaiaensis*, which coexist in the same geographical location,

occupy similar trophic levels, and have similar lifestyles. *C. maculifer* is a diploid, while *C. araguaiaensis* is tetraploid, having undergone a recent WGD event. Results showed that the tetraploid individuals had significantly fewer parasites on average than those of the diploid species. Additionally, the tetraploid species exhibited greater genetic diversity in their TLR1 and TLR2 genes.

Overall, the study of teleost fish offers an excellent opportunity to explore the impact of TSGD on immune system diversity and functions. Moreover, as WGD provides the foundation for the diversification of immunological features, studying teleost fish may aid in the identification of novel strategies used by this group for immune defenses.

2.3.1 Teleost immunoregulatory receptors of the IgSF

The identification of a broad range of teleost immune genes, coupled with the development of teleost immune cell isolation and *in-vitro* cultivation techniques, has significantly improved our understanding of teleost fish immunity (Montgomery et al., 2011). These developments have aided our investigation of immune cell functions in teleost fish. For instance, we now recognize that teleost immune cells can elicit a diverse range of immune cell responses, such as degranulation (Odaka et al., 2018), ADCC (Shen et al., 2003), phagocytosis (Li et al., 2006), antigen presentation (Vallejo et al., 1992), cellular cytotoxicity (Toda et al., 2009), cytokine secretion (Frenette et al., 2023), and NETosis (Li, Wang, et al., 2022). However, our knowledge of the immunoregulatory receptors governing these processes remains relatively limited.

Recent advances in genome-sequencing technologies have enabled the identification of a wide array of Ig-like-domain-based immunoregulatory receptor genes across various fish

species (Wcisel & Yoder, 2016). Among these receptors (Wcisel & Yoder, 2016) are novel immune-type receptors (NITRs), novel immunoglobulin-like transcripts (NILTs), diverse immunoglobulin domain-containing proteins (DICPs), and polymeric immunoglobulin receptor-like proteins (PIGRLs). Detailed reviews of these receptor-types can be found in the publications cited (Montgomery et al., 2011; Rodriguez-Nunez et al., 2014; Wcisel & Yoder, 2016).

Similar to their mammalian immunoregulatory receptor counterparts, teleost immunoregulatory genes commonly encode extracellular Ig-like domains of various types (i.e., V type, I type, and C2 type), TMs that anchor them in the phospholipid bilayer, and intracellular CYTs with a variety of tyrosine-based signaling motifs such as ITAMs, ITIMs, and ITSMs (Montgomery et al., 2011). These findings suggest that these receptors are likely involved in modulating various teleost immune cell effector functions by engaging evolutionarily conserved intracellular signaling pathways (Montgomery et al., 2011).

Another common feature among these genes is that they appear to be specific to teleost fish and share low sequence homologies with those found in mammals, which presents a challenge in assigning orthology. For example, NITRs have been proposed as functional equivalents of mammalian NK receptors as one of them has been found to recognize allogeneic targets (Cannon et al., 2008). However, these receptors are known to be exclusive to fish and do not share obvious sequence homology with any mammalian immunoregulatory receptor-types (Rast et al., 1995; Yoder, 2009). Additionally, this challenge is further compounded by considerable polymorphism (Wcisel & Yoder, 2016), which refers to sequence variability within the same gene between individuals. Furthermore, these genes generally exist as multiple gene copies (polygenicity) (Wcisel & Yoder, 2016). Teleost immunoregulatory receptor genes also have significant haplotypic variations in genetic polymorphism (Wcisel & Yoder, 2016), which

refers to combined genetic polymorphisms within a set of linked genes between individuals. Additionally, they also show haplotypic variations in gene content (Wcisel & Yoder, 2016), which refers to variable combinations and/or numbers of genes within a set of linked genes between individuals observed in these teleost immunoregulatory receptor families. Collectively, these features not only present obstacles to establishing orthologous connections between teleost fish and other vertebrates, but also add complexity in establishing such relationships among different teleost species (Wcisel & Yoder, 2016).

The genetic intricacies of the teleost immunoregulatory receptors, combined with the lack of reagents such as receptor-specific Abs, have also made the search for their ligands highly challenging. As a result, most of the identified teleost immunoregulatory receptors still lack known ligands, which significantly impedes our understanding of their physiological functions.

In the following sections, I will describe the discovery and transcript expression profiling of LITRs. The investigation of this unique family of receptors stemmed from comparative immunologists' specific interest in identifying catfish NK cell receptors that regulate allogeneic target cell-killing responses.

2.3.2 Discovery of LITRs

A search for immunoregulatory receptor candidates that regulate cytotoxic responses in channel catfish NK-like and cytotoxic T cells led to the discovery of LITRs. The first three prototype *iplitrs* (*iplitr1*, *iplitr2*, and *iplitr3*) transcripts identified belong to the IgSF and encode type 1 transmembrane proteins containing variable arrangements of C2-set Ig-like domains, TMs, and short or long CYTs (Stafford, Bengten, et al., 2006). Specifically, IpLITR1, a putative inhibitory receptor, is characterized by four extracellular Ig-like domains, an uncharged TM, and

a long CYT region containing two ITIMs and an ITIM-like motif. In contrast, IpLITR2 is a putative activating receptor with three Ig-like domains, a positively charged lysine within its TM, and a short CYT devoid of recognizable motifs. Similarly, IpLITR3 is predicted to be an activating receptor, displaying six Ig-like domains, a TM with a positively charged lysine, and a short cytoplasmic region. The *iplitr1* and *iplitr3* mRNA sequences were originally discovered from an EST cDNA library constructed from stimulated channel catfish cytotoxic lymphocytes, while the *iplitr2* transcript was identified from the channel catfish 42TA macrophage cell line (Stafford, Bengten, et al., 2006). Akin to other identified teleost immunoregulatory receptors of the IgSF, restriction fragment length polymorphism (RFLP) analysis using IpLITR domain-specific DNA probes on 16 channel catfish siblings revealed diverse hybridization patterns across these individuals (Stafford, Bengten, et al., 2006), indicating that IpLITRs belong to a large gene family characterized by high polymorphism and polygenicity.

Phylogenetic analysis of the three prototypic IpLITRs supported that they represented a novel family of receptors that are homologous to functionally and genomically disparate immunoregulatory receptor-types found in the FCR family and LRC-encoded receptors (Stafford, Bengten, et al., 2006). For example, the proximal D3 and D4 Ig-like domains of IpLITR1 and IpLITR3 clustered more closely with the Ig-like domains of mammalian KIRs, LILRs, and NKp46, members of the LRC known to be essential regulators of cell-mediated immunity (Martin et al., 2002). In contrast, the distal D1 and D2 Ig-like domains of IpLITR1, IpLITR2, and IpLITR3 grouped more closely with the Ig-like domains of mammalian FcRs and FCRLs, receptors of the FCR family known to be primarily antibody-binding receptors that play crucial roles in immune defenses and restoring immune balance (Rostamzadeh et al., 2018).

Therefore, IpLITRs showcased a unique “chimeric” composition of Ig-like domains reminiscent of multiple mammalian immunoregulatory receptor families with diverse functions.

2.3.3 Structural analyses of IpLITRs

As discussed, a variety of innate and adaptive immune cells such as NK and T lymphocytes utilize intricate arrays of cell surface receptors to survey classical and non-classical MHC-class 1 molecules present on diseased cells. This enables them to discriminate between self from non-self (Diefenbach & Raulet, 1999; Long & Rajagopalan, 2002). For instance, KIRs specifically engage with the α1 and α2 subunits of MHC class 1 proteins. The decision of KIR-bearing NK cells to attack or spare their targets relies on integrated signals they receive from activating and inhibitory KIRs (Debska-Zielkowska et al., 2021; Hilton & Parham, 2017). Similarly, select LILRs can also bind to the α3 and B2M domains of MHC class 1 molecules to regulate the cytotoxic activity of NK cells (Zhao et al., 2019). Interestingly, further sequence analysis of select IpLITR D1 and D2 domains (i.e., IpLITR1, IpLITR2, and TS32.17 L1.2b) revealed a putative MHC-class 1-binding site similar to the MHC 1 α3 domain-binding site within LILRB1 (Stafford et al., 2007). For instance, all six residues in LILRB1 D1 that are responsible for interacting with the MHC α3 domain were either identical or conserved across the various IpLITR D1s examined. However, none of the individual IpLITR D1 sequences contained all six MHC 1 contact residues that match with human LILRB1. Furthermore, comparative homology modeling of representative IpLITRs using LILRB1 as the template revealed that their D1 and D2 Ig-like domains shared similar folding patterns and relative coordinates of β-strands as human LILRs. Interestingly, a few IpLITRs analyzed were predicted to have a 3_{10}-helix within D1, a defining feature of the MHC class 1-binding LILRB1. Nonetheless, most of the IpLITRs were predicted to contain a C’ strand at the same position,

which was speculated as the reason for the incapability of group 2 LILRs to bind MHC 1. These results imply that some IpLITRs are potentially MHC 1 binding receptors, whereas others likely bind other non-MHC protein targets. Taken together, these findings further supported that select LITRs might be functional orthologs of mammalian LRC-encoded receptors that can distinguish self from non-self through binding MHC molecules (Stafford et al., 2007), but there is currently no experimental evidence demonstrating whether LITRs also bind to similar ligands as mammalian LILRs.

2.3.4 Expression analysis of IpLITRs in channel catfish

Examination of several channel catfish tissues with an *iplitr1* D1-specific RNA probe revealed high levels of *iplitr1* mRNA expression in the head and trunk kidney tissues (Stafford, Bengten, et al., 2006). In contrast, the spleen, heart, liver, gill, and muscle tissues showed relatively lower levels of *iplitr1* mRNA expression. In comparison, northern blotting experiments using an *iplitr2* D3-specific RNA probe revealed high mRNA expression levels of *iplitr2* in the channel catfish head kidney, trunk kidney, and gill tissues (Stafford, Bengten, et al., 2006). Conversely, the spleen, heart, muscle, and liver tissues showed lower mRNA levels of *iplitr2*. Reverse transcription polymerase chain reaction (RT-PCR) experiments using *iplitr*-specific primers reinforced that *iplitr1* and *iplitr2* transcripts were variably expressed in the tissues of the channel catfish (e.g., spleen, head kidney, trunk kidney, gill, heart, muscle, liver, intestine, and thymus) with the head and trunk kidneys displaying relatively high expression (Stafford, Bengten, et al., 2006). Channel catfish tissues also expressed different numbers of *iplitr1*- and *iplitr2*-like transcripts (Stafford, Bengten, et al., 2006). For instance, gill and heart tissues expressed three different-sized *Iplitr1*-like mRNA products, while the liver tissue expressed only a single *iplitr1*-like amplicon. *iplitr1*- and *iplitr2*-like transcripts were also

variably expressed in the immune cells of the channel catfish (42TA macrophages, 3B11 B cells, TS32.15 and TS32.17 cytotoxic cells, G14D T cells, mixed leukocyte culture (MLC), and 1F3 NK-like cells) with different cell-types expressing transcripts of distinct sizes (Stafford, Bengten, et al., 2006). Finally, no *iplitr* transcripts were observed in the fibroblast CCO cell line, suggesting that the *iplitrs* examined are primarily expressed in immune cells (Stafford, Bengten, et al., 2006).

Following stimulation of channel catfish peripheral blood leukocytes (PBLs) with LPS or concanavalin A (ConA), weak expressions of *iplitr1* and *iplitr2* transcripts were observed on day 0, but no detectable expression of transcripts was observed during the following 12 days (Stafford et al., 2007). In comparison, stimulation of catfish PBLs with irradiated 3B11 B cells (alloantigen) induced upregulation of *iplitr1* transcripts concomitantly with several different *iplitr2*-like transcripts of varying sizes (Stafford et al., 2007). Like channel catfish PBLs, alloantigen-stimulated TS32.15 and TS32.17 CTLs also featured upregulation of multiple *iplitr1*-like transcripts, as well as many *iplitr2*-like transcripts (Stafford et al., 2007). Overall, the CTLs yielded a total of 37 *iplitr* sequences that are closely related to the prototypical *iplitrs*, but that varied primarily in their number of extracellular Ig-like domains and showed variations in their TMs and CYT regions (Stafford et al., 2007). For example, TS32.15 L1.1a and the prototypic IpLITR1 share long CYTs that consist of three tyrosine-based motifs. However, TS32.15 L1.1a differs from IpLITR1 in that it has three additional ectodomains and an ITAM-like motif has replaced one of the ITIM motifs found in IpLITR1. Moreover, TS32.15 L2.1a and the prototypic IpLITR2 are both putative activating receptor-types, however, TS32.15 L2.1a displays two additional ectodomains relative to IpLITR2. Hence, the IpLITR receptors derived from the stimulated cytotoxic T cells may have variable ligands and/or affinities for their ligands, as well

as dynamic immunoregulatory capabilities. Whether or not the various *iplitrs* result from alternative splicing or different genes remains unknown. Further investigation is needed to determine the significance of the upregulation of *iplitr1* and *iplitr2* in channel catfish PBLs and CTLs; however, we hypothesize that multiple *iplitr* transcripts are upregulated to fine-tune inflammatory responses in these cells.

Immunoregulatory receptors are generally subject to complex transcriptional regulation dynamics (Rumpret et al., 2020). Some of these receptors are constitutively expressed, while others are either upregulated or downregulated following cellular activation (Rumpret et al., 2020). For instance, several KIRs are constitutively expressed to monitor perturbations in the expression of self-MHC class 1 molecules (Huard & Karlsson, 2000; Lanier, 2005; Mahaweni et al., 2018). In contrast, several LILRs (i.e., LILRB1, LILRB2, and LILRB4) are normally expressed at low levels in resting myeloid cells and are upregulated upon cellular activation (Young et al., 2008). Additionally, LAIR-1 expression on T cells decreases following *in vitro* stimulation (Jansen et al., 2007). To better understand the potential biological significance of these diverse immunoregulatory receptor expression patterns in immune defense against pathogens, researchers have developed mathematical models (Rumpret et al., 2020). Their models have allowed them to categorize inhibitory immunoregulatory receptors into two main types: 1) threshold receptors and 2) negative feedback receptors.

Specifically, threshold receptors are constitutively expressed on immune cells and help set a baseline for immune activation. Based on mathematical models, these receptors mainly function to filter out background noise (i.e., low-affinity receptor-ligand interactions), thereby preventing accidental triggering of the immune system in the absence of pathogenic ligands. In contrast, negative feedback receptors are upregulated upon immune activation and act during the

later phases of inflammatory responses. These receptors are postulated to help shut down the immune response in a timely manner to prevent excessive immunopathology. Furthermore, the delayed expression of negative feedback receptors allows for rapid pathogen clearance at the onset of inflammation. As the pathogen level declines, the increased inhibitory activity of the negative feedback receptors ensures the immune response is effectively terminated.

Based on this evidence, it's likely some of the upregulated putative inhibitory *iplitr* transcripts function as negative feedback receptors. Using similar logic, the increased gene expression of several putative activating *iplitrs* may provide further stimulatory signals to counter the ongoing insults. The precise roles of the upregulated *iplitr* transcripts await further experimental confirmation.

2.3.5 Functional characterization of IpLITRs overexpressed in mammalian cell lines

The absence of known ligands and antibody reagents at the time of LITR discovery presented a challenge for investigating their functional importance in teleost immunity. Consequently, our lab has relied on overexpressing putative activating and inhibitory LITR-types as epitope-tagged cell surface recombinant receptors in various cell lines (Fei et al., 2016). This strategy has allowed us to take advantage of commercial antibodies recognizing various epitope tags (i.e., hemagglutinin tag (HA-tag) and FLAG-tag (DYKDDDDK-tag)) to activate these receptors, bypassing the need for native IpLITR ligands or the development of IpLITR-specific Abs. Although this approach does not capture the native functions of LITRs in teleost immune cells, it has facilitated detailed and unambiguous biochemical analyses of IpLITRs, leading to the identification of both anticipated and unanticipated immunoregulatory potentials for these receptors (Fei et al., 2016).

In the next sections, I will summarize our findings regarding the conserved and unique aspects of IpLITR-mediated immunoregulatory potentials through the utilization of heterologous overexpression systems.

2.3.5.1 Immunoregulatory potentials of stimulatory IpLITR-types

2.3.5.1.1 IpLITR2.6b uniquely associates with ITAM-bearing adaptor molecules

Most of our research efforts have been devoted to studying the immunomodulatory potentials of IpLITR2.6b and IpLITR1.1b, predicted to be a stimulatory IpLITR-type and an inhibitory IpLITR-type, respectively. IpLITR2.6b has two Ig-like domains, a lysine-containing TM, and a short CYT (Cortes et al., 2012). As mentioned earlier, mammalian activating receptors typically have positively charged TMs with lysine or arginine residues and short CYTs. These receptors often depend on forming non-covalent interactions with negatively charged adaptor molecules containing ITAMs such as FcRγ and DAP12 to be expressed on the cell membrane and initiate ITAM-mediated signaling cascades (Call & Wucherpfennig, 2007). Furthermore, a variety of teleost adaptor molecules, homologous to mammalian DAP12 and FcRγ, have been identified (Yoder et al., 2007). These imply that teleost fish activating receptors likely use similar mechanisms for assembling activating receptor-adaptor complexes. Thus, we hypothesized that IpLITR2.6b would need to associate with adaptor molecules containing ITAMs to be expressed on the cell surface and transduce stimulatory signaling pathways.

Experiments performed using HEK cells overexpressing membrane recombinant HA-tagged IpLITR2.6b proteins revealed that IpLITR2.6b was capable of associating with several channel catfish ITAM-containing adaptor proteins, including IpFcRγ, IpFcRγ-like (IpFcRγ-L), and IpCD3ζ-L (Mewes et al., 2009). Furthermore, an increase in the surface expression of IpLITR2.6b was observed specifically in response to interactions with IpFcRγ and IpFcRγ-L, but

not IpCD3ζ-L (Mewes et al., 2009). These findings suggested that the surface assembly of IpLITR2.6b relies on the presence of appropriate adaptor molecules. Additionally, the preferential ability of IpLITR2.6b to associate with FcRγ molecules is unique, as mammalian activating receptors bearing lysine residues tend to favour DAP12 association (Feng et al., 2005). Interestingly, mutation of the TM lysine residue of IpLITR2.6b to an uncharged alanine residue or arginine had no impact on its membrane expression or adaptor recruitment (Mewes et al., 2009). Moreover, neutralization of the IpLITR2.6b TM not only preserved its association with IpFcRγ-L and IpCD3ζ-L, but also enabled it to interact with IpDAP12 (Mewes et al., 2009). These findings differ from mammalian activating receptor data (Call & Wucherpfennig, 2007) and suggest that the positively charged TM of IpLITR2.6b is not essential for adaptor recruitment. Additionally, these findings suggest that the nature of the positively charged residue within the TM of IpLITR2.6b can determine the types of adaptors with which this receptor can interact. Alternative experiments neutralizing the negatively charged TM of IpFcRγ-L prevented IpLITR2.6b-IpFcRγ-L complex formation and their surface expression (Mewes et al., 2009), highlighting the critical role of the negatively charged TM of IpFcRγ-L in facilitating the membrane assembly of the IpLITR2.6b-adaptor complex.

Overall, these studies showcased the unique features of the IpLITR2.6b membrane assembly mechanisms. In the next section, I will discuss the stimulatory potentials of IpLITR2.6b.

2.3.5.1.2 Stimulatory potentials of IpLITR2.6b

To investigate the functional implications of IpLITR2.6b-adaptor complex formation, we generated an N-terminal HA-tagged chimeric receptor construct. This construct consisted of the extracellular Ig-like domains of IpLITR2.6b fused with the TM and CYT of IpFcRγ-L

(Cortes et al., 2012). This chimeric construct was then transfected into RBL-2H3 cells to produce RBL-2H3 cells stably expressing membrane HA-tagged IpLITR2.6b/IpFcRγ-L (IpLITR2.6b) chimeric receptors (Cortes et al., 2012). Subsequent experiments using these cells showed that cross-linking of HA-tagged membrane IpLITR2.6b proteins with anti-HA Abs activated stimulatory signaling pathways and degranulation response in the RBL-2H3 cells (Cortes et al., 2012). Furthermore, mutation of the tyrosine residues within the ITAM of IpLITR2.6b to phenylalanine residues, blocked the functional responses elicited by IpLITR2.6b (Cortes et al., 2012), supporting that IpLITR2.6b operated in an ITAM-dependent manner to trigger stimulatory signaling cascades. Additional experiments showed that engagement of IpLITR2.6b leads to the phosphorylation of extracellular signal-regulated kinase 1/2 (ERK1/2) and protein kinase B (Akt) (Cortes et al., 2012). Moreover, pharmacological inhibitor experiments demonstrated that IpLITR2.6b-mediated degranulation response was effectively blocked by inhibitors of SFKs, mitogen-activated protein kinase (MAPK) kinase (MEK1 and MEK2), PKC, and PI3Ks (Cortes et al., 2012). However, inhibitors of c-Jun N-terminal kinases (JNKs) and p38 MAPK showed minimal effects on IpLITR2.6b-triggered degranulation response (Cortes et al., 2012). Taken together, these findings mark the first demonstration of the stimulatory potentials of an activating IpLITR-type, supporting that IpLITR2.6b uses a classical ITAM-based mechanism to control innate immune effector functions.

Using a MAPK signaling array, we then showed that cross-linking of HA-tagged IpLITR2.6b induced phosphorylation of a variety of intracellular signaling molecules, including glycogen synthase kinase 3-beta (GSK-3β), GSK-3α/β, ERK1/2, ribosomal S6 kinases (RSK1), cAMP-response element binding protein (CREB), JNK, MEK6, mitogen and stress-activated protein kinase (MSK)2, Akt2, and p38δ (Cortes et al., 2014). These observations provided a

more comprehensive understanding of the signaling pathways activated by IpLITR2.6b in RBL-2H3 cells. Furthermore, our cytokine secretion array experiment demonstrated that the ligation of IpLITR2.6b triggered RBL-2H3 cells to secrete levels of IL-4, IL-3, IL-6, TNF-α similar to those observed following activation of the cells using calcium ionophore, phorbol myristate acetate (PMA), or endogenous FcεRI crosslinking (Cortes et al., 2014). Furthermore, engagement of IpLITR2.6b by anti-HA-Ab-coated beads induced phagocytosis in RBL-2H3 cells (Cortes et al., 2014). This phagocytic process was inhibited by the calcium chelator EDTA and actin-polymerization inhibitor cytochalasin D (CytoD), suggesting that IpLITR2.6b-induced phagocytosis is dependent on the presence of calcium and actin-polymerization (Cortes et al., 2014).

As previously described, select mammalian FcRs rely on their association with FcRγ adaptor molecules to induce phagocytosis (Uribe-Querol & Rosales, 2020). When these receptors are engaged by their ligands, ITAMs in FcRγ are phosphorylated by SFKs, leading to the recruitment of Syk. Syk plays a critical role in FcR-mediated phagocytosis by activating a variety of downstream signaling molecules (Uribe-Querol & Rosales, 2020). For instance, Syk can induce the activation of Vav and Rho family small GTPases such as Cdc42 and Rac1. These GTPases are critical for actin polymerization and the formation of the phagocytic cup (Uribe-Querol & Rosales, 2020). Therefore, we set out to examine and compare whether IpLITR2.6b-mediated phagocytosis in RBL-2H3 relied on similar signaling intermediates as those in classical FcR-mediated phagocytosis, using pharmacological inhibitors.

Our pharmacological inhibitor experiments showed that the IpLITR2.6b-mediated phagocytosis was blocked by inhibitors targeting SFKs, Syk, PI3Ks, Rac1/2/3 Cdc42, MEK1/2, phosphoinositide-dependent kinase (PDK1), Akt, PKC, and F-actin polymerization (Lillico et al.,

2015). These results highlight the mechanistic similarities between classical FcR-mediated phagocytosis and IpLITR2.6b-induce phagocytosis, suggesting that select activating IpLITR-types likely use evolutionarily conserved ITAM-based mechanisms for controlling innate immune effector functions.

2.3.5.2 Immunoregulatory roles of inhibitory IpLITR-types

2.3.5.2.1 IpLITR1.1b contains ITIMs and is capable of recruiting PTPs

IpLITR1.1b has four Ig-like domains, a TM, and a long CYT containing several tyrosine-based motifs that match the consensus sequences of ITIM or ITSM, therefore, we hypothesized that IpLITR1.1b likely functions as an inhibitory receptor. To test this hypothesis, we initially examined its ability to recruit PTPs such as SHP-1 and SHP-2 (Montgomery et al., 2009). To address this, we generated chimeric constructs combining the ectodomain and TM of KIR2DL3 with the CYTs of two putative inhibitory IpLITR-types, IpLITR1.1b and IpLITR L1.2a. These constructs were initially transfected into HEK-293T cells. The ectodomain of KIR2DL3 was chosen because the native ligand of this receptor is known (Burshtyn et al., 1999). Our results showed that following phosphorylation, the CYTs of both IpLITR L1.2a and IpLITR1.1b recruited SHP-1 and SHP-2, and this recruitment was dependent on ITIMs (Montgomery et al., 2009).

The CYT of IpLITR1.1b contains a total of six tyrosine residues subdivided into proximal (Y^{433}, Y^{453}, and Y^{463}) and distal (Y^{477}, Y^{499}, and Y^{503}) regions (Montgomery et al., 2009). Specifically, the distal region contains two ITIMs (Y^{477} and Y^{499}) and an ITSM (Y^{503}). However, the tyrosine motifs within the proximal CYT region of IpLITR1.1b do not resemble classical activating and/or inhibitory motifs. Furthermore, our PTP-recruitment experiment showed that the proximal IpLITR1.1b CYT region was incapable of recruiting either SHP-1 or

SHP-2 (Montgomery et al., 2009). These data support that the distal CYT region of IpLITR1.1b was responsible for the recruitment of inhibitory phosphatases.

2.3.5.2.2 IpLITR1.1b uses SHP-dependent and -independent mechanisms to inhibit NK cell-mediated cellular cytotoxicity

To further evaluate the inhibitory potential of IpLITR1.1b on cell-mediated immune responses, we stably expressed the KIR/IpLITR$_{CYT}$ chimeric receptors on the surface of mouse lymphokine-activated killer (LAK) cells (NK-like cells) using vaccinia virus (Montgomery et al., 2012). This approach allowed us to examine the functional outcomes of the KIR/IpLITR$_{CYT}$ chimeric receptors by engaging them with HLA-Cw3 proteins (the native ligand of KIR2DL3) expressed on the surface of LAK-targets. Consistent with our hypothesis, both the CYTs of IpLITR L1.2a and IpLITR1.1b participated in the termination of LAK-mediated cellular cytotoxicity (Montgomery et al., 2012).

Since we previously showed that the CYTs of IpLITR L1.2a and IpLITR1.1b were capable of recruiting PTPs (Montgomery et al., 2009), we investigated if a catalytically inactive SHP-1 could block the inhibitory functions of IpLITR L1.2a and IpLITR1.1b. As predicted, the inhibitory potential of IpLITR L1.2a was shown to be dependent on SHP-1 (Montgomery et al., 2012). Unexpectedly, the inactive SHP-1 was incapable of blocking the IpLITR1.1b$_{CYT}$-mediated inhibitory effects (Montgomery et al., 2012). Further examination of a truncated version of IpLITR1.1b, containing only the proximal CYT region, showed that this region alone also inhibited the NK cell killing response, even though it does not contain any bona-fide ITIM/ITSM sequences (Montgomery et al., 2012; Montgomery et al., 2009). These findings support that IpLITR1.1b uses SHP-dependent and -independent mechanisms for inhibiting LAK-mediated cellular cytotoxicity.

Further analysis of the proximal CYT region of IpLITR1.1b revealed that it contained a peptide sequence (AVY^{453}AQV) resembling the consensus amino acid sequence of the Csk recruitment motif (Y (T/A/S) (K/R/Q/N) (M/I/V/I) (Songyang et al., 1994). In mammals, Csk is known as a negative regulator of SFK activities (Chong et al., 2005). Mechanistically, Csk inhibits SFKs by phosphorylating a conserved tyrosine residue found at their C-terminus (Nada et al., 1991). Additionally, Csk is recruited by several mammalian immunoregulatory receptors (Sayos et al., 2004; Veillette et al., 1998; Verbrugge et al., 2006), suggesting that this molecule may play essential roles in the control of immune responses. Based on this, we hypothesized that IpLITR1.1b likely also uses Csk for its inhibitory functions. Indeed, our mutagenesis and co-immunoprecipitation experiments confirmed that the Y^{453} of the CYT of IpLITR1.1b facilitated Csk recruitment and contributed to the inhibitory functions of IpLITR1.1b (Montgomery et al., 2012). Together, these findings mark the first functional demonstration of an ITIM-containing IpLITR and showcase the signaling versatility of IpLITR1.1b.

2.3.5.3 Functional plasticity of IpLITRs

2.3.5.3.1 IpLITR1.1b activates stimulatory signaling pathways and phagocytosis

As previously discussed, the classical definition of an activating receptor is defined by the presence of ITAMs in their CYTs, whereas ITIM-bearing immunoregulatory receptors commonly mediate inhibitory functions (Barrow & Trowsdale, 2006). However, this binary view of immunoregulatory receptor signaling has been challenged by several mammalian studies revealing that the functional outcomes of ITAM and ITIM-mediated signaling pathways are not as predictive as initially thought (Hamerman & Lanier, 2006). This phenomenon is known as functional plasticity. For example, several mammalian studies have shown that ITAM-bearing receptors can mediate inhibitory functions (Kane et al., 2014), while ITIM-bearing receptors can

sometimes activate immune responses (Kane et al., 2014). Furthermore, these studies indicate that the functional behaviour of immunoregulatory receptors is shaped not only by their activating and inhibitory motifs but also by the intracellular environments of various cell types and the magnitude and duration of immunoregulatory receptor activation by their native ligands (Bakema & van Egmond, 2011; Zhu et al., 2013). Thus, the functional plasticity of immunoregulatory receptors likely represents an important regulatory mechanism, allowing them to fine-tune immune responses and adjust their functions to suit the cellular and inflammatory context. Our studies of teleost IpLITRs also align with findings from mammalian studies, supporting that the activities of stimulatory (i.e., ITAM) and inhibitory (i.e., ITIM) motifs do not always correspond to their traditionally defined functions.

As described, when we overexpressed the KIR/IpLITR1.1$_{CYT}$ chimeric receptors in mammalian NK-like cells (a representative lymphoid cell line), activation of these receptors abolished NK-cell-mediated cellular cytotoxicity towards target cells expressing HLA-Cw3 ligands (Montgomery et al., 2012). Surprisingly, when these receptors were expressed in the RBL-2H3 cells (a representative myeloid cell line), their activation led to the phosphorylation of several stimulatory pathway intermediates, including ERK1/2 and Akt (Cortes et al., 2014). Moreover, activation of IpLITR1.1b also stimulated these cells to perform phagocytosis (Cortes et al., 2014). These results suggest that IpLITR1.1b functions in a cellular-context-dependent fashion to regulate immune effector functions.

However, in contrast to IpLITR2.6b/IpFcRγ-L, IpLITR1.1b did not induce the release of cytokines and displayed kinetics of IpLITR1.1b-stimulated ERK1/2 and Akt phosphorylation distinct from ITAM-induced responses (Cortes et al., 2014). Furthermore, IpLITR1.1b-mediated stimulatory functions were independent of ITAM-bearing adaptor molecules, and its induced

phagocytic activity was unaffected by EDTA treatment, suggesting a mode of signaling different from IpLITR2.6b-mediated responses (Cortes et al., 2014). Additionally, the removal of the CYT region of IpLITR1.1b did not affect its surface expression (Cortes et al., 2014); however, this alteration prevented it from activating phagocytosis, indicating that the phagocytic function of IpLITR1.1b relies on motifs present in its CYT region.

As the CYT of IpLITR1.1b lacks any recognizable stimulatory motifs, an ITAM-independent control of the phagocytosis mechanism was suggested. Drawing inspiration from mammalian studies, one plausible explanation for the functional plasticity of IpLITR1.1b involves its CYT ITSM motif. As previously explained, in some cases, ITSMs can recruit PTPs to suppress immune functions, but they can also promote positive signaling by recruiting activating signaling effectors such as SAP and EAT-2 (Veillette et al., 2009). Specifically, ITSMs can recruit SAP adaptors to activate p85 subunit of class 1A PI3Ks, leading to the downstream phosphorylation of Akt and the induction of phagocytosis (Mikhalap et al., 1999; Sidorenko & Clark, 2003).

Alternatively, SHP-2, recruited by ITIM and/or ITSMs, has also been reported to act as a scaffold molecule for interacting with stimulatory signaling intermediates (Buday & Tompa, 2010; Li et al., 2003). Upon SHP-2 recruitment by ITIMs and/or ITSMs, the C-terminal tyrosine of SHP-2 becomes phosphorylated, which serves as a binding site for growth factor receptor-bound 2 (Grb2) (Buday & Tompa, 2010). Subsequently, Grb2 interacts with and activates Grb2-associated binders (Gabs), which in turn stimulate class 1A PI3Ks to engage the phagocytic machinery (Bohdanowicz et al., 2010; Gotoh, 2008; Gu et al., 2001; Li et al., 1994). Based on this evidence, we proposed that following IpLITR1.1b engagement, phosphorylation of the distal

CYT region ITIMs and ITSM may lead to SHP-2 recruitment and subsequent binding of Grb2 and Gabs to induce the activation of PI3Ks (Fei et al., 2016).

Additional mechanisms of IpLITR1.1b-mediated phagocytosis have also been proposed (Fei et al., 2016). For instance, further analysis of the proximal CYT region of IpLITR1.1b revealed that Y^{463} bears a resemblance to the known Grb2 binding motif (YxN). This suggests that Grb2 may be recruited directly to the proximal CYT region of IpLITR1.1b to engage the Grb2-Gabs-PI3K pathway to induce phagocytosis. This hypothesis was further supported by our co-immunoprecipitation experiments, which showed that the IpLITR1.1b CYT recruited Grb2 and PI3K (Zwozdesky et al., 2017). For more information on proposed IpLITR1.1b-mediated signaling mechanisms, refer to the published graphical summary of the IpLITR1.1b signaling models (Fei et al., 2016).

2.3.5.3.2 IpLITR1.1b induces a unique phagocytosis phenotype

Confocal microscopy experiments further showed that RBL-2H3 cells expressing IpLITR1.1b exhibited a unique phagocytosis phenotype distinct from IpLITR2.6b-expressing RBL-2H3 cells (Lillico et al., 2015). Specifically, we observed that IpLITR1.1b-expressing cells frequently generated membrane extensions (filopodia-like) for capturing 4.5 μm beads and securing them in partially formed phagocytic cups (Lillico et al., 2015). However, these cells often struggled to fully engulf their targets (Lillico et al., 2015). This phenomenon, known as stalled phagocytosis, was predominately observed in IpLITR1.1b-expressing cells and rarely in IpLITR2.6b-expressing cells (Lillico et al., 2015). Even though IpLITR1.1b-expressing cells often displayed stalled phagocytic phenotype, approximately 30% of them were able to engulf at least one bead (Lillico et al., 2015). Interestingly, incubating IpLITR2.6b-expressing cells at 22 ˚C abolished their stimulated phagocytic activity (Lillico et al., 2015), whereas this temperature

had less pronounced effects on IpLITR1.1b-induced phagocytosis, suggesting that the phagocytic mechanism triggered by IpLITR2.6b is more temperature-sensitive than that of IpLITR1.1b.

Using pharmacological inhibitors, we further demonstrated that IpLITR1.1b and IpLITR2.6b activate distinct signaling pathways to initiate phagocytosis (Lillico et al., 2015). While inhibitors targeting the classic components of the mammalian FcR-dependent phagocytic pathways were highly effective at blocking IpLITR2.6b-mediated phagocytosis, IpLITR1.1b-induced phagocytosis was not affected by many of these inhibitors (Lillico et al., 2015). For instance, IpLITR1.1b-mediated phagocytosis was only effectively blocked by inhibitors of SFKs, Syk, and F-actin polymerization, whereas inhibitors targeting c, Rac, PI3Ks, PDK1, and PKCs had minimal effects (Lillico et al., 2015). These findings reinforce that IpLITR1.1b and IpLITR2.6b engage distinct molecular circuitries to induce phagocytosis. Considering these findings, we proposed that IpLITR1.1b likely uses a minimum set of actin polymerization machinery to engage phagocytosis (Lillico et al., 2015). Furthermore, these results suggested that actin polymerization is essential for IpLITR1.1b-mediated phagocytosis and may depend on the catalytic actions of SFKs and Syk.

Investigation into the binding partners of the IpLITR1.1b CYT using GST-pull-down assays showed that the IpLITR1.1b proximal and distal CYT regions differentially recruited various signaling molecules (Zwozdesky et al., 2017). For instance, the proximal CYT region recruited Nck, Vav1, and Grb2, while the distal CYT region interacted with Syk, PI3K, and SHP-2 (Zwozdesky et al., 2017). These findings have greatly expanded our understanding of the specific signaling molecules engaged by IpLITR1.1b to regulate phagocytosis and allowed us to formulate new hypotheses on how an inhibitory receptor can potentially drive dynamic actin

remodeling events. For additional information on the proposed signaling models, refer to this manuscript (Zwozdesky et al., 2017).

Overall, studies of IpLITRs using heterologous overexpression systems have provided detailed insights into the mechanisms behind the functional outputs of activated IpLITRs. These findings suggest that IpLITRs likely use both conserved and novel signaling mechanisms to control innate immune functions.

In the upcoming section, I will describe the development of a new receptor crosstalk model for investigating signaling interactions mediated by activating and inhibitory IpLITR-types.

2.3.5.3.3. IpLITR-mediated signaling crosstalk events

Immune cells rely on integrated signals from activating and inhibitory receptors to determine the optimal course of action for immune defense (Barrow & Trowsdale, 2006). In mammalian paired receptor systems, the activation of inhibitory immunoregulatory receptors relies on their co-engagement with their stimulatory counterparts through shared ligands (Takai, 2005b). These interactions prompt activating receptors to recruit SFKs, which then phosphorylate inhibitory motifs on the CYTs of inhibitory receptors. This phosphorylation enables the inhibitory receptors to recruit PTPs, which in turn dephosphorylate signaling intermediates triggered by activating receptors (Srivastava et al., 2003). As mentioned, activating and inhibitory IpLITR-types generally have similar ectodomains. Thus, we hypothesized that these receptors may interact with shared ligands to cooperatively regulate immune system functions. To address this question, we generated AD293 cells stably expressing both membrane HA-tagged IpLITR2.6b/FcRγ-L and FLAG-tagged IpLITR1.1b proteins (Fei et al., 2020). Using imaging flow cytometry, we initially examined the intracytoplasmic signaling potentials of these

receptors individually. To do this, we added 4.5 μm beads coated with either anti-HA-Abs to engage HA-tagged IpLITR2.6b proteins or anti-FLAG Abs to cross-link the anti-FLAG-tagged IpLITR1.1b proteins expressed on the surface of the AD293 cells (Fei et al., 2016). Consistent with the activating potential of IpLITR2.6b observed in RBL-2H3 cells, engagement of IpLITR2.6b by anti-HA-Ab-coated beads induced potent phagocytic activity in AD293 cells (Fei et al., 2020), further supporting the stimulatory roles of IpLITR2.6b. However, ligation of IpLITR1.1b alone did not induce significant phagocytic activity in the same cells (Fei et al., 2020). This contrasts with their functional activity observed in RBL-2H3s, suggesting that differences in intracellular environments likely contribute to varying functional outcomes of immunoregulatory receptors. Again, this highlights the context-dependent nature of receptor signaling in different cellular environments. Subsequently, we investigated whether co-engagement of IpLITR1.1b and IpLITR2.6b by beads co-opsonized with both anti-HA-Abs and anti-FLAG-Abs could result in IpLITR1.1b-mediated cross-inhibition of the stimulatory activity of IpLITR2.6b. As predicted, co-engagement of IpLITR1.1b and IpLITR2.6b resulted in significantly reduced phagocytotic activity compared to activation of IpLITR2.6b alone, supporting the ability of IpLITR1.1b to counteract signaling from IpLITR2.6b (Fei et al., 2020). This result is also consistent with findings in mammals whereby the activation of an inhibitory immunoregulatory receptor-type is facilitated by stimulatory signaling from activating receptors (Srivastava et al., 2003). Similar to previous findings, confocal microscopy and co-immunoprecipitation experiments further showed that the proximal and distal CYT segments of IpLITR1.1b recruited the inhibitory molecules Csk and SHP-2, respectively (Fei et al., 2020). Additionally, the recruitment of these molecules was shown to be required for sustaining IpLITR1.1b-mediated inhibition of phagocytosis and signaling transduction (Fei et al., 2020).

Overall, this model demonstrates that IpLITR1.1b uses a novel intra- and inter-cytoplasmic signaling mechanism to modulate immunoregulatory receptor functions.

2.3.6 Functional characterization of IpLITRs using IpLITR-specific monoclonal Abs (mAbs)

While a heterologous overexpression approach has provided detailed insights into the immunoregulatory potential of IpLITRs, their functional roles in teleost immunity remain largely elusive. Nevertheless, the limited literature on the native functions of IpLITRs has significantly improved our understanding of the immunomodulatory capabilities of IpLITRs in teleost immune cells. These studies have been made feasible using channel catfish immune cell lines, coupled with the generation of IpLITR-specific mAbs.

An IpLITR-reactive mAb termed CC41 was produced by immunizing BALB/c mice with the channel catfish NK cell line TS10.1 and has been shown to label fifteen NK cell lines from the channel catfish (Shen et al., 2002). Flow cytometry analysis also showed that CC41 mAb stains the TS32.15 CTLs, as well as cells in an MLC derived from PBL of a naïve outbred fish activated with irradiated allogeneic 3B11 B cells (Taylor et al., 2016). Additionally, sorted $CC41^{+}$ cells from the PBL of an unimmunized catfish showed potent cytotoxicity by lysing allogeneic 3B11 B cell targets (Taylor et al., 2016). Immunoprecipitation experiments using CC41 mAb isolated several peptides from TS32.15 CTL lysates matching the predicted Ig-like domains of many IpLITR transcripts found to be upregulated by TS32.15 cells stimulated with allogeneic cells (Taylor et al., 2016). Several of the precipitated peptides were identical to sequences within IpLITR1.1a, a seven Ig-like domain containing IpLITR with a TM and a long CYT containing an ITAM-like motif, two ITIMs, and an ITSM. In addition, the CC41 mAb also pulled down a peptide that matched sequences within IpLITR2, a putative activating receptor

with a positively charged arginine residue. Although the identity of each of the IpLITR peptides could not be determined with certainty due to the polygenic nature of the IpLITR family, these data support that the CC41 mAb is reactive against a collection of putative inhibitory and activating IpLITR forms in catfish TS32.15 CTLs (Taylor et al., 2016).

To determine if CCV infection leads to an increase in $CC41^+$ cells in PBLs isolated from CCV-immunized fish, catfish were intracoelomically immunized with either CCV-infected syngeneic G14D cells (G14D-CCV) or mock-infected G14D cells (Taylor et al., 2016). Results showed that G14D-CCV-immunized fish had a significantly higher percentage of $CC41^+$ cells in their PBL compared to fish injected with mock-infected G14D cells. Further experiments showed that $CC41^+$ cells isolated from G14D-CCV-immunized fish lysed more G14D-CCV targets than $CC41^-$ cells obtained from the same source (Taylor et al., 2016). Moreover, 2 h pre-treatment with CC41 mAb resulted in a 40% reduction in the lysis of irradiated G14D-CCV targets by an MLC (Taylor et al., 2016). Altogether, these findings support that a cohort of IpLITRs expressed on the surface of cytotoxic cells of the channel catfish are potentially capable of regulating cell-mediated cytotoxicity and immune responses against a viral infection.

Blackmon et al. (2020) developed an *in vitro* assay to monitor the proliferation of IpLITR-mAb-labeled cells in response to *Edwardsiella ictaluri*-infected channel catfish head kidney-derived macrophages (HKDM). The researchers initially generated recombinant IpLITR1.1a ectodomain fragments (LITR1.1a D2-D3, LITR1.1a D3-D5, and LITR1.1a D5-D7) and examined the abilities of the two mAbs (CC41 and CC34) to interact with these protein fragments (Blackmon et al., 2020). Their results showed that CC41 and CC34 mAbs only bound the LITR1.1a D2-D3 protein. Moreover, flow cytometry experiments

demonstrated that both CC41 and CC34 mAbs stained TS32.15 CTLs and cells in a channel catfish MLC stimulated with irradiated 3B11 B cells (Blackmon et al., 2020). However, the CC41 and CC34 mAbs differentially stained the channel catfish 28S.3 cell line (an autonomous T-cell line). These findings confirmed that both CC41 and CC34 mAbs recognized overlapping subsets of IpLITRs. To examine the growth of IpLITR-mAb-labeled PBLs in response to *E. ictaluri*-infected HKDM cells, channel catfish PBLs were stained with CellTrace Violet (a proliferation dye), whereas mock-infected and *E. ictaluri*-infected HKDM cells were labeled with CellTrace™ Far Red (Blackmon et al., 2020). The labeled PBLs and HKDMs cells were then combined and analyzed by flow cytometry after 2, 5, and 7 days in culture. These experiments showed a significantly higher $CC41^+$ PBL count when cultured with *E. ictaluri*-infected macrophages, compared to the mock-infected macrophage group. In contrast, the CC34 staining was variable between fish replicates, and no statistically significant increase in the number of $CC34^+$ cells was observed in these experiments. Therefore, these findings suggest that catfish PBLs bearing a specific subset of IpLITRs exhibit selective proliferation in response to *E. ictaluri*-infected cells. This is suggestive of their potential involvement in cell-mediated immunity against this bacterium, however, further research is required to verify the role of IpLITRs in regulating immune responses to microbial infections.

Crider et al. (2023) investigated the protein expression of IpLITRs in various channel catfish immune cell lines using 125.2 and CC41 mAbs and examined the potential of these mAbs to regulate phagocytosis in several cell lines. Their study showed that the 125.2 mAb immunoprecipitated several protein bands from G14D γδ T cell lysates ranging from 26 to 150 kDa (Crider et al., 2023). Mass spectrometry analysis of the 120 and 140 kDa bands retrieved 30 IpLITR peptides, 16 of which match sequences within the ectodomains of

IpLITR2.2.5, a putative activating receptor with eight Ig-like domains, a TM containing a lysine residue, and a short CYT region. Unlike the CC41-reactive IpLITRs (mostly long inhibitory IpLITR-types), which were shown to be phosphorylated in TS32.15 cells following pervanadate treatment (Crider et al., 2023), the 125.2-reactive IpLITRs were not detected using a phosphotyrosine-specific antibody (Crider et al., 2023). These results suggest that the 125.2 mAb recognizes a cohort of activating IpLITR-types that likely associate with adaptor molecules (i.e., FcRγ) to transduce downstream signaling responses. Flow cytometric analysis showed that the 125.2 and CC41 mAbs also differentially stained various channel catfish immune cell lines (TS32.15, 28S.3, G14D, 1G8, 3B11, and 42TA) and an MLC (Crider et al., 2023). For example, the 125.2 mAb weakly stained the 28S.3 αβ T cells, whereas it strongly stained the G14D γδ T cells. Conversely, the CC41 mAb strongly stained the 28S.3 αβ T cells but weakly stained the G14D γδ T cells. Taking advantage of the differential staining patterns observed in 28S.3 αβ T cells and G14D γδ T cells, the researchers examined the capacities of the 125.2 and CC41 mAbs to activate phagocytosis in G14D γδ T cells and 28S.3 αβ T cells, respectively (Crider et al., 2023). Cross-linking cell surface proteins with 125.2 mAb-coated beads was surprisingly shown to induce phagocytic activity in G14D T cells. Conversely, limited phagocytic activity was observed in 28S.3 T cells stimulated with CC41-conjugated beads. These findings were further confirmed by additional confocal microscopy experiments (Crider et al., 2023). As the 42TA macrophage line expresses both 125.2- and CC41-reactive IpLITRs, the researchers also investigated the crosstalk potential between the inhibitory and activating IpLITRs expressed by these cells (Crider et al., 2023). Pre-treatment of 42TA macrophages with CC41-conjugated beads significantly dampened 125.2 mAb-mediated phagocytic activity. In summary, these results have confirmed many of the IpLITR findings obtained using mammalian cell line

transfection-based studies and reinforce that activating and inhibitory IpLITR-types are capable of crosstalk regulation of phagocytosis in channel catfish immune cells.

2.3.7 The goldfish represents an ideal ex-vivo model system for studying teleost innate cellular immunity

The goldfish (*Carassius auratus*) was initially domesticated from the crucian carp in China thousands of years ago for its morphological variations and stunning beauty (Komiyama et al., 2009). However, it is only in the past century that its potential as a model system for biological research has been recognized. Today, the goldfish has emerged as a useful model for studying various aspects of biological systems, including immunology (Hodgkinson et al., 2015), cellular biology (Choresca et al., 2009), genetics (Kon et al., 2020), cardiac system (Filice et al., 2022), and endocrinology (Blanco et al., 2018). The versatility of the goldfish system in biological research is largely attributed to several factors (Blanco et al., 2018; Filice et al., 2022): 1) ease of maintenance and handling, 2) high tolerance to stress, 4) high reproductive capacity, and 5) suitability for extracting cells or tissues for various functional assays.

The goldfish has emerged as a prominent model for the study of the teleost immune system (Katzenback et al., 2016). For instance, many cytokines and their receptors have been identified and functionally characterized in this species (Grayfer et al., 2018). These studies collectively reveal that goldfish immune cells use intricate networks of both proinflammatory and anti-inflammatory cytokines for controlling inflammation, mirroring findings from mammalian studies. Furthermore, the goldfish is widely used as a model system for studying host-pathogen interactions due to the ease of observing disease manifestations (Talaat et al., 1998). For instance, the goldfish is currently being used for studying the pathogenesis of several fish microbes, such as *Edwardsiella piscicida* (Choe et al., 2017), *Aeromonas veronii* (Soliman

et al., 2021), *Mycobacterium marinum* (Talaat et al., 1998), and *Trypanosoma carassii* (McAllister et al., 2019). Beyond its role as an *in-vivo* model system for studying fish pathogens, researchers have also extensively characterized primary leukocyte cultures from the goldfish (Katzenback et al., 2016). These studies have been aided by the development of cultivation methods for culturing goldfish primary myeloid cells and a variety of immunological assays, such as nitric oxide production (Stafford et al., 2002), ROS production (Neumann & Belosevic, 1996), chemotaxis (Katzenback & Belosevic, 2009), degranulation (Katzenback & Belosevic, 2009), and phagocytosis assays (Rieger et al., 2010). In the sections below, I will briefly introduce the primary myeloid cells of the goldfish.

2.3.7.1 Goldfish primary kidney macrophage (PKM) culture

The goldfish primary kidney macrophage culture system was established in the 1990s with the aim of identifying factors controlling the development and activation of teleost macrophages (Neumann et al., 2000). These cultures were generated by growing mononuclear cells extracted from the goldfish kidney into flasks containing MGFL-15 (a specially designed incomplete medium) supplemented with 10% calf serum and 5% carp serum (Katzenback et al., 2016). Flow cytometry assays, using size and internal complexity as distinguishing factors, identified three populations of cells in PKM cultures after 8-11 days of incubation (Neumann et al., 2000). These cells were named R1, R2, and R3-type macrophages (Neumann et al., 2000).

Morphologically, R1-type macrophages were small cells with diameters ranging from 6 to 10 μm and had a high nucleus-to-cytoplasm ratio (Neumann et al., 2000), a phenotype resembling putative progenitor cells. Cytochemically, R1 cells showed positive staining for acid phosphatase but were negative for MPO and non-specific esterase (Neumann et al., 2000). In contrast, R2 cells were larger cells (approximately 12 to 20 μm in diameter), exhibited irregular

shapes, and had a low nucleus-to-cytoplasm ratio (Neumann et al., 2000). Additionally, these cells often displayed extensive vacuolization, reminiscent of mammalian macrophages (Neumann et al., 2000). Cytochemically, R2 cells demonstrated positive staining for acid phosphatase, localized staining for MPO, and variable staining for non-specific esterase (Neumann et al., 2000). Overall, the morphological features of the R2 cells suggest their similarity to mature mammalian tissue macrophages. Lastly, R3-type macrophages were large cells with a round morphology (approximately 12-15 μm in diameter), displayed a low nucleus-to-cytoplasm ratio, and often had kidney-shaped nuclei (Neumann et al., 2000). These cells were morphologically similar to mammalian monocytes and exhibited positive staining for acid phosphatase, diffuse staining for MPO, and variable staining for non-specific esterase (Neumann et al., 2000). Therefore, the PKM culture system is unique in that it simultaneously supports the presence of three distinct macrophage developmental stages within a single culture.

Functional assessment of the distinct stages of macrophages within PKM cultures demonstrated that R2-type macrophages had a limited ability to produce NO upon exposure to either macrophage activating factors (MAFs) or LPS alone. However, their NO production capacity was highly upregulated upon combined activation by MAFs and LPS (Neumann et al., 2000). Furthermore, exposure of R2-macrophages to MAF and/or LPS enhanced their ability to produce ROS after 6 h and 24 h (Neumann et al., 2000). In stark contrast, R3-type macrophages produced a limited amount of nitric oxide even with combined exposure to LPS and MAFs (Neumann et al., 2000). Moreover, exposure of R3 cells to MAF and/or LPS to R3 cells initially augmented their respiratory burst activity (ROS production) after 6 h, but they subsequently underwent de-priming and displayed lower respiratory burst activity at 48 h compared to 6 h (Neumann et al., 2000). Unfortunately, due to challenges in enriching the R1 population, their

functional activities were not examined. These observations underscore the functional heterogeneity of the distinct macrophage populations within PKM cultures.

The molecules and transcription factors involved in goldfish macrophage development and differentiation have also been extensively characterized (Katzenback et al., 2016). For example, the recombinant goldfish macrophage colony stimulatory factor 1 (rgCSF-1) has been shown to increase the proliferation of sorted goldfish monocytes and guide the differentiation of goldfish monocytes into macrophages (Hanington et al., 2007). Additionally, RNA interference (RNAi)-mediated knockdown of the expression of CSF-1 receptor (CSF-1R) abolished the biological activity of rgCSF-1 (Hanington et al., 2009), demonstrating the dependency of CSF-1 functions on its cognate receptor. Moreover, injection of rgCSF-1 into goldfish resulted in increased production of circulating monocytes (Hanington et al., 2009), further supporting the regulatory role of CSF-1 in macrophage development.

In contrast, a soluble version of CSF-1R (sCSF-1R) has also been identified from PKM cultures (Barreda et al., 2005). This soluble receptor was predominately expressed during the later stages of PKM cultures and was found to antagonize the activity of CSF-1R and inhibit PKM-mediated antimicrobial responses including chemotaxis, phagocytosis, and ROS production (Rieger et al., 2014). For more information on the molecules identified in regulating the development of goldfish macrophages, refer to this comprehensive review paper (Katzenback et al., 2016).

2.3.7.2 Goldfish primary kidney neutrophils (PKNs)

The goldfish primary neutrophil culture system was established following the development of PKM cultures. Like PKMs, PKNs were isolated from the goldfish kidney and constituted a population of cells with high purity (approximately 92% purity). Microscopic

examination of PKNs revealed them to be small cells (10-12 μm in size) with variable nuclear shapes, including indented, round, and kidney-shaped (Katzenback & Belosevic, 2009), and with cytoplasm filled with granules (Katzenback & Belosevic, 2009). Cytochemically, the goldfish PKNs were shown to be positive for Sudan black, MPO, and acid phosphatase, but they were negative for non-specific esterase (Katzenback & Belosevic, 2009). In contrast to mammalian neutrophils, which typically survive for less than 24 h following isolation from peripheral blood (Lahoz-Beneytez et al., 2016), goldfish PKNs are functional up to 96 h in culture (Katzenback & Belosevic, 2009). These findings support that the goldfish PKNs are longer-lived and well-suited for experiments requiring prolonged incubation periods compared to mammalian primary neutrophils. However, like mammalian neutrophils, the goldfish PKNs were found to be highly mobile and capable of performing a variety of innate immune effector functions, including degranulation, ROS production, and phagocytosis (Havixbeck et al., 2017; Katzenback & Belosevic, 2009). For instance, exposure of goldfish PKNs to a teleost pathogen, *Mycobacterium marinum*, induced significant upregulation of several pro-inflammatory genes (i.e., *tnf-α2* and *il-1β1*) in these cells (Hodgkinson et al., 2015). Moreover, these cells also exhibited chemotaxis towards mycobacteria and were shown to be capable of producing ROS and phagocytosing this pathogen (Hodgkinson et al., 2015). Additionally, goldfish neutrophils were shown to kill *Aeromonas veronii* by releasing ROS and performing phagocytosis (Havixbeck et al., 2017). Molecular analysis of the goldfish PKNs demonstrated that they expressed mRNAs for granulocyte colony-stimulating factor (G-CSFR), MPO, kit receptor, and prominin (Katzenback et al., 2016). Overall, the goldfish PKNs appear to exhibit similar morphological and functional characteristics as their mammalian counterparts. For a more comprehensive review of goldfish

neutrophils, please refer to these publications (Havixbeck & Barreda, 2015; Katzenback et al., 2016).

In summary, the availability of various molecular tools, combined with an in-depth understanding of the morphological and functional characteristics of goldfish PKMs and PKNs, makes the goldfish an ideal model system for studying teleost innate cellular immunity.

2.4 Conclusions

In conclusion, research on LITRs over the past two decades has yielded valuable insights into their diverse immunoregulatory potentials. We have shown that IpLITRs likely use both evolutionarily conserved and unique signaling mechanisms to control a variety of innate immune cell functions, including phagocytosis, degranulation, and cytokine secretion (Fei et al., 2016). Furthermore, our phylogenetic and structural analyses of IpLITRs (Stafford, Bengten, et al., 2006; Stafford et al., 2007) suggest that they may be evolutionary equivalents of the mammalian FcR family and LRC-encoded receptors, which are known to play crucial roles in maintaining immune system balance. However, our understanding of the evolutionary connections between LITRs and these mammalian immunoregulatory receptors is currently limited to amino acid sequence similarity. It is not known if these receptors also share similarities at levels of gene organizations, such as exon-intron organization or genomic synteny. Further complicating the matter is that the biological ligands of IpLITRs are not yet known, making it difficult to ascertain if IpLITRs are truly orthologous to either mammalian FcR family receptors or LRC-encoded receptors.

While our heterologous overexpression approach has enabled us to collect extensive data on IpLITR-mediated signaling mechanisms, their overall functional roles in teleost immune cells remain largely unexplored. Nonetheless, several studies of IpLITRs using the channel

catfish model system and IpLITR-specific mAbs have offered insights into their native functional capabilities (Wang et al., 2023). These studies have shown that specific subsets of IpLITRs likely participate in controlling immune responses against viral and bacterial infections (Wang et al., 2023). Furthermore, these findings support that select IpLITRs can regulate several innate immune effector functions, including cell-mediated cytotoxicity and phagocytosis (Wang et al., 2023). Thus, the development of IpLITR-specific-Abs has played a pivotal role in advancing our understanding of the immunobiology of LITRs in teleost fish.

To further investigate the native immunoregulatory functions of LITRs and their evolutionary relationships with immunoregulatory receptors found in the various aquatic and terrestrial vertebrates, my PhD project aimed to establish the goldfish as a new model system for studying LITRs. The choice of goldfish as a model system is based on several key factors. Firstly, the goldfish has a published genome (Chen et al., 2019), which allows me to examine the exon-intron organization of LITRs and compare their genomic organizations to the various immunoregulatory receptors found in other vertebrates. This comparison may shed new light into the evolutionary connections between LITRs and other vertebrate immunoregulatory receptor families. Secondly, as described, the goldfish has well-established primary myeloid cell culture systems (Katzenback et al., 2016), which enables me to examine the native immunoregulatory capabilities of LITRs in teleost monocytes, macrophages, and neutrophils. The specific aims of my thesis were as follows: i) identification of CaLITRs and examination of their genetic organization and transcript expression in various goldfish tissues, primary PKM, and PKN cultures; ii) examination of the syntenic relationships between LITRs and immunoregulatory receptors found in other vertebrates; iii) analysis of transcript expression of *calitrs* during PKM development and in activated goldfish kidney leukocyte cultures, and; iv) development of new

Ab-based tools for investigating the native functions of CaLITRs in goldfish primary myeloid cells.

CHAPTER III

MATERIALS AND METHODS

3.1 Ethics statement

All experiments adhered to the guidelines established by the Canadian Council of Animal Care guidelines and the University of Alberta Animal Care and Use Committee (animal use protocol# 069). Goldfish were subjected to anesthesia using Tricaine methanesulfonate (MS222) at a concentration of 15-30 mg/L (pH 7.4) and subsequently euthanized through cervical dislocation.

3.2 Maintenance of goldfish

Goldfish measuring 3-5 inches in length were purchased from Aquatic Imports in Calgary, Alberta, and were housed in the Department of Biological Sciences (University of Alberta) aquatic facility at a temperature of 17 ˚C, following a simulated natural period with a 12-hour light/dark cycle. Goldfish received daily feedings of trout pellets and allowed a minimum of 3 weeks to acclimate to this environment before being used in experiments.

3.3 Goldfish primary cells

3.3.1 PKM culture

The procedures for isolating and cultivating goldfish PKMs have previously been described (Neumann et al., 2000). Briefly, goldfish kidneys were aseptically extracted and placed in a homogenization solution (MGFL-15 medium 100 U/ml penicillin, 100 U/ml streptomycin, and 50 U/ml heparin). Subsequently, the kidneys were gently pressed through sterile mesh screens and rinsed with 10 ml of the homogenization solution. Large pieces of kidney tissues were allowed to separate from the smaller kidney cells through sedimentation for 5 min. The resulting cell suspension was layered on a 51% Percoll density gradient medium (Cytiva) and

centrifuged at 450 g for 25 min. Cells from the medium-Percoll interface were harvested, washed twice with MGFL-15 medium, and centrifuged at 350 g for 10 min. Finally, a combination of cell-conditioned medium (CCM, obtained from previous cultures and containing a complex mixture of growth factors) and C-MGFL-15 (MGFL-15 medium with 5% carp serum and 10% newborn calf serum from Gibco) was added to the kidney cells to facilitate cell growth. The cells were then incubated in a 20˚C incubator without CO_2.

3.3.2 Goldfish PKN culture

Primary kidney neutrophils were isolated according to previously described procedures (Havixbeck et al., 2017; Katzenback & Belosevic, 2009). Briefly, goldfish kidneys were macerated through screen meshes with 10 ml of homogenization solution. The resulting cell suspension was allowed to settle at the bottom of a conical tube for 5 min, and it was then carefully layered on top of a 51% Percoll density gradient medium (Cytiva). Subsequently, the supernatant and the cell suspension at the medium-Percoll interface were discarded, leaving behind the neutrophil-erythrocyte pellet. One ml of ACK lysis buffer (Life Technologies Inc) was then used to lyse the red blood cells, and the remaining neutrophils were washed with 10 ml of MGFL-15 before being centrifuged at 350 g for 10 min. Finally, the neutrophils bathed in C-MGFL-15 were incubated in a 20˚C incubator overnight (without CO_2) to allow for any remaining macrophages to adhere to the flask. The next day, non-adherent neutrophils were harvested for use in various experiments.

3.3.3 Isolation of splenocytes

The procedures for harvesting goldfish splenocytes were previously established (Grayfer & Belosevic, 2009). Briefly, spleens from goldfish were aseptically isolated and macerated through screen meshes with 10 ml of homogenization solution. The resulting cell

suspension was then allowed to settle for 5 min, and it was then layered over 51% Percoll before centrifugation at 400 g for 25 min. The cells from the Percoll-medium interface were removed and washed once with 10 ml of MGFL-15 before lysis for downstream western blotting experiments.

3.3.4 Isolation of mixed kidney leukocytes

The mixed kidney leukocytes were isolated following the protocols described in section 3.2.1. The kidney cell suspension was carefully layered over 51% Percoll before centrifugation at 400 g for 25 min. The cells from the Percoll-medium interface were harvested and washed once with 10 ml of MGFL-15. These cells were either pooled from ten goldfish to generate mixed leukocyte reaction (MLR) cultures (bathed in C-MGFL-15) or immediately lysed to generate whole cell lysates (WCLs) for Chapter VII western-blotting experiments.

3.3.5 Extraction of goldfish erythrocytes

Following goldfish blood collection via caudal vein puncture, the blood from each fish was diluted in 4 ml of homogenization solution and then carefully layered onto 3 ml of Ficoll®-Paque PREMIUM medium (catalog# GE17-5446-52, Sigma). After centrifugation at 400 g for 30 min, the blood plasma and the mononuclear cell layers were discarded, retaining only the erythrocyte pellet. The thin film of granulocytes on the surface of the erythrocyte pellet was then carefully removed.

3.4 Identification of *calitr* transcripts

A truncated sequence (CL16186.Contig2) for a putative *calitr* was initially identified from the goldfish transcriptome (generated in our lab) with BLAST+ (Camacho et al., 2009) using *iplitr1*, *iplitr2*, and *iplitr3* sequences as queries. Subsequently, it was used to search the

goldfish reference RNA database (refseq_rna) for putative *calitrs* with complete open reading frames (ORFs) using the Blastn algorithm on NCBI. Three putative *calitr* sequences, XM_026262093.1, XM_026236356.1, and XM_026218715.1, were obtained and renamed as *calitr1*, *calitr2*, and *calitr3*, respectively. To confirm the expression of these predicted *calitrs* in goldfish tissues and immune cells, RT-PCR was performed using primers (Table 2) that were designed to amplify the complete ORF of each predicted sequence. Using the same approach, *calitr4* and *calitr5* were later obtained by searching the goldfish reference RNA database using the *calitr2* and *calitr3* cDNA sequences as templates. Simple Modular Architecture Research Tool (SMART) (Letunic et al., 2004), PROSITE (de Castro et al., 2006), NetNGlyc1.0, NetOGlyc 4.0 (Steentoft et al., 2013), SignalP 5.0, TMHMM Server v. 2.0, and Phyre2 (Kelley et al., 2015) were used to identify signal peptides, Ig-like domains, TM, CYTs, secondary structures (beta-strands and alpha-helices), and post-translational modifications. All multiple sequence alignments were performed using Clustal Omega (Madeira et al., 2019) and presented with BoxShade v3.21 (https://embnet.vital-it.ch/software/BOX_form.html). The neighbor-joining (NJ) trees (10,000 bootstrap replicates) with complete deletions were drawn using MEGA7 (Kumar et al., 2016) using the No. of differences model.

3.5 RNA extraction

In Chapter VI, following the isolation of goldfish spleen, brain, muscle, gills, kidney, skin, intestine, and heart tissues, they were snap-frozen in liquid nitrogen. Total RNA from goldfish tissues (liver, spleen, kidney, heart, brain, intestine, muscle, and gills), PKMs (day 0, 2, 4, 6, 8, 10, and 12), and overnight cultured PKNs were extracted using Trizol reagent according to the manufacturer's instructions (Invitrogen). For Chapters VI and VII, total RNA was extracted using the RNeasy mini kit (Qiagen) according to the manufacturer's instructions.

3.6 cDNA synthesis

For all PCR-based experiments, RNA was treated with DNase 1 (Invitrogen) to eliminate contaminating genomic DNA and then reverse transcribed into cDNA using the SuperScript III First-Strand Synthesis System (Invitrogen).

3.7 RT-PCR analysis of the mRNA expression of *calitrs* in goldfish tissues and primary cells

RT-PCR was performed using specific primers for *calitrs* and the housekeeping gene elongation factor 1 alpha (*ef1a*; Accession number AB056104; Table 2). Typical cycling parameters were: 30 s 98 °C, followed by 36 cycles of 98 °C 30 s, 64 °C 30 s, and 72 °C 3 min, then an extension at 72 °C for 10 min. All PCR reactions were performed using the Phusion high-fidelity DNA polymerase (NEB). PCR products were visualized on 1.2 % Tris-acetate-EDTA agarose gels, excised, extracted, and then cloned into the pJET1.2/blunt vector (Thermo Scientific) for verification by sanger sequencing at the molecular biology facility located at the University of Alberta.

3.8 Real-time PCR assays and primer validation

All quantitative (q)PCR assays were run using the QuantStudio 6 Flex Real-Time PCR System located at the Molecular Biology Facility, University of Alberta. Each qPCR reaction mixture (10 µl total volume) has 5 µl of SYBR reagent mix, 0.5 µl of both forward and reverse primers (10 µM final concentrations), and 2.5 µl of cDNA (diluted in 1/10). *ef1α* was used as the endogenous control gene for all the experiments as it has been tested to be stably expressed (cycle threshold (Ct) values differ by ± 1) in goldfish PKMs and MLRs in my lab. Thermocycling parameters were 95 °C for 2 min, followed by 40 cycles of 95 °C for 15 s and 60 °C for 1 min. qPCR primers used in this study were purchased from Integrated DNA Technologies and are displayed in Table 6.1. The amplification efficiency of each primer pair

was assessed by running a serial dilution series of cDNA (1:2), and a ΔC_T (C_T target gene— C_T EF1α) versus the log of cDNA dilutions graph was plotted to determine the slope (acceptable values are between − 0.1 to 0.1). Melting curve analysis and amplicon sequencing were performed to evaluate the specificity of each primer pair.

3.8.1 Investigation of the expression levels of *calitr* transcripts during PKM development and in PKM subsets

To examine the expression profiles of *calitrs*, lymphoid markers, and myeloid-differentiation-associated transcription factors during PKM development, freshly isolated goldfish kidney cells from each fish were seeded in 24 well plates at a density of 2×10^5 cells/well (bathed in C-MGFL-15 medium with 33% CCM) and placed in a 20 °C incubator without CO_2. For each fish, total RNA from days 0, 2, 4, 6, 8, 10, and 12 culture wells were extracted using an RNeasy mini kit (Qiagen) according to the manufacturer's instructions. Insufficient goldfish kidney cells were obtained from each fish to have replicate culture wells at each time point. Therefore, RNA was extracted from one culture well per each time point for each fish. The sorting of cultured PKMs into progenitors, monocytes, and macrophages was done as described previously (Barreda et al., 2000; Neumann et al., 2000). On day 7, cultivated PKMs from three fish individuals were combined, centrifuged, and adjusted to a concentration of 5×10^6 cells/ml in a fresh C-MGFL-15 medium. FACS Aria flow cytometer (located at the flow cytometry facility, University of Alberta) was used for cell sorting based on distinct forward and side scatter characteristics of the three PKM subpopulations. Immediately after the sorting, cells were centrifuged and lysed using RLT buffer (RNeasy mini kit). Total RNA was then isolated and reversed transcribed into cDNA for downstream qPCR analysis.

3.8.2 Transcriptional profiling of *calitr3* in goldfish erythrocytes, mixed kidney leukocytes, and PKNs

Erythrocytes ($2x10^6$), mixed kidney leukocytes ($2x10^6$), and PKNs ($2x10^6$) from three goldfish individuals were lysed using the RLT buffer (Qiagen). Subsequently, total RNA was extracted using the RNeasy mini kit (Qiagen) according to the manufacturer's instructions. RNA (0.3 μg) was treated with DNase 1 (Invitrogen) to eliminate contaminating genomic DNA and then reverse transcribed into cDNA using the SuperScript III First-Strand Synthesis System (Invitrogen).

3.8.3 Analysis of the expression of inflammatory marker and *calitr* genes in goldfish mixed leukocyte reaction (MLR) cultures with/without T-cell mitogens

Goldfish MLR experiments were performed based on methods previously developed in our lab to generate macrophage activating factors (MAFs) (Neumann et al., 1995; Stafford et al., 2002). Ten goldfish individuals of similar sizes were euthanized and processed as described in section 3.2.4. Goldfish kidney cells from the medium-Percoll interface were washed with MGFL-15 medium and kept in separate tubes to prevent premature allogeneic reactions. Before the experiment, the isolated cells were combined and washed with MGFL-15. After centrifugation at 350 g for 5 min, the pooled cells were incubated in a C-MGFL-15 medium, enumerated using a hemocytometer, and stained with Trypan Blue to determine the percentage of viable cells. These cells were seeded into a 24 well-plate at a density of 1.5×10^6 cells/well with 0.2% DMSO/with mitogens including 10 μg/ml ConA (Sigma), 10 ng/ml PMA (Sigma), and 100 ng/ml calcium ionophore A23187 (Sigma). The RNeasy mini kit (Qiagen) was used to extract total RNA from cells at discrete time points of the MLR experiment (0, 6, 12, and 24 h). All MLR experiments have been replicated at least three times.

3.8.4 Assaying the effects of Cyclosporin A (CsA)/DMSO on mitogen-stimulated goldfish MLR cultures

MLR experiments were established as described in section 3.7.3. After pooling the freshly isolated goldfish kidney cells from ten goldfish, the C-MGFL-15 medium-bathed cells were enumerated and seeded into a 24 well-plate at a density of 1.5×10^6 cells/well. The mitogens mentioned in section 3.7.3 were added to the cells to further stimulate MLRs. Various concentrations of CsA (Sigma) or DMSO (CsA solvent, Sigma) were added to mitogen-stimulated MLRs, and total RNA was extracted from these cells using the RNeasy mini kit at the various time points examined (0, 6, 12, and 24 h).

3.9 Development of CaLITR3-epitope-specific pAbs

Anti-CaL3.D1 and Anti-CaL3.D2 pAbs were generated using the custom rabbit polyclonal antibody services from GenScript. Initially, multiple sequence alignment was conducted on all identified CaLITR cDNA sequences to pinpoint peptide sequences specific for CaLITR3. As a result, two unique CaLITR3 epitope sequences, GAERGGSRTSNISDE and DNKYNYQKLSG, were identified and designated as D1 and D2 peptides, respectively. The D1 and D2 cDNA sequences were cloned into an *E. coli* expression vector (pET30a), and the resulting plasmids were then used to transform BL21 Star™ (DE3) *E. coli* cells. IPTG was then added to induce the production of recombinant D1 and D2 peptides in the bacterial cells. To develop the pAbs, two rabbits were immunized with the purified D1 peptide, and an additional two rabbits were immunized with the purified D2 peptide. Each rabbit underwent a total of three immunizations with the respective peptides before being sacrificed for blood collection. Serum from the rabbits immunized with the D1 and D2 peptides were then separately pooled, and Abs

were purified from each pool. For simplicity, pAbs against the D1 and D2 peptides were named anti-CaL3.D1 and anti-CaL3.D2 pAbs, respectively.

3.10 Validating the specificity of anti-CaL3.D1 pAb

3.10.1 Generation of AD293 cells expressing HA-tagged recombinant CaLITR3 (rCaLITR3) and rIpLITR2.6b/6.1 proteins

AD293 cells expressing HA-tagged-LITR transmembrane proteins were generated according to our previously described methods (Fei et al., 2016). Briefly, full-length CaLITR3 and IpLITR2.6b/6.1CYT (a chimeric construct containing the ectodomains and TM of IpLITR2.6b fused to the CYT region of CaLITR6.1) cDNA sequences were cloned into pDisplay plasmids. Each plasmid (500 ng) was then transfected into parental AD293 cells ($2x10^5$) using TurboFect transfection reagent (catalog# R0531) following the manufacturer's instructions. Two days post-transfection, the AD293 cells were incubated with Dulbecco's Modified Eagle Medium (DMEM) containing 800 μg/ml G418 disulfate salt solution (Sigma-Aldrich) at 37 ˚C with 5% CO_2 for a week. Following selection, flow cytometry was used to sort out the LITR-positive AD293 cells into a 96-well plate to generate AD293 cells stably expressing LITR proteins using the Sony MA900 instrument located in the flow cytometry facility at the University of Alberta.

3.10.2 Flow cytometric analysis of the surface expression of HA-tagged rLITR proteins in AD293 cells

AD293 cells ($1x10^6$) expressing rCaLITR3 and rIpLITR2.6b/6.1CYT proteins were centrifuged at 1000 g for 2.5 min. After centrifugation, the cells were incubated with 50 μl FACS buffer (composed of 0.5% BSA, 1x PBS, 2 mM ethylenediaminetetraacetic acid (EDTA), and 0.05% NaN_3) containing either anti-HA mAb (1 μg/ml) or mouse IgG1 isotype control Ab (1 μg/ml) (catalog# 02-6100, Thermo Fisher Scientific) at 4 ˚C for 30 min. The AD293 cells were

then washed with 1 ml of ice-cold FACS buffer before being centrifuged at 1000 g for 2.5 min. Cells were then incubated with phycoerythrin (PE)-conjugated goat anti-mouse IgG (1 µg/ml) (catalog# 12-4010-82) for 30 min. Following washing with 1 ml of ice-cold FACS buffer and centrifugation at 1000 g for 2.5 min, the AD293 cells were resuspended in 250 µl of ice-cold FACS buffer. The Attune NxT flow cytometer, located in the flow cytometry facility at the University of Alberta, was used to examine the surface expression of LITR proteins, and all flow cytometry graphs in this study were analyzed and generated using FlowJo™ v10.10.

3.10.3 Analysis of the specificity of anti-CaL3.D1 pAb for rLITR proteins using confocal microscopy

Before staining the AD293 cells expressing HA-tagged recombinant LITR proteins, cells ($3x10^5$) (bathed in DMEM containing G418) from each treatment/control group were seeded onto a 12 mm coverslip placed in a well of a 24-well plate overnight to allow cell attachment. The next day, the DMEM medium was removed, and the cells were rinsed with 1x PBS before fixation with 4% paraformaldehyde in 1x PBS (Invitrogen) for 10 min at RT. Subsequently, the AD293 cells were washed with 200 µl PBS (twice) before being blocked with 1x PBST containing 1% BSA and 22.5 mg/ml glycine for 30 min. For staining, the AD293 cells were incubated with 1x PBST supplemented with 1% BSA, along with either the mouse IgG1 isotype control Ab (20 µg/ml), mouse anti-HA mAb (20 µg/ml) (catalog# 26183, Invitrogen), normal rabbit pAb (20 µg/ml), anti-CaL3.D1 pAb (20 µg/ml), or anti-CaL3.D2 pAb (20 µg/ml) at RT for an hour. After two PBS washes, the cells were incubated with either goat anti-mouse pAb conjugated to Alexa Fluor 647 (40 µg/ml) (catalog# A-21239, Invitrogen) or goat anti-rabbit pAb conjugated to Alexa Fluor 647 (40 µg/ml). Cells were then washed with PBS (twice), and the coverslips with cells were mounted on slides containing one drop of Prolong Gold Antifade

Mountant with DAPI (catalog# P36941, Invitrogen). Images were captured using an Olympus FLUOVIEW FV3000 Confocal Laser Scanning Microscope (Advanced Microscopy Facility, University of Alberta) with a 40x objective lens. Consistent laser settings were maintained across all acquisitions.

For the peptide blocking experiments, 1 µg of the anti-CaL3.D1 pAb was mixed with 50 µg of D1/D2 peptide to a final volume of 50 µl. These Ab-antigen complexes were then incubated at 4˚C overnight on a rotator. The following day, these were used as the primary Abs.

3.10.4 Evaluation of the specificity of anti-CaL3.D1 pAb using immunoprecipitation

AD293 cells ($3x10^5$) expressing rCaLITR3 or rIpLITR2.6b/6.1CYT proteins were lysed using 100 µl of Pierce™ IP Lysis Buffer containing a halt protease inhibitor cocktail. Subsequently, the lysates underwent processing and quantification as outlined in section 2.15. All immunoprecipitation experiments were performed using the Dynabeads™ Protein G Immunoprecipitation Kit (catalog# 10007D, Invitrogen) following the manufacturer's instructions. Briefly, to coat the magnetic Dynabeads with Abs, 5 µg of each immunoprecipitation Ab bathed in 200 µl of Ab binding buffer was incubated with the Dynabeads at RT for 10 min on a rotator. The resulting mixture was subsequently placed onto a magnetic stand to remove the supernatant. The Dynbeads were then resuspended in 200 µl Ab binding and washing buffer. Following the removal of the binding and washing buffer, the Dynabeads were incubated with 100 µl of each AD293 cell lysate on a rotator for 10 min at RT. Following supernatant removal, the Dynabeads were washed three times with 200 µl of washing buffer and then resuspended in 100 µl of washing buffer. After removing the supernatant, the Dynabead-protein complex was incubated with 20 µl elution buffer, 5 µl NuPAGE LDS Sample Buffer, and 5 µl NuPAGE Sample Reducing Agent. Prior to SDS-PAGE electrophoresis, the

Dynabead-protein-Ab mixture was heated at 70 ˚C for 10 min. Five µl of each reduced lysate was loaded onto a 10% polyacrylamide gel, and western blotting steps were carried out using the procedures described in section 2.15. The mouse β-actin mAb (catalog# AM4302) was used to verify the presence of proteins in AD293 WCLs in all immunoprecipitation experiments.

3.10.5 Analysis of the specificity of anti-CaL3.D1 pAb for the D1 peptide of CaLITR3

The goldfish neutrophil WCLs (20 µg) were reduced with DTT and then subjected to 10% SDS-PAGE gel electrophoresis. The separated proteins from the gel were subsequently transferred to a nitrocellulose membrane and cut into three identical parts with scissors. Each of the three sections was probed with either the anti-CaL3.D1 pAb alone (1µg/ml), anti-CaL3.D1 pAb (1 µg/ml) plus D1 peptide (in a 50 peptide:1 pAb ratio), or the anti-CaL3.D1 pAb (1 µg/ml) plus D2 peptide (in a 50 peptide:1 pAb ratio). The nitrocellulose membranes were visualized with SuperSignal West Pico PLUS Chemiluminescent Substrate (Thermo).

3.10.6 Examination of the reactivity of anti-CaL3.D1 pAb in goldfish PKN, PKM, and splenocyte lysates

Total cell lysates (15 µg) from resting goldfish primary immune cells (neutrophils, splenocytes, and mixed kidney leukocytes) were treated with DTT and separated on a 10% SDS-PAGE gel. Subsequently, the proteins were transferred onto a nitrocellulose membrane and probed with anti-CaL3.D1 pAb at a concentration of 1 µg/ml. To detect the bound primary antibody, a secondary antibody, goat anti-rabbit HRP IgG secondary antibody (Invitrogen) (1 µg/ml) was used. The nitrocellulose membrane was then visualized with SuperSignal West Pico PLUS Chemiluminescent Substrate (Thermo) and imaged via ChemiDoc MP Imaging System (Bio-Rad). Mouse anti-β-actin monoclonal antibody (Sigma) was used as the positive and loading controls for this experiment.

3.11 Isolation and processing of goldfish kidney for hematoxylin and eosin (H&E) and immunofluorescence staining

3.11.1 Fixation, paraffin embedding, and sectioning of goldfish kidney tissues

After extracting the kidney from each goldfish, the organ was immediately fixed in 10% formalin and left at 4 ˚C overnight on a rocker. The formalin-fixed kidney then underwent a series of dehydration steps in the following order: first immersed in 25% ethanol for 30 min, followed by 50% ethanol for another 30 min, and finally in 70% ethanol for an additional 30 min. The dehydrated kidney was then subjected to further dehydration steps with ethanol, followed by toluene washes using a Leica TP1020 tissue processor (Leica Biosystems, Concord, Canada). The tissue was then paraffin-embedded and cut into thin sections (5 μm thickness) using a Leica RM2125 RTS microtome (Leica Biosystems, Concord, Canada). Although the teleost kidney is anatomically subdivided into a head kidney and a trunk kidney, we did not differentiate between these sites, as the main focus of this study was to examine the overall patterns of anti-CaLITR-pAb-mediated staining in the whole kidney.

3.11.2 H&E staining of goldfish kidney tissue sections

Dewaxing of the paraffin-embedded goldfish tissue samples was performed by passing them through two rounds of toluene washes (5 min each), followed by a sequence of ethanol washes in the following order: 2 min in 100% ethanol (repeated twice), 2 min in 90% ethanol, 2 min in 70% ethanol, 2 min in 50% ethanol, and finally 2 min in distilled water. For H&E staining, the deparaffinized slides were incubated with Hematoxylin Gill III for 2 min, followed by rinsing with distilled water and tap water for a total of 15 min. The slides were then washed with 70% ethanol for 2 min, followed by eosin staining for 30 seconds. Following this, the slides

underwent two rounds of 100% ethanol washes (2 min each) and then toluene washes (2 min each) before being coverslipped with DPX. The H&E-stained slides were visualized using a ZEISS AXIO A1 compound light microscope, equipped with a SeBaCam 5.1MP camera.

3.11.3 Immunofluorescence staining of goldfish kidney sections

Following the dewaxing procedures described in section 3.10.2, the goldfish kidney sections were immersed in hot-boiling citrate buffer (10 mM citric acid, 0.05% Tween 20, pH 6.0) for 10 min to reverse formalin-induced protein crosslinking and unmask epitopes necessary for Ab binding. Subsequently, the slides were rinsed with PBS and then blocked with 5% bovine serum albumin (BSA) in PBST containing 22.5 mg/ml glycine for 30 min. Following the blocking step, the slides were incubated with either the normal rabbit pAb (5 µg/ml) (catalog# 02-6102, Thermo Fisher Scientific), anti-CaL3.D1 pAb (5 µg/ml), or anti-CaL3.D2 pAb (5 µg/ml) for an hour at room temperature (RT). The slides then underwent a PBS wash for 5 min (repeated three times). Subsequently, the slides were incubated with goat anti-rabbit pAb conjugated to Alexa Fluor 647 (40 µg/ml) (catalog# A21244, Thermo Fisher Scientific) for another hour at RT, followed by three washes with PBS for five min each. Finally, ProLong™ Antifade Mountant with DNA stain DAPI (Invitrogen) was applied to the tissue sections. All confocal microscopy images were acquired using an Olympus FLUOVIEW FV3000 Confocal Laser Scanning Microscope with a 40x objective lens. Consistent laser settings were maintained across all acquisitions. Kidney tissue sections from three distinct goldfish individuals were analyzed. Initially, a series of anti-CaL3.D1 pAb concentrations (5 µg/ml, 10 µg/ml, 15 µg/ml, and 20 µg/ml) were tested to establish the ideal antibody concentration for staining goldfish kidney tissue sections. Ultimately, 5 µg/ml was selected for our assays.

3.12 Microscopic examination of the specificity of anti-CaL3.D1 pAb in isolated goldfish leukocytes

The AD293 cell immunostaining protocol described in section 3.9.3 was also used for staining the goldfish PKNs and PKMs with some modifications to the sample preparation procedures. Briefly, PKNs and PKMs were combined from three individual goldfish. In each sample well of a 24-well plate, PKNs ($2x10^6$) were seeded onto a 12 mm coverslip coated with poly-L-lysine solution (Sigma-Aldrich) for one hour to facilitate cell adhesion. Conversely, for each sample well, PKMs ($1x10^6$) were seeded onto a 12 mm coverslip not coated with poly-L-lysine overnight to allow cell attachment. All microscopy experiments were replicated at least three times.

3.13 Flow cytometric analysis of anti-CaL3.D1-pAb staining of PKNs

The flow cytometry staining protocol for the goldfish PKNs was adapted from sections 3.9.2 and 3.11. Briefly, $1x10^6$ PKNs from each goldfish were centrifuged at 1000 g for 2.5 min. Following centrifugation, the cells were incubated with FACS buffer containing 20 μg/ml of either the normal rabbit IgG or anti-CaL3.D1 pAb at RT for one hour. After two washes with PBS, the PKNs were incubated with FACS buffer containing 40 μg/ml of goat anti-rabbit pAb conjugated to Alexa Fluor 647 at RT for an hour. Finally, following two washes with PBS, the cells were resuspended in 100 μl of FACS buffer. Protein expression profiles were obtained using Attune NxT and analyzed with FlowJo v10.10 software.

3.14 Anti-CaL3.D1-pAb-mediated cross-linking of PKN membrane proteins and western blotting analysis

PKNs from four goldfish individuals were pooled and for each time point of each sample well, PKNs ($1.5x10^6$) were transferred to a microtube containing phagocytosis buffer (consists of Opti-MEM, PBS, and 1% BSA-PBS). To sensitize the cells with the primary Abs, the PKNs were incubated with 40 µg/ml of either the normal rabbit IgG or anti-CaL3.D1 pAb at RT for 30 min. Following Ab sensitization, the cells were washed twice with PBS and then incubated with 50 µg/ml of unconjugated goat anti-rabbit pAb (catalog# A16098, Invitrogen) for 0-30 min. After centrifugation at 1000 g for 2.5 min, the PKNs were lysed with Pierce™ IP Lysis Buffer (catalog# 87787, Thermo Scientific) containing Halt Protease Inhibitor Cocktail (Thermo Scientific) and Halt Phosphatase Inhibitor Cocktail (Thermo Scientific). The PKN lysates were then centrifuged at 16900 g for 20 minutes. To quantify the amount of protein in each PKN lysate, a Micro BCA Protein Assay Kit (catalog# 23235) was used according to the manufacturer's instructions. For western blotting, 15 µg of protein lysate from each time point was reduced with Pierce Lane Marker Reducing Sample Buffer (catalog# 39000, Thermo Scientific) and then heated at 100˚C for 10 min. The samples were then loaded onto a 10% polyacrylamide gel and then subjected to gel electrophoresis using a PowerPac HC power supply (Bio-Rad) (100 volts for 90 min). The proteins from the polyacrylamide gel were subsequently transferred (90 volts for 90 min) onto a nitrocellulose membrane. Following protein transfer, the nitrocellulose membrane was blocked with 1x TBST containing 5% BSA for an hour at RT. After blocking, blots were probed with either Phospho-p38 MAPK (Thr180/Tyr182, (D3F9) XP® Rabbit mAb (1/1000) (catalog# 4511, Cell Signaling)), p38α MAPK (L53F8) Mouse mAb (1/1000) (catalog# 9228S), Phospho-p44/42 MAPK (Erk1/2) (1/1000) (catalog# 9101S), or p44/42 MAPK (Erk1/2) Antibody (1/1000) (catalog# 9102S) overnight at 4 ˚C. The following day, the blots were washed with 1x TBST buffer three times (5 min each) and then incubated

with either goat anti-rabbit IgG conjugated to horseradish peroxidase (HRP) (1/1000) (catalog# 65-6120) or goat anti-mouse IgG conjugated to HRP (1/1000) (catalog# 32430) at RT for an hour. Following three washes with 1x TBST (5 min each), SuperSignal West Pico PLUS Chemiluminescent Substrate (Thermo Fisher) was used to detect protein bands, and images were acquired using ChemiDoc MP Imaging System (Bio-Rad) (Molecular Biology Facility, University of Alberta). Relative protein band intensities were quantified using ImageJ software. Values of pp38 and pERK were normalized to total p38 and ERK1/2 levels and displayed as fold changes relative to the 0 min controls.

3.15 Statistical analysis

For Chapter VI, Shapiro–Wilk normality test was performed to determine if all data sets generated followed a normal distribution. One-way analysis of variance (ANOVA)/unpaired t-test was applied to determine significant differences between treatments at each timepoint examined (i.e., 6 h post-stimulation). For Chapter VII, ANOVA was used to calculate the statistical differences in the average transcript expression level of *calitr3* between erythrocytes, mixed kidney leukocytes, and PKNs. Additionally, unpaired t-test was conducted to examine differences in the phosphorylation levels of p38 and ERK1/2 across various time points. For all experiments, a p-value less than 0.05 was deemed statistically significant. All statistical analyses were performed using GraphPad Prism.

CHAPTER IV

IDENTIFICATION OF GOLDFISH (CARASSIUS AURATUS L.) LEUKOCYTE IMMUNE-TYPE RECEPTORS SHOWS ALTERNATIVE SPLICING AS A POTENTIAL MECHANISM FOR RECEPTOR DIVERSIFICATION

4.1 INTRODUCTION

The recognition and destruction of invading microbes require coordinated immune signaling networks that modulate the stimulation and suppression of vital innate immune cell effector responses. Over the last two decades, many teleost receptor gene families (i.e., LITRs, NITRs, NILTs, and DICPs) with diverse Ig-like domain architectures and immunoregulatory potentials have been identified (Wcisel & Yoder, 2016). The discovery of these receptors has provided new insights into the evolutionary mechanisms of immunoregulatory receptor diversification and has revealed that certain teleost immunoregulatory receptor-types use conserved as well as novel signaling mechanisms to control innate immune cell effector responses (Fei et al., 2016; Rodriguez-Nunez et al., 2014; Wcisel & Yoder, 2016; Yoder & Litman, 2011). For example, a representative member of the IpLITR family uses a novel combinatorial recruitment of Csk and SHP-1 to inhibit lymphocyte killing of targets. IpLITRs belong to the IgSF and are expressed by various channel catfish immune cell-types, including B cells, T cells, NK-like cells, and macrophages (Stafford, Bengten, et al., 2006; Stafford et al., 2007). Phylogenetic analyses and homology modeling have shown the distant relationships of the IpLITR extracellular Ig-like domains with members of the mammalian FcR family genes (i.e., FcRs and FCRLs) and LRC genes (i.e., KIRs, LILRs, and chicken Ig-like receptors (CHIRs)). In addition, a putative conserved MHC class 1 binding site was identified in the membrane distal Ig-like domains of certain IpLITR-types, further suggesting that functional similarities may exist between some IpLITR family members with

those that regulate important innate effector responses in mammals (Stafford, Bengten, et al., 2006; Stafford et al., 2007). To date, most of the biochemical and functional examination of IpLITRs have been performed using heterologous overexpression systems in mammalian cell lines. Specifically, representative IpLITR-types have been epitope-tagged (i.e., HA or FLAG tag) and then transfected into well-characterized mammalian cell lines (i.e., RBL-2H3 and AD-293 cells). Overall, this reductionist approach has significantly contributed to our present understanding of the diverse immunoregulatory capabilities of IpLITR family members (Cortes et al., 2014; Cortes et al., 2012; Lillico et al., 2015; Mewes et al., 2009; Montgomery et al., 2012; Montgomery et al., 2009; Zwozdesky et al., 2017). While select IpLITRs have been shown to exhibit potent immunoregulatory potentials in transfected cells, we have a limited understanding of the roles that LITRs play during immune reactions in fish.

Goldfish (*Carassius auratus*), with its well-characterized primary macrophage and neutrophil cultures (Katzenback et al., 2016), represents an excellent *ex vivo* model system for further exploring the functions of teleost LITRs. Consequently, the discovery of CaLITRs will help us gain further mechanistic insights into their immunoregulatory roles by providing a new model to specifically explore their actions in fish myeloid cells. The primary objectives of this thesis chapter were to identify and clone *calitr* transcripts from the goldfish. My subsequent aims were to compare these *calitr* transcripts with the published goldfish genome to analyze their exon-intron organizations. I also used RT-PCR to investigate the general expression patterns of *calitrs* in goldfish tissues as well as in PKN and PKM cultures.

Overall, I successfully cloned the complete ORFs of five different *calitrs* (*calitr1*, *calitr2*, *calitr3*, *calitr4*, and *calitr5*) from goldfish kidney tissue, primary macrophage, and neutrophil cDNAs. The discovered CaLITRs differed in their number of Ig-like domains and CYT signaling

motifs, demonstrating their potential variable immunomodulatory capabilities. Interestingly, my preliminary analysis of the exon-intron organizations of the five identified *calitrs* revealed that they all have a split signal peptide (encoded by two separate exons), a feature shared by both FcR family and LRC-encoded genes, further supporting the evolutionary links of LITRs to these receptor families (Davis, 2007). However, a closer examination of the *calitrs* exons showed that the second half of the signal peptide (S2) resides in a mini-exon of 36 base pairs (bp) long, a hallmark of LRC-encoded genes such as *fcar* (de Wit et al., 1995), *kirs* (Selvakumar et al., 1997; Wilson et al., 1997), *pirs* (Alley et al., 1998), and *chirs* (Viertlboeck et al., 2005). Additionally, phylogenetic analyses comparing the Ig-like domains of CaLITRs and IpLITRs indicated that they have unique membrane distal Ig-like domains, suggesting that these receptors may interact with different ligands or have variable affinities for their ligands. I also identified putative CaLITR splice variants with altered extracellular Ig-like domain compositions and variable CYT regions. Overall, these finding suggests that alternative splicing-mediated diversification of CaLITRs may generate forms with alternative binding and/or intracellular signaling potentials.

4.2 RESULTS

4.2.1 Genomic organizations of *calitrs* and their encoded domain architectures

Three putative *calitr* sequences (predicted by Gnomon) with significant similarities (e-value<1e-30) to prototypic *iplitrs* (*iplitr1*, *iplitr2*, and *iplitr3*) were retrieved from the goldfish reference RNA database and named as *calitr1*, *calitr2*, and *calitr3*. RT-PCR was then used to detect expression of the predicted sequences using primers that span the opening reading frames (from start codon to stop codon) of each putative *calitr*. To visualize the protein domain architectures of the cloned CaLITR PCR products, each sequence was analyzed using SMART.

The *calitr1* transcript was identified from goldfish PKM cDNA (Fig. 4.1) (GenBank Accession Number MT209979), and it precisely matches its genomic prediction (XM_026262093.1, NCBI genome data viewer). CaLITR1 appears as a functionally ambiguous CaLITR-type that contains no charged amino acids present in its TM, and it also has a short CYT region devoid of any recognizable tyrosine-based signaling motifs (Fig. 4.2A). The *calitr1* transcript also has a split signal peptide with a 36-bp-long S2, two Ig-like domains encoded by two separate exons, and a TM encoded by one exon (Fig. 4.2A). When the *calitr1* transcript was compared against the goldfish genome on NCBI, *calitr1* was shown to be unplaced; thus, its chromosomal location is currently unknown. I also compared the translated CaLITR1 sequences in three goldfish individuals. As shown in Fig. 4.2B, the CaLITR1 sequences from three separate goldfish show very little sequence variation between the individual fish, although a few amino acid differences were observed.

CaLITR2 is a putative inhibitory receptor-type cloned from goldfish PKM cDNA (Fig. 4.1) that contains predicted ITIM (LxYxxI) and ITSM (TxYxxL) motifs within its CYT region (Fig. 4.3B). The *calitr2* transcript (GenBank Accession Number MT209980) lacks exon1-exon14 when compared to its genomic prediction (XM_026236356.1, NCBI genome data viewer) (Fig. 4.3A), suggesting that it may be the product of alternative splicing. Like *calitr1*, the predicted genomic sequence of *calitr2* has a split signal peptide with a 36-bp-long S2. According to the NCBI genome data viewer and goldfish genome blast outputs, the *calitr2* transcript is located on Chr 47 in goldfish. Four sequence variants of *calitr2* were identified and named as *calitr2.1*-*calitr2.4* based on the chronological order of their discovery (Fig. 4.3C). *calitr2.1*, *calitr2.2*, and *calitr2.3* are similar in size and were cloned from the same RT-PCR band as *calitr2* (Fig. 4.1) in different individuals (F1, F2, and F3). Additionally, the *calitr2.4* transcript was cloned from a

day 0 PKM culture. Compared to CaLITR2, the CaLITR2.1 transcript (GenBank Accession Number MT209981) contains a variant D1 domain and a shorter CYT region (Fig. 4.4). Although the CYT region of CaLITR2.1 is shorter in length, it is otherwise identical to the CYT region of CaLITR2, and thus also appears to be an alternatively spliced product resulting from a deletion of 29 amino acid residues. Except for variations in the D1 domain, the rest of the Ig-like domains are identical between CaLITR2.1 and CaLITR2. CaLITR2.2 (GenBank Accession Number MT209982) is 79.59 % similar to CaLITR2 and it contains four extracellular Ig-like domains and a CYT region containing a putative STAT3 recruitment motif (YxxC) (Chakraborty et al., 1999) and an ITIM (LxYxxI) (Burshtyn et al., 1996; Daëron et al., 1995) and ITSM (TxYxxL) (Wilson et al., 2014). Finally, the amino acid sequences of CaLITR2.3 (GenBank Accession Number MT209983) and CaLITR2.4 (GenBank Accession Number MT209984) are 86.15 % and 72.41 % identical to CaLITR2, respectively, and they likely represent secretory and/or intracellular receptor-types since they have no identifiable TMs (Fig. 4.3C).

The *calitr3* transcript (GenBank Accession Number MT209985) was cloned from goldfish PKM cDNA (Fig. 4.1), and it lacks the D1 domain compared to its genomic prediction (XM_026218715.1, NCBI genome data viewer) (Fig. 4.5A). Both the NCBI data viewer and goldfish genome blast outputs indicate that *calitr3* is located on goldfish Chr 3. Like *calitr1 and calitr2*, *calitr3* has a split signal peptide with a S2 spanning 36 bp. Additionally, CaLITR3 has four extracellular Ig-like domains, a charged TM with a positively charged histidine residue, and a short CYT devoid of any tyrosine-based signaling motifs. Therefore, CaLITR3 is likely an activating receptor-type that may associate with ITAM-containing intracellular adaptor molecules. Interestingly, *calitr3* is also expressed as two additional variants (Fig. 4.5B), and these sequence variants were cloned from the same RT-PCR band as *calitr3* in the same three

goldfish individuals mentioned above (Fig. 4.1). As shown in Fig. 4.5C, CaLITR3.1 (GenBank Accession Number MT209986) contains four Ig-like domains; however, it has a different D1 domain. In comparison, CaLITR3.2 (GenBank Accession Number MT209987) is very similar to CaLITR3 except that it has an additional D1 domain identical to the one found in CaLITR3.1.

4.2.2 Phylogenetic analysis of CaLITRs and their relationships to mammalian immunoregulatory receptor-types

Phylogenetic trees were constructed to examine the evolutionary relationships between the Ig-like domains of CaLITRs and the Ig domains of mammalian FcRs, FCRLs, LILRs, and CHIRs. As shown in Fig. 4.6A, the D1 and D2 domains of CaLITR1 and CaLITR2 cluster with the D1 and D2 domains of mammalian FcRs and FCRLs. Alternatively, the membrane-proximal domains of CaLITR2 (D3 and D4) cluster with the mammalian LILRs and chicken CHIRs (Fig. 4.6B). Furthermore, when the extracellular regions of CaLITR1, CaLITR2, and CaLITR3 were used in PSI-blast analysis, various mammalian FCRLs and LRC members such as B-cell receptor CD22 and LILRs were retrieved as the top related matches (Table 4.1).

4.2.3 Transcript expression analysis of *calitr1*, *calitr2*, and *calitr3* in goldfish tissues, PKNs, and during PKM development

Although the “capture” primers were useful for “netting” *calitr* variants, they were inefficient at amplifying specific *calitr* transcripts and usually produced smears. To address this issue, specific primers were designed to amplify *calitr1*, *calitr2*, and *calitr3*, and RT-PCR was performed to preliminarily examine the expression patterns of *calitr1*, *calitr2*, and *calitr3* in goldfish tissues and immune cells (Table 2). As shown by the representative PCR gel, *calitr2* and *calitr3* are both expressed in the goldfish liver, spleen, kidney, heart, brain, gills, intestine, and

muscles, whereas *calitr1* was surprisingly not expressed in any of the tissues examined (Fig. 4.7A). Additionally, the *calitr3* gene-specific primers amplified two products, the top band corresponds to the predicted size of *calitr3* (i.e., 846 bp; GenBank Accession Number MT209991), whereas the bottom band at 597 bp (GenBank Accession Number MT209992) corresponds to another *calitr3* variant (partial sequence) that lacks the D4 domain found in *calitr3*. To determine whether *calitrs* are also expressed by goldfish myeloid cells, I examined the expression of these transcripts in goldfish primary neutrophils and during PKM development. As shown in Fig. 4.7B, the *calitr1*, *calitr2*, and *calitr3* transcripts were all detected in freshly isolated kidney leukocytes and over the course of PKM development. Additionally, all three *calitrs* are expressed by goldfish primary kidney neutrophils (Fig. 4.7C).

4.2.4 Mining of *calitr4* and *calitr5*

calitr4 (GenBank Accession Number MT209988) and *calitr5* (GenBank Accession Number MT209990) were recently identified using the *calitr2* and *calitr3* cDNA sequences as templates to search the goldfish reference RNA database. The *calitr4.0* transcript was cloned from goldfish kidney and intestine cDNA sequences (Fig. 4.8), and its protein product contains five Ig-like domains, a TM, and a CYT region with a putative endocytic signal (YxxL) (Li et al., 2000), an Nck recruitment motif (YDxV) (Blasutig et al., 2008; Jones et al., 2006), an ITIM motif (VxYxxI), an ITSM motif (TxYxxL) and an ITIM motif (VxYxxV) (Fig. 4.9B). Like *calitr1*, *calitr2*, and *calitr3*, *calitr4* appears to have a split signal peptide with a 36-bp-long S2. Relative to the predicted *calitr4* sequence, the amplified *calitr4* transcript lacks the D2 domain, due to a possible splicing event (Fig. 4.9A). Similar to the other three *calitrs*, a variant of *calitr4* was identified from goldfish intestine cDNA (Fig. 4.8) and named *calitr4.1* (GenBank Accession Number MT209989), which has identical D1, D2, D4, D5 Ig-like domains and CYT region when

compared with CaLITR4; however, it lacks the D3 domain (Fig. 4.9C). The *calitr5* transcript was cloned from the goldfish kidney (Fig. 4.8), and it differs from its prediction in the arrangements of its extracellular Ig-like domains and CYT region sequence (Fig. 4.10A). Like the previously identified *calitr* transcripts, the signal peptide of *calitr5* appears to be encoded by two separate exons with a 36-bp-long S2. CaLITR5 contains six Ig-like domains, a TM, and a complex CYT region with putative Nck (YDxV) and a STAT (YxxT) recruitment motif (Oates et al., 1999), as well as an ITIM motif (VxYxxI), an ITSM motif (TxYxxL), and ITIM (VxYxxV) (Fig. 4.10B). Based on the goldfish NCBI genome blast outputs, *calitr4* is located on Chr LG28B, whereas *calitr5* is located on an unplaced genomic scaffold.

4.2.5 CaLITRs encode for unique distal immunoglobulin-like domains

To determine the relative relatedness between the Ig-like domains of CaLITRs with prototypic IpLITR Ig-like domains, NJ trees were built with MEGA7. As shown in Fig. 4.11, CaLITR3, 4, and 5 share phylogenetically related Ig-like domain combinations (coded as gold, green, red, and blue Ig-like domains) with those of CaLITR2. However, CaLITR4 and CaLITR5 contain phylogenetically unique distal Ig-like domains (pink). Interestingly, the D1 of CaLITR1 is distinct among all the CaLITR currently identified, whereas the D2 (coded as light gold) of CaLITR1 is distantly related to the D1 of CaLITR2 and CaLITR3, D2 of CaLITR4, and D3 of CaLITR5 (Fig. 4.11).

I also examined the Ig-like domains of a prototypic IpLITR-type (i.e., IpLITR3) with the Ig-like domains of CaLITRs. As shown in Fig. 4.12, the TM proximal and distal Ig-like domains (blue, light purple, dark purple, and light orange domains) of CaLITR2, 3, 4, and 5 are related to the proximal domains (D4, D5, and D6) of IpLITR3. However, the distal domains of IpLITR3 (red, orange, and green domains) are not found in any of the CaLITRs identified,

reflecting their unique Ig domain composition. Furthermore, the D1 (yellow domain) of CaLITR1 and the distal domains (grey domains) of CaLITR4 and CaLITR5 do not group with any of the other Ig-like domains examined (Fig. 4.12).

4.2.6 DISCUSSION

In response to pathogen invasion, immunoregulatory receptors modulate the balance between immune activation and suppression to ensure clearance of infection and promote tissue healing. LITRs represent a large polymorphic and polygenic family of teleost immunoregulatory receptor-types that were originally discovered in the channel catfish. Although a few IpLITRs have been functionally characterized using heterologous overexpression systems, their roles in fish immunity remain largely unknown. Goldfish, along with its well-characterized primary kidney myeloid cell culture system (Katzenback et al., 2016), represents an ideal *ex vivo* model system for further investigating the immunoregulatory functions of teleost LITRs. This chapter describes the initial identification and molecular characterization of several CaLITR-types and their variants.

A *calitr*-like sequence fragment was initially identified from the goldfish transcriptome by Basic Local Alignment Search Tool (BLAST) searches using the prototypic *iplitr* sequences (*iplitr1*, *iplitr2*, and *iplitr3*) as templates. Subsequently, the *calitr*-like fragment was used to search the goldfish RNA reference database to identify putative *calitrs* with complete ORFs, and then RT-PCR was performed to verify the expression of these putative sequences in goldfish tissues and primary myeloid cell cultures. A total of 12 CaLITRs with diverse extracellular and intracellular domain architectures have now been identified. CaLITR1 represents an ambiguous receptor-type having a short CYT and a neutrally charged TM. CaLITR2 has an ITIM and ITSM within its CYT; thus, resembling a putative inhibitory receptor-

type. CaLITR3 is an activating receptor-type containing a positively charged histidine residue. Both CaLITR4 and CaLITR5 represent receptor-types with variable signaling capabilities as they contain several protein motifs in their CYT regions. For example, the CYT region of CaLITR4 has a putative endocytic motif, an Nck recruitment motif, two ITIMs, and an ITSM. Similarly, CaLITR5 has all the putative protein motifs possessed by CaLITR4 (except for the endocytic motif) with the addition of a predicted STAT recruitment motif (YxxT). Similar to CaLITR4 and CaLITR5, the distal portion of IpLITR1.1b also contains an Nck recruitment motif (YDTV); moreover, GST pulldown assays (Zwozdesky et al., 2017) and microscopic imaging experiments (Lillico et al., 2020) have shown that this tyrosine motif was capable of recruiting Nck, and that Nck was colocalized with the receptor during IpLITR1.1b-mediated regulation of the phagocytic process. Additionally, the phosphorylated YDxV motif of a nephrin adhesion protein was shown to recruit Nck to induce localized actin polymerization (Blasutig et al., 2008). Therefore, I hypothesize that the YDSV sequence within the CYT regions of CaLITR4 and CaLITR5 likely recruit Nck adaptor molecules to regulate actin polymerization and membrane remodeling events required for effector responses such as phagocytosis. Even though CaLITRs have protein motifs that closely match the consensus sequences of several protein motifs validated by other researchers, biochemical assays (i.e., co-immunoprecipitation) must be conducted to further validate the functional potential of each of the tyrosine modules contained with the newly identified CaLITR-types.

Genes of the mammalian FcR family and LRC are known to have similar exon-intron organizations, with some unique features distinguishing these different gene families (Davis, 2007). The classical *fcrs* and their distant relatives, *fcrls*, have a split signal peptide where the second exon of the signal peptide is consistently 21 bp long (Davis, 2007; Davis et al., 2001;

Pang et al., 1993; Qiu et al., 1990). Furthermore, this feature is also observed in several xenopus FCRL-like molecules (XFLs) (Guselnikov et al., 2008). In contrast, LRC-encoded genes also have a split signal peptide, but the second half of the signal peptide is 36-39 bp (Davis, 2007). Consistent with the exon organizations of vertebrate LRC-encoded genes, my preliminary analysis of the exon-intron-organizations of *calitr1-5* show that they also appear to have a split signal peptide, with the second exon being 36 bp in length. This supports their close evolutionary relationship to members of the LRC. However, it's important to note that although the 36-bp-long S2 is a common feature found in chicken *chirs*, mouse *Pirs*, and human *KIRs* and *LILRs* (Davis, 2007), it is not known whether this is a universal feature of the LRC in other vertebrates such as amphibians and teleost fish. Moreover, vertebrate FcR and LRC-encoded receptors have been hypothesized to be products of genome duplications during early vertebrate evolution (Sundstrom et al., 2008; Zucchetti et al., 2009). This hypothesis is supported by several lines of evidence (Akula et al., 2014): 1) several signaling molecules, including DAP10, DAP12, FcεRIγ, and TCRζ chains, are located in both the FcR family and LRC gene loci; 2) the Ig-like domains of both the FcR family and LRC members are C2-type and are phylogenetically related (N. Nikolaidis et al., 2005). Therefore, I hypothesize that the 36-bp-long S2 observed in the teleost *calitrs* may reflect an ancestral feature that predates the divergence of the vertebrate FcR family and LRC genes. Additionally, it is yet to be determined if the 36-bp-long S2 of the *calitrs* is unique to goldfish or a general characteristic of all *litrs*.

Like IpLITRs, the *calitr1-5* cDNA sequences are predicted to be type 1 transmembrane receptors containing variable numbers of extracellular C2 type Ig-like ectodomains. Additionally, CaLITRs share key phylogenetic characteristics with IpLITRs having proximal and distal Ig-like domains that are distantly related to the mammalian FCR and LRC family genes,

respectively. When the individual Ig-like domains of CaLITRs were compared to the individual Ig-like domains of IpLITR3, it became clear that the CaLITRs encode distinct distal Ig-like domains from their IpLITR counterparts. Furthermore, five different types of distal domain arrangements of CaLITRs were observed, suggesting that the newly identified CaLITRs may interact with ligands that are different from those bound by IpLITRs or that they use different mechanisms and/or have variable affinities for extracellular targets, however this hypothesis requires further exploration.

In addition to the discovery of the five CaLITR sequences (CaLITR1-5), variant forms of these receptors were also identified. These CaLITR variants contain highly similar amino acid sequences in relation to the five CaLITR sequences and mostly differ in terms of the presence or absence of entire Ig-like domains, TM regions, or CYT segments. For instance, the translated CaLITR3.1 and CaLITR3.2 sequences resemble exon-skipped isoforms of CaLITR3 having a variant D1 domain and an addition of the same variant D1 domain relative to CaLITR3, respectively. Similarly, CaLITR4.1 lacks the D3 domain of CaLITR4, likely representing another exon-skipped protein isoform. The ability of transmembrane receptors to selectively include or exclude exons encoding extracellular domains is a commonly observed phenomenon in the immune system (Martinez & Lynch, 2013; Sahoo & Im, 2010) that has been implicated to play a role in fine-tuning immune responses (Lynch, 2004). A well-studied example of an immune receptor that alternatively splices extracellular domains to regulate immune functions is CD45, which is an important player in T-cell immunity (Zikherman & Weiss, 2008). Specifically, mammalian CD45 produces long isoforms in resting T-cells and short isoforms (by excluding exons encoding a few extracellular domains) in activated T-cells; the shorter isoforms have been shown to dampen T-cell signaling to prevent T-cell hyperactivation (Trowbridge &

Thomas, 1994; Xu & Weiss, 2002). Similarly, alternatively spliced forms of CD45 have also been identified in the channel catfish (Kountikov et al., 2010; Kountikov et al., 2005), although their functions are not well understood. Additionally, alternative splicing of receptor extracellular regions has been observed in numerous IgSF members such as FCRLs (Hatzivassiliou et al., 2001; Kulemzin et al., 2011), KIRs (Bruijnesteijn et al., 2018), Down syndrome cell adhesion molecule (Dscam) (Kurtz & Armitage, 2006; Watson et al., 2005), receptor for advanced glycation end products (RAGE) (Kalea et al., 2011), and Carcinoembryonic antigen-related cell adhesion molecule 1 (CAECAM1) (Missbach et al., 2018). Among these examples, Dscam is well-known for its remarkable ability to generate large repertoires of alternatively spliced protein variants (more than 30,000 isoforms in theory). Furthermore, extracellular variants of Dscam have been shown to have different binding affinities for pathogen molecules (Dong et al., 2006; Li et al., 2019). Based on these findings, I hypothesize that the extracellular variants of CaLITRs likely differ in their binding affinities and may have varying immunomodulatory functions. I also identified putative secretory or intracellular CaLITR-types (CaLITR2.3 and CaLITR2.4) lacking both TMs and CYT regions. Similar to other soluble IgSF (i.e., LILR) (Jones et al., 2009) and cytokine receptors (i.e., IL-1RII) (Mantovani et al., 2001), expression of the soluble forms of CaLITRs may exist to serve as a negative feedback mechanism to control immune responses. Interestingly, a soluble human FCRL receptor (FCRLA) lacking a TM domain was shown to associate with intracellular IgA, IgG, and IgM, and has been suggested to assist the assembly of these intracellular antibodies (Santiago et al., 2011; Wilson et al., 2010). Since the distal Ig-like domains of FCRs are distantly related to mammalian FCRLs, the soluble CaLITR-types may also be expressed as intracellular receptors that interact with intracellular proteins such as Abs. Compared to the CaLITR variants

with variable extracellular domains, only one putative CaLITR intracellular splice variant was observed. Specifically, CaLITR2.1 represents a cytoplasmic spliced variant of CaLITR2 lacking 29 amino acid residues containing a tyrosine motif (YAEI). It is worth noting that CYT region variants of LITRs resembling spliced forms may also exist in the channel catfish (Stafford et al., 2007). Specifically, the CYT regions of the translated TS32.15 L1.2a1-3 sequences are highly identical to the CYT region of IpLITR1, although their CYTs appear to have a deletion of two blocks of amino acids. Alternative splicing of cytoplasmic regions of IgSF receptors have also been observed in a few family members such as RAGE (Jules et al., 2013), Platelet endothelial cell adhesion molecule-1 (PECAM-1) (Yan et al., 1995), and CAECAM1 (Gaur et al., 2008); the cytoplasmic splicing of these receptors have been shown to impact cellular functions such as cell migration, cell adhesion, tumor formation, and apoptosis. Since CaLITR2.1 lacks one of the tyrosine motifs found in the CYT region of CaLITR2, this results in the loss of a tyrosine phosphorylation site, which may significantly alter the ability of this variant to interact with specific downstream signaling molecules.

In conclusion, this chapter describes the initial identification of goldfish LITR transcripts, and I provide evidence that alternative splicing may contribute to the diversification of the signaling potentials and/or ligand-binding capabilities of goldfish LITRs. The recently published goldfish genome (Chen et al., 2019) has allowed me to examine and compare the CaLITR transcripts with their predicted genomic sequences, which has revealed new information supporting the evolutionary links of CaLITRs to immunoregulatory receptors of the vertebrate FcR family and LRC. While phylogenetic analysis and investigations into the genetic organization of LITRs have provided intriguing clues about their evolutionary relatedness to various vertebrate immunoregulatory receptors, it remains unknown whether these genes also

share conserved synteny (conservation of the relative arrangement of genes on two Chrs across different species). In addition to phylogenetic analysis, several teleost studies have highlighted that syntenic analysis can be useful for inferring orthologous relationships among genes (Soderberg et al., 2000; Sundstrom et al., 2008). Therefore, the objective of my next chapter is to further investigate the evolutionary connections among LITRs and their sequence relatives, using both phylogenetic and syntenic analyses. Overall, the well-characterized primary macrophage and neutrophil cultures (Katzenback et al., 2016) of the goldfish model system offer us an exciting opportunity to examine the immunoregulatory functions of CaLITRs as well as their putative isoforms in goldfish myeloid cells. The goldfish model system, along with the recently developed techniques for examining the functional potential of IpLITRs, represents an important platform for further examining the immunoregulatory roles of teleost LITRs with the goal of determining how they ultimately participate in fish immune cell-mediated defense from microbes.

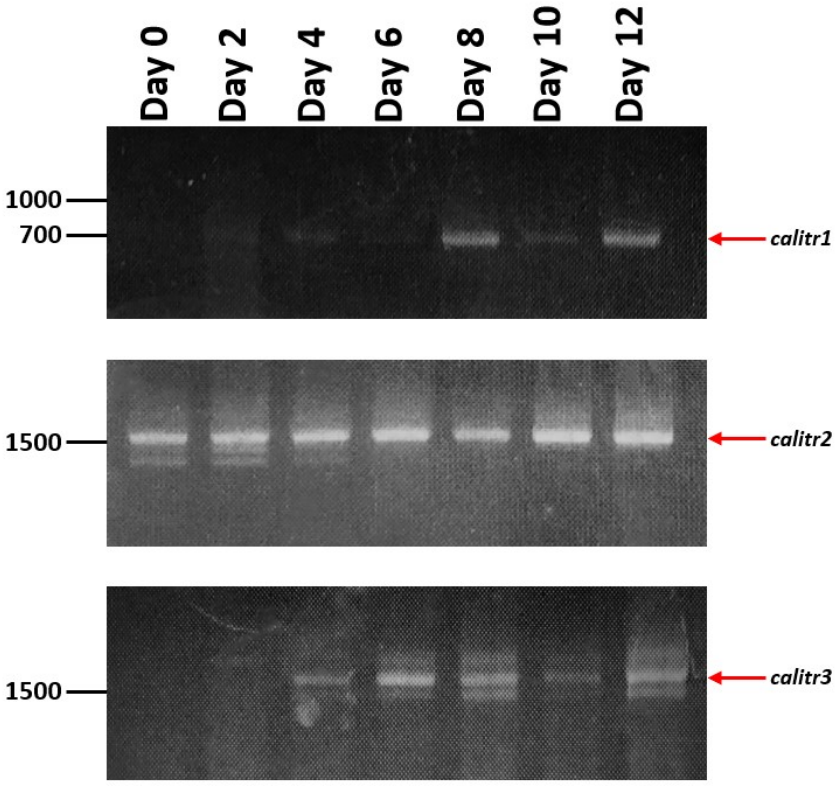

Figure 4.1. RT-PCR gels showing the expression of *calitrs* over the course of PKM development. The RT-PCR was performed using *calitr*1, 2, and 3 "capture" primers. Each "capture" primer was designed for amplifying all possible transcripts of each *calitr* gene. The bands cloned and sequenced are indicated by red arrows.

(A)

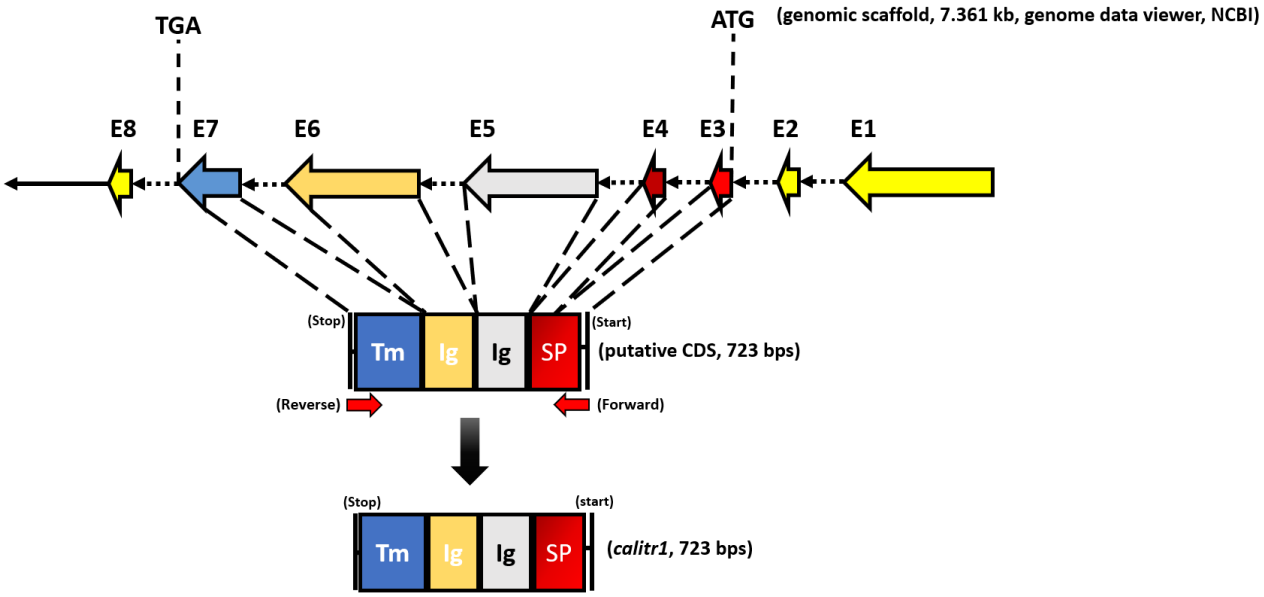
TGA
ATG
(genomic scaffold, 7.361 kb, genome data viewer, NCBI)
E8
E7
E6
E5
E4
E3
E2
E1
(Stop)
Tm
Ig
Ig
SP
(Start)
(putative CDS, 723 bps)
(Reverse)
(Forward)
(Stop)
(start)
Tm
Ig
Ig
SP
(calitr1, 723 bps)

(B)

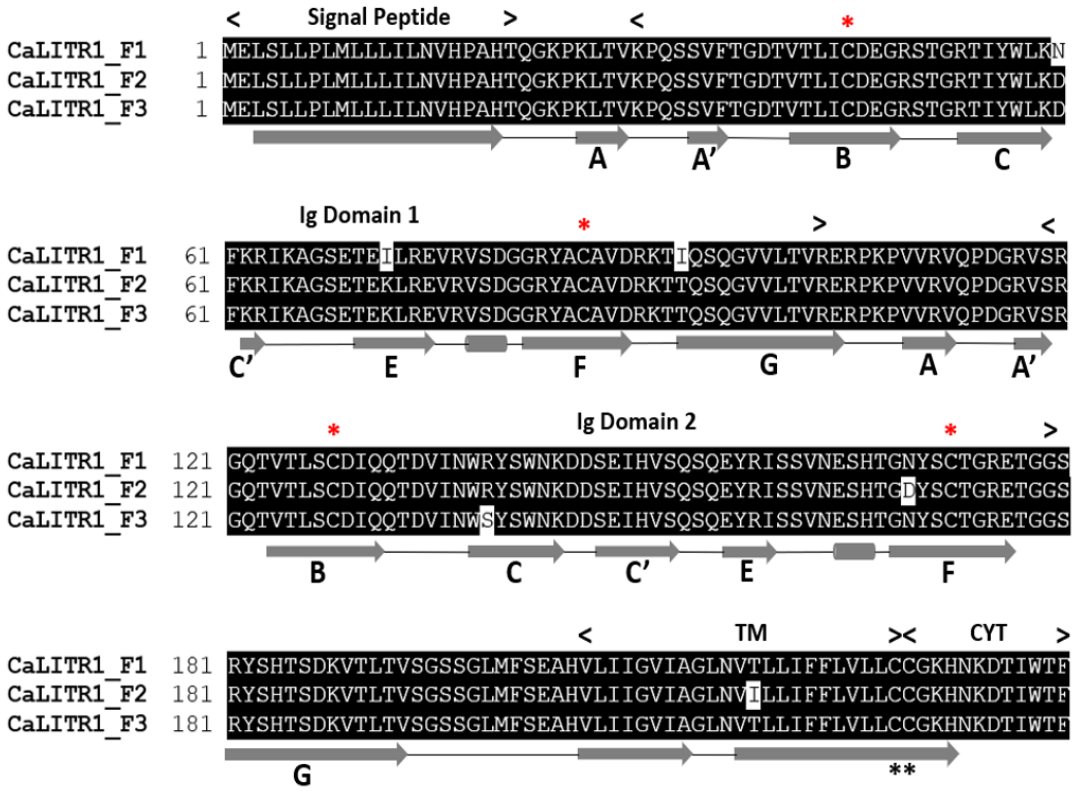
Signal Peptide
CaLITR1_F1 1 MELSLLPLMLLLILNVHPAHTQGKPKLTVKPQSSVFTGDTVTLICDEGRSTGRTIYWLKN
CaLITR1_F2 1 MELSLLPLMLLLILNVHPAHTQGKPKLTVKPQSSVFTGDTVTLICDEGRSTGRTIYWLKD
CaLITR1_F3 1 MELSLLPLMLLLILNVHPAHTQGKPKLTVKPQSSVFTGDTVTLICDEGRSTGRTIYWLKD
A
A'
B
C
Ig Domain 1
CaLITR1_F1 61 FKRIKAGSETEILREVRVSDGGRYACAVDRKTIQSQGVVLTVRERPKPVVRVQPDGRVSR
CaLITR1_F2 61 FKRIKAGSETEKLREVRVSDGGRYACAVDRKTTQSQGVVLTVRERPKPVVRVQPDGRVSR
CaLITR1_F3 61 FKRIKAGSETEKLREVRVSDGGRYACAVDRKTTQSQGVVLTVRERPKPVVRVQPDGRVSR
C'
E
F
G
A
A'
Ig Domain 2
CaLITR1_F1 121 GQTVTLSCDIQQTDVINWRYSWNKDDSEIHVSQSQEYRISSVNESHTGNYSCTGRETGGS
CaLITR1_F2 121 GQTVTLSCDIQQTDVINWRYSWNKDDSEIHVSQSQEYRISSVNESHTGDYSCTGRETGGS
CaLITR1_F3 121 GQTVTLSCDIQQTDVINWSYSWNKDDSEIHVSQSQEYRISSVNESHTGNYSCTGRETGGS
B
C
C'
E
F
TM
CYT
CaLITR1_F1 181 RYSHTSDKVTLTVSGSSGLMFSEAHVLIIGVIAGLNVTLLIFFLVLLCCGKHNKDTIWTF
CaLITR1_F2 181 RYSHTSDKVTLTVSGSSGLMFSEAHVLIIGVIAGLNVILLIFFLVLLCCGKHNKDTIWTF
CaLITR1_F3 181 RYSHTSDKVTLTVSGSSGLMFSEAHVLIIGVIAGLNVTLLIFFLVLLCCGKHNKDTIWTF
G
**

Figure 4.2. Genomic organization and identified variants of CaLITR1. (A) Schematic comparison of putative *calitr1* (predicted by Gnomon, NCBI eukaryotic gene prediction tool) and its RT-PCR amplified product. The signal peptide, Ig-like domains, TMs, and CYT regions were predicted using SMART (Letunic et al., 2004). The Ig-like domains of the CaLITR1 genomic sequence and cDNA transcript are coloured according to their phylogenetic relatedness. Locations of the "capture" primers are indicated by mini red arrows. Exons of *calitr1* are designated by arrows on the top of the diagram, whereas the intervening introns are represented by dashed arrows. Yellow portions of the genomic scaffold indicate the untranslated regions. Base pair (bp) sizes of the *calitr1* genomic scaffold, putative gene, and cDNA are shown. **(B)** Amino acid alignment of CaLITR1 from goldfish 1 (F1; GenBank Accession Number MT209979), goldfish 2 (F2; GenBank Accession Number MT209993), and goldfish 3 (F3; GenBank Accession Number MT209994).The predicted signal peptide, Ig-like domains, TM, and CYT region are labeled. Conserved amino acids are highlighted in black. The cysteine residues predicted to form the intrachain disulfide bonds are marked with red asterisks. Black asterisks represent conserved cysteine residues. Predicted beta sheets and helixes are designated by grey arrows and cylinders, respectively. Sequence alignment was performed using Clustal Omega and presented with Boxshade 3.21.

(A)

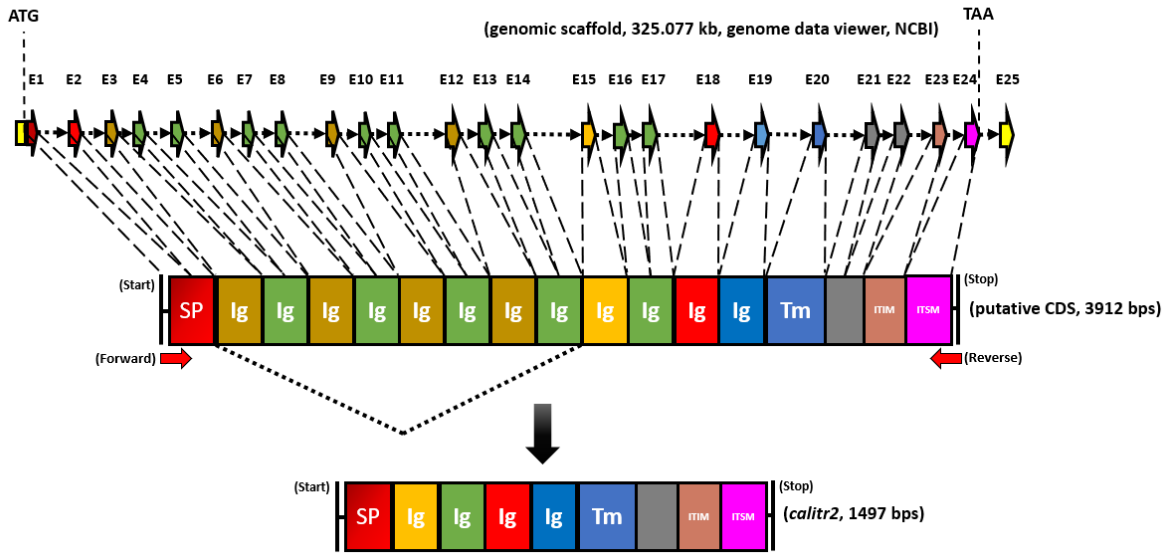
ATG
TAA
(genomic scaffold, 325.077 kb, genome data viewer, NCBI)
E1 E2 E3 E4 E5 E6 E7 E8 E9 E10 E11 E12 E13 E14 E15 E16 E17 E18 E19 E20 E21 E22 E23 E24 E25
(Start)
SP
Ig
Tm
ITIM
ITSM
(Stop)
(putative CDS, 3912 bps)
(Forward)
(Reverse)
(calitr2, 1497 bps)

(B)

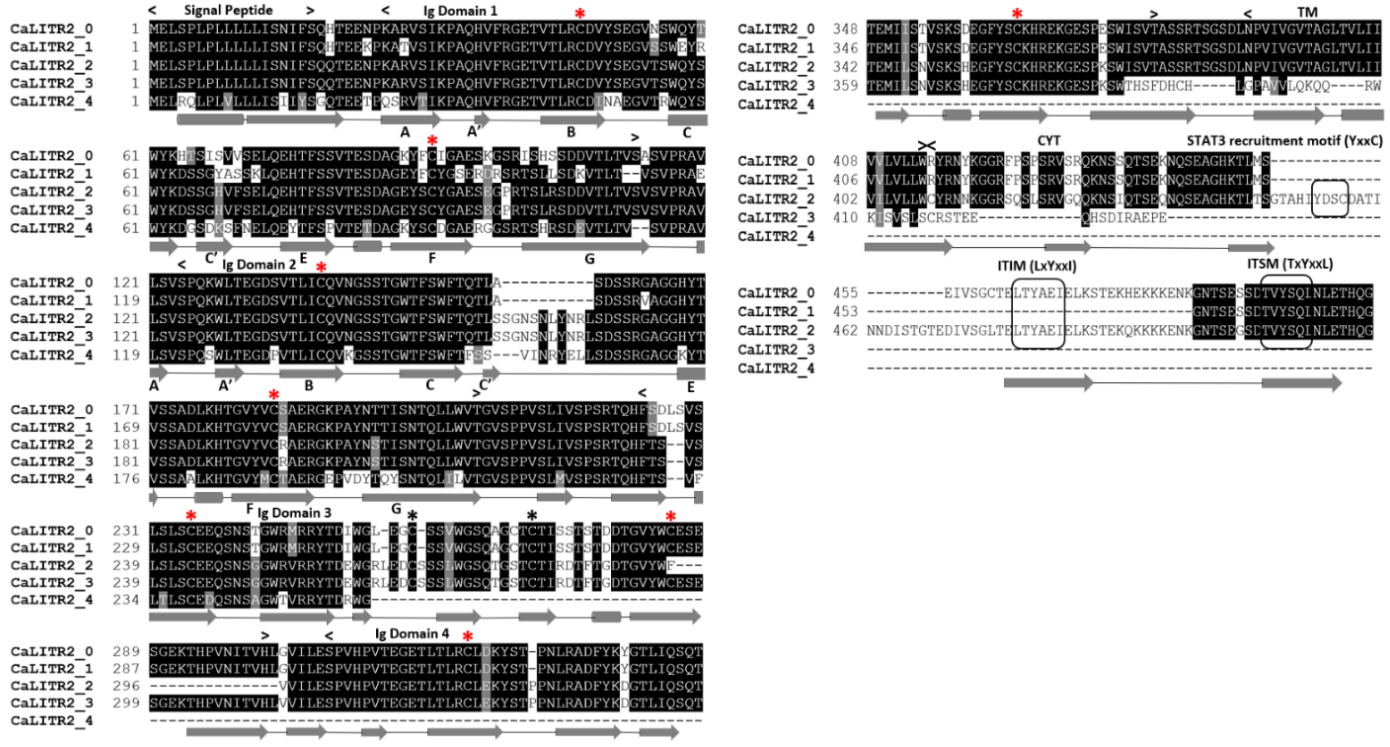
Signal Peptide
Ig Domain 1
Ig Domain 2
Ig Domain 3
Ig Domain 4
TM
CYT
STAT3 recruitment motif (YxxC)
ITIM (LxYxxI)
ITSM (TxYxxL)
CaLITR2_0
CaLITR2_1
CaLITR2_2
CaLITR2_3
CaLITR2_4

(C)

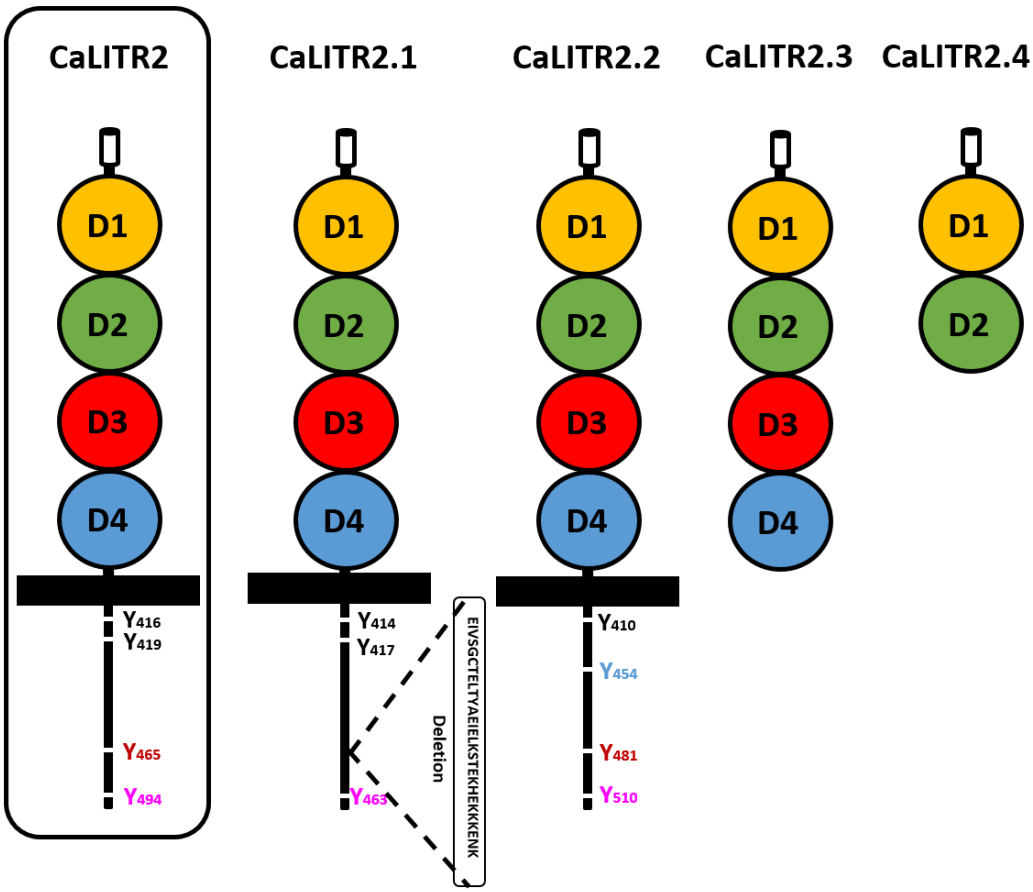

Figure 4.3. Genomic organization and identified variants of CaLITR2/2.0. (A) Schematic comparison of putative *calitr2* (predicted by Gnomon, NCBI eukaryotic gene prediction tool) and its RT-PCR amplified product. The signal peptide, Ig-like domains, TMs, and CYT regions were predicted using SMART. The Ig-like domains of the *calitr1* genomic sequence and cDNA transcript are coloured according to their phylogenetic relatedness. The dashed triangular lines represent the absence of Ig-like domains in the predicted *calitr2* genomic sequence relative to its cDNA product, indicating a potential splicing event. Locations of the "capture" primers are indicated by mini red arrows. Exons of *calitr2* are designated by arrows on the top of the diagram, whereas the intervening introns are represented by dashed arrows. Yellow portions of the genomic scaffold indicate the untranslated regions. Base pair (bp) sizes of the *calitr2* genomic scaffold, putative gene, and cDNA product are shown. **(B)** Amino acid alignment comparing CaLITR2 variants. The predicted signal peptide, Ig-like domains, TM, and CYT region are labeled. CYT containing putative ITIM, ITSM, and STAT3 recruitment motifs are boxed. Conserved amino acids are highlighted in black and similar residues in gray. Gaps in the alignment are indicated by dashes. Cysteine residues that are predicted to form the intrachain disulfide bonds are marked with red asterisks. Black asterisks represent conserved cysteine residues. Predicted beta sheets and helixes are designated by grey arrows and cylinders, respectively. The Sequence alignment was performed using Clustal Omega and presented with Boxshade 3.21. **(C)** Schematic representation of CaLITR2 variants. CaLITR2.1 represents a

putative isoform of CaLITR2, and the deleted portion relative to CaLITR2 is highlighted in a box. Both CaLITR2.3 and 2.4 lack TM regions, and thus represent secreted and/or intracellular forms. The signal peptide, Ig-like domains, TM region, and CYT regions were predicted using SMART. CaLITR2, the originally identified sequence, is boxed. Individual CaLITR domains are coloured according to their phylogenetic relatedness with the CaLITR2 variants (Fig. 4.13). Tyrosine residues in the CYT of each sequence are shown and are numbered based on the length from the start codon to each tyrosine residue. The blue, red, and purple tyrosine residues represent putative STAT3 recruitment, ITIM, and ITSM motifs, respectively.

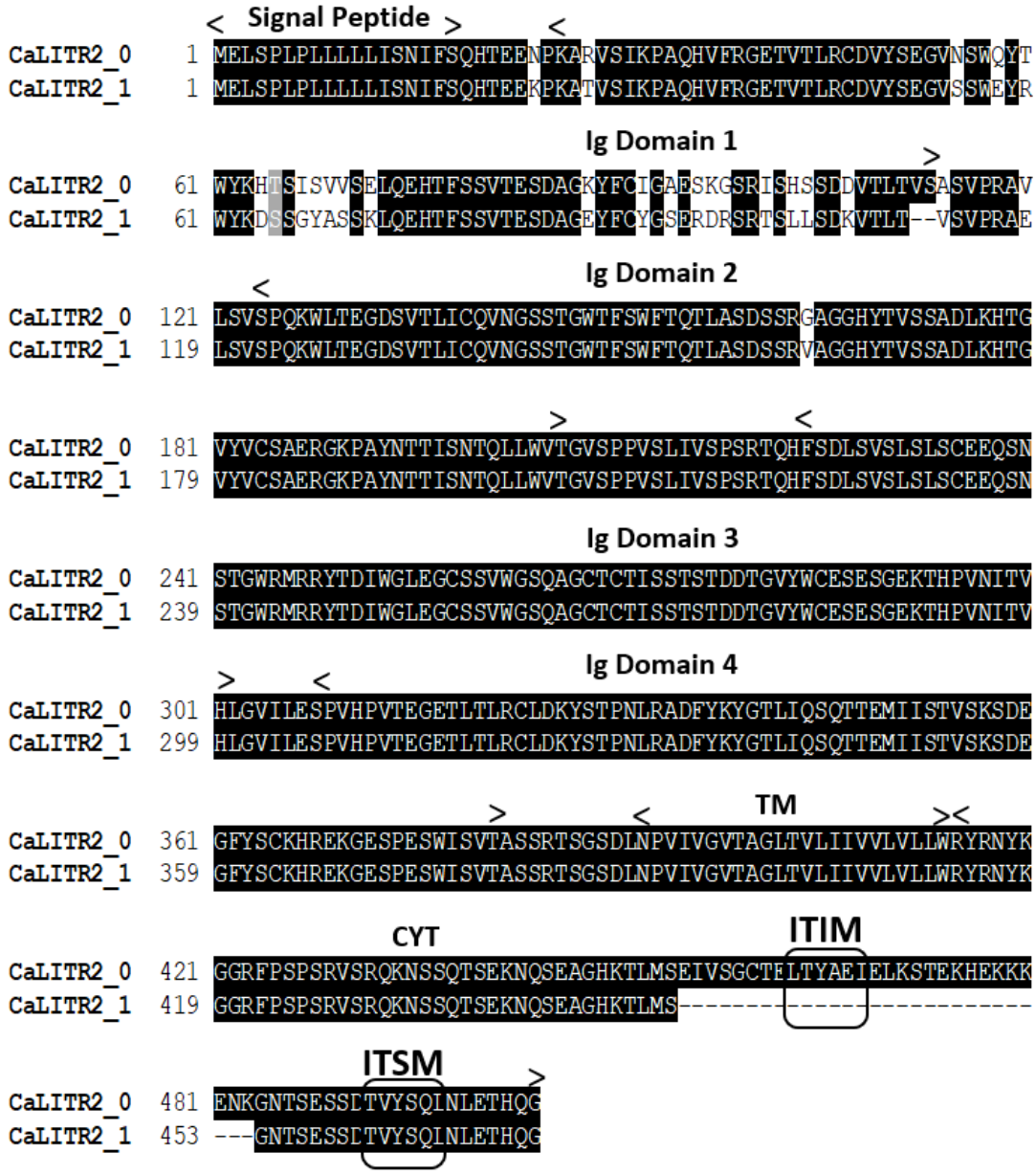

Figure 4.4. Alignment of the predicted amino acid sequences of CaLITR2 and CaLITR2.1. The predicted signal peptide, Ig domains, TM, and CYT are labeled. The putative ITIM and ITSM motifs of CaLITR2.0 are boxed. Conserved amino acids are highlighted in black and similar residues in gray. Gaps in the alignment are indicated by dashes. The Sequence alignment was performed using Clustal Omega and presented with Boxshade 3.21.

(A)

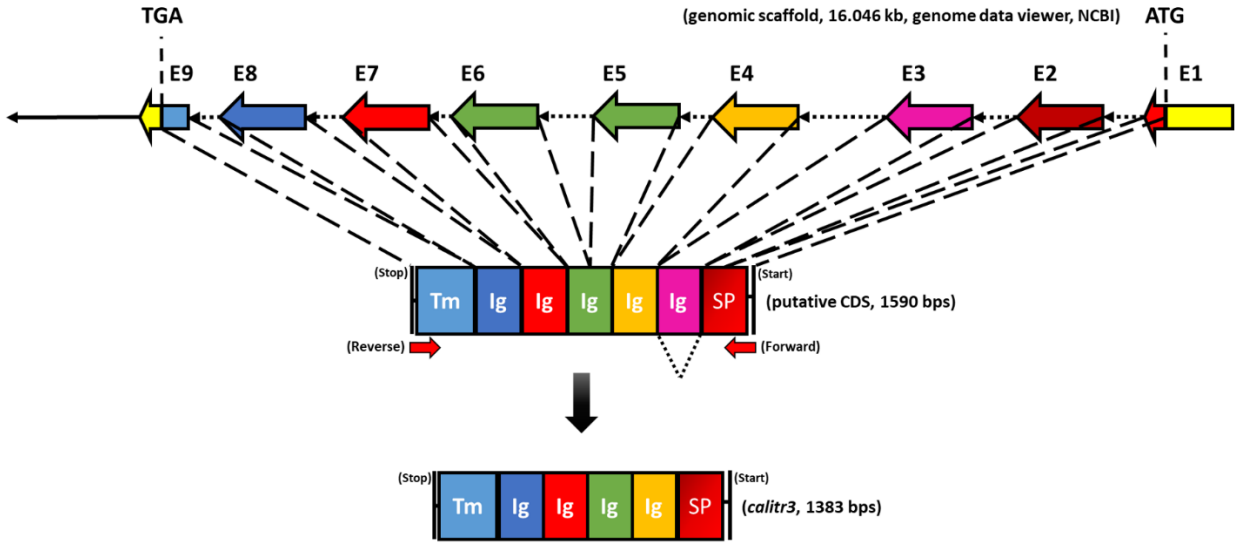
TGA
(genomic scaffold, 16.046 kb, genome data viewer, NCBI)
ATG
E9
E8
E7
E6
E5
E4
E3
E2
E1
(Stop)
Tm
Ig
Ig
Ig
Ig
Ig
SP
(Start)
(putative CDS, 1590 bps)
(Reverse)
(Forward)
(Stop)
Tm
Ig
Ig
Ig
Ig
SP
(Start)
(calitr3, 1383 bps)

(B)

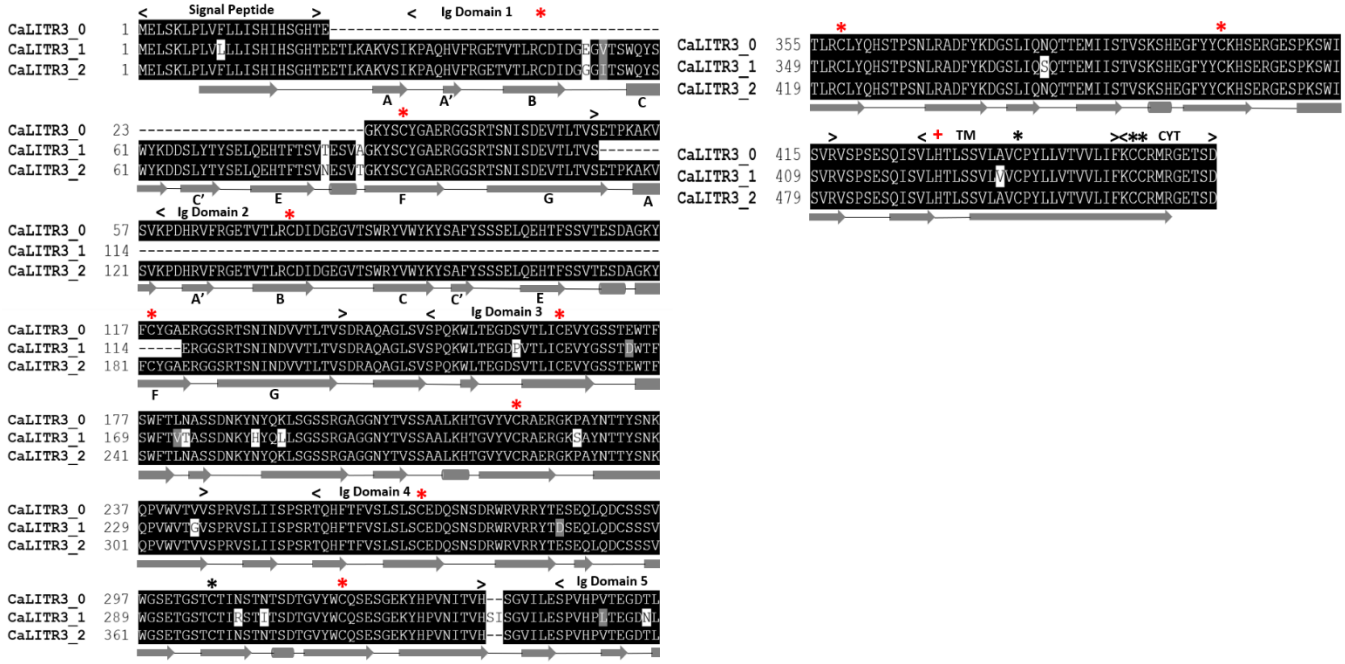
Signal Peptide
Ig Domain 1
Ig Domain 2
Ig Domain 3
Ig Domain 4
Ig Domain 5
TM
CYT
CaLITR3_0
CaLITR3_1
CaLITR3_2

(C)

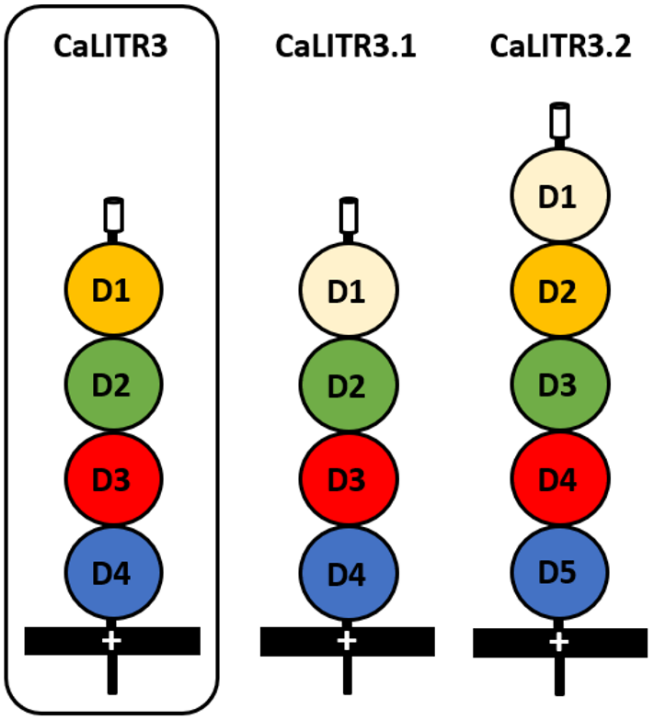

Figure 4.5. Genomic organization and identified variants of CaLITR3/3.0. (A) Schematic comparison of putative *calitr3* (predicted by Gnomon, NCBI eukaryotic gene prediction tool) and its RT-PCR amplified product. The signal peptide, Ig-like domains, TMs, and CYT regions were predicted using SMART. The Ig-like domains of the *calitr3* genomic sequence and cDNA transcript are coloured according to their phylogenetic relatedness. The dashed triangular lines represent the absence of Ig-like domain in the predicted *calitr3* genomic sequence relative to its cDNA product, indicating a potential splicing event. Locations of the "capture" primers are indicated by mini red arrows. Exons of *calitr3* are designated by arrows on the top of the diagram, whereas the intervening introns are represented by dashed arrows. Yellow portions of the genomic scaffold indicate the untranslated regions. Base pair (bp) sizes of the *calitr3* genomic scaffold, putative gene, and cDNA product are shown. **(B)** Amino acid alignment comparing CaLITR3 variants. The predicted signal peptide, Ig-like domains, TM, and CYT region are labeled. The positively charged histidine residue in the CYT of each receptor is marked with a red plus sign. Conserved amino acids are highlighted in black and similar residues in gray. Gaps in alignment are indicated by dashes. Cysteine residues that are predicted to form the intrachain disulfide bonds are marked with red asterisks. Black asterisks represent conserved cysteine residues. Predicted beta sheets and helixes are designated by grey arrows and cylinders, respectively. The Sequence alignment was performed using Clustal Omega and presented with Boxshade 3.21. **(C)** Schematic representations of CaLITR3 variants. The signal peptide, Ig-like domains, TM, and CYT regions were predicted using SMART. The positively charged histidine residue in the CYT of each receptor is marked as a white plus sign. CaLITR3, the originally identified sequence, is boxed. Individual CaLITR Ig-like domains are coloured according to their phylogenetic relatedness with the CaLITR3 variants (Fig. 4.14).

(A)

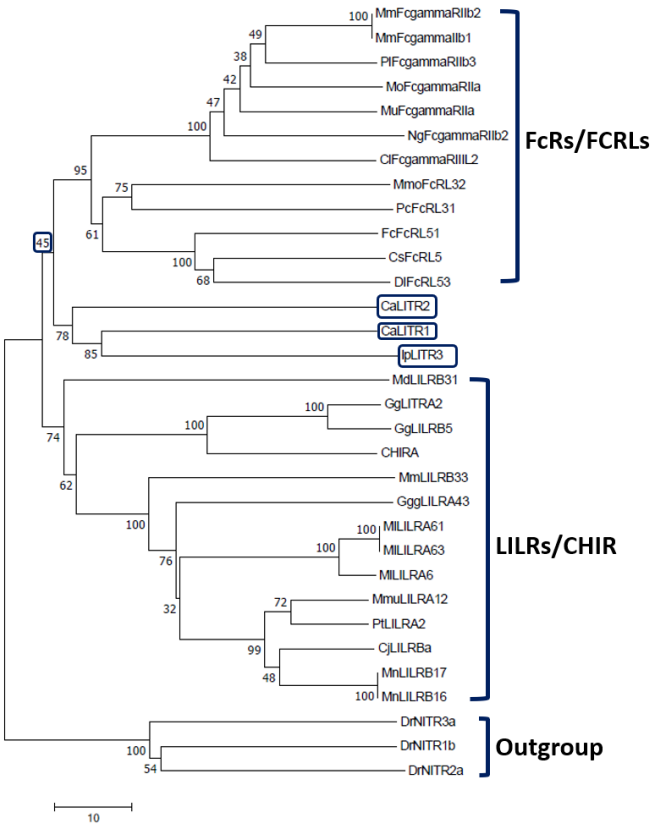
MmFcgammaRIIb2
MmFcgammaIIb1
PlFcgammaRIIb3
MoFcgammaRIIa
MuFcgammaRIIa
NgFcgammaRIIb2
ClFcgammaRIIIL2
MmoFcRL32
PcFcRL31
FcFcRL51
CsFcRL5
DlFcRL53
CaLITR2
CaLITR1
IpLITR3
MdLILRB31
GgLITRA2
GgLILRB5
CHIRA
MmLILRB33
GggLILRA43
MILILRA61
MILILRA63
MILILRA6
MmuLILRA12
PtLILRA2
CjLILRBa
MnLILRB17
MnLILRB16
DrNITR3a
DrNITR1b
DrNITR2a
FcRs/FCRLs
LILRs/CHIR
Outgroup
10

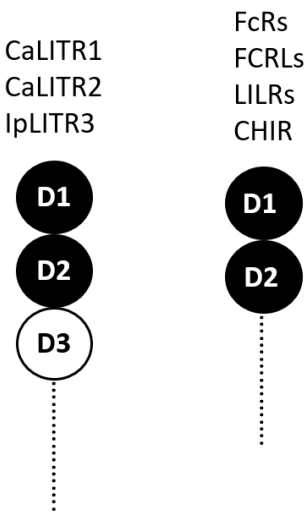
CaLITR1
CaLITR2
IpLITR3
D1
D2
D3
FcRs
FCRLs
LILRs
CHIR
D1
D2

(B)

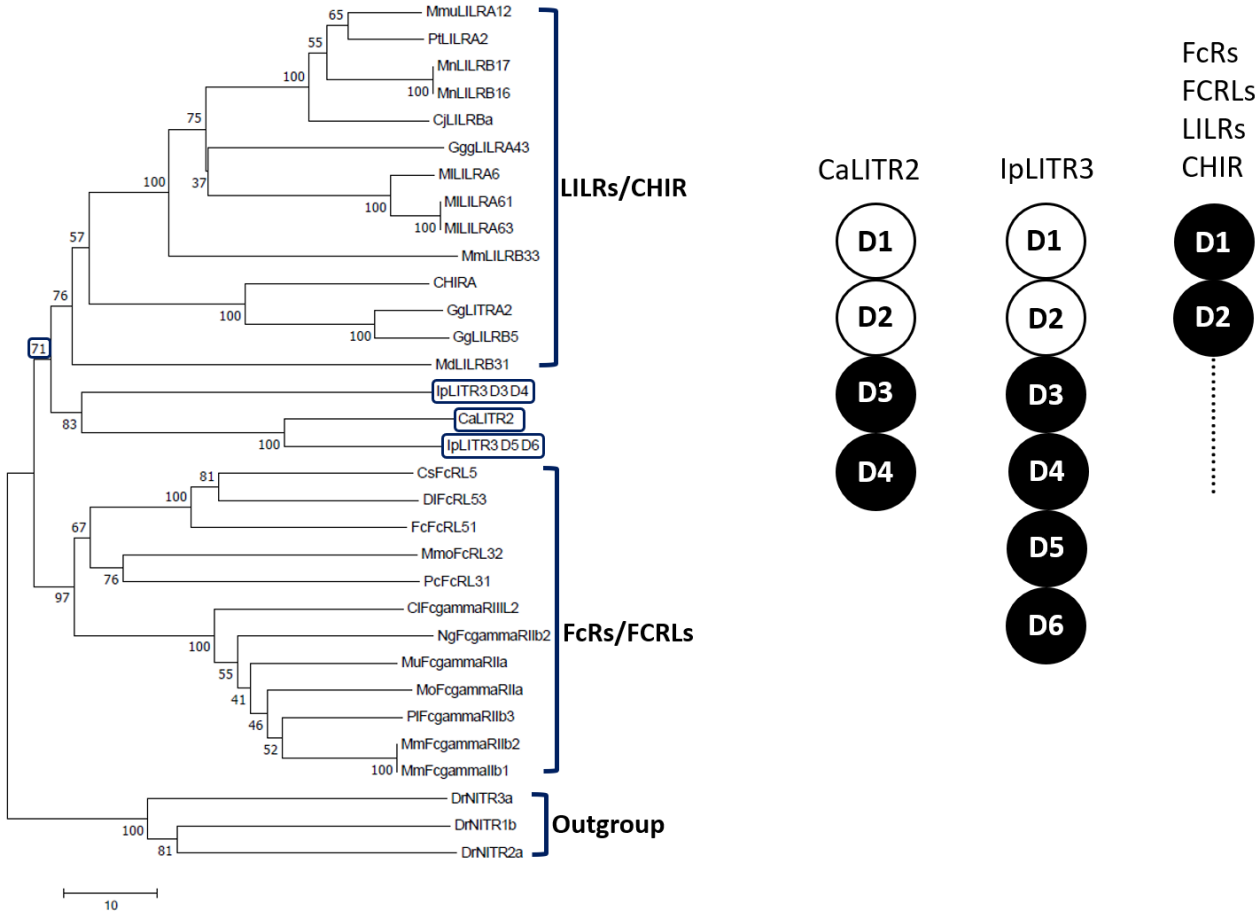

Figure 4.6. Phylogenetic relationships of the extracellular transmembrane proximal and distal Ig-like domains of CaLITRs in comparison with the proximal and distal Ig-like domains of FcR family genes, LRC-encoded genes, and representative chicken IgSF members. The Ig-like domains compared are indicated by black shading to the right of each phylogenetic tree. **(A)** Comparison of the D1 and D2 (black shaded) of CaLITR1, CaLITR2, and IpLITR3 with the D1 and D2 (black shaded) of representative FCR, FCRL, LILR, and CHIR sequences. **(B)** Comparison of the proximal Ig-like domains of CaLITR (D3 and D4) and IpLITR3 (D3, D4, D5, and D6) with the D1 and D2 of FCRs, FCRLs, LILRs, and CHIR. The accession numbers for the sequences compared are: *Gallus gallus* (Gg)LITRA2 (XP_025001793.1), GgLILRB5 (XP_025002060.1), CHIRA (AAG37067.1), *Mus musculus* (Mm)FcgammaRIIb2 (NP_034317.1), MmFcgammaIIb1 (AAA92707.1), *Peromyscus leucopus* (Pl)FcgammaRIIb3 (XP_028720159.1), *Microtus ochrogaster* (Mo)FcgammaRIIa (XP_005348844.1), *Meriones unguiculatus* (Mu)FcgammaRIIa (XP_021502762.1), *Nannospalax galili* (Ng)FcgammaRIIb2 (XP_008847285.1), *Chinchilla lanigera* (Cl)FcgammaRIIIL2 (XP_005398367.1), *Monodon monoceros* (Mmo)FcRL32 (XP_029083037.1), *Phascolarctos cinereus* (Pc)FcRL31 (XP_020847115.1), *Felis catus* (Fc)FcRL51 (XP_023103005.1), *Carlito syrichta* (Cs)FcRL5 (XP_021566497.1), *Delphinapterus leucas* (Dl)FcRL53 (XP_022415050.1), *Monodelphis domestica* (Md)LILRB31 (XP_007492558.1), MmLILRB33 (XP_006539698.1), *Gorilla gorilla gorilla* (Ggg)LILRA43

(XP_018870369.1), *Myotis lucifugus* (Ml)LILRA61 (XP_014304669.1), MlLILRA63 (XP_014304671.1), MlLILRA6 (XP_023603176.1), *Macaca mulatta* (Mmu)LILRA12 (XP_028694177.1), (*Pan troglodytes*) (Pt)LILRA2, *Callithrix jacchus* (Cj)LILRBa (ABZ80230.1), (*Macaca nemestrina*) (Mn)LILRB17 (XP_024653420.1), MnLILRB16 (XP_024653419.1), CaLITR1 (MT209979), CaLITR2 (MT209980), CaLITR3 (MT209985), IpLITR3 (AAW82354.1), *Danio rerio* (Dr)NITR3a (AAK60110.1), DrNITR1b (NP_001296748.1), and DrNITR2a (NP_001122263.1). For all analyses, DrNITR sequences (outgroups) were used for rooting the phylogenetic trees. NJ trees with complete deletions were constructed using MEGA7 with 10000 bootstrap replications. Branch lengths represent distance, and the scale bar indicates the number of amino acid substitutions per site.

(A)

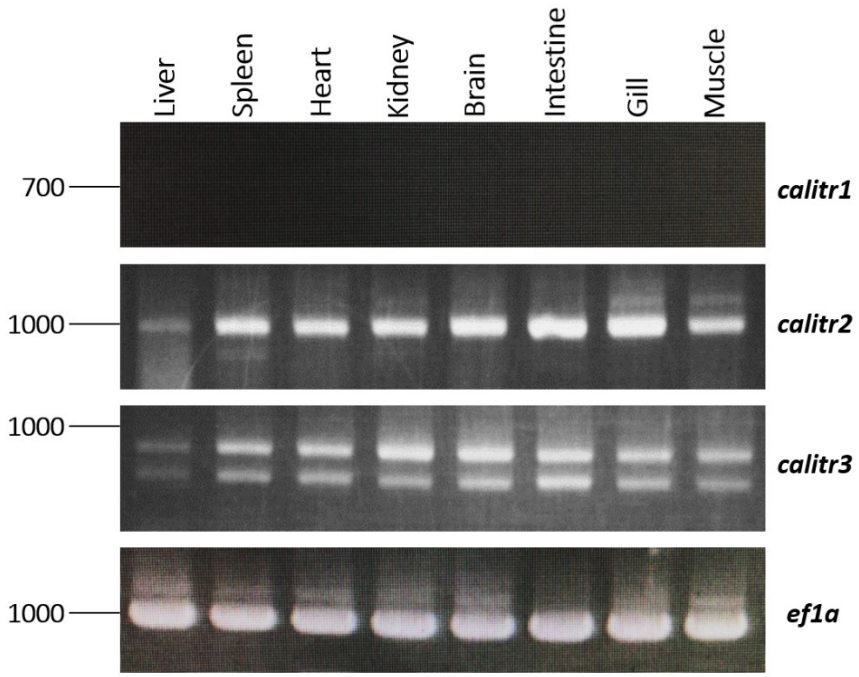
Liver
Spleen
Heart
Kidney
Brain
Intestine
Gill
Muscle
700
calitr1
1000
calitr2
1000
calitr3
1000
ef1a

(B)

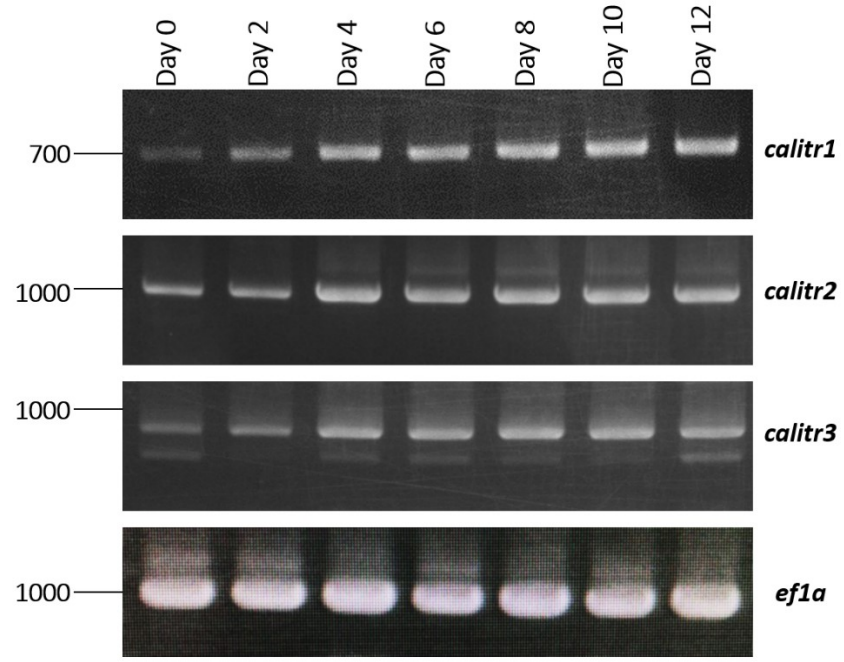
Day 0
Day 2
Day 4
Day 6
Day 8
Day 10
Day 12
700
calitr1
1000
calitr2
1000
calitr3
1000
ef1a

(C)

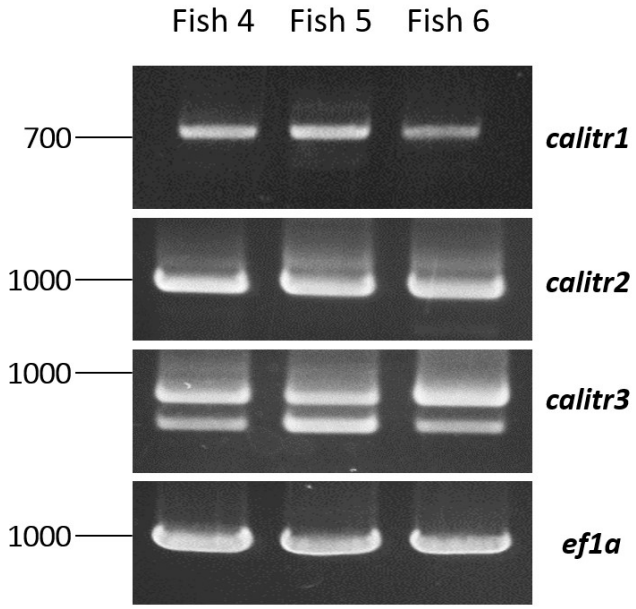

Figure 4.7. RT-PCR analyses of *calitr* expression in various goldfish tissues (A), over the course of goldfish PKM development **(B)**, and in primary kidney neutrophils **(C)**. The RT-PCR was performed using primers specific for each *calitr* indicated and *ef1α* expression was used as a positive cDNA loading control, loading control. All experiments have been replicated at least three times and only representative gels are shown.

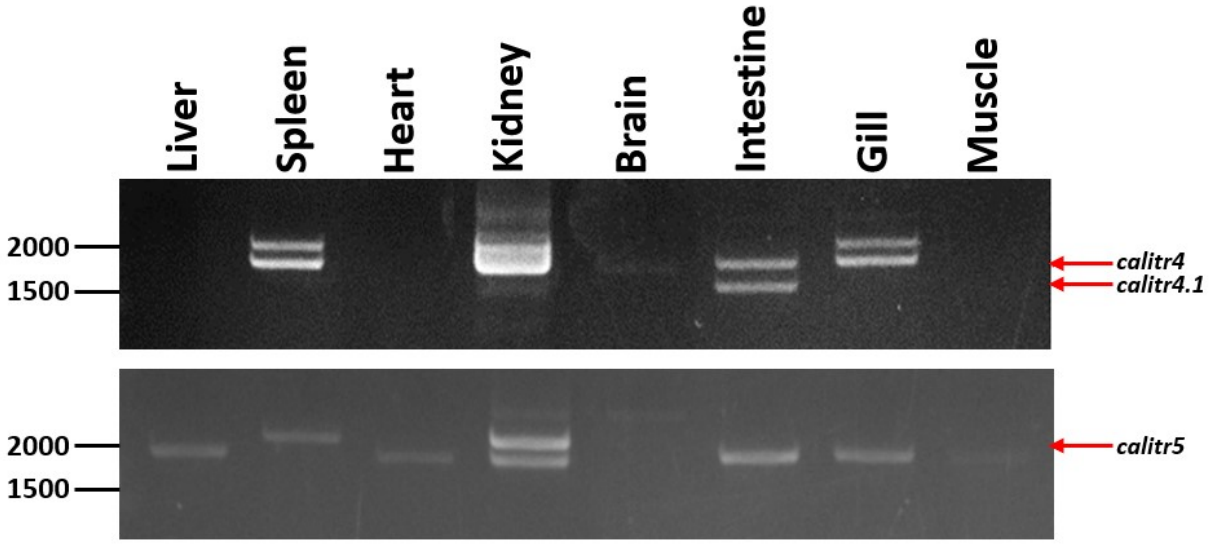

Figure 4.8. RT-PCR gels showing the expression of *calitrs* in various goldfish tissues. The RT-PCR was performed using *calitr4* and *calitr5* "capture" primers. Each "capture" primer was designed for amplifying all possible transcripts of each *calitr* gene. The bands cloned and sequenced are indicated by red arrows.

(A)

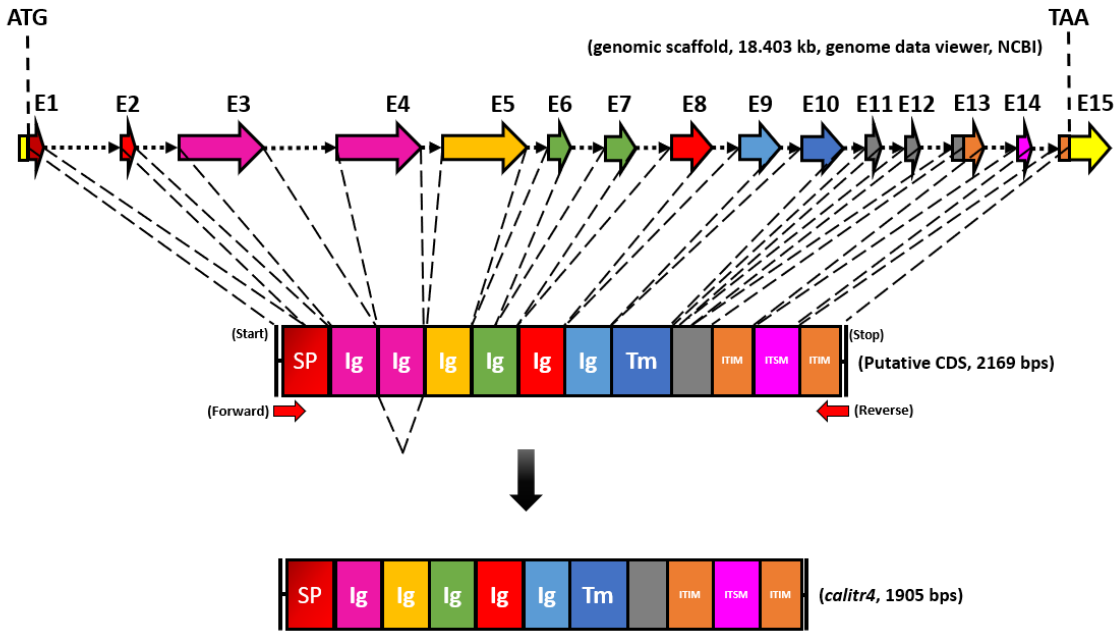
ATG
TAA
(genomic scaffold, 18.403 kb, genome data viewer, NCBI)
E1
E2
E3
E4
E5
E6
E7
E8
E9
E10
E11
E12
E13
E14
E15
(Start)
SP
Ig
Ig
Ig
Ig
Ig
Ig
Tm
ITIM
ITSM
ITIM
(Stop)
(Putative CDS, 2169 bps)
(Forward)
(Reverse)
SP
Ig
Ig
Ig
Ig
Ig
Tm
ITIM
ITSM
ITIM
(calitr4, 1905 bps)

(B)

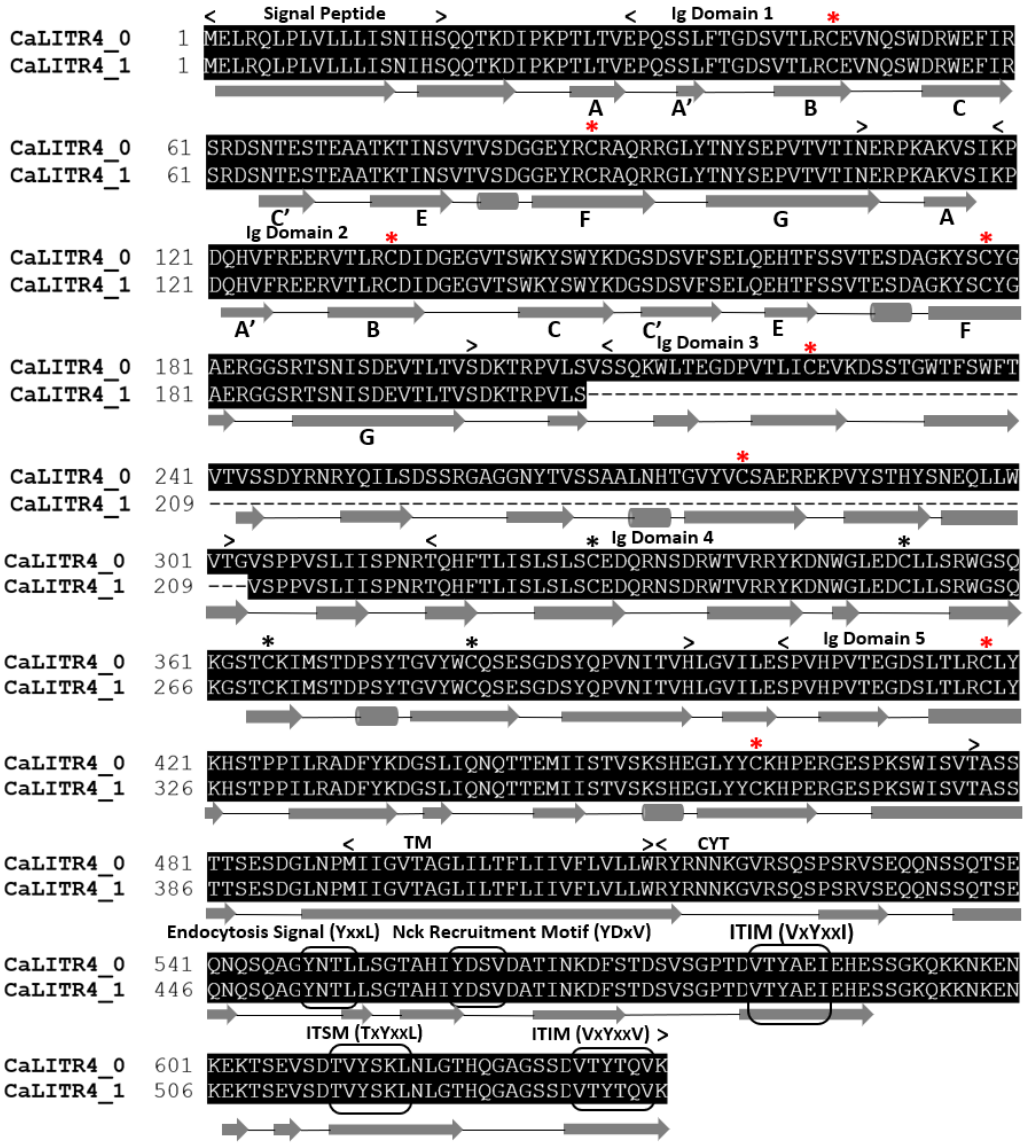
Signal Peptide
Ig Domain 1
Ig Domain 2
Ig Domain 3
Ig Domain 4
Ig Domain 5
TM
CYT
Endocytosis Signal (YxxL)
Nck Recruitment Motif (YDxV)
ITIM (VxYxxI)
ITSM (TxYxxL)
ITIM (VxYxxV)
CaLITR4_0
CaLITR4_1

(C)

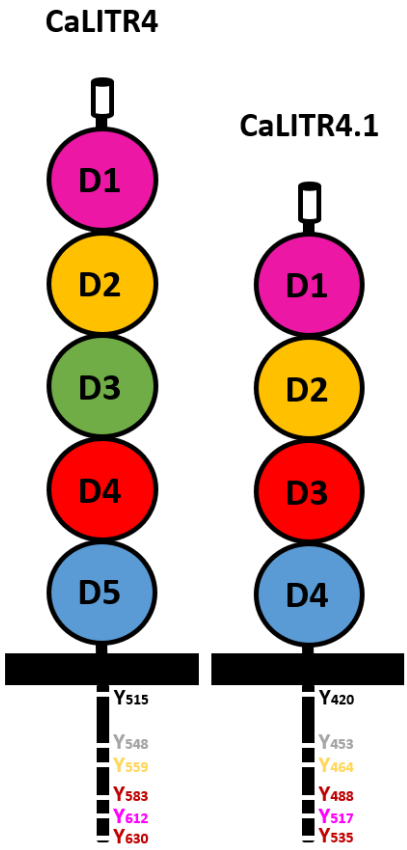

Figure 4.9. Genomic organization and identified variants of CaLITR4/4.0. (A) Schematic comparison of putative *calitr4* (predicted by Gnomon, NCBI eukaryotic gene prediction tool) and its RT-PCR amplified product. The signal peptide, Ig-like domains, TMs, and CYT regions were predicted using SMART. The Ig-like domains of the *calitr4* genomic sequence and cDNA transcript are coloured according to their phylogenetic relatedness. The dashed triangular lines represent the absence of an Ig-like domain in the predicted *calitr4* genomic sequence relative to its cDNA product, indicating a potential splicing event. Locations of the "capture" primers are indicated by mini red arrows. Exons of *calitr4* are designated by arrows on the top of the diagram, whereas the intervening introns are represented by dashed arrows. Yellow portions of the genomic scaffold indicate the untranslated regions. Base pair sizes (bp) of the *calitr4* genomic scaffold, putative gene, and cDNA product are shown. **(B)** Alignment comparing CaLITR4 with its isoform, CaLITR4.1. The predicted signal peptide, Ig-like domains, TM, and CYT region are labeled. CYT containing putative endocytosis signal, Nck recruitment motif, ITAM-like motif, and ITIM motif are labeled and boxed. Conserved amino acids are highlighted in black. Gaps in alignment are indicated by dashes. Cysteine residues that are predicted to form the intrachain disulfide bonds are marked with red asterisks. Black asterisks represent conserved cysteine residues. Predicted beta sheets and helixes are designated by grey arrows and cylinders, respectively. The Sequence alignment was performed using Clustal Omega and presented with Boxshade 3.21. **(C)** Schematic representations of CaLITR4 and its isoform, CaLITR4.1. The

signal peptide, Ig-like domains, TM, and CYT regions were predicted using SMART. CaLITR4, the originally identified sequence, is boxed. Individual CaLITR Ig-like domains are coloured according to their phylogenetic relatedness (Fig. 4.15). The gray, yellow, red, and purple tyrosine residues in the CYT of each receptor denote the putative endocytosis signal, Nck recruitment domain, ITIM motif, and ITSM motif, respectively.

(A)

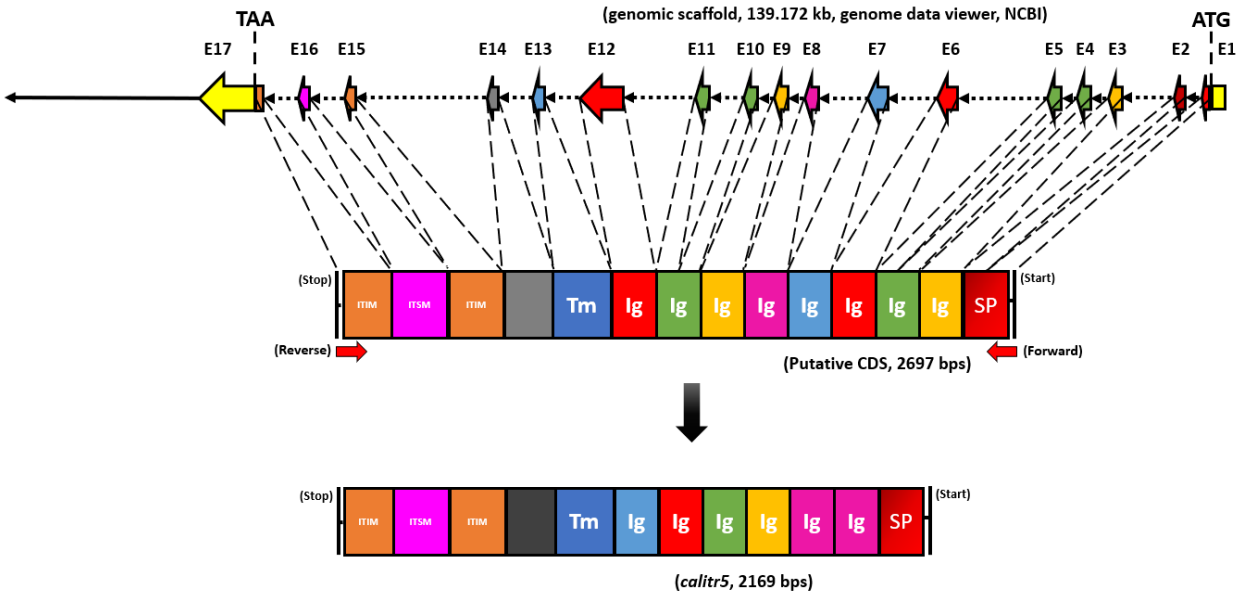
TAA
(genomic scaffold, 139.172 kb, genome data viewer, NCBI)
ATG
E17
E16
E15
E14
E13
E12
E11
E10
E9
E8
E7
E6
E5
E4
E3
E2
E1
(Stop)
ITIM
ITSM
ITIM
Tm
Ig
Ig
Ig
Ig
Ig
Ig
Ig
Ig
SP
(Start)
(Reverse)
(Forward)
(Putative CDS, 2697 bps)
(Stop)
ITIM
ITSM
ITIM
Tm
Ig
Ig
Ig
Ig
Ig
Ig
SP
(Start)
(*calitr5*, 2169 bps)

(B)

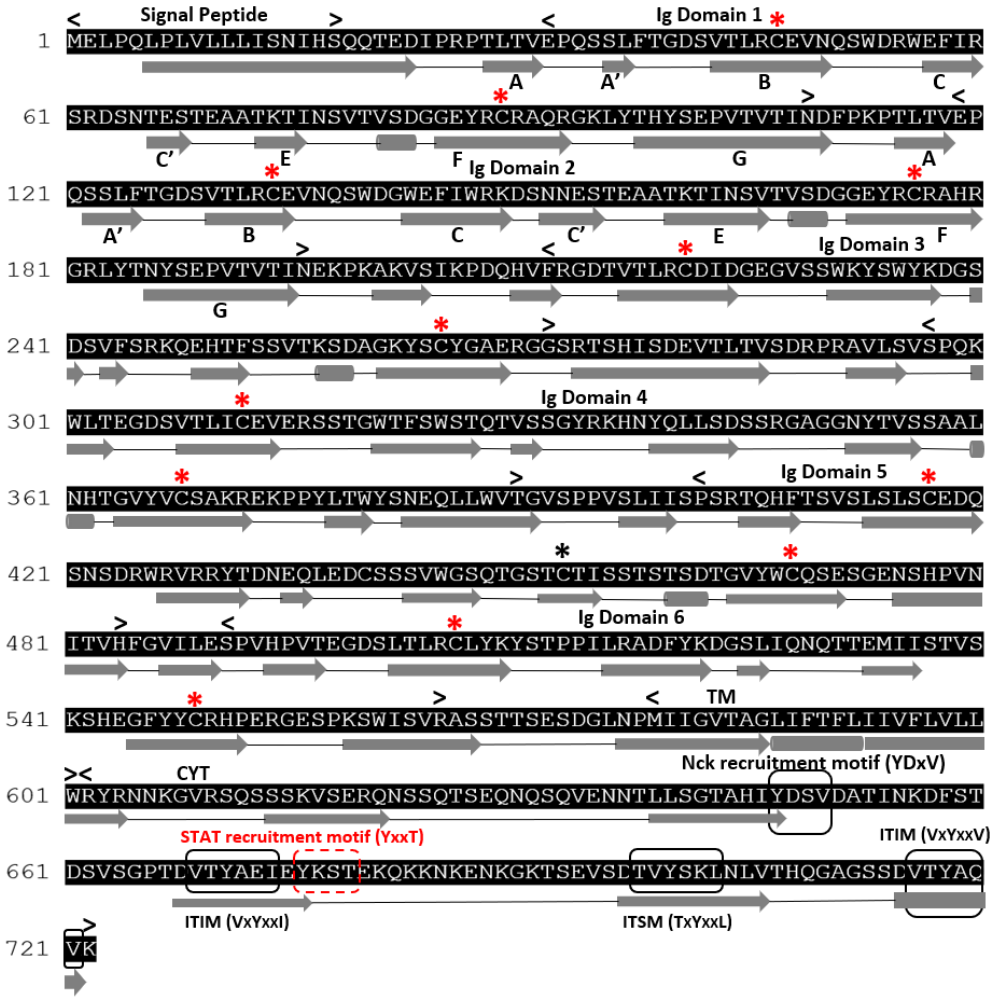

Figure 4.10. Genomic organization and amino acid sequence of CaLITR5. (A) Schematic comparison of putative *calitr5* (predicted by Gnomon, NCBI eukaryotic gene prediction tool) and its RT-PCR amplified product. The signal peptide, Ig-like domains, TMs, and CYT regions were predicted using SMART. The Ig-like domains of the *calitr5* genomic sequence and cDNA transcript are coloured according to their phylogenetic relatedness. Locations of the "capture" primers are indicated by mini red arrows. Exons of *calitr5* are designated by arrows on the top of the diagram, whereas the intervening introns are represented by dashed arrows. Yellow portions of the genomic scaffold indicate the untranslated regions. Base pair sizes (bp) of the *calitr5* genomic scaffold, putative gene, and cDNA product are shown. **(B)** Sequence features of CaLITR5. The predicted signal peptide, Ig-like domains, TM, and CYT regions are labeled. CYT containing putative Nck recruitment motif, STAT recruitment motif, ITSM, and ITIM motifs are labeled and boxed. Cysteine residues that are predicted to form the intrachain disulfide bonds are marked with red asterisks. Black asterisks represent conserved cysteine residues. Predicted beta sheets and helixes are designated by grey arrows and cylinders, respectively.

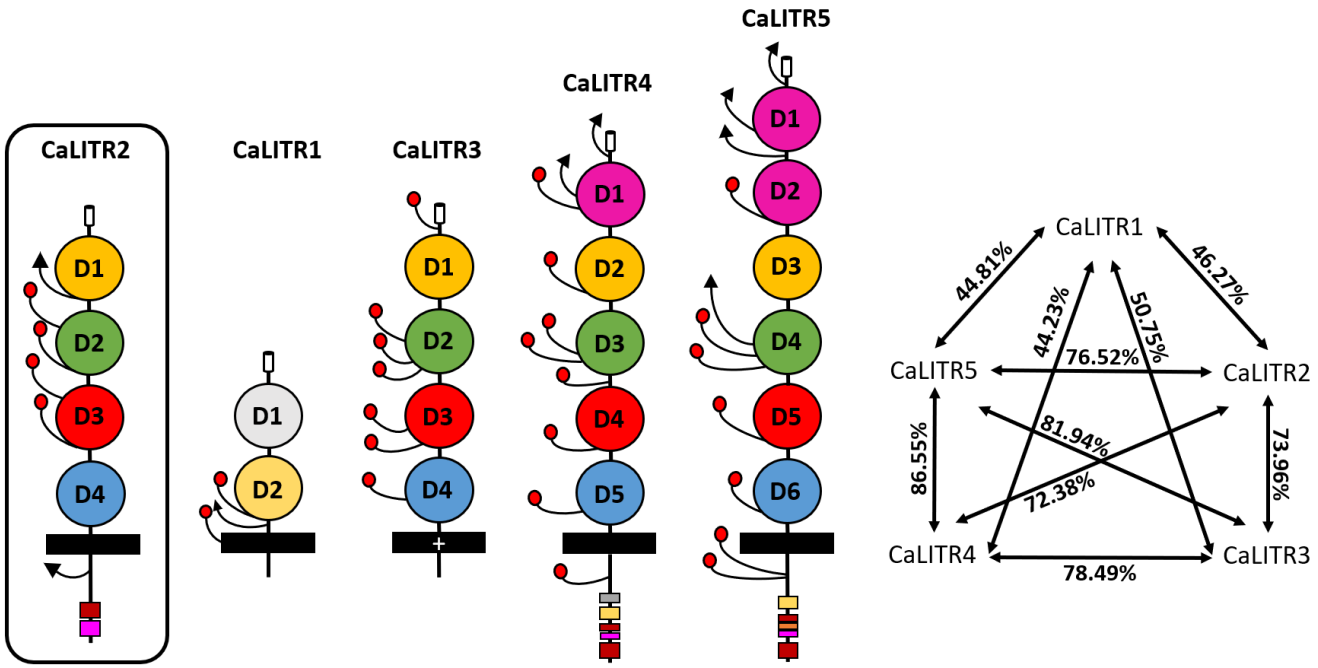

Figure 4.11. Schematic representations of CaLITRs. CaLITR2 is boxed and used as a reference for comparing individual Ig-like domains between CaLITRs. A diagram comparing amino acid percent identity between CaLITR Ig-like domains is shown to the right (the Ig-like domains were used for comparison). The signal peptide, Ig-like domains, TM, and CYT regions were predicted using SMART. N-linked and O-linked glycosylation sites are marked as red ballpoint lines and black arrows, respectively. Individual CaLITR Ig-like domains are coloured according to their phylogenetic relatedness (Fig. 4.16). The red and purple squares in the CYT of CaLITR2 represent ITIM and ITSM, respectively. The white plus sign in the TM region of CaLITR3 represents a charged histidine. The gray, yellow, purple, and red boxes in the CYT of CaLITR4 represent putative endocytosis signal, Nck recruitment domain, ITSM, and ITIM, respectively. The CYT of CaLITR5 contains putative Nck recruitment, STAT recruitment, ITSM, and ITIM motifs; these are indicated by the yellow, orange, purple, and red boxes, respectively.

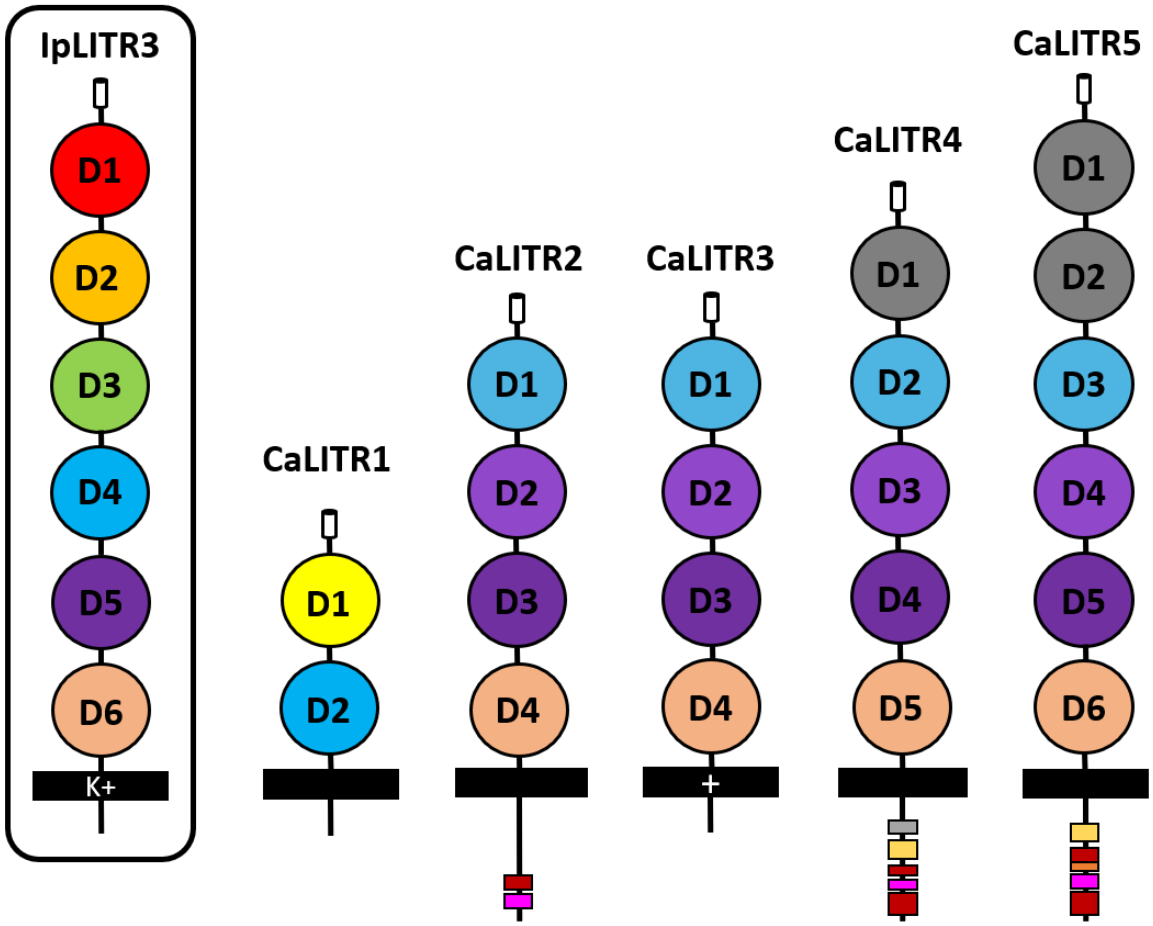

Figure 4.12. Schematics comparing CaLITR Ig-like domains to prototypic IpLITR Ig-like domains. The signal peptide, Ig-like domains, TMs, and CYT regions were predicted using SMART (Letunic, 2004). Individual CaLITR Ig-like domains are coloured according to their phylogenetic relatedness with the Ig-like domains of IpLITR3 (Fig. 4.17). The red and purple squares in the CYT of CaLITR2 represent ITIM and ITSM, respectively. The white plus sign in the TM region of CaLITR3 represents a charged histidine. The gray, yellow, purple, and red boxes in the CYT of CaLITR4 denote putative endocytosis signal, Nck recruitment domain, ITSM, and ITIM, respectively. The CYT of CaLITR5 contains putative Nck recruitment, STAT recruitment, ITSM, and ITIM motifs; these are indicated by the yellow, orange, purple, and red boxes, respectively.

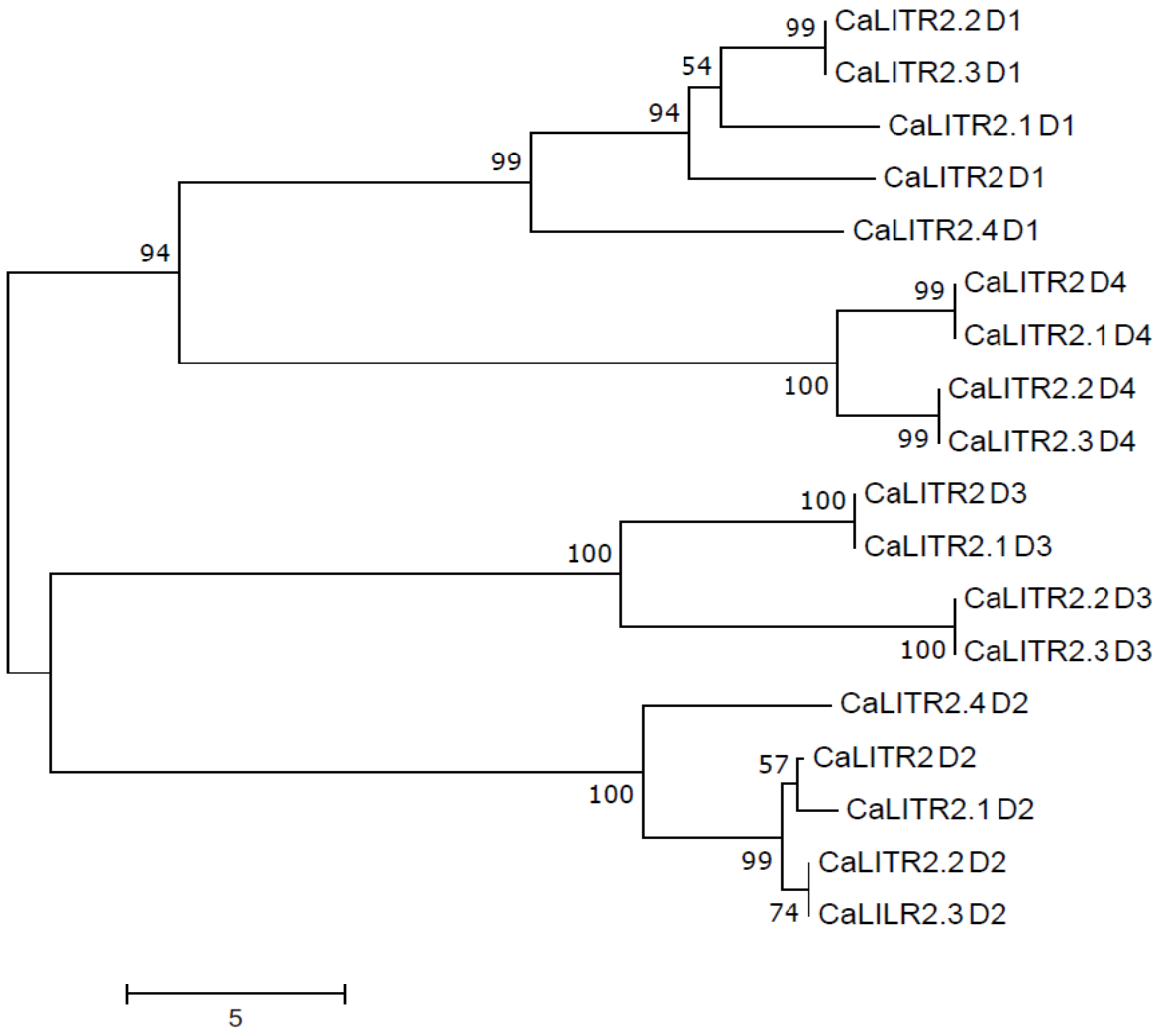

Figure 4.13. Phylogenetic analysis of the individual Ig-like domains of CaLITR2 and its variants. The NJ tree with complete deletions was constructed using MEGA7 with 10000 replications. Branch lengths represent distance, and the scale bar indicates the number of amino acid substitutions per site.

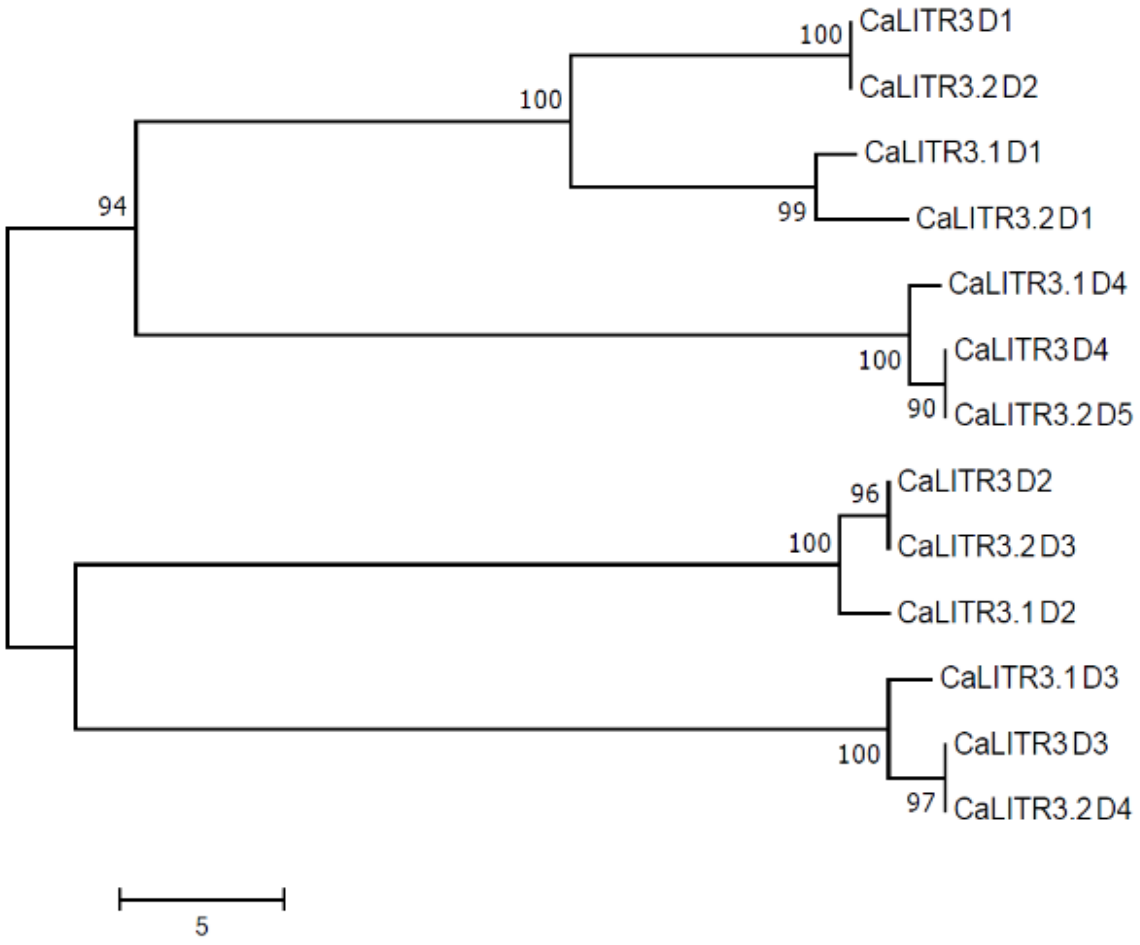

Figure 4.14. Phylogenetic analysis of the individual Ig-like domains of CaLITR3 and its variants. The NJ tree with complete deletions was constructed using MEGA7 with 10000 replications. Branch lengths represent distance, and the scale bar indicates the number of amino acid substitutions per site.

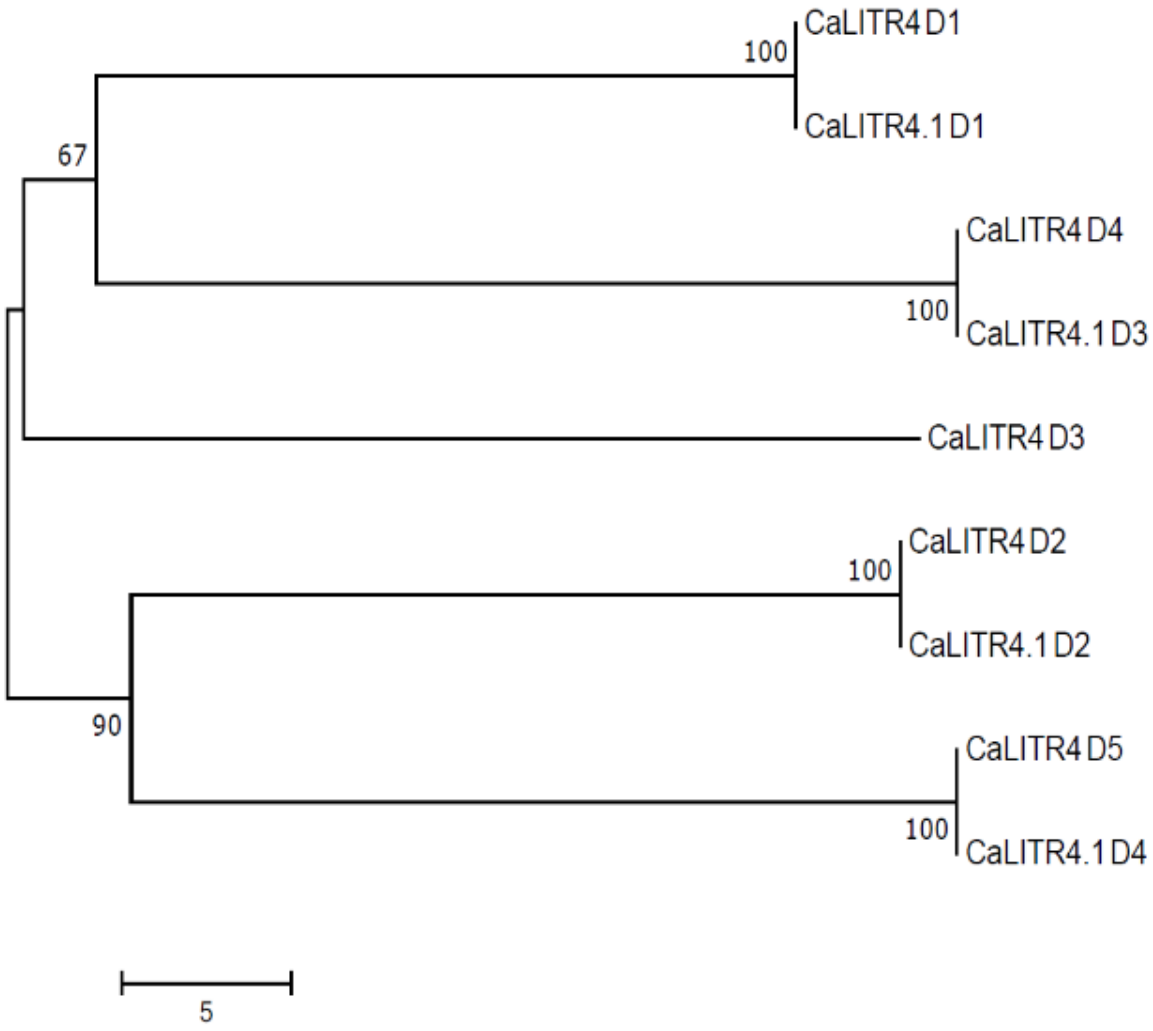

Figure 4.15. Phylogenetic analysis of the individual Ig-like domains of CaLITR4 and its variant. The NJ tree with complete deletions was constructed using MEGA7 with 10000 replications. Branch lengths represent distance, and the scale bar indicates the number of amino acid substitutions per site.

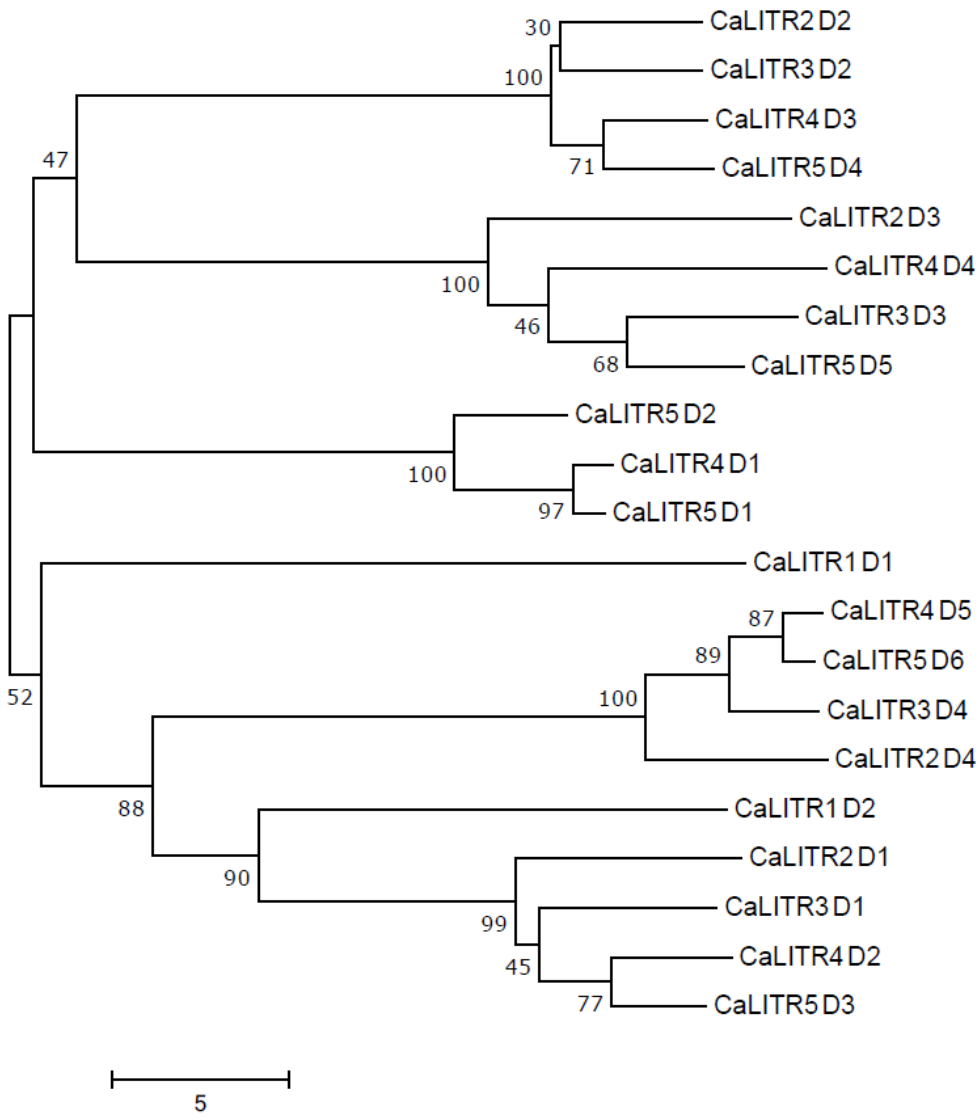

Figure 4.16. Phylogenetic analysis of the individual Ig-like domains of CaLITRs. NJ trees with complete deletions were drawn using MEGA7 with 10000 bootstrap replications. Branch lengths indicate distance. The scale bar below the tree indicates the number of amino acid substitutions per site.

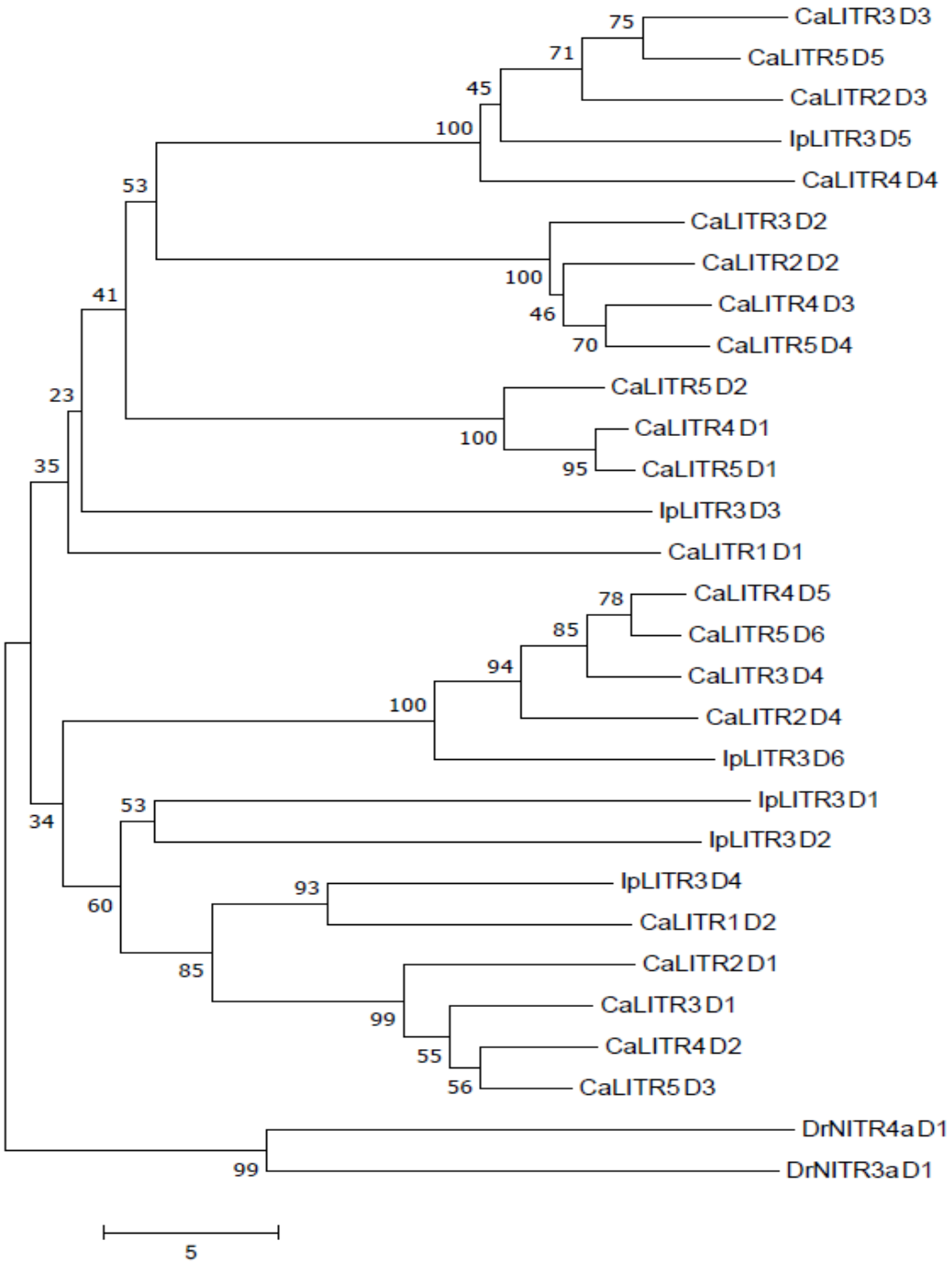

Figure 4.17. Phylogenetic comparison of the individual Ig-like domains of CaLITRs (CaLITR1, 2, 3, 4, and 5) and the individual Ig-like domains of IpLITR3. NJ trees with complete deletions were drawn using MEGA7 with 10000 bootstrap replications. Branch lengths indicate distance. The scale bar below the tree indicates the number of amino acid substitutions per site.

Receptor	Top Matching Sequences	Accession	Per.Ident	E-value
CaLITR1	FcγRIII-like (common carp)	XP_018928314.1	88.00%	1.00E-89
	sialoadhesin-like (barbel)	XP_016111186.1	88.00%	5.00E-89
	FCRL5 (*S. rhinocerous*)	XP_016414874.1	86.75%	4.00E-88
	sialoadhesin-like (common carp)	XP_018978296.1	87.33%	1.00E-87
	B-cell receptor CD22 (elephant)	XP_023395630.1	28.57%	5.00E-12
	FCRL2 (chinese hamster)	EGW07026.1	32.35%	3.00E-10
	B-cell receptor CD22 (mole-rat)	KFO32379.1	27.45%	1.00E-09
	sialoadhesin (great galago)	XP_003788097.1	30.72%	1.00E-09
	sialoadhesin (koala)	XP_020856706.1	28.21%	1.00E-09
Receptor	**Top Matching Sequences**	**Accession**	**Per.Ident**	**E-value**
CaLITR2	LILRB1 (*S. anshuiensis*)	XP_016305063.1	77.22%	0.00E+00
	FCRL5 (barbel)	XP_016117234.1	76.02%	0.00E+00
	FCRL4 (*S. anshuiensis*)	XP_016308871.1	74.86%	2.00E-179
	FCRL5 (common carp)	XP_018919999.1	75.07%	2.00E-179
	FCRL5 (*S. rhinocerous*)	XP_016386865.1	73.96%	6.00E-179
	FCRL2 (Lynx)	XP_030157702.1	25.30%	4.00E-15
	FCRL5 (Puma)	XP_025770938.1	25.30%	2.00E-14
	FCRL5 (polecat)	XP_012902985.1	26.63%	4.00E-13
	FCRL5 (rabbit)	XP_008262488.1	27.47%	9.00E-13
	FCRL5 (seal)	XP_006748221.2	27.50%	1.00E-12
Receptor	**Top Matching Sequences**	**Accession**	**Per.Ident**	**E-value**
CaLITR3	FCRL5 (common carp)	XP_018930228.1	86.91%	0.00E+00
	B-cell CD22-like (*S. anshuiensis*)	XP_016323040.1	83.01%	0.00E+00
	FCRL2 (*S. anshuiensis*)	XP_016295637.1	84.33%	0.00E+00
	FCRL5 (*S. anshuiensis*)	XP_016348498.1	84.66%	0.00E+00
	FCRL2 (cheetah)	XP_026904166.1	26.03%	1.00E-12
	FCRL5 (puma)	XP_025770938.1	26.03%	2.00E-12
	FCRL2 (lynx)	XP_030157702.1	25.07%	3.00E-12
	FCRL5 (leopard)	XP_019294099.1	25.21%	8.00E-11
	FCRL4 (narwhale)	XP_029083042.1	26.97%	1.00E-10
Receptor	**Top Matching Sequences**	**Accession**	**Per.Ident**	**E-value**
CaLITR4	FCRL5 (common carp)	XP_018919999.1	81.80%	0.00E+00
	FCRL2 (barbel)	XP_016146377.1	77.63%	0.00E+00
	FCRL2 (barbel)	XP_016106352.1	84.01%	0.00E+00
	LILRA2 (*S. rhinocerous*)	XP_016382685.1	78.34%	0.00E+00
	FCRL2 (*S. anshuiensis*)	XP_016295637.1	82.42%	0.00E+00
	FCRL5 (crab-eating macaque)	XP_005541425.1	26.88%	1.00E-19
	FCRL5 (sabaeus monkey)	XP_007974856.1	27.50%	2.00E-19
	FCRL5 (sooty mangabey)	XP_011934188.1	26.15%	3.00E-19
	FCRL5 (pig-tailed macaque)	XP_011768234.1	27.08%	5.00E-19
	FCRL5 (puma)	XP_025770939.1	25.22%	8.00E-19
Receptor	**Top Matching Sequences**	**Accession**	**Per.Ident**	**E-value**
CaLITR5	FCRL5 (common carp)	XP_018930228.1	75.88%	0.00E+00
	FCRL2 (barbel)	XP_018919999.1	83.80%	0.00E+00
	FCRL2 (common carp)	XP_018950620.1	69.01%	0.00E+00
	BCR CD22-like (*S. anshuiensis*)	XP_016323040.1	83.83%	0.00E+00
	LILRA3 (baboon)	XP_031516101.1	23.89%	3.00E-27
	LILRA4 (gorilla)	XP_018870348.1	27.52%	1.00E-24
	FCRL3 (star-nosed mole)	XP_012588718.1	27.49%	4.00E-24
	LILRA2 (bleeding-heart monkey)	XP_025225110.1	24.29%	5.00E-24
	LILRA3 (baboon)	XP_031516112.1	25.62%	9.00E-24

Table 4.1. Representative CaLITR PSI-BLAST results. The protein sequences of the identified five CaLITRs were used as queries to search the non-redundant protein sequence databases for vertebrates (taxid:7742, excluding the goldfish taxid:7957) and mammals (taxid:40674) by PSI-BLAST at http://blast.ncbi.nlm.nih.gov/Blast; For each receptor, a line is used to divide the top hits retrieved by limiting searches to vertebrates (above the boundary line) and mammals (below the boundary line); All searches were performed using the predicted extracellular regions of each receptor sequence (i.e. TM and CYT regions were excluded).

Primer name	Forward sequences (5′ to 3′)	Reverse sequences (5′ to 3′)
*calitr1*_capture[a]	ATGGGTTACACTCATACTGCTACA	TCAGTGACATGAGATTTGAAGTTTCTTCT
*calitr2*_capture[a]	CATCATTCAGTCAGTATGGAGCTC	TTAACCTTGATGGGTTTCCGAATTCAGC
*calitr3*_capture[a]	ATGGAGCTCAGTAAACTTCCTCTT	TCAGTCAGATGTTTCACCTCTCAT
*calitr4*_capture[a]	ATGGAGCTCCGTCAACTTCCTCTTG	CTCGTCTGGGCATTTATTTAACCTGA
*calitr5*_capture[a]	ATGGAGCTCCCTCAACTTCCTC	CTGGGCATTTATTTAACCTGAGCATACGT
calitr1[b]	CTTCCTCTAATGCTCTTGCTGAT	AGTGTCTTTGTTGTGTTTGCC
calitr2[b]	AAGCCAGAGTGAGCATCAAA	CTCTGTGTTTGCAGGAGTAGAA
calitr3[b]	GTGAGGTTTATGGCTCCTCTAC	CGACTGTCACTAGCAGATATGG
ef1a[c]	TCGAGGCTGGTATCTCCAAGAA	GTGGCATCAGGTGCAGTTCTAA

Table 4.2. List of RT-PCR primers used in this study. Primers with superscript (a) were designed against the start and stop codons of predicted calitr sequences and were used for "netting" *calitr* variants. Primers with superscript (b) are specific for *calitr* sequences and were designed against a portion of each "captured" sequence to increase primer specificity. The *ef1α* primer pair was used to check for RNA integrity and loading levels, serving as a positive control.

CHAPTER V

IDENTIFICATION OF DISTINCT LRC- AND FC RECEPTOR COMPLEX-LIKE CHROMOSOMAL REGIONS IN FISH SUPPORTS THAT TELEOST LEUKOCYTE IMMUNE-TYPE RECEPTORS ARE DISTANT RELATIVES OF MAMMALIAN FC RECEPTOR-LIKE MOLECULES

5.1 INTRODUCTION

Proper functioning of the immune system requires intricately coordinated immunoregulatory receptor networks to activate and suppress immune cell effector responses. Defects in these regulatory circuits have been linked to numerous autoimmune and inflammatory diseases (de la Fuente et al., 2012; Rostamzadeh et al., 2018). In vertebrates, evolutionarily related immunoregulatory receptor gene families are generally found in large genomic clusters with specific genomic organizations, including physical linkage of genes and their neighbors, gene content, and orientation of transcription (Ohta et al., 2019; Trowsdale et al., 2001). In many cases, genomic organizations of these gene clusters are preserved across phylogeny (Akula et al., 2014; Barten et al., 2001; Davis et al., 2002). For example, the human classical *fcrs* and their homologs, the *fcrls*, are found in large genomic clusters on human Chr 1q21-23 (Davis, 2007). The distal Ig-like domains (D1, D2, and D3) of FCRL family members are distantly related to the Ig-like domains (D1, D2, D3) of the classical FcRs (i.e., CD64, CD32, and CD16), which are genomically linked to genes of the CD2 superfamily (i.e., SLAM family genes), and a wide variety of other genes (i.e., *dusp12*, *etv3*, *CD5l*, and *nges*) (Davis, 2007). These physical linkage relationships are also shared by FCRL and FcR homologs found in mice (*Mus musculus*) and the tropical clawed frog (*Xenopus tropicalis*), indicating that FCRLs and FcRs belong to a complex conserved syntenic group in mammals and amphibians (Fayngerts et al., 2007; Guselnikov et al., 2008). Similarly, the LRC is located on Chr 19q13.4, which contains a large number of highly related immunoregulatory receptor genes including the *lilrs*, *kirs*, and others (i.e., *fcar*, *ncr1*,

and *oscar*), which are clustered among several phylogenetically unrelated genes such as tweety family member 1 (*ttyh1*), leukocyte receptor cluster member 8 (*leng8*), and leukocyte receptor cluster member 9 (*leng9*) (Sambrook et al., 2006). In mice, the paired immunoglobulin-like receptors (*pirs*) are also located on a chromosomal region among relatives of the human *ttyh1*, *leng8*, *leng9*, as well as several other genes found in the human LRC region (Martin et al., 2002). Beyond mammals, human *lilr* and mouse *pir* relatives have been described within an LRC-like region in the tropical clawed frog (*Silurana tropicalis* immunoglobulin-like receptor (*silrs*)) that are located next to several relatives of the mammalian genes *ttyh1*, *leng8*, and *leng9* (Guselnikov et al., 2010). Therefore, like the *fcrs* and *fcrls*, human *lilrs* and their mouse and amphibian relatives belong to a genomic complex that have conserved synteny.

Initially identified in the channel catfish, LITRs belong to the IgSF and are a family of polymorphic and polygenic immunoregulatory receptor-types expressed in various channel catfish myeloid and lymphoid cell lines (Stafford, Bengten, et al., 2006; Stafford et al., 2007). Original phylogenetic analyses of IpLITRs showed that they have a unique chimeric composition of domains. For example, representative IpLITR membrane-proximal Ig-like domains (e.g., D3, D4, D5, etc.) cluster with the Ig domain sequences found among mammalian LRC members, whereas IpLITR membrane-distal domains (e.g., D1 and D2) feature phylogenetic relationships with the mammalian FCR family genes (Stafford, Bengten, et al., 2006). Furthermore, comparative homology modeling of the Ig-like domains of select IpLITRs using LILRB1 as a template showed that they share similar overall tertiary protein structures with group 1 LILRs, which can bind MHC class 1 molecules (Stafford et al., 2007). Additionally, further sequence analysis revealed a putative MHC class 1 binding site within the D1 of specific IpLITR-types

(Stafford et al., 2007) supporting the hypothesis that some IpLITRs may be capable of recognizing MHC class 1 molecules.

In the previous chapter, I detailed the initial discovery of several *calitr* transcripts and their variants from the goldfish primary macrophage and neutrophil cultures (Wang et al., 2020). As expected, CaLITRs share similar phylogenetic characteristics with IpLITRs as their membrane-proximal Ig-like domains are distantly related to mammalian LRC receptors and their membrane-distal Ig-domains appear to be related to the FCR family members (Wang et al., 2020). Additionally, my preliminary examination of the exon organization of several *calitrs* indicated that their signal peptides are encoded by two separate exons, with the second exon being 36-bp-long, a specific feature observed in vertebrate LRC-encoded members. This suggests a possible evolutionary relationship to receptors of the LRC.

Collectively, phylogenetic analyses and investigations into the exon organization of LITRs have provided some interesting clues about their possible relationships with several important immunoregulatory receptor families in mammals. However, with limited *in vivo* functional data and no known ligands, classification of LITRs as Fc/FCRL and/or LRC-like receptor-types has not been established. By examining their genomic organization and syntenic relationships, new information into their evolutionary connections with immunoregulatory receptors systems found in other vertebrates can be uncovered. Therefore, using a comparative genomics approach, the main objective of this chapter was to comprehensively investigate the possible syntenic relationships between teleost LITRs and the FCR and LRC family genes found in the genomes of representative vertebrates (e.g., elephant shark (*Callorhinchus milii*), tropical clawed frog (*Xenopus tropicalis*), chicken (*Gallus gallus*), mouse (*Mus musculus*), and humans

(*Homo sapiens*). Further understanding of the evolutionary history of LITRs will help to piece together the evolutionary processes shaping the immunoregulatory repertoires of vertebrates, and aid in designing more effective experiments to help elucidate the functional roles of teleost LITR family members.

5.2 RESULTS

5.2.1 Syntenic *litr* genomic clusters are linked to *arhgeff*, *vangl2*, *myadm*, and *cd2*

To examine the genomic location and organization of teleost *litrs*, I searched the Ensembl genome database (https://uswest.ensembl.org/index.html; Ensembl release 100) for possible orthologs of IpLITRs and CaLITRs in the fugu (*Takifugu rubripes*, fTakRub1.2 assembly), zebrafish (*Danio rerio*, GRCz11 assembly), channel catfish (*Ictalurus punctatus*, IpCoco_1.2 assembly), and goldfish (*Carassius auratus L.*, ASM336829v1) genome databases. BLASTP searches (near match option) of the teleost genomes were performed using representative IpLITR and CaLITR amino acid sequences (CaLITR1-5 and IpLITR1-3) (Wang et al., 2020) as queries to identify possible *litr* gene hits with E-values ≤ 1e−30. Multiple reiterations of the BLAST searches were performed using identified *litr* genes each time as queries to capture additional *litr* sequences. Next, the longest transcript of each gene hit (annotated from the Havana project/by genebuild) was selected, and its predicted amino acids were visualized using SMART (Letunic & Bork, 2018). Then, to validate the identity of each *litr*, phylogenetic analyses were performed by comparing all individual Ig-like domains of each *litr* hit with existing *litr* cDNAs using MEGA7 (Kumar et al., 2016). In this study, only amino acid sequences (aligned by ClustalW) were used for phylogenetic analyses and all of the phylogenetic trees were constructed using the NJ method (p-distance model, pairwise deletion,

and 10,000 bootstrap replicates). As shown in Fig. 5.1, teleost *litrs* are linked (often < 1 million base pairs apart) and present on more than one Chrs in each teleost species. Specifically, my searches for *litrs* identified 23 different genes distributed across six different goldfish Chrs; Chr 3, 7, 15, 22, 40, 47, and LG28B (Fig. 5.1A). Fourteen *litrs* were found on zebrafish Chr 7 and three *litrs* on zebrafish Chr 3 (Fig. 5.1B). In channel catfish, twenty-four *litrs* on channel catfish Chr 7 and one *litr* on Chr 6 (Fig. 5.1C) were identified and seven *litrs* on Fugu Chr 8 were retrieved (Fig. 5.1D). Although located on different Chrs, the majority of the *litr* sequences in each teleost are found on a single Chr (e.g., goldfish, zebrafish, and catfish Chr 7). This raises the possibility that *litrs* were likely located on a single Chr in the teleost ancestor and subsequent genomic processes (i.e., teleost-specific genome duplication (TGD), gene conversion, and chromosomal translocation) relocated *litrs* to other Chrs. Furthermore, the presence of *litrs* distributed across seven different goldfish Chrs is likely the result of an allotetraploidization event (David et al., 2003; Yuan et al., 2010). Further analyses of the selected teleost genomes have also identified numerous unplaced *litr* contigs in the goldfish and channel catfish (Fig. 5.2), indicating that the number of *litrs* reported in Fig. 5.1 is an underestimation of the total gene content.

5.2.2 Teleost LITRs encode diverse Ig-like domain architectures and signaling potentials

To visually represent the diversity of Ig-like domain architectures and signaling potentials of teleost *litrs*, their nucleotide sequences were translated into amino acid sequences and then analyzed using ORF Finder (https://www.bioinformatics.org/sms2/orf_find.html) and SMART, respectively. Phylogenetic analyses was then performed to compare the individual Ig-like domain sequences of the newly identified goldfish *litrs* (i.e., the genome annotated sequences) with the Ig-like domains of the previously reported CaLITR sequences (CaLITR1-5)

(Wang et al., 2020) using MEGA7 (pairwise deletion and 10,000 bootstrap replicates). Subsequently, the Ig-like domains of the predicted CaLITRs found on the different goldfish Chrs were then color-coded based on their phylogenetic relationships, which allowed for the identification and categorization of the various Ig-domain types expressed by these receptors. Using the color schemes of the CaLITRs as a reference, the Ig-like domains of the other teleost were then color-coded according to their overall phylogenetic relatedness with the CaLITRs. Phylogenetic trees with the most persistent branching patterns and high bootstrap supports were selected for color-coding to ensure accuracy and consistency in the reported relationships of the Ig-like domains (a representative tree is shown in Fig. 5.3). Using this approach, the Ig-like domain architectures that exist among the various teleost LITR-types is detailed in Fig. 5.4 and described further below.

Overall, CaLITRs differ significantly in the number, types, and arrangements of their extracellular Ig-like domains (Fig. 5.4A). Specifically, CaLITRs have five major Ig-like domain-types colored as pink, gold, green, red, and blue domains (Fig. 5.4A). Most of these domains are arranged in a consistent membrane distal to proximal order among the various CaLITRs: gold (distal), green, red, and blue (proximal). The pink, gold, and green Ig-like domains of the CaLITRs are often expressed at the membrane-distal regions of the receptors indicated possible ligand-binding potentials. Conversely, the red and blue CaLITR Ig-like domains are primarily expressed proximal to the transmembrane segments, suggesting that they serve structural or other accessory functions, but unlikely to directly interact with extracellular ligands. Some CaLITR-types also have distinct Ig-like domain arrangements. For example, ENSCARG00000012407, which is indicated with an “a” in Fig. 5.4A, has four Ig-like domains, which are all of the gold Ig-like domain-type. Additionally, ENSCARG00000001135 (identified as “b” in Fig. 5.4A) has

three dark-shaded gold Ig-like domains (e.g., D1, D2, and D4), one lightly shaded pink D3, one dark-shaded red D5, and one dark-shaded blue D6. Furthermore, ENSCARG00000036842 (identified as "c" in Fig. 5.4A) has the common CaLITR domain architecture of gold, green, red, and blue, but with the unique addition of tandem repeats of gold and green Ig-like domains in its membrane-distal region. The different Ig-like domain arrangements and Ig-like domain subsets present in the repertoire of CaLITRs identified highlight the overall intraspecies diversity of this immunoregulatory receptor family.

I also observed that the predicted *calitr* genomic sequences found on the different goldfish Chrs frequently do not precisely match with the previously reported expressed *calitr* cDNA sequences (Wang et al., 2020). For example, ENSCARG00000012374 (identified as "d" in Fig. 5.4A; a gene with the highest match to *calitr3* cDNA (Fig. 5.5), has an additional membrane-distal gold domain of CALITR3. Although ENSCARG00000036842 ("c" in Fig. 5.4A) is the highest matching hit to *calitr2* (Fig. 5.5), it has an additional array of gold and green domains in its membrane-proximal region that are absent in the *calitr2* cDNA. The observed discrepancies between the predicted *calitr* gene sequences and the cDNAs is likely due to annotation errors, the nature of the outbred goldfish (high haplotypic diversity and polymorphic genes), and/or posttranscriptional events such as exon splicing.

Based on their predicted TMs and array of tyrosine-based protein motifs within their CYT regions, CaLITRs can be tentatively classified as putative activating, inhibitory, secreted, or functionally ambiguous receptor-types (Fig. 5.4A). For example, activating goldfish LITR-types have positively charged histidine, lysine, or arginine residues located in their TMs (indicated with "+" symbols in the TMs of ENSCARG00000022980, ENSCARG00000001127,

and ENSCARG00000012435; Fig. 5.4A), which may facilitate their associations with various intracellular adaptor signaling molecules (i.e., FcRγ and DAP12) containing ITAMs. Additionally, ITAM-like sequences (Barrow & Trowsdale, 2006) were also encoded within the CYT regions of certain CaLITR-types (see "c" and "e" in Fig. 5.4A). Putative secreted and ambiguous forms of CaLITRs either lack predicted TMs entirely or they have neutrally charged TMs and CYT regions devoid of recognizable signaling motifs, respectively. Interestingly, some CaLITR-types ("f" and "g" in Fig. 5.4A) have CYT regions containing multiple signaling motifs matching the consensus sequences of the Nck recruitment motif (Blasutig et al., 2008), ITAM-like sequences, ITIM-like sequences (Barrow & Trowsdale, 2006), ITSM (Liu et al., 2015), STAT recruitment motifs (Chakraborty et al., 1999; Oates et al., 1999), and endocytic signals (Traub & Bonifacino, 2013). A few of the CaLITRs also have non-canonical-tyrosine-based protein motifs (e.g., YSLR and YKGK; indicated as yellow circles in the CYT regions of "h" and "i" in Fig. 5.4A).

When compared with CaLITRs as the reference sequences, phylogenetical analyses show that zebrafish LITRs feature related Ig-like domain-types and similar Ig-like domain arrangements. For example, the majority of the *Danio rerio* (Dr)-LITRs have the same five major Ig-domain types (pink, gold, green, red, and blue Ig-like domains) and these domains are arranged in the same general order as observed for many of the CaLITRs (gold-green-red-blue; Fig. 5.4B). Select DrLITRs also have variable Ig-like domain arrangements or Ig-like domain subsets. For example, si:cabz01036022.1 (indicated as "a" in Fig. 5.4B) has one dark shaded gold D1, four brightly shaded gold domains (e.g., D2, D3, D6, and D7), a lightly shaded pink D4, and a classic gold-colored D5. In comparison, the ectodomains of si:ch211-165f21.7 (indicated as "b" in Fig. 5.4B) are all the gold Ig-like domain-type.

DrLITRs are also predicted to have variable signaling abilities, and some may also represent secreted forms. Specifically, the putative activating DrLITR-types (indicated with "+" in their TMs; si:ch211-220f21.3 and si:ch211-165f21.7; Fig. 5.4B) all have charged lysine residues in their TMs and feature short CYT regions devoid of signaling motifs. Functionally ambiguous DrLITR-types also exist, which have uncharged TMs plus CYT regions devoid of signaling motifs (indicated as "c," "d," "e," and "f" in Fig. 5.4B). Some DrLITRs appear to have variable functional potentials, encoding several tyrosine-based motifs within their CYT regions such as ITAM, ITIM, and ITSM-like sequences (see receptors "g" and "h" in Fig. 5.4B). Finally, putative secreted DrLITR-types lack TMs (see receptor "i"; Fig. 5.4B).

IpLITRs also vary significantly in their number of Ig-like domains as well as their overall Ig-like domain arrangements (Fig. 5.4C). However, as shown for goldfish and zebrafish, IpLITRs encode the same five main Ig-like domain-types (pink, gold, green, red, and blue) found in the CaLITRs. Uniquely, several of the predicted *iplitr* genomic sequences also encode domains that are highly similar to the previously reported Ig-like domains found in the expressed cDNA sequences of the originally discovered *iplitr* prototypes (i.e., IpLITR1, 2, and 3; Fig. 5.5). Specifically, the extracellular region of ENSIPUG00000009559 (identified as "a" in Fig. 5.4C) shares 91% amino acid similarity with IpLITR1 and contains two highly related membrane-distal gold D1 and D2, a rose-shaded D3, and a gold D4, which perfectly matches the domain organization of the *iplitr1* expressed cDNA sequence. Furthermore, the ectodomains of ENSIPUG00000009496 (see "b" in Fig. 5.4C) share 88% sequence similarity with the ectodomains of IpLITR2, and it encodes two membrane distal D1 and D2 (gold) and a pink D3, which matches the domain organization of IpLITR2. In contrast, ENSIPUG00000010182 (see "c" in Fig. 5.4C) shares 90% sequence similarity with the extracellular region of IpLITR3 and

has two membrane-distal gold D1 and D2, a rose-shaded D3, a gold D4, and a red D5; however, it lacks the blue D6 found in IpLITR3. Several of the identified IpLITRs also share similar Ig-like domain arrangements with those in the CaLITR1-5 sequences (Fig. 5.5). For example, the extracellular region of ENSIPUG00000014440 (see "d" in Fig. 5.4C) shares 57% amino acid sequence similarity with the ectodomains of CaLITR2 and CaLITR3 and has a membrane-distal gold D1, green D2, red D3, and blue D4, which matches the Ig-like domain architectures of CaLITR2 and CaLITR3. In comparison, the ectodomain of ENSIPUG00000014166 (see "e" in Fig. 5.4C) shares 57% sequence similarity with the ectodomains of CaLITR2 and CaLITR3; however, its extracellular domains are arranged in the reverse order compared to those of CaLITR2 and CaLITR3 (Fig. 5.5).

The ectodomains of several IpLITR sequences resemble truncated versions of the ectodomains of CaLITR2. Specifically, ENSIPUG00000010226 (see "f" in Fig. 5.4C) and ENSIPUG00000013778 (see "g" in Fig. 5.4C) both lack the membrane-distal gold D1 of CaLITR2. The ectodomains of ENSIPUG00000014210 (see "h" in Fig. 5.4C) are also inversely arranged when compared with the ectodomains of CaLITR2, and it also lacks the blue domain-type found in CaLITR2. ENSIPUG00000014948 (see "i" in Fig. 5.4C) lacks the membrane-proximal red D3 and blue D4 of CaLITR2, whereas ENSIPUG00000002918 (see "j" in Fig. 5.4C) lacks the membrane-proximal gold D1 and green D2 of CaLITR2. Select IpLITR-types also have unique Ig-like domain architectures relative to the CaLITRs and DrLITRs. Notably, ENSIPUG00000016218 (see "k" in Fig. 5.4C) encodes a distinct mixture of pink and gold Ig-like domains, whereas ENSIPUG00000009781 (see "l" in Fig. 5.4C) has two membrane proximal domains (red D11 and blue D12) followed by five tandem repeats of gold and pink domains showing that the patterns and distributions of Ig-like domains among teleost LITRs are

quite dynamic. Unsurprisingly, several of the newly identified IpLITR genes are predicted to have variable signaling potentials that covers the same dynamic range of putative functions detailed for CaLITRs and DrLITRs, which are documented in Fig. 5.4C.

There are only a few *Takifugu rubripes* (Tr)-LITRs, which have limited diversity of Ig-like domain arrangements and putative functional-types when compared to other teleost LITRs (Fig. 5.4D). Additionally, the Ig-like domains of TrLITRs are most distantly related (lightly colored Ig-like domains) to the Ig-like domains of CaLITRs, which is likely the result of the long evolutionary distance between the fugu and the more closely related goldfish, zebrafish, and channel catfish. For example, the red D1 and blue D2 of ENSTRUG00000032148 (see "a" in Fig. 5.4D) share 38% overall amino acid sequence similarity with the membrane proximal red D3 and blue D4 of CaLITR2 (Fig. 5.5). Additionally, ENSTRUG00000032664 (see "b" in Fig. 5.4D) shares 40% overall amino acid sequence similarity with the D3 and D4 of CaLITR2 (Fig. 5.5). Although only a small repertoire of LITRs exists in the fugu, the five major Ig-like domain-types (pink, gold, green, red, and blue) that I identified in the other teleost LITRs are all present in the TrLITRs. However, most of the TrLITRs encode only the red and blue Ig-like domain-types and they exist as putative secreted receptors (i.e., ENSTRUG00000009011 and ENSTRUG00000029328; see "c" and "d" in Fig. 5.4D). Two putative activating TrLITR-types (ENSTRUG00000030157 and ENSTRUG00000027550) also exist in the fugu genome with positively charged arginine residues in their TMs (see "e" and "f" in Fig. 5.4D).

5.2.3 Identification of classical FcR-like sequences in the goldfish, zebrafish, and channel catfish genomes

Beyond *litrs*, my genomic surveys also uncovered a total of six sequences with Ig-like domains that are more closely related with the Ig-like domains of the various mammalian classical *fcrs* (Fig. 5.6). Specifically, I identified an *fcr*-like sequence (ENSCARG00000011633, marked with asterisk) on goldfish Chr 24 (Fig. 5.4A), two *fcr*-like sequences on zebrafish Chr 24 (si:ch1073-66l23.1 and zgc:154125, marked with asterisks in Fig. 5.4B), and one classical *fcr*-like sequence on channel catfish Chr 20 (ENSIPUG00000005005, marked with asterisk in Fig. 5.4C). ENSCARG00000011633 is a putative activating receptor bearing multiple ITAMs in its CYT and it has two Ig-like domains that are distantly related to the gold and blue domain-types of the teleost LITRs. The zebrafish zgc:154125 shares ~ 57% overall amino acid sequence similarity with the goldfish ENSCARG00000011633, and it contains two Ig-like domains that are also distantly related to the gold and blue domain-types found among the various teleost LITRs. Structurally, zgc:154125 resembles an ambiguous receptor-type bearing no recognizable signaling motifs. The zebrafish si:ch1073-66l23.1 shares ~ 82% amino acid sequence similarity with zgc:154125 and its putative function is unknown as the sequence has a truncated CYT region. Channel catfish ENSIPUG00000005005 has three Ig-like domains, which are distantly related to the blue domain-type of the teleost LITRs, and its amino acid sequence matches the previously described IpFcR1 protein that was shown to bind catfish IgM (Stafford, Wilson, et al., 2006). I also identified two unplaced goldfish FcR-like sequences (ENSCARG00000034619 and ENSCARG00000032136, marked with asterisks in Fig. 5.2) in the genome database.

While these teleost FcR-like receptors are distinct from the LITR family, their Ig-like domains are distantly related to those found among the LITRs. However, all the teleost FcR-like receptors are located on separate Chrs from the *litrs* and do not appear to be members of an extended gene family. The gold D1 of ENSCARG00000011633 (marked with an asterisk in

Fig. 5.4A) shares only 28% amino acid sequence similarity with the gold D1 of CaLITR2 (Fig. 5.5), whereas the blue D2 of ENSCARG00000011633 shares 38% sequence similarity with the blue D4 of CaLITR2. Another major distinction observed between the teleost FcR-like receptors and LITR family members is that the FcR-like receptor CYT regions contain bonafide ITAMs instead of the ITAM-like motifs sequences often found in the CYTs of putative stimulatory LITR-types. For example, ENSCARG00000011633 has five ITAMs (green circles; Fig. 5.4A) in its CYT region and ENSCARG00000034619 (marked with asterisk in Fig. 5.2) has three bona-fide ITAMs present in its CYT region. Comparatively, only one of the LITR sequences (ENSCARG00000050887; Fig. 5.4A) contains a true ITAM motif. Interestingly, stimulatory FcRs in mammals (i.e., FcγRIIA and FcγRIIC; (Gillis et al., 2014)) also contain bona-fide ITAMs, indicating that the preferential use of ITAMs may be a conserved feature shared by the teleost FcR-like sequences and the mammalian FcRs. On the other hand, the ITAM-like sequences found among representative teleost LITR-types are also a distinguishing feature shared among several of the human FCRLs (Li et al., 2014).

5.2.4 Teleost *litrs* display conserved synteny with amphibian and mammalian *fcrls*

As described earlier, the goldfish *litr* genomic cluster located on Chr 7 is linked to a group of *litr*-unrelated genes (*arhgef11*, *vangl2*, *myadm*, and *cd2*) and this linkage relationship was also observed in the zebrafish *litr* genomic cluster on Chr 7, two of the channel catfish *litr* genomic clusters on Chr 7, and the small *litr* genomic cluster on the fugu Chr 8. These conserved syntenic *litr* genomic regions are all highlighted with blue circles on Fig. 5.7, which are located next to the series of *litr*-unrelated genes on the different teleost Chrs.

With the establishment of the conserved syntenic *litr* genomic regions in the teleost fishes, I then investigated if *arhgef11*, *vangl2*, *myadm*, and *cd2* are also linked to the *fcrl* genomic regions present in the tropical clawed frog (Xenopus_tropicalis_v9.1 assembly), chicken (GRCg6a assembly), mouse (GRCm38 assembly), and human (GRCh38 assembly) genomes. As shown in Fig. 5.7, genes related to teleost *cd2*, *vangl2*, and *arhgef11* genes are also linked (< 1 million base pairs apart) to *fcrl* gene clusters in the other representative vertebrate genomes with the unique exception of chicken. Specifically, BLAST searches (BLASTP) of the tropical clawed frog Ensembl genome database using the previously described XFL sequence (AY293305.1; (Guselnikov et al., 2008)) as a query, identified two large *fcrl* genomic clusters on Chr 8 (highlighted as blue and gray clusters; Fig. 5.7). Interestingly, the blue cluster of Xenopus *fcrls* is linked to four Xenopus SLAM family genes, *vangl2*, and *arghef11*. This linkage relationship mirrors what I observed for selected teleost *litr* genomic clusters, supporting that these are likely to be conserved syntenic regions between teleost fish and frogs (Fig. 5.7). The other identified tropical clawed frog *fcrl* cluster identified on Chr 8 (highlighted in gray; Fig. 5.7) is located at a distance from the *fcrl* cluster that is linked with the SLAM family genes, *vangl2*, and *arghef11*, suggesting that this region of amphibian *fcrls* is present within a non-conserved syntenic region.

Consistent with previous reports (Fayngerts et al., 2007; Taylor et al., 2007), the FCRL repertoire in chickens is significantly reduced, and this is likely due to the reported massive loss of protein-coding genes in the chicken relative to mammals (Hughes & Friedman, 2008). However, in addition to the previously characterized chFCR/L/FCRL4 gene (Taylor et al., 2007) found on Chr 25, a second *fcrl* gene (ENSGALG00000054978) was also identified on the same Chr at a location remote from chFCR/L (Fig. 5.7). Interestingly, the only two *fcrl* genes in the

chicken genome are located on the same Chr as the SLAM family, *Arhgef11*, and *Vangl2* genes; therefore, the remoteness of the chicken *fcrls* from these genes might be due to the loss of the ancestral chicken *fcrl* gene clusters.

Examination of the mouse Ensembl genome database shows that mouse *fcrls* are located on Chr 1 and Chr 3 (Fig. 5.7), which is consistent with previous findings (Li et al., 2014; Maltais et al., 2006). Specifically, *fcrlb*, *fcrla*, *fcer1a*, *fcrl6*, and a small classical FcR genomic cluster (highlighted blue; Fig. 5.7) are present on the mouse Chr 1 and are flanked by nine CD2 superfamily/SLAM family genes (*cd244*, *ly9*, *slamf7*, *cd48*, *slamf1*, *cd84*, *slamf6*, *slamf9*, and *slamf8*) and *vangl2*, whereas the other *fcrl* cluster on mouse Chr 3 (highlighted blue; Fig. 5.7) is positioned next to a single *arhgef11* gene (Fig. 5.7). These results indicate that the mouse *fcr* cluster (along with the four *fcrl*s) on Chr 1, and the *fcrl* cluster on Chr 3 both share conserved synteny with the tropical clawed frog *fcrl* cluster and the various *litr* clusters identified in teleost fish.

When compared to the mouse FCR loci on Chr 1 and Chr 3, the human *fcer1a*, *fcrl6*, *fcrla*, and *fcrlb* genes are located next to nine human CD2 superfamily/SLAM family genes (*cd244*, *ly9*, *slamf7*, *cd48*, *slamf1*, *cd84*, *slamf6*, *slamf9*, and *slamf8*) and *vangl2* (Fig. 5.7). Similar to the mouse FCR locus, a group of human *fcrls* are also positioned next to *arhgef11*. Therefore, the human FCR loci share conserved synteny with the mouse FCR loci distributed on Chr1 and Chr3. The consistently observed physical linkage relationships between the *cd2* superfamily genes, *arhgef11*, *vangl2*, and the various teleost *litr* clusters and amphibian and mammalian *fcrl*/*fcr* clusters strongly suggest that these

genes originated from a complex chromosomal region in the common ancestor of teleost fishes and tetrapod that has subsequently diversified during the various vertebrate speciation events.

5.2.5 LITRs are phylogenetically related to amphibian, avian, and mammalian FCRL members

To further investigate the evolutionary relationships between teleost LITRs and FCRLs in other vertebrates, I performed phylogenetic analyses to compare the Ig-like domains of CaLITRs with the Ig-like domains of FCRLs found in the tropical clawed frog, chicken, mouse, and human. As shown in Fig. 5.8, two of the established CaLITR Ig-like domain-types (gold and blue) are related to the distal Ig-like domains (gold D1, light blue D2, and dark blue D3) found within most of the tropical clawed frog, chicken, mouse, and human FCRLs examined (Fig. 5.8). Specifically, five major Ig-like domain-types (gold, light blue, dark blue, turquoise, dark brown, and dark purple domains) are present in representative tropical clawed frog FCRLs and the majority of these XFLs share similar Ig-like domain arrangements (i.e., gold D1, light blue D2, and dark blue D3). The turquoise, dark brown, and dark purple domain-types found in snx22 (marked with asterisk; Fig. 5.8) appear to be amphibian specific as these Ig-like domains are not found in any of the other vertebrate FCRLs. Phylogenetic comparison of the individual Ig-like domains of select XFLs and the teleost LITRs clearly show the clustering of the gold domain-types of the teleost LITRs and the gold domain-types of select XFLs (Fig. 5.9). Additionally, the light blue and dark blue Ig-like domains of all representative XFLs cluster with the blue domain-type of the teleost LITRs (Fig. 5.9). Phylogenetic comparisons of the teleost Ig-like domains and those found in chicken FCRLs indicate that the chicken FCRLs also have gold, light blue, and dark blue Ig domain-types that are like the ones found in XFLs (Fig. 5.8). Chicken FCRLs also

encode an additional Ig-like domain-type, shown as the yellow ectodomain. Similar to the chicken FCRLs, representative mouse and human FCRLs have gold, light blue, dark blue, and yellow ectodomains (Fig. 5.8); however, they also have an additional Ig-like domain-type, indicated as the dark yellow domain. The dark yellow Ig-like domain-types found in the mouse and human FCRLs seem to be specific to mammals as it is not found in any of the other vertebrate FCRLs examined.

To reinforce the evolutionary relationships between the Ig-like domains of LITRs and Ig-like domains of the mammalian FCRLs, I performed additional phylogenetic analyses to evaluate if the complete extracellular domains (rather than the individual Ig-like domains) of representative LITRs also cluster with the full-length extracellular domains of representative mammalian FCRLs. Overall, my results support the individual Ig-like domain phylogenetic trees (Fig. 5.10) and clearly show that the two representative LITRs (CaLITR5 and IpLITR3) preferentially cluster with the representative mammalian FCRLs, but not with selected members of the mammalian LRC (Fig. 5.10).

5.2.6 A newly identified teleost LRC-like region does not contain *litrs*

Original phylogenetic analyses of LITR prototype cDNAs showed that they are composed of variable combinations of Ig-like domains and that some of these (i.e., the membrane-proximal domains) are distantly related to various genes found in the mammalian LRC (i.e., *lilrs*). Therefore, I hypothesized that various *litr*-types may be present in a teleost chromosomal region akin to the mammalian LRC. Therefore, to identify an LRC-like region in teleost, I used the built-in synteny program at the Ensembl Web site to compare the already established LRC genomic regions of humans, mouse, and the tropical clawed frog with the zebrafish Ensembl genome database. Using this approach, I identified a putative teleost LRC-like

genomic region located on the zebrafish Chr 16, which resembles the mammalian LRC as it contains many of the hallmark genes found in the mammalian LRC region including *ttyh1*, *leng9*, *cdc42ep5*, *rps9*, *mboat7*, *tmc4*, and *leng1* (Fig. 5.11).

After uniquely establishing that a teleost LRC-like genomic region possibly exists in zebrafish, I next examined if the teleost LRC-like genomic region contains any *litrs* and/or perhaps other *lilr*-related teleost sequences. Surprisingly, the LRC-like syntenic region on the zebrafish Chr 16 is devoid of *litrs* and/or any teleost relatives of *lilrs*, *kirs*, or other known immunoregulatory receptors-types (Fig. 5.11). I also did not identify any *nitrs* at this location. Specifically, the human *kir/lilr*-related genes are located next to a large group of LRC-unrelated genes (i.e., *ttyh1*, *leng8*, and *rps9*; Fig. 5.11) (Guselnikov & Taranin, 2019; Martin et al., 2002). Similarly, the murine *lilr* orthologs, the *pirs*, are also located next to a similar array of LRC-unrelated genes (Fig. 5.11; (Chen et al., 1999)). Additionally, the *lilr* relatives in frog (i.e., *silrs*) are tightly linked to the mammalian orthologs of *ttyh1*and *leng8* (Fig. 5.11; (Guselnikov et al., 2009; Guselnikov et al., 2010)). In chickens, CHIRs are well-known to be syntenically linked to G-protein coupled receptors (homologs found in the human LRC extended region; not shown in Fig. 5.11; (Nikolas Nikolaidis et al., 2005; Viertlboeck et al., 2005)); therefore, they are the exception among the vertebrates examined. Although the human orthologs of the LRC-flanking genes (i.e., *ttyh1*, *leng8*, and *leng9*) are present on zebrafish Chr 16, *litrs* are absent from this chromosomal region, indicating that teleost immunoregulatory receptor-types belonging to the IgSF are either lost from this syntenic LRC-like region, or they are located elsewhere in the genome. Importantly, the absence of *litrs* from the teleost LRC-like region reinforces their evolutionary connections with vertebrate FCRLs, although it is plausible that their immunoregulatory roles may still overlap with representative LRC members (Fei et al., 2016).

To investigate if select Ig-like domains found among the various LITRs are related to the Ig-like domains present in the various mammalian LRC genes, I performed detailed phylogenetic analyses by comparing the domains of the LILR homologs found in the tropical clawed frog, chicken, mouse, and humans to the Ig-like domains of LITRs. Overall, I found no evidence for phylogenetic relationships between the Ig-like domains of LITRs with those of the domains in the representative LRC members shown in Fig. 5.12. This is reinforced by the unique patterns displayed for each Ig-like domain shown, which are completely distinct from the coloured Ig-like domains used to establish LITR domain relationships with the FCRLs.

5.2.7 The spotted gar genome lacks *lilr*/*kir*-related genes

To examine if the lack of *kir*/*lilr*-related genes is possibly a teleost lineage-specific phenomenon, I searched the Ensembl genome database of the spotted gar (*Lepisosteus oculatus*; LepOcu1 assembly), a representative basal ray-finned fish. As previously published (Wcisel et al., 2017), using CaLITR2 and human FCRL5 amino acids as search queries, six *fcrl*-like genes (ENSLOCG00000009857, ENSLOCG00000009867.1, ENSLOCG00000009848.1, ENSLOCG00000000344, ENSLOCG00000000629, and ENSLOCG00000000699) were identified among two different spotted gar Chrs (LG3 and LG5) as well on an unplaced scaffold (JH591510.1) (Fig. 5.13). Consistent with teleost *litrs*, two of the spotted gar *fcrl*-like genes (highlighted in blue) are closely linked (approximately 1 mb apart) to the two SLAM family genes, *arhgeff11* and *myadm*; however, the spotted gar *fcrl*-like gene cluster (highlighted in gray) on Chr LG3 is not syntenic with any of these genes (Fig. 5.13). Furthermore, all of the identified spotted gar *fcrl*-like sequences share low amino acid similarities (28 to 30%) with CaLITR2 and human FCRL5. Similar to the zebrafish, I was unable to retrieve any *lilr*/*kir* relatives from the

spotted gar genome, indicating that a loss of the *lilr*/*kir*-related genes may be a specific event that occurred in ray-finned fishes. However, additional ray-finned fish genomes (e.g., sturgeons and bichirs) should be examined to validate this claim.

5.2.8 The elephant shark genome contains *fcrl*-like and *kir*/*lilr*-related genes

To determine the absence of *lilr*-related genes in the LRC is specific to ray-finned fish, I examined the Ensembl genome database of the elephant shark, a representative cartilaginous fish, and an outgroup to the ray-finned fish. BLAST searches (BLASTP) of the elephant shark genome using the human FCRL5 and LILRB1 amino acid sequences as queries identified two *fcrl*-like sequences (ENSCMIG00000019933 and ENSCMIG00000019130) and one *lilr*-like sequence (ENSCMIG00000001801) in the genome database. Specifically, ENSCMIG00000019933 has four Ig-like domains, a neutrally charged TM, and a long cytoplasmic tail containing two ITIM and one ITAM sequences, representing a putative receptor-type with dual-signaling potentials, whereas ENSCMIG00000019130 is a putative functionally ambiguous receptor-type containing two Ig-like domains, a neutrally charged TM, and a short cytoplasmic tail devoid of signaling motifs (Fig. 5.14A). In contrast to these identified elephant shark *fcrl*-like sequences, ENSCMIG00000001801 is a putative secreted protein having only a single Ig-like domain (Fig. 5.15A). To further validate the identities of the elephant shark *fcrl*-like and *lilr*-like sequences, I performed both PSI-BLAST (NCBI Website) searches of the mammalian database (taxid: 40674) using these sequences as queries and conducted phylogenetic analyses using MEGA7. My results show that in the elephant shark these putative *fcrl*-like sequence share approximately 25–30% amino acid sequence similarities with the mammalian FCRLs and the ectodomains of these sequences appear to cluster with the

ectodomains of representative mammalian FCRLs (Fig. 5.14B). In comparison, PSI-BLAST searches of the putative elephant shark *lilr*-like sequence retrieved mostly mammalian LRC members as top hits; this receptor appears to share ~ 30–40% sequence similarities with various mammalian LRC members such as OSCAR, LILRs, and alpha-1B-glycoproteins (A1BGs). Additionally, phylogenetic analysis of the single Ig-like domain of the elephant shark *lilr*-like sequence indicates that it is indeed a *lilr*-related gene as it clusters with the chicken CHIRs (Fig. 5.15B). Interestingly, further BLAST searches of the elephant shark genome (Ensembl) using ENSCMIG00000001801 as the query identified two additional putative *lilr*-like sequences (ENSCMIG00000003331 and ENSCMIG00000003333). Specifically, ENSCMIG00000001801 shares 66.3% and 54.4% amino acid sequence similarities with ENSCMIG00000003331 and ENSCMIG00000003333, respectively. Since the elephant shark Ensembl genome database contains mostly isolated contigs, I was unable to examine the genomic organizations of the elephant shark *fcrl*-like and *lilr*-like sequences. However, the apparent presence of *lilr*-like sequences in the elephant shark genome suggests that these sequences may have been specifically lost in ray-finned fish.

5.2.9 DISCUSSION

Immunoregulatory receptors are important for maintaining physiological homeostasis by regulating the balance between immune activation and suppression to effectively eliminate foreign invaders while controlling inflammation-mediated tissue damage. Teleost LITRs belong to the IgSF and represent a large group of immunoregulatory receptors with diverse Ig-like domain configurations and signaling potentials. Although our original phylogenetic analyses provided some clues about the relatedness of LITRs to various mammalian FCR family and LRC

genes, their overall genomic organizations and syntenic relationships with immunoregulatory receptor gene families found in representative aquatic and terrestrial vertebrates were unknown.

Here, I have shown that teleost *litrs* are found in distinct gene clusters and they exist on multiple Chrs in the different teleost species examined. Specifically, a total of twenty-three *litrs* were distributed on seven different goldfish Chrs. Additionally, three *litrs* on Chr 3 and fourteen *litrs* on Chr 7 were identified in the zebrafish. In channel catfish, twenty-five *litrs* were primarily grouped among three different clusters on Chr 7 and a single *litr* was also identified on Chr 6. Lastly, seven *litrs* were found on fugu Chr 8. I also identified sixteen different unplaced goldfish *litr* contigs and eight unplaced *litr* contigs in the channel catfish. These results emphasize the multigene nature of the LITR family and show that the number of *litrs* can vary significantly between different teleost species The variable number of *litrs* observed in the genomes of the different teleost fishes is likely the result of a combination of teleost genome duplications and subsequent lineage-specific gene losses, which is a common fate for duplicated genes.

Teleost LITRs encode five major Ig-like domain-types that are variably arranged among the different LITR members of each teleost. Consequently, each of the teleost species examined has a diverse and unique repertoire of predicted LITRs (Fig. 5.4), likely representing lineage-specific diversification due in part to different evolutionary pressures (i.e., pathogens and environments) exerted on these genes in the different species. Several of the teleost LITRs are predicted to function as putative activating or inhibitory receptor-types with highly related Ig-like domains and Ig-like domain configurations, suggesting that these receptors may have

evolved to interact with similar ligands required for stimulation, inhibition, and/or the fine-tuning of immune responses (Akkaya & Barclay, 2013).

Using a comparative genomics approach, I have shown that teleost have conserved syntenic *litr* regions that are linked to a variety of *litr*-unrelated genes including SLAM family, *arhgef11*, *vangl2*, and *myadm*. Additionally, I have also shown that non-syntenic *litr* genes/gene clusters are also present in the goldfish, zebrafish, channel catfish, and fugu. The presence of the conserved *litr* genomic regions suggests that these are homologous regions that have been preferentially selected to keep some degree of their ancestral organization due to unknown evolutionary constraints. Interestingly, genes within conserved syntenic regions are often functionally conserved (Takeda & Nakamura, 2017; Yu et al., 2001). For example, human phosphatase and tensin homolog (*pten*) and fugu *pten* both exist in conserved syntenic regions and share conserved functions as a tumor suppressor (Yu et al., 2001). In addition, mouse *pirs* and human *lilrs* share conserved synteny and feature similar immunomodulatory roles such as inhibiting axonal growth (Takeda & Nakamura, 2017). Studies have also shown that syntenically linked genes often interact with each other and share similar cis-regulatory elements (Ghanbarian & Hurst, 2015; Hurst et al., 2004; Makino & McLysaght, 2008). Based on this evidence, I speculate that the preservation of the teleost *litrs* and their neighboring genes may have been evolutionarily selected to retain their genomic organization due to functional constraints. On the other hand, *litrs* located outside of the conserved *litr* syntenic regions likely evolved from dynamic chromosomal processes (e.g., gene conversion and genomic rearrangements) and these may have divergent functions. Surprisingly, when I compared the teleost conserved syntenic *litr* regions to the *fcrl* chromosomal regions in the tropical clawed frog, chicken, mouse, and humans, homologs of the teleost *arhgef11*, *vangl2*, and *cd2* genes were

also found to be linked (< 1 million base pairs apart) to one of the *fcrl* cluster on the tropical clawed frog Chr 8 and the FCR locus (*fcrs* and *fcrls*) in mouse and humans. These results indicate that the teleost *litrs* share conserved synteny with the *fcrls*/*fcrs* found in the various vertebrates, which strongly suggests that the teleost *litrs* are distant relatives of *fcrls*.

Comparing the Ig-like domains of the teleost LITRs and the Ig-like domains of FCRLs in other vertebrates showed that distant relatives of several Ig-like domains of the teleost LITRs are present in several representative vertebrates, which further supports the common evolutionary origin of these receptors. Functionally, human FCRL4 and FCRL5 are receptors for IgA and IgG antibodies, respectively (Wilson et al., 2012). The D1 and D3 of the human FCRL5 were also demonstrated to be mainly responsible for its IgG binding activity (Franco et al., 2013) . Furthermore, the D2 of the classical FCRs (i.e., human FcγR1), which are related to the light blue domain-type of FCRLs, have also been implicated as the key domain for interacting with antibody proteins (Kiyoshi et al., 2015). Previously, the Ig-like domains of channel catfish IpFcR1 (blue-colored; Fig. 5.4C) were shown to bind to catfish IgM (Stafford, Wilson, et al., 2006). As identified relatives of FCRLs, it is possible that teleost LITR-types also interact with antibodies, but this long-standing speculation has yet to be confirmed experimentally. Complicating the matter is the fact that human FCRL6 and murine FCRL5 were also shown to interact with MHC class II and orthopoxvirus MHC class 1-like protein (OMCP), respectively (Campbell et al., 2010; Schreeder et al., 2010), and that MHC class I-binding residues were also identified in the membrane distal Ig-like domains of various IpLITR-types (Stafford et al., 2007). Therefore, although some LITRs may be the teleost relatives of mammalian FCRLs, identifying their binding partners remains a formidable challenge.

Another common theme observed among *litrs*, *fcrls*, and *lilr*-relatives is that the repertoires of these receptors seem to be contracting or expanding relative to each other. For example, I have shown that many *litrs* are present in the various teleost fishes examined; however, no obvious *lilr* homologs were found in these species. In comparison, the tropical clawed frog genome contains as many as seventy-five *fcrls* (Guselnikov et al., 2008). In stark contrast, only three *lilr* relatives, the *silrs*, were found in the frog genome (based on my study). Alternatively, chicken has more than a hundred *chirs* in its genome (Nikolas Nikolaidis et al., 2005); however, only two chicken *fcrls* were found. One hypothesis for this observed trend is that *fcrls* and *lilr* relatives may share redundant regulatory functions in the various vertebrates and some of these receptors would be preferentially selected over the others due to specific evolutionary pressures. Evidence supporting this hypothesis is the similar binding partners shared by FCRLs and LILR/LILR relatives. As previously mentioned, the human FCRLs are known to interact with both MHC-like proteins and various antibody classes (e.g., IgA and IgG; (Li et al., 2014)), whereas the Fc fragment of IgA receptor (FCAR), a human LILR related sequence, binds IgA (Bakema & van Egmond, 2011). Similarly, the immunoglobulin A FcR from cattle (bFcaR), a human FCAR homolog, also binds IgA (Morton et al., 2004). Furthermore, mouse PIRs have been shown to bind MHC class I molecules (Takai, 2005a) and despite the fact that the CHIRs belong to the chicken LRC, they actually function as variable affinity IgY receptors (Viertlboeck et al., 2007; Viertlboeck et al., 2009). Although the majority of the human FCRLs and LILR-relatives remain to be functionally characterized, the shared ability for these gene families to bind to antibodies and MHC-like molecules may imply that they have redundant regulatory functions in vertebrates. Additionally, the expansion of teleost *litrs*, amphibian *fcrls*, and avian *chirs* might be explained by gene compensation. For example, the

lack of *lilr* relatives in the different teleost may have exerted evolutionary pressures on fish to positively select for the expansion of the potentially functionally redundant *litrs*, although this is purely speculation at this time. Notably, contraction and expansions of immune genes have been observed in vertebrates. For example, the loss of MHC class II molecules in Atlantic cod coincides with a subsequent expansion of MHC class I and toll-like receptors (TLR) receptors, which may have occurred due to specific environmental pressures (Star & Jentoft, 2012).

I also showed that zebrafish Chr 16 contains orthologs of many signature genes found in the LRC regions of other vertebrates, including humans, supporting the notion that teleost fish contain an LRC-like genomic region. The lack of *litrs* and/or *lilr*-related sequences in the identified zebrafish LRC-like region, combined with the fact that the Ig-like domains of LITRs are not phylogenetically related with the Ig-like domains of representative LILRs or LILR-related genes, further emphasizes that teleost LITRs are likely homologs of FCRLs and not LILR relatives. Additionally, the absence of *lilr*-like genes in the spotted gar genome and their presence in the elephant shark genome suggest that the *lilr*-relatives may have been lost in the ray-finned fish lineage.

In summary, I have presented evidence supporting that LITRs are likely homologs of vertebrate FCRLs, based on their shared conserved synteny and phylogenetic relationships. The data in this chapter provides a comprehensive overview of the various potential LITR-types and their signaling capabilities across different teleost species. Notably, additional to the identified conserved syntenic *calitr* cluster on goldfish Chr7, I have also located multiple non-conserved syntenic *calitr* regions on other goldfish Chrs (e.g., Chr 3, Chr 47, LG28B). This raises the possibility that the *calitr* genes on different Chrs may be regulated by distinct cis and/or trans-

regulatory elements, potentially leading to differential expression, a topic that will be further explored in the next chapter.

(A)

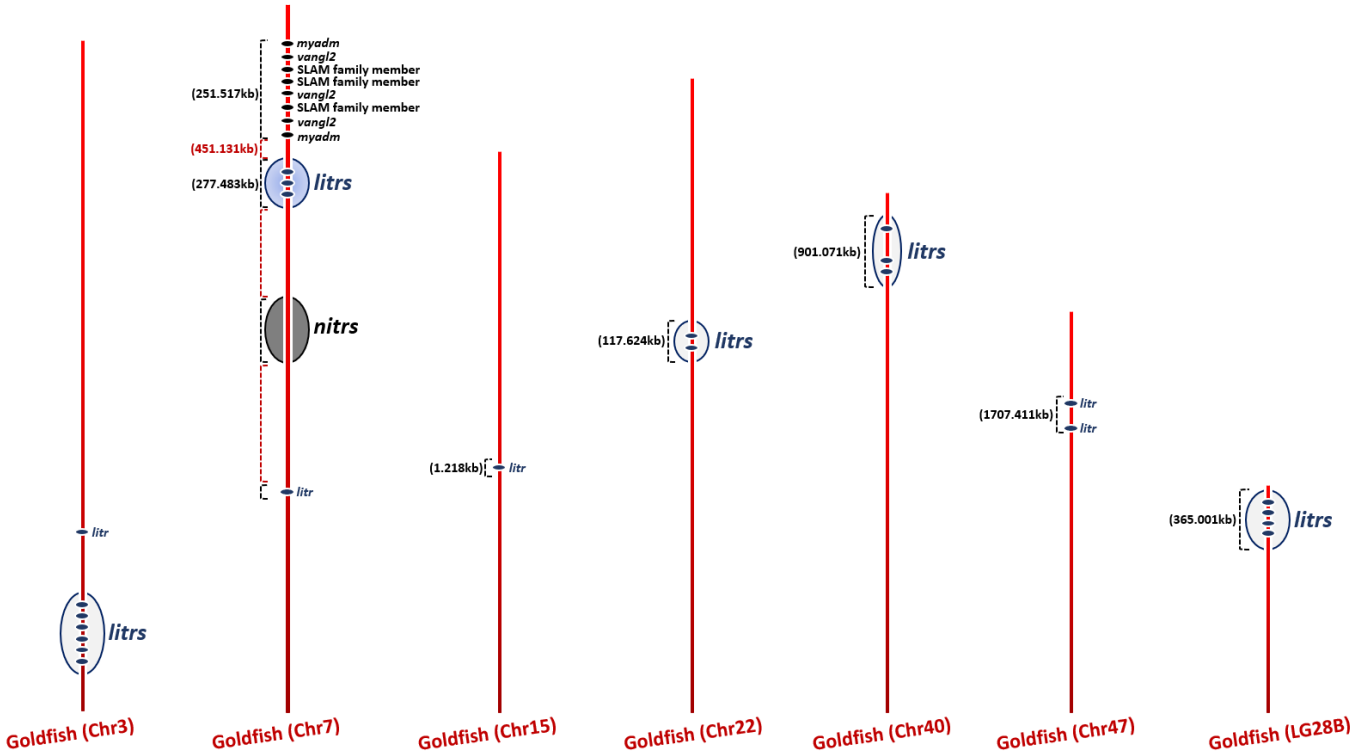
myadm
vangl2
SLAM family member
SLAM family member
vangl2
SLAM family member
vangl2
myadm
(251.517kb)
(451.131kb)
(277.483kb)
litrs
nitrs
litr
litr
litrs
Goldfish (Chr3)
Goldfish (Chr7)
(1.218kb)
litr
Goldfish (Chr15)
(117.624kb)
litrs
Goldfish (Chr22)
(901.071kb)
litrs
Goldfish (Chr40)
(1707.411kb)
litr
litr
Goldfish (Chr47)
(365.001kb)
litrs
Goldfish (LG28B)

(B)

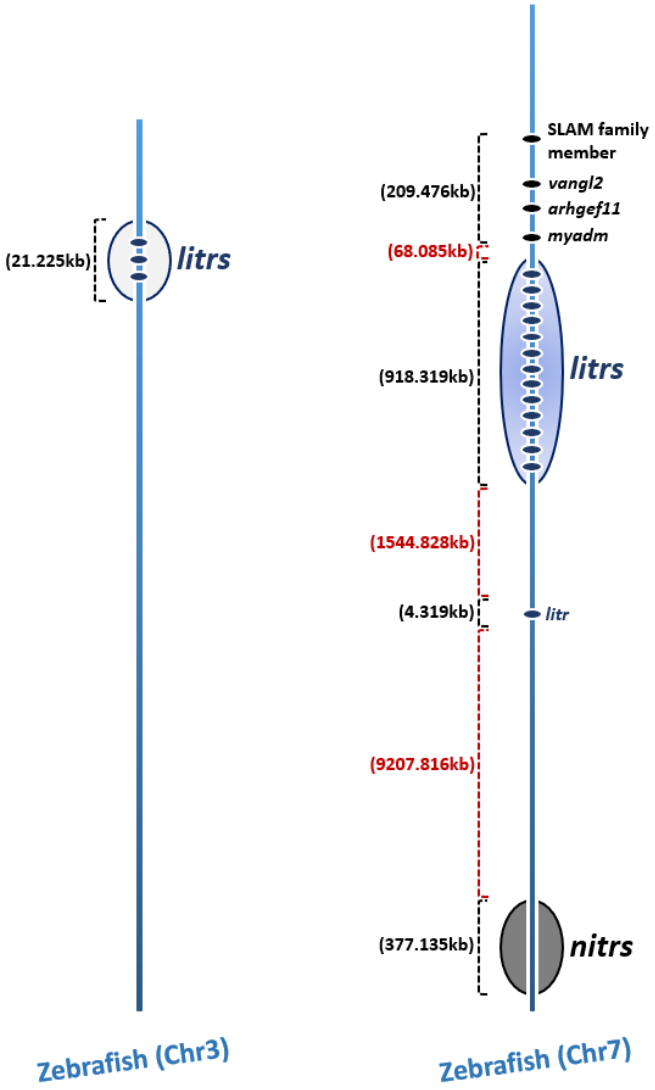
(21.225kb)
litrs
Zebrafish (Chr3)
(209.476kb)
SLAM family member
vangl2
arhgef11
myadm
(68.085kb)
(918.319kb)
litrs
(1544.828kb)
(4.319kb)
litr
(9207.816kb)
(377.135kb)
nitrs
Zebrafish (Chr7)

(C)

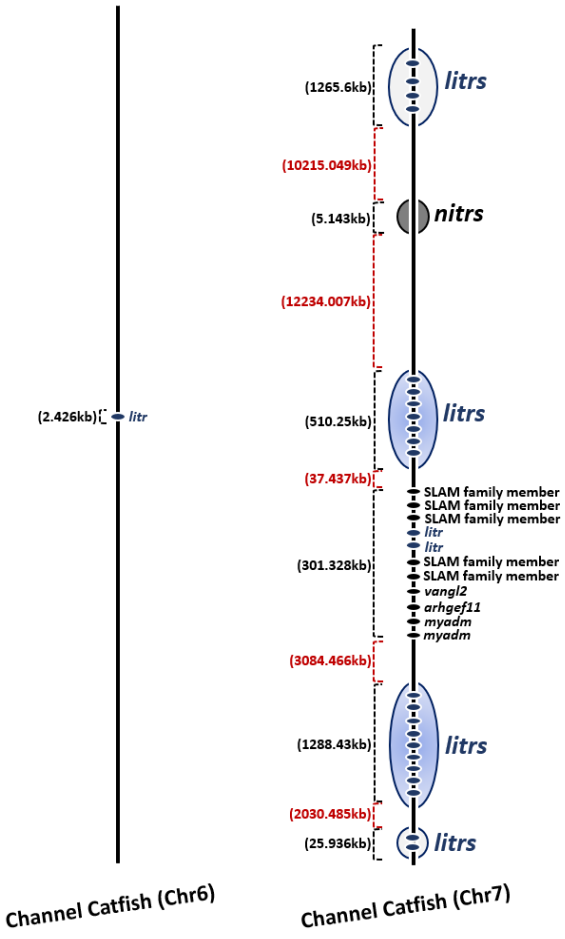
(2.426kb)
litr
Channel Catfish (Chr6)
(1265.6kb)
litrs
(10215.049kb)
(5.143kb)
nitrs
(12234.007kb)
(510.25kb)
litrs
(37.437kb)
SLAM family member
SLAM family member
SLAM family member
litr
litr
(301.328kb)
SLAM family member
SLAM family member
vangl2
arhgef11
myadm
myadm
(3084.466kb)
(1288.43kb)
litrs
(2030.485kb)
(25.936kb)
litrs
Channel Catfish (Chr7)

(D)

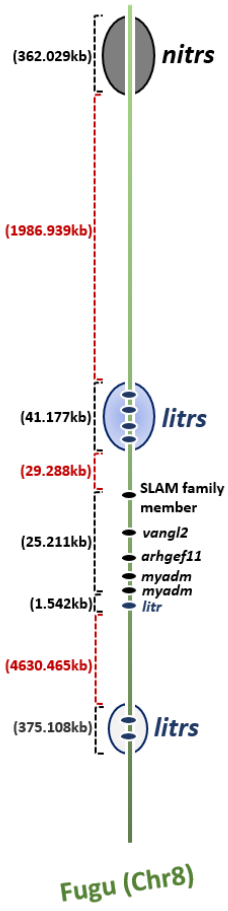

Figure 5.1. Genomic organization of *litrs* and their neighboring genes on various Chrs in the goldfish (A), zebrafish (B), channel catfish (C), and fugu (D). *litr* clusters (syntenic *litr* regions) that are linked to the SLAM family, *vangl2*, *arhgef11*, and *myadm* genes are circled and highlighted in blue in each teleost, whereas the distantly located *litr* clusters are circled and highlighted in light grey. The size (kilobases (kb)) of each gene and gene cluster is indicated to the left of each diagram and is illustrated using a black dashed bracket. Genomic distances between genes and gene clusters are illustrated using red dashed brackets. For each teleost Chr, the *nitr* cluster is circled and highlighted in dark gray.

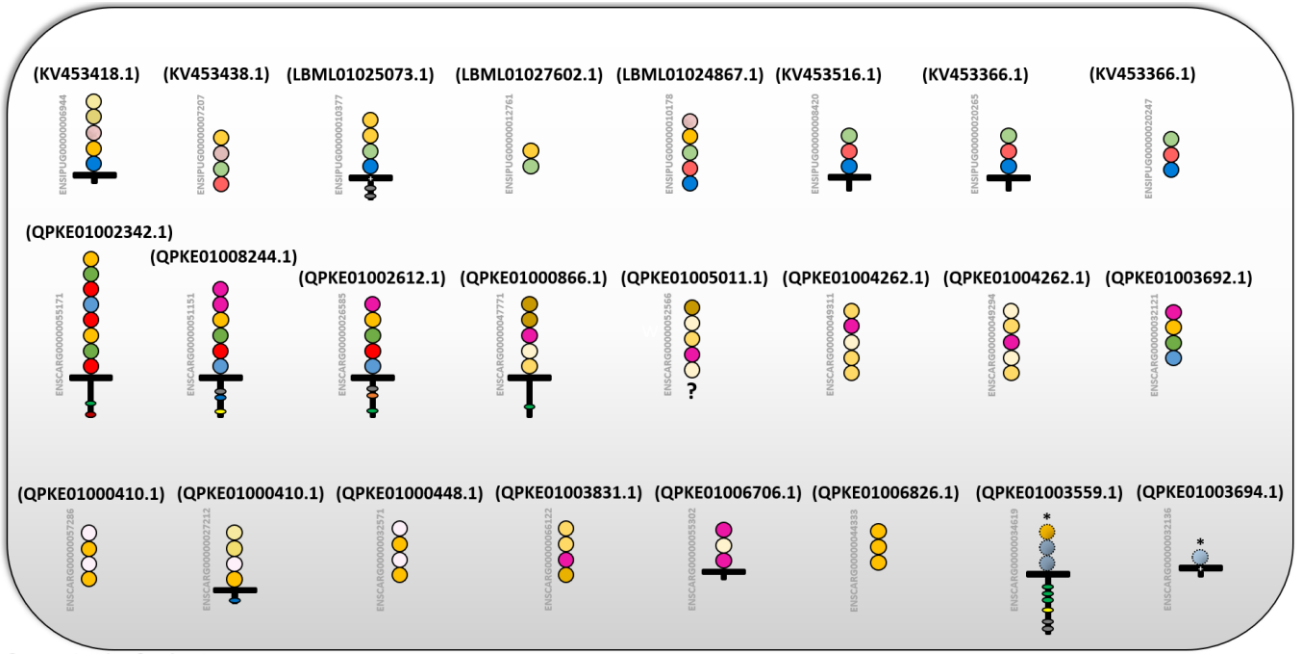

Figure 5.2. Schematic representations of unplaced LITR contigs in the channel catfish and goldfish genomes. Receptors in the first row represent the LITR sequences found in the channel catfish. The goldfish LITRs are placed in the second and third rows. The goldfish classical-FcR-like sequences have dashed Ig-like domains (circles) and are also marked with asterisks. The Ig-like domains, TMs, and CYT regions were predicted using SMART. Individual Ig-like domains are coloured according to their phylogenetic relatedness with CaLITR1-5. The gene name is placed to the left of each receptor. The name of the primary assembly is placed at the top of each receptor. Positively charged amino acid residues in the TMs are designated by the white plus sign. Gray circles in the CYTs represent the endocytosis signal. ITAM/ITAM-like sequences in the CYTs are indicated by green circles. Red circles in the CYTs represent ITIM/ITIM-like sequences. Non-canonical tyrosine-based motifs in the CYTs are designated by yellow circles. Orange circles in the CYTs represent Nck recruitment motifs. STAT recruitment motifs in the CYTs are represented by blue circles.

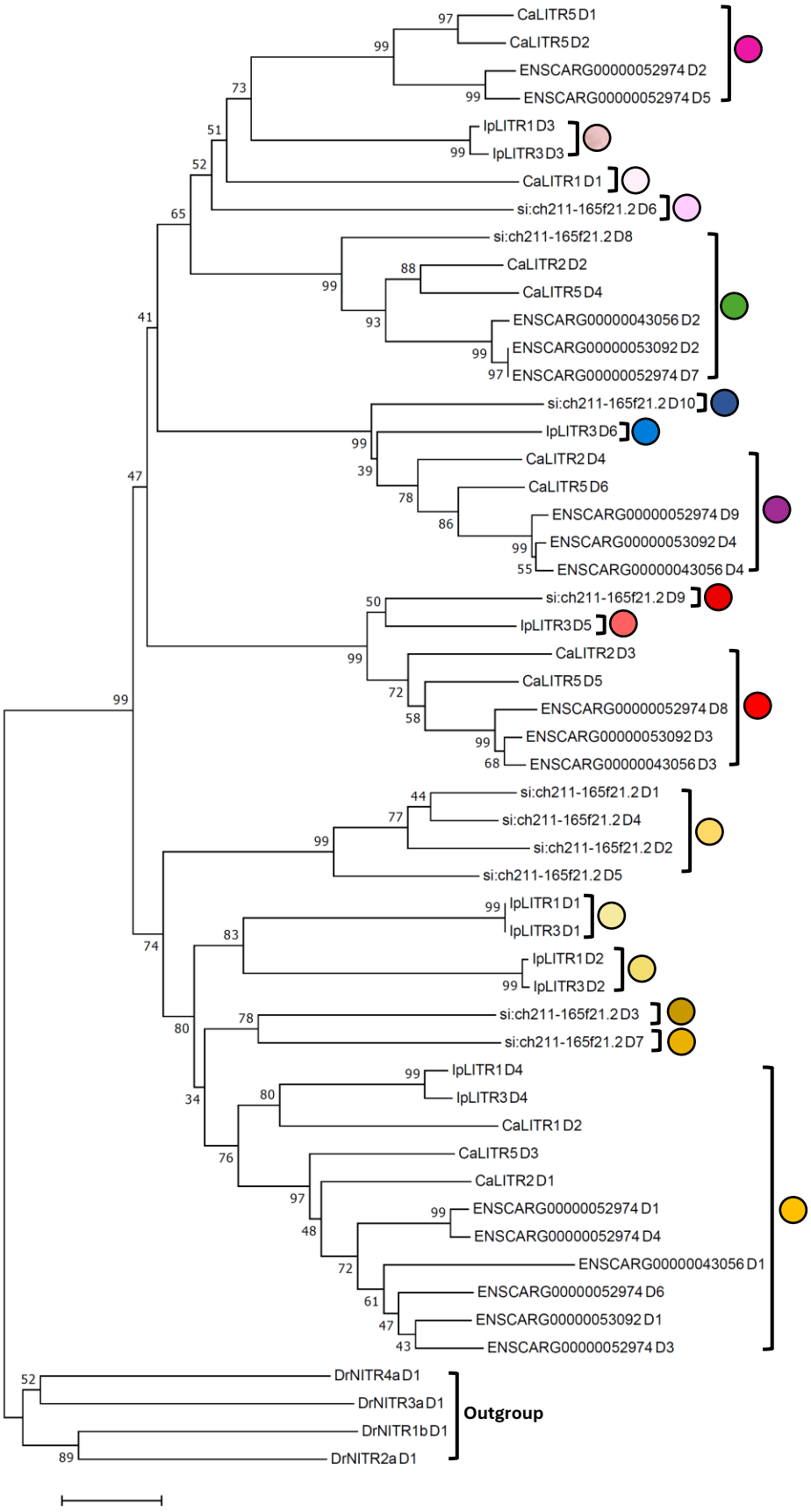
CaLITR5 D1
CaLITR5 D2
ENSCARG00000052974 D2
ENSCARG00000052974 D5
lpLITR1 D3
lpLITR3 D3
CaLITR1 D1
si:ch211-165f21.2 D6
si:ch211-165f21.2 D8
CaLITR2 D2
CaLITR5 D4
ENSCARG00000043056 D2
ENSCARG00000053092 D2
ENSCARG00000052974 D7
si:ch211-165f21.2 D10
lpLITR3 D6
CaLITR2 D4
CaLITR5 D6
ENSCARG00000052974 D9
ENSCARG00000053092 D4
ENSCARG00000043056 D4
si:ch211-165f21.2 D9
lpLITR3 D5
CaLITR2 D3
CaLITR5 D5
ENSCARG00000052974 D8
ENSCARG00000053092 D3
ENSCARG00000043056 D3
si:ch211-165f21.2 D1
si:ch211-165f21.2 D4
si:ch211-165f21.2 D2
si:ch211-165f21.2 D5
lpLITR1 D1
lpLITR3 D1
lpLITR1 D2
lpLITR3 D2
si:ch211-165f21.2 D3
si:ch211-165f21.2 D7
lpLITR1 D4
lpLITR3 D4
CaLITR1 D2
CaLITR5 D3
CaLITR2 D1
ENSCARG00000052974 D1
ENSCARG00000052974 D4
ENSCARG00000043056 D1
ENSCARG00000052974 D6
ENSCARG00000053092 D1
ENSCARG00000052974 D3
DrNITR4a D1
DrNITR3a D1
DrNITR1b D1
DrNITR2a D1
Outgroup

Figure 5.3. Phylogenetic analysis comparing the individual Ig-like domains of CaLITRs and the Ig-like domains of IpLITRs and DrLITRs. The NJ tree with pairwise deletions was constructed using MEGA v7. Numbers at the nodes indicate the level of bootstrap support based on 10000 replicates. Branch lengths represent distance, and the scale bar indicates the number of amino acid substitutions per site.

(A)

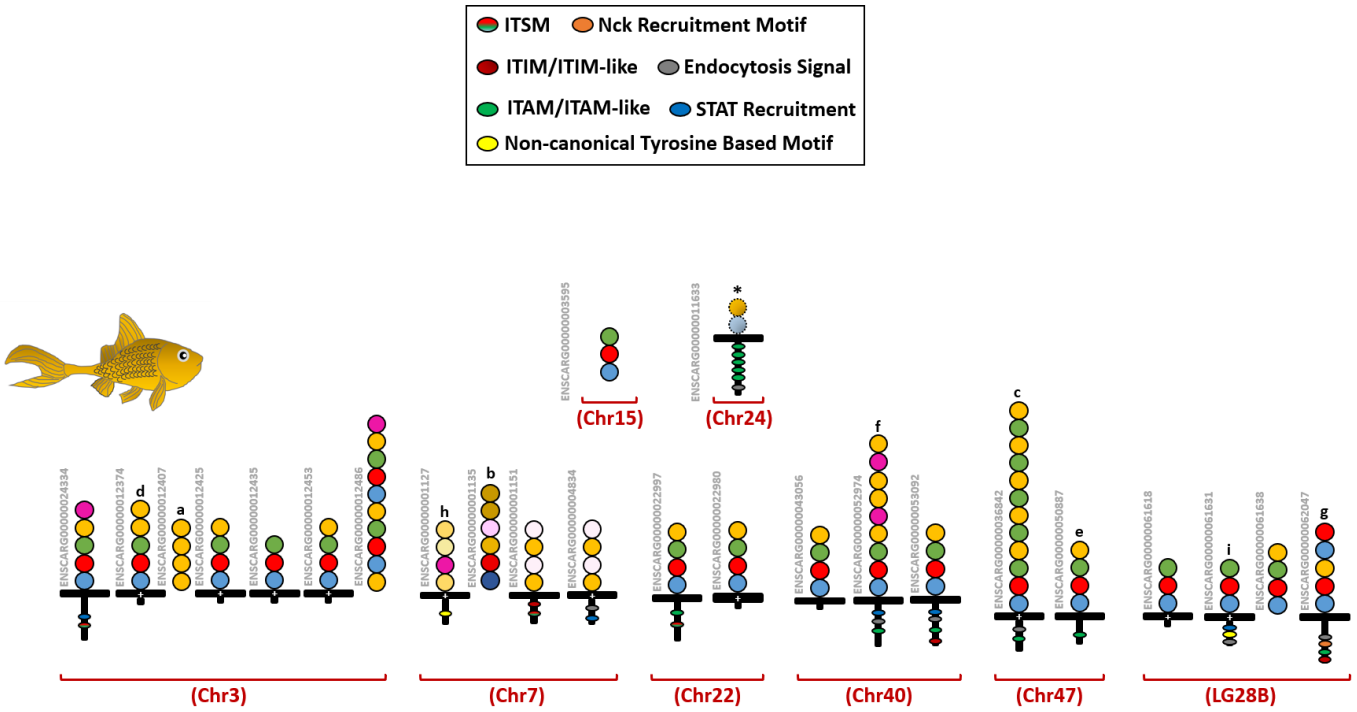
ITSM
Nck Recruitment Motif
ITIM/ITIM-like
Endocytosis Signal
ITAM/ITAM-like
STAT Recruitment
Non-canonical Tyrosine Based Motif
(Chr15)
(Chr24)
(Chr3)
(Chr7)
(Chr22)
(Chr40)
(Chr47)
(LG28B)

(B)

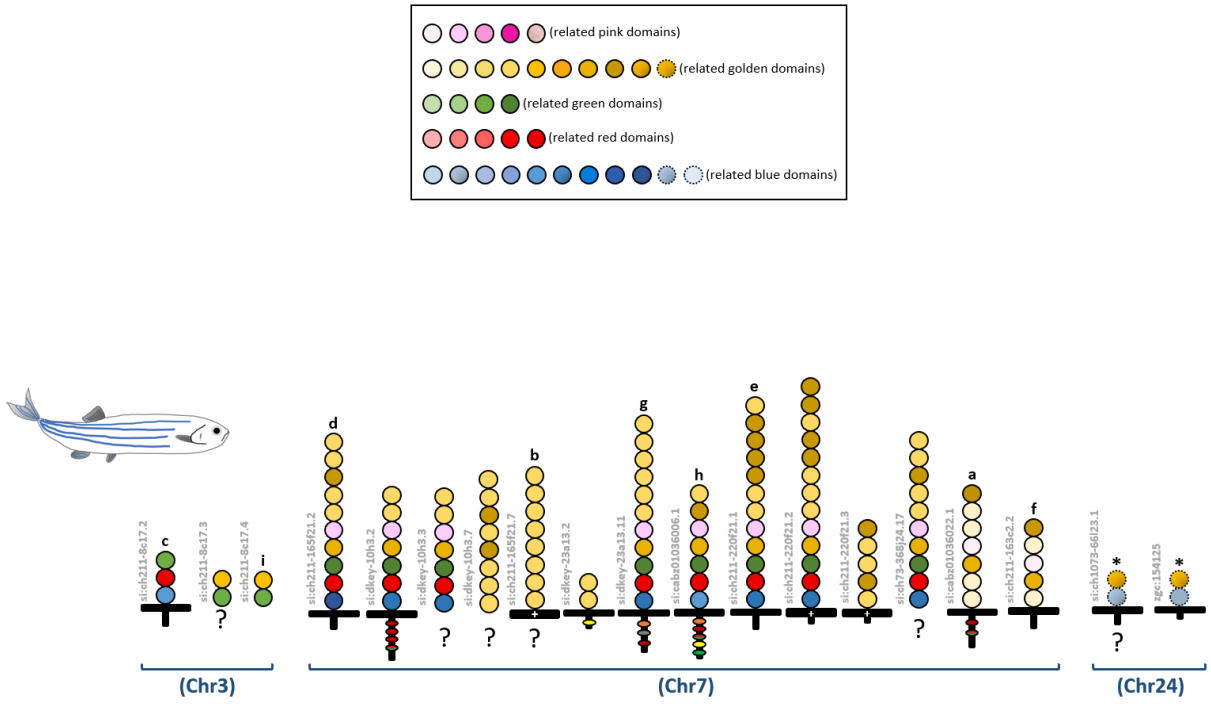
(related pink domains)
(related golden domains)
(related green domains)
(related red domains)
(related blue domains)
si:ch211-8c17.2
si:ch211-8c17.3
si:ch211-8c17.4
si:ch211-165f21.2
si:dkey-10h3.2
si:dkey-10h3.3
si:dkey-10h3.7
si:ch211-165f21.7
si:dkey-23a13.2
si:dkey-23a13.11
si:cabz01036006.1
si:ch211-220f21.1
si:ch211-220f21.2
si:ch211-220f21.3
si:ch73-368j24.17
si:cabz01036022.1
si:ch211-163e2.2
si:ch1073-66i23.1
zgc:154125
(Chr3)
(Chr7)
(Chr24)

(C)

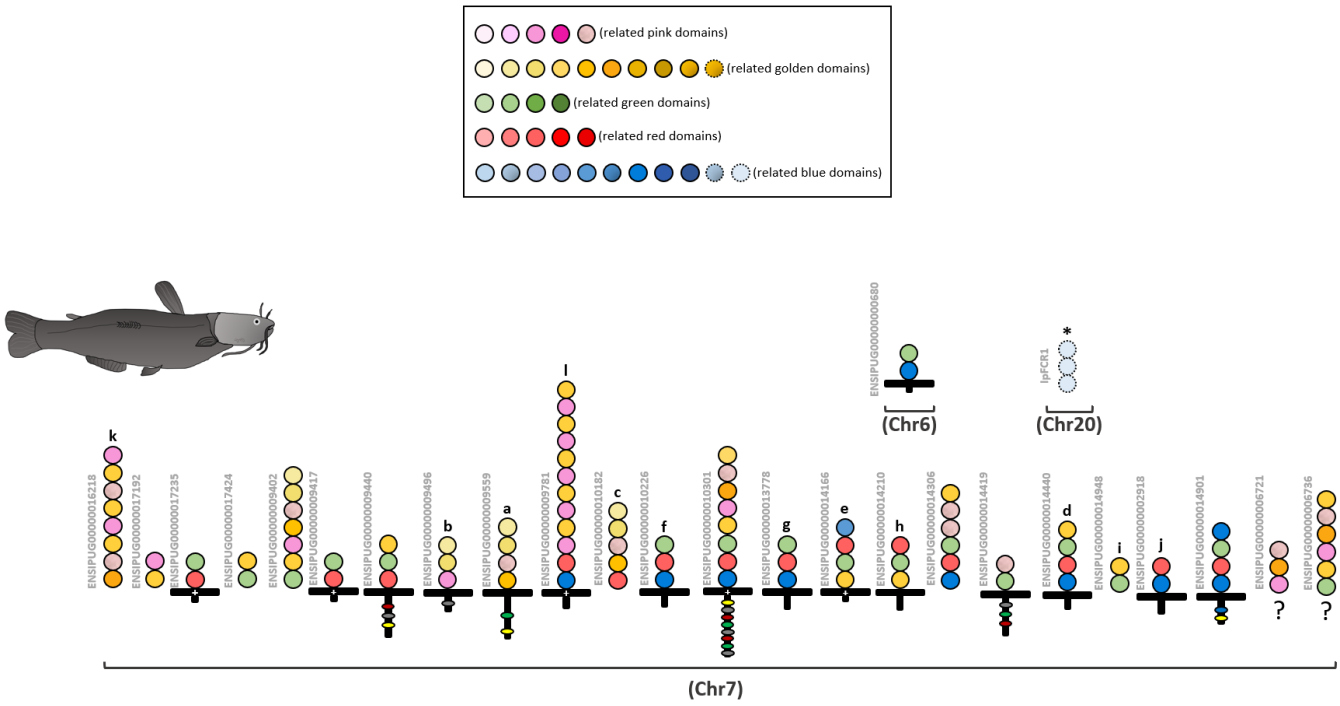
(related pink domains)
(related golden domains)
(related green domains)
(related red domains)
(related blue domains)
ENSIPUG00000000680
(Chr6)
IpFCR1
*
(Chr20)
k
l
c
b
a
f
e
h
d
i
j
?
?
(Chr7)

(D)

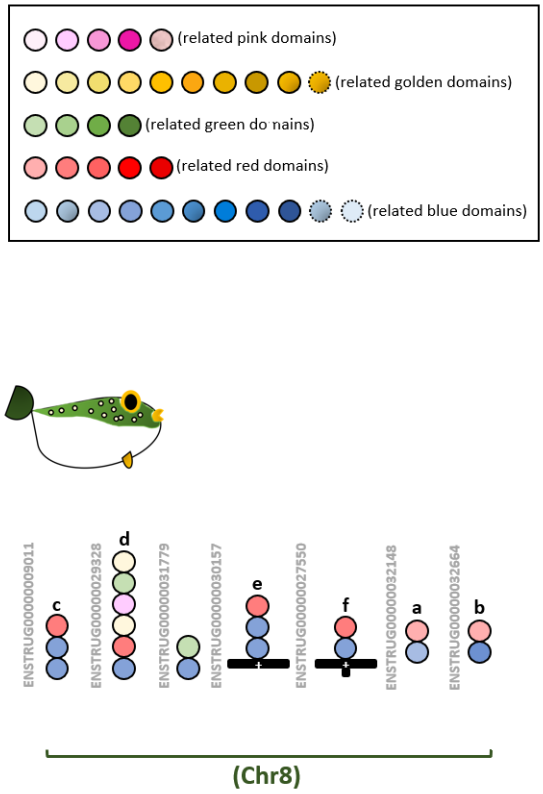

Figure 5.4. Graphical representations of the diversity of Ig-like domains and signaling potentials of putative LITR and classical FcR-like proteins in the goldfish (A), zebrafish (B), channel catfish (C), and fugu genomes (D). Colorations of the Ig-like domains reflect their phylogenetic relatedness with one another (the amino acid sequences of goldfish LITRs are used as a basis of comparison). Phylogenetic analyses of all of the individual Ig-like domains of LITRs were conducted using MEGA7 and a representative tree is shown in Fig. 5.3. The Ig-like domains of the predicted teleost classical FCR-like proteins are depicted as dashed circles and are color-coded according to phylogenetic relatedness to those of CaLITRs and IpLITRs. The positive signs in the TMs of LITRs represent positively charged amino acid residues. Partial sequences are labeled with question marks. All of the predicted sequences presented in this figure are based on the current genomic annotations (Ensembl release 100, April 2020) at the Ensembl Website, and their Ensembl gene names are placed to the left of each putative protein (IpFCR1 = ENSIPUG00000005005). The signaling motif legend on the top of this figure will be used consistently throughout this chapter. The letters placed above a few of the putative protein structures are genes that will be specifically mentioned in this chapter.

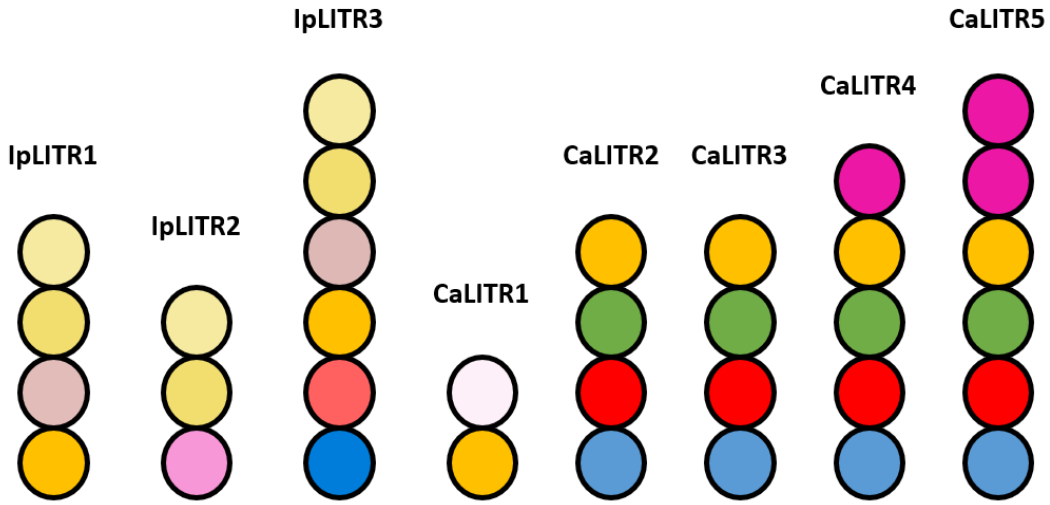

Figure 5.5. Schematic representations of the Ig-like domains of IpLITRs and CaLITRs. Individual Ig-like domains are coloured according to their phylogenetic relatedness.

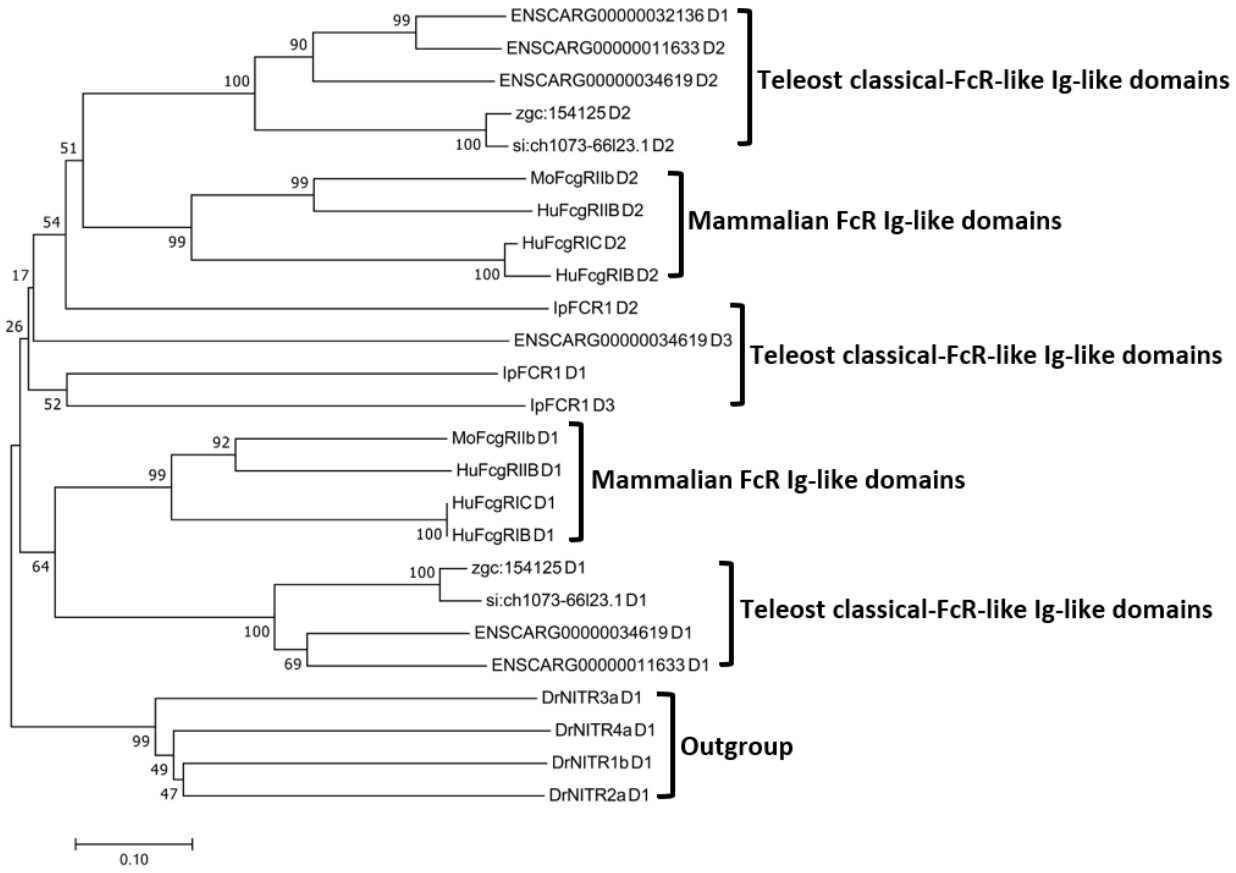

Figure 5.6. Phylogenetic comparison of the individual Ig-like domains of teleost classical-FcR-like sequences and the individual Ig-like domains of mammalian classical-FcR-like sequences. The NJ tree with pairwise deletions was constructed using MEGA v7. Numbers at the nodes indicate the level of bootstrap support based on 10000 replicates. Branch lengths represent distance, and the scale bar indicates the number of amino acid substitutions per site.

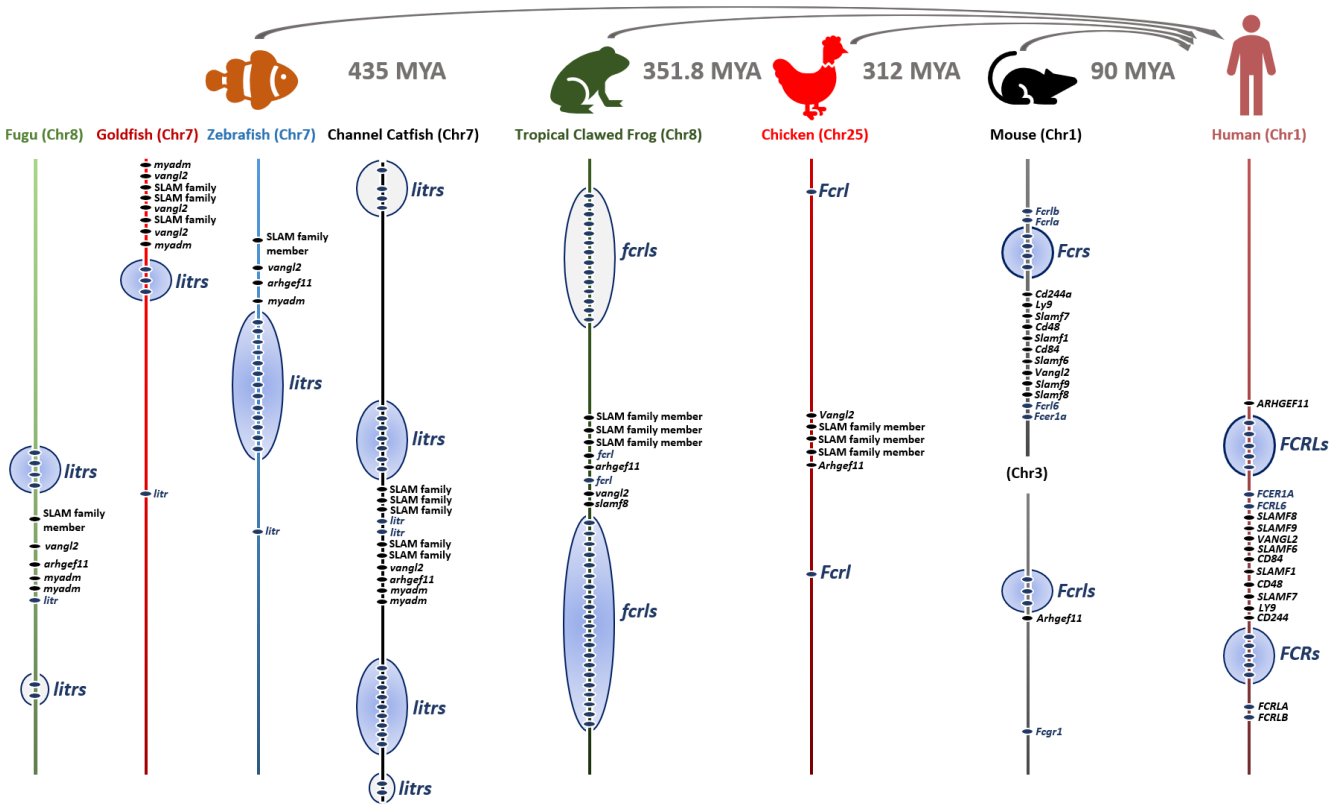

Figure 5.7. Visualization of the synteny between teleost *litrs* and the FCR family genes in representative amphibian, avian, and mammalian genomes. The conserved syntenic gene clusters are circled and colored blue, whereas the non-syntenic regions are colored gray. Evolutionary divergence times (mya) between humans and the other compared taxa were estimated using TIMETREE (http://www.timetree.org/). Information presented in this figure is based on the current genomic annotations (Ensembl release 100, April 2020) in the Ensembl database.

(A)

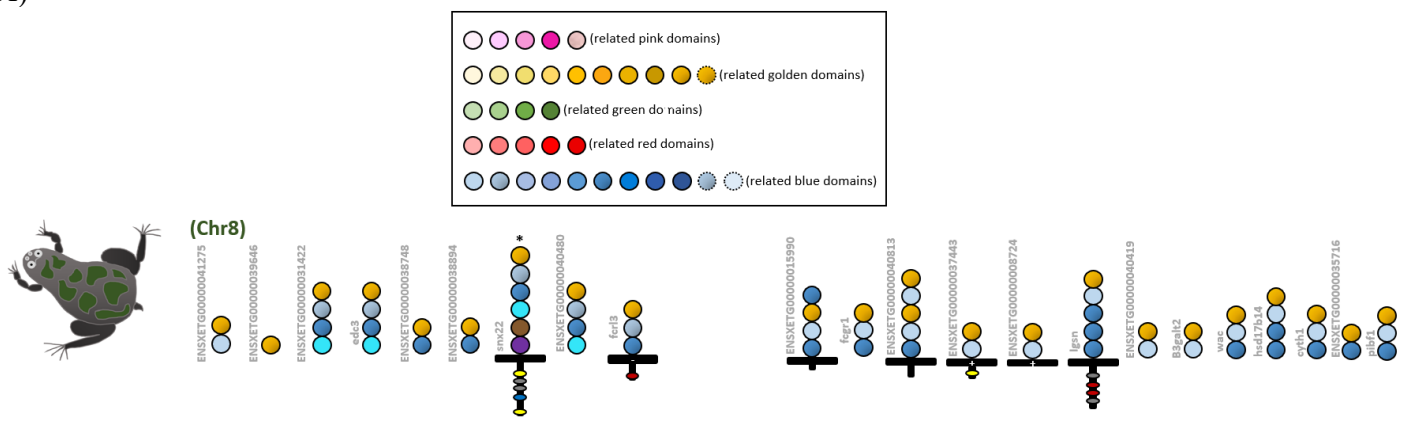
(related pink domains)
(related golden domains)
(related green do nains)
(related red domains)
(related blue domains)
(Chr8)
ENSXETG00000041275
ENSXETG00000039646
ENSXETG00000031422
cd8
ENSXETG00000038748
ENSXETG00000038894
snx22
ENSXETG00000040480
fcrl3
ENSXETG00000015990
fcgr1
ENSXETG00000040813
ENSXETG00000037443
ENSXETG00000008724
lgsn
ENSXETG00000040419
B3galt2
wac
hsd17b14
cyth1
ENSXETG00000035716
pibf1

(B)

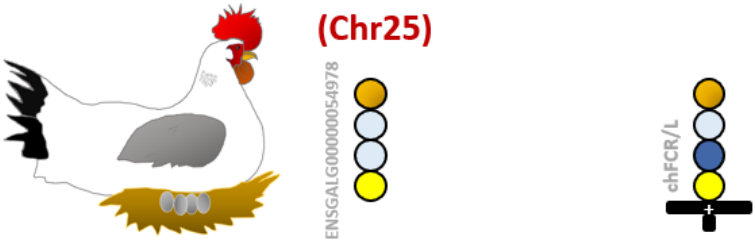
(Chr25)
ENSGALG00000054978
chFCR/L

(C)

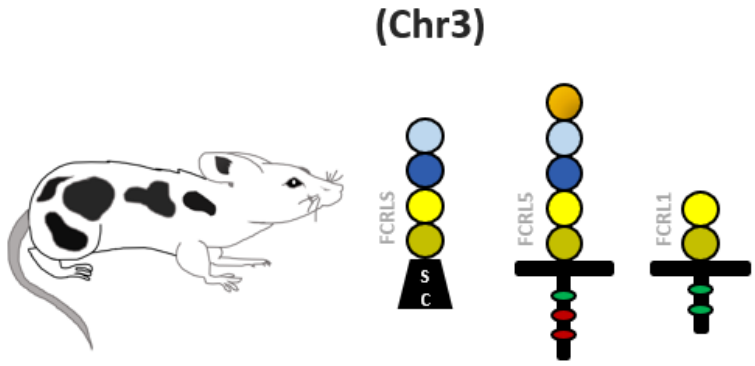
(Chr3)
FCRL5
S
C
FCRL5
FCRL1

(D)

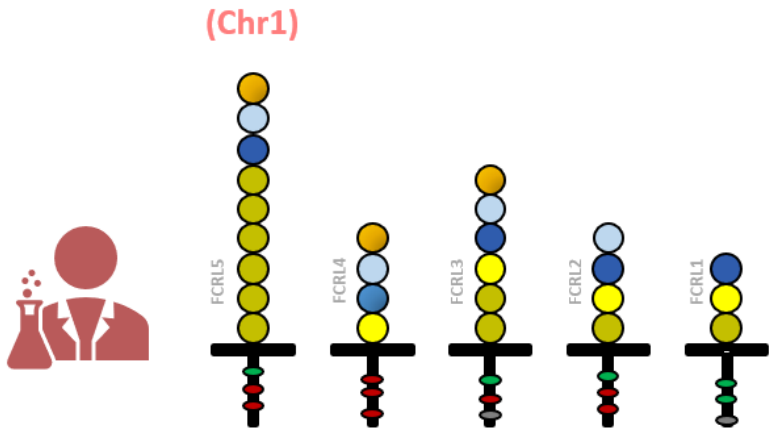

Figure 5.8. Representative FCRL molecules in the tropical clawed frog (A), chicken (B), mouse (C), and human genomes (D). The Ig-like domains of the FCRL proteins are color-coded based on their phylogenetic relatedness and a representative phylogenetic tree is shown in Fig. 5.9. All of the FCRL proteins presented in this figure are based on the current genomic annotations (Ensembl release 100, April 2020) at the Ensembl Web site and their Ensembl gene names are placed to the left of each protein (chFCR/L = FCRL4).

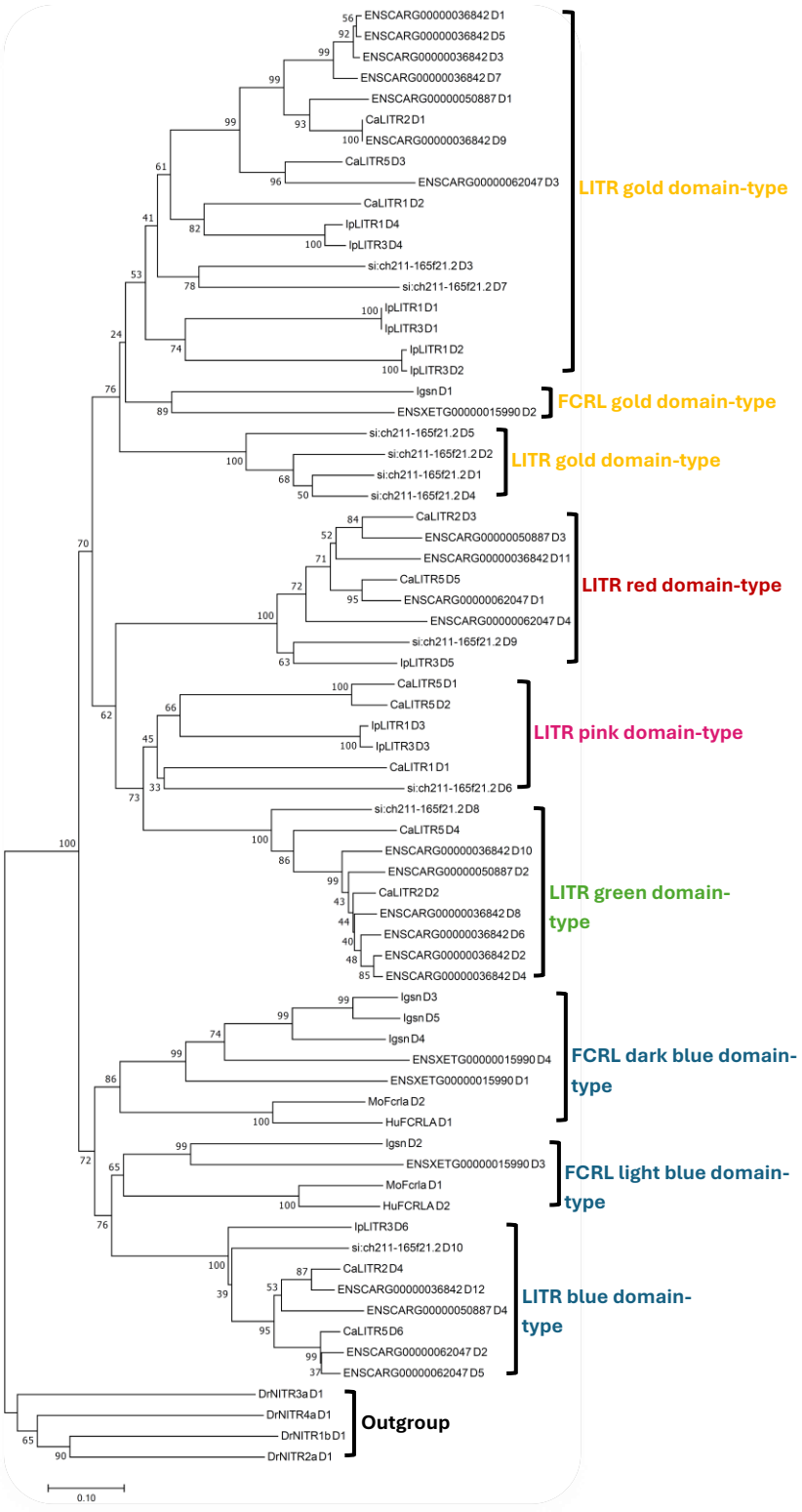

Figure 5.9. Phylogenetic comparison of the individual Ig-like domains of teleost LITRs with those of amphibian and mammalian FCRLs. The NJ tree with pairwise deletions was constructed using MEGA v7. Numbers at the nodes indicate the level of bootstrap support based

on 10000 replicates. Branch lengths represent distance, and the scale bar indicates the number of amino acid substitutions per site.

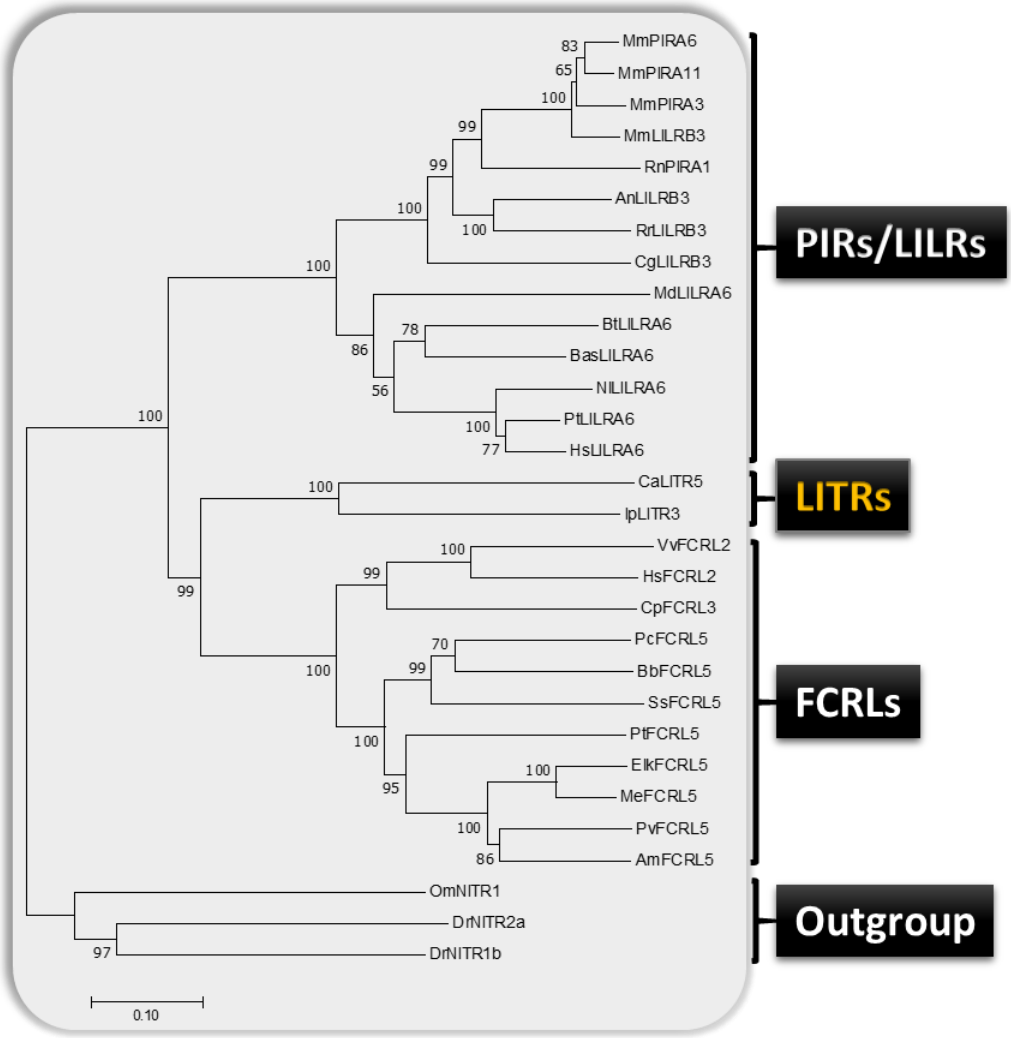

Figure 5.10. Phylogenetic analysis comparing the full-length extracellular regions of teleost LITRs and the full-length extracellular regions of mammalian FCRLs and PIRs/LILRs. The NJ tree with pairwise deletions was constructed using MEGA v7. Numbers at the nodes indicate the level of bootstrap support based on 10000 replicates. Branch lengths represent distance, and the scale bar indicates the number of amino acid substitutions per site.

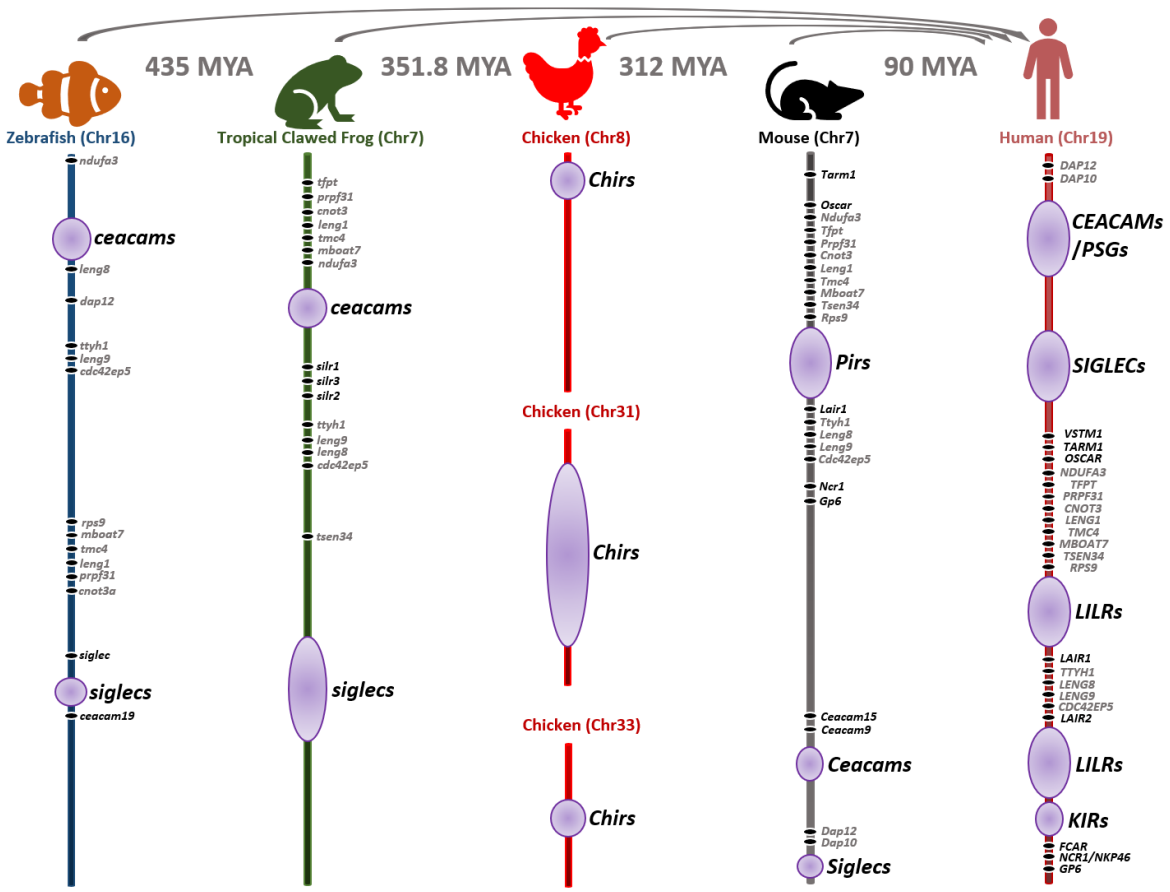

Figure 5.11.Visual representations of the LRC and LRC extended regions in the zebrafish, tropical clawed frog, chicken, mouse, and humans. Genes and gene clusters belonging to the LRC, and their evolutionary relatives are bolded and depicted as purple circles, respectively. Information presented in this figure is based on the current genomic annotations (Ensembl release 100, April 2020) in the Ensembl database. Evolutionary divergence times (mya) between humans and the other compared taxa were estimated using TIMETREE (http://www.timetree.org/).

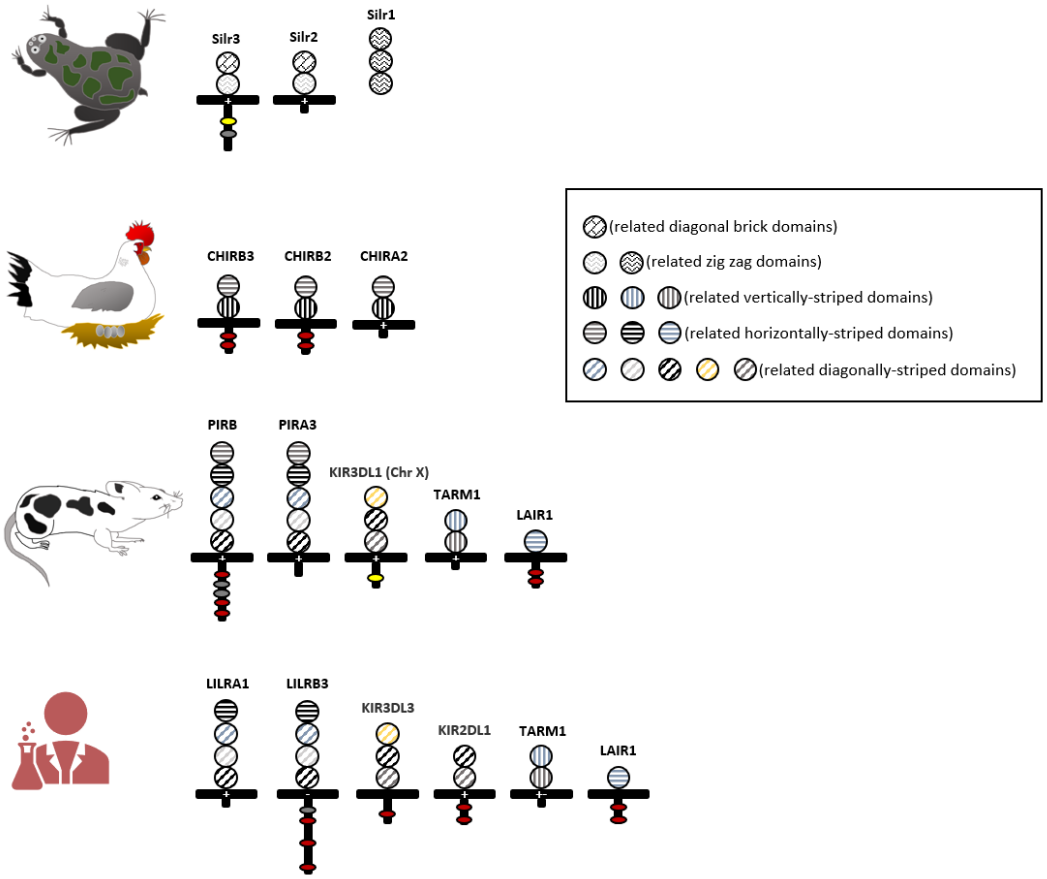

Figure 5.12. Schematic depictions of the diversity of Ig-like domains and signaling potentials of LRC proteins in the tropical clawed frog, chicken, mouse, and humans. Phylogenetic relatedness between the individual Ig-like domains of the LRC proteins is indicated by their colours and patterns. Information presented in this figure is based on the current genomic annotations (Ensembl release 100, April 2020) in the Ensembl database. The Ensembl gene names of the receptors are shown on the top (sILR3 = ENSXETG00000035217, sILR2 = ENSXETG00000032533, sILR1 = ENSXETG00000032630).

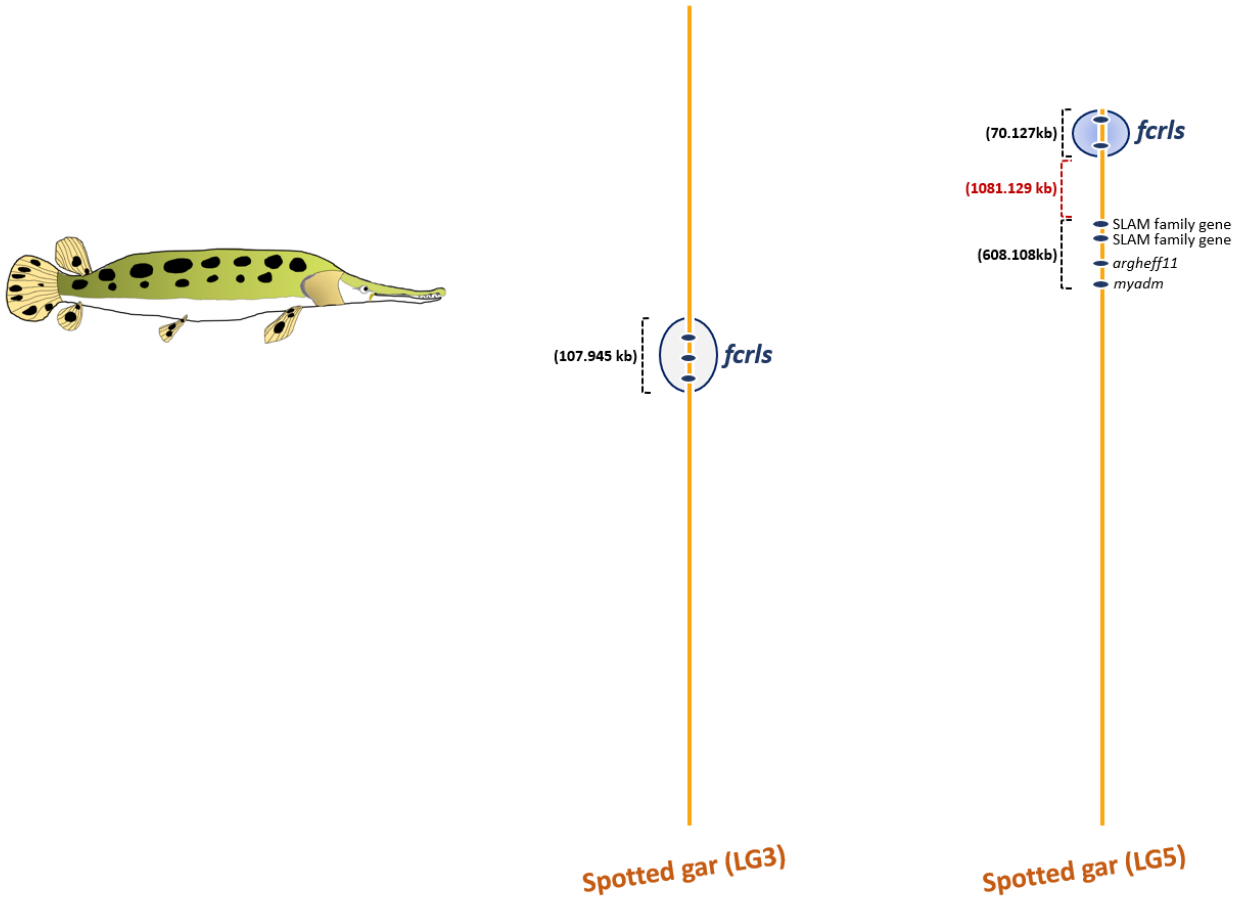

Figure 5.13. Genomic organization of *fcrl*-like genes and their neighboring genes on various Chrs in the spotted gar. The syntenic *fcrl*-like gene cluster that is linked to the SLAM family, *arhgef11*, and *myadm* genes is circled and highlighted in blue, whereas the distantly located *fcrl*-like genomic cluster is circled and highlighted in light grey. The size (kb) of each gene cluster is indicated to the left of each diagram and is illustrated using a black dashed bracket. Genomic distances between genes and gene clusters are illustrated using red dashed brackets.

(A)

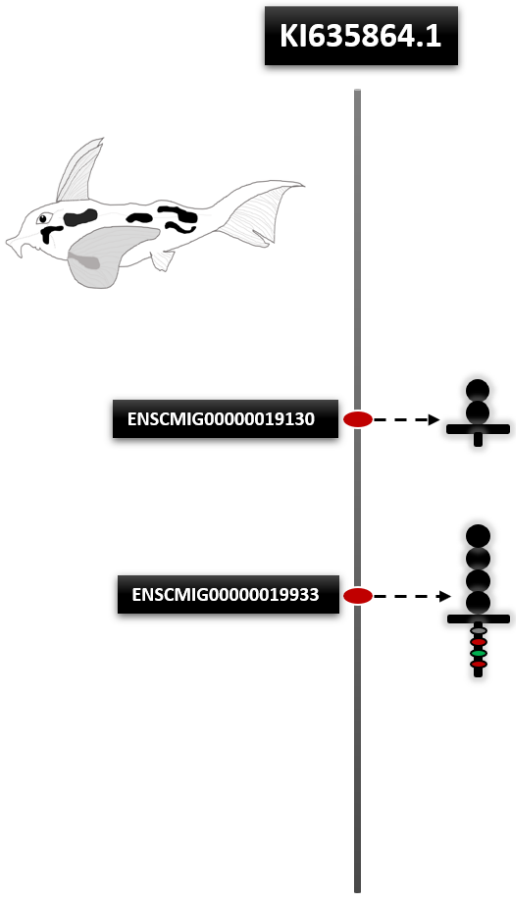

(B)

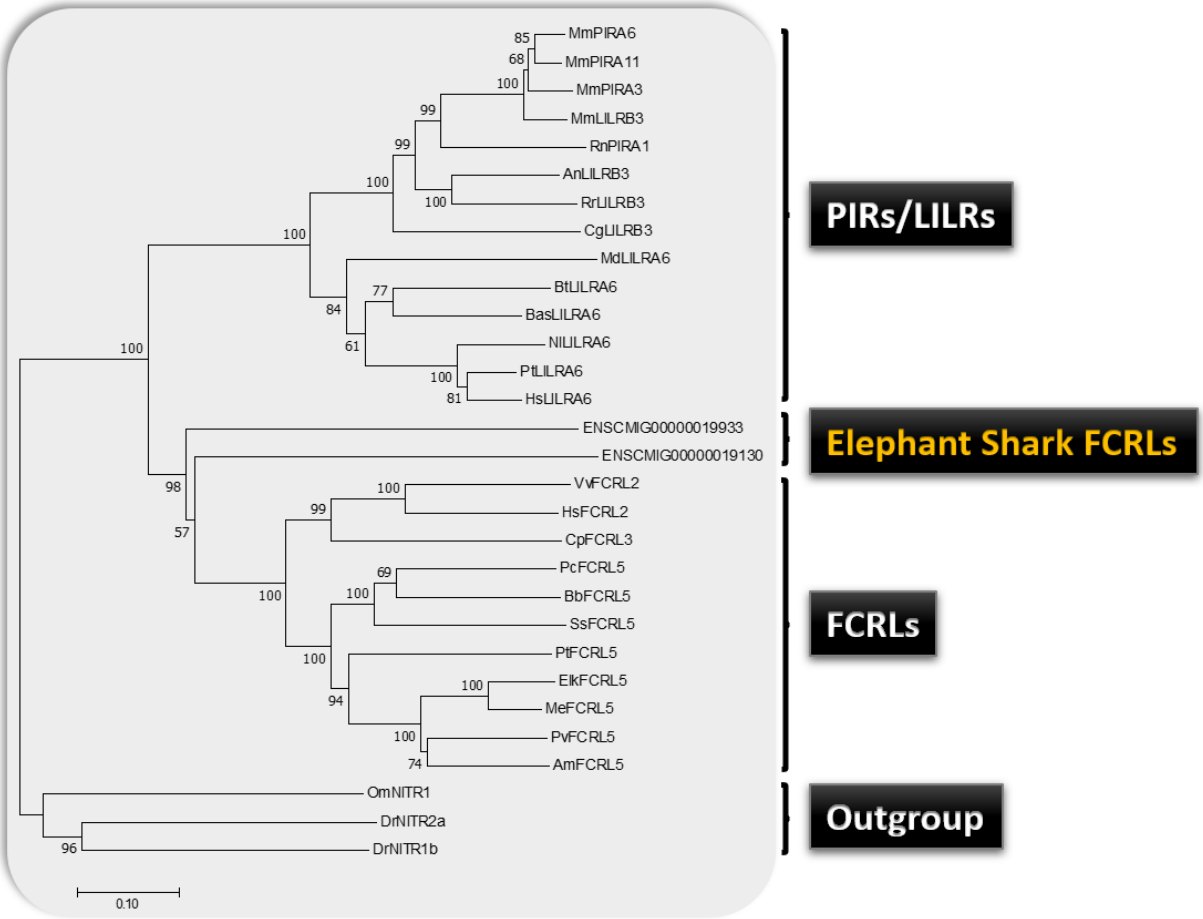

Figure 5.14. Schematic representations and phylogenetic analysis of the elephant shark FCRL-like sequences. (A) Graphical representations of the predicted elephant shark FCRL-like sequences. The Ig-like domains, TMs, and CYT regions were predicted using SMART. The Ensembl gene names are boxed and placed to the left of the receptors, whereas the name of the Ensembl primary assembly is placed at the top of the receptors. ITIM motifs in the TMs are designated by red circles. The ITAM motif is represented as a green circle. The gray circle in the CYT represents the endocytosis signal. **(B)** Phylogenetic analysis comparing the full-length extracellular regions of the predicted elephant shark FCRLs and the full-length ectodomains of the mammalian FCRLs, PIRs, and LILRs. The NJ tree with pairwise deletions was constructed using MEGA v7. Numbers at the nodes indicate the level of bootstrap support based on 10000 replicates. Branch lengths represent distance, and the scale bar indicates the number of amino acid substitutions per site.

(A)

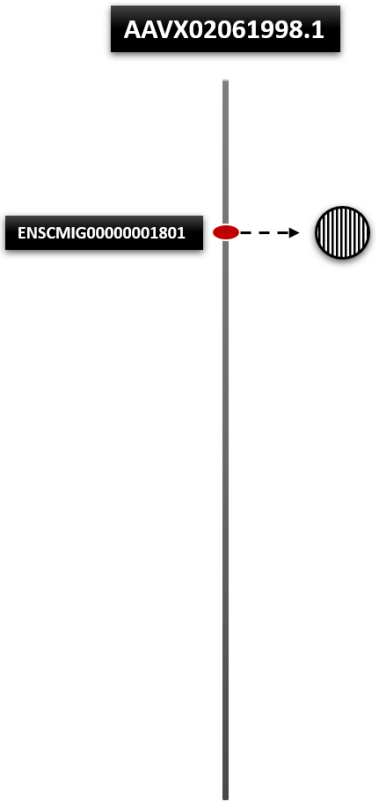

(B)

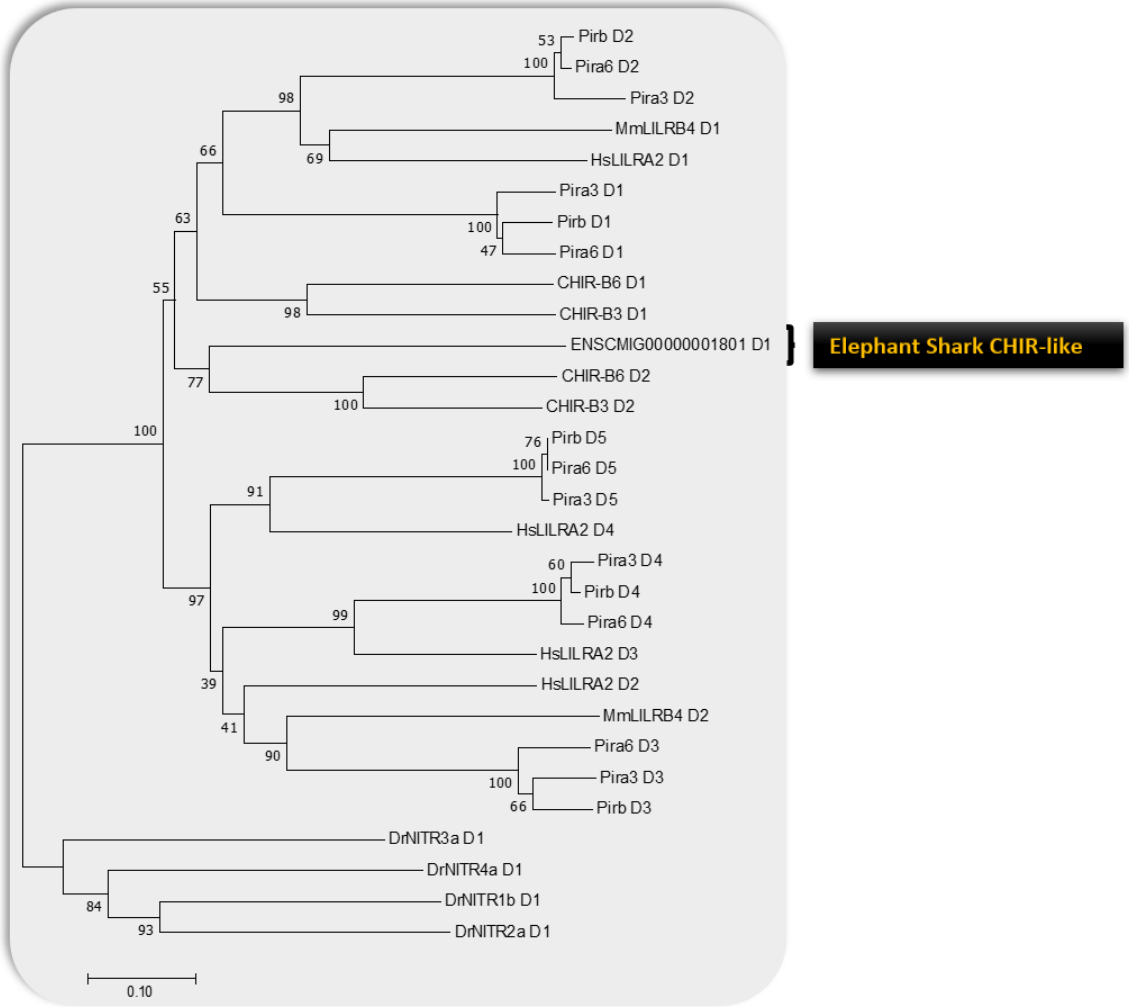

Figure 5.15. **Schematic representations and phylogenetic analysis of the predicted elephant shark LILR-like sequence. (A)** Schematic of the single Ig-like domain of the predicted elephant shark LILR-like sequence. The Ig-like domain of the receptor was predicted using SMART. The Ensembl gene name is boxed and placed to the left of the Ig-like domain. The name of the Ensembl primary assembly is placed at the top of the Ig-like domain. **(B)** Phylogenetic analysis comparing the individual Ig-like domain of the predicted elephant shark LILR-like sequence and the individual Ig-like domains of mammalian PIRs and LILRs. The NJ tree with pairwise deletions was constructed using MEGA v7. Numbers at the nodes indicate the level of bootstrap support based on 10000 replicates. Branch lengths represent distance, and the scale bar indicates the number of amino acid substitutions per site.

CHAPTER VI

EXPRESSION ANALYSIS OF CALITRS DURING GOLDFISH PKM DEVELOPMENT AND IN ACTIVATED KIDNEY LEUKOCYTE CULTURES

6.1 INTRODUCTION

calitr genes are primarily organized into gene clusters located on various goldfish Chrs (e.g., Chr 3, Chr 47, and Chr LG28B) (Wang et al., 2021). This organization is like the clustering observed in their mammalian FcR family gene counterparts. Several studies have shown that linked genes often have similar expression profiles (Ghanbarian & Hurst, 2015) due to their shared cis and/or trans-regulatory elements. Generally, cis-regulatory sequences, such as promoters and enhancers, are relatively close in distance to the gene of interest, while trans-regulatory sequences, such as genes encoding for transcription factors, are randomly distributed throughout the genome. For example, one study transfected HEK293 cells with a lentiviral vector containing a green fluorescent protein (GFP) gene driven by a human phosphoglycerate kinase (PGK) promoter (Gierman et al., 2007). After mapping the randomly distributed transgene insertion sites onto their respective Chrs and analyzing GFP expression at each insertion site, it was shown that the integrated GFP genes, on average, acquired expression levels similar to up to 80 adjacent genes. This strongly supports the hypothesis that linked genes share similar genetic regulatory mechanisms that act over long distances. Similarly, another group developed an effective *in vivo* transposition system to introduce a *lacZ* reporter gene (driven by a weak promoter carried in a *sleeping beauty* transposon) into mouse embryos (Symmons et al., 2014). By mapping hundreds of transposon insertion sites and analyzing the expression level of each reporter gene, they demonstrated that the closer a reporter gene is to an enhancer, the greater the impact the enhancer has on the reporter gene expression. Additionally, they showed that enhancers typically control the transcription of nearby genes in a non-discriminatory fashion

over long distances (~ hundreds of kb). Moreover, they found that mouse Chrs are subdivided into distinct regulatory domains (RDs), where genes from the same RD (range from 3.8 kb to 2.1 megabase pair (Mb)) generally show similar expression patterns. Besides these two studies, others have also demonstrated that eukaryotic genes with similar expression profiles tend to be clustered in genomes (Ghanbarian & Hurst, 2015).

It is reasonable to speculate that *calitrs* gene clusters on different goldfish Chrs may be regulated by distinct cis and/or trans-regulatory elements. To better understand whether the different *calitr* genes from distinct chromosomal locations are potentially differentially expressed, I set out to examine the transcriptional activities of several *calitrs* located on different goldfish Chrs, during the development of goldfish PKM cultures and in activated goldfish MLR cultures.

The goldfish PKM culture system is unique in that it supports the growth of three distinct macrophage developmental stages simultaneously (Belosevic et al., 2006). Furthermore, the goldfish PKM cultures are known to progress through distinct phases (Barreda et al., 2004; Belosevic et al., 2006; Katzenback et al., 2016). From day 1 to day 4, PKM cultures consist primarily of a mixed population of putative progenitors, and this early phase is characterized by minimal cell growth and the dying of non-macrophage cells (i.e., T and B cells) (Belosevic et al., 2006). The putative progenitors isolated from day 0 PKMs are small cells (6–10 μm in diameter) having a high nucleus-to-cytoplasm ratio (Neumann et al., 2000). Biochemical analyses showed that these cells stained positively for acid phosphatase, but not myeloperoxidase/non-specific esterase (Neumann et al., 2000). Moreover, these progenitor cells highly express transcription factors (i.e., *cmyb* and *gata2*) involved in the maintenance of HSCs/hematopoietic progenitor

cells (HPCs), as well as many other transcription factor mRNAs (i.e., *egr1*, *cjun*, and *mafb*) (Katzenback et al., 2011; Soza-Ried et al., 2010). From day 5 to day 9 (proliferation phase), macrophage progenitor-like cells proliferate and give rise to monocytes and mature macrophages (Belosevic et al., 2006). Compared with the progenitor cells, monocytes are larger cells (~ 12–15 μm in diameter) having a low nucleus to cytoplasm ratio and a crescent-moon-shaped nucleus (Neumann et al., 2000). Unlike the progenitors, monocytes stained positively for acid phosphatase and showed diffuse and variable staining patterns for myeloperoxidase and non-specific esterase, respectively (Neumann et al., 2000). Goldfish kidney monocytes also expressed relatively higher levels of transcription factors directing macrophage differentiation (i.e., *runx1*, *pu.1*, and *irf8*), relative to the progenitors (Katzenback et al., 2013). In comparison to monocytes, goldfish kidney macrophages (~ 12–20 μm) are irregularly shaped and highly vacuolated (Neumann et al., 2000). These cells stained positively for acid phosphatase while displaying localized staining for myeloperoxidase and variable staining for non-specific esterase (Neumann et al., 2000). Overall, goldfish macrophages maintained an increased expression of the myeloid-differentiation transcription factor (*pu.1*) while significantly reducing the mRNA expression levels of other transcription factors (i.e., *mafb*, *egr1*, and *cjun*) (Katzenback et al., 2013). Finally, from day 10 to day 15, PKM cultures undergo a senescence phase of growth characterized by cell clumping and apoptosis (Belosevic et al., 2006). Overall, this well-established PKM culture system provides an opportunity to study the expression of *calitrs* during PKM culture development.

The specific objective of this chapter was to use a qPCR-based approach to examine the expression patterns of select *calitr* genes (*calitr1*, *calitr2*, *calitr3*, *calitr4*) from different genomic regions during goldfish PKM development and in goldfish MLRs (analogous to allogeneic-

antigen activated channel catfish PBLs). Specifically, *calitr1*, *calitr2*, *calitr3*, and *calitr4* are located on an unplaced genomic scaffold, Chr47, Chr3, and ChrLG28B, respectively. My results showed that the *calitr* transcripts examined were differentially expressed during goldfish PKM development and in goldfish MLR cultures. I also showed that the mRNA expression level of the functionally ambiguous receptor-type (*calitr1*) is uniquely and differentially expressed in goldfish MLRs following exposure to a T cell mitogen cocktail (ConA, calcium ionophore A23187, and PMA) and immunosuppressive drugs (Dimethyl Sulfoxide (DMSO) and Cyclosporin A (CsA)), respectively. In contrast, *calitr2*, *calitr3*, and *calitr4* were all shown to be constitutively expressed during PKM differentiation/maturation, and their transcriptional activities remain largely unchanged in goldfish MLRs stimulated with the T cell mitogen cocktail containing ConA, PMA, and calcium ionophore. Their expression kinetics also remained static during MLRs following exposure to DMSO and CsA. Overall, my results suggest that *calitr1*, *calitr2*, *calitr3*, and *calitr4* transcripts are likely under the regulation of variable cis- and/or trans-regulatory elements, and the transcription of *calitr1* is likely regulated by inflammation-associated transcription factors.

6.2 RESULTS

6.2.1 Expression of myeloid-differentiation associated transcription factor genes during PKM development

To monitor transcriptional activities during the temporal culturing of goldfish PKM, I initially investigated the gene expression profile of c-myeloblastosis (*cmyb*) and runt-related transcription factor 1 (*runx1*), T-cell receptor alpha chain (*tcrα*) T cell marker), and *igm* (B cell marker). The transcripts of *runx1* and *cmyb* were reported to be differentially expressed in

goldfish macrophage subsets (Katzenback et al., 2013) and act as essential regulators of myelopoiesis (Duprey & Boettiger, 1985; Gonda & Metcalf, 1984; Studzinski & Brelvi, 1987). As shown in Fig. 6.1A, all three goldfish examined displayed similar overall gene expression kinetics of *cmyb*. In short, the gene expression level of *cmyb* increased during the early phase of PKM development (around days 0–4), followed by a decrease and stabilization as the PKM remained in culture. The *runx1* gene expression kinetics were the opposite of what I observed for the *cmyb* expression kinetics during PKM development (Fig. 6.1A). The transcript level of *runx1* was initially stable (around days 0–6), which was followed by an increase and then a decline (the decline phase in fish 2 was not captured). Similar to previously reported findings (Frampton, 2004), the expression level of the goldfish *cmyb* gene consistently increased during the early phase of PKM development (around days 0–4, coinciding with the proliferation of myeloid progenitors) and then rapidly decreased during the later phases of PKM development (around days 4–12, the emergence of monocytes and macrophages).

6.2.2 Expression of lymphoid markers during PKM development

Freshly isolated goldish PKMs contain a mixed population of myeloid progenitors and other cell types (i.e., T and B cells); however, non-macrophage cells usually die out shortly following the introduction of CCM, which selects for the growth and differentiation of the macrophage lineage (Neumann et al., 1998). To indirectly track the relative presence/absence of immune cells growing in PKM cultures over time, I monitored the gene expressions of T-cell and B-cell markers (*tcrα* and *igm*) in PKM cultures for 12 days. As shown in Fig. 6.1B, the *igm* transcript was present on day 0 of the fish 1 and 2 PKM cultures, but its expression level dropped to undetectable levels from day 2 to day 12. In comparison, the *igm* transcript (Fig. 6.1B) persisted for 4 days in the fish 3 PKM culture. However, its expression levels dropped to

undetectable levels by day 8 and remained undetectable for the rest of the PKM culture period. The gene expression kinetics of *tcrα* matched that of the *igm* (Fig. 6.1B). Specifically, the *tcrα* transcript was present at day 0 of the PKM cultures in fish 1 and 2, but it became undetectable after day 2. Interestingly, the expression level of the *tcrα* gene sharply decreased from day 0 to day 2 in the fish 3 PKM culture. However, it showed a slight rebound from day 2 to day 6 but its expression was undetectable after day 6. These data indicate that T and B cells likely exist in PKM cultures for a short period.

The relatively consistent expression patterns of the control genes (*cmyb*, *runx1*, *tcrα*, and *igm*) observed across the different fish examined further support previous findings (Katzenback et al., 2013) showing that the goldfish PKM cultures initially consisted of a heterogenous population of immune cell-types (i.e., T cells, B cells, and myeloid progenitors) that subsequently developed into a homogenous population of myeloid cells consisting of mostly monocytes and macrophages. These findings have confirmed the reproducibility of the PKM culture system and verified that *cmyb*, *runx1*, *tcrα*, and *igm* are reliable markers for monitoring the development of PKM cultures over time.

6.2.3 *calitr* transcripts are variably expressed in cultured PKMs over time

With the establishment of the expression profile of the myeloid-differentiation and lymphoid marker genes, I proceeded to examine the expression kinetics of *calitr1*, *calitr2*, *calitr3*, and *calitr4* in the same three PKM cultures for 12 days. As shown in Fig. 6.1C, the gene expression kinetics of *calitr1* is similar between the three fish examined. Specifically, in fish 1 and fish 2, the expression level of *calitr1* remained relatively static during the first 4 days of

PKM culture. However, its expression level increased around day 6, followed by a rapid decline. In contrast, the *calitr1* mRNA expression in the fish 3 PKM culture peaked around day 4, followed by a decrease.

Compared with *calitr1* expression, *calitr2*, *calitr3*, and *calitr4* levels were relatively constant (except for the *calitr3* expression peak observed around day 10 in fish 1) (Fig. 6.1C and Fig. 6.1D) during the development of the three goldfish PKM cultures examined. Specifically, in the fish 1 PKM culture (Fig. 6.1C), *calitr2* expression level stayed consistent for the first 2 days. It was then slightly upregulated from day 2 to day 8, followed by a decrease (days 8–10) and then an increase (days 10–12). In the fish 2 cultured PKMs, the *calitr2* transcript was downregulated early (days 0–2), but after day 2, the gene expression level of *calitr2* increased gradually (days 2–8) up to a plateau (days 8–12). In fish 3, the *calitr2* gene expression showed an upward trend (days 0–10), which peaked around day 10 and then decreased (days 10–12).

In the fish 1 cultured PKM, the *calitr3* transcript expression level (Fig. 6.1D) remained unchanged for eight days (days 0–8), followed by an increase (days 8–10) and then a decrease (days 10–12). In fish 2, the *calitr3* expression level increased from day 0 to day 2 of the PKM culture. It was then reduced (days 2–4) before returning to baseline (days 4–12). In fish 3, the expression level of *calitr3* peaked around day 4 of the PKM culture, which was followed by a decrease (days 4–8) before reaching a stable level (days 8–12).

The *calitr4* transcript level (Fig. 6.1D) from the fish 1 cultured PKMs showed a rapid decline (from day 0 to day 2, and then remained at low levels (days 2–12). In fish 2, the *calitr4* expression peaked around day 8 (days 0–8), which was then decreased from day 8 to day 12. In

fish 3, the *calitr4* expression peaked around day 4, followed by a decrease (days 4–8) and stabilization (days 8–12). In summary, compared with *calitr1*, which showed a unique unimodal gene expression trend during PKM development, the expressions of *calitr2*, *calitr3*, and *calitr4* remained relatively constant in each fish culture for 12 days.

6.2.4 *calitrs* are differentially expressed in goldfish MLRs upon exposure to T-cell mitogens

To examine the transcriptional activities of *calitr1*, *calitr2*, *calitr3*, and *calitr4* in activated immune cells, I used qPCR to measure the gene expression levels of these *calitrs* in goldfish MLR cultures stimulated with a specific mixture of T-cell mitogens (ConA, PMA, calcium ionophore), a set up previously used by our lab to generate macrophage activating factors (MAFs) (Neumann et al., 1995). For these experiments, I used goldfish *tnf-α2* and *ifn-γ* genes as inflammatory markers based on the immune pathways known to be activated by ConA (NFAT pathway) (Bemer & Truffa-Bachi, 1996; Dwyer & Johnson, 1981; Lei & Chang, 2009), PMA (PKC pathway) (Robinson, 1992; Tahara et al., 2009), and calcium ionophore (calcium signaling and NFAT pathway) (Canellada et al., 2008; Luckasen et al., 1974; Tomita et al., 2002). As shown in Fig. 6.2A, the *tnf-α2* gene was upregulated at 6, 12, and 24 h in goldfish MLRs following mitogen stimulation. Furthermore, the gene expression level of *tnf-α2* was significantly higher in mitogen-stimulated MLRs, compared to MLRs treated with 0.2% DMSO vehicle at 6, 12, and 24 h post-stimulation. Similarly, the goldfish *ifn-γ* gene (Fig. 6.3A) showed a higher rate of transcription activation in mitogen-stimulated MLRs, relative to DMSO-vehicle-stimulated MLRs at all the time points examined (6, 12, and 24 h).

Compared to *tnf-α2* and *ifn-γ*, the gene expression level of *calitr1* (Fig. 6.2B) was significantly higher in mitogen-activated MLRs than in DMSO-treated MLRs at 6 h and 12 h.

However, no statistically significant difference in the expression of *calitr1* was observed between these treatment conditions at 24 h. The expression of *calitr2* (Fig. 6.2B) was not induced in both mitogen-activated MLRs and DMSO-treated MLRs and no significant differences in the expression level of *calitr2* were observed between the two MLR conditions at 6 h, 12 h, and 24 h. Like *calitr2*, the *calitr3* transcript level (Fig. 6.2C) remained unchanged in both mitogen-activated MLRs and DMSO-treated MLRs. The gene expression level of *calitr4* (Fig. 6.2C) was slightly higher (0.61-fold) in DMSO-treated MLRs relative to mitogen-activated MLRs (0.29-fold) at 6 h and 12 h, but no differences were observed at 24 h. Overall, these results show that the mRNA expression patterns of *calitr1* are uniquely correlated with the expression kinetics of *tnf-α2* and *ifn-γ* in mitogen-activated MLRs.

6.2.5 Effects of CsA on the transcriptional activities of *calitr1*, *calitr2*, *calitr3* and *calitr4* in goldfish mitogen-activated MLRs

CsA is a potent inhibitor of calcineurin-mediated activation of the NFAT family of transcription factors and their downstream target genes (i.e., *il-2*, *ifn-γ*, and *tnf-α*), which negatively regulate T-cell functions in mammals (Eckstein et al., 2005; Emmel et al., 1989; Thomson, 1992). As a result, CsA is commonly used for suppressing organ rejection in transplant patients (Colombo & Ammirati, 2011; Miach, 1986). As T-cells are known to be the principal responder cells in mammalian and fish MLRs (Cantor & Boyse, 1975; Caspi & Avtalion, 1984; Meloni et al., 2006; Miller et al., 1986), I investigated if CsA could downregulate the expression of proinflammatory marker genes (*tnf-α2* and *ifn-γ*) and the select *calitr* genes (*calitr1*, *calitr2*, *calitr3*, and *calitr4*) in goldfish mitogen-activated MLRs.

To determine the concentration of CsA from the 1 mg/mL stock solution (dissolved in DMSO) that effectively inhibits goldfish mitogen-activated MLRs, I initially examined the effects of 5 μg/mL of CsA and 10 μg/mL of CsA on goldfish mitogen-activated MLRs. These concentrations were chosen based on a previously published study (Meloni et al., 2006). As shown in Fig. 6.3A, CsA downregulated the expression level of *tnf-α2* in goldfish mitogen-activated MLRs in a dose-dependent manner. Specifically, both 5 μg/mL and 10 μg/mL of CsA significantly reduced the mean expression level of *tnf-a2* in mitogen-activated MLRs after 6, 12, and 24 h. However, 10 μg/mL of CsA reduced the level of *tnf-α2* in mitogen-activated MLRs to a greater extent than 5 μg/mL of CsA (Fig. 6.3A). I also examined if the DMSO vehicle affected the mRNA expression of *tnf-α2*. Unexpectedly, the addition of small volumes of DMSO (0.5 and 1%) to mitogen-activated MLRs also reduced the expression level of *tnf-α2* after 6 and 12 h (Fig. 6.3A). Although DMSO (0.5 and 1%) reduced the expression of *tnf-α2* in mitogen-activated MLRs after 24 h, these were not statistically significant (Fig. 6.3A).

The transcriptional activity of *ifn-γ* in mitogen-treated MLRs was also supressed by both CsA and DMSO (Fig. 6.3B). Specifically, 5 μg/mL of CsA significantly reduced the transcript level of *ifn-γ* in mitogen-treated MLRs after 6 and 12 h, although no significant difference was observed at 24 h (Fig. 6.3B). In comparison, 10 μg/mL of CsA caused a significant drop in the transcript level of *ifn-γ* at every time point examined. Relative to CsA, DMSO caused a statistically significant reduction of *ifn-γ* expression in mitogen-treated MLRs at the 12- and 24-h time points.

Similar to goldfish *ifn-γ* and *tnf-α2*, the *calitr1* expression in mitogen-activated MLRs was significantly reduced by CsA and DMSO. As shown in Fig. 6.3C, 5 μg/mL of CsA

significantly inhibited *calitr1* expression in mitogen-treated MLRs after 6 and 12 h (24 h time point was not significant), whereas 10 μg/mL of CsA significantly repressed the expression level of *calitr1* at every time point examined (Fig. 6.3C). The transcript level of *calitr1* was also significantly reduced by 0.5 and 1% DMSO concentrations (Fig. 6.3C). Overall, the expression patterns of *calitr1* in DMSO-treated samples matched that of the CsA-treated samples.

Compared to *calitr1*, the mRNA expression level of *calitr2* in mitogen-treated MLRs (Fig. 6.3D) was unaffected by the various concentrations of CsA/DMSO applied at all time points examined. Likewise, *calitr3* (Fig. 6.3E) and *calitr4* (Fig. 6.3F) transcripts remained static in mitogen-activated MLRs treated with the various concentrations of CsA/DMSO and they did not display any significant differences between the treatment groups at 6, 12, and 24 h. These results show that the *calitr1* transcript displays similar expression kinetics as *tnf-α2* and *ifn-γ*. As the DMSO vehicle also inhibits the mRNA expression level of *calitr1* in mitogen-activated MLRs, it is unclear how much CsA contributes to the suppression of *calitr1* levels in these cultures.

6.2.6 Effects of CsA on the transcriptional activities of *calitr1*, *calitr2*, *calitr3*, and *calitr4*

To delineate the effects of CsA on the mRNA expression of *calitr1*, I used a concentrated stock of the CsA solution (10 mg/mL) and compared the expression level of *calitr1* in mitogen-activated-MLRs treated with 0.3% DMSO vehicle with mitogen-activated-MLRs treated with a high dose of CsA (30 μg/mL). As shown in Fig. 6.4A, 30 μg/mL of CsA slightly downregulated the mRNA expression level of *tnf-α2* in mitogen-activated MLRs relative to the DMSO vehicle control group after 6, 12, and 24 h. In contrast, this CsA concentration

significantly inhibited the transcription of *ifn-γ* (Fig. 6.4A) in the experimental group after 6, 12, and 24 h, compared with the DMSO vehicle control. The expression of *calitr1* (Fig. 6.4B) was also lower in the CsA-treated-MLR group relative to the DMSO control. However, a statistically significant difference in the expression level of *calitr1* between the treatment and control groups was only observed after 12 h. In contrast, the expression of *calitr2* (Fig. 6.4B), *calitr3* (Fig. 6.4C), and *calitr4* (Fig. 6.4C) were unaffected by the CsA treatment. Overall, these results show that the mRNA expression of *ifn-γ* is highly sensitive to CsA, whereas the transcriptional activities of *tnf-α2* and *calitr1* are less affected by CsA treatments.

6.2.7 DISCUSSION

Immunoregulatory receptors generally use ITAMs or ITIMs in their CYTs to modulate the activation status of immune cells (Barrow & Trowsdale, 2006). Furthermore, the mRNA and protein expression of these receptors are often tightly regulated during the maturation of various myeloid and lymphoid cells (Jansen et al., 2007; Poggi et al., 1998; Tedla et al., 2008; Verbrugge et al., 2006). For example, LILRB1, an inhibitory receptor from the LRC, is significantly upregulated on the cell surface during dendritic cell (DC) development from monocyte precursors (Young et al., 2008). Furthermore, activation of LILRB1 induced DC cells to display a phenotype characterized by a reduced ability to stimulate T-cell responses (Young et al., 2008). The cell-surface expression of Leukocyte associated Immunoglobulin-like receptor 1 (LAIR-1, an inhibitory receptor encoded by the LRC) decreased as HL-60 cells (human promyeloid tumor cell line) differentiated into neutrophils (Verbrugge et al., 2006). Additionally, the surface expression of LAIR-1 was known to be differentially expressed in T-cell subsets. Activation of

LAIR-1 by cross-linking also inhibited T-cell functions, suggesting LAIR-1 likely regulates the functional activities of the T-cell subsets (Jansen et al., 2007).

Currently, it is not known how *calitr* transcripts from the distinct goldfish Chrs are regulated, what conditions regulate their expression, are these genes differentially expressed in resting and/or activated goldfish immune cells, do *calitr* transcripts show similar expression kinetics as pro-inflammatory markers, and are select *calitrs* markers of specific goldfish immune cells. To investigate if select *calitrs* are developmentally regulated in goldfish immune cells, I examined the mRNA expressions of *calitr1*, *calitr2*, *calitr3*, and *calitr4* during the development of goldfish PKM cultures. To monitor the progression of the PKM cultures, I also surveyed the transcriptional activities of several myeloid-differentiation-associated transcription factors, including *cmyb* and *runx1*, over 12 days. C-Myb and Runx1 are essential regulators of myelopoiesis. For example, c-Myb modulates the proliferation of myeloid progenitors, and its transcription level significantly diminishes following the differentiation of myeloid progenitors to monocytes (Frampton, 2004). In comparison, Runx1 has been known to cooperate with other myeloid transcription factors, such as PU.1, to direct macrophage differentiation (Hu et al., 2011; Huang et al., 2008; Imperato et al., 2015). I also tracked the expression of *igm* and *tcrα*, markers of B-cells and T-cells, respectively. The PKM cultures, derived from genetically outbred goldfish, were demonstrated to proliferate at varying rates in the presence of goldfish CCM. This variability is reflected by the different expression kinetics, including variable gene expression levels and peak expression times, observed for the different genes examined (i.e., *cmyb* and *runx1*) in the three PKM cultures.

My results showed that the mRNA expression level of *calitr1* significantly increases during the early phase of PKM development (i.e., days 0–6), followed by a decrease during the later time points (days 6–12). Conversely, the expressions of *calitr2*, *calitr3*, and *calitr4* stayed relatively constant during PKM development. These expression patterns suggest that the transcriptional activity of *calitr1* is likely developmentally regulated in PKMs and support that the select *calitrs* examined are likely under the regulation of distinct cis- and/or trans-regulatory elements. I also examined the mRNA expression level of *calitr1* in the PKM subsets (progenitors, monocytes, and macrophages) obtained from day 7 PKM cultures. However, no differences in the mRNA expression levels of *calitr1*, *calitr2*, *calitr3*, and *calitr4* between these cell subsets, suggesting that the increased mRNA expression of *calitr1* is not strictly dependent on the maturation status of goldfish macrophages. Further experiments are required to examine the expression level of *calitr1* in progenitors, monocytes, and macrophages isolated from the early and late time points of PKM development (i.e., day 0, day 4, and day 8) to verify if the increased expression of *calitr1* is dependent on developing macrophage subsets. The recombinant proteins of several key PKM growth factors have been generated in goldfish (Barreda et al., 2005; Hanington et al., 2006; Hanington et al., 2009). For example, the goldfish recombinant (colony stimulating factor-1) CSF-1 was shown to induce the proliferation and differentiation of goldfish monocytes and macrophages, whereas the recombinant soluble-CSF-1 receptor (sCSF1R) negatively regulated PKM proliferation (Barreda et al., 2005; Hanington et al., 2009). These will be useful tools for further elucidating the mechanism of the increased *calitr1* expression during PKM development.

In vertebrates, the expression of immunoregulatory receptor genes that are localized in large genomic complexes (i.e., LRC-encoded receptors) is often regulated by diverse cis- and/or

trans-regulatory elements (Cichocki et al., 2009; Goettsch et al., 2011; Huang et al., 2020; Nakajima et al., 2003). For example, the transcription factors, PU.1 and Sp1 (specificity protein 1), are known to bind to the proximal core promoter (~ 160 bp) of LILRB1/LILRB2 to regulate their transcriptional activity (Nakajima et al., 2003). In comparison, PU.1 and Runx1 collaborate to transactivate the promoter of LILRA2 (Nakajima et al., 2003). OSCAR, a sequence relative of LILRs, was shown to be transcriptionally regulated by the nuclear factor of activated T-cells 1 (NFATc1) (Goettsch et al., 2011). Moreover, the transcription factor, cMyc, regulates the transcription of multiple KIRs (Cichocki et al., 2009). In addition to cis- and/or trans-regulatory elements, immunoregulatory receptors from large genomic complexes can also be regulated through epigenetic processes. For instance, TSA- (inhibitor of histone deacetylases) stimulated THP-1 cells (a human monocyte cell line) enhanced the expression of LILRB2 (Nakajima et al., 2003). Additionally, HDAC (histone deacetylase) inhibitor elevated the transcription level of Siglec-7 (a member of the LRC) (Huang et al., 2020). Since many CaLITR genes are also located in gene complexes and spread across multiple goldfish Chrs (Wang et al., 2021), their transcription is likely regulated by diverse cis- and/or trans-regulatory elements as well as epigenetic processes.

The *calitr1* transcript was upregulated in MLRs stimulated with a T-cell mitogen cocktail containing ConA, PMA, and calcium ionophore, whereas the mRNA expressions of *calitr2*, *calitr3*, and *calitr4* remained constitutively expressed in mitogen-stimulated MLRs and unaffected by mitogens. ConA, originally isolated from the jack bean (*Canavalia ensiformis*), is well-known to crosslink TCRs to activate the NFAT family of transcription factors required for the transcription of several genes (i.e., *il-2*) involved in T-cell proliferation and activation (Bemer & Truffa-Bachi, 1996; Dwyer & Johnson, 1981; Lei & Chang, 2009). Moreover, calcium

ionophore activates T-cells by raising intracellular calcium levels to activate NFAT family of transcription factors (Canellada et al., 2008; Luckasen et al., 1974; Tomita et al., 2002), whereas PMA activates T-cells by stimulating PKC signaling pathways to activate several transcription factors including activator protein (AP-1) and NFκB (Brignall et al., 2017; Robinson, 1992; Tahara et al., 2009). Based on these findings, the increased transcription levels of *calitr1* in mitogen-activated MLRs are likely due to inflammation-associated transcription factors such as NFAT, AP-1, and NFκB. However, epigenetic changes in PKMs upon exposure to T-cell mitogens might also contribute to the upregulation of the *calitr1* transcript. Since the cellular basis of goldfish MLRs is currently not well understood, I cannot attribute the increased *calitr1* mRNA expression to specific immune cell types, although goldfish T-cells or other immune cells (i.e., NK cells) are likely responsible for the upregulation of *calitr1*. In the previous chapters, I reported (Wang et al., 2020) that *calitr1* was minimally expressed/undetectable in most of the goldfish tissues that I investigated (spleen, liver, muscles, kidney, intestine, brain, heart, and gills), but its mRNA expression increases in freshly isolated PKM cultures, suggesting that the transcriptional activity of *calitr1* is normally repressed under homeostatic conditions. Thus, the upregulation of *calitr1* transcript in PKM cultures might be due to the culturing conditions or the growth factors present in the goldfish PKM media (i.e., CCM, calf serum, and carp serum). In contrast to *calitr1*, transcripts of *calitr2*, *calitr3*, and *calitr4* are highly expressed in various goldfish tissues and during PKM development, indicating that their genetic circuits are continuously active and likely not influenced by the PKM media and culturing conditions.

The addition of low concentrations of DMSO (0.5 and 1%) to mitogen-activated MLRs downregulated the expression of *ifn-γ*, *tnfα*, and *calitr1* while having no detectable effects on the transcription of *calitr2*, *calitr3*, and *calitr4*. It is important to note that these DMSO

concentrations are not toxic to cells within goldfish MLRs (% cells stained by trypan blue remained roughly the same pre- and post-DMSO treatments). This is likely the first report for the ability of DMSO to suppress cytokine gene expressions in teleost fish. Low concentrations of DMSO have been frequently reported to suppress the functions of various immune cells in mammals (Ahn et al., 2014; de Abreu Costa et al., 2017; Elisia et al., 2016). For example, 0.5 to 2% DMSO concentrations potently suppressed the secretion of various cytokines (i.e., TNF-α, IL-6, IFN-γ, and IFN-α) in *E. coli*- and Herpes simplex virus-1 (HSV-1)-stimulated whole human blood (Elisia et al., 2016). Furthermore, DMSO has been shown to inhibit various inflammation-associated signaling pathways including JNK, p38 MAP kinase, ERK1/2, and PI3K/Akt pathways (Elisia et al., 2016). Additional experiments have shown that 5 and 10% DMSO inhibited the production of IL-2, TNF-α, and IFN-γ produced by lymphocytes (de Abreu Costa et al., 2017). Moreover, DMSO (2 to 4%) repressed the mRNA expressions of *il-1α* and *il-6* (Ahn et al., 2014). Therefore, DMSO-mediated suppression of the mRNA expression of *calitr1* further supports that *calitr1* transcription is likely modulated by inflammation-associated signaling pathways and their downstream transcription factors. The fact that DMSO inhibited the mRNA expressions of *tnf-α* and *calitr1* to a much greater extent than CsA is likely explained by the broader immunosuppressive mechanisms of DMSO, relative to CsA that primarily inhibits lymphocyte activity through the inhibition of calcineurin-NFAT pathway (Eckstein et al., 2005). Conversely, the inability of T-cell mitogens and immunosuppressive drugs (DMSO and CsA) to influence the mRNA expression levels of *calitr2*, *calitr3*, and *calitr4* suggests that the transcription of these genes might be independent of the specific inflammation-associated transcription factors regulated by the immunomodulatory drugs.

To further investigate potential differences in the gene regulatory regions of the various *calitrs*, I performed BLAST searches on the goldfish genome using Ensembl (version 112) with the various *calitr* cDNA sequences as queries (unpublished observations). For each gene, the BLAST hit with the highest score was selected, and a 1000 bp sequence upstream of the first exon of each *calitr* gene was identified. These sequences were then analyzed with PROMO (Farre et al., 2003; Messeguer et al., 2002) to identify putative transcription factor binding sites (TFBS). To maximize accuracy, only human TFBS were used as a basis for comparison, and factors predicted with minimal differences (≤2% dissimilarity margin) to the human TFBS were considered. My preliminary examination of the putative promoter regions of the *calitrs* (unpublished data) revealed that, while all the *calitr* genes of interest share a similar set of core TFBS, including sites for glucocorticoid receptor (GR)-β, CCAAT enhancing binding protein (C/EBP)β, transcription factor II D (TFIID), GATA binding factor 1 (GATA-1), estrogen receptor (ER)-α, forkhead box p3 (FOXP3), and IRF-2, the predicted promoter region of *calitr1* uniquely contains TFBS for STAT4 and CREB, transcription factors known to regulate inflammatory processes (Wen et al., 2010; Yang et al., 2020). Using the same approach, I have also analyzed the putative promoter sequence of goldfish *tnf-α2* gene. Although the predicted promoter region of *tnf-α2* contains a similar set of core TFBS as the *calitrs*, it also features additional TFBS such as AP-1 and c-Jun, which are transcription factors well-recognized for their association with inflammation (Atsaves et al., 2019). Overall, these findings provide a first look at the possible TFBS that may be involved in the transcriptional regulation of the various *calitrs*.

Among the *calitrs* studied, the mRNA expression of *calitr1*, encoding a transmembrane receptor without obvious signaling potentials, was the only receptor strongly influenced by T-

cell mitogens/immunosuppressive drugs. Although the functions of CALITR1 in teleost immune cells remain to be elucidated, I can speculate on the possible roles that CaLITR1 may play in teleost immune cells based on CaLITR1-like receptors found in other vertebrate systems. For example, CD200, an IgSF receptor with a neutrally charged TM and a short CYT devoid of signaling motifs, is known to interact with inhibitory CD200Rs expressed on the surface of various myeloid cells (i.e., mast cells and macrophages) as well as T-cells to downregulate the functions of these cells (Kotwica-Mojzych et al., 2021). CD80 and CD86, receptors with neutrally charged TMs and CYTs seemingly devoid of signaling motifs, are well known to interact with the T-cell costimulatory receptor CD28 to further activate T-cell functions (Carreno & Collins, 2002). Lastly, the murine UL-16-binding protein-like transcript (MULT)-1 glycoprotein, a stress-induced receptor with a neutrally charged TM and a CYT devoid of recognizable signaling motifs, has a high affinity for the stimulatory receptor NKG2D expressed on the surface of various lymphocytes (i.e., NK and T-cells) (Krmpotic et al., 2005). Based on these reports, CaLITR1 might also act as a ligand for unknown immunoregulatory receptors in the context of the goldfish MLRs, although I can't exclude the possibility that CaLITR1 might have intrinsic signaling properties that are independent of tyrosine-based motifs.

Molecules of the immune system generally display two main patterns of expressions, constitutive and inducible expressions (Paludan et al., 2021). Many pro-inflammatory molecules (i.e., TNF-α and IFN-γ) are induced only under inflammatory conditions as continuous production of these molecules even at a low level are not beneficial for the well-being of an organism (i.e., autoimmune diseases) (Zhang & An, 2007). On the other hand, many immune system molecules are also constitutively expressed (Paludan et al., 2021). For example, NKG2D, an activating receptor, is constitutively expressed on the surface of NK cells (Lanier, 2015). This

receptor interacts with a variety of stress-induced molecules (i.e., MHC class 1 polypeptide-related sequence A (MIC-A) and MIC-B) presented on the surface of virally infected and cancer cells (Lanier, 2015). Furthermore, Nkp46 and Nkp30, natural cytotoxicity receptors, are also constitutively expressed on NK cells and play critical roles in viral and cancer immunosurveillance (Barrow et al., 2019). Therefore, it may be that *calitr2*, *calitr3*, and *calitr4* are constitutively expressed by goldfish immune cells for monitoring the expression of cellular stress-related ligands or constitutively positioned on immune cells to perform their immunoregulatory roles without required inducible expression mechanism for their functions.

Since *calitrs* are highly polygenic, I cannot exclude the possibility that my qPCR primers (Table 6.1) may also target different splice variants of the same gene or genes sharing highly similar sequences with my *calitrs* of interest. I acknowledge that this is a limitation of the qPCR approach. To address this, future experiments should be performed using non-biased gene detection methods, such as RNA sequencing or DNA microarray, to validate the expression patterns of *calitrs* observed in my study. These techniques will provide a more comprehensive view of mRNA expression for *calitrs* located on distinct goldfish Chrs and enable monitoring of their overall expression patterns under various conditions. Up to this point, my experiments have focused solely on the genes of *calitrs*, and currently, there are no reagents available for examining their protein expression or functions within the goldfish model system. This gap will be addressed in the next chapter.

In summary, I have provided evidence that the select CaLITRs from distinct goldfish chromosomal regions are likely regulated by distinct cis- and/or trans-regulatory elements. This provides a reasonable step forward for further investigations focused on deciphering the complex

signaling pathways and transcription factors potentially involved in the transcriptional regulation of teleost *litrs*.

(A)

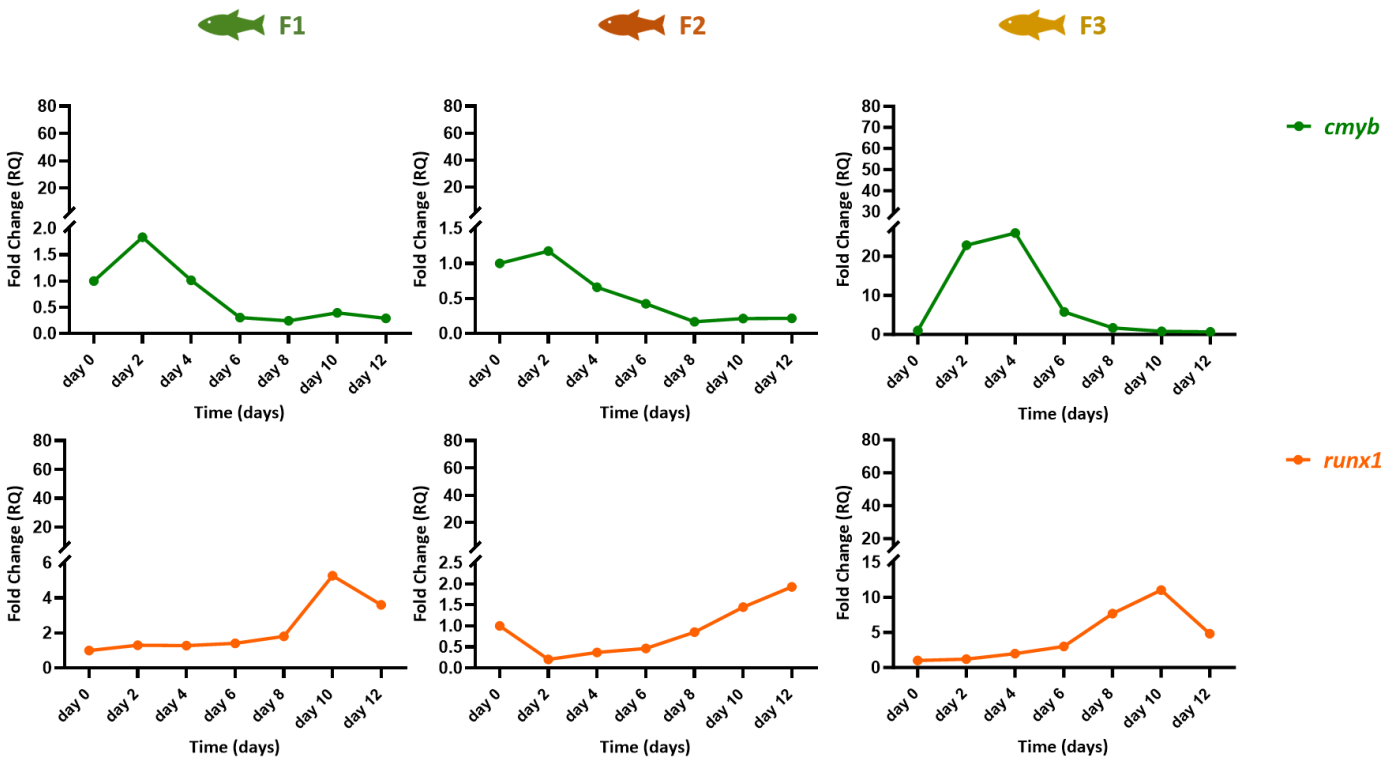
F1
F2
F3
cmyb
runx1
Fold Change (RQ)
Time (days)
day 0
day 2
day 4
day 6
day 8
day 10
day 12

(B)

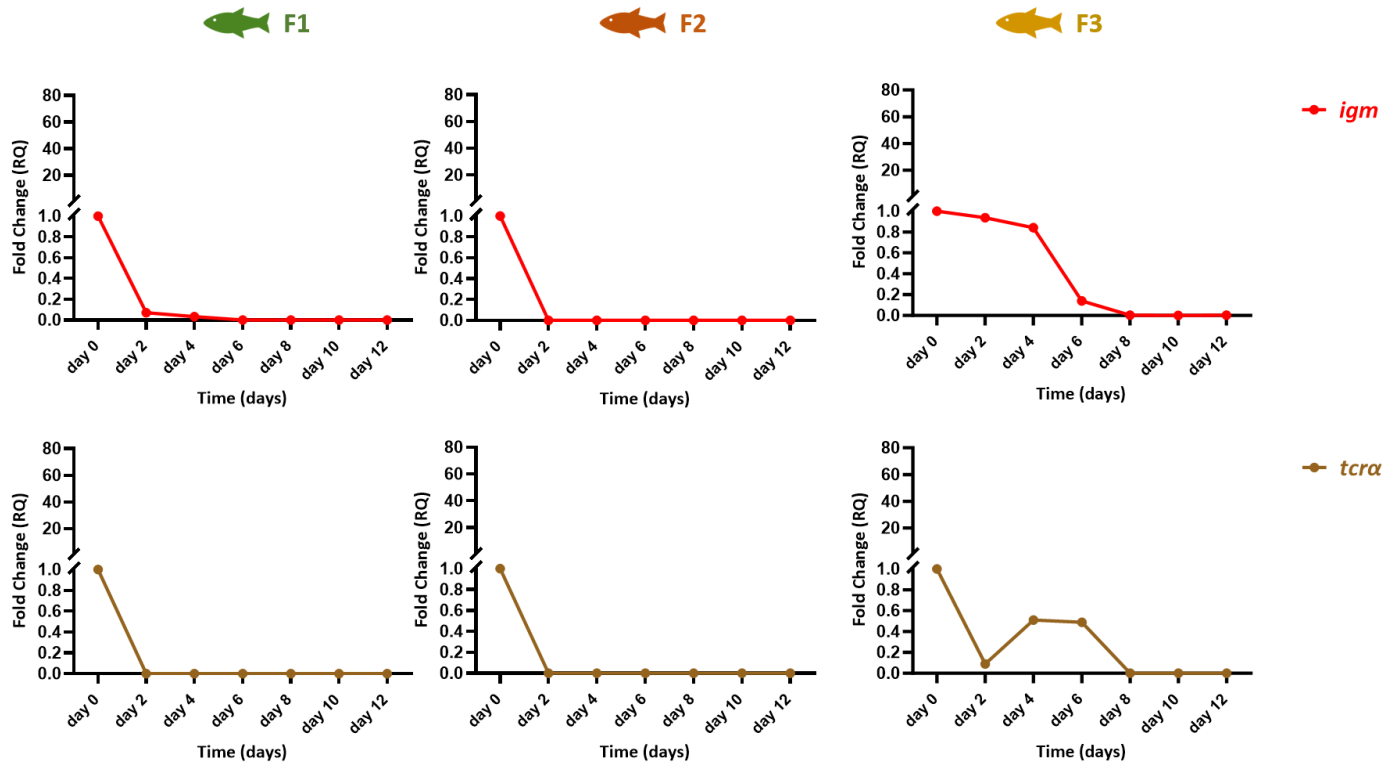
F1
F2
F3
igm
tcrα
Fold Change (RQ)
Time (days)
day 0
day 2
day 4
day 6
day 8
day 10
day 12

(C)

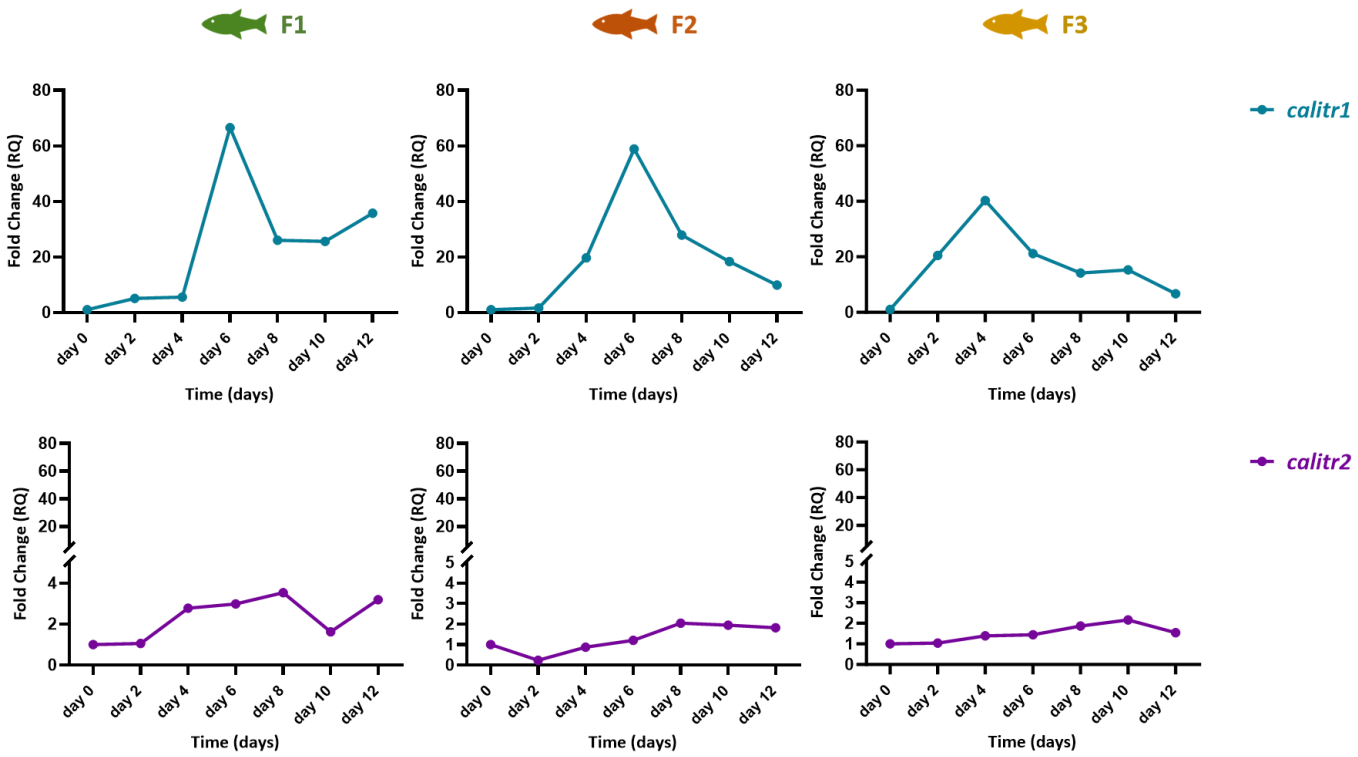
F1
F2
F3
calitr1
calitr2
Fold Change (RQ)
Time (days)
day 0
day 2
day 4
day 6
day 8
day 10
day 12

(D)

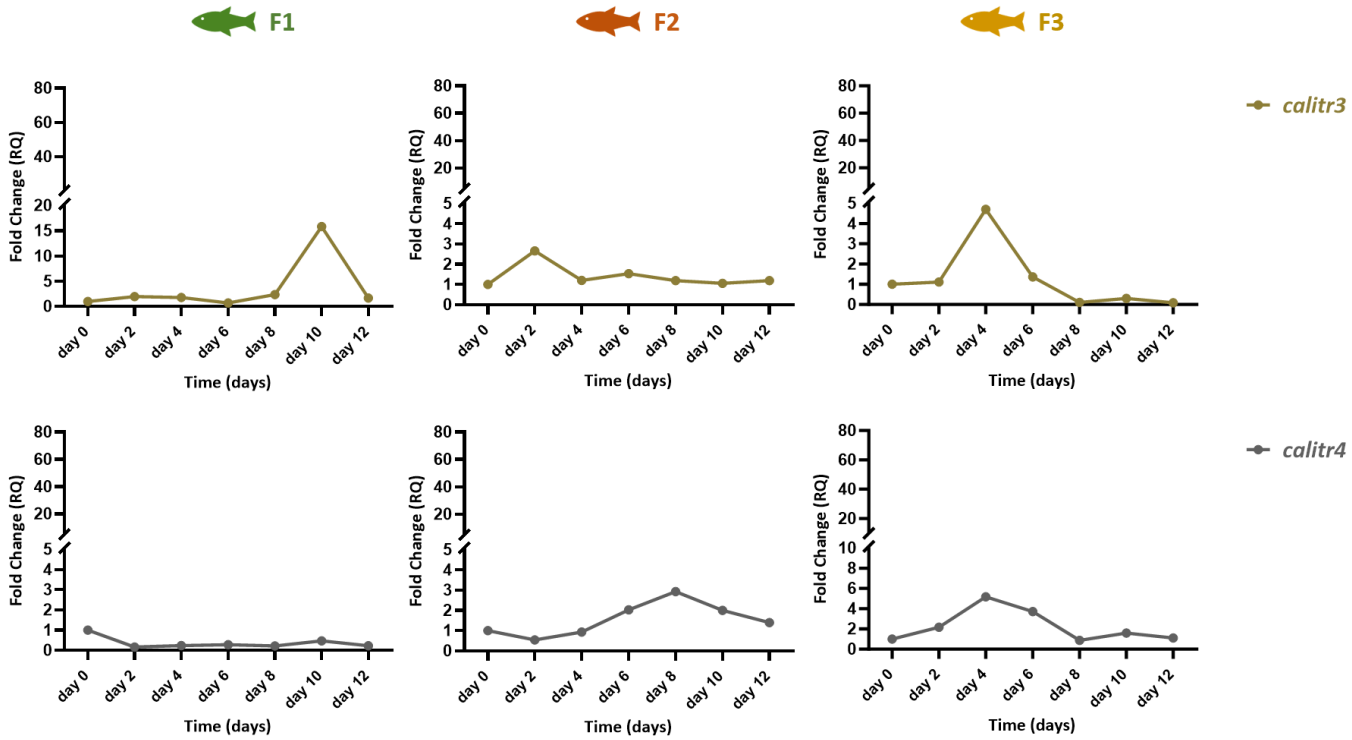

Figure 6.1. Expression profiles of myeloid-differentiation-associated transcription factors, lymphoid markers, and *calitrs* during the development of three goldfish PKM cultures. Freshly isolated PKMs were seeded into a 24-well plate at a density of 2×10^5 cells per well. Total RNAs were extracted from the respective time points (day 0, day 2, day 4, day 6, day 8, day 10, and day 12) using the RNeasy mini kit (Qiagen). **(A)** Transcriptional activities of myeloid-differentiation-associated transcription factors *cmyb* and *runx1* in cultured PKMs for 12 days. **(B)** Quantitative expression analysis of the transcript levels of *Igm* and *tcrα* during PKM development. **(C)** Expression patterns of *calitr1* and *calitr2* during PKM development. **(D)** Expression patterns of *calitr3* and *calitr4* during PKM development. Relative fold change was normalized to the endogenous control gene, *ef1α*, and then displayed as fold change in expression relative to day 0 control (RQ = 1) for each gene.

(A)

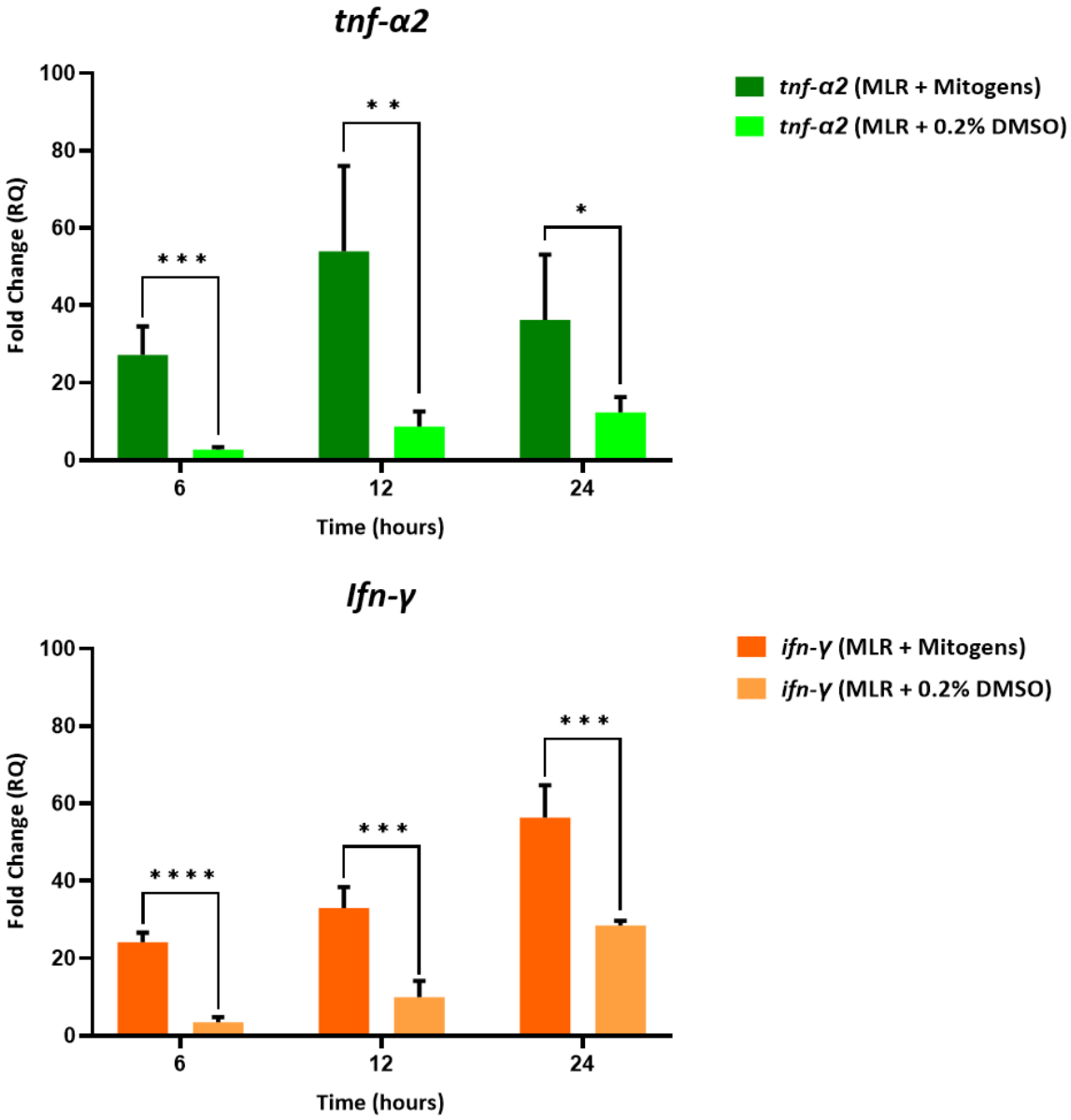
tnf-α2
Fold Change (RQ)
100
80
60
40
20
0
* *
* * *
*
6
12
24
Time (hours)
tnf-α2 (MLR + Mitogens)
tnf-α2 (MLR + 0.2% DMSO)
Ifn-γ
Fold Change (RQ)
100
80
60
40
20
0
* * * *
* * *
* * *
6
12
24
Time (hours)
ifn-γ (MLR + Mitogens)
ifn-γ (MLR + 0.2% DMSO)

(B)

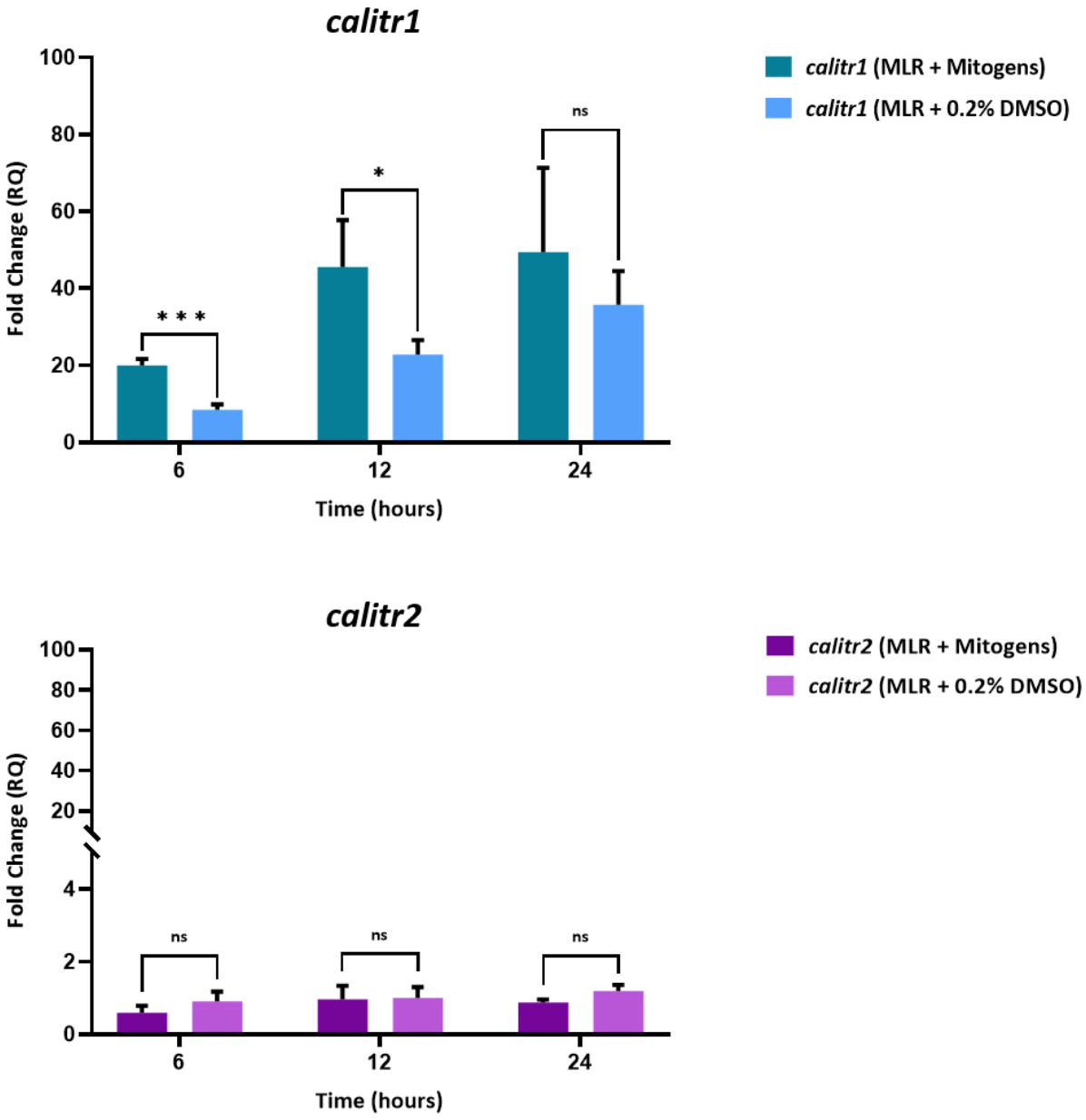
calitr1
Fold Change (RQ)
100
80
60
40
20
0
* * *
*
ns
6
12
24
Time (hours)
calitr1 (MLR + Mitogens)
calitr1 (MLR + 0.2% DMSO)
calitr2
Fold Change (RQ)
100
80
60
40
20
4
2
0
ns
ns
ns
6
12
24
Time (hours)
calitr2 (MLR + Mitogens)
calitr2 (MLR + 0.2% DMSO)

(C)

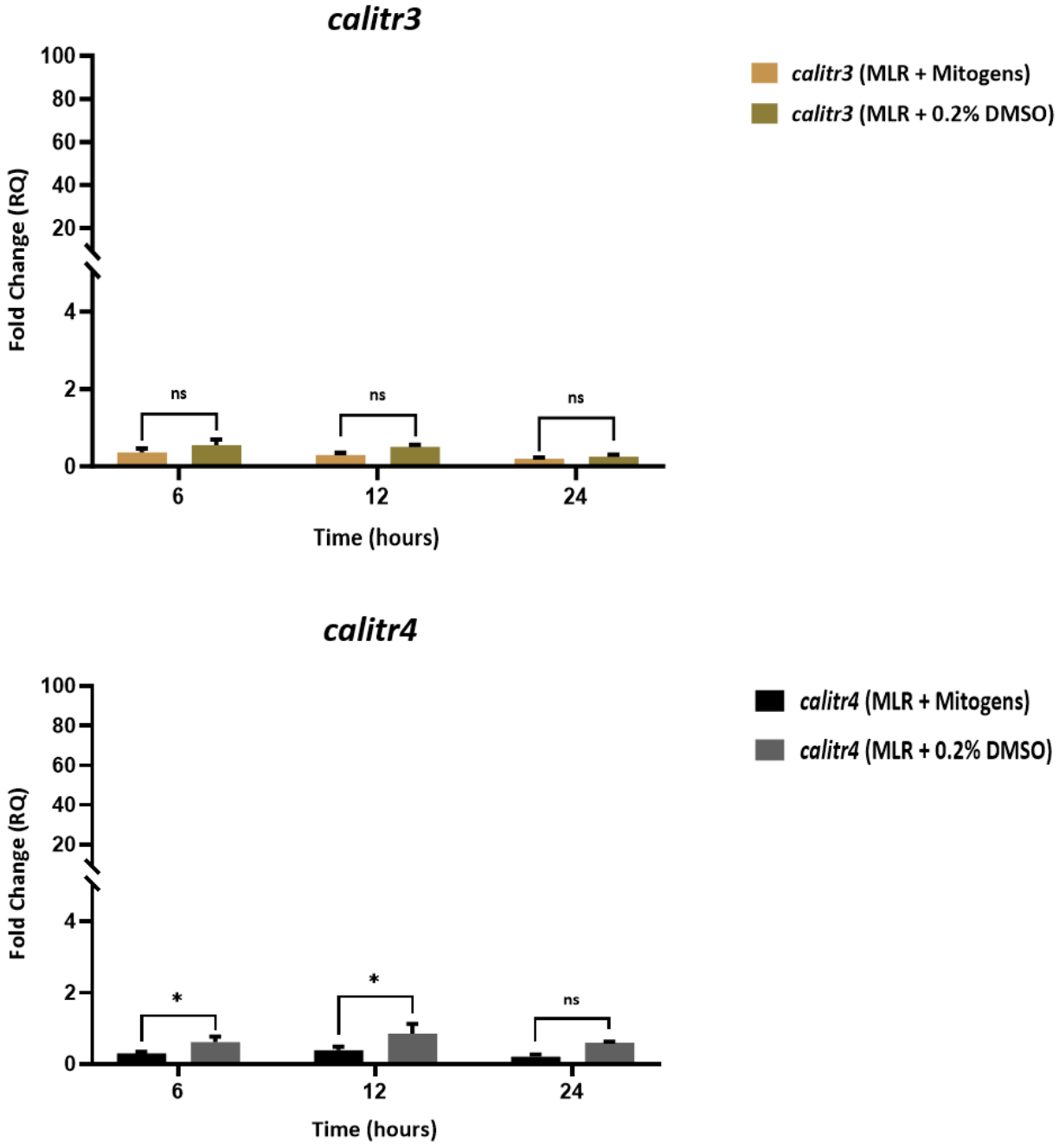

Figure 6.2. Expression patterns of pro-inflammatory markers and *calitrs* in goldfish MLRs upon exposure to T-cell mitogens. (A) The mRNA expressions of goldfish *tnf-α2* and *ifn-γ* in DMSO-vehicle-treated MLRs/mitogen-activated MLRs over time. **(B)** The transcript levels of *calitr1* and *calitr2* in DMSO-vehicle-treated MLRs/mitogen-activated MLRs over time. **(C)** The mRNA expression levels of *calitr3* and *calitr4* in DMSO-treated MLRs/mitogen-activated MLRs over time. Freshly isolated PKMs from ten separate goldfish individuals were combined into one tube and subsequently seeded into a 24-well plate at a density of 1.5×10^6 cells/well and incubated in 0.2% DMSO with complete C-MGFL-15 medium or stimulated with a T-cell

mitogen cocktail containing 10 μg/mL ConA, 10 ng/mL of PMA, and 100 ng/mL of calcium ionophore A23187. Relative fold change was normalized to the endogenous control gene, *ef1α*, and then displayed as fold change in expression relative to the 0-h time point (RQ = 1) for each gene. This experiment has been replicated three times ($n = 3$). Each bar graph represents the mean value. Each error bar indicates the standard deviation (SD). *P*-values are illustrated as $^{ns}p > 0.05$, $^{*}p \leq 0.05$, $^{**}p \leq 0.01$, $^{***}p \leq 0.001$, and $^{****}p \leq 0.0001$.

(A)

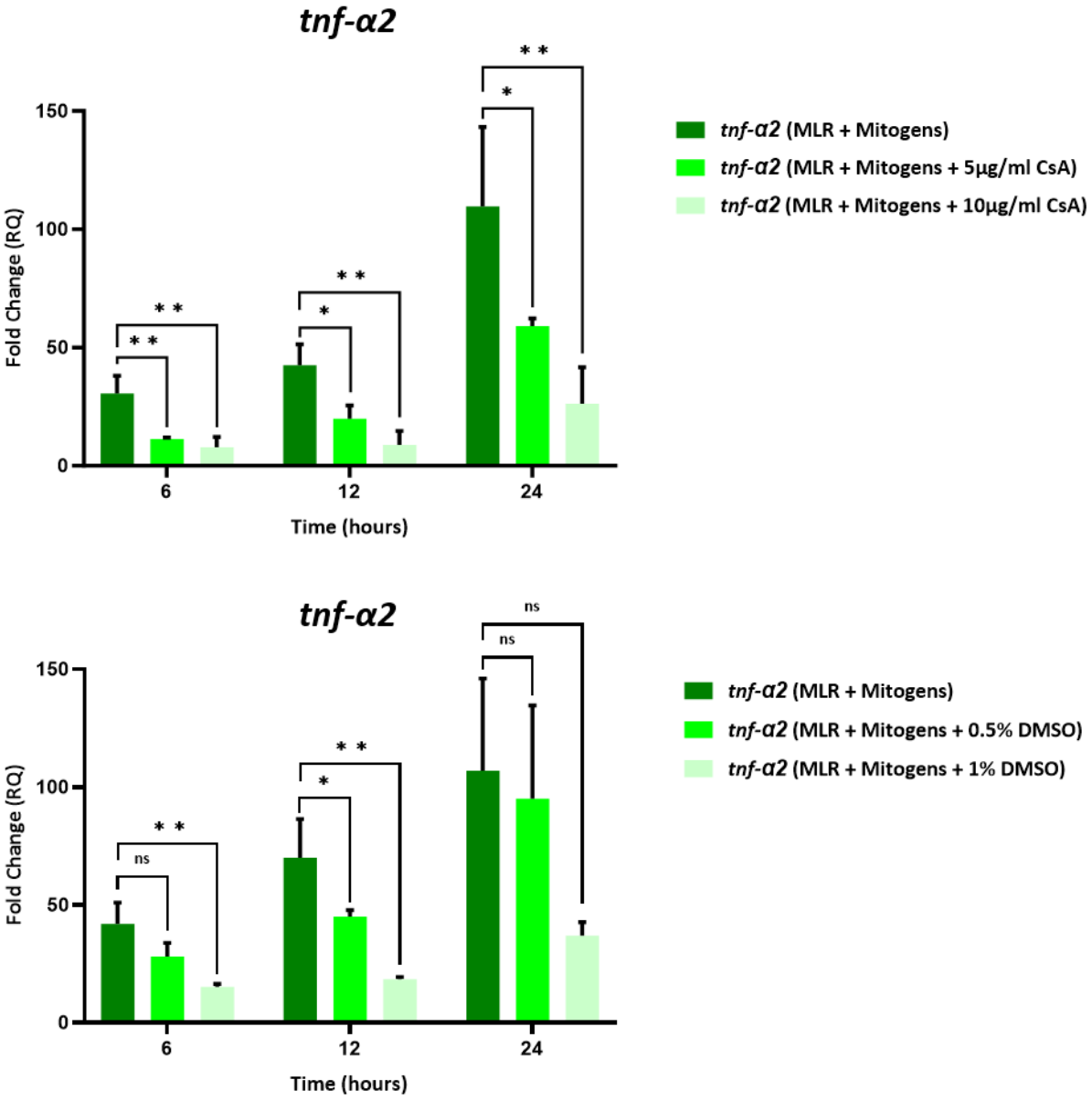
tnf-α2
Fold Change (RQ)
150
100
50
0
6
12
24
Time (hours)
* *
*
* *
*
* *
tnf-α2 (MLR + Mitogens)
tnf-α2 (MLR + Mitogens + 5µg/ml CsA)
tnf-α2 (MLR + Mitogens + 10µg/ml CsA)
tnf-α2
Fold Change (RQ)
150
100
50
0
6
12
24
Time (hours)
ns
ns
* *
*
* *
tnf-α2 (MLR + Mitogens)
tnf-α2 (MLR + Mitogens + 0.5% DMSO)
tnf-α2 (MLR + Mitogens + 1% DMSO)

(B)

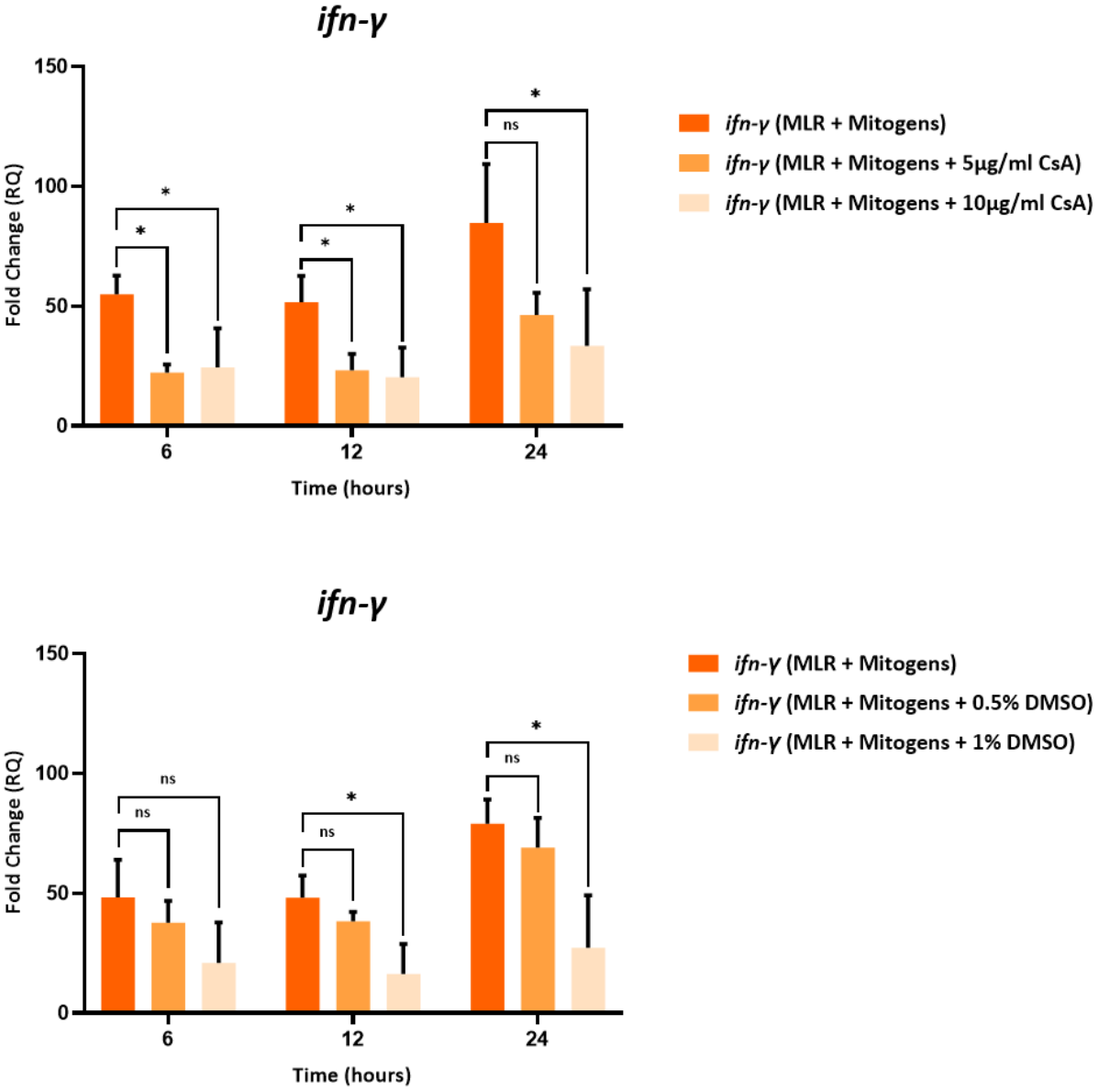
ifn-γ
150
100
50
0
Fold Change (RQ)
*
*
*
*
ns
*
6
12
24
Time (hours)
ifn-γ (MLR + Mitogens)
ifn-γ (MLR + Mitogens + 5µg/ml CsA)
ifn-γ (MLR + Mitogens + 10µg/ml CsA)
ifn-γ
150
100
50
0
Fold Change (RQ)
ns
ns
*
ns
*
ns
6
12
24
Time (hours)
ifn-γ (MLR + Mitogens)
ifn-γ (MLR + Mitogens + 0.5% DMSO)
ifn-γ (MLR + Mitogens + 1% DMSO)

(C)

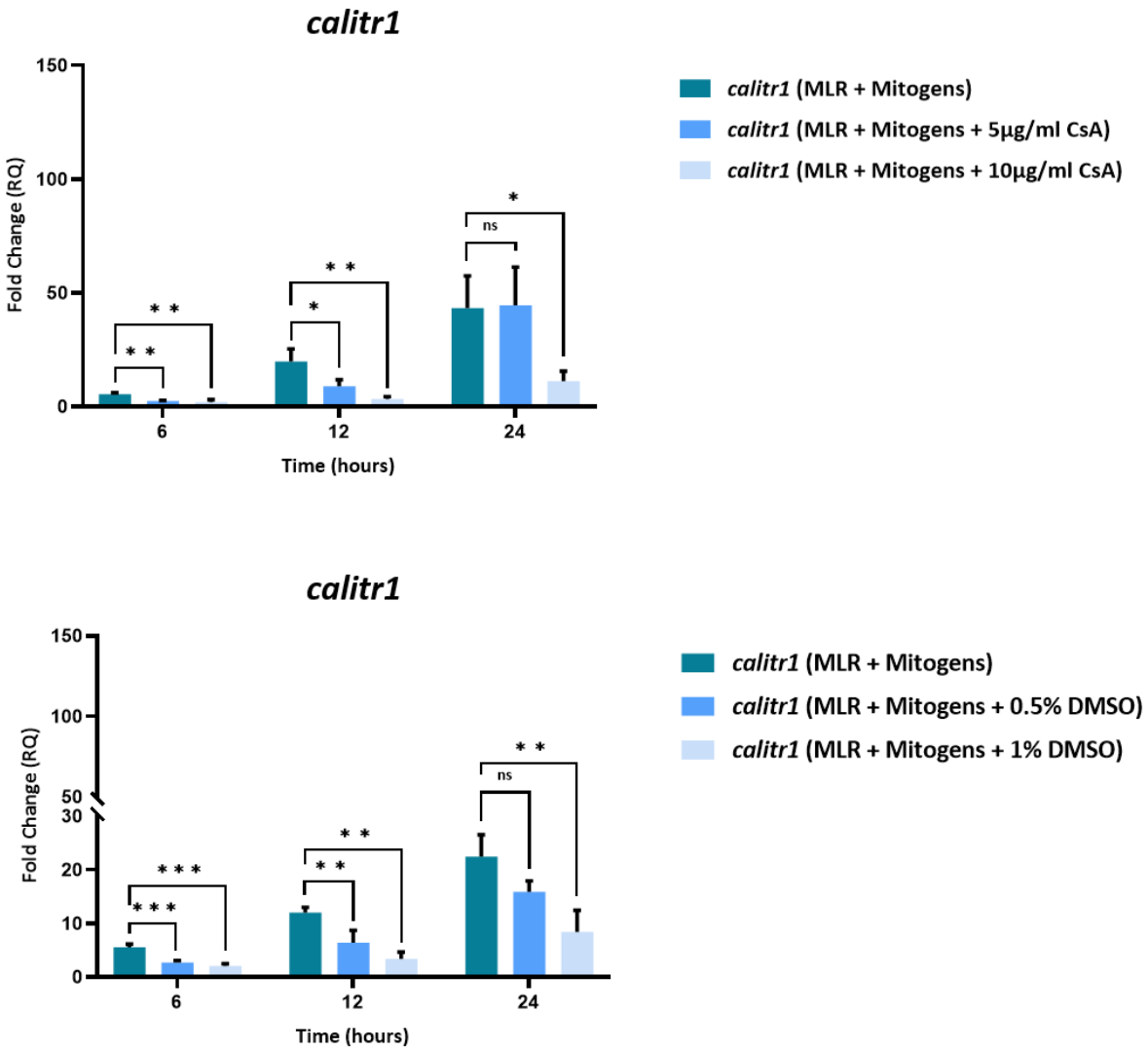
calitr1
Fold Change (RQ)
150
100
50
0
6
12
24
Time (hours)
* *
* *
* *
*
*
ns
calitr1 (MLR + Mitogens)
calitr1 (MLR + Mitogens + 5µg/ml CsA)
calitr1 (MLR + Mitogens + 10µg/ml CsA)
calitr1
Fold Change (RQ)
150
100
50
30
20
10
0
6
12
24
Time (hours)
* * *
* * *
* *
* *
* *
ns
calitr1 (MLR + Mitogens)
calitr1 (MLR + Mitogens + 0.5% DMSO)
calitr1 (MLR + Mitogens + 1% DMSO)

(D)

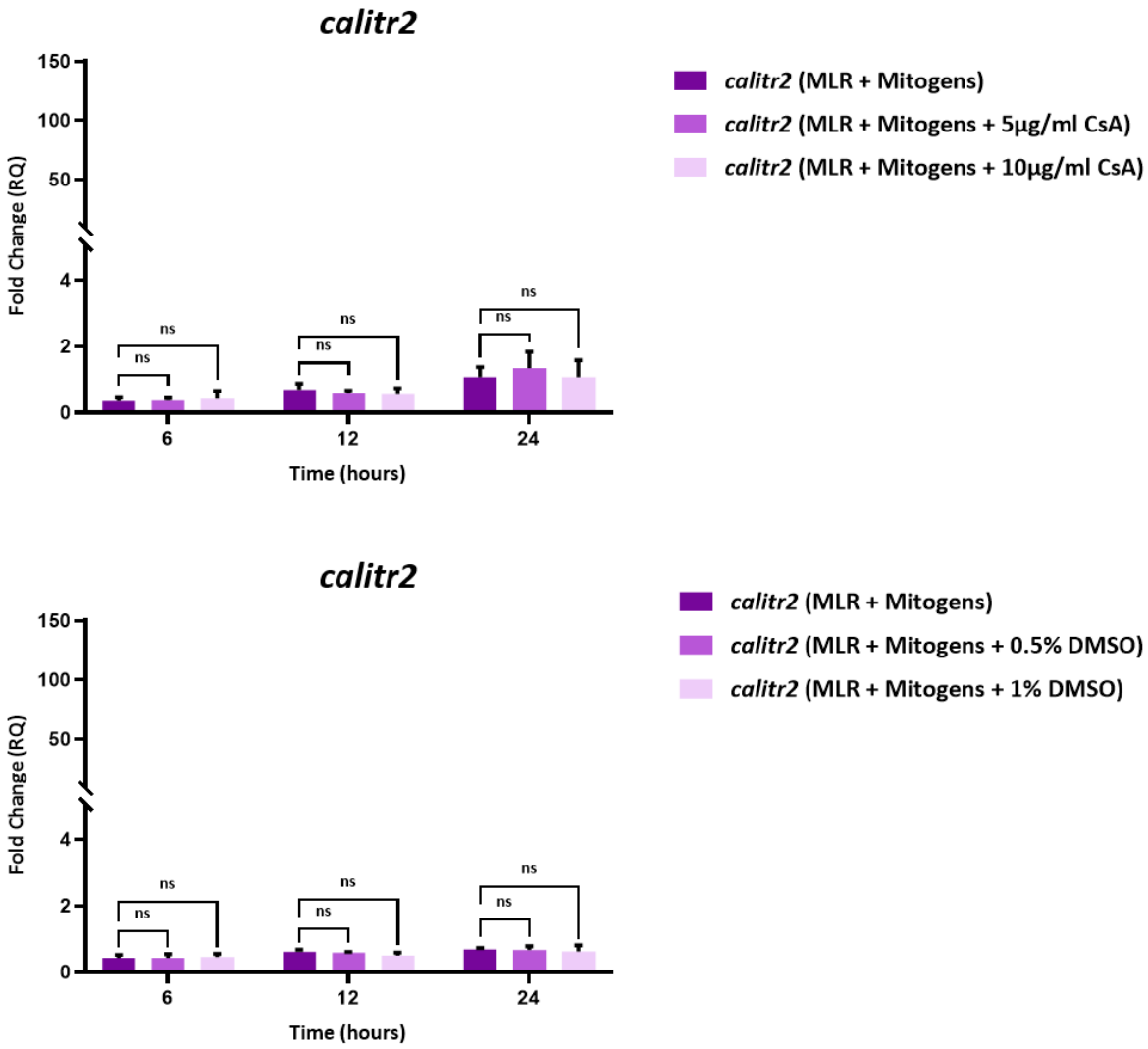
calitr2
150
100
50
4
2
0
Fold Change (RQ)
ns
ns
ns
ns
ns
ns
6
12
24
Time (hours)
calitr2 (MLR + Mitogens)
calitr2 (MLR + Mitogens + 5µg/ml CsA)
calitr2 (MLR + Mitogens + 10µg/ml CsA)
calitr2
150
100
50
4
2
0
Fold Change (RQ)
ns
ns
ns
ns
ns
ns
6
12
24
Time (hours)
calitr2 (MLR + Mitogens)
calitr2 (MLR + Mitogens + 0.5% DMSO)
calitr2 (MLR + Mitogens + 1% DMSO)

(E)

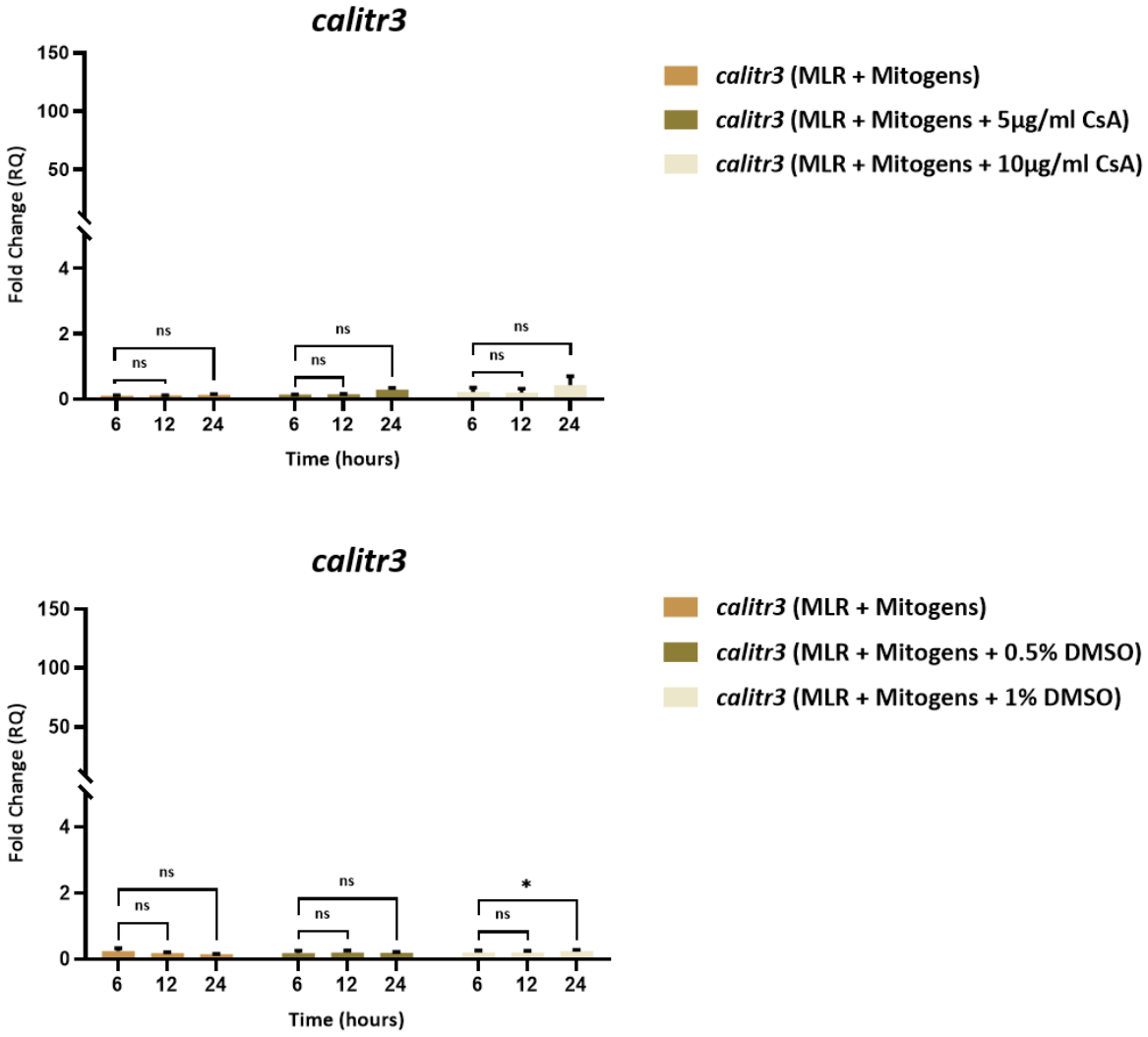
calitr3
150
100
50
4
2
0
Fold Change (RQ)
ns
ns
ns
ns
ns
ns
6
12
24
6
12
24
6
12
24
Time (hours)
calitr3 (MLR + Mitogens)
calitr3 (MLR + Mitogens + 5µg/ml CsA)
calitr3 (MLR + Mitogens + 10µg/ml CsA)
calitr3
150
100
50
4
2
0
Fold Change (RQ)
ns
ns
ns
ns
*
ns
6
12
24
6
12
24
6
12
24
Time (hours)
calitr3 (MLR + Mitogens)
calitr3 (MLR + Mitogens + 0.5% DMSO)
calitr3 (MLR + Mitogens + 1% DMSO)

(F)

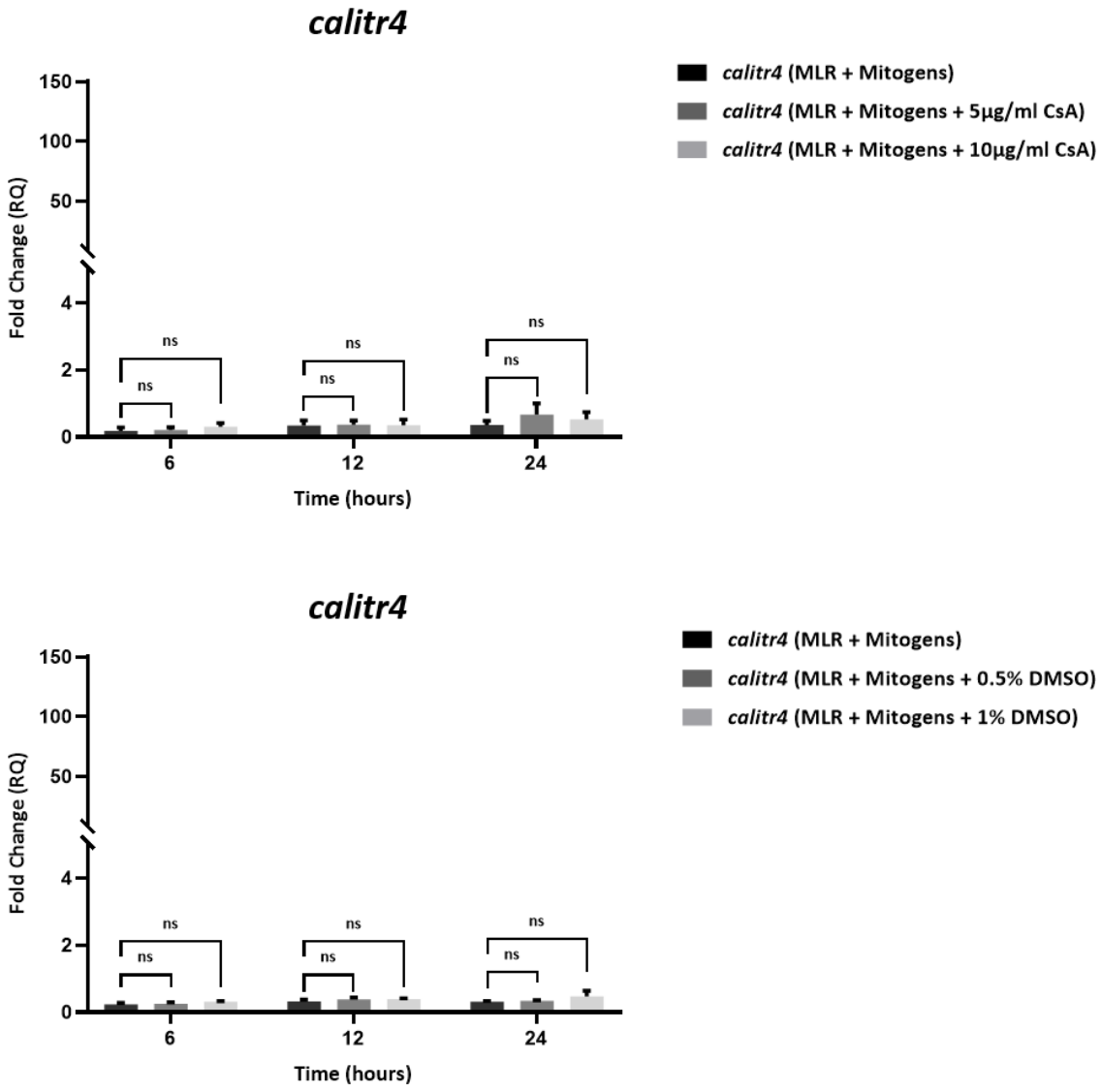

Figure 6.3. RT-qPCR analysis of the expression patterns of pro-inflammatory markers and *calitrs* in mitogen-activated MLRs treated with the various concentrations of CsA (dissolved in DMSO) or mitogen-stimulated MLRs treated with the various concentrations of DMSO vehicle controls over time. (A) Expressions of goldfish *tnf-α2*. **(B)** Expressions of goldfish *ifn-γ*. **(C)** Expressions of *calitr1*. **(D)** Expressions of *calitr2*. **(E)** Expressions of *calitr3*. **(F)** Expressions of *calitr4*. Relative fold change was normalized to the endogenous control gene, *ef1α*, and then displayed as fold change in expression relative to the 0-h time point (RQ = 1) for each gene. All experiments have been replicated three times ($n = 3$). Each bar graph represents the mean value. Each error bar indicates the standard deviation (SD). *P*-values are illustrated as $^{ns}p > 0.05$, $^{*}p \leq 0.05$, $^{**}p \leq 0.01$, $^{***}p \leq 0.001$, and $^{****}p \leq 0.0001$.

(A)

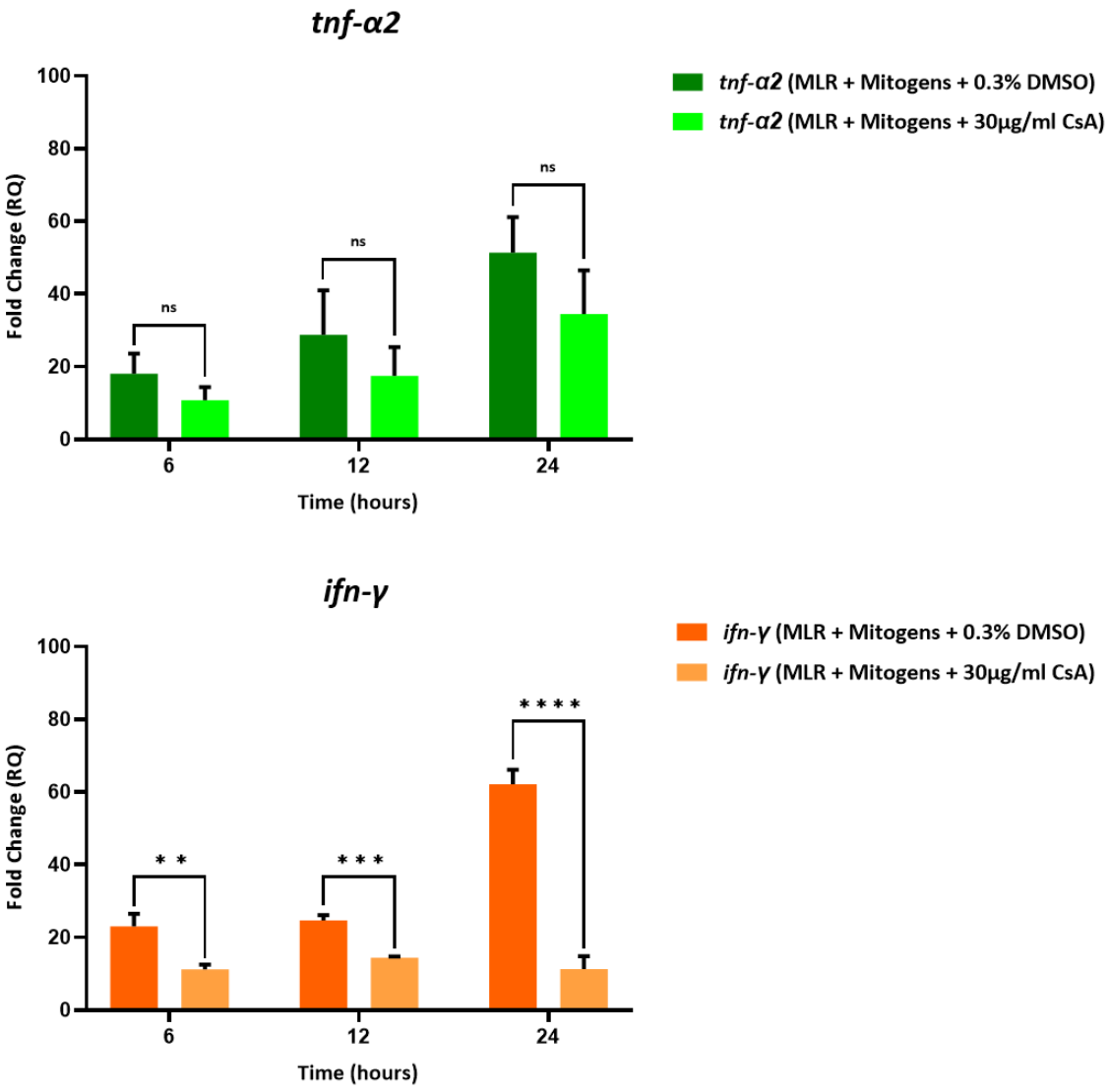
tnf-α2
Fold Change (RQ)
100
80
60
40
20
0
ns
ns
ns
6
12
24
Time (hours)
tnf-α2 (MLR + Mitogens + 0.3% DMSO)
tnf-α2 (MLR + Mitogens + 30µg/ml CsA)
ifn-γ
Fold Change (RQ)
100
80
60
40
20
0
* *
* * *
* * * *
6
12
24
Time (hours)
ifn-γ (MLR + Mitogens + 0.3% DMSO)
ifn-γ (MLR + Mitogens + 30µg/ml CsA)

(B)

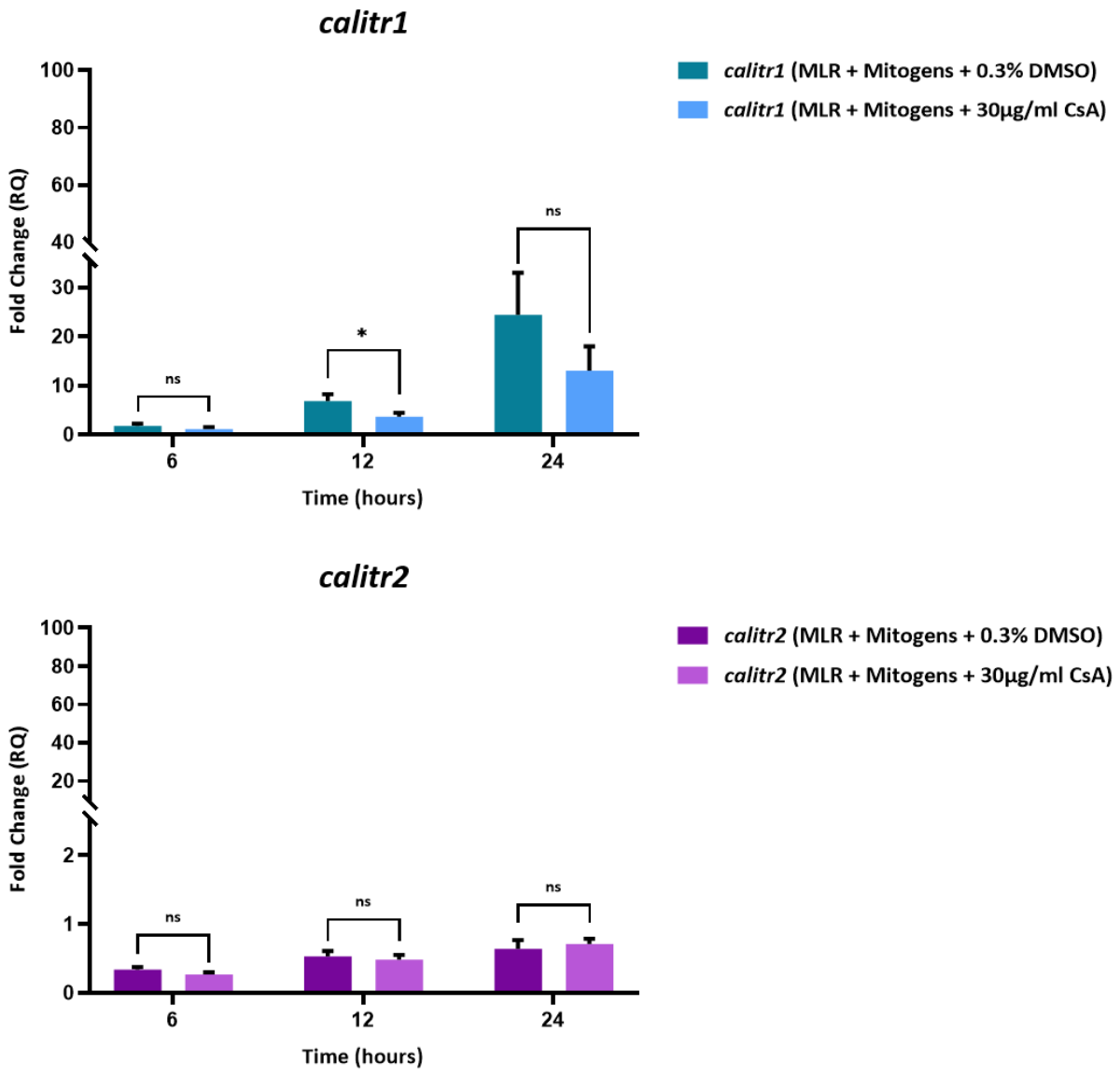
calitr1
Fold Change (RQ)
100
80
60
40
30
20
10
0
ns
*
ns
6
12
24
Time (hours)
calitr1 (MLR + Mitogens + 0.3% DMSO)
calitr1 (MLR + Mitogens + 30µg/ml CsA)
calitr2
Fold Change (RQ)
100
80
60
40
20
2
1
0
ns
ns
ns
6
12
24
Time (hours)
calitr2 (MLR + Mitogens + 0.3% DMSO)
calitr2 (MLR + Mitogens + 30µg/ml CsA)

(C)

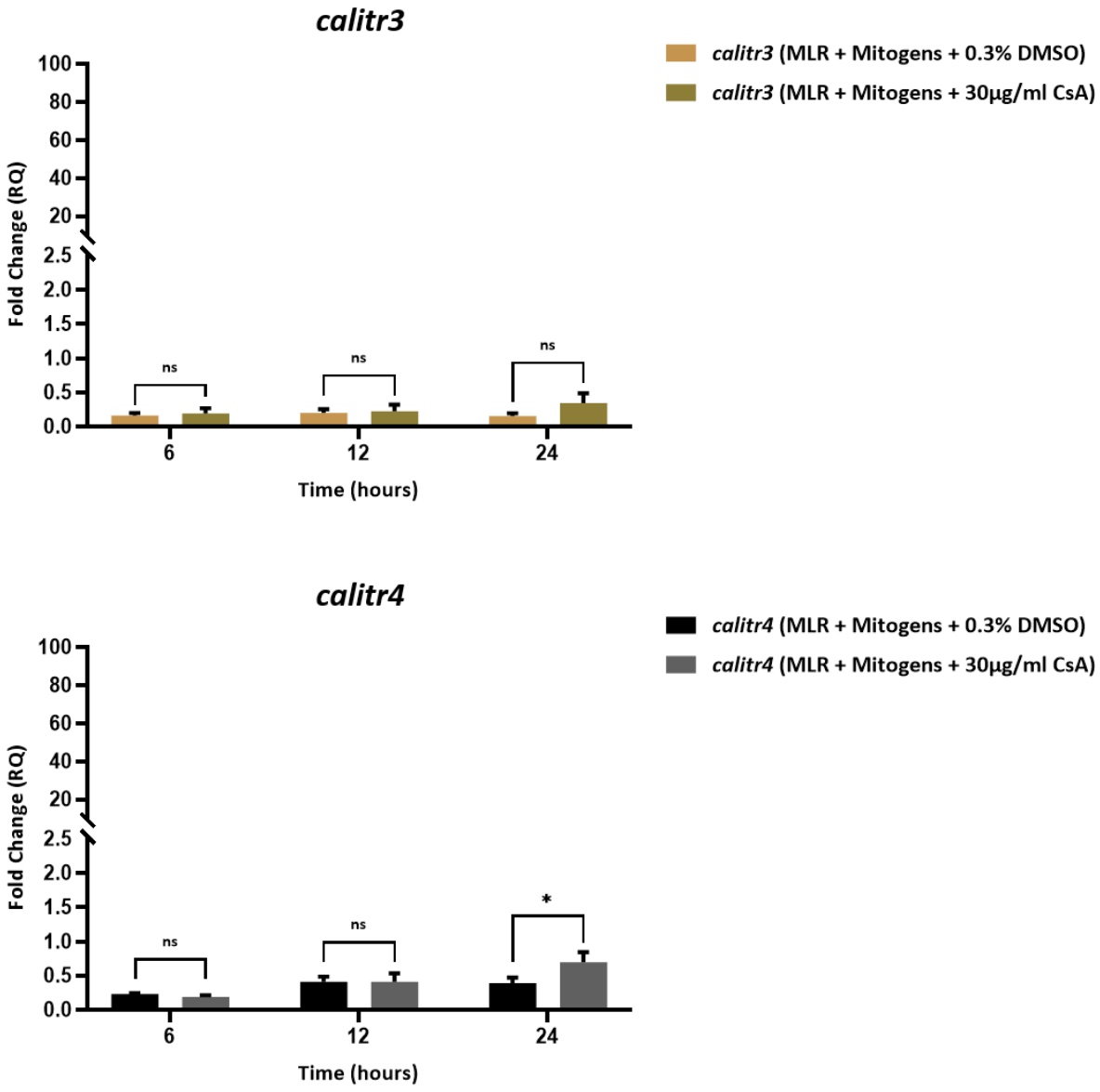

Figure 6.4. Expression profiles of pro-inflammatory markers and *calitrs* in mitogen-activated MLRs treated with 0.3% DMSO vehicle or mitogen-activated MLRs exposed to 30 µg/mL of CsA. (A) The mRNA expression levels of *tnf-α2* and *ifn-γ*. **(B)** The transcript levels of *calitr1* and *calitr2*. **(C)** The transcript levels of *calitr3* and *calitr4*. Relative fold change was normalized to the endogenous control gene, *ef1α*, and then displayed as fold change in expression relative to the 0-h time point (RQ = 1) for each gene. This experiment has been replicated three times ($n = 3$). Each bar graph represents the mean value. Each error bar indicates the standard deviation (SD). *P*-values are illustrated as $^{ns}p > 0.05$, $^{*}p \leq 0.05$, $^{**}p \leq 0.01$, $^{***}p \leq 0.001$, and $^{****}p \leq 0.0001$.

Genes	Forward primer sequences (5’ to 3’)	Reverse primer sequences (5’ to 3’)
*ef1α**	CCGTTGAGATGCACCAT	TTGACAGACACGTTCTTCACGTT
ifn-γ’	GAAACCCTATGGGCGATCAA	GTAGACACGCTTCAGCTCAAACA
tnf-α2’	TCATTCCTTACGACGGCATTT	CAGTCACGTCAGCCTTGCAG
*cmyb**	GGGCTTACGGATGCATTAAAGA	GAGCAGGGATGCCTTCCA
*runx1**	TCAAGGTAGTTGCCCTTGGTGATA	TTGAGGAGGGTTTGTGAAGACGGT
igm	CAGCATCTAAGGACAGCTCTAATC	TCAGGAGTACACTGGGACAT
tcrα	GCCTCTGGAACATCATTGACT	GCTTTCTCCTCGCATTCTTCT
calitr1	GAGAGTCTCTGATGGAGGAAGA	GATGACGTCTGTCTGCTGTATG
calitr2	AAAGTCAGACGAGGGTTTCTAC	CAGGACCAAGACGACAATGA
calitr3	CCAGTATGGGTCACTGTTGTT	GCTGTTCACTCTCTGTGTATCTT
calitr4	AGAGGAGCTGGAGGAAACTA	AGCTCAGAGAGAGAGAGATCAA

Table 6.1. qPCR Primers used for amplification of the endogenous control, inflammatory marker, and *calitr* genes. *Primers and ‘primers were acquired from these publications (Grayfer et al., 2011; Katzenback et al., 2011).

CHAPTER VII

A LEUKOCYTE IMMUNE-TYPE RECEPTOR SPECIFIC POLYCLONAL ANTIBODY STAINS GOLDFISH KIDNEY LEUKOCYTES AND ACTIVATES THE MAPK PATHWAY IN ISOLATED GOLDFISH KIDNEY NEUTROPHIL-LIKE CELLS

7.1 INTRODUCTION

In the previous chapter, I described findings regarding the transcriptional activities of several *calitrs* from distinct goldfish Chrs. However, without CaLITR-specific Abs, I cannot examine the protein expression profiles of these CaLITRs or investigate their functional implications. As previously described, the *calitr3* transcript was cloned from the goldfish kidney and was shown to be expressed during goldfish PKM development and in goldfish neutrophil-like cells. Furthermore, CaLITR3 represents a putative activating receptor-type, having four Ig-like domains, a TM containing a positively charged histidine residue, and a short CYT. Therefore, it's possible that CaLITR3 participates in the regulation of innate immune effector responses in the various goldfish myeloid cells.

In this chapter, I describe the development of a polyclonal antibody (pAb) specific for CaLITR3 and its application in investigating the immunoregulatory roles of CaLITRs in goldfish myeloid cells. This Ab was produced by immunizing rabbits with the recombinant D1 peptide (GAERGGSRTSNISDEC) of CaLITR3 (Fig. 7.1), as blast searches (tblastn) of the goldfish reference genome (goldfish (taxid:7957)) database confirmed that the D1 peptide is relatively specific for CaLITR3. For simplicity, I have renamed the anti-GAERGGSRTSNISDEC pAb to anti-CaL3.D1 pAb. My findings showed that the anti-CaL3.D1 pAb recognized a prominent 70 kDa protein in goldfish neutrophil lysates. Additionally, this interaction was effectively blocked when the anti-CaL3.D1 pAb was pre-incubated with an excess amount of the D1 peptide. In contrast, an excess amount of the D2 peptide (DNKYNYQKLSGC, a peptide located within the

D2 of CaLITR3) of CaLITR3 could not block the anti-CaL3.D1 pAb from interacting with the 70 kDa protein, supporting the specificity of anti-CaL3.D1 pAb for the D1 peptide.

Further experiments showed that the anti-CaL3.D1 pAb stained neutrophil-like cells and various other hematopoietic cell-types within the goldfish kidney. Using confocal microscopy, I also confirmed the staining capability of anti-CaL3.D1 pAb in both PKNs and PKMs. Additionally, my flow cytometry experiments identified the presence of anti-CaL3.D1-pAb-reactive proteins on the cell surface of goldfish neutrophils. Importantly, the cross-linking of anti-CaL3.D1-pAb-reactive membrane proteins in goldfish neutrophils using anti-CaL3.D1 pAb triggered the phosphorylation of 38-kDa mitogen-activated protein kinase (p38) and extracellular signal-regulated kinase 1/2 (ERK1/2), supporting the activating functions of CaLITR3 proteins. Overall, these data suggest that surface-expressed CaLITRs can activate the ERK and p38 signaling pathways, which are associated with a variety of antimicrobial immune responses such as reactive oxygen species (ROS) production, NETosis, degranulation, and production of proinflammatory cytokines. Furthermore, these findings imply that upon ligand binding, stimulatory LITR-types may trigger teleost neutrophil antimicrobial responses.

7.2 RESULTS

7.2.1 Anti-CaL3.D1 pAb stains rCaLITR3-expressing AD293 cells and shows specificity for recombinant CaLITR3

To characterize the specificity of anti-CaL3.D1 pAb, I initially examined its ability to distinguish between AD293 cells overexpressing HA-tagged recombinant (r)CaLITR3 proteins and parental AD293 cells lacking expression of any HA-tagged proteins. Using flow cytometry and confocal microscopy, I confirmed the presence of HA-tagged rCaLITR3 proteins on the

surface of AD293 cells (Fig. 7.2A; Fig. 7.2B). Specifically, in comparison to the mouse IgG1 isotype control group that displayed no staining, rCaLITR3-expressing AD293 cells showed significantly higher levels of immunofluorescence after staining with an anti-HA mAb. With the expression of HA-tagged rCaLITR3 proteins established using AD293 cells, I then evaluated the ability of anti-CaL3.D1 pAb to label rCaLITR3-expressing AD293 cells. Consistent with the results obtained using the anti-HA mAb, rCaLITR3-expressing AD293 cells were strongly stained by anti-CaL3.D1 pAb (Fig. 7.2C). Conversely, no immunofluorescence of rCaLITR3-expressing cells was observed for the normal rabbit pAb control group (Fig. 7.2C). The anti-CaL3.D2 pAb, a rabbit pAb developed against a peptide (the D2 peptide) located in the D2 ectodomain of CaLITR3, also failed to stain rCaLITR3-expressing AD293 cells (Fig. 7.2D).

Following validation that the anti-CaL3.D1 pAb binds to rCaLITR3 proteins on the membrane of AD293 cells, I examined whether these interactions could be blocked by the D1 peptide (the peptide used to initially generate the anti-CaL3.D1 pAb). As shown in Fig. 7.2C (bottom panels), overnight preincubation of anti-CaL3.D1 pAb with the D1 peptide at a ratio of 1 to 50, blocked the reactivity of anti-CaL3.D1 pAb towards rCaLITR3-expressing AD293 cells. In contrast, preincubating anti-CaL3.D1 pAb with the D2 peptide (a CaLITR3 peptide distinct from D1) overnight at a 1 to 50 ratio did not prevent the anti-CaL3.D1 pAb from staining rCaLITR3-expressing AD293 cells (Fig. 7.2D).

As shown in Fig. 7.3A, the anti-HA mAb did not stain parental AD293 cells, confirming that these cells do not express any HA-tagged proteins. Importantly, no staining of parental AD293 cells was observed with the anti-CaL3.D1 pAb and anti-CaL3.D2 pAb (Fig. 7.3B; Fig. 7.3C). To rule out the possibility of a chance interaction between anti-CaL3.D1 pAb and overexpressed rCaLITR3 proteins, which may occur due to increased availability of substrates

for protein interactions in overexpressed proteins, I investigated if the anti-CaL3.D1 pAb could also stain AD293 cells overexpressing a different LITR protein. The ectodomains of rIpLITR2.6b/6.1CYT share roughly 42% percent identity with those of CaLITR3. Despite observing high levels of immunofluorescence in AD293 cells expressing HA-tagged rIpLITR2.6b/6.1CYT proteins (Fig. 7.4A), the anti-CaL3.D1 pAb did not stain rIpLITR2.6b/6.1CYT-expressing AD293 cells (Fig. 7.4B).

I also performed immunoprecipitation experiments to determine if the anti-CaL3.D1 pAb could pull down rCaLITR3 proteins from the lysates of rCaLITR3-expressing AD293 cells. As shown in Fig. 7.5A, the anti-HA mAb did not precipitate proteins from parental AD293 cell lysate. Likewise, the mouse IgG1 isotype control antibody had no reactivity towards HA-tagged rCaLITR3 proteins (Fig. 7.5A). In comparison, the anti-HA mAb effectively precipitated rCaLITR3 proteins from rCaLITR3-expressing AD293 cell lysate (Fig. 7.5A). Compared to the normal-rabbit-IgG-coated magnetic Dynabeads, which did not capture rCaLITR3 proteins from rCaLITR3-expressing AD293 cell lysate (Fig. 7.5B), the anti-CaL3.D1 pAb clearly precipitated rCaLITR3 proteins from this lysate (Fig. 7.5B). In line with the confocal microscopy findings, the anti-HA mAb effectively pulled down rIpLITR2.6b/6.1CYT proteins (Fig. 7.6A), whereas the anti-CaL3.D1 pAb demonstrated no reactivity towards rIpLITR2.6b/6.1CYT proteins (Fig. 7.6B).

7.2.2 Assessment of the reactivity of anti-CaL3.D1 pAb in goldfish primary cell lysates

To investigate whether the anti-CaL3.D1 pAb is also capable of binding putative CaLITR3 proteins expressed in goldfish cells, I initially examined its ability to interact with proteins in the lysates of various goldfish primary cell populations. As shown in Fig. 7.7, the anti-CaL3.D1 pAb recognizes a prominent 70 kDa protein band in goldfish neutrophils lysates.

Additionally, pre-incubation of the anti-CaL3.D1 pAb with the D1 peptide at a 1 to 50 ratio blocked the interaction between the anti-CaL3.D1 pAb and the putative 70 kDa CaLITR3 protein (Fig. 7.7). In contrast, pre-incubation of the anti-CaL3.D1 pAb with the anti-D2 peptide did not interfere with the binding of anti-CaL3.D1 pAb to the putative CaLITR3 protein (Fig. 7.7). Further western blotting experiments (Fig. 7.8) showed that the anti-CaL3.D1 pAb reacts with a 70 kDa protein in goldfish neutrophil and kidney leukocyte lysates, however, the 70 kDa protein band was not detected when a goldfish splenocyte lysate was probed with the anti-CaL3.D1 pAb (Fig. 7.8).

7.2.3 Anti-CaL3.D1 pAb labels haematopoietic cells within the goldfish kidney

To determine if the anti-CaL3.D1 pAb can recognize putative native CaLITR3 proteins expressed in goldfish tissues, I then explored its potential for staining cells within the goldfish kidney, given that the CaLITR3 cDNA was originally cloned from this organ (Wang et al., 2020). Prior to examining the reactivity of anti-CaL3.D1 pAb in the goldfish kidney, I performed H&E staining on several goldfish kidney tissue sections to visualize the general histological features of the organ. As reported by others , the goldfish kidney contains numerous glomeruli and renal tubules, which are the functional units of the teleost urinary system (Fig. 7.9A).

In accordance with the goldfish kidney as also a major hematopoietic site (Kobayashi et al., 2008; Kondera, 2019), I noted that the goldfish kidney tissue sections had a high abundance of dark-purple-stained leukocyte-like cells (Fig. 7.9A). These cells were often situated near glomeruli and renal tubules. Similar to earlier findings (Katzenback & Belosevic, 2009; Watson, 1963), upon closer inspection of the pool of hematopoietic cells, many tissue-resident neutrophil-like cells were identifiable (Fig. 7.9B), as these cells predominately featured kidney-shaped nuclei. Additionally, I observed a variety of other leukocyte cell types containing round nuclei

reminiscent of lymphocytes and/or progenitor cells. I then examined whether the anti-CaL3.D1 pAb stained any of these leukocyte-like cells within the goldfish kidney tissue. As shown in Fig. 7.10B, kidney tissue sections displayed strong staining with the anti-CaL3.D1 pAb, while the normal rabbit control group showed no staining (Fig. 7.10A). Likewise, no staining was observed for the anti-CaL3.D2 pAb treatment group (Fig. 7.10C).

Upon further analysis of the tissue sections stained with anti-CaL3.D1 pAb, I observed that the anti-CaL3.D1 pAb reacted with diverse structures in the goldfish kidney (Fig. 7.11). Notably, various types of leukocytes located between the renal tubules were strongly stained by the anti-CaL3.D1 pAb (Fig. 7.11). For example, neutrophil-like cells with kidney-shaped nuclei were clearly labeled by the anti-CaL3.D1 pAb (Fig. 7.11, panels i and iv). Furthermore, the immunofluorescence signals appeared diffuse throughout the cytoplasm of these cells. These immunofluorescence patterns were also present in other hematopoietic cell types with round or spindle-shaped nuclei ((Fig. 7.11, panels i and iv). Unfortunately, due to the lack of any immune cell-type-specific antibody reagents, the identity of the goldfish immune cell types stained by the anti-CaL3.D1 pAb is unknown. I also detected anti-CaL3.D1-pAb-based immunofluorescence signals in melanomacrophage structures (Fig. 7.11, panel ii), as well as on both the apical and basal sides of renal tubules (Fig. 7.11, panel iii). However, since melanomacrophages consistently had strong autofluorescence in the Alexa Fluor 647 channel (Fig. 7.12), I was uncertain if these cells were specifically stained by the anti-CaL3.D1 pAb.

I also examined a kidney tissue section containing several large melanomacrophage clusters (MMCs) and erythrocytes (Fig. 7.13, panel i). Like the other goldfish kidney sections examined, I observed intense immunofluorescence in the hematopoietic cells surrounding the auto-fluorescent MMCs. Intriguingly, none of the erythrocytes examined displayed anti-

CaL3.D1-pAb-based staining (Fig. 7.13, panel ii). However, in contrast, a neutrophil-like cell with a kidney-shaped nucleus (Fig. 7.13, panel ii) was distinctive among the erythrocyte population in that it showed positive staining with the anti-CaL3.D1 pAb. The absence of anti-CaL3.D1-pAb-based staining in erythrocytes was once again observed in another large mass of erythrocytes (Fig. 7.14, panel i). This contrasted markedly with the immunofluorescent renal structures and hematopoietic cells (Fig. 7.14, panels ii and iii) adjacent to the erythrocyte mass.

As shown in Fig. 7.15, like the erythrocytes, glomeruli were also consistently unstained when treated with the anti-CaL3.D1 pAb (Fig. 7.15, panel i). Conversely, hematopoietic cells situated next to renal tubules were observed to be immunofluorescent (Fig. 7.15, panel ii). Specifically, the anti-CaL3.D1 pAb stained hematopoietic cells with spindle-shaped and kidney-shaped nuclei (Fig. 7.15, panel ii), showing a diffuse cytoplasmic staining pattern within these cells. These findings reinforce that the anti-CaL3.D1 pAb stains various lineages of hematopoietic cells brighter than erythrocytes and glomeruli.

7.2.4 Goldfish PKNs have higher *calitr3* transcript expression levels in comparison to mixed kidney leukocytes and erythrocytes

The overall anti-CaL3.D1-pAb-based immunofluorescence staining observed in goldfish kidney tissues suggests a potential higher expression of putative CaLITR3 proteins in neutrophil-like cells and cells resembling lymphocytes/progenitors relative to erythrocytes and glomerular cells. To further examine this possibility, I investigated the mRNA expression of *calitr3* in isolated PKNs, mixed kidney leukocytes predominately comprising small cells reminiscent of lymphocytes and/or progenitors, and erythrocytes. These specific cell populations were selected due to their relatively easier isolation compared to glomerular cells. As shown in Fig. 7.16, PKNs exhibited approximately a 30-fold higher *calitr3* expression compared to the

erythrocytes. Although mixed kidney leukocytes displayed a four-fold increase in *calitr3* mRNA expression compared to erythrocytes, this difference was not statistically significant.

7.2.5 The anti-CaL3.D1 pAb stains isolated PKNs and PKMs

To further validate the neutrophil staining profiles observed in the goldfish kidney tissue sections, I isolated PKNs and subjected them to staining with the anti-CaL3.D1 pAb. As shown in Fig. 7.17 and Fig. 7.18B, the anti-CaL3.D1 pAb readily stained PKNs, thus verifying the immunofluorescence staining results in the goldfish kidney tissue. Specifically, immunofluorescence signals from the anti-CaL3.D1 pAb appeared to span across the entire surface area of the PKNs (Fig. 7.17, panel i). Also, some of the cells appeared to have a punctate staining pattern around their cytoplasm, indicative of potential granular staining. Like the AD293 cell and goldfish kidney tissue staining experiments, both the normal rabbit (Fig. 7.18A) and anti-CaL3.D2 (Fig. 7.18E) pAbs showed no staining in the PKNs. Moreover, preincubation of the anti-CaL3.D1 pAb and D1 peptide at a 1 to 50 ratio (Fig. 7.18C) eliminated the immunofluorescence signals of anti-CaL3.D1 pAb in the PKNs, whereas the D2 peptide failed to block the anti-CaL3.D1 pAb from interacting with these cells (Fig. 7.18D).

As previously mentioned, besides staining the goldfish neutrophils, the anti-CaL3.D1 pAb also marked various other leukocyte-like cells in the goldfish kidney tissue (Fig. 7.11). Therefore, I investigated if the anti-CaL3.D1 pAb was capable of staining PKMs, another well-characterized myeloid cell type in goldfish. Consistent with the PKN staining results, the anti-CaL3.D1 pAb strongly stained the PKMs (Fig. 7.19). For the majority of the PKMs observed, the immunofluorescence signals generated by anti-CaL3.D1 pAb seemed to be dispersed throughout the cells rather than confined to specific cellular compartments (Fig. 7.19, panel i). Furthermore, highly immunofluorescent dot-like patterns were occasionally observed near the nuclei and/or

cytoplasm of some PKMs, suggestive of potential staining of granular and nuclear proteins. Additionally, I also noted that not all cells from the PKM cultures had strong staining with the anti-CaL3.D1 pAb, as weakly stained PKMs were also observed (Fig. 7.19, panel i). Like the PKN microscopy experiments, I further evaluated the specificity of the anti-CaL3.D1 pAb in the PKMs. Unlike the anti-CaL3.D1-pAb-treated PKMs, which showed strong staining (Fig. 7.20B), the normal rabbit and anti-CaL3.D2 pAbs produced no staining in these cells (Fig. 7.20A; Fig. 7.20E). Furthermore, quenching of the anti-CaL3.D1 pAb with the D1 peptide abolished the reactivity of the anti-CaL3.D1 pAb towards the PKMs (Fig. 7.20C). Conversely, the D2 peptide did not block the anti-CaL3.D1 pAb from staining the PKMs (Fig. 7.20D).

7.2.6 Anti-CaL3.D1 pAb stains proteins on the surface of PKNs

To confirm that the anti-CaL3.D1 pAb stains proteins on the surface of PKNs, I conducted flow cytometry staining experiments. As shown in Fig. 7.21, compared to PKNs treated with normal rabbit pAb, the addition of anti-CaL3.D1 pAb resulted in a rightward shift of the entire immunofluorescence histogram in each fish examined (Fig. 7.21). To quantify the percentage of cells positively stained with anti-CaL3.D1 pAb, we set up a positive gate based on the normal rabbit control histogram for each fish. Specifically, the percentage of anti-CaL3.D1-pAb-positive cells in fish 1, 2, 3, are 57.7%, 36.3%, and 39.5%, respectively. Therefore, PKNs from different goldfish individuals show some variation in the expression of anti-CaL3.D1-pAb-reactive membrane proteins.

7.2.7 Cross-linking of anti-CaL3.D1-pAb-reactive membrane proteins triggers phosphorylation of ERK1/2 and p38 in PKNs

Given that the TM of CaLITR3 contains a positively charged histidine residue (Wang et al., 2020), I hypothesized that it may facilitate the association of the receptor with negatively charged adaptor molecules containing ITAMs (i.e., FcRγ) to transmit stimulatory signals. To test this hypothesis, I examined the phosphorylation status of ERK1/2 and p38 following PKN membrane-protein crosslinking with either the rabbit control pAb or anti-CaL3.D1 pAb. In mammals, ERK1/2 and p38 play crucial roles as mediators of innate immune effector responses and are known to be downstream targets of ITAM-mediated signaling pathways (Chen et al., 2021; Rosales & Uribe-Querol, 2018) in neutrophils. Hence, I focused specifically on these two proteins as functional readouts. As shown in Fig. 7.22A, I observed a low level of baseline p38 phosphorylation in PKNs treated with the normal rabbit pAb across all examined time points (0, 5, 10, 15, and 30 min) (Fig. 7.22A). In contrast, treatment with anti-CaL3.D1 pAb caused a significant increase of over 20-fold in p38 phosphorylation as early as 5 min post-treatment (Fig. 7.22A; Fig. 7.22B). This elevated p38 phosphorylation persisted for the remaining time points. Interestingly, I also detected an additional anti-p38-mAb-reactive band at a lower molecular weight (~35kDa) compared to the canonical p38 protein (38kDa) in this experiment (Fig. 7.22A). I speculate that this band may correspond to a goldfish p38 isoform. Moreover, this putative p38 isoform exhibited comparable activation kinetics to its canonical counterpart. Notably, the p38 isoform protein displayed a basal level of phosphorylation after treatment with the rabbit control pAb, and a markedly increased level of phosphorylation following treatment with the anti-CaL3.D1 pAb. In line with the activation dynamics of p38, I noted a minimal baseline level of ERK1/2 phosphorylation in the normal-rabbit-pAb-treatment group throughout all time points examined (Fig. 7.22C; Fig. 7.22D). However, the anti-CaL3.D1-pAb treatment induced a

significantly higher level of ERK1/2 phosphorylation in PKNs at 5-, 10-, 15-, and 30-min post-treatment.

7.2.8 DISCUSSION

Immunoregulatory receptors serve as important regulators of innate immune cell functions. While it is firmly established that teleost innate immune cells can elicit a range of immune effector responses like degranulation, phagocytosis, and ROS production (Graves et al., 1984; Rieger et al., 2010; Stafford et al., 2002; Utke et al., 2007), our understanding of the specific immunoregulatory receptors responsible for controlling these processes remains limited. LITRs are a large family of teleost immunoregulatory receptor-types that have been shown to have a variety of immunoregulatory potentials. To further investigate LITR-mediated control of teleost innate immune cell functions, I developed and characterized the anti-CaL3.D1 pAb, an Ab specific for a D1 epitope within CaLITR3, a predicted stimulatory receptor-type. Microscopy experiments revealed that the goldfish kidney contains a high abundance of neutrophil-like cells as well as various other leukocytes. While the exact proportions of the hematopoietic cells in the goldfish kidney remains undocumented, insights can be drawn from closely related species like the crucian carp (*Carassius auratus gibelio*) and common carp (*Cyprinus carpio*). Analysis of the common carp head kidney revealed a diverse array of haematopoietic cells (Kondera, 2011), including approximately 13% erythroid cells, 24% neutrophil-like cells, 39% lymphoid cells, 0.98% monocytoid cells, and 18% thrombocytes. Similarly, the head kidney of the crucian carp has a variety of hematopoietic cell lineages, with proportions of approximately 17% neutrophils, 22% myelocytes, 13% blast cells, and 56.4% lymphocytes (Kutyrev et al., 2011). Thus, the kidneys of the crucian carp and common carp display a notable high abundance of neutrophil-like cells and lymphocytes. Considering the relatedness of goldfish to crucian carp and common

carp, it is reasonable to infer that the goldfish kidney likely shares comparable hematopoietic characteristics. Previous research supports the presence of a relatively large reserve of functional neutrophils in the goldfish kidney. Specifically, during inflammation, many neutrophils have been shown to exit the goldfish kidney and enter circulation (Bielek et al., 1999; Havixbeck et al., 2017; Havixbeck et al., 2016). Moreover, neutrophils isolated from the goldfish kidney exhibit similar morphological, cytochemical, and functional characteristics to their mammalian counterparts (Katzenback & Belosevic, 2009, 2012). H&E-stained PKNs are 10-12 μm and possess kidney shaped-nuclei resembling mammalian metamyelocyte or monocytes, although some PKNs appear to also contain unsegmented nuclei. Moreover, these PKNs are stained by Sudan Black and acid phosphatase, and express myeloperoxidase and granulocyte colony stimulating factor receptor (GCSFR) mRNAs (Katzenback & Belosevic, 2009, 2012). Lastly, PKNs induce respiratory burst, degranulation, and chemotactic responses when exposed to a goldfish pathogen (Katzenback & Belosevic, 2009). Therefore, these studies further support the presence of a substantial reserve of functionally mature neutrophil-like cells in the goldfish kidney.

My previous findings revealed a high expression level of the CaLITR3 transcript in both the goldfish kidney and isolated PKNs (Wang et al., 2020). In this study, the anti-CaL3.D1 pAb effectively identified a single protein band of approximately 70 kDa in goldfish neutrophil lysates, similar in size to the rCaLITR3 protein produced by AD293 cells. Moreover, these protein interactions were blocked by the CaLITR3 D1 peptide, whereas the CaLITR3 D2 peptide had no effect. Hence, these data support the specificity of the anti-CaL3.D1 pAb for the CaLITR3 D1 peptide and align with the strong anti-CaL3.D1-pAb-mediated staining observed in

goldfish kidney neutrophil-like cells. Additionally, these results imply the presence of membrane and/or intracellular CaLITR3 proteins in goldfish neutrophils.

I also observed anti-CaL3.D1-pAb-based staining in goldfish kidney hematopoietic cells with a high nucleus-to-cytoplasm ratio, resembling lymphocytes or hematopoietic progenitor cells. Multiple IpLITR1 and IpLITR2 transcripts were also detected in both the channel catfish kidney and several channel catfish lymphocyte cell lines, including TS32.15 and TS32.17 cytotoxic T cell lines, G14D T cells, 3B11 B cells, and IF3 NK-like cells (Stafford, Bengten, et al., 2006). Furthermore, stimulation of channel catfish PBLs with irradiated 3B11 B cells (alloantigen) induced upregulation of multiple *iplitr1* and I *iplitr2* transcripts (Stafford et al., 2007). Additionally, the CC41 mAb, an Ab known to recognize a collection of putative activating and inhibitory IpLITR-types, stained channel catfish PBLs (Taylor et al., 2016). Pre-treatment of these cells with CC41 hindered their ability to lyse allogeneic targets (Taylor et al., 2016). Therefore, it is plausible that putative CaLITR3 proteins are also expressed by goldfish lymphocytes.

Given the documented expression of IpLITR and CaLITR transcripts and proteins in various types of teleost immune cells, I hypothesized that the expression pattern of putative CaLITR3 proteins might also be confined to goldfish immune cells. However, I detected anti-CaL3.D1-pAb-based immunofluorescence in goldfish renal tubular cells. Whether this indicates non-specific binding has not been conclusively established. Immune receptors such as toll-like receptors (i.e., TLR2 and TLR4) are known to be expressed by human and mice renal tubular epithelial cells (TECs) and participate in the recognition and elimination of urinary tract bacterial infections (Chassin et al., 2006; Chowdhury et al., 2006; Liu et al., 2023; Patole et al., 2005). Considering that tubular epithelial cells constitute the frontline of immune defense against

microbial invaders in the goldfish kidney, it is possible that putative CaLITR3 proteins might serve as sensors for microbial intruders within renal tubules. However, further confirmation of the mRNA and protein expression of CaLITRs in TECs is required using an approach such as laser capture microscopy, followed by subsequent analysis of the isolated TECs using RT-PCR. Alternatively, fluorescent in situ hybridization (FISH) could be used to examine the transcript expression of *calitr3* in TECs. Our lab is currently developing *calitr3*-mRNA-specific probes for this purpose.

Contrary to goldfish TECs, no anti-CaL3.D1-pAb-based immunofluorescence was detected in goldfish glomerular cells and erythrocytes, suggesting a potential absence or low levels of putative CaLITR3 proteins in these cell types. qPCR experiments further supported this observation, revealing a significantly higher level of c*alitr3* mRNA expression in the goldfish PKNs compared to erythrocytes and mixed kidney leukocytes. Unfortunately, due to challenges in isolating goldfish glomerular cells, I was unable to determine the relative transcript level of *calitr3* in these cells.

Consistent with the confocal microscopy results, the anti-CaL3.D1 pAb also strongly labeled the goldfish PKNs. Interestingly, a punctate immunofluorescence staining pattern was observed in the cytoplasm of some PKNs, indicative of granular staining. In mammals, it is well-established that a variety of transmembrane receptor proteins are stored within the secretory vesicles of neutrophils (Faurschou & Borregaard, 2003). Upon sensing chemokines or other inflammatory mediators, receptors located within secretory granule, such as CD16, CD14, CR1, and Mac-1, have been shown to undergo rapid mobilization to the cell surface of neutrophils (Detmers et al., 1995; Sengeløv et al., 1995; Sengeløv et al., 1993; Sengeløv et al., 1994). Moreover, these proteins play critical roles in facilitating neutrophil adhesion to vascular

endothelium and phagocytosis (Borregaard et al., 1993; Faurschou & Borregaard, 2003; Othman et al., 2022; Yin & Heit, 2018). Considering that secretory vesicles are formed via endocytosis of membrane proteins (Borregaard et al., 1992) and based on the demonstration of the likely presence of putative CaLITR3 proteins on the cell surface of goldfish neutrophils, it is possible that putative CaLITR3 proteins may also be localized in goldfish neutrophil granules. In addition to PKNs, I also observed strong anti-CaL3.D1-pAb-mediated immunofluorescence in day 7 goldfish PKM cultures. This is unsurprising as the CaLITR3 transcript was shown to be highly expressed during PKM development (Wang et al., 2020). Like PKNs, I also observed a punctate anti-CaL3.D1-pAb-based immunofluorescence pattern in goldfish PKMs, further reinforcing the possibility of an intracellular localization of putative CaLITR3 proteins.

In general, activating immunoregulatory receptor-types feature positively charged TMs and short CYT regions. Consequently, they rely on physical association with adaptor molecules bearing activating tyrosine-based motifs (e.g., ITAMs) to enable the transmission of stimulatory signals (Call & Wucherpfennig, 2007). Since the TM of CaLITR3 contains a positively charged histidine residue, I hypothesized that ligation of putative CaLITR3 proteins on the membrane of goldfish neutrophils with anti-CaL3.D1 pAb could potentially trigger intracellular signaling events. As predicted, anti-CaL3.D1-pAb-mediated cross-linking of PKN membrane proteins induced the phosphorylation of ERK1/2 and p38 proteins in goldfish neutrophils.

In mammals, p38 and ERK1/2 induce the phosphorylation of $p67^{phox}$ and $p47^{phox}$, integral components of NADPH oxidase essential for the production of ROS (El Benna et al., 1996; Sheppard et al., 2005). Furthermore, these proteins have been implicated in the regulation of NETosis in both mammalian and teleost neutrophils (Aleman et al., 2016; Hakkim et al., 2011; Khan & Palaniyar, 2017; Li, Ma, et al., 2022; Simard et al., 2010). Additionally, p38 and ERK1/2

have been shown to cooperate in controlling the transcription and release of cytokines such as IL-6 and TNF in human neutrophils (Carter et al., 1999; Cloutier et al., 2007; Zarubin & Han, 2005). Based on these studies, I hypothesize that the activation of p38 and ERK1/2 in goldfish neutrophils may trigger various downstream neutrophil-mediated inflammatory responses such as ROS production, NETosis, and cytokine release. Given the diverse array of biological processes regulated by pERK and p38, it is plausible that they may also modulate non-inflammatory processes in goldfish neutrophils like cellular survival and migration (Alvarado-Kristensson et al., 2004; Liu et al., 2012). Overall, the activation of p38 and ERK1/2 by anti-CaL3.D1 pAb further supports the ability of anti-CaL3.D1 pAb to recognize putative CaLITR3 proteins on the cell-surface of goldfish neutrophils. These findings represent the second documented instance of activating LITR types transmitting stimulatory signals in teleost immune cells.

In mammals, activating receptors containing a TM lysine residue preferentially associate with DAP12, while those with an arginine residue favour FcRγ interactions (Feng et al., 2006). Although activating receptors with a TM histidine residue have been identified in a few species like birds (i.e., CHIR-A) (Dennis Jr et al., 2000) and humans (i.e., FcγRI) (Morton et al., 1995), little is known about their adaptor assembly mechanism. For example, the TM histidine of FcγRI has been suggested to associate with FcRγ to control phagocytosis and ligand affinity (Miller et al., 1996; Morton et al., 1995; van Vugt et al., 1996). Moreover, replacement of the TM arginine residue of human FcαR with histidine showed no effect on its ability to assemble with FcRγ and regulate downstream signaling responses (Morton et al., 1995). Therefore, I hypothesize that CaLITR3, which also has a TM histidine residue may associate with negatively charged goldfish adaptor molecules, such as FcRγ, to trigger ITAM-mediated signaling

pathways. Interestingly, deletion of a short stretch of amino acids (Lysine, Threonine, Asparagine, and Isoleucine) from the proximal CYT region of human FcγRIIIAα negatively impacted its ability to transduce stimulatory signals (Hou et al., 1996). Additionally, while the neutrophil GPI-anchored protein, FcγRIIIb, appears to lack inherent signaling capability, it has been shown to collaborate with FcγRIIA and complement receptors to transduce activating signals (Daëron, 1997; Edberg & Kimberly, 1994). Thus, I cannot exclude the possibility that putative CaLITR3 proteins may also utilize their short CYTs or the signaling apparatus of other goldfish activating receptors to transmit signals.

Unlike the anti-CaL3.D1 pAb, the anti-CaL3.D2 pAb did not recognize the rCaLITR3 proteins produced by AD293 cells. The reason for this discrepancy is unclear, considering that both pAbs were generated using similar methods, and both the D1 and D2 peptides from CaLITR3 proteins were predicted to be exposed (i.e., using DeepREx-WS). Consistent with the AD293 cell experiments, the anti-CaL3.D2 pAb also failed to stain goldfish PKNs and PKMs, in stark contrast to the strong staining observed with the anti-CaL3.D1 pAb in these cell types. These findings support that the anti-CaL3.D1 pAb likely recognizes putative CaLITR3 proteins in goldfish PKNs and PKNs. Additionally, this hypothesis is reinforced by the observation of the inability of the D2 peptide to block anti-CaL3.D1-pAb-based staining of goldfish PKNs and PKMs, while the D1 peptide completely quenched the reactivity of the anti-CaL3.D1 pAb towards these cells. Although my Ab validation experiments support the specificity of anti-CaL3.D1 pAb for putative CaLITR3 proteins, the identities of the anti-CaL3.D1-pAb-reactive proteins in goldfish PKNs and PKMs have yet to be confirmed. Due to the polygenic nature of the CaLITRs, I cannot exclude the possibility that the anti-CaL3.D1 pAb may also interact with other CaLITR types.

In summary, this study has provided evidence that stimulatory CaLITR-types can transmit activating signals in goldfish PKNs. This lays the groundwork for a more comprehensive investigation of the immunoregulatory functions of CaLITRs in goldfish myeloid cells.

CaLITR3
Amino acid length: **460**
Prediction protein weight: **51.06 kD**

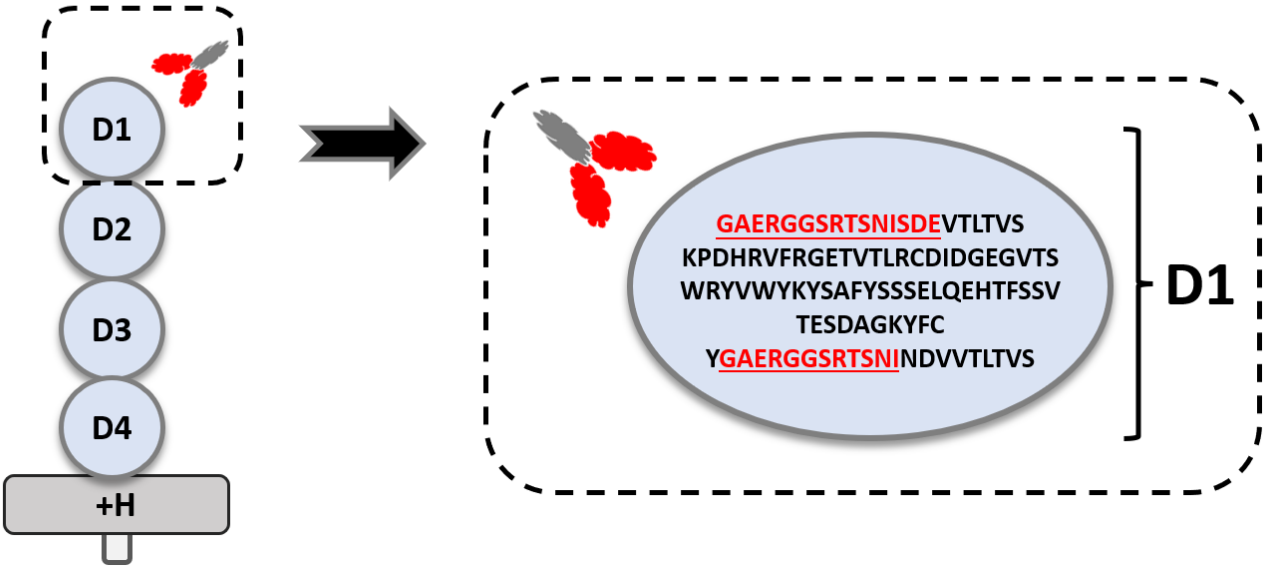

Figure 7.1. Graphical illustrations of the predicted binding site (dashed box) of the anti-CaL3.D1 pAb in CaLITR3.0, as well as the CaLITR3 peptide sequences (underlined in red) predicted to interact with the anti-CaL3.D1 pAb. CaLITR3 is a putative activating receptor-type consisted of a TM containing a positively charged histidine (H) residue.

(A)

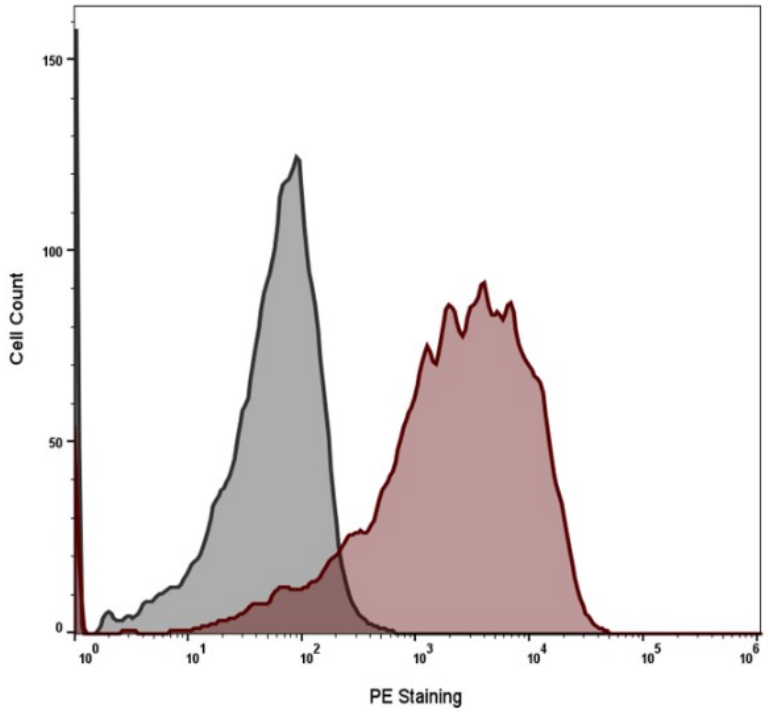

(B)

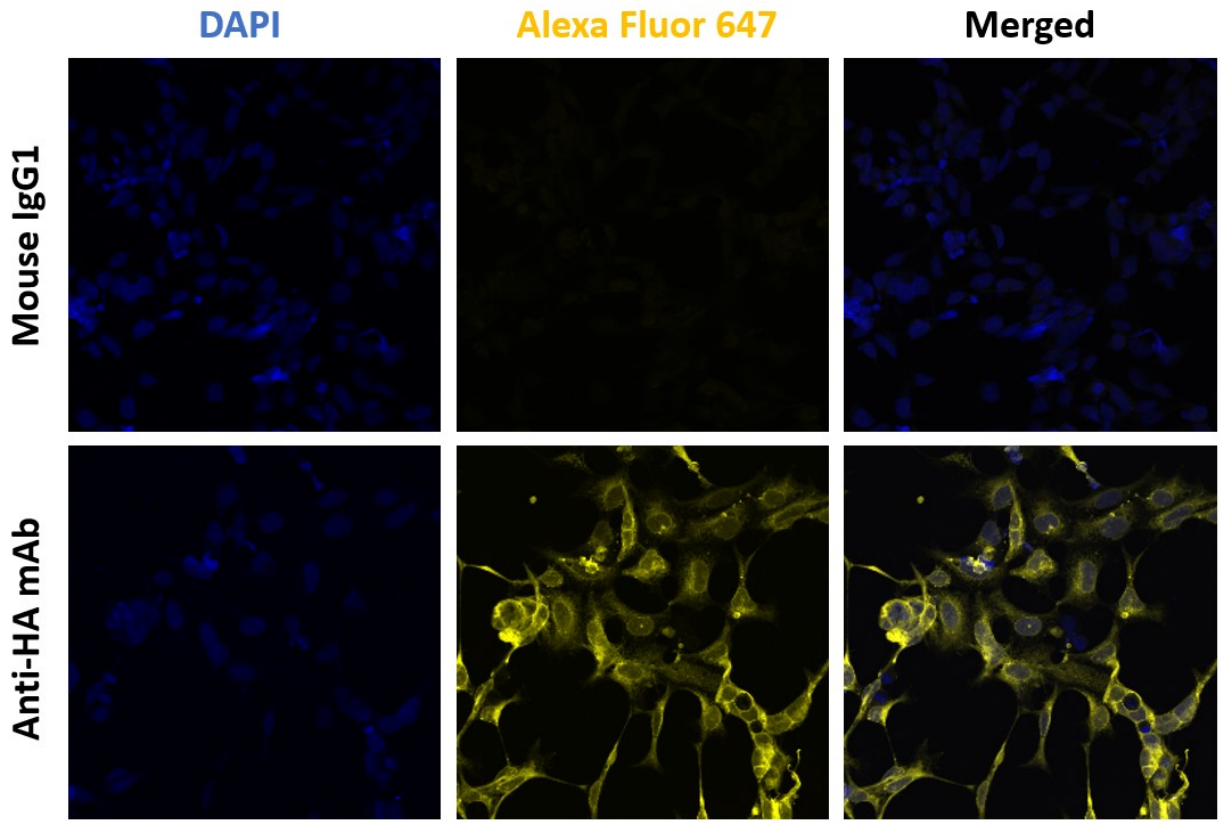

(C)

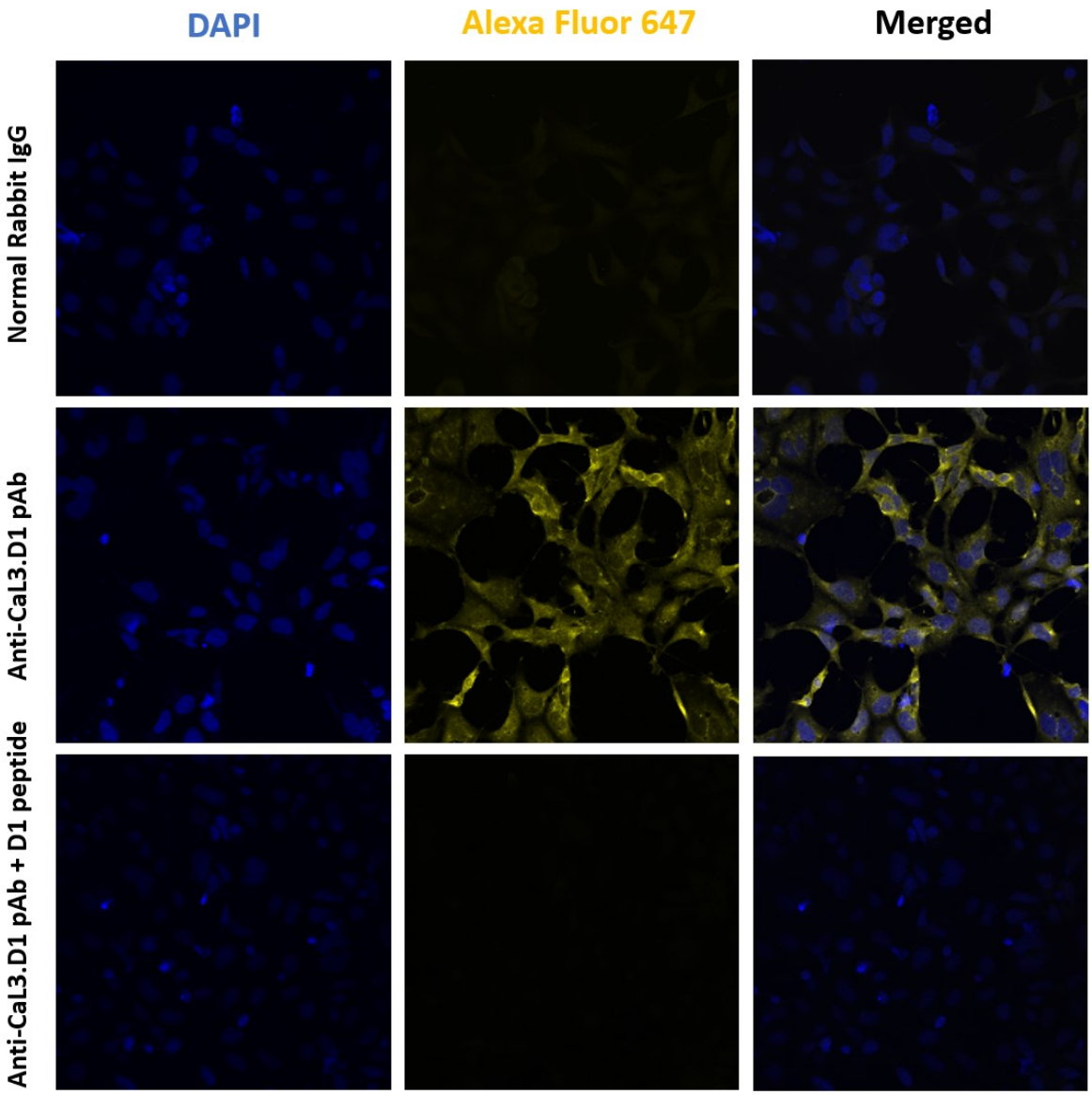
DAPI
Alexa Fluor 647
Merged
Normal Rabbit IgG
Anti-CaL3.D1 pAb
Anti-CaL3.D1 pAb + D1 peptide

(D)

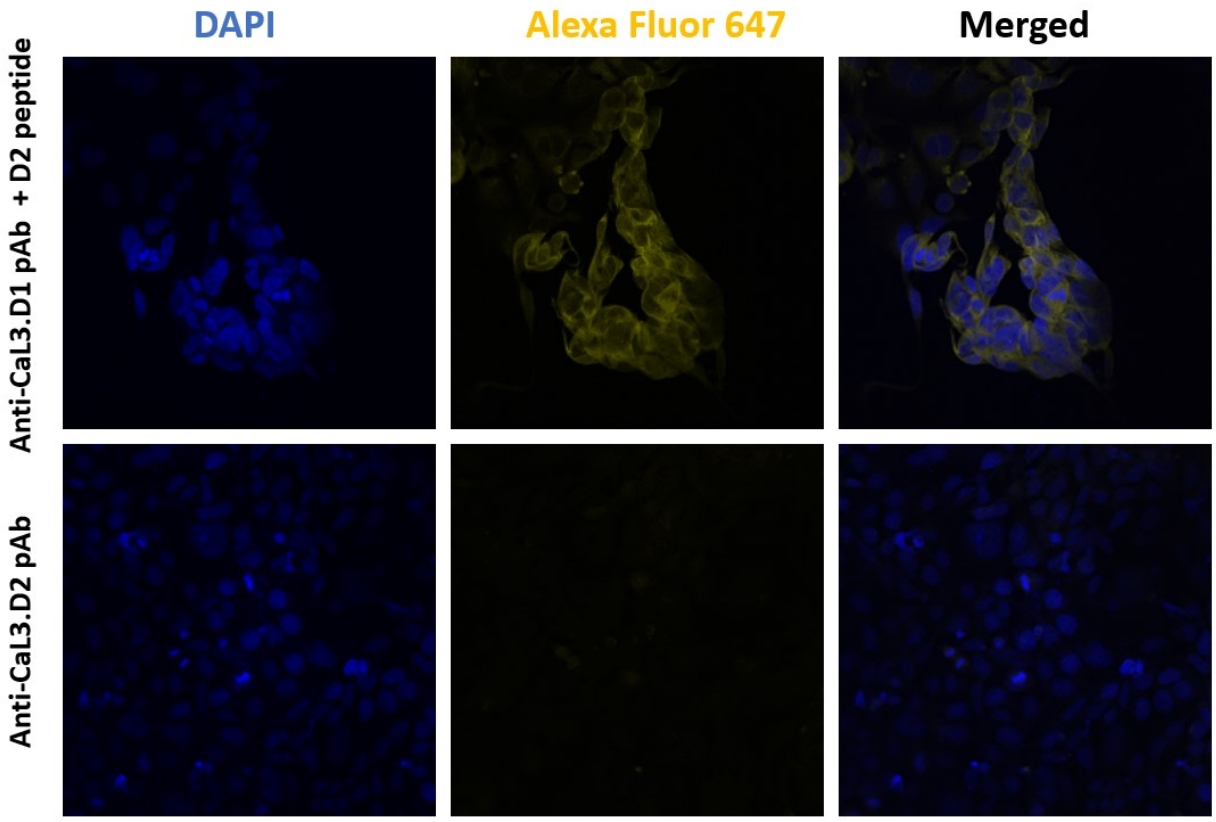

Figure 7.2. Immunofluorescence staining of AD293 cells expressing HA-tagged rCaLITR3 proteins. (A) Examination of the surface expression of rCaLITR3 proteins in AD293 cells using a flow cytometer. The grey and red histograms represent mouse IgG1 isotype Ab (1 µg/ml) and anti-HA mAb staining (1 µg/ml), respectively. Image was captured using Attune NxT and analyzed with FlowJo v10.10 software. **(B)** Fluorescence confocal microscopy images of rCaLITR3-expressing AD293 cells stained with mouse IgG1 (20 µg/ml) or anti-HA Abs (20 µg/ml). **(C)** rCaLITR3-expressing AD293 cells stained with normal rabbit IgG (20 µg/ml) or Anti-CaL3.D1 pAb (20 µg/ml) or Anti-CaL3.D1 pAb plus D1 peptide (50:1 peptide to pAb ratio). **(D)** rCaLITR3-expressing AD293 cells stained with Anti- pAb plus D2 peptide (50:1 peptide to pAb ratio) or anti-CaL3.D2 pAb (20 µg/ml). For each antibody treatment group, parental AD293 cells ($3x10^5$) were seeded onto a 12 mm coverslip overnight to facilitate cell attachment. The following day, the cells were formalin-fixed and then blocked with 1% BSA in 1x PBST containing 22.5 mg/ml glycine. Subsequently, the cells were incubated with various primary Abs, followed by secondary antibodies: either rabbit anti-mouse or goat-anti-rabbit Alexa Fluor 647 pAb (40 µg/ml). All antibody incubation steps were performed at RT. The coverslips were then mounted on slides containing ProLong Gold Antifade Mountant with DAPI (Invitrogen). All images were captured using an Olympus FLUOVIEW FV3000 Confocal Laser Scanning Microscope with a 40x objective lens. Consistent laser settings were maintained across all acquisitions.

(A)

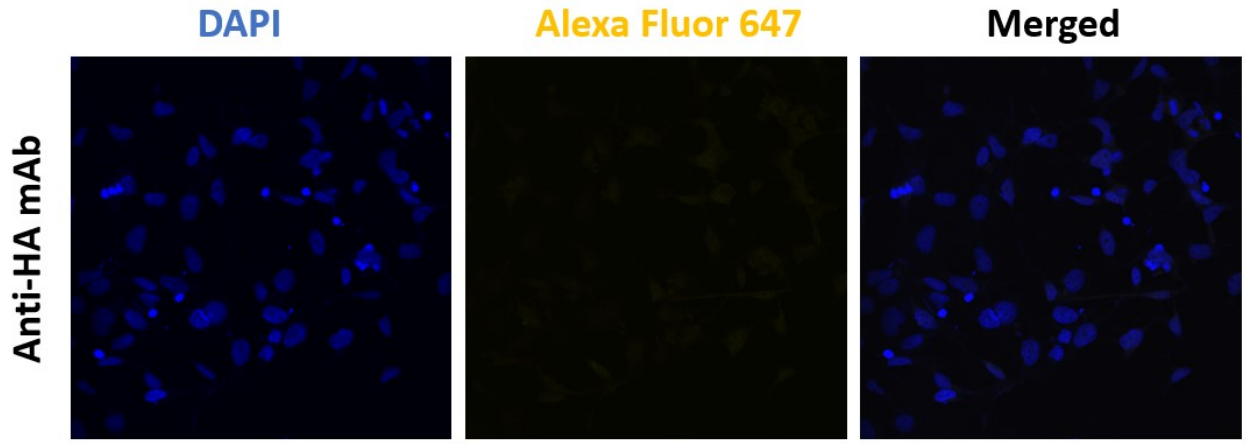
DAPI
Alexa Fluor 647
Merged
Anti-HA mAb

(B)

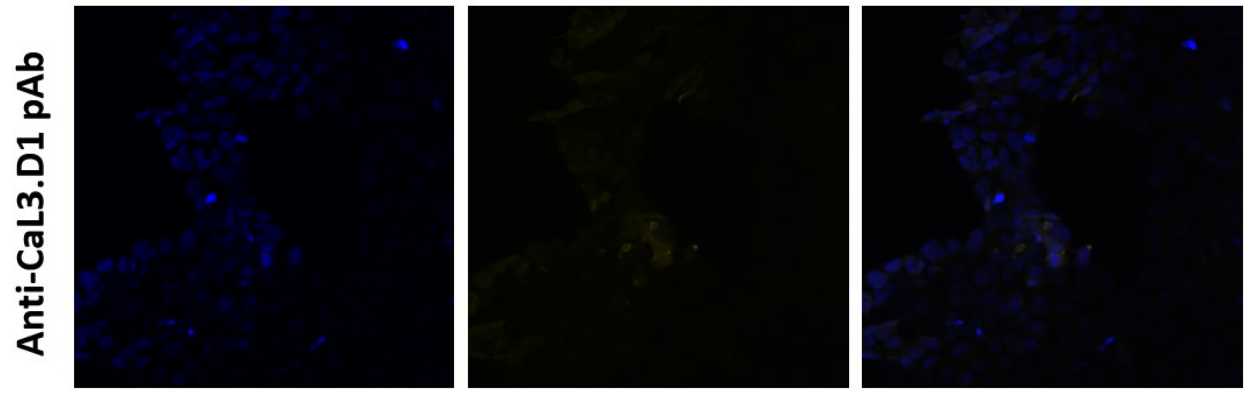
Anti-CaL3.D1 pAb

(C)

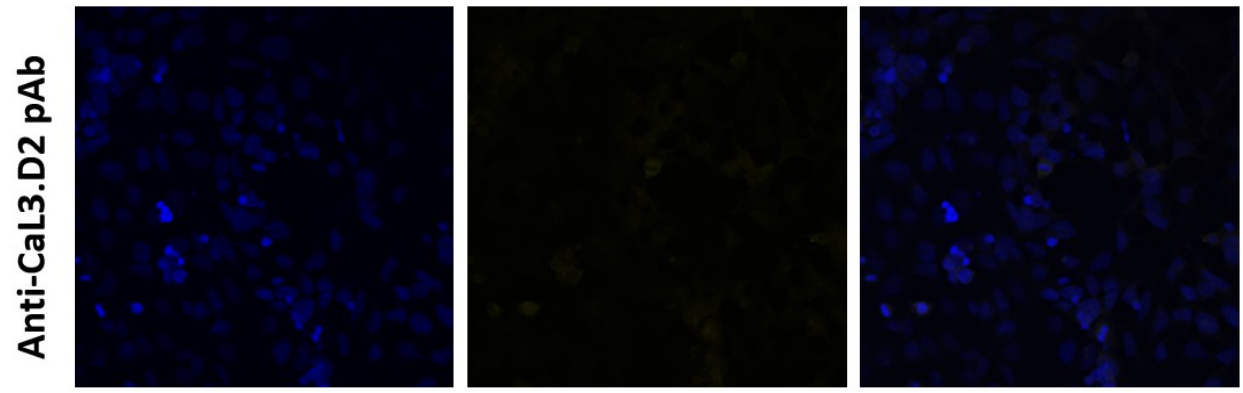
Anti-CaL3.D2 pAb

Figure 7.3. Immunofluorescence staining of parental AD293 cells with various mouse and rabbit Abs. (A) Staining with anti-HA mAb (20 µg/ml). **(B)** Staining with anti-CaL3.D1 pAb (20 µg/ml). **(C)** Staining with anti-CaL3.D2 pAb (20 µg/ml). For each antibody treatment group, parental AD293 cells ($3x10^5$) were seeded onto a 12 mm coverslip overnight to facilitate cell attachment. The following day, the cells were formalin-fixed and then blocked with 1% BSA in 1x PBST containing 22.5 mg/ml glycine. Subsequently, the cells were incubated with various primary Abs, followed by secondary antibodies: either rabbit anti-mouse or goat-anti-rabbit Alexa Fluor 647 pAb (40 µg/ml). All antibody incubation steps were performed at RT. The coverslips were then mounted on slides containing ProLong Gold Antifade Mountant with DAPI (Invitrogen). All images were captured using an Olympus FLUOVIEW FV3000 Confocal Laser Scanning Microscope with a 40x objective lens. Consistent laser settings were maintained across all acquisitions.

(A)

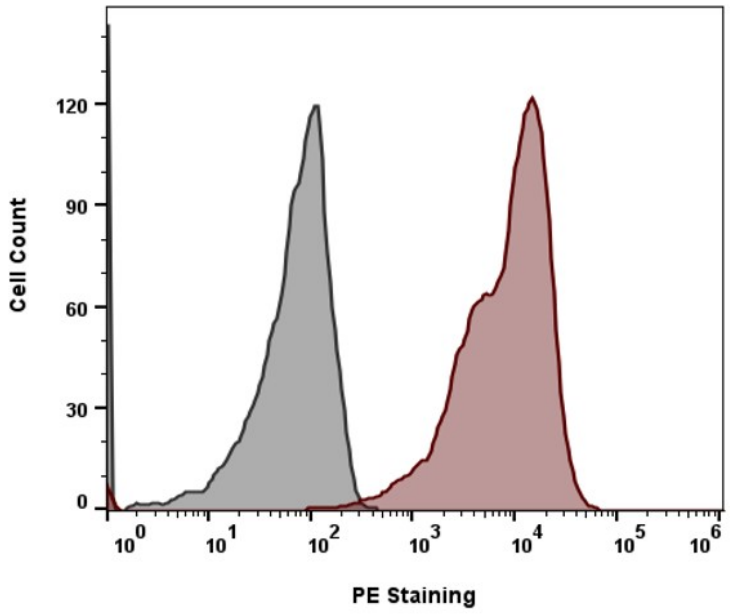

(B)

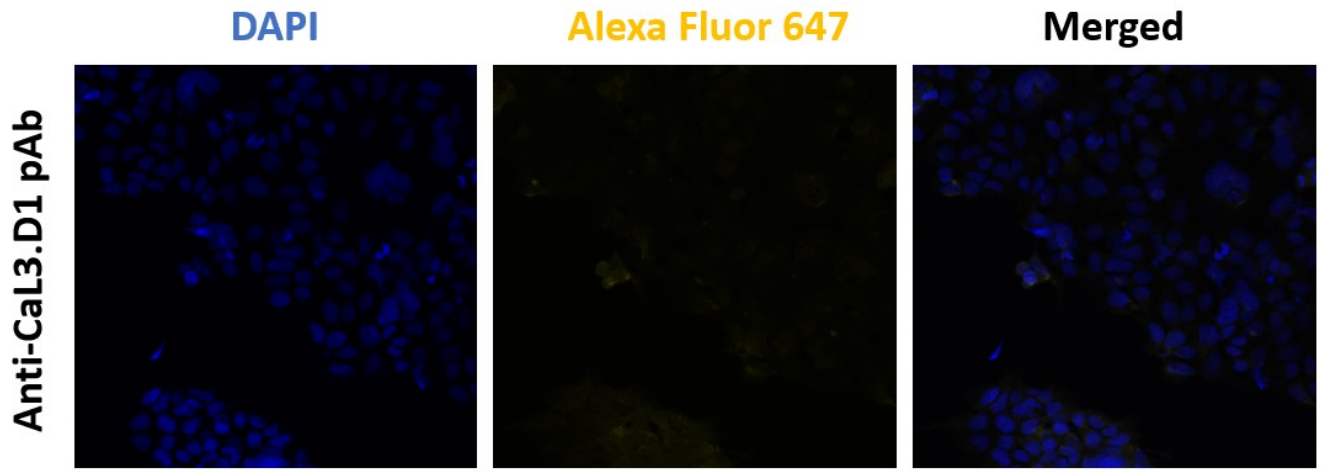

Figure 7.4. Immunofluorescence staining of AD293 cells expressing HA-tagged rIpLITR2.6b/6.1CYT proteins. (A) Flow cytometric analysis of the surface expression of rIpLITR2.6b/6.1CYT proteins in AD293 cells. The grey and red histograms represent data obtained from mouse IgG1 isotype control Ab (1 µg/ml) and anti-HA mAb (1 µg/ml) staining, respectively. Image was acquired using Attune NxT and analyzed with FlowJo v10.10 software **(B)** Fluorescence confocal microscopy images of IpLITR2.6b/6.1CYT-expressing AD293 cells stained with the anti-CaL3.D1 pAb. AD293 cells ($3x10^5$) expressing rIpLITR2.6b/6.1CYT proteins were seeded onto a 12 mm coverslip overnight to facilitate cell attachment. The following day, the cells were formalin-fixed and then blocked with 1% BSA in 1x PBST

containing 22.5 mg/ml glycine. Subsequently, the cells were incubated with the anti-CaL3.D1 pAb (20 µg/ml), followed by secondary goat-anti-rabbit Alexa Fluor 647 pAb (40 µg/ml). All antibody incubation steps were performed at RT. The coverslip was then mounted on a slide containing ProLong Gold Antifade Mountant with DAPI (Invitrogen). Images were captured using an Olympus FLUOVIEW FV3000 Confocal Laser Scanning Microscope with a 40x objective lens.

(A)

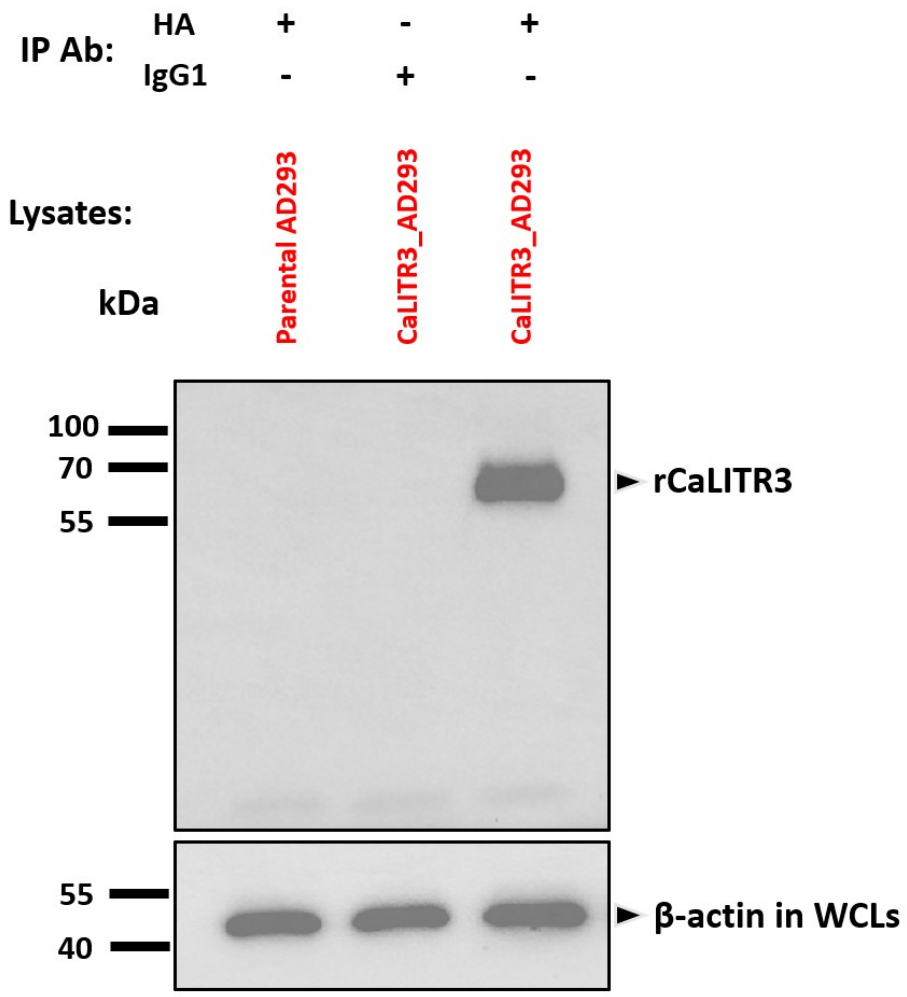
IP Ab:
HA
IgG1
+
-
-
+
+
-
Lysates:
kDa
Parental AD293
CaLITR3_AD293
CaLITR3_AD293
100
70
55
rCaLITR3
55
40
β-actin in WCLs

(B)

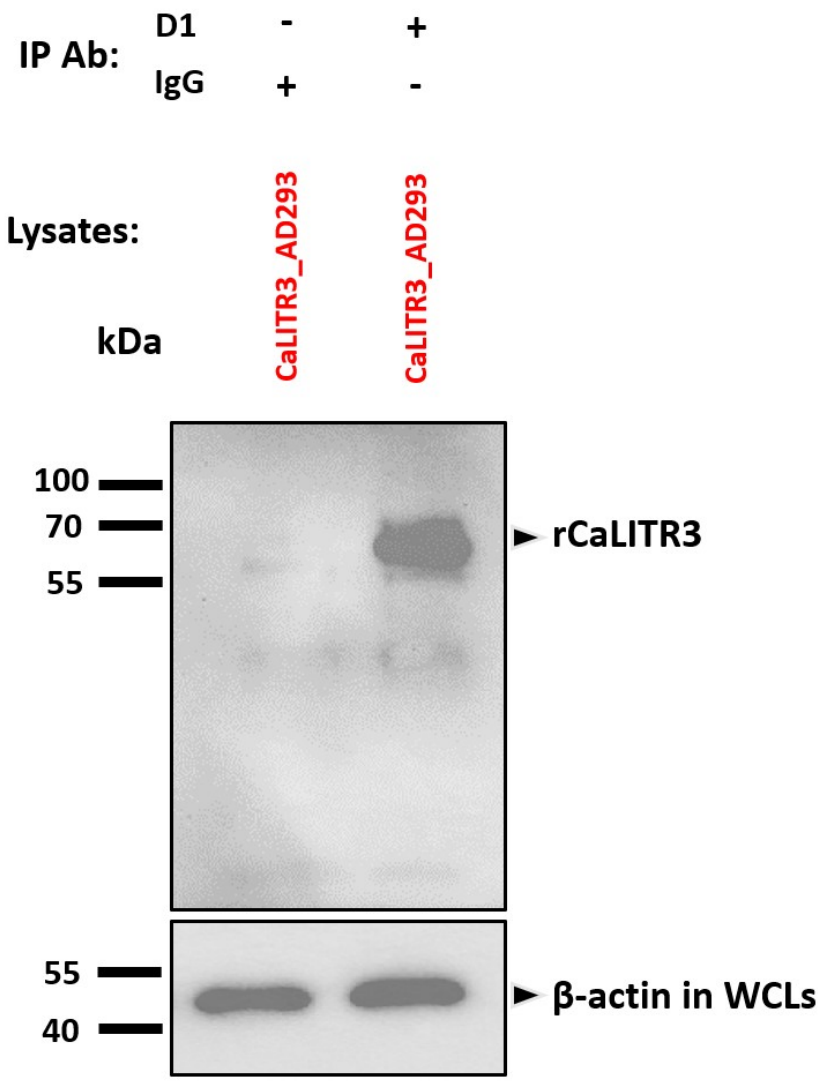

Figure 7.5. Immunoprecipitation experiments validating the selectivity of the anti-CaL3.D1 pAb for rCaLITR3 proteins. (A) Control experiments confirming pulldown of HA-tagged rCaLITR3 proteins from rCaLITR3-expressing AD293 WCL using mouse-anti-HA-mAb-coated Dynabeads. From left to right, the first lane represents the immunoprecipitation of proteins from parental AD293 cell lysate using mouse-anti-HA-mAb-coated Dynabeads. The second lane displays the pulldown of proteins from rCaLITR3-expressing AD293 WCL with mouse-IgG-isotype-control-Ab-coated Dynabeads. The third lane illustrates the immunoprecipitation of rCaLITR3 proteins from rCaLITR3-expressing AD293 WCL with mouse-anti-HA-mAb-coated Dynabeads. **(B)** Immunoprecipitation of rCaLITR3 proteins from rCaLITR3-expressing AD293 cells with anti-CaL3.D1-pAb-coated Dynabeads. From left to right, the first lane represents the immunoprecipitation of proteins from rCaLITR3-expressing AD293 cells with normal-rabbit-

pAb-coated Dynabeads. The second lane shows the pulldown of proteins from rCaLITR3-expressing AD293 WCL with anti-CaL3.D1-pAb-coated Dynabeads. For all pulldown experiments, mouse anti-β-actin mAb was used to verify the presence of proteins in each AD293 WCL. The presence (+) and absence (-) of antibodies used for pull-down assays are indicated.

(A)

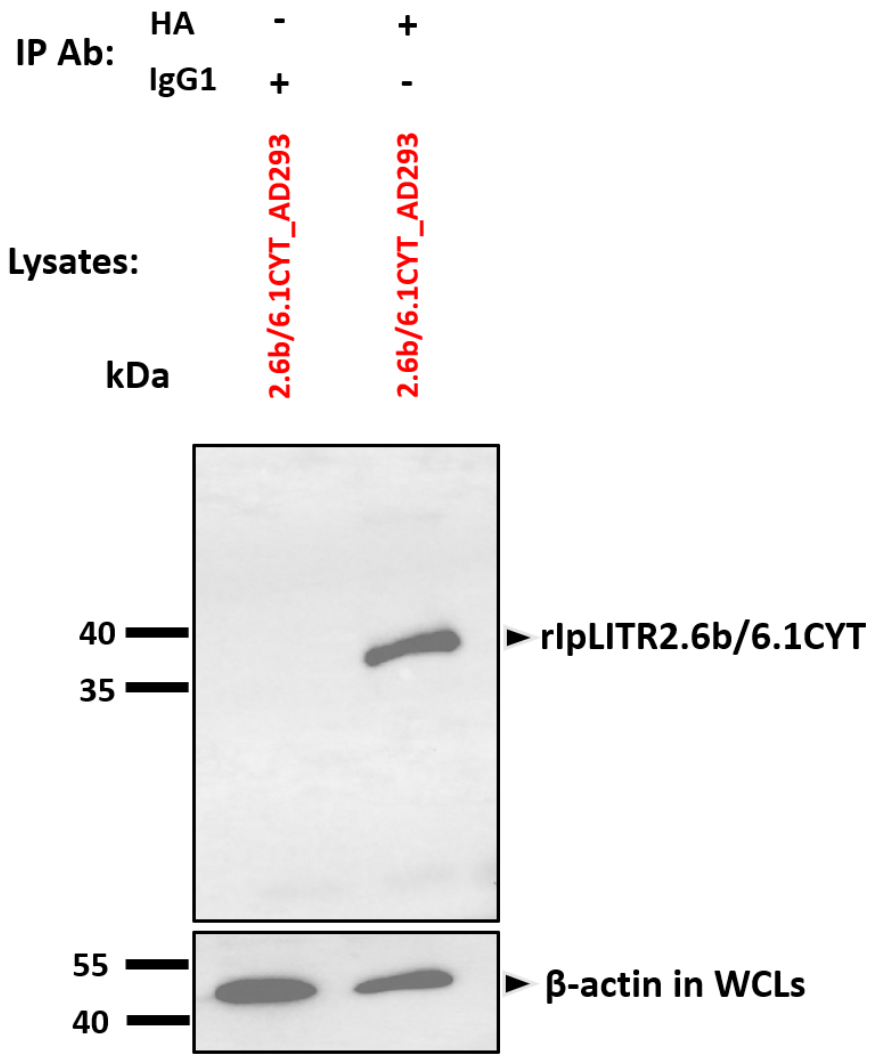
IP Ab:
HA
IgG1
-
+
+
-
Lysates:
2.6b/6.1CYT_AD293
2.6b/6.1CYT_AD293
kDa
40
35
rIpLITR2.6b/6.1CYT
55
40
β-actin in WCLs

(B)

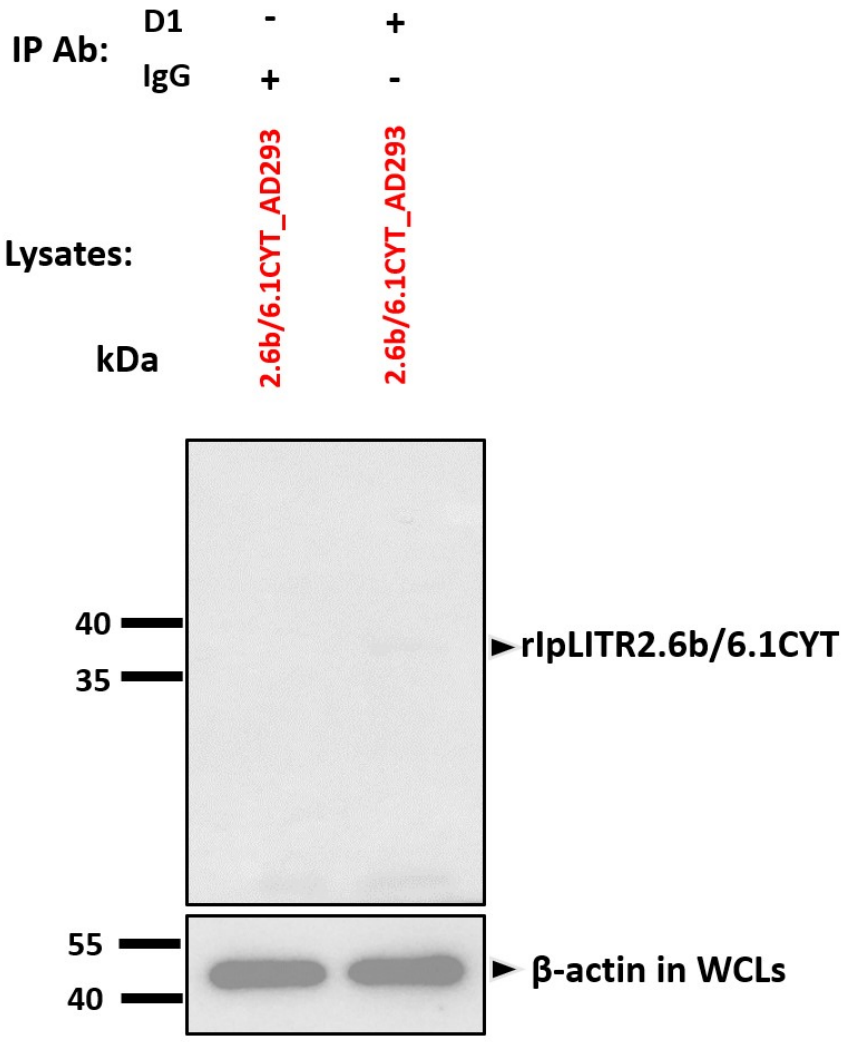

Figure 7.6. Immunoprecipitation assays verifying the selectivity of the anti-CaL3.D1 pAb for rIpLITR2.6b/6.1CYT proteins using Dynabeads coated with various Abs. (A) Control experiments confirming the pulldown of rIpLITR2.6b/6.1CYT proteins from rIpLITR2.6b/6.1CYT-expressing AD293 WCL with anti-HA mAb. From left to right, the first lane represents the immunoprecipitation of proteins from rIpLITR2.6b/6.1CYT-expressing AD293 WCL with mouse IgG1 isotype control Ab. The second lane shows the pulldown of rIpLITR2.6b/6.1 proteins from rIpLITR2.6b/6.1-expressing AD293 WCL with mouse anti-HA mAb. **(B)** Pulldown of proteins from rIpLITR2.6b/6.1CYT-expressing AD293 WCL using anti-CaL3.D1-pAb-coated Dynabeads. From left to right, the first lane illustrates the immunoprecipitation of proteins from rIpLITR2.6b/6.1CYT-expressing AD293 WCL with normal rabbit IgG. The second lane shows the pulldown of proteins from rIpLITR2.6b/6.1CYT-expressing AD293 WCL with anti-CaL3.D1 pAb. For all pulldown experiments, mouse anti-β-actin mAb was used to verify the presence of proteins in each AD293 WCL. The presence (+) and absence (-) of antibodies used for pull-down assays are indicated.

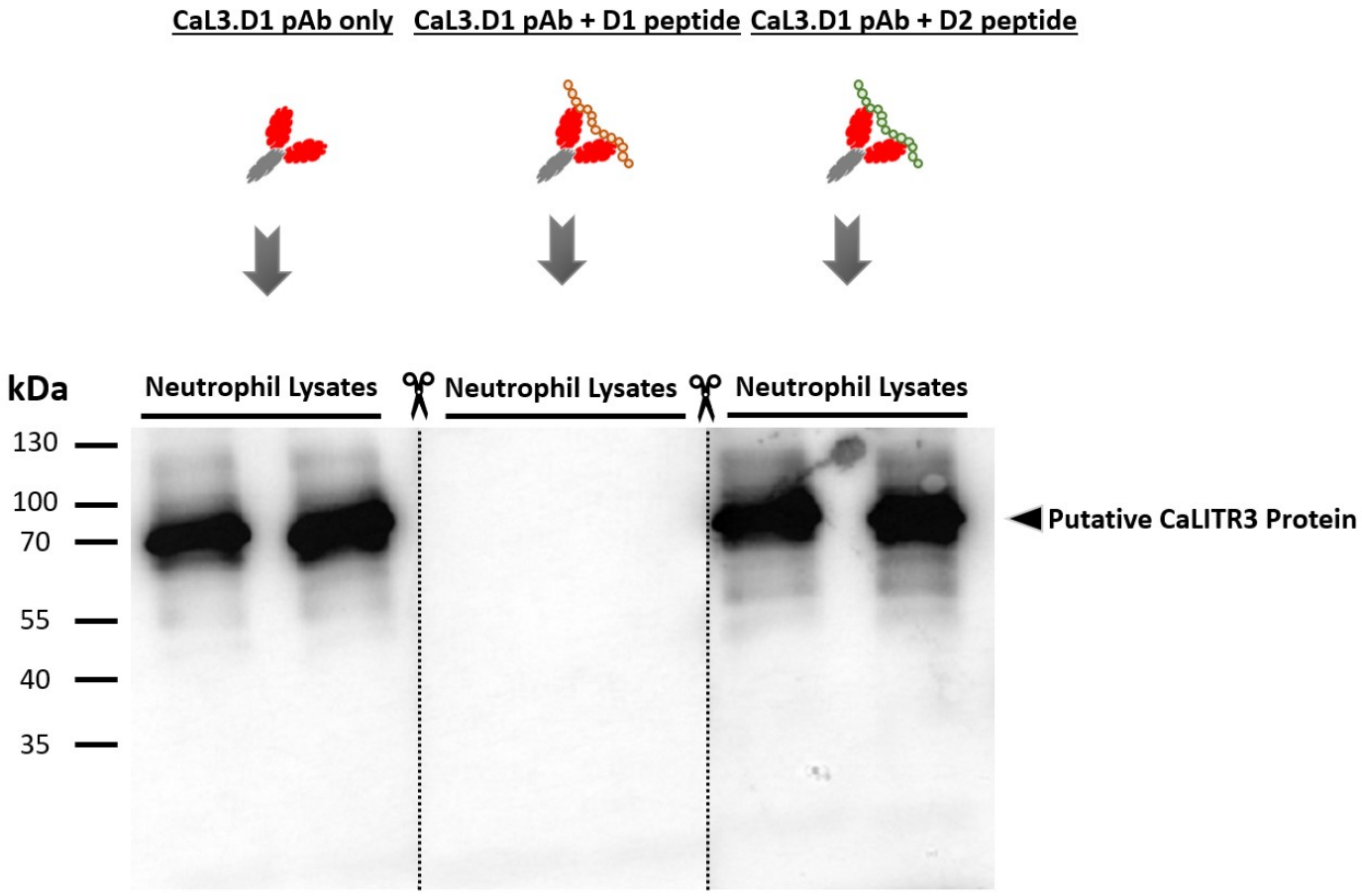

Figure 7.7. Peptide competition assay validating the specificity of the rabbit anti-CaL3.D1 pAb for the recombinant CaLITR3.0 D1 peptide. The goldfish neutrophil WCLs (20 µg) were reduced with DTT and then subjected to 10% SDS-PAGE gel electrophoresis. The separated proteins from the gel were subsequently transferred to a nitrocellulose membrane and cut into three identical parts with scissors. Each of the three sections was probed with either the anti-CaL3.D1 pAb alone (1 µg/ml), anti-CaL3.D1 pAb (1 µg/ml) plus D1 peptide (in a 50 peptide:1 pAb ratio), or the anti-CaL3.D1 pAb (1 µg/ml) plus D2 peptide (in a 50 peptide:1 pAb ratio). The nitrocellulose membranes were visualized with SuperSignal West Pico PLUS Chemiluminescent Substrate (Thermo).

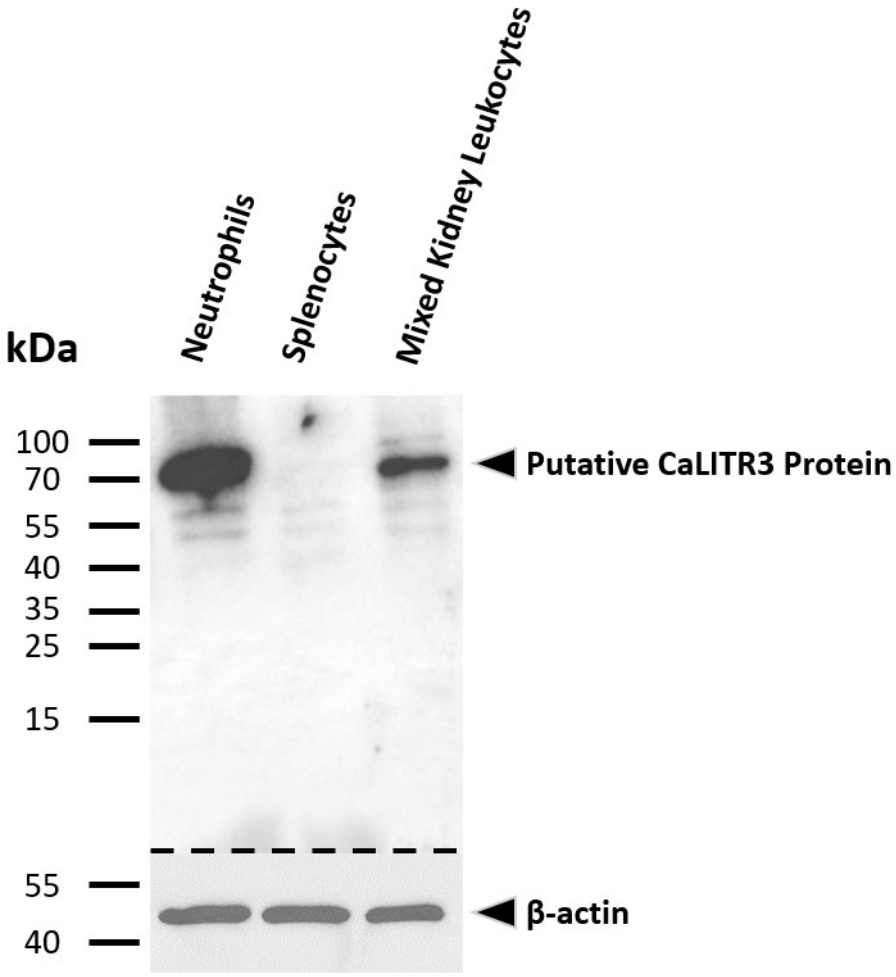

Figure 7.8. Visualization of anti-CaL3.D1-pAb-reactive bands using western blotting. Total cell lysates from resting goldfish primary immune cells (neutrophils, splenocytes, and kidney leukocytes) were treated with DTT and separated on a 10% SDS-PAGE gel. Subsequently, the proteins were transferred onto a nitrocellulose membrane and probed with anti-CaL3.D1 pAb at a concentration of 1 μg/mL. To detect the bound primary antibody, a secondary antibody, goat anti-rabbit HRP IgG secondary antibody (Invitrogen) (1 μg/mL) was used. The nitrocellulose membrane was then visualized with SuperSignal West Pico PLUS Chemiluminescent Substrate (Thermo) and imaged via ChemiDoc MP Imaging System (Bio-Rad). Mouse anti-β-actin monoclonal antibody (Sigma) was used as the positive and loading controls for this experiment. This experiment was replicated three times using three distinct goldfish individuals.

(A)

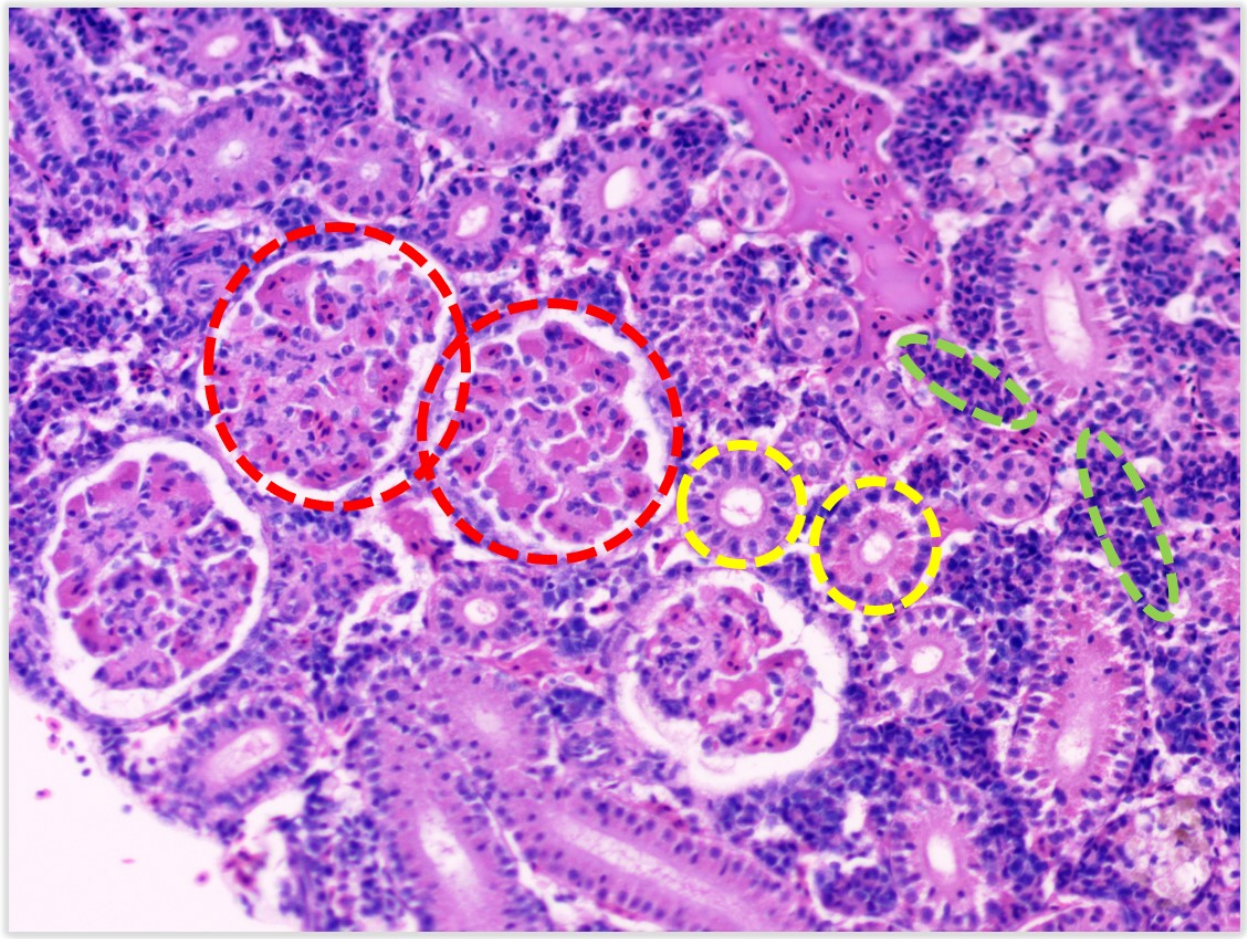

(B)

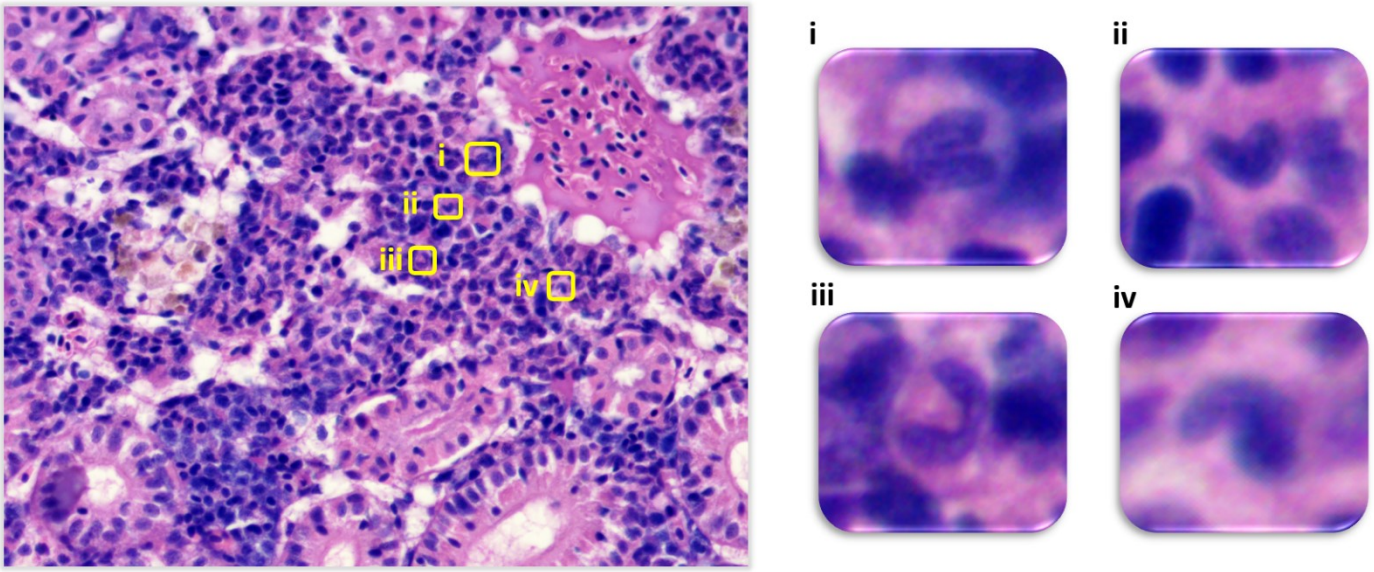

Figure 7.9. Representative hematoxylin and eosin (H&E) staining of kidney tissue from a healthy goldfish. (A) A section of goldfish kidney tissue containing glomeruli, renal tubules, and numerous darkly-stained hematopoietic cells (20x). The dotted red, yellow, and green circles denote glomeruli, renal tubules, and hematopoietic cells, respectively. **(B)** A close-up view of hematopoietic cells (40x). Goldfish neutrophils are boxed in yellow squares (i, ii, iii, and iv). These cells feature crescent-moon-shaped nuclei. All images were captured using a ZEISS AXIO A1 compound light microscope equipped with a SeBaCam 5.1MP camera.

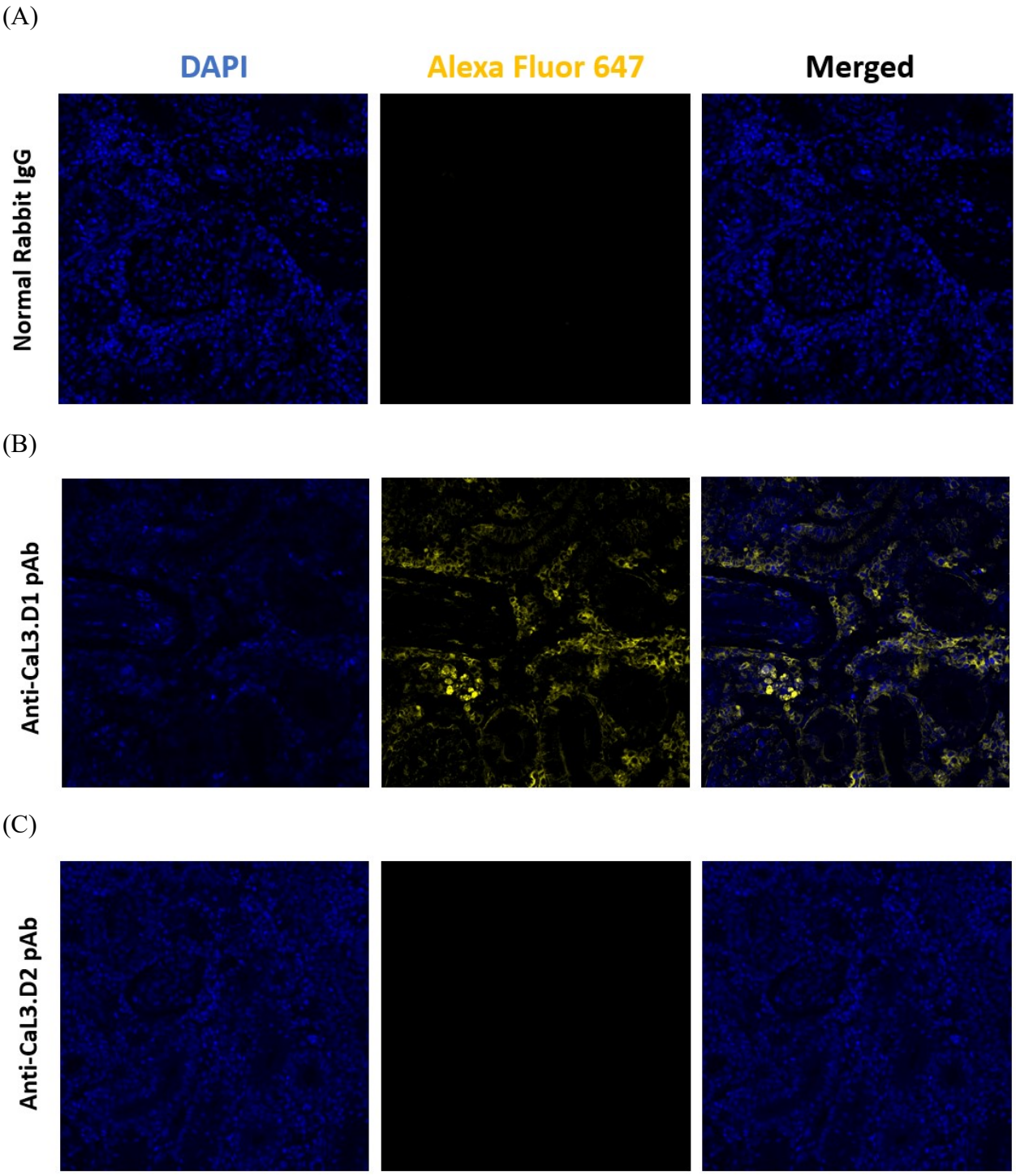

Figure 7.10. Fluorescence microscopy images of goldish kidney tissue stained with various rabbit pAbs. (A) goldfish kidney tissue stained with normal rabbit IgG (5 µg/ml). **(B)** Staining with anti-CaL3.D1 pAb (5 µg/ml). **(C)** Staining with anti-CaL3.D2 pAb (5 µg/ml). Positively charged glass slides with formalin-fixed and paraffin-embedded goldfish kidney sections (5 µm thickness) were subjected to dewaxing, followed by a 10-minute treatment with hot-boiling citric acid buffer (pH 6.0) to reverse formalin-mediated protein cross-linking and expose necessary

epitopes for pAb recognition. Subsequently, the slides were rinsed with PBS and blocked with 5% BSA in PBST for 30 min at RT. The slides were then stained with various primary pAbs (5 µg/ml), followed by incubation with secondary goat-anti-rabbit pAb conjugated to Alexa Fluor 647 (40 µg/ml) (Thermo Fisher). All antibody-incubation steps were performed at RT. ProLong Gold Antifade Mountant with DAPI (Invitrogen) was used to stain cell nuclei. All images were acquired using an Olympus FLUOVIEW FV3000 Confocal Laser Scanning Microscope with a 40x objective lens. Consistent laser settings were applied for all acquisitions.

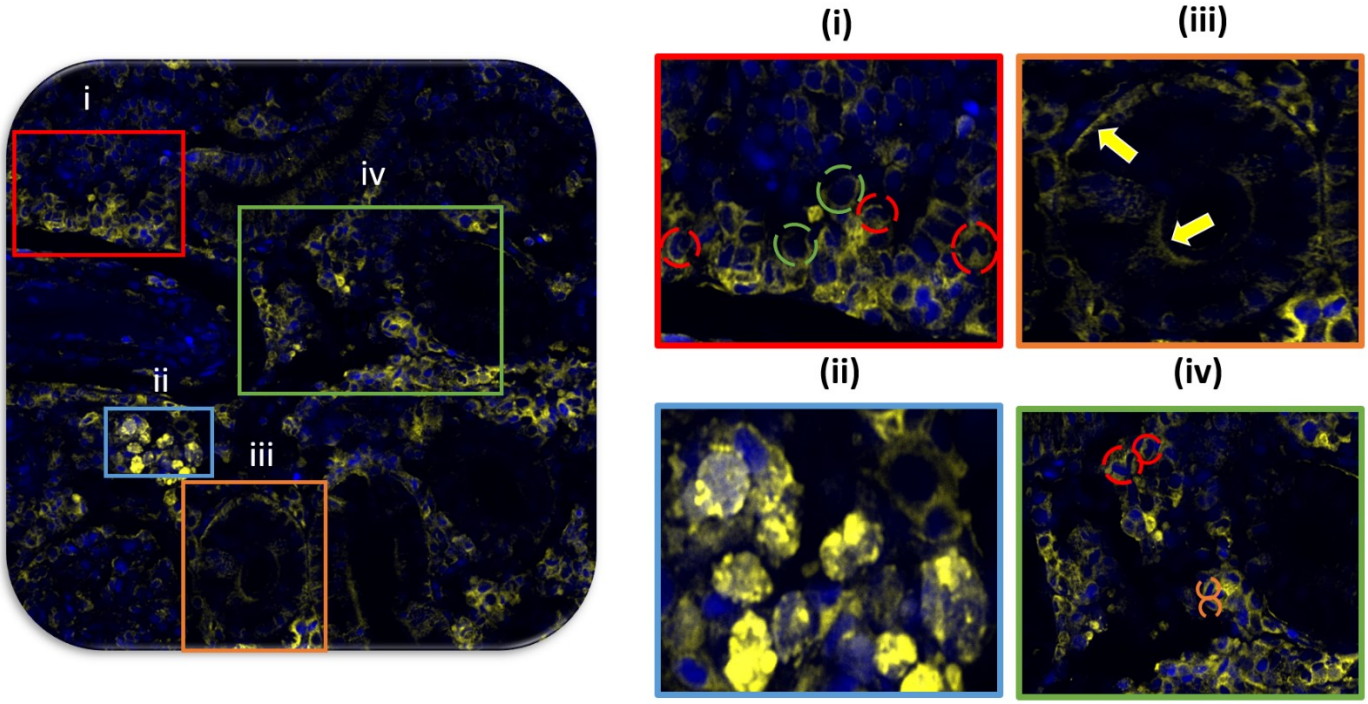

Figure 7.11. Representative fluorescence microscopy image of a goldfish kidney tissue section stained with anti-CaL3.D1 pAb. (i) Enlarged image illustrating the membrane or intracellular expression (yellow) of anti-CaL3.D1-pAb-reactive proteins in a cluster of hematopoietic cells. Neutrophils containing crescent-moon-shaped nuclei (blue) are highlighted in red dashed circles, while cells with round nuclei are outlined in green dashed circles. **(ii)** Magnified view of a section of (A) showing an auto-fluorescent MMC. **(iii)** Close-up view of the expression of anti-CaL3.D1-pAb-reactive proteins in columnar epithelial cells of a renal tubule. The yellow arrows indicate the expression of anti-CaL3.D1-pAb-reactive proteins in epithelial linings of a renal tubule. **(iv)** Expression of anti-CaL3.D1-pAb-reactive proteins in hematopoietic cells. The cells with spindle-shaped nuclei are highlighted in orange dashed circles. Neutrophils are highlighted in red dashed circles. Positively charged glass slide with formalin-fixed and paraffin-embedded goldfish kidney section (5 µm thickness) was subjected to dewaxing, followed by a 10-minute treatment with hot-boiling citric acid buffer (pH 6.0) to reverse formalin-mediated protein cross-linking and expose necessary epitopes for pAb recognition. Subsequently, the slide was rinsed with PBS and blocked with 5% BSA in PBST for 30 min at RT. The slide was then stained with the anti-CaL3.D1 pAb (5 µg/ml), followed by incubation with secondary goat-anti-rabbit pAb conjugated to Alexa Fluor 647 (40 µg/ml) (Thermo Fisher). All antibody-incubation steps were performed at RT. ProLong Gold Antifade Mountant with DAPI (Thermo Fisher) was used to stain cell nuclei. All images were acquired using an Olympus FLUOVIEW FV3000 Confocal Laser Scanning Microscope with a 40x objective lens.

Figure 7.12. Representative image of a goldfish kidney tissue section displaying three autofluorescent MMCs. The autofluorescent MMCs are highlighted in dashed black circles. No dyes or fluorescent Abs were added. Positively charged glass slide with formalin-fixed and paraffin-embedded goldfish kidney section (5 µm thickness) underwent dewaxing prior to treatment with Prolong Gold antifade reagent for preservation. The image was acquired using an Olympus FLUOVIEW FV3000 Confocal Laser Scanning Microscope with a 40x objective lens.

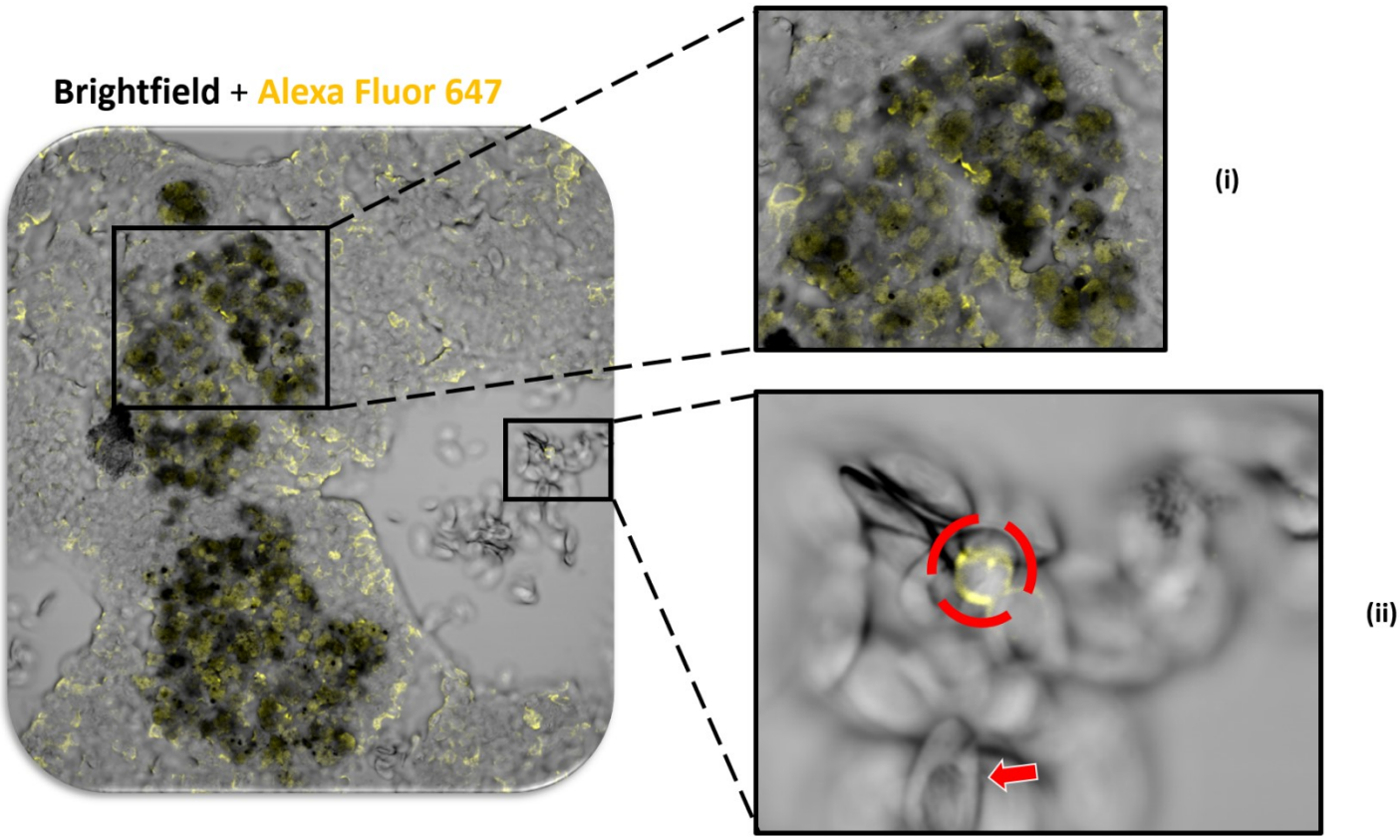

Figure 7.13. Fluorescence microscopy images of a goldfish kidney tissue section stained with anti-CaL3.D1 pAb. (i) Close-up examination of a large MMC. Melanomacrophages exhibit pigmentation due to melanin and lipofuscin (source of autofluorescence) (Diaz-Satizabal & Magor, 2015). **(ii)** Magnified view of a cluster of erythrocytes and a neutrophil-like cell stained with anti-CaL3.D1 pAb (yellow). The anti-CaL3.D1-pAb-labeled neutrophil is delineated by a red dashed circle, while an erythrocyte is indicated by a red arrow. Positively charged glass slide with formalin-fixed and paraffin-embedded goldfish kidney section (5 µm thickness) was subjected to dewaxing, followed by a 10-minute treatment with hot-boiling citric acid buffer (pH 6.0) to reverse formalin-mediated protein cross-linking and expose necessary epitopes for pAb recognition. Subsequently, the slide was rinsed with PBS and blocked with 5% BSA in PBST for 30 min at RT. The slide was then stained with the anti-CaL3.D1 pAb (5 µg/ml), followed by incubation with secondary goat-anti-rabbit pAb conjugated to Alexa Fluor 647 (40 µg/ml) (Thermo Fisher). All antibody-incubation steps were performed at RT. ProLong Gold Antifade Mountant with DAPI (Thermo Fisher) was used to stain cell nuclei. All images were acquired using an Olympus FLUOVIEW FV3000 Confocal Laser Scanning Microscope with a 40x objective lens.

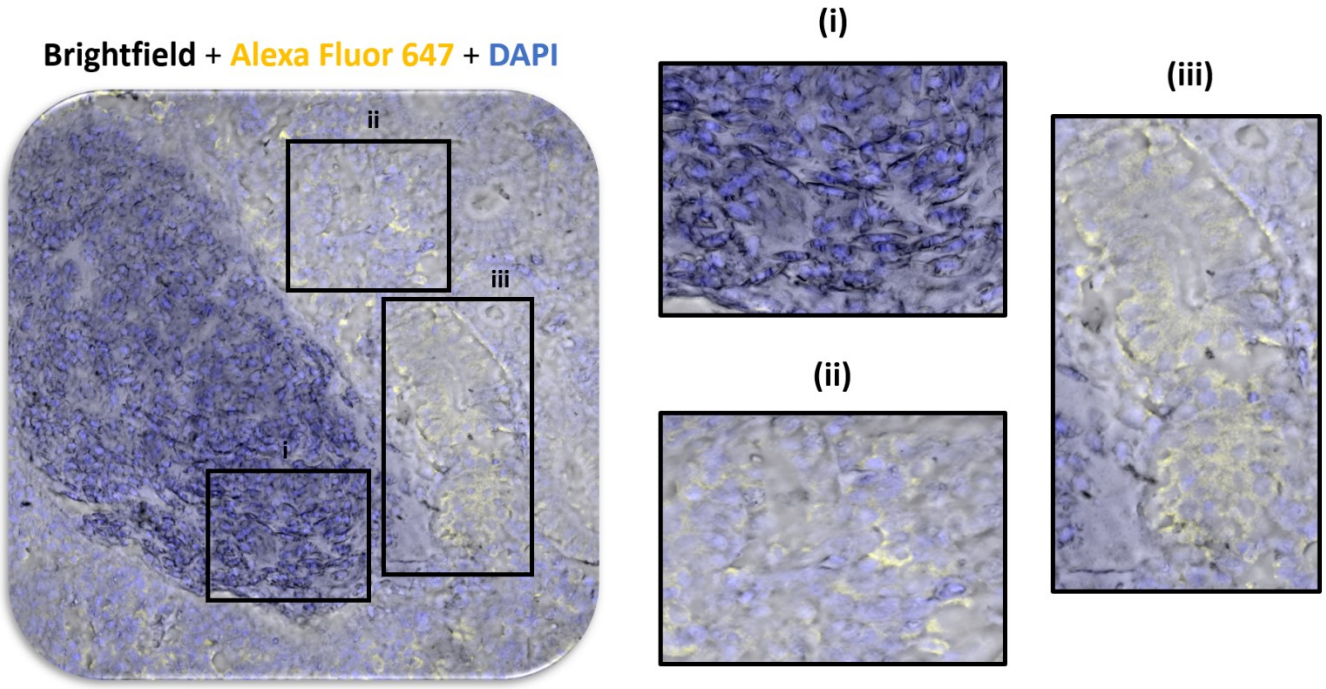

Figure 7.14. Fluorescence microscopy image of a goldfish kidney tissue section treated with anti-CaL3.D1 pAb. (i) Magnified image illustrating the mass of unstained erythrocytes. **(ii)** hematopoietic cells positively stained with anti-CaL3.D1 pAb. **(iii)** Renal tubular epithelial cells stained with anti-CaL3.D1 pAb. Positively charged glass slide with formalin-fixed and paraffin-embedded goldfish kidney section (5 µm thickness) was subjected to dewaxing, followed by a 10-minute treatment with hot-boiling citric acid buffer (pH 6.0) to reverse formalin-mediated protein cross-linking and expose necessary epitopes for pAb recognition. Subsequently, the slide was rinsed with PBS and blocked with 5% BSA in PBST for 30 min at RT. The slide was then stained with the anti-CaL3.D1 pAb (5 µg/ml), followed by incubation with secondary goat-anti-rabbit pAb conjugated to Alexa Fluor 647 (40 µg/ml) (Thermo Fisher). All antibody-incubation steps were performed at RT. ProLong Gold Antifade Mountant with DAPI (Thermo Fisher) was used to stain cell nuclei. All images were acquired using an Olympus FLUOVIEW FV3000 Confocal Laser Scanning Microscope with a 40x objective lens.

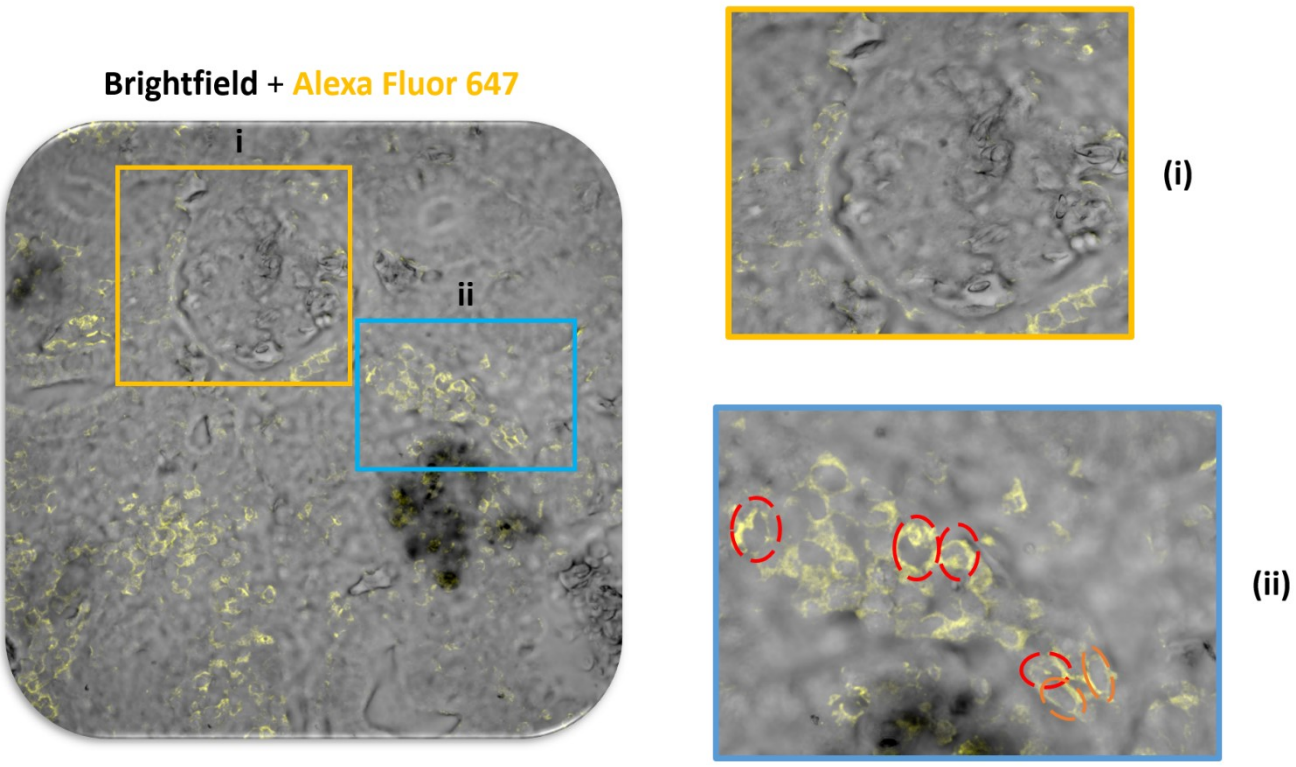

Figure 7.15. Anti-CaL3.D1-pAb-labeled kidney section showing a glomerulus surrounded by renal tubules and hematopoietic cells. (i) Close-up examination of the glomerulus revealing minimal staining by anti-CaL3.D1 pAb. **(ii)** Cluster of hematopoietic cells labeled with anti-CaL3.D1 pAb. Neutrophil-like cells with "c"- shaped nuclei are indicated by red dashed circles. Cells with spindle-shaped nuclei are highlighted in orange dashed circles. Positively charged glass slide with formalin-fixed and paraffin-embedded goldfish kidney section (5 µm thickness) was subjected to dewaxing, followed by a 10-minute treatment with hot-boiling citric acid buffer (pH 6.0) to reverse formalin-mediated protein cross-linking and expose necessary epitopes for pAb recognition. Subsequently, the slide was rinsed with PBS and blocked with 5% BSA in PBST for 30 min at RT. The slide was then stained with the anti-CaL3.D1 pAb (5 µg/ml), followed by incubation with secondary goat-anti-rabbit pAb conjugated to Alexa Fluor 647 (40 µg/ml) (Thermo Fisher). All antibody-incubation steps were performed at RT. ProLong Gold Antifade Mountant with DAPI (Thermo Fisher) was used to stain cell nuclei. All images were acquired using an Olympus FLUOVIEW FV3000 Confocal Laser Scanning Microscope with a 40x objective lens.

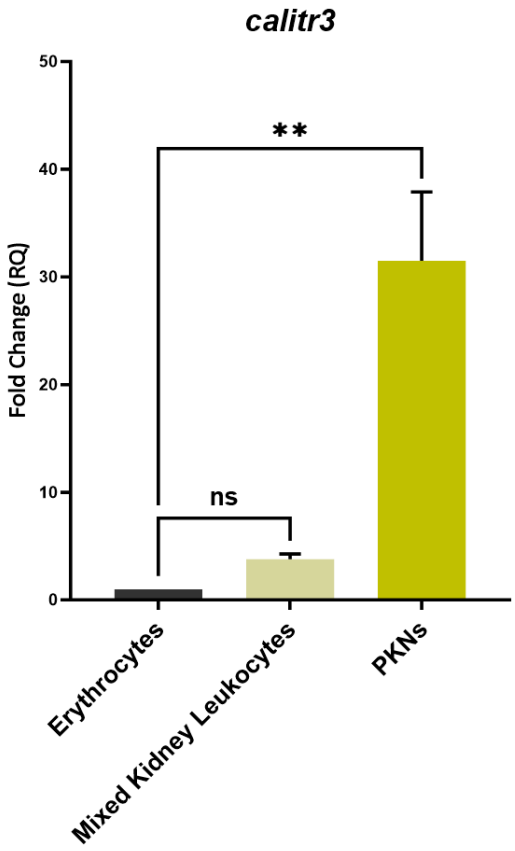

Figure 7.16. RT-qPCR analysis of the transcript level of *calitr3* in erythrocytes, mixed kidney leukocytes, and PKNs of the goldfish (n=3). Relative fold-change was normalized to the endogenous control gene, *ef1α*, and then displayed as fold change in expression relative to erythrocyte control (RQ=1) for each gene. Each bar graph represents the mean value. Each error bar indicates the standard error mean. P-values are illustrated as $^{ns}p > 0.05$, $*p \leq 0.05$, $**p \leq 0.01$, $***p \leq 0.001$, and $****p \leq 0.0001$.

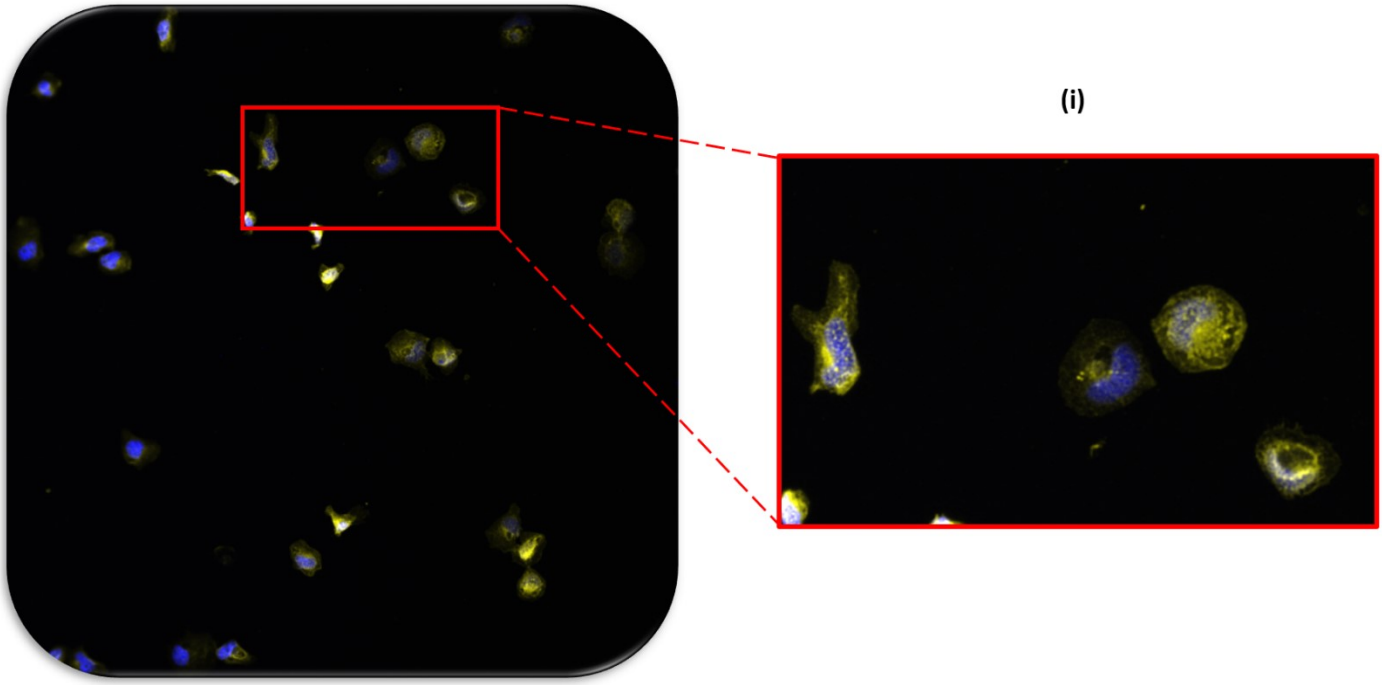

Figure 7.17. Immunofluorescence staining of goldfish PKNs with anti-CaL3.D1 pAb. (i) Close-up examination of the membrane or intracellular expression of anti-CaL3.D1-reactive proteins in multiple neutrophils. Neutrophils were isolated from three goldfish individuals and then pooled before experiments. In a well of a 24-well plate, neutrophils ($2x10^6$) were seeded onto a 12 mm coverslip coated with poly-L-lysine for 1 h at RT to facilitate neutrophil attachment. Afterward, the cells were formalin-fixed and then blocked with 1% BSA in 1x PBST containing 22.52 mg/ml glycine for 30 min at RT. The cells were subsequently probed with anti-CaL3.D1 pAb (20 µg/ml), followed by secondary goat-anti-rabbit Alexa Fluor 647 pAb (40 µg/ml). All antibody-incubation steps were performed at RT. The coverslips were then mounted on slides containing ProLong Gold Antifade Mountant with DAPI (Thermo Fisher). All images were captured using an Olympus FLUOVIEW FV3000 Confocal Laser Scanning Microscope with a 40x objective lens.

(A)

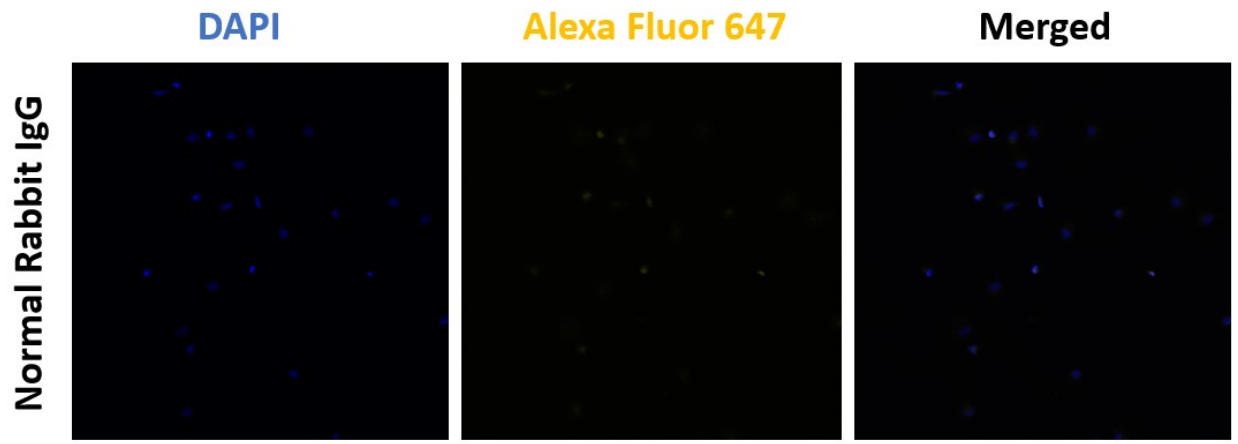
DAPI
Alexa Fluor 647
Merged
Normal Rabbit IgG

(B)

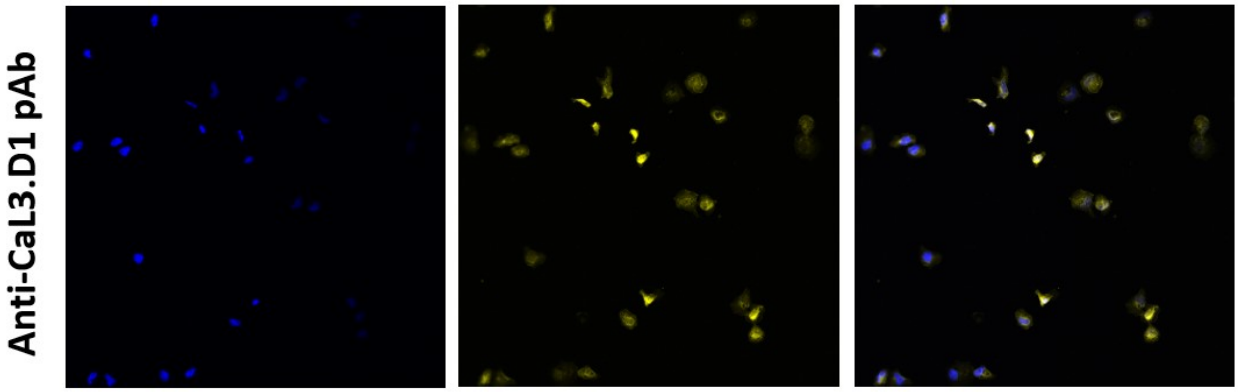
Anti-CaL3.D1 pAb

(C)

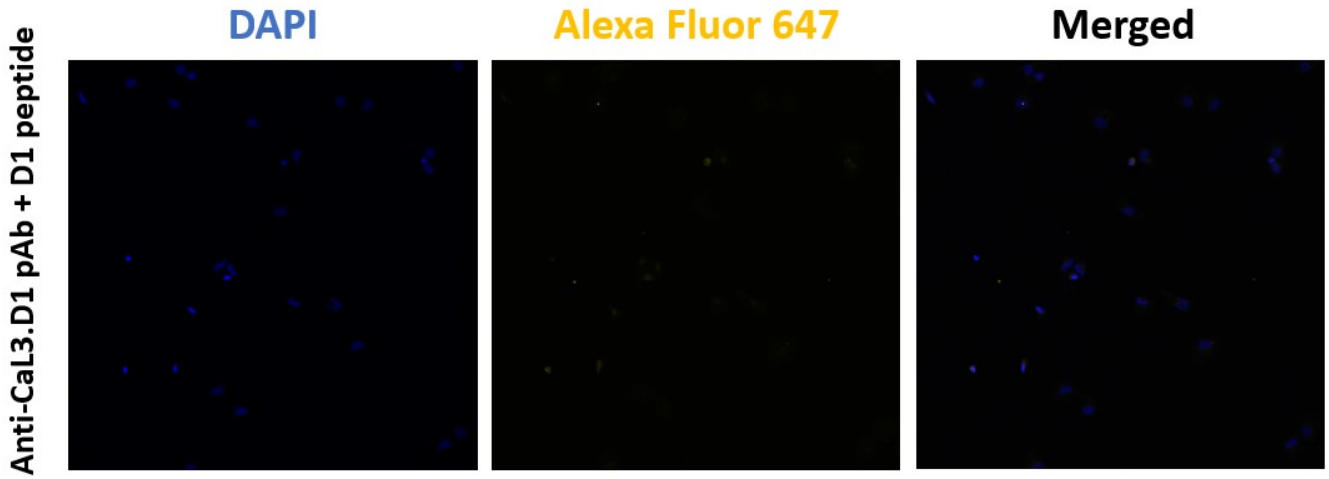
DAPI
Alexa Fluor 647
Merged
Anti-CaL3.D1 pAb + D1 peptide

(D)

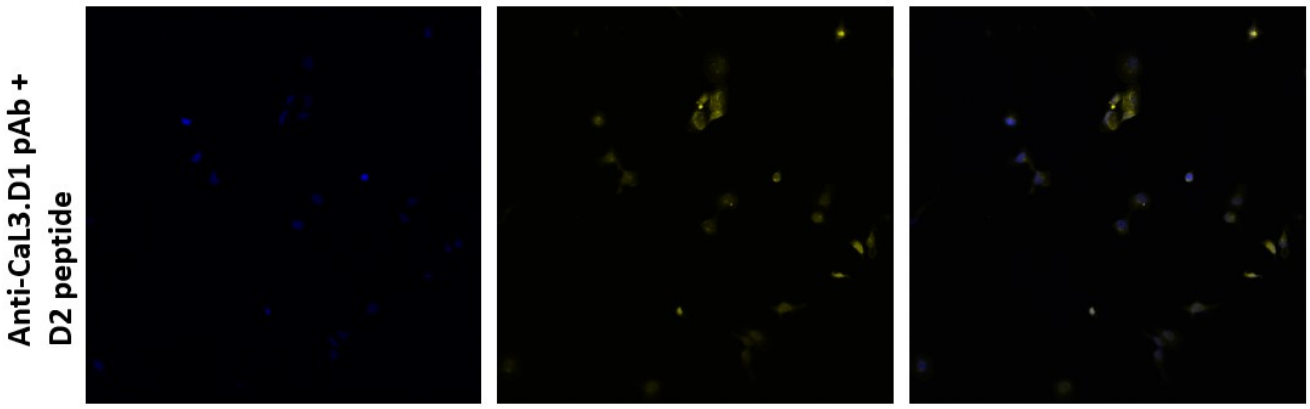
Anti-CaL3.D1 pAb +
D2 peptide

(E)

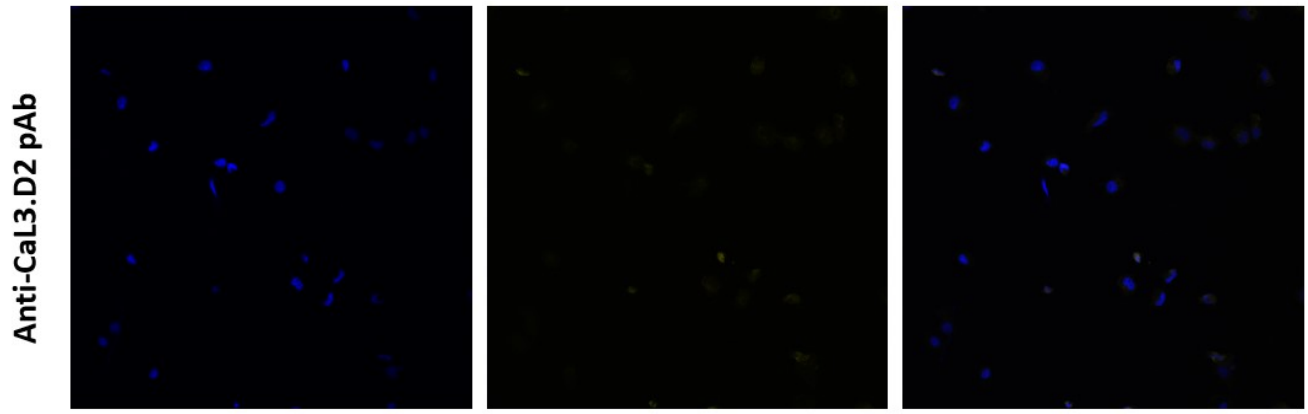

Figure 7.18. Fluorescence images of goldfish PKNs labeled with various rabbit pAbs. (A) Neutrophils stained with normal rabbit IgG (20 µg/ml). **(B)** Anti-CaL3.D1 pAb staining (20 µg/ml). **(C)** Staining with anti-CaL3.D1 pAb plus D1 peptide (50:1 peptide to pAbs ratio). **(D)** Staining with anti-CaL3.D1 pAb plus D2 peptide (50:1 peptide to pAb ratio). **(E)** Anti-CaL3.D2 pAb staining (20 µg/ml). Neutrophils were isolated from three goldfish individuals and then pooled before experiments. In each sample well of a 24-well plate, neutrophils ($2x10^6$) were seeded onto a 12 mm coverslip coated with poly-L-lysine for 1 h at RT to facilitate neutrophil attachment. Afterward, the cells were formalin-fixed and then blocked with 1% BSA in 1x PBST containing 22.5 mg/ml glycine for 30 min at RT. The cells were subsequently probed with various primary rabbit pAbs (20 µg/ml for all), followed by secondary goat-anti-rabbit Alexa Fluor 647 pAb (40 µg/ml). All antibody-incubation steps were performed at RT. The coverslips were then mounted on slides containing ProLong Gold Antifade Mountant with DAPI (Invitrogen). All images were captured using an Olympus FLUOVIEW FV3000 Confocal Laser Scanning Microscope with a 40x objective lens. Consistent laser settings were maintained across all acquisitions.

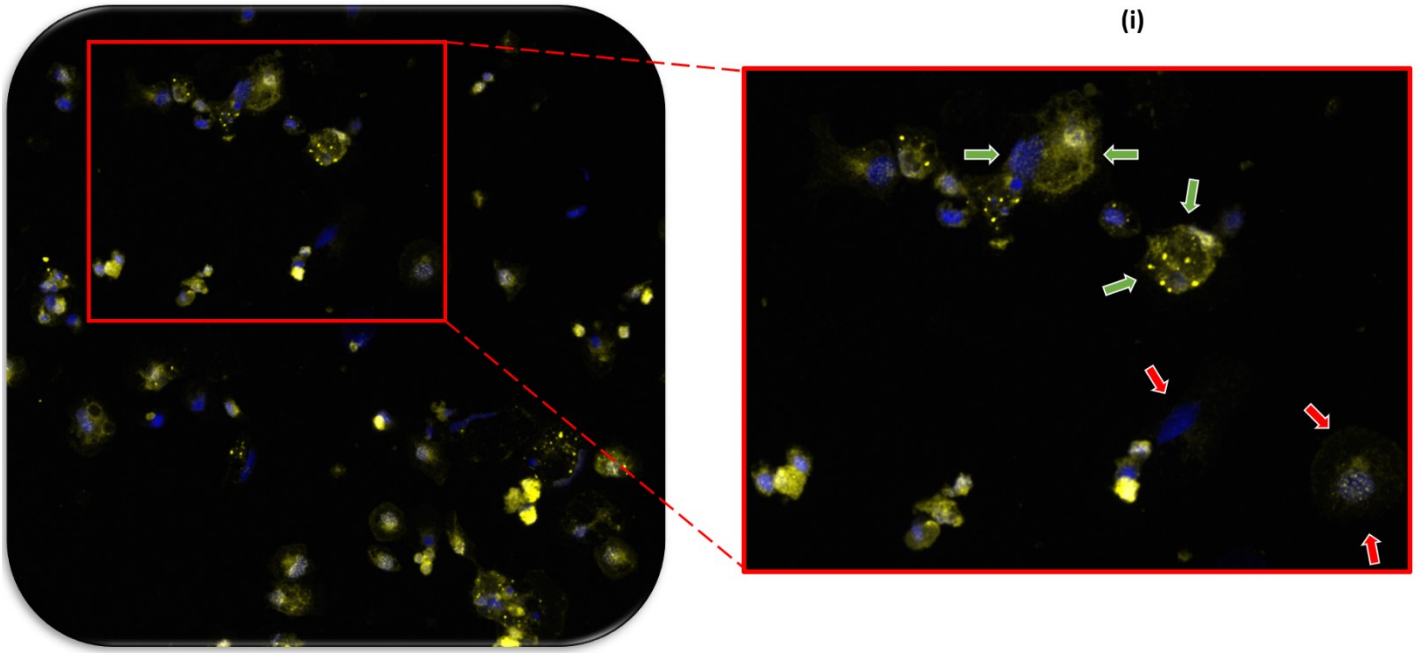

Figure 7.19. Immunofluorescence staining of day 7 goldfish PKMs with anti-CaL3.D1 pAb. **(i)** Enlarged image displaying anti-CaL3.D1-pAb-stained PKMs. The green arrows denote PKMs with strong anti-CaL3.D1-pAb staining. The red arrows represent PKMs with weak anti-CaL3.D1-pAb staining. In a well of a 24-well plate, PKMs ($1x10^6$) were seeded onto a 12 mm coverslip overnight to allow PKM attachment. The following day, the cells were fixed and then blocked with 1% BSA in 1x PBST containing 22.52 mg/ml glycine for 30 min at RT. The cells were subsequently probed with anti-CaL3.D1 pAb (20 µg/ml), followed by secondary goat-anti-rabbit Alexa Fluor 647 pAb (40 µg/ml). All antibody-incubation steps were performed at RT. The coverslips were then mounted on slides containing ProLong Gold Antifade Mountant with DAPI (Thermo Fisher). All images were captured using an Olympus FLUOVIEW FV3000 Confocal Laser Scanning Microscope with a 40x objective lens.

(A)

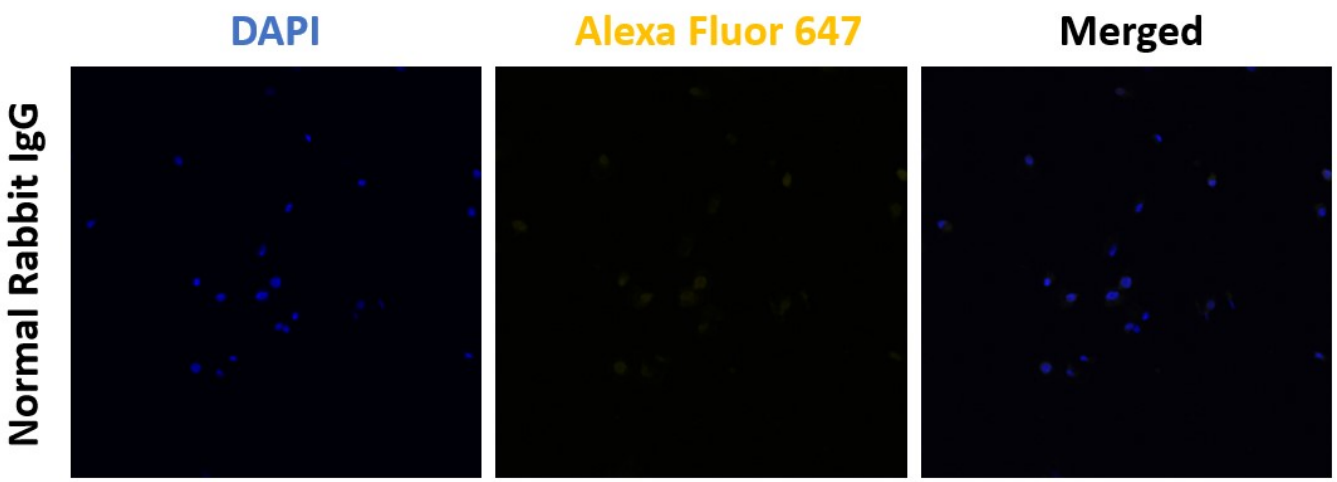
DAPI
Alexa Fluor 647
Merged
Normal Rabbit IgG

(B)

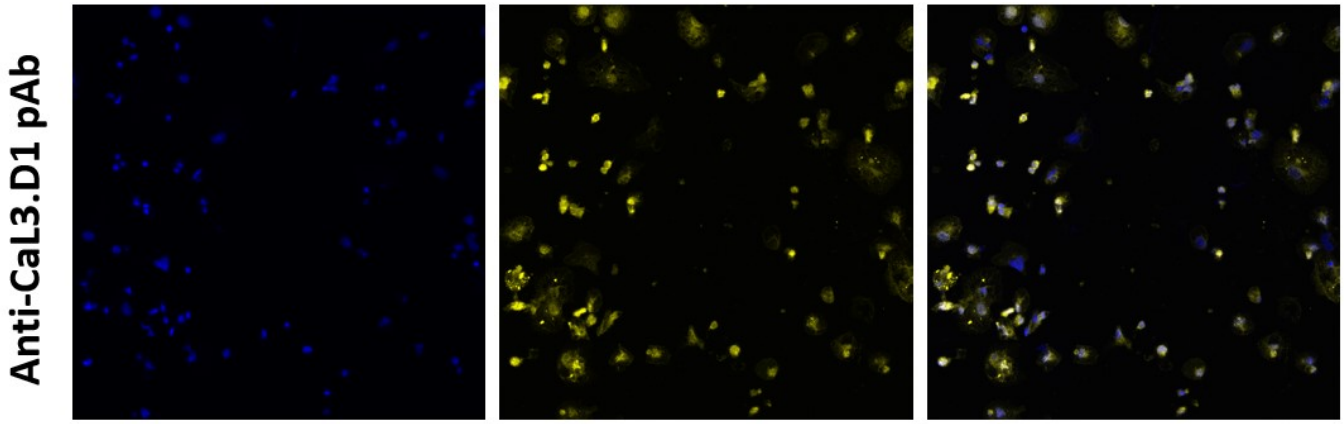
Anti-CaL3.D1 pAb

(C)

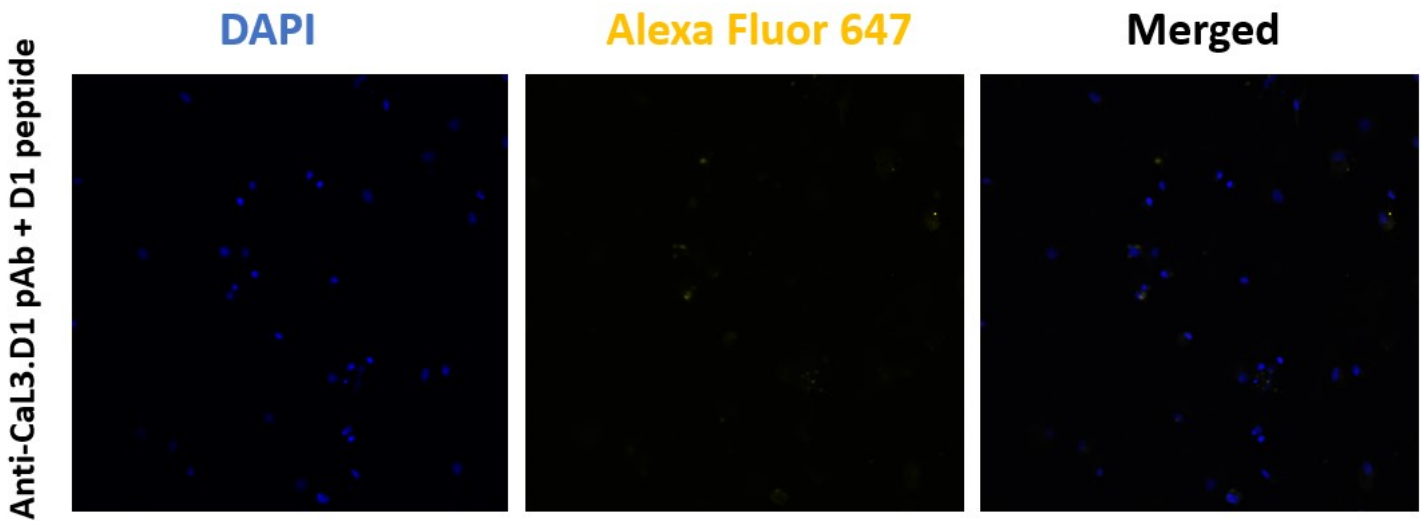
DAPI
Alexa Fluor 647
Merged
Anti-CaL3.D1 pAb + D1 peptide

(D)

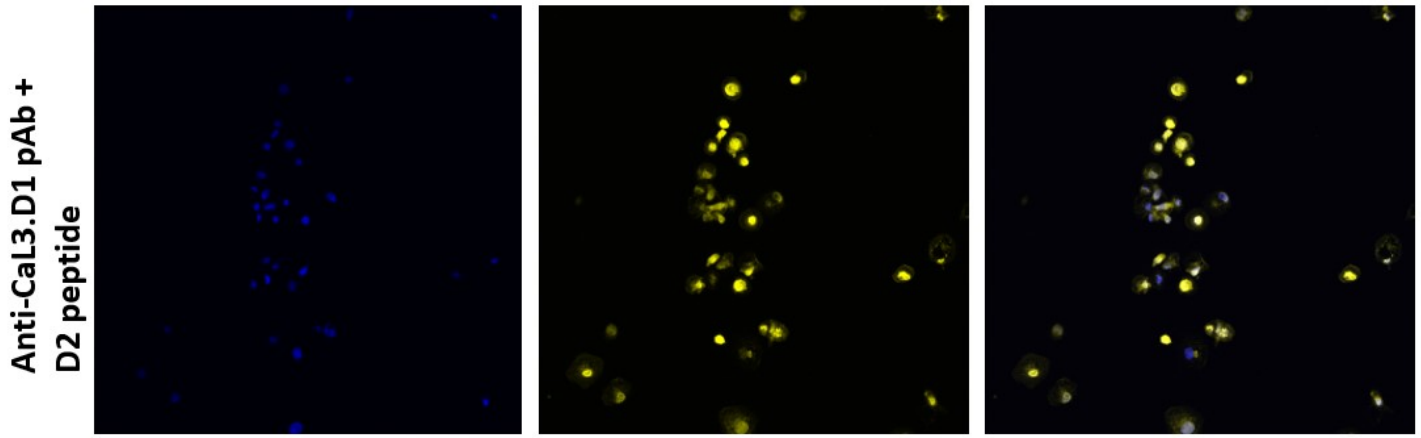
Anti-CaL3.D1 pAb + D2 peptide

(E)

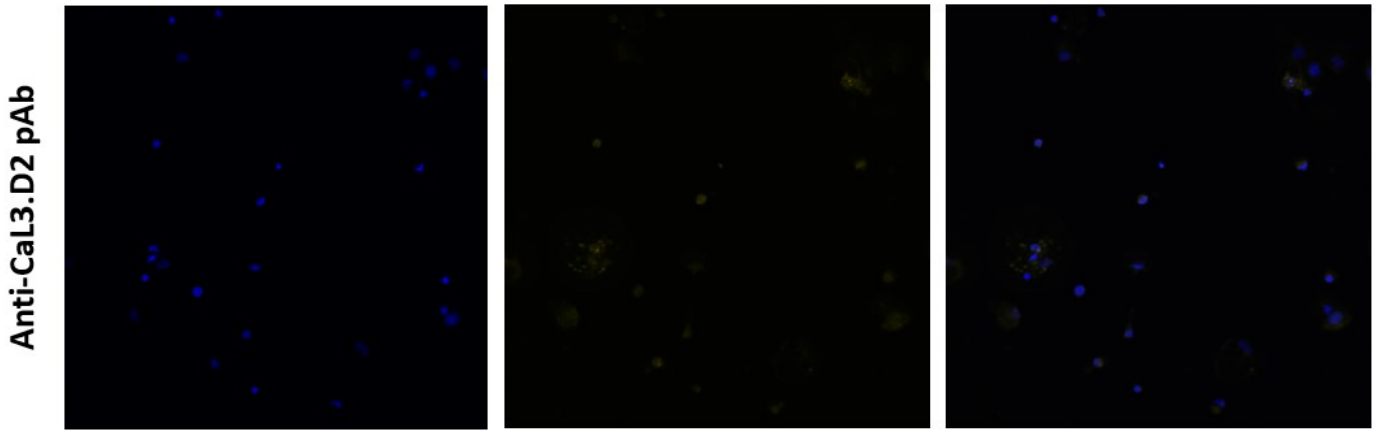

Figure 7.20. Immunofluorescence staining of day 7 goldfish PKMs with various rabbit pAbs. (A) Day 7 PKMs stained with normal rabbit IgG (20 µg/ml). **(B)** Staining with anti-CaL3.D1 pAb (20 µg/ml). **(C)** Staining with anti-CaL3.D1 pAb plus D1 peptide (50:1 peptide to pAbs ratio). **(D)** Staining with anti-CaL3.D1 pAb plus D2 peptide (50:1 peptide to pAb ratio). **(E)** Staining with anti-CaL3.D2 pAb (20 µg/ml). Day 7 PKMs from three separate goldfish cultures were pooled prior to experiments. In each sample well of a 24-well plate, PKMs ($1x10^6$) were seeded onto a 12 mm coverslip overnight to allow PKM attachment. The following day, the cells were fixed and then blocked with 1% BSA in 1x PBST containing 22.5 mg/ml glycine for 30 min at RT. The cells were subsequently probed with various primary rabbit pAbs (20 µg/ml for all), followed by secondary goat-anti-rabbit Alexa Fluor 647 pAb (40 µg/ml). All antibody-incubation steps were performed at RT. The coverslips were then mounted on slides containing ProLong Gold Antifade Mountant with DAPI (Invitrogen). All images were captured using an Olympus FLUOVIEW FV3000 Confocal Laser Scanning Microscope with a 40x objective lens. Consistent laser settings were maintained across all acquisitions.

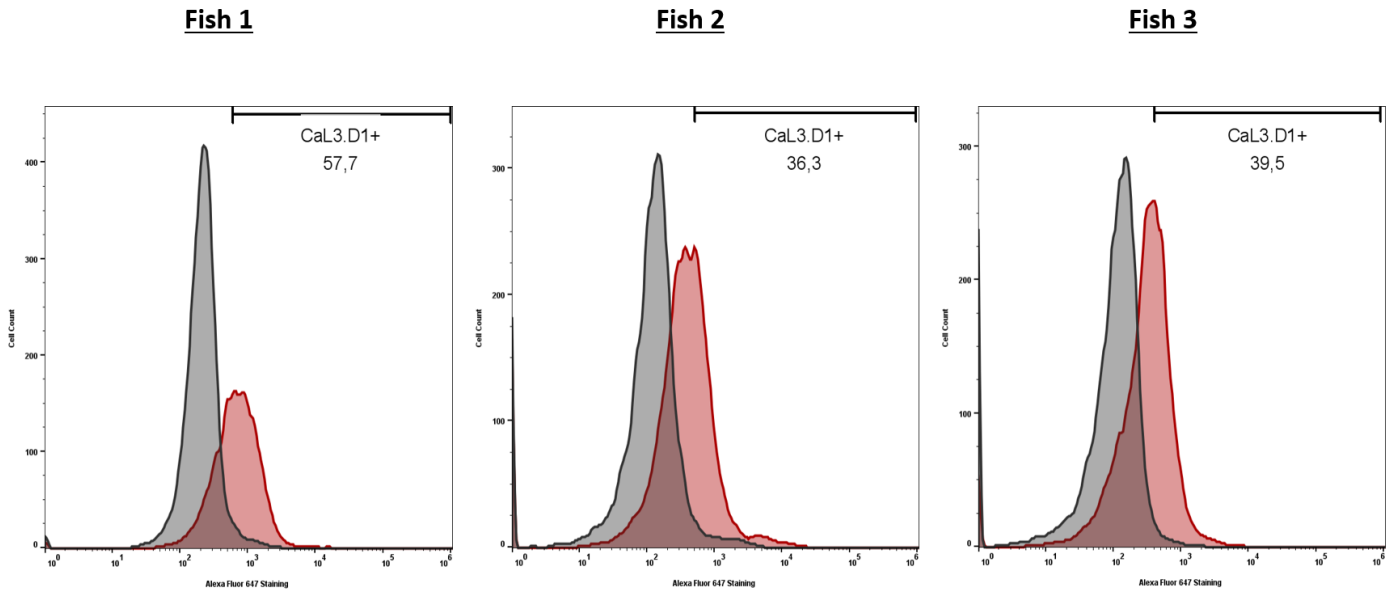

Figure 7.21. Flow cytometric analysis of the cell-surface expression of anti-CaL3.D1-pAb-reactive proteins in PKNs collected from three distinct goldfish individuals. Neutrophils ($1x10^6$) were treated with either normal rabbit IgG (20 µg/ml) or anti-CaL3.D1 pAb (20 µg/ml) in FACS buffer containing sodium azide (0.05%), followed by incubation with secondary goat-anti-rabbit Alexa Fluor 647 pAb (40 µg/ml). All antibody-incubation steps were carried out at RT. Protein expression profiles were obtained using Attune NxT and analyzed with FlowJo v10.10 software. The x-axis represents the fluorescence intensity of Alexa Fluor 647, while the y-axis indicates cell count. Grey and red histograms represent data obtained from rabbit control pAb and anti-CaL3.D1 pAb treatments, respectively. The percentage of anti-CaL3.D1-pAb-positive cells is indicated on each graph.

(A)

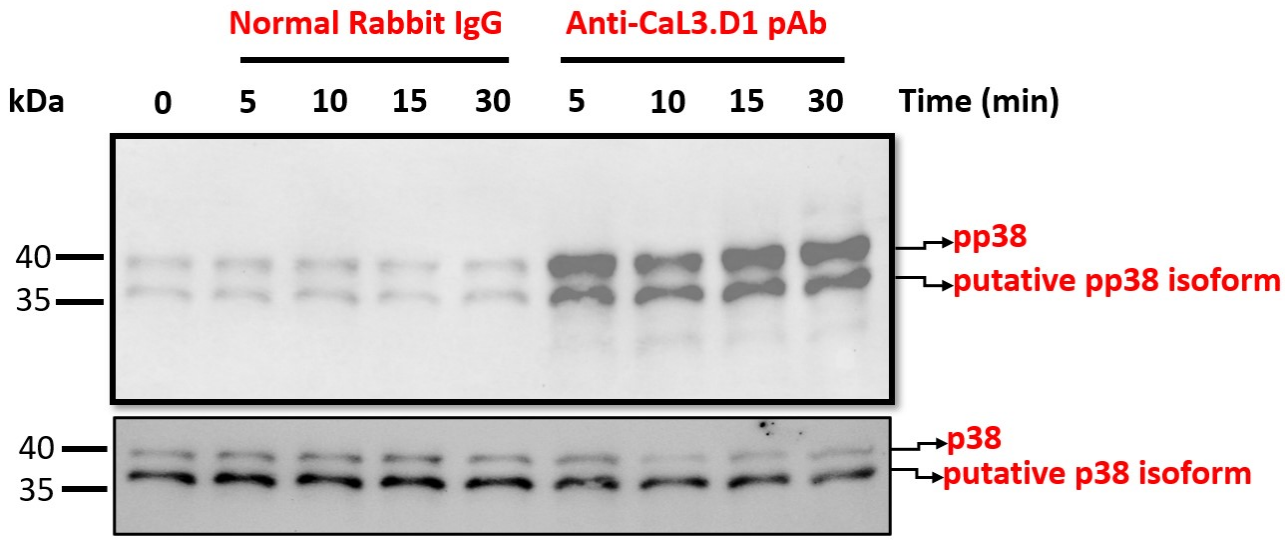
Normal Rabbit IgG
Anti-CaL3.D1 pAb
kDa
0
5
10
15
30
5
10
15
30
Time (min)
40
35
pp38
putative pp38 isoform
40
35
p38
putative p38 isoform

(B)

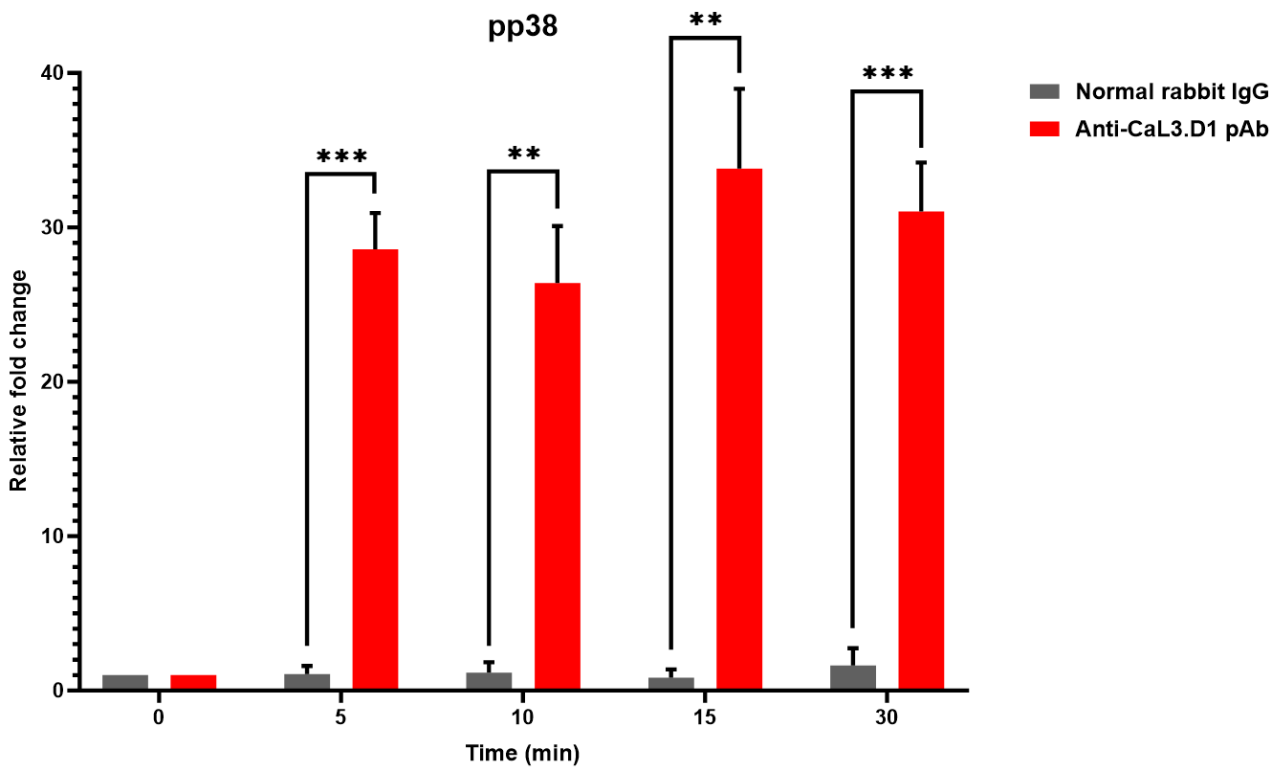
pp38
Relative fold change
Time (min)
0
5
10
15
30
0
10
20
30
40
***
**
**
***
Normal rabbit IgG
Anti-CaL3.D1 pAb

(C)

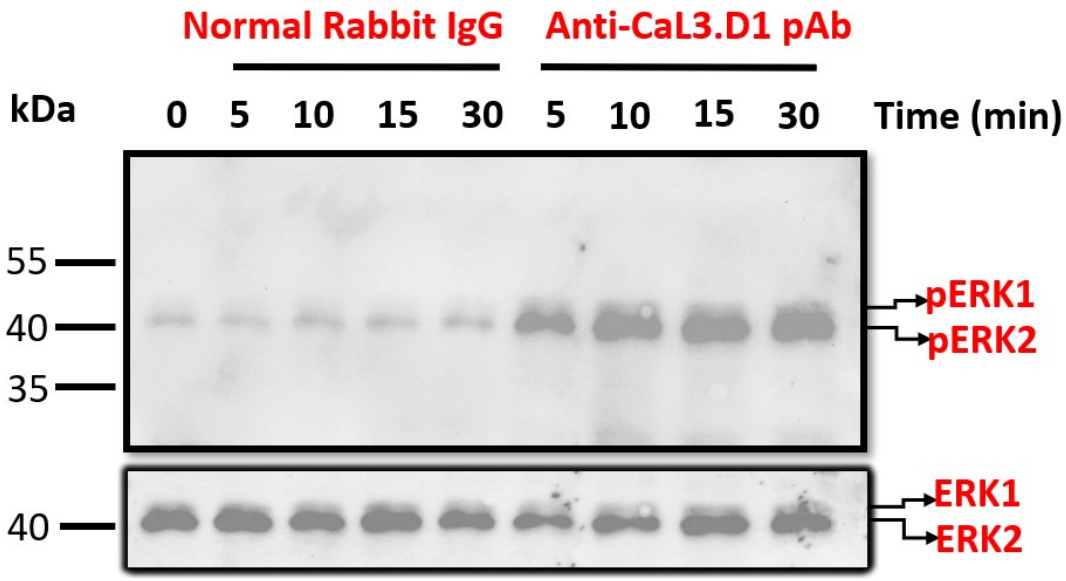
Normal Rabbit IgG
Anti-CaL3.D1 pAb
kDa
0
5
10
15
30
5
10
15
30
Time (min)
55
40
35
40
pERK1
pERK2
ERK1
ERK2

(D)

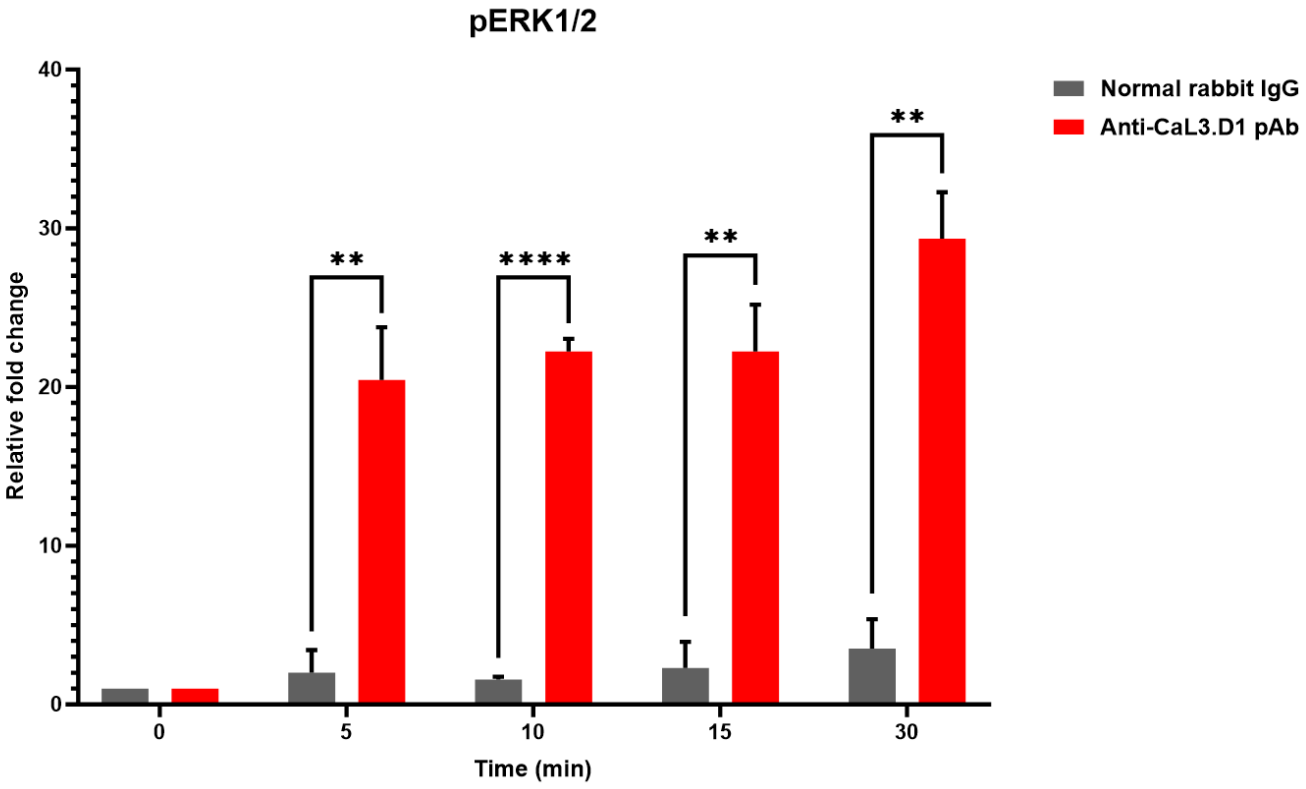

Figure 7.22. Western blot analysis of the protein expression levels of pERK1/2 and pp38 following anti-CaL3.D1-pAb/normal-rabbit-pAb-mediated cross-linking of cell-surface proteins in goldfish PKNs. (A) Representative blot illustrating the phosphorylation status of p38 in neutrophils treated with either normal rabbit IgG or anti-CaL3.D1 pAb for 30 min. The top panels are probed with an Ab to specific phosphotyrosines of p38, while the bottom panels are probed with an Ab that recognizes both phosphorylated and non-phosphorylated p38 proteins. **(B)** Densitometric analysis of the protein expression levels of pp38 in goldfish neutrophils following cross-linking of cell-surface proteins with either normal rabbit IgG or anti-CaL3.D1 pAb (n=3). **(C)** Representative blot depicting the phosphorylation status of ERK1/2 in neutrophils treated with either normal rabbit IgG or anti-CaL3.D1 pAb for 30 min. The top panels are probed with an Ab to specific phosphotyrosines of ERK1/2, while the bottom panels are probed with an Ab that recognizes both phosphorylated and non-phosphorylated ERK1/2 proteins. **(D)** Densitometric analysis of the protein expression levels of pERK1/2 in goldfish neutrophils following cross-linking of cell-surface proteins with either normal rabbit IgG or anti-CaL3.D1 pAb (n=3). Neutrophils from four separate PKN cultures were pooled before experiments. For each time point, neutrophils ($1.5x10^6$) were transferred to a microtube and bathed in phagocytosis buffer. These cells were then sensitized with either normal rabbit IgG (40 µg/ml) or anti-CaL3.D1 pAb (40 µg/ml) for 30 min at RT. Following two washes with PBS, neutrophils were treated with 50 µg/ml of unconjugated goat-anti-rabbit pAb for durations of 0, 5, 10, 15, and 30 min. Lastly, neutrophils were quickly centrifuged, and the resulting cell pellets

were lysed with Pierce IP Lysis Buffer containing protease and phosphatase inhibitor cocktails. WCLs were quantified using a Micro BCA protein assay kit. Subsequently, 15 µg of proteins from each time point were subjected to SDS-PAGE electrophoresis. Total proteins were transferred onto a nitrocellulose membrane and then blocked with 5% BSA in 1x TBST for 1 h at RT. Blots were subsequently probed with either primary antibodies reactive against pp38 (Phospho-p38 MAPK (Thr180/Tyr182, (D3F9) XP® Rabbit mAb) or endogenous p38 (p38α MAPK (L53F8) Mouse mAb) or pERK1/2 (Phospho-p44/42 MAPK (Erk1/2) (Thr202/Tyr204) Antibody) or endogenous ERK (p44/42 MAPK (Erk1/2) Antibody). Afterward, blots were probed with either goat-anti-rabbit or goat-anti-mouse HRP conjugated antibodies. SuperSignal West Pico PLUS Chemiluminescent Substrate was used to detect protein bands, and images were acquired using the ChemiDoc MP Imaging System. Relative protein band intensities were quantified using ImageJ software. Values of pp38 and pERK were normalized to total p38 and ERK1/2 levels and displayed as fold changes relative to 0-minute controls. Data from (C) and (D) are represented as means ± standard errors from three biological replicates. Significant differences between treatments were determined by unpaired T-tests. P-values are illustrated as $^{ns}p > 0.05$, $*p \leq 0.05$, $**p \leq 0.01$, $***p \leq 0.001$, and $****p \leq 0.0001$.

CHAPTER VIII

GENERAL DISCUSSION AND FUTURE DIRECTIONS

8.1 Summary of thesis findings

IpLITRs are a large family of immunoregulatory receptors that share phylogenetic relationships with the mammalian FcR family and LRC-encoded receptors. Due to the lack of reagents and the absence of native IpLITR ligands at the time of their discovery, research on these receptors has primarily relied on overexpressing specific IpLITRs in various mammalian cell lines. These studies have provided significant insights into the immunoregulatory potentials of several IpLITRs and suggest that select IpLITRs likely use dynamic signaling mechanisms to control various innate immune effector responses. While there is considerable knowledge regarding the immunomodulatory potentials of IpLITRs, their native functions in teleost immunity remain largely unknown. To address this knowledge gap, the overall aim of my thesis was to establish the goldfish as a new model system for studying LITRs and their functions.

In Chapter IV, I used the goldfish genome to design primers against several predicted *calitr* transcripts. This approach allowed me to successfully clone a total of seventeen *calitr* transcripts with complete ORFs (a few are not shown in Chapter IV) without relying on the relatively laborious rapid amplification of cDNA ends (RACE) PCR method. Using RT-PCR, I showed that several transcripts (*calitr2* and *calitr3*) are expressed in a wide range of goldfish tissues, including spleen, kidney, intestine, heart, brain, liver, muscle, and gills. In contrast, the *calitr1* mRNA was not expressed in any of these tissues. Additionally, the transcripts of *calitr1*, *calitr2*, and *calitr3* were shown to be expressed during PKM development and in PKNs. Sequence analysis of the various identified CaLITRs revealed that they have variable

arrangements of extracellular Ig-like domains and CYTs containing different tyrosine-based signaling motifs. Overall, these CaLITRs can be broadly classified into putative activating receptor-types, putative inhibitory receptor-types, predicted functionally ambiguous receptor-types, putative secreted/intracellular CaLITR forms, and receptors with multiple signaling potentials. For instance, CaLITR1 has a short CYT and an uncharged TM. Thus, it's currently unknown if this receptor has any signaling capabilities. The CYT of CaLITR2 contains tandem ITIM and ITSM motifs, suggesting that this receptor may recruit PTPs to dampen immune activities. CaLITR3 is predicted to be an activating receptor-type characterized by a positively charged TM and a short CYT. Furthermore, this receptor is also unique in that its TM features a histidine residue, whereas the majority of mammalian activating receptors typically have a TM with either lysine or arginine residues (Feng et al., 2005). CaLITR2.3 is closely related to CaLITR2 but lacks a TM and CYT; therefore, this receptor may be secreted or have an intracellular localization. Finally, CaLITR4 represents a putative multi-functional receptor-type with a CYT containing various tyrosine-based motifs, including endocytosis, Nck recruitment, ITIM, and ITSM motifs, suggestive of their potential dynamic immunoregulatory capabilities.

I also identified several *calitr* transcript variants. Sequence comparisons of these CaLITRs revealed that they share high sequence similarity and mostly differ in the presence or absence of Ig-like domains, akin to protein isoforms. Further comparison with their respective genomic sequences indicated that most of these sequences resemble exon-skipped splice variants. These results suggest that these putative extracellular domain splice variants may have different ligands or affinities for their ligands. In addition, I discovered a pair of CaLITR sequences resembling CYT splice variants. Specifically, CaLITR2.1 has a CYT containing a single ITSM motif. Overall, this sequence is highly similar to CaLITR2, except that the CYT

region of CaLITR2.1 lacks a 29-amino-acid-long signalling cassette containing the ITIM motif of CaLITR2. This CYT alteration was hypothesized to impact the ability of CaLITR2.1 to engage downstream signaling molecules. Indeed, triggering of HA-tagged recombinant chimeric IpLITR2.6b receptors containing the CYT regions of CaLITR2/2.1 expressed on the surface of AD293 cells showed that the CaLITR2.1 CYT induced a higher rate of phagocytosis of both anti-HA-Ab-coated 4.5 μm and 2.0 μm beads compared to the CaLITR2 CYT (Al-Rikabi, 2024). Additionally, we have shown that the CaLITR2.1 CYT induced AD293 cells to display a unique delayed phagocytosis phenotype relative to the ITAM-containing CaLITR6.1 (Al-Rikabi, 2024), suggesting that CaLITR2.1 uses a novel ITAM-independent mechanism to control phagocytosis. Altogether, these findings support that alternative splicing likely plays a significant role in diversifying the ligand-binding abilities and/or signaling potentials of CaLITRs. The discovery of the unique CaLITR forms and sequence variants opens up new avenues for exploring how these sequences may contribute to controlling the goldfish immune system.

Initial phylogenetic analysis revealed that IpLITRs share phylogenetic relationships with mammalian immunoregulatory receptors of the FcR family and LRC, however, their syntenic relationships with these receptors were unknown. To gain a better understanding of the evolutionary connections between *litrs* and immunoregulatory receptors in various aquatic and terrestrial vertebrates, I used a comparative genomics approach to comprehensively investigate whether *litrs* share conserved synteny with the various vertebrate FcR family and LRC-encoded receptor genes. As shown in Chapter V, the genomic analysis revealed that *litrs* from the goldfish, zebrafish, channel catfish, and Fugu, are organized within gene complexes, similar to their mammalian FcR family or LRC-encoded counterparts. Additionally, I demonstrated that select *litr* genomic clusters from each of the fish species examined are linked to *arhgef11*,

vangl2, and genes of the CD2 family; features that are also shared by amphibian, mouse, and human *fcrls*. Moreover, phylogenetic analysis showed that select individual Ig-like domains from LITRs (gold and light blue domains) are also related to those from amphibian, mouse, and human *fcrls*. Collectively, these results further consolidate the evolutionary relationships between LITRs and FCRLs. I also identified an LRC-like genomic region on zebrafish Chr16 that contains several hallmark genes (i.e., *ttyh1*, *leng9*, *cdc42ep5*) found in well-established LRC regions of amphibians and mammals. However, no *lilr* or *litr* relatives were found in this region. The absence of these genes on zebrafish Chr 16 further strengthens the hypothesis that LITRs are more closely related to FCR family receptors than to receptors encoded within the LRC. Interestingly, others have identified several *fcrls* on zebrafish Chr 7, Chr 3, and Chr 23 (Akula et al., 2014). Further analysis indicated that these zebrafish *fcrls* share phylogenetically related Ig-like domains with those of the human and mouse FcR family receptors (Akula et al., 2014). Specifically, sequence relatives of the D1 and D2 Ig-like domains (correspond to the gold and light blue domains in my study, respectively) of human and mouse FCRLs were shown to be present in the zebrafish FCRLs. Thus, these results align with my findings and reinforce that LITRs are likely to be relatives of vertebrate FCRLs.

As previously described, mammalian FCRLs play diverse roles in regulating immune responses in different innate and adaptive immune cell types (Li et al., 2014). Additionally, they are known to recognize various sub-types of antibodies (i.e., IgA and IgG) and MHC/MHC-like molecules (i.e., OMCP and MHC-class II molecules) (Campbell et al., 2010; Rostamzadeh et al., 2018; Schreeder et al., 2010). Therefore, future experiments should focus on examining the potential for LITRs derived from the various conserved syntenic clusters to interact with either teleost Abs or MHC/MHC-like molecules.

Due to the fact that *calitr* genes are widely distributed across the goldfish genome (i.e., Chr 3, Chr 47, and LG28B), I hypothesized that the various *calitr* genes on the distinct goldfish Chrs may be under the influence of different cis- and/or trans-regulatory elements. To test this hypothesis, Chapter VI examined the transcriptional activities of several *calitrs* originated from different goldfish Chrs during goldfish PKM development and in activated goldfish MLR cultures. For instance, *calitr1*, *calitr2*, *calitr3*, and *calitr4* are located on an unplaced genomic scaffold, Chr 47, Chr 3, and LG28B, respectively. Using a qPCR-based approach, I showed that the various *calitr* transcripts were variably expressed during PKM development over a twelve-day culture period. Interestingly, *calitr1* mRNA was upregulated during early PKM development (days 2–4), while the expression levels of *calitr2*, *calitr3*, and *calitr4* stayed relatively stable over the course of PKM development. These results suggest that *calitr1* is likely developmentally regulated in goldfish macrophages, and that select CaLITRs from different goldfish Chrs may share distinct *cis*- and/or *trans*-regulatory elements. Further investigations showed that the mRNA expressions of *calitr1* and proinflammatory markers *tnf-α* and *ifnγ* were upregulated in goldfish MLRs at 6 and 12 h following stimulation with a mitogen cocktail containing ConA, PMA, and calcium ionophore A23187, whereas the expression levels of *calitr2*, *calitr3*, and *calitr4* showed no observable changes. Moreover, I showed that the transcriptional activity of *calitr1*, *ifnγ*, and *tnf-α* in mitogen-activated MLRs were significantly reduced when treated with DMSO, and to a lesser extent with CsA. Conversely, the expression levels of *calitr2*, *calitr3*, and *calitr4* remained constant. These findings suggest in part that CaLITR1 has distinct expression kinetics akin to that of classical proinflammatory genes (i.e., *tnf-α* and *ifnγ*) and provided additional evidence to suggest that select CaLITR genes from distinct goldfish Chrs might be regulated via different *cis*- and/or *trans*-regulatory elements.

Examination of the putative promoter regions of the various *calitrs* also showed that *calitr1* and *tnf-α2* have additional inflammation-associated TFBS (i.e., STAT-4), which may explain the more active transcriptional profiles of these genes in activated goldfish leukocyte cultures. However, the exact size of the various *calitr* promoter regions and their associated transcription factors will need to be further confirmed with additional experiments. For example, Assay for Transposase Accessible Chromatin Sequencing (ATAC-seq) can be used for investigating the chromatin accessibility of the putative *calitr* promoter regions. Additionally, chromatin immunoprecipitation sequencing (ChIP-seq) can be used for examining specific transcription factor binding (i.e., STAT4) to the various putative *calitr* promoter regions, Alternatively, other techniques, including DNase footprinting and electrophoretic mobility shift assays (EMSA), can also be used for examining transcription factor protein binding events. Overall, the availability of the goldfish genome allows for an initial analysis of the putative promoter regions of the various *calitrs*. Furthermore, this study has shed light on the transcriptional patterns of several *calitrs* from distinct goldfish Chrs and paves the way for more detailed investigations into the complex signaling pathways and transcription factors regulating the transcription of *calitrs*.

In Chapter VII, I described the development of a LITR-specific polyclonal antibody for the characterization of the functions of CaLITR3 in goldfish primary myeloid cells. As noted earlier, CaLITR3 was selected as it represents a putative activating receptor-type, with a TM containing a positively charged histidine residue and a short CYT. Thus, I hypothesized that this receptor may require physical associations with negatively charged adaptor molecules containing ITAMs (i.e., FcRγ) to transduce stimulatory signals. Another reason for studying CaLITR3 is that activating receptor-types with TM histidine residues are rarely studied compared to those with

TM lysine or arginine residues. To my knowledge, only one FcαR study (Morton et al., 1995) has investigated the adaptor recruitment potential of a TM histidine residue.

To specifically characterize CaLITR3 in the goldfish, I developed two pAbs that target epitopes located in the D1 (GAERGGSRTSNISDE) and D2 (DNKYNYQKLSGC) of CaLITR3. These particular peptides were selected as they exhibit relatively high specificity for CaLITR3 when aligned with all identified CaLITR transcript sequences. Additionally, they were predicted to be exposed and linear. This increases the likelihood that these pAbs can interact with both denatured and native CaLITR3 proteins, rendering them suitable for various downstream applications such as western blotting and flow cytometry. As shown in Chapter VII, my initial pAb validation experiments demonstrated that the anti-CaL3.D1 pAb was capable of interacting with rCaLITR3 proteins expressed on the surface of AD293 cells. However, the anti-CaL3.D2 and normal rabbit control pAbs showed no reactivity towards rCaLITR3 proteins. Furthermore, my peptide-blocking experiments showed that the D1 peptide was effective at blocking the interaction between anti-CaL3.D1 pAb and rCaLITR3 proteins, whereas the D2 peptide failed to block these protein interactions. These results support the specificity of anti-CaL3.D1 pAb for rCaLITR3 proteins. In addition, my immunoprecipitation experiments also showed that the anti-CaL3.D1 pAb was capable of recognizing rCaLITR3 proteins. However, this pAb was unable to recognize overexpressed rIpLITR2.6b proteins, reinforcing the selectivity of anti-CaL3.D1 pAb for rCaLITR3 proteins.

I investigated the ability of the CaLITR pAbs to detect putative CaLITR3 proteins in the lysates of various goldfish primary cells, including PKNs, splenocytes, and mixed kidney leukocytes. These experiments showed that the anti-CaL3.D1 pAb recognized a 70 kDa protein in the lysates of PKNs and mixed kidney leukocytes, which corresponds to approximately the

size of rCaLITR3 proteins observed in AD293 cell lysates. However, this protein was not detected in goldfish splenocyte lysates. Moreover, peptide-blocking experiments further confirmed the specificity of anti-CaL3.D1 pAb for the putative 70 kDa CaLITR3 protein expressed in PKN lysates, supporting its specificity for the D1 peptide.

To further investigate the ability of CaLITR3 pAbs to interact with putative native CaLITR3 proteins in goldfish cells, I initially examined staining in the goldfish kidney, as the *calitr3* transcript was originally cloned from this organ (Wang et al., 2020). These experiments revealed that the anti-CaL3.D1 pAb brightly stained neutrophil-like cells with kidney-shaped nuclei and putative lymphocytes/progenitor cells within the goldfish kidney tissue. Surprisingly, this pAb also stained renal tubular epithelial cells. Consistent with the inability of the normal rabbit control and anti-CaL3.D1 pAbs to interact with rCaLITR3 proteins, these pAbs showed minimal reactivities within the goldfish kidney. Interestingly, the anti-CaL3.D1 pAb consistently showed no reactivity towards kidney erythrocytes and glomeruli. Overall, these findings suggest a potential higher expression of CaLITR3 proteins in kidney neutrophil-like cells and putative lymphocytes/progenitor cells compared to erythrocytes and glomerular cells. These results were further supported by a 30-fold higher expression of the *calitr3* transcript in PKNs relative to mixed kidney leukocytes and erythrocytes.

To further validate the staining patterns of the CaLITR pAbs observed within the goldfish kidney, I isolated goldfish PKNs and examined the potential of these pAbs for staining these cells. Consistent with the high anti-CaL3.D1-pAb-based immunofluorescence observed in kidney neutrophil-like cells, PKNs were strongly stained by the anti-CaL3.D1 pAb, reinforcing its ability to label neutrophil-like cells. Additionally, the anti-CaL3.D1 pAb also brightly stained PKMs, demonstrating its preferential staining for goldfish leukocytes. To investigate the

potential of anti-CaL3.D1 pAb to recognize putative CaLITR3 proteins on the membrane of goldfish neutrophil-like cells, I used a flow cytometry cell surface staining protocol to examine the anti-CaL3.D1-pAb-based immunofluorescence in these cells. The results showed that the anti-CaL3.D1 pAb variably stained PKN surface proteins in three goldfish individuals, indicating that putative CaLITR3 proteins are present on the surface of PKNs.

As discussed, CaLITR3 is a predicted activating receptor with a TM containing a positively charged histidine residue. Therefore, I postulated that this receptor may form non-covalent associations with adaptor molecules bearing ITAMs to stimulate ITAM-based signaling pathways. To investigate this possibility, I examined the ability of anti-CaL3.D1 pAb to induce the phosphorylation of ERK1/2 and p38 following cross-linking of putative PKN membrane CaLITR3 proteins. These signaling molecules were selected as they are well-known downstream targets of ITAM-based signaling pathways (Rosales, 2017). Consistent with my predictions, upon PKN membrane protein crosslinking by the anti-CaL3.D1 pAb, this Ab induced a rapid and persistent phosphorylation of ERK1/2 and p38 proteins, confirming the stimulatory potential of putative CaLITR3 proteins. These findings imply that upon ligand recognition, activating CaLITR-types may trigger neutrophil-mediated innate immune effector responses.

In summary, I have identified a total of seventeen *calitr* transcripts. Sequence analysis of these genes has provided novel insights into the exon organization of *litrs*, revealing that alternative splicing may serve as a significant mechanism driving the diversification of ligand recognition and/or immunoregulatory potentials in LITRs. Most importantly, the discoveries of the various unique CaLITR forms have created opportunities for asking new questions and testing new hypotheses on how these receptors may contribute to the regulation of teleost immunity. Additionally, genomic analysis of *calitrs* and *litrs* from other teleost species

demonstrates that *litrs* are syntenically related to vertebrate *fcrls*. These findings expand our understanding of the diverse forms of LITRs present across different teleost species and may be useful for further elucidation of the binding partners of LITRs. Furthermore, expression analysis of several *calitrs* from distinct goldfish Chrs revealed that these genes are differentially expressed in activated goldfish leukocytes and during PKM development, suggesting that they are likely regulated by distinct cis and/or trans-regulatory elements. These data provide the foundation for a more in-depth analysis of the transcriptional regulation of *calitrs*. Finally, I have successfully developed an Ab-based reagent for characterizing CaLITRs in goldfish. This tool will be useful for further investigation of the native functions of LITRs in various goldfish immune cells. Collectively, my thesis work has established the goldfish as a valuable and versatile model system for investigating various aspects of LITR immunobiology and laid the groundwork for further investigation of the native immunoregulatory roles of LITRs.

8.2 Future directions

8.2.1 Investigation of the downstream functional consequences of anti-CaL3.D1-pAb-mediated triggering of the MAPK pathway in goldfish neutrophils

Crosslinking of the anti-CaL3.D1-pAb-reactive membrane proteins was shown to induce rapid phosphorylation of ERK1/2 and p38 in goldfish PKNs, confirming the stimulatory potential of putative CaLITR3 proteins. However, the functional outcomes downstream of these MAPK pathway signaling molecules are unknown. As previously discussed, studies in mammals have shown that ERK1/2 and p38 are associated with the activation of various neutrophil-mediated innate immune effector functions, such as ROS production (Rosales & Uribe-Querol, 2018), NETosis (Rosales & Uribe-Querol, 2018), and transcriptional upregulation of various cytokine genes (Rosales & Uribe-Querol, 2018), and degranulation (Lacy, 2006). Based on this

evidence, I have provided a summary figure (Fig. 8.1) to illustrate the potential signaling events triggered by anti-CaL3.D1-pAb-mediated protein cross-linking. Several methods are available for investigating the potential anti-CaL3.D1-pAb-mediated activation of ROS production in goldfish PKNs. For example, dihydrorhodamine (DHR) reacts with ROS to produce Rhodamine 123, a fluorescent compound that can be detected by confocal microscopy or flow cytometry. Moreover, this probe has been used to quantify the respiratory burst activity in goldfish PKNs upon exposure to the teleost pathogen *A. salmonicida* (Katzenback & Belosevic, 2009). Additionally, it has been used to measure the percentage of ROS-positive cells in isolated intraperitoneal leukocyte infiltrates from the goldfish (Havixbeck et al., 2016). Alternatively, techniques such as nitroblue tetrazolium (NBT) assay (Javvaji et al., 2020) and commercially available fluorescent dyes (i.e., CellRox) may be used for detecting general respiratory burst activity in goldfish PKNs following receptor crosslinking by the anti-CaL3.D1 pAb.

The activation of ERK1/2 is often followed by the stimulation of NETosis (Rosales & Uribe-Querol, 2018) (Fig. 8.1), thus, future experiments should also investigate this possibility. One approach for visualizing NET release is to use the nucleic acid dye, SYTOX Green (Palic et al., 2007). Since SYTOX Green is impermeant to live cells, it effectively stains released DNA during the process of NETosis in goldfish PKNs. Indeed, using SYTOX Green, I have confirmed that the majority of goldfish PKNs can release DNA NETs following stimulation with either 5 µg/ml of calcium ionophore A23187 and 1 µg/ml PMA as early as 1 h post-mitogen stimulation (Appendix Fig. 1). Furthermore, I have set up the experimental protocols for visualizing or quantifying PKN NETosis using confocal microscopy (Appendix Fig. 1) and flow cytometry (not shown), respectively. These established assays would be useful not only for elucidating the

functions of putative CaLITR3 proteins but also for studying other goldfish LITR types, such as the ITAM domain-containing CaLITR6.1.

ERK1/2 and p38 may also regulate the transcription of cytokine genes (Fig. 8.1) in goldfish PKNs. To investigate this possibility, qPCR can be used to measure transcriptional changes in goldfish cytokine genes such as *tnf-α2*, *ifnγ*, and *il-6*. Additionally, high-throughput sequencing technologies (i.e., RNA-seq) can be to detect broad-spectrum changes in goldfish PKN mRNA expressions following receptor triggering. This approach would help us quickly identify other potential signaling pathways or functional outcomes triggered by anti-CaL3.D1 pAb and gain a more comprehensive understanding of anti-CaL3.D1-pAb-mediated triggering of signaling pathways and their associated downstream functional responses.

p38 has been shown to regulate neutrophil degranulation. Therefore, I hypothesize that anti-CaL3.D1-pAb-mediated crosslinking may also induce PKN degranulation. This can be tested using a published 3,3',5,5'-tetramethylbenzidine (TMB)-based assay for measuring MPO release activity in teleost neutrophils (Palic et al., 2005). In this assay, MPO catalyzes the oxidation of TMB to form a blue-coloured product in the presence of H_2O_2. This method has also been previously demonstrated to be effective at measuring myeloperoxidase release activity in goldfish PKNs (Katzenback & Belosevic, 2009).

8.2.2 Identification of the potential goldfish adaptor molecules associating with putative CaLITR3 proteins following receptor cross-linking

As discussed, since CaLITR3 contains a TM containing with a positively charged histidine residue, I postulated that these putative proteins may associate with adaptor molecules containing ITAMs for signaling transduction. To my knowledge, only one study has investigated

the adaptor recruitment potential of a TM histidine residue (Morton et al., 1995). This study revealed that replacing the native arginine residue of FcαR with histidine did not prevent this receptor from interacting with FcRγ. Interestingly, BLAST searches of the goldfish genome identified more putative activating CaLITR-types containing TM histidine residues compared to TM lysine or arginine residues (Wang et al., 2021). Although the reason for this preference for histidine remains unknown, this observation suggests that these TM-histidine-bearing receptors may play a crucial role in the immune system of the goldfish. Therefore, it's important to investigate the adaptor recruitment potential of putative CaLITR3 proteins. One approach would be to perform a co-immunoprecipitation assay using the anti-CaL3.D1 pAb. Based on the established assay for isolating CC41-reactive channel catfish proteins (Crider et al., 2023), PKN membrane proteins would be initially biotinylated by incubating PKNs with a Sulfo-NHS-Biotin solution. Subsequently, this reaction would be terminated by adding a cold 100 mM glycine solution to the cell mixture. These cells would then be lysed for downstream co-immunoprecipitation experiments. Following this, Dynabeads coated with either the normal rabbit control pAb (negative control) or anti-CaL3.D1 pAb would be used to pull down biotinylated membrane proteins in resting PKN cells to examine if any adaptor proteins constitutively interact with the putative CaLITR3 proteins.

Alternatively, these procedures would be performed on PKN cells following membrane crosslinking by either the normal rabbit pAb or anti-CaL3.D1 pAb. To prevent co-elution of the rabbit Abs that would potentially interfere with downstream western blotting experiments, both the normal rabbit control and anti-CaL3.D1 pAbs should be cross-linked to Dynabeads before using them for the pull-down assay. This could be achieved using the Pierce^{TM} Crosslink IP kit (Thermo Fisher). Running the immunoprecipitated anti-CaL3.D1-pAb-reactive proteins on an

SDS-PAGE gel and comparing the resulting immunoreactive bands to those from the normal rabbit control pAb group may allow for the identification of proteins that can interact with the putative CaLITR3 proteins using a streptavidin Ab. To verify the identities of the immunoprecipitated proteins, these immunoreactive bands should be examined with silver staining, which is highly sensitive for detecting low concentrations of native proteins. Finally, the specific anti-CaL3.D1-pAb-reactive bands would be purified and validated by mass spectrometry.

The methods described above would facilitate the identification of all possible binding partners of putative CaLITR3 proteins. Once the identities of the immunoprecipitated proteins are known, a more specific approach would be used to confirm these protein interactions. For example, our established protocols (Mewes et al., 2009) for examining the adaptor recruitment potential of IpLITR2.6b are highly suitable for this task.

8.2.3 Confirmation of the identities of the anti-CaL3.D1-pAb-reactive proteins in goldfish neutrophils

Overall, my Chapter VII results support that the anti-CaL3.D1 pAb interacts with putative CaLITR3 proteins expressed on the membrane of PKNs to transduce stimulatory signals; however, the identities of these proteins are currently unknown. Further verification of these proteins are necessary for confirming the specificity of the anti-CaL3.D1 pAb. Using the methods described in 8.2.2, the anti-CaL3.D1 pAb can be used to pull down any biotinylated anti-CaL3.D1-pAb-reactive CaLITR proteins from PKN membranes. These immunoreactive proteins would then be run on an SDS-PAGE gel and visualized with silver staining. The specific anti-CaL3.D1-pAb bands could then be excised and sent for mass spectrometry analysis.

8.2.4 The search for CaLITR ligands

Even though LITRs were discovered in 2006, their biological ligands remain elusive. This greatly hinders our understanding of their native functions and predicted roles as immunoregulatory receptor-types. As mentioned earlier, select *calitrs* and *litrs* from several other teleost species were shown to share conserved synteny with the vertebrate *fcrls*, suggesting that they are likely to be relatives of these receptors. However, it remains unknown if any of these LITRs also share similar ligands as mammalian FCRLs. Without this information, their possible orthologous relationships to the FCRLs cannot be established.

To increase our likelihood of discovering the ligands of LITRs, I propose the use of a combination of biased and unbiased approaches. One approach is to covalently fuse select ectodomains of LITRs (i.e., CaLITR3 or IpLITR1.1b) to the Fc region of human IgG2 molecules to generate LITR-Fc-fusion proteins. This approach offers several key advantages (Czajkowsky et al., 2012). Firstly, the resulting LITR-Fc-fusion proteins form homodimers, which provides a more natural platform for ligand binding compared to monomeric LITR proteins. Secondly, these LITR-Fc-fusion proteins can be used as Abs. For instance, they can be effectively purified by protein-G-based methods. Additionally, the LITR-Fc-fusion proteins can be immobilized on magnetic Dynabeads for immunoprecipitation experiments. Moreover, coating beads with these Fc fusion proteins would significantly increase their overall avidity for ligand binding. For this experiment, I propose using fluorescently labeled LITR-fusion proteins to explore their potential ligands on the surface of various goldfish leukocytes, such as goldfish PKNs, PKMs, and splenocytes. Additionally, flow cytometry should be used to facilitate rapid screening of all potential endogenous ligand-bearing cells. Notably, this approach enabled researchers to identify the ligand of FCRL6 (Schreeder et al., 2010). The next step is to use the LITR-fusion proteins to

pull down potential ligands from fluorescent cells. As with any Abs or Fc fusion proteins, it is crucial to include a negative control Fc fusion protein to assess background protein-protein interactions.

Since LITRs may interact with Abs due to their shared phylogenetic and syntenic relationships with FCRLs, I propose using teleost IgM molecules as bait proteins to "fish" for any potential LITR prey. Previous findings have shown that the putative activating IpLITR2.6b can form homo- or heterodimers with other IpLITR forms (Schreeder et al., 2010), suggesting that LITR-ligand interactions may require the formation of multi-LITR-protein complexes. In contrast, teleost IgM molecules are structurally intact, eliminating concerns about whether these proteins need to bind to other proteins for ligand interactions. For this experiment, teleost IgM can be isolated and purified from the goldfish serum using an IgM purification kit. These IgM molecules would then be immobilized onto protein-L-coated Dynabeads. Subsequently, the resulting immunoprecipitated products would then be analyzed with mass spectrometry.

The two unbiased methods described above would allow us to identify all potential LITR-ligand and IgM-binding-LITR candidates. In addition to co-immunoprecipitation, I recommend the use of several proximity ligation assays to verify these protein interactions. These assays operate on the principle of bringing two proteins or substrates into close proximity to generate a chemiluminescent/fluorescent product. For example, the Amplified Luminescent Proximity Homogenous Assay Screen (AlphaScreen) technology can be used to validate LITR-ligand-binding events (Yasgar et al., 2016). In this assay, LITR-ligand candidates would be coated onto "donor beads" containing the photosensitive chemical, phthalocyanine. This chemical can be excited by a 680 nm wavelength light, which subsequently initiates the conversion of ambient oxygen into oxygen singlets. Meanwhile, LITR-fusion proteins would be

attached to “acceptor beads” containing dyes, including thioxene, anthracene, and rubrene. If LITR-fusion proteins and their ligand candidates interact, the singlet oxygen molecules produced by the “donor” beads would activate the dyes on the “acceptor” beads, resulting in fluorescence emission. Additionally, other technologies similar to AlphaScreen, including split luciferase technology and the CoralHue™ Fluo-chase kit, can also be useful tools for validating LITR-ligand interactions.

8.3 Concluding remarks

In conclusion, my thesis work has contributed to a better understanding of the evolutionary relationship between teleost LITRs and the other vertebrate immunoregulatory receptor families. Additionally, this work has provided insights into the transcriptional regulation of several *calitr* genes. Most importantly, the development of CaLITR-specific pAbs will enable further investigation of the native immunoregulatory functions of CaLITRs in various goldfish immune cells. Overall, these findings establish the goldfish as a valuable model system for the study of LITRs.

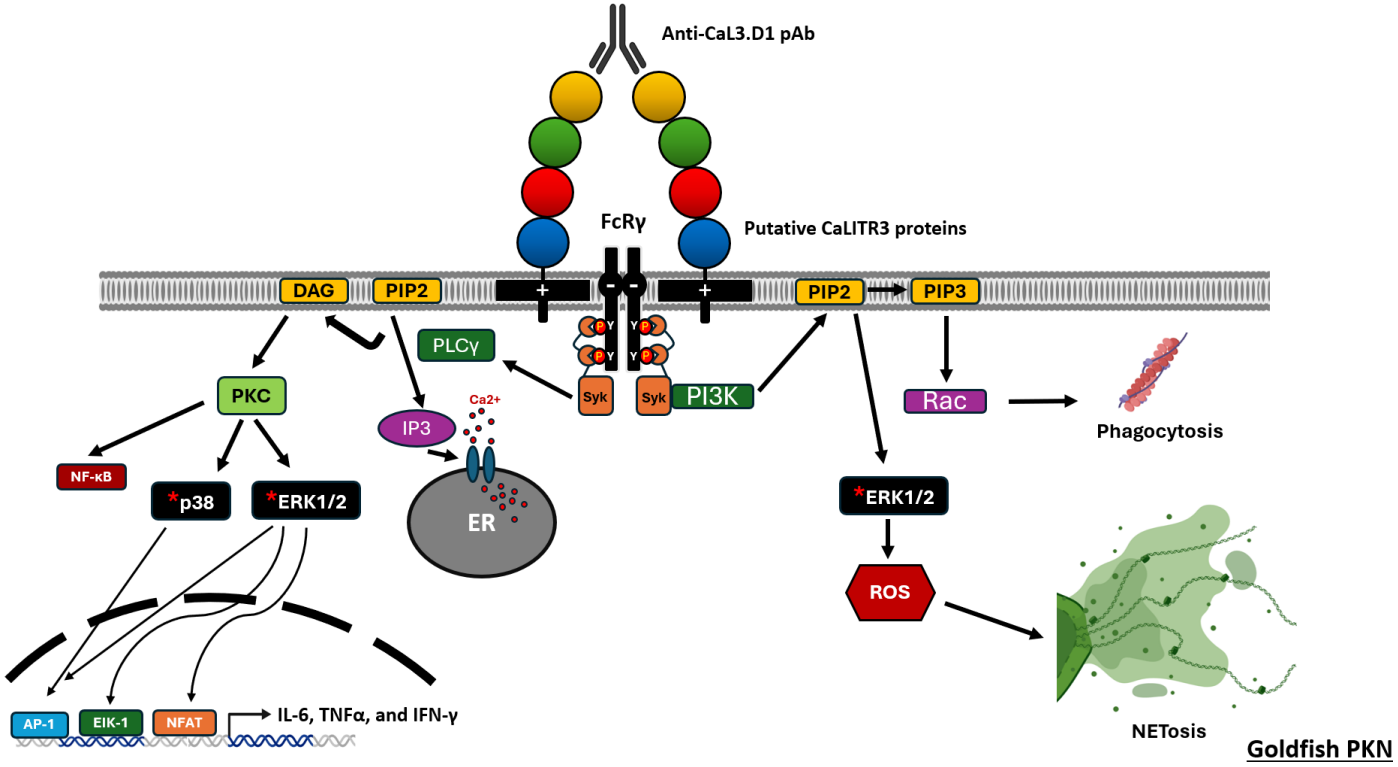

Figure 8.1. Confirmed and predicted signaling pathways activated by the anti-CaL3.D1-pAb-mediated crosslinking of PKN membrane proteins. This signaling model was constructed based on the signaling transduction events known to be induced by various activating FcRs, including FcγRIIa and FcγRIIIb, expressed in mammalian neutrophils (Rosales & Uribe-Querol, 2018). Upon crosslinking of putative CaLITR3 proteins expressed on the membrane of goldfish PKNs by the anti-CaL3.D1 pAb, the putative CaLITR3 proteins may form non-covalent associations with negatively charged goldfish adaptor molecules bearing ITAMs (i.e., FcRγ). Following this event, SFKs phosphorylate the ITAM motifs within the CYTs of FcRγ. This leads to the recruitment and activation of Syk. Subsequently, the activated Syk molecules stimulate PLCγ to convert PIP2 to DAG and IP3. From here, DAG activates the PKC pathway and its downstream targets, including ERK1/2, p38, and possibly NFκB. Phosphorylated ERK1/2 and p38 may induce the upregulation of several cytokine genes by

stimulating various inflammation-associated transcription factors, including NFAT, AP-1, and ElK-1. Meanwhile, IP3 binds to its cognate receptor expressed on the membrane of ER to trigger calcium release. Syk can also activate PI3K to mediate the conversion of PIP2 into PIP3, which leads to the activation of Rac, subsequently stimulating Arp2/3 to promote F-actin polymerization and phagocytosis. In addition to regulating the transcription of inflammatory cytokine genes, ERK1/2 controls ROS production and NETosis in mammalian neutrophils. The experimentally validated signaling mediators are marked with red asterisks. This diagram was created with the help of BioRender.

REFERENCES

Aderem, A., & Underhill, D. M. (1999). Mechanisms of phagocytosis in macrophages. *Annual review of immunology*, *17*(1), 593-623.

Agarwal, S., Kraus, Z., Dement-Brown, J., Alabi, O., Starost, K., & Tolnay, M. (2020). Human Fc Receptor-like 3 Inhibits Regulatory T Cell Function and Binds Secretory IgA. *Cell Rep*, *30*(5), 1292-1299 e1293. https://doi.org/10.1016/j.celrep.2019.12.099

Ahn, H., Kim, J., Jeung, E. B., & Lee, G. S. (2014). Dimethyl sulfoxide inhibits NLRP3 inflammasome activation. *Immunobiology*, *219*(4), 315-322. https://doi.org/10.1016/j.imbio.2013.11.003

Akkaya, M., & Barclay, A. N. (2013). How do pathogens drive the evolution of paired receptors? *Eur J Immunol*, *43*(2), 303-313. https://doi.org/10.1002/eji.201242896

Akula, S., Mohammadamin, S., & Hellman, L. (2014). Fc receptors for immunoglobulins and their appearance during vertebrate evolution. *PLoS One*, *9*(5), e96903. https://doi.org/10.1371/journal.pone.0096903

Al-Rikabi, H. I. (2024). Examining the Effects of Cytoplasmic Tail Splicing Event in Goldfish (Carassius auratus) Leukocyte Immune-type receptors.

Alabi, O., Dement-Brown, J., & Tolnay, M. (2017). Human Fc receptor-like 5 distinguishes IgG2 disulfide isoforms and deamidated charge variants. *Mol Immunol*, *92*, 161-168. https://doi.org/10.1016/j.molimm.2017.10.020

Alblas, J., Honing, H., de Lavalette, C. R., Brown, M. H., Dijkstra, C. D., & van den Berg, T. K. (2005). Signal regulatory protein alpha ligation induces macrophage nitric oxide production through JAK/STAT- and phosphatidylinositol 3-kinase/Rac1/NAPDH

oxidase/H2O2-dependent pathways. *Mol Cell Biol*, *25*(16), 7181-7192. https://doi.org/10.1128/MCB.25.16.7181-7192.2005

Aleman, O. R., Mora, N., Cortes-Vieyra, R., Uribe-Querol, E., & Rosales, C. (2016). Differential Use of Human Neutrophil Fcgamma Receptors for Inducing Neutrophil Extracellular Trap Formation. *J Immunol Res*, *2016*, 2908034. https://doi.org/10.1155/2016/2908034

Alley, T. L., Cooper, M. D., Chen, M., & Kubagawa, H. (1998). Genomic structure of PIR-B, the inhibitory member of the paired immunoglobulin-like receptor genes in mice. *Tissue Antigens*, *51*(3), 224-231. https://doi.org/10.1111/j.1399-0039.1998.tb03096.x

Alvarado-Kristensson, M., Melander, F., Leandersson, K., Rönnstrand, L., Wernstedt, C., & Andersson, T. (2004). p38-MAPK signals survival by phosphorylation of caspase-8 and caspase-3 in human neutrophils. *The Journal of experimental medicine*, *199*(4), 449-458.

Ángeles Esteban, M. (2012). An Overview of the Immunological Defenses in Fish Skin. *ISRN Immunology*, *2012*, 1-29. https://doi.org/10.5402/2012/853470

Atsaves, V., Leventaki, V., Rassidakis, G. Z., & Claret, F. X. (2019). AP-1 Transcription Factors as Regulators of Immune Responses in Cancer. *Cancers (Basel)*, *11*(7). https://doi.org/10.3390/cancers11071037

Arnold, V., Cummings, J.-S., Moreno-Nieves, U. Y., Didier, C., Gilbert, A., Barré-Sinoussi, F., & Scott-Algara, D. (2013). S100A9 protein is a novel ligand for the CD85j receptor and its interaction is implicated in the control of HIV-1 replication by NK cells. *Retrovirology*, *10*, 1-11.

Bakema, J. E., & van Egmond, M. (2011). The human immunoglobulin A Fc receptor FcalphaRI: a multifaceted regulator of mucosal immunity. *Mucosal Immunol*, *4*(6), 612-624. https://doi.org/10.1038/mi.2011.36

Barreda, D. R., Hanington, P. C., Stafford, J. L., & Belosevic, M. (2005). A novel soluble form of the CSF-1 receptor inhibits proliferation of self-renewing macrophages of goldfish (Carassius auratus L.). *Dev Comp Immunol*, *29*(10), 879-894. https://doi.org/10.1016/j.dci.2005.02.006

Barreda, D. R., Hanington, P. C., Walsh, C. K., Wong, P., & Belosevic, M. (2004). Differentially expressed genes that encode potential markers of goldfish macrophage development in vitro. *Dev Comp Immunol*, *28*(7-8), 727-746. https://doi.org/10.1016/j.dci.2003.11.005

Barreda, D. R., Neumann, N. F., & Belosevic, M. (2000). Flow cytometric analysis of PKH26-labeled goldfish kidney-derived macrophages. *Developmental & Comparative Immunology*, *24*(4), 395-406.

Barrow, A. D., Astoul, E., Floto, A., Brooke, G., Relou, I. A., Jennings, N. S., Smith, K. G., Ouwehand, W., Farndale, R. W., Alexander, D. R., & Trowsdale, J. (2004). Cutting edge: TREM-like transcript-1, a platelet immunoreceptor tyrosine-based inhibition motif encoding costimulatory immunoreceptor that enhances, rather than inhibits, calcium signaling via SHP-2. *J Immunol*, *172*(10), 5838-5842. https://doi.org/10.4049/jimmunol.172.10.5838

Barrow, A. D., Martin, C. J., & Colonna, M. (2019). The Natural Cytotoxicity Receptors in Health and Disease. *Front Immunol*, *10*, 909. https://doi.org/10.3389/fimmu.2019.00909

Barrow, A. D., & Trowsdale, J. (2006). You say ITAM and I say ITIM, let's call the whole thing off: the ambiguity of immunoreceptor signalling. *Eur J Immunol*, *36*(7), 1646-1653. https://doi.org/10.1002/eji.200636195

Barten, R., Torkar, M., Haude, A., Trowsdale, J., & Wilson, M. J. (2001). Divergent and convergent evolution of NK-cell receptors. *Trends in immunology*, *22*(1), 52-57.

Bayne, C. J., & Gerwick, L. (2001). The acute phase response and innate immunity of fish. *Developmental & Comparative Immunology*, *25*(8-9), 725-743.

Belosevic, M., Hanington, P. C., & Barreda, D. R. (2006). Development of goldfish macrophages in vitro. *Fish Shellfish Immunol*, *20*(2), 152-171. https://doi.org/10.1016/j.fsi.2004.10.010

Bemer, V., & Truffa-Bachi, P. (1996). T cell activation by concanavalin A in the presence of cyclosporin A: immunosuppressor withdrawal induces NFATp translocation and interleukin-2 gene transcription. *Eur J Immunol*, *26*(7), 1481-1488. https://doi.org/10.1002/eji.1830260712

Ben Mkaddem, S., Benhamou, M., & Monteiro, R. C. (2019). Understanding Fc Receptor Involvement in Inflammatory Diseases: From Mechanisms to New Therapeutic Tools. *Front Immunol*, *10*, 811. https://doi.org/10.3389/fimmu.2019.00811

Bielek, E., Bigaj, J., Chadzinska, M., & Plytycz, B. (1999). Depletion of head kidney neutrophils and cells with basophilic granules during peritoneal inflammation in the goldfish, Carassius auratus. *FOLIA BIOLOGICA-KRAKOW-*, *47*, 33-42.

Billadeau, D. D., & Leibson, P. J. (2002). ITAMs versus ITIMs: striking a balance during cell regulation. *Journal of Clinical Investigation*, *109*(2), 161-168. https://doi.org/10.1172/jci0214843

Blackmon, L. E., Quiniou, S. M. A., Wilson, M., & Bengten, E. (2020). Catfish lymphocytes expressing CC41-reactive leukocyte immune-type receptors (LITRs) proliferate in response to Edwardsiella ictaluri infection in vitro. *Dev Comp Immunol*, *106*, 103610. https://doi.org/10.1016/j.dci.2020.103610

Blanco, A. M., Sundarrajan, L., Bertucci, J. I., & Unniappan, S. (2018). Why goldfish? Merits and challenges in employing goldfish as a model organism in comparative endocrinology research. *Gen Comp Endocrinol*, *257*, 13-28. https://doi.org/10.1016/j.ygcen.2017.02.001

Blank, U., Launay, P., Benhamou, M., & Monteiro, R. C. (2009). Inhibitory ITAMs as novel regulators of immunity. *Immunol Rev*, *232*(1), 59-71. https://doi.org/10.1111/j.1600-065X.2009.00832.x

Blasutig, I. M., New, L. A., Thanabalasuriar, A., Dayarathna, T. K., Goudreault, M., Quaggin, S. E., Li, S. S., Gruenheid, S., Jones, N., & Pawson, T. (2008). Phosphorylated YDXV motifs and Nck SH2/SH3 adaptors act cooperatively to induce actin reorganization. *Mol Cell Biol*, *28*(6), 2035-2046. https://doi.org/10.1128/MCB.01770-07

Bohdanowicz, M., Cosio, G., Backer, J. M., & Grinstein, S. (2010). Class I and class III phosphoinositide 3-kinases are required for actin polymerization that propels phagosomes. *J Cell Biol*, *191*(5), 999-1012. https://doi.org/10.1083/jcb.201004005

Borregaard, N., Kjeldsen, L., Rygaard, K., Bastholm, L., Nielsen, M., Sengeløv, H., Bjerrum, O., & Johnsen, A. (1992). Stimulus-dependent secretion of plasma proteins from human neutrophils. *The Journal of clinical investigation*, *90*(1), 86-96.

Borregaard, N., Lollike, K., Kjeldsen, L., Sengelov, H., Bastholm, L., Nielsen, M. H., & Bainton, D. F. (1993). Human neutrophil granules and secretory vesicles. *Eur J Haematol*, *51*(4), 187-198. https://doi.org/10.1111/j.1600-0609.1993.tb00629.x

Breedveld, A., & van Egmond, M. (2019). IgA and FcalphaRI: Pathological Roles and Therapeutic Opportunities. *Front Immunol*, *10*, 553. https://doi.org/10.3389/fimmu.2019.00553

Brignall, R., Cauchy, P., Bevington, S. L., Gorman, B., Pisco, A. O., Bagnall, J., Boddington, C., Rowe, W., England, H., Rich, K., Schmidt, L., Dyer, N. P., Travis, M. A., Ott, S., Jackson, D. A., Cockerill, P. N., & Paszek, P. (2017). Integration of Kinase and Calcium Signaling at the Level of Chromatin Underlies Inducible Gene Activation in T Cells. *J Immunol*, *199*(8), 2652-2667. https://doi.org/10.4049/jimmunol.1602033

Bruhns, P., & Jönsson, F. (2015). Mouse and human FcR effector functions. *Immunological reviews*, *268*(1), 25-51.

Bruijnesteijn, J., van der Wiel, M. K. H., de Groot, N., Otting, N., de Vos-Rouweler, A. J. M., Lardy, N. M., de Groot, N. G., & Bontrop, R. E. (2018). Extensive Alternative Splicing of KIR Transcripts. *Front Immunol*, *9*, 2846. https://doi.org/10.3389/fimmu.2018.02846

Buday, L., & Tompa, P. (2010). Functional classification of scaffold proteins and related molecules. *FEBS J*, *277*(21), 4348-4355. https://doi.org/10.1111/j.1742-4658.2010.07864.x

Burn, G. L., Foti, A., Marsman, G., Patel, D. F., & Zychlinsky, A. (2021). The Neutrophil. *Immunity*, *54*(7), 1377-1391. https://doi.org/10.1016/j.immuni.2021.06.006

Burshtyn, D. N., Lam, A. S., Weston, M., Gupta, N., Warmerdam, P. A., & Long, E. O. (1999). Conserved residues amino-terminal of cytoplasmic tyrosines contribute to the SHP-1-mediated inhibitory function of killer cell Ig-like receptors. *The Journal of Immunology*, *162*(2), 897-902.

Burshtyn, D. N., Scharenberg, A. M., Wagtmann, N., Rajagopalan, S., Berrada, K., Yi, T., Kinet, J.-P., & Long, E. O. (1996). Recruitment of tyrosine phosphatase HCP by the killer cell inhibitory receptor. *Immunity*, *4*(1), 77-85.

Bell, E. A., Cable, J., Oliveira, C., Richardson, D. S., Yant, L., & Taylor, M. I. (2020). Help or hindrance? The evolutionary impact of whole-genome duplication on immunogenetic diversity and parasite load. *Ecol Evol*, *10*(24), 13949-13956. https://doi.org/10.1002/ece3.6987

Bonapace, L., Coissieux, M. M., Wyckoff, J., Mertz, K. D., Varga, Z., Junt, T., & Bentires-Alj, M. (2014). Cessation of CCL2 inhibition accelerates breast cancer metastasis by promoting angiogenesis. *Nature*, *515*(7525), 130-133. https://doi.org/10.1038/nature13862

Boyington, J. C., & Sun, P. D. (2002). A structural perspective on MHC class I recognition by killer cell immunoglobulin-like receptors. *Mol Immunol*, *38*(14), 1007-1021. https://doi.org/10.1016/s0161-5890(02)00030-5

Burshtyn, D. N., & Morcos, C. (2016). The Expanding Spectrum of Ligands for Leukocyte Ig-like Receptors. *J Immunol*, *196*(3), 947-955. https://doi.org/10.4049/jimmunol.1501937

Caligiuri, M. A. (2008). Human natural killer cells. *Blood*, *112*(3), 461-469. https://doi.org/10.1182/blood-2007-09-077438

Call, M. E., & Wucherpfennig, K. W. (2007). Common themes in the assembly and architecture of activating immune receptors. *Nat Rev Immunol*, *7*(11), 841-850. https://doi.org/10.1038/nri2186

Camacho, C., Coulouris, G., Avagyan, V., Ma, N., Papadopoulos, J., Bealer, K., & Madden, T. L. (2009). BLAST+: architecture and applications. *BMC Bioinformatics*, *10*, 421. https://doi.org/10.1186/1471-2105-10-421

Campbell, J. A., Davis, R. S., Lilly, L. M., Fremont, D. H., French, A. R., & Carayannopoulos, L. N. (2010). Cutting edge: FcR-like 5 on innate B cells is targeted by a poxvirus MHC class I-like immunoevasin. *J Immunol*, *185*(1), 28-32. https://doi.org/10.4049/jimmunol.1000240

Canellada, A., Ramirez, B. G., Minami, T., Redondo, J. M., & Cano, E. (2008). Calcium/calcineurin signaling in primary cortical astrocyte cultures: Rcan1-4 and cyclooxygenase-2 as NFAT target genes. *Glia*, *56*(7), 709-722. https://doi.org/10.1002/glia.20647

Cannon, J. P., Haire, R. N., Magis, A. T., Eason, D. D., Winfrey, K. N., Hernandez Prada, J. A., Bailey, K. M., Jakoncic, J., Litman, G. W., & Ostrov, D. A. (2008). A bony fish immunological receptor of the NITR multigene family mediates allogeneic recognition. *Immunity*, *29*(2), 228-237. https://doi.org/10.1016/j.immuni.2008.05.018

Cannon, J. P., Haire, R. N., Mueller, M. G., Litman, R. T., Eason, D. D., Tinnemore, D., Amemiya, C. T., Ota, T., & Litman, G. W. (2006). Ancient divergence of a complex family of immune-type receptor genes. *Immunogenetics*, *58*(5-6), 362-373. https://doi.org/10.1007/s00251-006-0112-7

Cantor, H., & Boyse, E. A. (1975). Functional subclasses of T lymphocytes bearing different Ly antigens. II. Cooperation between subclasses of Ly+ cells in the generation of killer activity. *The Journal of experimental medicine*, *141*(6), 1390-1399.

Carreno, B. M., & Collins, M. (2002). The B7 family of ligands and its receptors: new pathways for costimulation and inhibition of immune responses. *Annu Rev Immunol*, *20*, 29-53. https://doi.org/10.1146/annurev.immunol.20.091101.091806

Carter, A. B., Monick, M. M., & Hunninghake, G. W. (1999). Both Erk and p38 kinases are necessary for cytokine gene transcription. *American journal of respiratory cell and molecular biology*, *20*(4), 751-758.

Caspi, R. R., & Avtalion, R. R. (1984). The mixed leukocyte reaction (MLR) in carp: bidirectional and unidirectional MLR responses. *Developmental & Comparative Immunology*, *8*(3), 631-637.

Chakraborty, A., Dyer, K. F., Cascio, M., Mietzner, T. A., & Tweardy, D. J. (1999). Identification of a novel Stat3 recruitment and activation motif within the granulocyte colony-stimulating factor receptor. *Blood, The Journal of the American Society of Hematology*, *93*(1), 15-24.

Chassin, C., Goujon, J. M., Darche, S., du Merle, L., Bens, M., Cluzeaud, F., Werts, C., Ogier-Denis, E., Le Bouguenec, C., Buzoni-Gatel, D., & Vandewalle, A. (2006). Renal collecting duct epithelial cells react to pyelonephritis-associated Escherichia coli by activating distinct TLR4-dependent and -independent inflammatory pathways. *J Immunol*, *177*(7), 4773-4784. https://doi.org/10.4049/jimmunol.177.7.4773

Chen, C.-C., Hurez, V., Brockenbrough, J. S., Kubagawa, H., & Cooper, M. D. (1999). Paternal monoallelic expression of the paired immunoglobulin-like receptors PIR-A and PIR-B. *Proceedings of the National Academy of Sciences*, *96*(12), 6868-6872.

Chen, S. N., Zou, P. F., & Nie, P. (2017). Retinoic acid-inducible gene I (RIG-I)-like receptors (RLRs) in fish: current knowledge and future perspectives. *Immunology*, *151*(1), 16-25. https://doi.org/10.1111/imm.12714

Chen, T., Li, Y., Sun, R., Hu, H., Liu, Y., Herrmann, M., Zhao, Y., & Munoz, L. E. (2021). Receptor-Mediated NETosis on Neutrophils. *Front Immunol*, *12*, 775267. https://doi.org/10.3389/fimmu.2021.775267

Chen, Z., Omori, Y., Koren, S., Shirokiya, T., Kuroda, T., Miyamoto, A., Wada, H., Fujiyama, A., Toyoda, A., & Zhang, S. (2019). De novo assembly of the goldfish (Carassius auratus) genome and the evolution of genes after whole-genome duplication. *Science Advances*, *5*(6), eaav0547.

Choe, Y., Yu, J. E., Park, J., Park, D., Oh, J. I., Kim, S., Moon, K. H., & Kang, H. Y. (2017). Goldfish, Carassius auratus, as an infection model for studying the pathogenesis of Edwardsiella piscicida. *Vet Res Commun*, *41*(4), 289-297. https://doi.org/10.1007/s11259-017-9700-2

Choresca, C. H., Jr., Koo, O. J., Oh, H. J., Hong, S. G., Gomez, D. K., Kim, J. H., Lee, B. C., & Park, S. C. (2009). Different culture conditions used for arresting the G0/G1 phase of the cell cycle in goldfish (Carassius auratus) caudal fin-derived fibroblasts. *Cell Biol Int*, *33*(1), 65-70. https://doi.org/10.1016/j.cellbi.2008.09.015

Chowdhury, P., Sacks, S. H., & Sheerin, N. S. (2006). Toll-like receptors TLR2 and TLR4 initiate the innate immune response of the renal tubular epithelium to bacterial products. *Clin Exp Immunol*, *145*(2), 346-356. https://doi.org/10.1111/j.1365-2249.2006.03116.x

Cichocki, F., Hanson, R. J., Lenvik, T., Pitt, M., McCullar, V., Li, H., Anderson, S. K., & Miller, J. S. (2009). The transcription factor c-Myc enhances KIR gene transcription through

direct binding to an upstream distal promoter element. *Blood*, *113*(14), 3245-3253. https://doi.org/10.1182/blood-2008-07-166389

Cloutier, A., Ear, T., Blais-Charron, E., Dubois, C. M., & McDonald, P. P. (2007). Differential involvement of NF-kappaB and MAP kinase pathways in the generation of inflammatory cytokines by human neutrophils. *J Leukoc Biol*, *81*(2), 567-577. https://doi.org/10.1189/jlb.0806536

Colombo, D., & Ammirati, E. (2011). Cyclosporine in transplantation-a history of converging timelines. *Journal of biological regulators and homeostatic agents*, *25*(4), 493-504.

Cortes, H. D., Lillico, D. M., Zwozdesky, M. A., Pemberton, J. G., O'Brien, A., Montgomery, B. C., Wiersma, L., Chang, J. P., & Stafford, J. L. (2014). Induction of phagocytosis and intracellular signaling by an inhibitory channel catfish leukocyte immune-type receptor: evidence for immunoregulatory receptor functional plasticity in teleosts. *J Innate Immun*, *6*(4), 435-455. https://doi.org/10.1159/000356963

Cortes, H. D., Montgomery, B. C., Verheijen, K., Garcia-Garcia, E., & Stafford, J. L. (2012). Examination of the stimulatory signaling potential of a channel catfish leukocyte immune-type receptor and associated adaptor. *Dev Comp Immunol*, *36*(1), 62-73. https://doi.org/10.1016/j.dci.2011.06.004

Coxon, C. H., Geer, M. J., & Senis, Y. A. (2017). ITIM receptors: more than just inhibitors of platelet activation. *Blood*, *129*(26), 3407-3418. https://doi.org/10.1182/blood-2016-12-720185

Crider, J., Wilson, M., Felch, K. L., Dupre, R. A., Quiniou, S. M. A., & Bengten, E. (2023). A subset of leukocyte immune-type receptors (LITRs) regulates phagocytosis in channel

catfish (Ictalurus punctatus) leukocytes. *Mol Immunol*, *154*, 33-44. https://doi.org/10.1016/j.molimm.2022.12.009

Czajkowsky, D. M., Hu, J., Shao, Z., & Pleass, R. J. (2012). Fc-fusion proteins: new developments and future perspectives. *EMBO Mol Med*, *4*(10), 1015-1028. https://doi.org/10.1002/emmm.201201379

Cain, K., & Swan, C. (2010). Barrier function and immunology. In *The multifunctional gut of fish* (pp. 111-134). https://doi.org/10.1016/s1546-5098(10)03003-7

Chen, C., Hu, Y. H., Xiao, Z. Z., & Sun, L. (2013). SmCCL19, a CC chemokine of turbot Scophthalmus maximus, induces leukocyte trafficking and promotes anti-viral and anti-bacterial defense. *Fish Shellfish Immunol*, *35*(5), 1677-1682. https://doi.org/10.1016/j.fsi.2013.08.020

Chong, Y. P., Mulhern, T. D., & Cheng, H. C. (2005). C-terminal Src kinase (CSK) and CSK-homologous kinase (CHK)--endogenous negative regulators of Src-family protein kinases. *Growth Factors*, *23*(3), 233-244. https://doi.org/10.1080/08977190500178877

Daëron, M. (1997). Fc receptor biology. *Annual review of immunology*, *15*(1), 203-234.

Daëron, M., Latour, S., Malbec, O., Espinosa, E., Pina, P., Pasmans, S., & Fridman, W. H. (1995). The same tyrosine-based inhibition motif, in the intra-cytoplasmic domain of FcγRIIB, regulates negatively BCR-, TCR-, and FcR-dependent cell activation. *Immunity*, *3*(5), 635-646.

David, L., Blum, S., Feldman, M. W., Lavi, U., & Hillel, J. (2003). Recent duplication of the common carp (Cyprinus carpio L.) genome as revealed by analyses of microsatellite loci. *Mol Biol Evol*, *20*(9), 1425-1434. https://doi.org/10.1093/molbev/msg173

Davis, R. S. (2007). Fc receptor-like molecules. *Annu Rev Immunol*, *25*, 525-560. https://doi.org/10.1146/annurev.immunol.25.022106.141541

Davis, R. S., Dennis, G., Jr., Odom, M. R., Gibson, A. W., Kimberly, R. P., Burrows, P. D., & Cooper, M. D. (2002). Fc receptor homologs: newest members of a remarkably diverse Fc receptor gene family. *Immunol Rev*, *190*, 123-136. https://doi.org/10.1034/j.1600-065x.2002.19009.x

Davis, R. S., Wang, Y.-H., Kubagawa, H., & Cooper, M. D. (2001). Identification of a family of Fc receptor homologs with preferential B cell expression. *Proceedings of the National Academy of Sciences*, *98*(17), 9772-9777.

de Abreu Costa, L., Henrique Fernandes Ottoni, M., Dos Santos, M. G., Meireles, A. B., Gomes de Almeida, V., de Fatima Pereira, W., Alves de Avelar-Freitas, B., & Eustaquio Alvim Brito-Melo, G. (2017). Dimethyl Sulfoxide (DMSO) Decreases Cell Proliferation and TNF-alpha, IFN-gamma, and IL-2 Cytokines Production in Cultures of Peripheral Blood Lymphocytes. *Molecules*, *22*(11). https://doi.org/10.3390/molecules22111789

de Buhr, N., & von Kockritz-Blickwede, M. (2016). How Neutrophil Extracellular Traps Become Visible. *J Immunol Res*, *2016*, 4604713. https://doi.org/10.1155/2016/4604713

de Castro, E., Sigrist, C. J., Gattiker, A., Bulliard, V., Langendijk-Genevaux, P. S., Gasteiger, E., Bairoch, A., & Hulo, N. (2006). ScanProsite: detection of PROSITE signature matches and ProRule-associated functional and structural residues in proteins. *Nucleic Acids Res*, *34*(Web Server issue), W362-365. https://doi.org/10.1093/nar/gkl124

de la Fuente, H., Cibrian, D., & Sanchez-Madrid, F. (2012). Immunoregulatory molecules are master regulators of inflammation during the immune response. *FEBS Lett*, *586*(18), 2897-2905. https://doi.org/10.1016/j.febslet.2012.07.032

de Wit, T. P., Morton, H. C., Capel, P. J., & van de Winkel, J. G. (1995). Structure of the gene for the human myeloid IgA Fc receptor (CD89). *The Journal of Immunology*, *155*(3), 1203-1209. https://doi.org/10.4049/jimmunol.155.3.1203

Debska-Zielkowska, J., Moszkowska, G., Zielinski, M., Zielinska, H., Dukat-Mazurek, A., Trzonkowski, P., & Stefanska, K. (2021). KIR Receptors as Key Regulators of NK Cells Activity in Health and Disease. *Cells*, *10*(7). https://doi.org/10.3390/cells10071777

Dennis Jr, G., Kubagawa, H., & Cooper, M. D. (2000). Paired Ig-like receptor homologs in birds and mammals share a common ancestor with mammalian Fc receptors. *Proceedings of the National Academy of Sciences*, *97*(24), 13245-13250.

Detmers, P. A., Zhou, D., Powell, D., Lichenstein, H., Kelley, M., & Pironkova, R. (1995). Endotoxin receptors (CD14) are found with CD16 (Fc gamma RIII) in an intracellular compartment of neutrophils that contains alkaline phosphatase. *The Journal of Immunology*, *155*(4), 2085-2095. https://doi.org/10.4049/jimmunol.155.4.2085

Dickson, C., Fletcher, A. J., Vaysburd, M., Yang, J. C., Mallery, D. L., Zeng, J., Johnson, C. M., McLaughlin, S. H., Skehel, M., Maslen, S., Cruickshank, J., Huguenin-Dezot, N., Chin, J. W., Neuhaus, D., & James, L. C. (2018). Intracellular antibody signalling is regulated by phosphorylation of the Fc receptor TRIM21. *Elife*, *7*. https://doi.org/10.7554/eLife.32660

Diefenbach, A., & Raulet, D. H. (1999). Natural killer cells: stress out, turn on, tune in. *Current biology*, *9*(22), R851-R853.

Dong, Y., Taylor, H. E., & Dimopoulos, G. (2006). AgDscam, a hypervariable immunoglobulin domain-containing receptor of the Anopheles gambiae innate immune system. *PLoS Biol*, *4*(7), e229. https://doi.org/10.1371/journal.pbio.0040229

Duan, T., Du, Y., Xing, C., Wang, H. Y., & Wang, R. F. (2022). Toll-Like Receptor Signaling and Its Role in Cell-Mediated Immunity. *Front Immunol*, *13*, 812774. https://doi.org/10.3389/fimmu.2022.812774

Duprey, S. P., & Boettiger, D. (1985). Developmental regulation of c-myb in normal myeloid progenitor cells. *Proceedings of the National Academy of Sciences*, *82*(20), 6937-6941.

Dwyer, J., & Johnson, C. (1981). The use of concanavalin A to study the immunoregulation of human T cells. *Clinical and experimental immunology*, *46*(2), 237.

Dong, Z., & Veillette, A. (2010). How do SAP family deficiencies compromise immunity? *Trends Immunol*, *31*(8), 295-302. https://doi.org/10.1016/j.it.2010.05.008

Eckstein, L. A., Van Quill, K. R., Bui, S. K., Uusitalo, M. S., & O'Brien, J. M. (2005). Cyclosporin a inhibits calcineurin/nuclear factor of activated T-cells signaling and induces apoptosis in retinoblastoma cells. *Invest Ophthalmol Vis Sci*, *46*(3), 782-790. https://doi.org/10.1167/iovs.04-1022

Edberg, J. C., & Kimberly, R. P. (1994). Modulation of Fc gamma and complement receptor function by the glycosyl-phosphatidylinositol-anchored form of Fc gamma RIII. *The Journal of Immunology*, *152*(12), 5826-5835. https://doi.org/10.4049/jimmunol.152.12.5826

Ehrhardt, G. R., Davis, R. S., Hsu, J. T., Leu, C.-M., Ehrhardt, A., & Cooper, M. D. (2003). The inhibitory potential of Fc receptor homolog 4 on memory B cells. *Proceedings of the National Academy of Sciences*, *100*(23), 13489-13494.

Ehrhardt, G. R., Hsu, J. T., Gartland, L., Leu, C. M., Zhang, S., Davis, R. S., & Cooper, M. D. (2005). Expression of the immunoregulatory molecule FcRH4 defines a distinctive

tissue-based population of memory B cells. *J Exp Med*, *202*(6), 783-791. https://doi.org/10.1084/jem.20050879

El Benna, J., Han, J., Park, J.-W., Schmid, E., Ulevitch, R. J., & Babior, B. M. (1996). Activation of p38 in stimulated human neutrophils: phosphorylation of the oxidase component p47phoxby p38 and ERK but not by JNK. *Archives of biochemistry and biophysics*, *334*(2), 395-400.

Elisia, I., Nakamura, H., Lam, V., Hofs, E., Cederberg, R., Cait, J., Hughes, M. R., Lee, L., Jia, W., Adomat, H. H., Guns, E. S., McNagny, K. M., Samudio, I., & Krystal, G. (2016). DMSO Represses Inflammatory Cytokine Production from Human Blood Cells and Reduces Autoimmune Arthritis. *PLoS One*, *11*(3), e0152538. https://doi.org/10.1371/journal.pone.0152538

Emmel, E. A., Verweij, C. L., Durand, D. B., Higgins, K. M., Lacy, E., & Crabtree, G. R. (1989). Cyclosporin A specifically inhibits function of nuclear proteins involved in T cell activation. *Science*, *246*(4937), 1617-1620.

Evans, D., LEARY III, J., Weisman, Z., Warren, J., & JASO‐FRIEDMANN, L. (1996). Mapping of the Epitope Recognized by Non‐Specific Cytotoxic Cells: Determination of the Fine Specificity Using Synthetic Peptides. *Scandinavian journal of immunology*, *43*(5), 556-565.

Evans, D. L., & Jaso-Friedmann, L. (1992). Nonspecific cytotoxic cells as effectors of immunity in fish. *Annual Review of Fish Diseases*, *2*, 109-121.

Evans, D. L., Jaso-Friedmann, L., Smith, E. E., St John, A., Koren, H. S., & Harris, D. T. (1988). Identification of a putative antigen receptor on fish nonspecific cytotoxic cells with

monoclonal antibodies. *The Journal of Immunology*, *141*(1), 324-332. https://doi.org/10.4049/jimmunol.141.1.324

Eissmann, P., Beauchamp, L., Wooters, J., Tilton, J. C., Long, E. O., & Watzl, C. (2005). Molecular basis for positive and negative signaling by the natural killer cell receptor 2B4 (CD244). *Blood*, *105*(12), 4722-4729. https://doi.org/10.1182/blood-2004-09-3796

Farre, D., Roset, R., Huerta, M., Adsuara, J. E., Rosello, L., Alba, M. M., & Messeguer, X. (2003). Identification of patterns in biological sequences at the ALGGEN server: PROMO and MALGEN. *Nucleic Acids Res*, *31*(13), 3651-3653. https://doi.org/10.1093/nar/gkg605

Faurschou, M., & Borregaard, N. (2003). Neutrophil granules and secretory vesicles in inflammation. *Microbes Infect*, *5*(14), 1317-1327. https://doi.org/10.1016/j.micinf.2003.09.008

Fayngerts, S. A., Najakshin, A. M., & Taranin, A. V. (2007). Species-specific evolution of the FcR family in endothermic vertebrates. *Immunogenetics*, *59*(6), 493-506. https://doi.org/10.1007/s00251-007-0208-8

Fei, C., Pemberton, J. G., Lillico, D. M., Zwozdesky, M. A., & Stafford, J. L. (2016). Biochemical and Functional Insights into the Integrated Regulation of Innate Immune Cell Responses by Teleost Leukocyte Immune-Type Receptors. *Biology (Basel)*, *5*(1). https://doi.org/10.3390/biology5010013

Fei, C., Zwozdesky, M. A., & Stafford, J. L. (2020). A Fish Leukocyte Immune-Type Receptor Uses a Novel Intracytoplasmic Tail Networking Mechanism to Cross-Inhibit the Phagocytic Response. *Int J Mol Sci*, *21*(14). https://doi.org/10.3390/ijms21145146

Feng, J., Call, M. E., & Wucherpfennig, K. W. (2006). The assembly of diverse immune receptors is focused on a polar membrane-embedded interaction site. *PLoS Biol*, *4*(5), e142. https://doi.org/10.1371/journal.pbio.0040142

Feng, J., Garrity, D., Call, M. E., Moffett, H., & Wucherpfennig, K. W. (2005). Convergence on a distinctive assembly mechanism by unrelated families of activating immune receptors. *Immunity*, *22*(4), 427-438. https://doi.org/10.1016/j.immuni.2005.02.005

Filice, M., Cerra, M. C., & Imbrogno, S. (2022). The goldfish Carassius auratus: an emerging animal model for comparative cardiac research. *J Comp Physiol B*, *192*(1), 27-48. https://doi.org/10.1007/s00360-021-01402-9

Fitzgerald, K. A., & Kagan, J. C. (2020). Toll-like Receptors and the Control of Immunity. *Cell*, *180*(6), 1044-1066. https://doi.org/10.1016/j.cell.2020.02.041

Frampton, J. (2004). *MYB transcription factors: their role in growth, differentiation and disease*. Springer.

Franco, A., Damdinsuren, B., Ise, T., Dement-Brown, J., Li, H., Nagata, S., & Tolnay, M. (2013). Human Fc receptor-like 5 binds intact IgG via mechanisms distinct from those of Fc receptors. *J Immunol*, *190*(11), 5739-5746. https://doi.org/10.4049/jimmunol.1202860

Frenette, A. P., Rodriguez-Ramos, T., Zanuzzo, F., Ramsay, D., Semple, S. L., Soulliere, C., Rodriguez-Cornejo, T., Heath, G., McKenzie, E., Iwanczyk, J., Bruder, M., Aucoin, M. G., Gamperl, A. K., & Dixon, B. (2023). Expression of Interleukin-1beta protein in vitro,exvivo and in vivo salmonid models. *Dev Comp Immunol*, *147*, 104767. https://doi.org/10.1016/j.dci.2023.104767

Fu, Y. L., & Harrison, R. E. (2021). Microbial Phagocytic Receptors and Their Potential Involvement in Cytokine Induction in Macrophages. *Front Immunol*, *12*, 662063. https://doi.org/10.3389/fimmu.2021.662063

Fan, Q. R., Long, E. O., & Wiley, D. C. (2001). Crystal structure of the human natural killer cell inhibitory receptor KIR2DL1–HLA-Cw4 complex. *Nature immunology*, *2*(5), 452-460.

Faure, M., & Long, E. O. (2002). KIR2DL4 (CD158d), an NK cell-activating receptor with inhibitory potential. *J Immunol*, *168*(12), 6208-6214. https://doi.org/10.4049/jimmunol.168.12.6208

Favor, O. K., Pestka, J. J., Bates, M. A., & Lee, K. S. S. (2021). Centrality of Myeloid-Lineage Phagocytes in Particle-Triggered Inflammation and Autoimmunity. *Front Toxicol*, *3*, 777768. https://doi.org/10.3389/ftox.2021.777768

Franco, A., Kraus, Z., Li, H., Seibert, N., Dement-Brown, J., & Tolnay, M. (2018). CD21 and FCRL5 form a receptor complex with robust B-cell activating capacity. *Int Immunol*, *30*(12), 569-578. https://doi.org/10.1093/intimm/dxy052

Gabay, C., & Kushner, I. (1999). Acute-phase proteins and other systemic responses to inflammation. *New England journal of medicine*, *340*(6), 448-454.

Gaur, S., Shively, J. E., Yen, Y., & Gaur, R. K. (2008). Altered splicing of CEACAM1 in breast cancer: identification of regulatory sequences that control splicing of CEACAM1 into long or short cytoplasmic domain isoforms. *Mol Cancer*, *7*, 46. https://doi.org/10.1186/1476-4598-7-46

Ghanbarian, A. T., & Hurst, L. D. (2015). Neighboring Genes Show Correlated Evolution in Gene Expression. *Mol Biol Evol*, *32*(7), 1748-1766. https://doi.org/10.1093/molbev/msv053

Gierman, H. J., Indemans, M. H., Koster, J., Goetze, S., Seppen, J., Geerts, D., van Driel, R., & Versteeg, R. (2007). Domain-wide regulation of gene expression in the human genome. *Genome Res*, *17*(9), 1286-1295. https://doi.org/10.1101/gr.6276007

Gillis, C., Gouel-Cheron, A., Jonsson, F., & Bruhns, P. (2014). Contribution of Human FcgammaRs to Disease with Evidence from Human Polymorphisms and Transgenic Animal Studies. *Front Immunol*, *5*, 254. https://doi.org/10.3389/fimmu.2014.00254

Glasauer, S. M., & Neuhauss, S. C. (2014). Whole-genome duplication in teleost fishes and its evolutionary consequences. *Mol Genet Genomics*, *289*(6), 1045-1060. https://doi.org/10.1007/s00438-014-0889-2

Goettsch, C., Rauner, M., Sinningen, K., Helas, S., Al-Fakhri, N., Nemeth, K., Hamann, C., Kopprasch, S., Aikawa, E., Bornstein, S. R., Schoppet, M., & Hofbauer, L. C. (2011). The osteoclast-associated receptor (OSCAR) is a novel receptor regulated by oxidized low-density lipoprotein in human endothelial cells. *Endocrinology*, *152*(12), 4915-4926. https://doi.org/10.1210/en.2011-1282

Gonda, T. J., & Metcalf, D. (1984). Expression of myb, myc and fos proto-oncogenes during the differentiation of a murine myeloid leukaemia. *Nature*, *310*(5974), 249-251.

Gong, T., Liu, L., Jiang, W., & Zhou, R. (2020). DAMP-sensing receptors in sterile inflammation and inflammatory diseases. *Nat Rev Immunol*, *20*(2), 95-112. https://doi.org/10.1038/s41577-019-0215-7

Gotoh, N. (2008). Regulation of growth factor signaling by FRS2 family docking/scaffold adaptor proteins. *Cancer Sci*, *99*(7), 1319-1325. https://doi.org/10.1111/j.1349-7006.2008.00840.x

Graves, S. S., Evans, D. L., Cobb, D., & Dawe, D. L. (1984). Nonspecific cytotoxic cells in fish (Ictaluruspunctatus) I. Optimum requirements for target cell lysis. *Developmental & Comparative Immunology*, *8*(2), 293-302.

Grayfer, L., & Belosevic, M. (2009). Molecular characterization of novel interferon gamma receptor 1 isoforms in zebrafish (Danio rerio) and goldfish (Carassius auratus L.). *Mol Immunol*, *46*(15), 3050-3059. https://doi.org/10.1016/j.molimm.2009.06.004

Grayfer, L., & Belosevic, M. (2012). Cytokine regulation of teleost inflammatory responses. *New Advances and Contributions to Fish Biology*, 11281-11286.

Grayfer, L., Hodgkinson, J. W., & Belosevic, M. (2011). Analysis of the antimicrobial responses of primary phagocytes of the goldfish (Carassius auratus L.) against Mycobacterium marinum. *Dev Comp Immunol*, *35*(11), 1146-1158. https://doi.org/10.1016/j.dci.2011.04.007

Grayfer, L., Kerimoglu, B., Yaparla, A., Hodgkinson, J. W., Xie, J., & Belosevic, M. (2018). Mechanisms of Fish Macrophage Antimicrobial Immunity. *Front Immunol*, *9*, 1105. https://doi.org/10.3389/fimmu.2018.01105

Gu, H., Saito, K., Klaman, L. D., Shen, J., Fleming, T., Wang, Y., Pratt, J. C., Lin, G., Lim, B., & Kinet, J.-P. (2001). Essential role for Gab2 in the allergic response. *Nature*, *412*(6843), 186-190.

Guselnikov, S. V., Ramanayake, T., Erilova, A. Y., Mechetina, L. V., Najakshin, A. M., Robert, J., & Taranin, A. V. (2008). The Xenopus FcR family demonstrates continually high diversification of paired receptors in vertebrate evolution. *BMC Evol Biol*, *8*, 148. https://doi.org/10.1186/1471-2148-8-148

Guselnikov, S. V., Ramanayake, T., Robert, J., & Taranin, A. V. (2009). Diversity of the FcR-and KIR-related genes in an amphibian Xenopus. *Front Biosci*, *14*, 130-140.

Guselnikov, S. V., Reshetnikova, E. S., Najakshin, A. M., Mechetina, L. V., Robert, J., & Taranin, A. V. (2010). The amphibians Xenopus laevis and Silurana tropicalis possess a family of activating KIR-related Immunoglobulin-like receptors. *Dev Comp Immunol*, *34*(3), 308-315. https://doi.org/10.1016/j.dci.2009.10.010

Guselnikov, S. V., & Taranin, A. V. (2019). Unraveling the LRC Evolution in Mammals: IGSF1 and A1BG Provide the Keys. *Genome Biol Evol*, *11*(6), 1586-1601. https://doi.org/10.1093/gbe/evz102

Gregory, C. D., & Devitt, A. (2004). The macrophage and the apoptotic cell: an innate immune interaction viewed simplistically? *Immunology*, *113*(1), 1-14. https://doi.org/10.1111/j.1365-2567.2004.01959.x

Grimholt, U. (2018). Whole genome duplications have provided teleosts with many roads to peptide loaded MHC class I molecules. *BMC Evol Biol*, *18*(1), 25. https://doi.org/10.1186/s12862-018-1138-9

Hakkim, A., Fuchs, T. A., Martinez, N. E., Hess, S., Prinz, H., Zychlinsky, A., & Waldmann, H. (2011). Activation of the Raf-MEK-ERK pathway is required for neutrophil extracellular trap formation. *Nat Chem Biol*, *7*(2), 75-77. https://doi.org/10.1038/nchembio.496

Hamerman, J. A., & Lanier, L. L. (2006). Inhibition of immune responses by ITAM-bearing receptors. *Science's STKE*, *2006*(320), re1-re1.

Hanington, P. C., Barreda, D. R., & Belosevic, M. (2006). A novel hematopoietic granulin induces proliferation of goldfish (Carassius auratus L.) macrophages. *J Biol Chem*, *281*(15), 9963-9970. https://doi.org/10.1074/jbc.M600631200

Hanington, P. C., Hitchen, S. J., Beamish, L. A., & Belosevic, M. (2009). Macrophage colony stimulating factor (CSF-1) is a central growth factor of goldfish macrophages. *Fish Shellfish Immunol*, *26*(1), 1-9. https://doi.org/10.1016/j.fsi.2008.09.020

Hanington, P. C., Wang, T., Secombes, C. J., & Belosevic, M. (2007). Growth factors of lower vertebrates: characterization of goldfish (Carassius auratus L.) macrophage colony-stimulating factor-1. *J Biol Chem*, *282*(44), 31865-31872. https://doi.org/10.1074/jbc.M706278200

Hatzivassiliou, G., Miller, I., Takizawa, J., Palanisamy, N., Rao, P. H., Iida, S., Tagawa, S., Taniwaki, M., Russo, J., & Neri, A. (2001). IRTA1 and IRTA2, novel immunoglobulin superfamily receptors expressed in B cells and involved in chromosome 1q21 abnormalities in B cell malignancy. *Immunity*, *14*(3), 277-289.

Havixbeck, J. J., & Barreda, D. R. (2015). Neutrophil Development, Migration, and Function in Teleost Fish. *Biology (Basel)*, *4*(4), 715-734. https://doi.org/10.3390/biology4040715

Havixbeck, J. J., Rieger, A. M., Churchill, L. J., & Barreda, D. R. (2017). Neutrophils exert protection in early Aeromonas veronii infections through the clearance of both bacteria and dying macrophages. *Fish Shellfish Immunol*, *63*, 18-30. https://doi.org/10.1016/j.fsi.2017.02.001

Havixbeck, J. J., Rieger, A. M., Wong, M. E., Hodgkinson, J. W., & Barreda, D. R. (2016). Neutrophil contributions to the induction and regulation of the acute inflammatory response in teleost fish. *J Leukoc Biol*, *99*(2), 241-252. https://doi.org/10.1189/jlb.3HI0215-064R

Hilton, H. G., & Parham, P. (2017). Missing or altered self: human NK cell receptors that recognize HLA-C. *Immunogenetics*, *69*(8-9), 567-579. https://doi.org/10.1007/s00251-017-1001-y

Hodgkinson, J. W., Ge, J. Q., Katzenback, B. A., Havixbeck, J. J., Barreda, D. R., Stafford, J. L., & Belosevic, M. (2015). Development of an in vitro model system to study the interactions between Mycobacterium marinum and teleost neutrophils. *Dev Comp Immunol*, *53*(2), 349-357. https://doi.org/10.1016/j.dci.2015.07.016

Hogan, R. J., Taylor, W. R., Cuchens, M. A., Naftel, J. P., Clem, L. W., Miller, N. W., & Chinchar, V. G. (1999). Induction of target cell apoptosis by channel catfish cytotoxic cells. *Cellular immunology*, *195*(2), 110-118.

Holland, M. C. H., & Lambris, J. D. (2002). The complement system in teleosts. *Fish & shellfish immunology*, *12*(5), 399-420.

Hou, X., Dietrich, J., & Geisler, C. (1996). The cytoplasmic tail of FcγRIIIAα is involved in signaling by the low affinity receptor for immunoglobulin G. *Journal of Biological Chemistry*, *271*(37), 22815-22822.

Hu, Z., Gu, X., Baraoidan, K., Ibanez, V., Sharma, A., Kadkol, S., Munker, R., Ackerman, S., Nucifora, G., & Sauntharajah, Y. (2011). RUNX1 regulates corepressor interactions of PU.1. *Blood*, *117*(24), 6498-6508. https://doi.org/10.1182/blood-2010-10-312512

Huang, G., Zhang, P., Hirai, H., Elf, S., Yan, X., Chen, Z., Koschmieder, S., Okuno, Y., Dayaram, T., Growney, J. D., Shivdasani, R. A., Gilliland, D. G., Speck, N. A., Nimer, S. D., & Tenen, D. G. (2008). PU.1 is a major downstream target of AML1 (RUNX1) in adult mouse hematopoiesis. *Nat Genet*, *40*(1), 51-60. https://doi.org/10.1038/ng.2007.7

Huang, H. T., Su, S. C., Chiou, T. J., Lin, Y. H., Shih, Y. C., Wu, Y. X., Fan, T. H., & Twu, Y. C. (2020). DNA methylation-mediated Siglec-7 regulation in natural killer cells via two 5' promoter CpG sites. *Immunology*, *160*(1), 38-51. https://doi.org/10.1111/imm.13179

Huard, B., & Karlsson, L. (2000). KIR expression on self-reactive CD8+ T cells is controlled by T-cell receptor engagement. *Nature*, *403*(6767), 325-328.

Hughes, A. L., & Friedman, R. (2008). Genome size reduction in the chicken has involved massive loss of ancestral protein-coding genes. *Mol Biol Evol*, *25*(12), 2681-2688. https://doi.org/10.1093/molbev/msn207

Hughes, C. E., & Nibbs, R. J. B. (2018). A guide to chemokines and their receptors. *FEBS J*, *285*(16), 2944-2971. https://doi.org/10.1111/febs.14466

Hurst, L. D., Pal, C., & Lercher, M. J. (2004). The evolutionary dynamics of eukaryotic gene order. *Nat Rev Genet*, *5*(4), 299-310. https://doi.org/10.1038/nrg1319

Hirayasu, K., Saito, F., Suenaga, T., Shida, K., Arase, N., Oikawa, K., Yamaoka, T., Murota, H., Chibana, H., Nakagawa, I., Kubori, T., Nagai, H., Nakamaru, Y., Katayama, I., Colonna, M., & Arase, H. (2016). Microbially cleaved immunoglobulins are sensed by the innate immune receptor LILRA2. *Nat Microbiol*, *1*(6), 16054. https://doi.org/10.1038/nmicrobiol.2016.54

Hudson, L. E., & Allen, R. L. (2016). Leukocyte Ig-Like Receptors - A Model for MHC Class I Disease Associations. *Front Immunol*, *7*, 281. https://doi.org/10.3389/fimmu.2016.00281

Imperato, M. R., Cauchy, P., Obier, N., & Bonifer, C. (2015). The RUNX1-PU.1 axis in the control of hematopoiesis. *Int J Hematol*, *101*(4), 319-329. https://doi.org/10.1007/s12185-015-1762-8

Jansen, C. A., Cruijsen, C. W., de Ruiter, T., Nanlohy, N., Willems, N., Janssens-Korpela, P. L., & Meyaard, L. (2007). Regulated expression of the inhibitory receptor LAIR-1 on human peripheral T cells during T cell activation and differentiation. *Eur J Immunol*, *37*(4), 914-924. https://doi.org/10.1002/eji.200636678

Jaso-Friedmann, L., Leary III, J. H., & Evans, D. L. (1997). NCCRP-1: a novel receptor protein sequenced from teleost nonspecific cytotoxic cells. *Molecular immunology*, *34*(12-13), 955-965.

Javvaji, P. K., Dhali, A., Francis, J. R., Kolte, A. P., Mech, A., Roy, S. C., Mishra, A., & Bhatta, R. (2020). An Efficient Nitroblue Tetrazolium Staining and Bright-Field Microscopy Based Method for Detecting and Quantifying Intracellular Reactive Oxygen Species in Oocytes, Cumulus Cells and Embryos. *Front Cell Dev Biol*, *8*, 764. https://doi.org/10.3389/fcell.2020.00764

Jones, D. C., Roghanian, A., Brown, D. P., Chang, C., Allen, R. L., Trowsdale, J., & Young, N. T. (2009). Alternative mRNA splicing creates transcripts encoding soluble proteins from most LILR genes. *Eur J Immunol*, *39*(11), 3195-3206. https://doi.org/10.1002/eji.200839080

Jones, N., Blasutig, I. M., Eremina, V., Ruston, J. M., Bladt, F., Li, H., Huang, H., Larose, L., Li, S. S., Takano, T., Quaggin, S. E., & Pawson, T. (2006). Nck adaptor proteins link nephrin to the actin cytoskeleton of kidney podocytes. *Nature*, *440*(7085), 818-823. https://doi.org/10.1038/nature04662

Jules, J., Maiguel, D., & Hudson, B. I. (2013). Alternative splicing of the RAGE cytoplasmic domain regulates cell signaling and function. *PLoS One*, *8*(11), e78267. https://doi.org/10.1371/journal.pone.0078267

Ji, J., Rao, Y., Wan, Q., Liao, Z., & Su, J. (2018). Teleost-Specific TLR19 Localizes to Endosome, Recognizes dsRNA, Recruits TRIF, Triggers both IFN and NF-kappaB Pathways, and Protects Cells from Grass Carp Reovirus Infection. *J Immunol*, *200*(2), 573-585. https://doi.org/10.4049/jimmunol.1701149

Kalea, A. Z., Schmidt, A. M., & Hudson, B. I. (2011). Alternative splicing of RAGE: roles in biology and disease. *Front Biosci*, *17*, 2756-2770.

Kane, B. A., Bryant, K. J., McNeil, H. P., & Tedla, N. T. (2014). Termination of immune activation: an essential component of healthy host immune responses. *J Innate Immun*, *6*(6), 727-738. https://doi.org/10.1159/000363449

Katzenback, B. A., & Belosevic, M. (2009). Isolation and functional characterization of neutrophil-like cells, from goldfish (Carassius auratus L.) kidney. *Dev Comp Immunol*, *33*(4), 601-611. https://doi.org/10.1016/j.dci.2008.10.011

Katzenback, B. A., & Belosevic, M. (2012). Characterization of granulocyte colony stimulating factor receptor of the goldfish (Carassius auratus L.). *Dev Comp Immunol*, *36*(1), 199-207. https://doi.org/10.1016/j.dci.2011.07.005

Katzenback, B. A., Foroutanpay, B. V., & Belosevic, M. (2013). Expressions of transcription factors in goldfish (Carassius auratus L.) macrophages and their progenitors. *Dev Comp Immunol*, *41*(2), 230-239. https://doi.org/10.1016/j.dci.2013.05.019

Katzenback, B. A., Karpman, M., & Belosevic, M. (2011). Distribution and expression analysis of transcription factors in tissues and progenitor cell populations of the goldfish (Carassius auratus L.) in response to growth factors and pathogens. *Mol Immunol*, *48*(9-10), 1224-1235. https://doi.org/10.1016/j.molimm.2011.03.007

Katzenback, B. A., Katakura, F., & Belosevic, M. (2016). Goldfish (Carassius auratus L.) as a model system to study the growth factors, receptors and transcription factors that govern myelopoiesis in fish. *Dev Comp Immunol*, *58*, 68-85. https://doi.org/10.1016/j.dci.2015.10.024

Kelley, L. A., Mezulis, S., Yates, C. M., Wass, M. N., & Sternberg, M. J. (2015). The Phyre2 web portal for protein modeling, prediction and analysis. *Nat Protoc*, *10*(6), 845-858. https://doi.org/10.1038/nprot.2015.053

Khan, M. A., & Palaniyar, N. (2017). Transcriptional firing helps to drive NETosis. *Sci Rep*, *7*, 41749. https://doi.org/10.1038/srep41749

Kiyoshi, M., Caaveiro, J. M., Kawai, T., Tashiro, S., Ide, T., Asaoka, Y., Hatayama, K., & Tsumoto, K. (2015). Structural basis for binding of human IgG1 to its high-affinity human receptor FcgammaRI. *Nat Commun*, *6*, 6866. https://doi.org/10.1038/ncomms7866

Kobayashi, I., Kuniyoshi, S., Saito, K., Moritomo, T., Takahashi, T., & Nakanishi, T. (2008). Long-term hematopoietic reconstitution by transplantation of kidney hematopoietic stem cells in lethally irradiated clonal ginbuna crucian carp (Carassius auratus langsdorfii). *Dev Comp Immunol*, *32*(8), 957-965. https://doi.org/10.1016/j.dci.2008.01.006

Komiyama, T., Kobayashi, H., Tateno, Y., Inoko, H., Gojobori, T., & Ikeo, K. (2009). An evolutionary origin and selection process of goldfish. *Gene*, *430*(1-2), 5-11. https://doi.org/10.1016/j.gene.2008.10.019

Kon, T., Omori, Y., Fukuta, K., Wada, H., Watanabe, M., Chen, Z., Iwasaki, M., Mishina, T., Matsuzaki, S. S., Yoshihara, D., Arakawa, J., Kawakami, K., Toyoda, A., Burgess, S. M., Noguchi, H., & Furukawa, T. (2020). The Genetic Basis of Morphological Diversity in

Domesticated Goldfish. *Curr Biol*, *30*(12), 2260-2274 e2266. https://doi.org/10.1016/j.cub.2020.04.034

Kondera, E. (2011). Haematopoiesis in the head kidney of common carp (Cyprinus carpio L.): a morphological study. *Fish Physiol Biochem*, *37*(3), 355-362. https://doi.org/10.1007/s10695-010-9432-5

Kondera, E. (2019). Haematopoiesis and haematopoietic organs in fish. *Roczniki Naukowe Polskiego Towarzystwa Zootechnicznego*, *15*(1), 9-16. https://doi.org/10.5604/01.3001.0013.4535

Kotwica-Mojzych, K., Jodlowska-Jedrych, B., & Mojzych, M. (2021). CD200:CD200R Interactions and Their Importance in Immunoregulation. *Int J Mol Sci*, *22*(4). https://doi.org/10.3390/ijms22041602

Kountikov, E., Nayak, D., Wilson, M., Miller, N. W., & Bengten, E. (2010). Expression of alternatively spliced CD45 isoforms by channel catfish clonal T and B cells is dependent on activation state of the cell and regulated by protein synthesis and degradation. *Dev Comp Immunol*, *34*(10), 1109-1118. https://doi.org/10.1016/j.dci.2010.06.003

Kountikov, E., Wilson, M., Quiniou, S., Miller, N., Clem, W., & Bengtén, E. (2005). Genomic organization of the channel catfish CD45 functional gene and CD45 pseudogenes. *Immunogenetics*, *57*, 374-383.

Krmpotic, A., Hasan, M., Loewendorf, A., Saulig, T., Halenius, A., Lenac, T., Polic, B., Bubic, I., Kriegeskorte, A., Pernjak-Pugel, E., Messerle, M., Hengel, H., Busch, D. H., Koszinowski, U. H., & Jonjic, S. (2005). NK cell activation through the NKG2D ligand MULT-1 is selectively prevented by the glycoprotein encoded by mouse cytomegalovirus gene m145. *J Exp Med*, *201*(2), 211-220. https://doi.org/10.1084/jem.20041617

Kubagawa, H., Oka, S., Kubagawa, Y., Torii, I., Takayama, E., Kang, D. W., Gartland, G. L., Bertoli, L. F., Mori, H., Takatsu, H., Kitamura, T., Ohno, H., & Wang, J. Y. (2009). Identity of the elusive IgM Fc receptor (FcmuR) in humans. *J Exp Med*, *206*(12), 2779-2793. https://doi.org/10.1084/jem.20091107

Kulemzin, S. V., Zamoshnikova, A. Y., Yurchenko, M. Y., Vitak, N. Y., Najakshin, A. M., Fayngerts, S. A., Chikaev, N. A., Reshetnikova, E. S., Kashirina, N. M., Peclo, M. M., Rutkevich, P. N., Shevelev, A. Y., Yanushevskaya, E. V., Baranov, K. O., Mamonkin, M., Vlasik, T. N., Sidorenko, S. P., Taranin, A. V., & Mechetina, L. V. (2011). FCRL6 receptor: expression and associated proteins. *Immunol Lett*, *134*(2), 174-182. https://doi.org/10.1016/j.imlet.2010.09.023

Kumar, S., Stecher, G., & Tamura, K. (2016). MEGA7: Molecular Evolutionary Genetics Analysis Version 7.0 for Bigger Datasets. *Mol Biol Evol*, *33*(7), 1870-1874. https://doi.org/10.1093/molbev/msw054

Kurtz, J., & Armitage, S. A. (2006). Alternative adaptive immunity in invertebrates. *Trends Immunol*, *27*(11), 493-496. https://doi.org/10.1016/j.it.2006.09.001

Kutyrev, I. A., Pronin, N. M., & Dugarov, Z. N. (2011). Composition of leucocytes of the head kidney of the crucian carp (Carassius auratus gibelio, Cypriniformes: Cyprinidae) as affected by invasion of cestode Digramma interrupta (Cestoda; Pseudophyllidea). *Biology Bulletin*, *38*(6), 653-657. https://doi.org/10.1134/s1062359011060069

Kim, T., Vidal, G. S., Djurisic, M., William, C. M., Birnbaum, M. E., Garcia, K. C., Hyman, B. T., & Shatz, C. J. (2013). Human LilrB2 is a beta-amyloid receptor and its murine homolog PirB regulates synaptic plasticity in an Alzheimer's model. *Science*, *341*(6152), 1399-1404. https://doi.org/10.1126/science.1242077

Ko, Y. P., & Flick, M. J. (2016). Fibrinogen Is at the Interface of Host Defense and Pathogen Virulence in Staphylococcus aureus Infection. *Semin Thromb Hemost*, *42*(4), 408-421. https://doi.org/10.1055/s-0036-1579635

Krumbholz, M., Theil, D., Steinmeyer, F., Cepok, S., Hemmer, B., Hofbauer, M., Farina, C., Derfuss, T., Junker, A., Arzberger, T., Sinicina, I., Hartle, C., Newcombe, J., Hohlfeld, R., & Meinl, E. (2007). CCL19 is constitutively expressed in the CNS, up-regulated in neuroinflammation, active and also inactive multiple sclerosis lesions. *J Neuroimmunol*, *190*(1-2), 72-79. https://doi.org/10.1016/j.jneuroim.2007.07.024

Kuroki, K., Furukawa, A., & Maenaka, K. (2012). Molecular recognition of paired receptors in the immune system. *Front Microbiol*, *3*, 429. https://doi.org/10.3389/fmicb.2012.00429

Lacy, P. (2006). Mechanisms of degranulation in neutrophils. *Allergy, Asthma & Clinical Immunology*, *2*, 1-11.

Lahoz-Beneytez, J., Elemans, M., Zhang, Y., Ahmed, R., Salam, A., Block, M., Niederalt, C., Asquith, B., & Macallan, D. (2016). Human neutrophil kinetics: modeling of stable isotope labeling data supports short blood neutrophil half-lives. *Blood*, *127*(26), 3431-3438. https://doi.org/10.1182/blood-2016-03-700336

Lanier, L. L. (2005). NK cell recognition. *Annu Rev Immunol*, *23*, 225-274. https://doi.org/10.1146/annurev.immunol.23.021704.115526

Lanier, L. L. (2015). NKG2D Receptor and Its Ligands in Host Defense. *Cancer Immunol Res*, *3*(6), 575-582. https://doi.org/10.1158/2326-6066.CIR-15-0098

Lawrence, T., & Natoli, G. (2011). Transcriptional regulation of macrophage polarization: enabling diversity with identity. *Nat Rev Immunol*, *11*(11), 750-761. https://doi.org/10.1038/nri3088

Lei, H. Y., & Chang, C. P. (2009). Lectin of Concanavalin A as an anti-hepatoma therapeutic agent. *J Biomed Sci*, *16*(1), 10. https://doi.org/10.1186/1423-0127-16-10

Lemaitre, B. (2004). The road to Toll. *Nature Reviews Immunology*, *4*(7), 521-527.

Lemaitre, B., Nicolas, E., Michaut, L., Reichhart, J.-M., & Hoffmann, J. A. (1996). The dorsoventral regulatory gene cassette spätzle/Toll/cactus controls the potent antifungal response in Drosophila adults. *Cell*, *86*(6), 973-983.

Letunic, I., & Bork, P. (2018). 20 years of the SMART protein domain annotation resource. *Nucleic Acids Res*, *46*(D1), D493-D496. https://doi.org/10.1093/nar/gkx922

Letunic, I., Copley, R. R., Schmidt, S., Ciccarelli, F. D., Doerks, T., Schultz, J., Ponting, C. P., & Bork, P. (2004). SMART 4.0: towards genomic data integration. *Nucleic Acids Res*, *32*(Database issue), D142-144. https://doi.org/10.1093/nar/gkh088

Levin, R., Grinstein, S., & Schlam, D. (2015). Phosphoinositides in phagocytosis and macropinocytosis. *Biochim Biophys Acta*, *1851*(6), 805-823. https://doi.org/10.1016/j.bbalip.2014.09.005

Li, C., Iosef, C., Jia, C. Y., Han, V. K., & Li, S. S. (2003). Dual functional roles for the X-linked lymphoproliferative syndrome gene product SAP/SH2D1A in signaling through the signaling lymphocyte activation molecule (SLAM) family of immune receptors. *J Biol Chem*, *278*(6), 3852-3859. https://doi.org/10.1074/jbc.M206649200

Li, D., Wan, Z., Li, X., Duan, M., Yang, L., Ruan, Z., Wang, Q., & Li, W. (2019). Alternatively spliced down syndrome cell adhesion molecule (Dscam) controls innate immunity in crab. *J Biol Chem*, *294*(44), 16440-16450. https://doi.org/10.1074/jbc.RA119.010247

Li, D., & Wu, M. (2021). Pattern recognition receptors in health and diseases. *Signal Transduct Target Ther*, *6*(1), 291. https://doi.org/10.1038/s41392-021-00687-0

Li, F. J., Won, W. J., Becker, E. J., Jr., Easlick, J. L., Tabengwa, E. M., Li, R., Shakhmatov, M., Honjo, K., Burrows, P. D., & Davis, R. S. (2014). Emerging roles for the FCRL family members in lymphocyte biology and disease. *Curr Top Microbiol Immunol*, *382*, 29-50. https://doi.org/10.1007/978-3-319-07911-0_2

Li, J., Barreda, D. R., Zhang, Y. A., Boshra, H., Gelman, A. E., Lapatra, S., Tort, L., & Sunyer, J. O. (2006). B lymphocytes from early vertebrates have potent phagocytic and microbicidal abilities. *Nat Immunol*, *7*(10), 1116-1124. https://doi.org/10.1038/ni1389

Li, M. F., & Zhang, H. Q. (2022). An overview of complement systems in teleosts. *Dev Comp Immunol*, *137*, 104520. https://doi.org/10.1016/j.dci.2022.104520

Li, S., Ma, Y., Ye, S., Hu, D., & Xiao, F. (2022). ERK/p38/ROS burst responses to environmentally relevant concentrations of diphenyl phosphate-evoked neutrophil extracellular traps formation: Assessing the role of autophagy. *J Hazard Mater*, *421*, 126758. https://doi.org/10.1016/j.jhazmat.2021.126758

Li, S., Wang, Y., Yu, D., Zhang, Y., Wang, X., Shi, M., Xiao, Y., Li, X., Xiao, H., Chen, L., & Xiong, X. (2022). Triclocarban evoked neutrophil extracellular trap formation in common carp (Cyprinus carpio L.) by modulating SIRT3-mediated ROS crosstalk with ERK1/2/p38 signaling. *Fish Shellfish Immunol*, *129*, 85-95. https://doi.org/10.1016/j.fsi.2022.08.060

Li, W., Nishimura, R., Kashishian, A., Batzer, A. G., Kim, W. J., Cooper, J. A., & Schlessinger, J. (1994). A new function for a phosphotyrosine phosphatase: linking GRB2-Sos to a receptor tyrosine kinase. *Molecular and cellular biology*.

Li, Y., Marzolo, M. P., van Kerkhof, P., Strous, G. J., & Bu, G. (2000). The YXXL motif, but not the two NPXY motifs, serves as the dominant endocytosis signal for low density

lipoprotein receptor-related protein. *J Biol Chem*, *275*(22), 17187-17194. https://doi.org/10.1074/jbc.M000490200

Liao, Z., & Su, J. (2021). Progresses on three pattern recognition receptor families (TLRs, RLRs and NLRs) in teleost. *Dev Comp Immunol*, *122*, 104131. https://doi.org/10.1016/j.dci.2021.104131

Lillico, D. M., Zwozdesky, M. A., Pemberton, J. G., Deutscher, J. M., Jones, L. O., Chang, J. P., & Stafford, J. L. (2015). Teleost leukocyte immune-type receptors activate distinct phagocytic modes for target acquisition and engulfment. *J Leukoc Biol*, *98*(2), 235-248. https://doi.org/10.1189/jlb.2A0215-039RR

Lillico, D. M. E., Pemberton, J. G., Niemand, R., & Stafford, J. L. (2020). Selective recruitment of Nck and Syk contribute to distinct leukocyte immune-type receptor-initiated target interactions. *Cell Signal*, *66*, 109443. https://doi.org/10.1016/j.cellsig.2019.109443

Liston, A., & Masters, S. L. (2017). Homeostasis-altering molecular processes as mechanisms of inflammasome activation. *Nat Rev Immunol*, *17*(3), 208-214. https://doi.org/10.1038/nri.2016.151

Liu, F., Chen, H., Cao, C., Liang, Y., & Zhou, Y. (2023). The role of toll-like receptors (TLRs) and their therapeutic applications in glomerulonephritis. *Int Urol Nephrol*, *55*(11), 2845-2856. https://doi.org/10.1007/s11255-023-03592-3

Liu, H., Li, L., Voss, C., Wang, F., Liu, J., & Li, S. S. (2015). A Comprehensive Immunoreceptor Phosphotyrosine-based Signaling Network Revealed by Reciprocal Protein-Peptide Array Screening. *Mol Cell Proteomics*, *14*(7), 1846-1858. https://doi.org/10.1074/mcp.M115.047951

Liu, X., Ma, B., Malik, A. B., Tang, H., Yang, T., Sun, B., Wang, G., Minshall, R. D., Li, Y., Zhao, Y., Ye, R. D., & Xu, J. (2012). Bidirectional regulation of neutrophil migration by mitogen-activated protein kinases. *Nat Immunol*, *13*(5), 457-464. https://doi.org/10.1038/ni.2258

Liu, Y., McDaniel, J. R., Khan, S., Campisi, P., Propst, E. J., Holler, T., Grunebaum, E., Georgiou, G., Ippolito, G. C., & Ehrhardt, G. R. A. (2018). Antibodies Encoded by FCRL4-Bearing Memory B Cells Preferentially Recognize Commensal Microbial Antigens. *J Immunol*, *200*(12), 3962-3969. https://doi.org/10.4049/jimmunol.1701549

Long, E. O., & Rajagopalan, S. (2002). Stress signals activate natural killer cells. *J Exp Med*, *196*(11), 1399-1402. https://doi.org/10.1084/jem.20021747

Luckasen, J. R., White, J. G., & Kersey, J. H. (1974). Mitogenic properties of a calcium ionophore, A23187. *Proceedings of the National Academy of Sciences*, *71*(12), 5088-5090.

Lynch, K. W. (2004). Consequences of regulated pre-mRNA splicing in the immune system. *Nat Rev Immunol*, *4*(12), 931-940. https://doi.org/10.1038/nri1497

Le Morvan, C., Troutaud, D., & Deschaux, P. (1998). Differential effects of temperature on specific and nonspecific immune defences in fish. *J Exp Biol*, *201*(Pt 2), 165-168. https://doi.org/10.1242/jeb.201.2.165

Lee, F. F., Chuang, H. C., Chen, N. Y., Nagarajan, G., & Chiou, P. P. (2015). Toll-Like Receptor 9 Alternatively Spliced Isoform Negatively Regulates TLR9 Signaling in Teleost Fish. *PLoS One*, *10*(5), e0126388. https://doi.org/10.1371/journal.pone.0126388

Li, D., Hong, A., Lu, Q., Gao, G. F., Jin, B., Screaton, G. R., & Xu, X. N. (2012). A novel role of CD1c in regulating CD1d-mediated NKT cell recognition by competitive binding to Ig-like transcript 4. *Int Immunol*, *24*(11), 729-737. https://doi.org/10.1093/intimm/dxs082

Li, D., Wang, L., Yu, L., Freundt, E. C., Jin, B., Screaton, G. R., & Xu, X. N. (2009). Ig-like transcript 4 inhibits lipid antigen presentation through direct CD1d interaction. *J Immunol*, *182*(2), 1033-1040. https://doi.org/10.4049/jimmunol.182.2.1033

Li, F. J., Schreeder, D. M., Li, R., Wu, J., & Davis, R. S. (2013). FCRL3 promotes TLR9-induced B-cell activation and suppresses plasma cell differentiation. *Eur J Immunol*, *43*(11), 2980-2992. https://doi.org/10.1002/eji.201243068

Ljunggren, H.-G., & Kärre, K. (1990). In search of the 'missing self': MHC molecules and NK cell recognition. *Immunology today*, *11*, 237-244.

Lu, I. N., Chiang, B. L., Lou, K. L., Huang, P. T., Yao, C. C., Wang, J. S., Lin, L. D., Jeng, J. H., & Chang, B. E. (2012). Cloning, expression and characterization of CCL21 and CCL25 chemokines in zebrafish. *Dev Comp Immunol*, *38*(2), 203-214. https://doi.org/10.1016/j.dci.2012.07.003

Ma, C. S., Nichols, K. E., & Tangye, S. G. (2007). Regulation of cellular and humoral immune responses by the SLAM and SAP families of molecules. *Annu Rev Immunol*, *25*, 337-379. https://doi.org/10.1146/annurev.immunol.25.022106.141651

Ma, Y., Kemp, S. S., Yang, X., Wu, M. H., & Yuan, S. Y. (2023). Cellular mechanisms underlying the impairment of macrophage efferocytosis. *Immunol Lett*, *254*, 41-53. https://doi.org/10.1016/j.imlet.2023.02.001

Madeira, F., Park, Y. M., Lee, J., Buso, N., Gur, T., Madhusoodanan, N., Basutkar, P., Tivey, A. R. N., Potter, S. C., Finn, R. D., & Lopez, R. (2019). The EMBL-EBI search and

sequence analysis tools APIs in 2019. *Nucleic Acids Res*, *47*(W1), W636-W641. https://doi.org/10.1093/nar/gkz268

Mahapatra, S., Ganguly, B., Pani, S., Saha, A., & Samanta, M. (2023). A comprehensive review on the dynamic role of toll-like receptors (TLRs) in frontier aquaculture research and as a promising avenue for fish disease management. *Int J Biol Macromol*, *253*(Pt 1), 126541. https://doi.org/10.1016/j.ijbiomac.2023.126541

Mahaweni, N. M., Ehlers, F. A. I., Bos, G. M. J., & Wieten, L. (2018). Tuning Natural Killer Cell Anti-multiple Myeloma Reactivity by Targeting Inhibitory Signaling via KIR and NKG2A. *Front Immunol*, *9*, 2848. https://doi.org/10.3389/fimmu.2018.02848

Makino, T., & McLysaght, A. (2008). Interacting gene clusters and the evolution of the vertebrate immune system. *Mol Biol Evol*, *25*(9), 1855-1862. https://doi.org/10.1093/molbev/msn137

Maltais, L. J., Lovering, R. C., Taranin, A. V., Colonna, M., Ravetch, J. V., Dalla-Favera, R., Burrows, P. D., Cooper, M. D., & Davis, R. S. (2006). New nomenclature for Fc receptor–like molecules. *Nature immunology*, *7*(5), 431-432.

Mantovani, A., & Garlanda, C. (2023). Humoral Innate Immunity and Acute-Phase Proteins. *N Engl J Med*, *388*(5), 439-452. https://doi.org/10.1056/NEJMra2206346

Mantovani, A., Locati, M., Vecchi, A., Sozzani, S., & Allavena, P. (2001). Decoy receptors: a strategy to regulate inflammatory cytokines and chemokines. *Trends in immunology*, *22*(6), 328-336.

Martin, A. M., Kulski, J. K., Witt, C., Pontarotti, P., & Christiansen, F. T. (2002). Leukocyte Ig-like receptor complex (LRC) in mice and men. *Trends in immunology*, *23*(2), 81-88.

Martinez, N. M., & Lynch, K. W. (2013). Control of alternative splicing in immune responses: many regulators, many predictions, much still to learn. *Immunol Rev*, *253*(1), 216-236. https://doi.org/10.1111/imr.12047

McAllister, M., Phillips, N., & Belosevic, M. (2019). Trypanosoma carassii infection in goldfish (Carassius auratus L.): changes in the expression of erythropoiesis and anemia regulatory genes. *Parasitol Res*, *118*(4), 1147-1158. https://doi.org/10.1007/s00436-019-06246-5

Mellman, I., Turley, S. J., & Steinman, R. M. (1998). Antigen processing for amateurs and professionals. *Trends in cell biology*, *8*(6), 231-237.

Meloni, S., Zarletti, G., Benedetti, S., Randelli, E., Buonocore, F., & Scapigliati, G. (2006). Cellular activities during a mixed leucocyte reaction in the teleost sea bass Dicentrarchus labrax. *Fish Shellfish Immunol*, *20*(5), 739-749. https://doi.org/10.1016/j.fsi.2005.10.001

Messeguer, X., Escudero, R., Farré, D., Nuñez, O., Martínez, J., & Albà, M. M. (2002). PROMO: detection of known transcription regulatory elements using species-tailored searches. *Bioinformatics*, *18*(2), 333-334.

Mewes, J., Verheijen, K., Montgomery, B. C., & Stafford, J. L. (2009). Stimulatory catfish leukocyte immune-type receptors (IpLITRs) demonstrate a unique ability to associate with adaptor signaling proteins and participate in the formation of homo- and heterodimers. *Mol Immunol*, *47*(2-3), 318-331. https://doi.org/10.1016/j.molimm.2009.09.014

Miach, P. J. (1986). Cyclosporin A in organ transplantation. *Medical Journal of Australia*, *145*(3-4), 146-150.

Mikhalap, S. V., Shlapatska, L. M., Berdova, A. G., Law, C.-L., Clark, E. A., & Sidorenko, S. P. (1999). CDw150 Associates with Src-Homology 2-Containing Inositol Phosphatase and

Modulates CD95-Mediated Apoptosis. *The Journal of Immunology*, *162*(10), 5719-5727. https://doi.org/10.4049/jimmunol.162.10.5719

Miller, K. L., Duchemin, A.-M., & Anderson, C. L. (1996). A novel role for the Fc receptor gamma subunit: enhancement of Fc gamma R ligand affinity. *The Journal of experimental medicine*, *183*(5), 2227-2233.

Miller, N., Deuter, A., & Clem, L. (1986). Phylogeny of lymphocyte heterogeneity: the cellular requirements for the mixed leucocyte reaction with channel catfish. *Immunology*, *59*(1), 123.

Missbach, S., Aleksic, D., Blaschke, L., Hassemer, T., Lee, K. J., Mansfeld, M., Hanske, J., Handler, J., & Kammerer, R. (2018). Alternative splicing after gene duplication drives CEACAM1-paralog diversification in the horse. *BMC Evol Biol*, *18*(1), 32. https://doi.org/10.1186/s12862-018-1145-x

Mold, C., Gewurz, H., & Du Clos, T. W. (1999). Regulation of complement activation by C-reactive protein. *Immunopharmacology*, *42*(1-3), 23-30.

Montgomery, B. C., Cortes, H. D., Burshtyn, D. N., & Stafford, J. L. (2012). Channel catfish leukocyte immune-type receptor mediated inhibition of cellular cytotoxicity is facilitated by SHP-1-dependent and -independent mechanisms. *Dev Comp Immunol*, *37*(1), 151-163. https://doi.org/10.1016/j.dci.2011.09.005

Montgomery, B. C., Cortes, H. D., Mewes-Ares, J., Verheijen, K., & Stafford, J. L. (2011). Teleost IgSF immunoregulatory receptors. *Dev Comp Immunol*, *35*(12), 1223-1237. https://doi.org/10.1016/j.dci.2011.03.010

Montgomery, B. C., Mewes, J., Davidson, C., Burshtyn, D. N., & Stafford, J. L. (2009). Cell surface expression of channel catfish leukocyte immune-type receptors (IpLITRs) and

recruitment of both Src homology 2 domain-containing protein tyrosine phosphatase (SHP)-1 and SHP-2. *Dev Comp Immunol*, *33*(4), 570-582. https://doi.org/10.1016/j.dci.2008.10.006

Morton, H. C., Pleass, R. J., Storset, A. K., Dissen, E., Williams, J. L., Brandtzaeg, P., & Woof, J. M. (2004). Cloning and characterization of an immunoglobulin A Fc receptor from cattle. *Immunology*, *111*(2), 204-211.

Morton, H. C., van den Herik-Oudijk, I. E., Vossebeld, P., Snijders, A., Verhoeven, A. J., Capel, P. J., & van de Winkel, J. G. (1995). Functional Association between the Human Myeloid Immunoglobulin A Fc Receptor (CD89) and FcR γChain: MOLECULAR BASIS FOR CD89/FcR γCHAIN ASSOCIATION (∗). *Journal of Biological Chemistry*, *270*(50), 29781-29787.

Magnadottir, B. (2010). Immunological control of fish diseases. *Mar Biotechnol (NY)*, *12*(4), 361-379. https://doi.org/10.1007/s10126-010-9279-x

Mao, Y., & Finnemann, S. C. (2015). Regulation of phagocytosis by Rho GTPases. *Small GTPases*, *6*(2), 89-99. https://doi.org/10.4161/21541248.2014.989785

Marshall, J. S., Warrington, R., Watson, W., & Kim, H. L. (2018). An introduction to immunology and immunopathology. *Allergy Asthma Clin Immunol*, *14*(Suppl 2), 49. https://doi.org/10.1186/s13223-018-0278-1

Matsuo, A., Oshiumi, H., Tsujita, T., Mitani, H., Kasai, H., Yoshimizu, M., Matsumoto, M., & Seya, T. (2008). Teleost TLR22 recognizes RNA duplex to induce IFN and protect cells from birnaviruses. *J Immunol*, *181*(5), 3474-3485. https://doi.org/10.4049/jimmunol.181.5.3474

Middleton, D., & Gonzelez, F. (2010). The extensive polymorphism of KIR genes. *Immunology*, *129*(1), 8-19.

Moradi, S., Berry, R., Pymm, P., Hitchen, C., Beckham, S. A., Wilce, M. C., Walpole, N. G., Clements, C. S., Reid, H. H., Perugini, M. A., Brooks, A. G., Rossjohn, J., & Vivian, J. P. (2015). The structure of the atypical killer cell immunoglobulin-like receptor, KIR2DL4. *J Biol Chem*, *290*(16), 10460-10471. https://doi.org/10.1074/jbc.M114.612291

Mosser, D. M., & Edwards, J. P. (2008). Exploring the full spectrum of macrophage activation. *Nat Rev Immunol*, *8*(12), 958-969. https://doi.org/10.1038/nri2448

Munoz-Atienza, E., Aquilino, C., Syahputra, K., Al-Jubury, A., Araujo, C., Skov, J., Kania, P. W., Hernandez, P. E., Buchmann, K., Cintas, L. M., & Tafalla, C. (2019). CK11, a Teleost Chemokine with a Potent Antimicrobial Activity. *J Immunol*, *202*(3), 857-870. https://doi.org/10.4049/jimmunol.1800568

Nakajima, H., Asai, A., Okada, A., Ping, L., Hamajima, F., Sata, T., & Isobe, K. (2003). Transcriptional regulation of ILT family receptors. *J Immunol*, *171*(12), 6611-6620. https://doi.org/10.4049/jimmunol.171.12.6611

Neumann, N., Fagan, D., & Belosevic, M. (1995). Macrophage activating factor (s) secreted by mitogen stimulated goldfish kidney leukocytes synergize with bacterial lipopolysaccharide to induce nitric oxide production in teleost macrophages. *Developmental & Comparative Immunology*, *19*(6), 473-482.

Neumann, N. F., Barreda, D., & Belosevic, M. (1998). Production of a macrophage growth factor (s) by a goldfish macrophage cell line and macrophages derived from goldfish kidney leukocytes. *Developmental & Comparative Immunology*, *22*(4), 417-432.

Neumann, N. F., Barreda, D. R., & Belosevic, M. (2000). Generation and functional analysis of distinct macrophage sub-populations from goldfish (Carassius auratus L.) kidney leukocyte cultures. *Fish & shellfish immunology*, *10*(1), 1-20.

Neumann, N. F., & Belosevic, M. (1996). Deactivation of primed respiratory burst response of goldfish macrophages by leukocyte-derived macrophage activating factor (s). *Developmental & Comparative Immunology*, *20*(6), 427-439.

Nguyen, G. T., Green, E. R., & Mecsas, J. (2017). Neutrophils to the ROScue: Mechanisms of NADPH Oxidase Activation and Bacterial Resistance. *Front Cell Infect Microbiol*, *7*, 373. https://doi.org/10.3389/fcimb.2017.00373

Nikolaidis, N., Klein, J., & Nei, M. (2005). Origin and evolution of the Ig-like domains present in mammalian leukocyte receptors: insights from chicken, frog, and fish homologues. *Immunogenetics*, *57*(1-2), 151-157. https://doi.org/10.1007/s00251-004-0764-0

Nikolaidis, N., Makalowska, I., Chalkia, D., Makalowski, W., Klein, J., & Nei, M. (2005). Origin and evolution of the chicken leukocyte receptor complex. *Proceedings of the National Academy of Sciences*, *102*(11), 4057-4062.

Nada, S., Okada, M., MacAuley, A., Cooper, J. A., & Nakagawa, H. (1991). Cloning of a complementary DNA for a protein-tyrosine kinase that specifically phosphorylates a negative regulatory site of p60c-src. *Nature*, *351*(6321), 69-72.

Oates, A. C., Wollberg, P., Pratt, S. J., Paw, B. H., Johnson, S. L., Ho, R. K., Postlethwait, J. H., Zon, L. I., & Wilks, A. F. (1999). Zebrafish stat3 is expressed in restricted tissues during embryogenesis and stat1 rescues cytokine signaling in a STAT1‐deficient human cell line. *Developmental dynamics: an official publication of the American Association of Anatomists*, *215*(4), 352-370.

Odaka, T., Suetake, H., Maeda, T., & Miyadai, T. (2018). Teleost Basophils Have IgM-Dependent and Dual Ig-Independent Degranulation Systems. *J Immunol*, *200*(8), 2767-2776. https://doi.org/10.4049/jimmunol.1701051

Ohta, Y., Kasahara, M., O'Connor, T. D., & Flajnik, M. F. (2019). Inferring the "Primordial Immune Complex": Origins of MHC Class I and Antigen Receptors Revealed by Comparative Genomics. *J Immunol*, *203*(7), 1882-1896. https://doi.org/10.4049/jimmunol.1900597

Ostrakhovitch, E. A., & Li, S. S. (2006). The role of SLAM family receptors in immune cell signaling. *Biochem Cell Biol*, *84*(6), 832-843. https://doi.org/10.1139/o06-191

Othman, A., Sekheri, M., & Filep, J. G. (2022). Roles of neutrophil granule proteins in orchestrating inflammation and immunity. *FEBS J*, *289*(14), 3932-3953. https://doi.org/10.1111/febs.15803

Opazo, J. C., Butts, G. T., Nery, M. F., Storz, J. F., & Hoffmann, F. G. (2013). Whole-genome duplication and the functional diversification of teleost fish hemoglobins. *Mol Biol Evol*, *30*(1), 140-153. https://doi.org/10.1093/molbev/mss212

Palic, D., Andreasen, C. B., Menzel, B. W., & Roth, J. A. (2005). A rapid, direct assay to measure degranulation of primary granules in neutrophils from kidney of fathead minnow (Pimephales promelas Rafinesque, 1820). *Fish Shellfish Immunol*, *19*(3), 217-227. https://doi.org/10.1016/j.fsi.2004.12.003

Palic, D., Ostojic, J., Andreasen, C. B., & Roth, J. A. (2007). Fish cast NETs: neutrophil extracellular traps are released from fish neutrophils. *Dev Comp Immunol*, *31*(8), 805-816. https://doi.org/10.1016/j.dci.2006.11.010

Paludan, S. R., Pradeu, T., Masters, S. L., & Mogensen, T. H. (2021). Constitutive immune mechanisms: mediators of host defence and immune regulation. *Nat Rev Immunol*, *21*(3), 137-150. https://doi.org/10.1038/s41577-020-0391-5

Pang, J., Taylor, G., Munroe, D. G., Ishaque, A., Fung-Leung, W.-P., Lau, C. Y., Liu, F.-T., & Zhou, L. (1993). Characterization of the gene for the human high affinity IgE receptor (Fc epsilon RI) alpha-chain. *Journal of immunology (Baltimore, Md.: 1950)*, *151*(11), 6166-6174.

Pasquier, B., Launay, P., Kanamaru, Y., Moura, I. C., Pfirsch, S., Ruffié, C., Hénin, D., Benhamou, M., Pretolani, M., & Blank, U. (2005). Identification of FcαRI as an inhibitory receptor that controls inflammation: dual role of FcRγ ITAM. *Immunity*, *22*(1), 31-42.

Patole, P. S., Schubert, S., Hildinger, K., Khandoga, S., Khandoga, A., Segerer, S., Henger, A., Kretzler, M., Werner, M., Krombach, F., Schlondorff, D., & Anders, H. J. (2005). Toll-like receptor-4: renal cells and bone marrow cells signal for neutrophil recruitment during pyelonephritis. *Kidney Int*, *68*(6), 2582-2587. https://doi.org/10.1111/j.1523-1755.2005.00729.x

Poggi, A., Tomasello, E., Ferrero, E., Zocchi, M. R., & Moretta, L. (1998). p40/LAIR-1 regulates the differentiation of peripheral blood precursors to dendritic cells induced by granulocyte-monocyte colony-stimulating factor. *European Journal of Immunology*, *28*(7), 2086-2091. https://doi.org/10.1002/(sici)1521-4141(199807)28:07<2086::Aid-immu2086>3.0.Co;2-t

Pasquier, L. D. (1982). Antibody diversity in lower vertebrates—why is it so restricted? *Nature*, *296*(5855), 311-313.

Pende, D., Falco, M., Vitale, M., Cantoni, C., Vitale, C., Munari, E., Bertaina, A., Moretta, F., Del Zotto, G., Pietra, G., Mingari, M. C., Locatelli, F., & Moretta, L. (2019). Killer Ig-Like Receptors (KIRs): Their Role in NK Cell Modulation and Developments Leading to Their Clinical Exploitation. *Front Immunol*, *10*, 1179. https://doi.org/10.3389/fimmu.2019.01179

Pijanowski, L., Golbach, L., Kolaczkowska, E., Scheer, M., Verburg-van Kemenade, B. M., & Chadzinska, M. (2013). Carp neutrophilic granulocytes form extracellular traps via ROS-dependent and independent pathways. *Fish Shellfish Immunol*, *34*(5), 1244-1252. https://doi.org/10.1016/j.fsi.2013.02.010

Qiu, W. Q., De Bruin, D., Brownstein, B. H., Pearse, R., & Ravetch, J. V. (1990). Organization of the human and mouse low-affinity FcγR genes: duplication and recombination. *Science*, *248*(4956), 732-735.

Rahman, M., & Bordoni, B. (2023). Histology, natural killer cells. In *StatPearls [Internet]*. StatPearls Publishing.

Rast, J. P., Haire, R. N., Litman, R. T., Pross, S., & Litman, G. W. (1995). Identification and characterization of T-cell antigen receptor-related genes in phylogenetically diverse vertebrate species. *Immunogenetics*, *42*, 204-212.

Rehwinkel, J., & Gack, M. U. (2020). RIG-I-like receptors: their regulation and roles in RNA sensing. *Nat Rev Immunol*, *20*(9), 537-551. https://doi.org/10.1038/s41577-020-0288-3

Reth, M. (1989). Antigen receptor tail clue. *Nature*, *338*, 383.

Rieger, A. M., Hall, B. E., & Barreda, D. R. (2010). Macrophage activation differentially modulates particle binding, phagocytosis and downstream antimicrobial mechanisms. *Dev Comp Immunol*, *34*(11), 1144-1159. https://doi.org/10.1016/j.dci.2010.06.006

Rieger, A. M., Hanington, P. C., Belosevic, M., & Barreda, D. R. (2014). Control of CSF-1 induced inflammation in teleost fish by a soluble form of the CSF-1 receptor. *Fish Shellfish Immunol*, *41*(1), 45-51. https://doi.org/10.1016/j.fsi.2014.03.035

Riera Romo, M., Perez-Martinez, D., & Castillo Ferrer, C. (2016). Innate immunity in vertebrates: an overview. *Immunology*, *148*(2), 125-139. https://doi.org/10.1111/imm.12597

Robinson, N. E., & Robinson, A. B. (2001a). Molecular clocks. *Proceedings of the National Academy of Sciences*, *98*(3), 944-949.

Robinson, N. E., & Robinson, A. B. (2001b). Prediction of protein deamidation rates from primary and three-dimensional structure. *Proceedings of the National Academy of Sciences*, *98*(8), 4367-4372.

Robinson, P. J. (1992). Differential stimulation of protein kinase C activity by phorbol ester or calcium/phosphatidylserine in vitro and in intact synaptosomes. *Journal of Biological Chemistry*, *267*(30), 21637-21644. https://doi.org/10.1016/s0021-9258(19)36659-1

Rodriguez-Nunez, I., Wcisel, D. J., Litman, G. W., & Yoder, J. A. (2014). Multigene families of immunoglobulin domain-containing innate immune receptors in zebrafish: deciphering the differences. *Dev Comp Immunol*, *46*(1), 24-34. https://doi.org/10.1016/j.dci.2014.02.004

Rosales, C. (2017). Fcgamma Receptor Heterogeneity in Leukocyte Functional Responses. *Front Immunol*, *8*, 280. https://doi.org/10.3389/fimmu.2017.00280

Rosales, C. (2018). Neutrophil: A Cell with Many Roles in Inflammation or Several Cell Types? *Front Physiol*, *9*, 113. https://doi.org/10.3389/fphys.2018.00113

Rosales, C., & Uribe-Querol, E. (2017). Phagocytosis: A Fundamental Process in Immunity. *Biomed Res Int*, *2017*, 9042851. https://doi.org/10.1155/2017/9042851

Rosales, C., & Uribe-Querol, E. (2018). Neutrophil activation by antibody receptors. In *Neutrophils*. IntechOpen.

Rostamzadeh, D., Kazemi, T., Amirghofran, Z., & Shabani, M. (2018). Update on Fc receptor-like (FCRL) family: new immunoregulatory players in health and diseases. *Expert Opin Ther Targets*, *22*(6), 487-502. https://doi.org/10.1080/14728222.2018.1472768

Rumpret, M., Drylewicz, J., Ackermans, L. J. E., Borghans, J. A. M., Medzhitov, R., & Meyaard, L. (2020). Functional categories of immune inhibitory receptors. *Nat Rev Immunol*, *20*(12), 771-780. https://doi.org/10.1038/s41577-020-0352-z

Radwan, J., Babik, W., Kaufman, J., Lenz, T. L., & Winternitz, J. (2020). Advances in the Evolutionary Understanding of MHC Polymorphism. *Trends Genet*, *36*(4), 298-311. https://doi.org/10.1016/j.tig.2020.01.008

Redondo-Garcia, S., Barritt, C., Papagregoriou, C., Yeboah, M., Frendeus, B., Cragg, M. S., & Roghanian, A. (2023). Human leukocyte immunoglobulin-like receptors in health and disease. *Front Immunol*, *14*, 1282874. https://doi.org/10.3389/fimmu.2023.1282874

Sahoo, A., & Im, S.-H. (2010). Interleukin and Interleukin Receptor Diversity: Role of Alternative Splicing. *International Reviews of Immunology*, *29*(1), 77-109. https://doi.org/10.3109/08830180903349651

Sakai, M., Hikima, J.-i., & Kono, T. (2020). Fish cytokines: current research and applications. *Fisheries Science*, *87*(1), 1-9. https://doi.org/10.1007/s12562-020-01476-4

Sambrook, J. G., Bashirova, A., Andersen, H., Piatak, M., Vernikos, G. S., Coggill, P., Lifson, J. D., Carrington, M., & Beck, S. (2006). Identification of the ancestral killer

immunoglobulin-like receptor gene in primates. *BMC Genomics*, *7*, 209. https://doi.org/10.1186/1471-2164-7-209

Santiago, T., Kulemzin, S. V., Reshetnikova, E. S., Chikaev, N. A., Volkova, O. Y., Mechetina, L. V., Zhao, M., Davis, R. S., Taranin, A. V., Najakshin, A. M., Hendershot, L. M., & Burrows, P. D. (2011). FCRLA is a resident endoplasmic reticulum protein that associates with intracellular Igs, IgM, IgG and IgA. *Int Immunol*, *23*(1), 43-53. https://doi.org/10.1093/intimm/dxq456

Sarma, J. V., & Ward, P. A. (2011). The complement system. *Cell Tissue Res*, *343*(1), 227-235. https://doi.org/10.1007/s00441-010-1034-0

Schoen, J., Euler, M., Schauer, C., Schett, G., Herrmann, M., Knopf, J., & Yaykasli, K. O. (2022). Neutrophils' Extracellular Trap Mechanisms: From Physiology to Pathology. *Int J Mol Sci*, *23*(21). https://doi.org/10.3390/ijms232112855

Schreeder, D. M., Cannon, J. P., Wu, J., Li, R., Shakhmatov, M. A., & Davis, R. S. (2010). Cutting edge: FcR-like 6 is an MHC class II receptor. *J Immunol*, *185*(1), 23-27. https://doi.org/10.4049/jimmunol.1000832

Selvakumar, A., Steffens, U., Palanisamy, N., Chaganti, R. S., & Dupont, B. (1997). Genomic organization and allelic polymorphism of the human killer cell inhibitory receptor gene KIR103. *Tissue Antigens*, *49*(6), 564-573. https://doi.org/10.1111/j.1399-0039.1997.tb02803.x

Sengeløv, H., Follin, P., Kjeldsen, L., Lollike, K., Dahlgren, C., & Borregaard, N. (1995). Mobilization of granules and secretory vesicles during in vivo exudation of human neutrophils. *The Journal of Immunology*, *154*(8), 4157-4165. https://doi.org/10.4049/jimmunol.154.8.4157

Sengeløv, H., Kjeldsen, L., Diamond, M. S., Springer, T. A., & Borregaard, N. (1993). Subcellular localization and dynamics of Mac-1 (alpha m beta 2) in human neutrophils. *The Journal of clinical investigation*, *92*(3), 1467-1476.

Sengeløv, H., Kjeldsen, L., Kroeze, W., Berger, M., & Borregaard, N. (1994). Secretory vesicles are the intracellular reservoir of complement receptor 1 in human neutrophils. *Journal of immunology (Baltimore, Md.: 1950)*, *153*(2), 804-810.

Shen, L., Stuge, T. B., Evenhuis, J. P., Bengten, E., Wilson, M., Chinchar, V. G., Clem, L. W., & Miller, N. W. (2003). Channel catfish NK-like cells are armed with IgM via a putative FcmicroR. *Dev Comp Immunol*, *27*(8), 699-714. https://doi.org/10.1016/s0145-305x(03)00042-9

Shen, L., Stuge, T. B., Zhou, H., Khayat, M., Barker, K. S., Quiniou, S. M., Wilson, M., Bengtén, E., Chinchar, V. G., & Clem, L. W. (2002). Channel catfish cytotoxic cells: a mini-review. *Developmental & Comparative Immunology*, *26*(2), 141-149.

Sheppard, F. R., Kelher, M. R., Moore, E. E., McLaughlin, N. J., Banerjee, A., & Silliman, C. C. (2005). Structural organization of the neutrophil NADPH oxidase: phosphorylation and translocation during priming and activation. *J Leukoc Biol*, *78*(5), 1025-1042. https://doi.org/10.1189/jlb.0804442

Shibuya, A., Sakamoto, N., Shimizu, Y., Shibuya, K., Osawa, M., Hiroyama, T., Eyre, H. J., Sutherland, G. R., Endo, Y., & Fujita, T. (2000). Fcα/μ receptor mediates endocytosis of IgM-coated microbes. *Nature immunology*, *1*(5), 441-446.

Sidorenko, S. P., & Clark, E. A. (2003). The dual-function CD150 receptor subfamily: the viral attraction. *Nature immunology*, *4*(1), 19-24.

Simard, J. C., Girard, D., & Tessier, P. A. (2010). Induction of neutrophil degranulation by S100A9 via a MAPK-dependent mechanism. *J Leukoc Biol*, *87*(5), 905-914. https://doi.org/10.1189/jlb.1009676

Smith, J. L. (2003). The role of gastric acid in preventing foodborne disease and how bacteria overcome acid conditions. *J Food Prot*, *66*(7), 1292-1303. https://doi.org/10.4315/0362-028x-66.7.1292

Smith, N. C., Rise, M. L., & Christian, S. L. (2019). A Comparison of the Innate and Adaptive Immune Systems in Cartilaginous Fish, Ray-Finned Fish, and Lobe-Finned Fish. *Front Immunol*, *10*, 2292. https://doi.org/10.3389/fimmu.2019.02292

Soderberg, C., Wraith, A., Ringvall, M., Yan, Y. L., Postlethwait, J. H., Brodin, L., & Larhammar, D. (2000). Zebrafish genes for neuropeptide Y and peptide YY reveal origin by chromosome duplication from an ancestral gene linked to the homeobox cluster. *J Neurochem*, *75*(3), 908-918. https://doi.org/10.1046/j.1471-4159.2000.0750908.x

Soliman, A. M., Yoon, T., Wang, J., Stafford, J. L., & Barreda, D. R. (2021). Isolation of Skin Leukocytes Uncovers Phagocyte Inflammatory Responses During Induction and Resolution of Cutaneous Inflammation in Fish. *Front Immunol*, *12*, 725063. https://doi.org/10.3389/fimmu.2021.725063

Songyang, Z., Shoelson, S., McGlade, J., Olivier, P., Pawson, T., Bustelo, X., Barbacid, M., Sabe, H., Hanafusa, H., & Yi, T. (1994). Specific motifs recognized by the SH2 domains of Csk, 3BP2, fps/fes, GRB-2, HCP, SHC, Syk, and Vav. *Molecular and cellular biology*, *14*(4), 2777-2785.

Soza-Ried, C., Hess, I., Netuschil, N., Schorpp, M., & Boehm, T. (2010). Essential role of c-myb in definitive hematopoiesis is evolutionarily conserved. *Proc Natl Acad Sci U S A*, *107*(40), 17304-17308. https://doi.org/10.1073/pnas.1004640107

Srivastava, R. M., Savithri, B., & Khar, A. (2003). Activating and inhibitory receptors and their role in natural killer cell function.

Stafford, J. L., Bengten, E., Du Pasquier, L., McIntosh, R. D., Quiniou, S. M., Clem, L. W., Miller, N. W., & Wilson, M. (2006). A novel family of diversified immunoregulatory receptors in teleosts is homologous to both mammalian Fc receptors and molecules encoded within the leukocyte receptor complex. *Immunogenetics*, *58*(9), 758-773. https://doi.org/10.1007/s00251-006-0134-1

Stafford, J. L., Bengten, E., Du Pasquier, L., Miller, N. W., & Wilson, M. (2007). Channel catfish leukocyte immune-type receptors contain a putative MHC class I binding site. *Immunogenetics*, *59*(1), 77-91. https://doi.org/10.1007/s00251-006-0169-3

Stafford, J. L., Galvez, F., Goss, G. G., & Belosevic, M. (2002). Induction of nitric oxide and respiratory burst response in activated goldfish macrophages requires potassium channel activity. *Developmental & Comparative Immunology*, *26*(5), 445-459.

Stafford, J. L., Wilson, M., Nayak, D., Quiniou, S. M., Clem, L. W., Miller, N. W., & Bengten, E. (2006). Identification and characterization of a FcR homolog in an ectothermic vertebrate, the channel catfish (Ictalurus punctatus). *J Immunol*, *177*(4), 2505-2517. https://doi.org/10.4049/jimmunol.177.4.2505

Star, B., & Jentoft, S. (2012). Why does the immune system of Atlantic cod lack MHC II? *Bioessays*, *34*(8), 648-651. https://doi.org/10.1002/bies.201200005

Steentoft, C., Vakhrushev, S. Y., Joshi, H. J., Kong, Y., Vester-Christensen, M. B., Schjoldager, K. T., Lavrsen, K., Dabelsteen, S., Pedersen, N. B., Marcos-Silva, L., Gupta, R., Bennett, E. P., Mandel, U., Brunak, S., Wandall, H. H., Levery, S. B., & Clausen, H. (2013). Precision mapping of the human O-GalNAc glycoproteome through SimpleCell technology. *EMBO J*, *32*(10), 1478-1488. https://doi.org/10.1038/emboj.2013.79

Studzinski, G. P., & Brelvi, Z. S. (1987). Changes in proto-oncogene expression associated with reversal of macrophage-like differentiation of HL 60 cells. *Journal of the National Cancer Institute*, *79*(1), 67-76.

Stuge, T., Miller, N., & Clem, L. (1995). Channel catfish cytotoxic effector cells from peripheral blood and pronephroi are different. *Fish & shellfish immunology*, *5*(6), 469-471.

Sundstrom, G., Larsson, T. A., Brenner, S., Venkatesh, B., & Larhammar, D. (2008). Evolution of the neuropeptide Y family: new genes by chromosome duplications in early vertebrates and in teleost fishes. *Gen Comp Endocrinol*, *155*(3), 705-716. https://doi.org/10.1016/j.ygcen.2007.08.016

Symmons, O., Uslu, V. V., Tsujimura, T., Ruf, S., Nassari, S., Schwarzer, W., Ettwiller, L., & Spitz, F. (2014). Functional and topological characteristics of mammalian regulatory domains. *Genome Res*, *24*(3), 390-400. https://doi.org/10.1101/gr.163519.113

Sayos, J., Martinez-Barriocanal, A., Kitzig, F., Bellon, T., & Lopez-Botet, M. (2004). Recruitment of C-terminal Src kinase by the leukocyte inhibitory receptor CD85j. *Biochem Biophys Res Commun*, *324*(2), 640-647. https://doi.org/10.1016/j.bbrc.2004.09.097

Shiroishi, M., Kajikawa, M., Kuroki, K., Ose, T., Kohda, D., & Maenaka, K. (2006). Crystal structure of the human monocyte-activating receptor, "Group 2" leukocyte Ig-like

receptor A5 (LILRA5/LIR9/ILT11). *J Biol Chem*, *281*(28), 19536-19544. https://doi.org/10.1074/jbc.M603076200

Sihombing, M., Safitri, M., Zhou, T., Wang, L., McGinty, S., Zhang, H. J., Yin, Y., Peng, Q., Qiu, J., & Wang, G. (2021). Unexpected Role of Nonimmune Cells: Amateur Phagocytes. *DNA Cell Biol*, *40*(2), 157-171. https://doi.org/10.1089/dna.2020.5647

Sims, R., Vandergon, V. O., & Malone, C. S. (2012). The mouse B cell-specific mb-1 gene encodes an immunoreceptor tyrosine-based activation motif (ITAM) protein that may be evolutionarily conserved in diverse species by purifying selection. *Mol Biol Rep*, *39*(3), 3185-3196. https://doi.org/10.1007/s11033-011-1085-7

Sohn, H. W., Krueger, P. D., Davis, R. S., & Pierce, S. K. (2011). FcRL4 acts as an adaptive to innate molecular switch dampening BCR signaling and enhancing TLR signaling. *Blood*, *118*(24), 6332-6341. https://doi.org/10.1182/blood-2011-05-353102

Tahara, E., Kadara, H., Lacroix, L., Lotan, D., & Lotan, R. (2009). Activation of protein kinase C by phorbol 12-myristate 13-acetate suppresses the growth of lung cancer cells through KLF6 induction. *Cancer Biol Ther*, *8*(9), 801-807. https://doi.org/10.4161/cbt.8.9.8186

Takai, T. (2005a). A novel recognition system for MHC class I molecules constituted by PIR. *Adv Immunol*, *88*, 161-192. https://doi.org/10.1016/S0065-2776(05)88005-8

Takai, T. (2005b). Paired immunoglobulin-like receptors and their MHC class I recognition. *Immunology*, *115*(4), 433-440. https://doi.org/10.1111/j.1365-2567.2005.02177.x

Takeda, K., & Nakamura, A. (2017). Regulation of immune and neural function via leukocyte Ig-like receptors. *J Biochem*, *162*(2), 73-80. https://doi.org/10.1093/jb/mvx036

Talaat, A. M., Reimschuessel, R., Wasserman, S. S., & Trucksis, M. (1998). Goldfish, Carassius auratus, a novel animal model for the study of Mycobacterium marinum pathogenesis. *Infection and Immunity*, *66*(6), 2938-2942.

Taylor, A. I., Gould, H. J., Sutton, B. J., & Calvert, R. A. (2007). The first avian Ig-like Fc receptor family member combines features of mammalian FcR and FCRL. *Immunogenetics*, *59*(4), 323-328. https://doi.org/10.1007/s00251-007-0195-9

Taylor, E. B., Moulana, M., Stuge, T. B., Quiniou, S. M., Bengten, E., & Wilson, M. (2016). A Leukocyte Immune-Type Receptor Subset Is a Marker of Antiviral Cytotoxic Cells in Channel Catfish, Ictalurus punctatus. *J Immunol*, *196*(6), 2677-2689. https://doi.org/10.4049/jimmunol.1502166

Tedla, N., Lee, C. W., Borges, L., Geczy, C. L., & Arm, J. P. (2008). Differential expression of leukocyte immunoglobulin-like receptors on cord-blood-derived human mast cell progenitors and mature mast cells. *J Leukoc Biol*, *83*(2), 334-343. https://doi.org/10.1189/jlb.0507314

Thielens, A., Vivier, E., & Romagne, F. (2012). NK cell MHC class I specific receptors (KIR): from biology to clinical intervention. *Curr Opin Immunol*, *24*(2), 239-245. https://doi.org/10.1016/j.coi.2012.01.001

Thomson, A. (1992). The effects of cyclosporin A on non-T cell components of the immune system. *Journal of autoimmunity*, *5*, 167-176.

Toda, H., Shibasaki, Y., Koike, T., Ohtani, M., Takizawa, F., Ototake, M., Moritomo, T., & Nakanishi, T. (2009). Alloantigen-specific killing is mediated by CD8-positive T cells in fish. *Dev Comp Immunol*, *33*(4), 646-652. https://doi.org/10.1016/j.dci.2008.11.008

Tolnay, M. (2022). Lymphocytes sense antibodies through human FCRL proteins: Emerging roles in mucosal immunity. *J Leukoc Biol*, *111*(2), 477-487. https://doi.org/10.1002/JLB.4RU0221-102RR

Tomita, M., Reinhold, M. I., Molkentin, J. D., & Naski, M. C. (2002). Calcineurin and NFAT4 induce chondrogenesis. *J Biol Chem*, *277*(44), 42214-42218. https://doi.org/10.1074/jbc.C200504200

Traub, L. M., & Bonifacino, J. S. (2013). Cargo recognition in clathrin-mediated endocytosis. *Cold Spring Harb Perspect Biol*, *5*(11), a016790. https://doi.org/10.1101/cshperspect.a016790

Trowbridge, I. S., & Thomas, M. L. (1994). CD45: an emerging role as a protein tyrosine phosphatase required for lymphocyte activation and development. *Annual review of immunology*, *12*(1), 85-116.

Trowsdale, J., Barten, R., Haude, A., Stewart, C. A., Beck, S., & Wilson, M. J. (2001). The genomic context of natural killer receptor extended gene families. *Immunol Rev*, *181*, 20-38. https://doi.org/10.1034/j.1600-065x.2001.1810102.x

Trowsdale, J., Jones, D. C., Barrow, A. D., & Traherne, J. A. (2015). Surveillance of cell and tissue perturbation by receptors in the LRC. *Immunol Rev*, *267*(1), 117-136. https://doi.org/10.1111/imr.12314

Turula, H., & Wobus, C. E. (2018). The Role of the Polymeric Immunoglobulin Receptor and Secretory Immunoglobulins during Mucosal Infection and Immunity. *Viruses*, *10*(5). https://doi.org/10.3390/v10050237

Takiishi, T., Fenero, C. I. M., & Camara, N. O. S. (2017). Intestinal barrier and gut microbiota: Shaping our immune responses throughout life. *Tissue Barriers*, *5*(4), e1373208. https://doi.org/10.1080/21688370.2017.1373208

Tort, L., Balasch, J., & Mackenzie, S. (2003). Fish immune system. A crossroads between innate and adaptive responses. *Inmunología*, *22*(3), 277-286.

Tsujita, T., Tsukada, H., Nakao, M., Oshiumi, H., Matsumoto, M., & Seya, T. (2004). Sensing bacterial flagellin by membrane and soluble orthologs of Toll-like receptor 5 in rainbow trout (Onchorhynchus mikiss). *J Biol Chem*, *279*(47), 48588-48597. https://doi.org/10.1074/jbc.M407634200

Underhill, D. M., & Goodridge, H. S. (2007). The many faces of ITAMs. *Trends Immunol*, *28*(2), 66-73. https://doi.org/10.1016/j.it.2006.12.004

Uribe-Querol, E., & Rosales, C. (2020). Phagocytosis: Our Current Understanding of a Universal Biological Process. *Front Immunol*, *11*, 1066. https://doi.org/10.3389/fimmu.2020.01066

Uribe, C., Folch, H., Enriquez, R., & Moran, G. (2011). Innate and adaptive immunity in teleost fish: a review. *Veterinární medicína*, *56*(10), 486-503. https://doi.org/10.17221/3294-vetmed

Utke, K., Bergmann, S., Lorenzen, N., Kollner, B., Ototake, M., & Fischer, U. (2007). Cell-mediated cytotoxicity in rainbow trout, Oncorhynchus mykiss, infected with viral haemorrhagic septicaemia virus. *Fish Shellfish Immunol*, *22*(3), 182-196. https://doi.org/10.1016/j.fsi.2006.04.008

Vallejo, A. N., Miller, N. W., Harvey, N. E., Cuchens, M. A., Warr, G. W., & Clem, L. W. (1992). Cellular Pathway (S) of Antigen Processing and Presentation in Fish APC: Endosomal

Involvement and Cell‐Free Antigen Presentation. *Journal of Immunology Research*, *3*(1), 51-65.

van Vugt, M. J., Heijnen, I. A., Capel, P. J., Park, S. Y., Ra, C., Saito, T., Verbeek, J. S., & van de Winkel, J. G. (1996). FcR gamma-chain is essential for both surface expression and function of human Fc gamma RI (CD64) in vivo. *Blood*, *87*(9), 3593-3599. https://doi.org/10.1182/blood.V87.9.3593.bloodjournal8793593

Vandooren, J., & Itoh, Y. (2021). Alpha-2-Macroglobulin in Inflammation, Immunity and Infections. *Front Immunol*, *12*, 803244. https://doi.org/10.3389/fimmu.2021.803244

Veillette, A., Dong, Z., Perez-Quintero, L. A., Zhong, M. C., & Cruz-Munoz, M. E. (2009). Importance and mechanism of 'switch' function of SAP family adapters. *Immunol Rev*, *232*(1), 229-239. https://doi.org/10.1111/j.1600-065X.2009.00824.x

Verbrugge, A., de Ruiter, T., Geest, C., Coffer, P. J., & Meyaard, L. (2006). Differential expression of leukocyte-associated Ig-like receptor-1 during neutrophil differentiation and activation. *J Leukoc Biol*, *79*(4), 828-836. https://doi.org/10.1189/jlb.0705370

Viertlboeck, B. C., Habermann, F. A., Schmitt, R., Groenen, M. A., Du Pasquier, L., & Gobel, T. W. (2005). The chicken leukocyte receptor complex: a highly diverse multigene family encoding at least six structurally distinct receptor types. *J Immunol*, *175*(1), 385-393. https://doi.org/10.4049/jimmunol.175.1.385

Viertlboeck, B. C., Schweinsberg, S., Hanczaruk, M. A., Schmitt, R., Du Pasquier, L., Herberg, F. W., & Göbel, T. W. (2007). The chicken leukocyte receptor complex encodes a primordial, activating, high-affinity IgY Fc receptor. *Proceedings of the National Academy of Sciences*, *104*(28), 11718-11723.

Viertlboeck, B. C., Schweinsberg, S., Schmitt, R., Herberg, F. W., & Gobel, T. W. (2009). The chicken leukocyte receptor complex encodes a family of different affinity FcY receptors. *J Immunol*, *182*(11), 6985-6992. https://doi.org/10.4049/jimmunol.0803060

Veillette, A., Thibaudeau, E., & Latour, S. (1998). High expression of inhibitory receptor SHPS-1 and its association with protein-tyrosine phosphatase SHP-1 in macrophages. *J Biol Chem*, *273*(35), 22719-22728. https://doi.org/10.1074/jbc.273.35.22719

Verbrugge, A., Rijkers, E. S., de Ruiter, T., & Meyaard, L. (2006). Leukocyte-associated Ig-like receptor-1 has SH2 domain-containing phosphatase-independent function and recruits C-terminal Src kinase. *Eur J Immunol*, *36*(1), 190-198. https://doi.org/10.1002/eji.200535226

Volff, J. N. (2005). Genome evolution and biodiversity in teleost fish. *Heredity (Edinb)*, *94*(3), 280-294. https://doi.org/10.1038/sj.hdy.6800635

Wang, J., Belosevic, M., & Stafford, J. L. (2020). Identification of goldfish (Carassius auratus L.) leukocyte immune-type receptors shows alternative splicing as a potential mechanism for receptor diversification. *Mol Immunol*, *125*, 83-94. https://doi.org/10.1016/j.molimm.2020.06.024

Wang, J., Belosevic, M., & Stafford, J. L. (2021). Identification of distinct LRC- and Fc receptor complex-like chromosomal regions in fish supports that teleost leukocyte immune-type receptors are distant relatives of mammalian Fc receptor-like molecules. *Immunogenetics*, *73*(1), 93-109. https://doi.org/10.1007/s00251-020-01193-3

Wang, J., Gurupalli, H. V., & Stafford, J. L. (2023). Teleost leukocyte immune-type receptors. *Dev Comp Immunol*, *147*, 104768. https://doi.org/10.1016/j.dci.2023.104768

Watson, F. L., Püttmann-Holgado, R., Thomas, F., Lamar, D. L., Hughes, M., Kondo, M., Rebel, V. I., & Schmucker, D. (2005). Extensive diversity of Ig-superfamily proteins in the immune system of insects. *Science*, *309*(5742), 1874-1878.

Watson, L. S., IL. Jackson, LL. (1963). The hematology of goldfish, Carassius auratus. *Cytologia*, *28*(2), 118-130.

Wcisel, D. J., Ota, T., Litman, G. W., & Yoder, J. A. (2017). Spotted Gar and the Evolution of Innate Immune Receptors. *J Exp Zool B Mol Dev Evol*, *328*(7), 666-684. https://doi.org/10.1002/jez.b.22738

Wcisel, D. J., & Yoder, J. A. (2016). The confounding complexity of innate immune receptors within and between teleost species. *Fish Shellfish Immunol*, *53*, 24-34. https://doi.org/10.1016/j.fsi.2016.03.034

Wen, A. Y., Sakamoto, K. M., & Miller, L. S. (2010). The role of the transcription factor CREB in immune function. *J Immunol*, *185*(11), 6413-6419. https://doi.org/10.4049/jimmunol.1001829

Wilson, M. J., Torkar, M., & Trowsdale, J. (1997). Genomic organization of a human killer cell inhibitory receptor gene. *Tissue Antigens*, *49*(6), 574-579. https://doi.org/10.1111/j.1399-0039.1997.tb02804.x

Wilson, T. J., Fuchs, A., & Colonna, M. (2012). Cutting edge: human FcRL4 and FcRL5 are receptors for IgA and IgG. *J Immunol*, *188*(10), 4741-4745. https://doi.org/10.4049/jimmunol.1102651

Wilson, T. J., Garner, L. I., Metcalfe, C., King, E., Margraf, S., & Brown, M. H. (2014). Fine specificity and molecular competition in SLAM family receptor signalling. *PLoS One*, *9*(3), e92184. https://doi.org/10.1371/journal.pone.0092184

Wilson, T. J., Gilfillan, S., & Colonna, M. (2010). Fc receptor-like A associates with intracellular IgG and IgM but is dispensable for antigen-specific immune responses. *J Immunol*, *185*(5), 2960-2967. https://doi.org/10.4049/jimmunol.1001428

Wynn, T. A., Chawla, A., & Pollard, J. W. (2013). Macrophage biology in development, homeostasis and disease. *Nature*, *496*(7446), 445-455. https://doi.org/10.1038/nature12034

Willcox, B. E., Thomas, L. M., & Bjorkman, P. J. (2003). Crystal structure of HLA-A2 bound to LIR-1, a host and viral major histocompatibility complex receptor. *Nat Immunol*, *4*(9), 913-919. https://doi.org/10.1038/ni961

Xu, Z., & Weiss, A. (2002). Negative regulation of CD45 by differential homodimerization of the alternatively spliced isoforms. *Nat Immunol*, *3*(8), 764-771. https://doi.org/10.1038/ni822

Xu, H., & Liu, F. (2024). Advances in chemokines of teleost fish species. *Aquaculture and Fisheries*, *9*(2), 115-125. https://doi.org/10.1016/j.aaf.2023.01.008

Yan, H.-C., Baldwin, H. S., Sun, J., Buck, C. A., Albelda, S. M., & DeLisser, H. M. (1995). Alternative Splicing of a Specific Cytoplasmic Exon Alters the Binding Characteristics of Murine Platelet/Endothelial Cell Adhesion Molecule-1 (PECAM-1)(∗). *Journal of Biological Chemistry*, *270*(40), 23672-23680.

Yang, C., Mai, H., Peng, J., Zhou, B., Hou, J., & Jiang, D. (2020). STAT4: an immunoregulator contributing to diverse human diseases. *Int J Biol Sci*, *16*(9), 1575-1585. https://doi.org/10.7150/ijbs.41852

Yasgar, A., Jadhav, A., Simeonov, A., & Coussens, N. P. (2016). AlphaScreen-Based Assays: Ultra-High-Throughput Screening for Small-Molecule Inhibitors of Challenging

Enzymes and Protein-Protein Interactions. *Methods Mol Biol*, *1439*, 77-98. https://doi.org/10.1007/978-1-4939-3673-1_5

Yin, C., & Heit, B. (2018). Armed for destruction: formation, function and trafficking of neutrophil granules. *Cell Tissue Res*, *371*(3), 455-471. https://doi.org/10.1007/s00441-017-2731-8

Yoder, J. A. (2009). Form, function and phylogenetics of NITRs in bony fish. *Dev Comp Immunol*, *33*(2), 135-144. https://doi.org/10.1016/j.dci.2008.09.004

Yoder, J. A., & Litman, G. W. (2011). The phylogenetic origins of natural killer receptors and recognition: relationships, possibilities, and realities. *Immunogenetics*, *63*(3), 123-141. https://doi.org/10.1007/s00251-010-0506-4

Yoder, J. A., Orcutt, T. M., Traver, D., & Litman, G. W. (2007). Structural characteristics of zebrafish orthologs of adaptor molecules that associate with transmembrane immune receptors. *Gene*, *401*(1-2), 154-164.

Yoo, E. M., Trinh, K. R., Lim, H., Wims, L. A., & Morrison, S. L. (2011). Characterization of IgA and IgM binding and internalization by surface-expressed human Fcalpha/mu receptor. *Mol Immunol*, *48*(15-16), 1818-1826. https://doi.org/10.1016/j.molimm.2011.05.011

Young, N. T., Waller, E. C., Patel, R., Roghanian, A., Austyn, J. M., & Trowsdale, J. (2008). The inhibitory receptor LILRB1 modulates the differentiation and regulatory potential of human dendritic cells. *Blood*, *111*(6), 3090-3096. https://doi.org/10.1182/blood-2007-05-089771

Yu, W.-P., Pallen, C. J., Tay, A., Jirik, F. R., Brenner, S., Tan, Y., & Venkatesh, B. (2001). Conserved synteny between the Fugu and human PTEN locus and the evolutionary conservation of vertebrate PTEN function. *Oncogene*, *20*(39), 5554-5561.

Yuan, J., He, Z., Yuan, X., Jiang, X., Sun, X., & Zou, S. (2010). Speciation of polyploid Cyprinidae fish of common carp, crucian carp, and silver crucian carp derived from duplicated Hox genes. *J Exp Zool B Mol Dev Evol*, *314*(6), 445-456. https://doi.org/10.1002/jez.b.21350

Yamazaki, R., Furukawa, A., Hirayasu, K., Yumoto, K., Fukuhara, H., Arase, H., & Maenaka, K. (2020). Molecular mechanism of the recognition of bacterially cleaved immunoglobulin by the immune regulatory receptor LILRA2. *J Biol Chem*, *295*(28), 9531-9541. https://doi.org/10.1074/jbc.RA120.013354

Yu, L., & Feng, Z. (2018). The Role of Toll-Like Receptor Signaling in the Progression of Heart Failure. *Mediators Inflamm*, *2018*, 9874109. https://doi.org/10.1155/2018/9874109

Yu, Y., Wang, Q., Huang, Z., Ding, L., & Xu, Z. (2020). Immunoglobulins, Mucosal Immunity and Vaccination in Teleost Fish. *Front Immunol*, *11*, 567941. https://doi.org/10.3389/fimmu.2020.567941

Yung, S. C., & Murphy, P. M. (2012). Antimicrobial chemokines. *Front Immunol*, *3*, 276. https://doi.org/10.3389/fimmu.2012.00276

Zarubin, T., & Han, J. (2005). Activation and signaling of the p38 MAP kinase pathway. *Cell research*, *15*(1), 11-18.

Zhang, C., Merana, G. R., Harris-Tryon, T., & Scharschmidt, T. C. (2022). Skin immunity: dissecting the complex biology of our body's outer barrier. *Mucosal Immunol*, *15*(4), 551-561. https://doi.org/10.1038/s41385-022-00505-y

Zhang, J. M., & An, J. (2007). Cytokines, inflammation, and pain. *Int Anesthesiol Clin*, *45*(2), 27-37. https://doi.org/10.1097/AIA.0b013e318034194e

Zhao, J., Zhong, S., Niu, X., Jiang, J., Zhang, R., & Li, Q. (2019). The MHC class I-LILRB1 signalling axis as a promising target in cancer therapy. *Scand J Immunol*, *90*(5), e12804. https://doi.org/10.1111/sji.12804

Zhu, Z., Li, R., Li, H., Zhou, T., & Davis, R. S. (2013). FCRL5 exerts binary and compartment-specific influence on innate-like B-cell receptor signaling. *Proc Natl Acad Sci U S A*, *110*(14), E1282-1290. https://doi.org/10.1073/pnas.1215156110

Zikherman, J., & Weiss, A. (2008). Alternative splicing of CD45: the tip of the iceberg. *Immunity*, *29*(6), 839-841. https://doi.org/10.1016/j.immuni.2008.12.005

Zou, J., & Secombes, C. J. (2016). The Function of Fish Cytokines. *Biology (Basel)*, *5*(2). https://doi.org/10.3390/biology5020023

Zucchetti, I., De Santis, R., Grusea, S., Pontarotti, P., & Du Pasquier, L. (2009). Origin and evolution of the vertebrate leukocyte receptors: the lesson from tunicates. *Immunogenetics*, *61*(6), 463-481. https://doi.org/10.1007/s00251-009-0373-z

Zwozdesky, M. A., Fei, C., Lillico, D. M. E., & Stafford, J. L. (2017). Imaging flow cytometry and GST pulldown assays provide new insights into channel catfish leukocyte immune-type receptor-mediated phagocytic pathways. *Dev Comp Immunol*, *67*, 126-138. https://doi.org/10.1016/j.dci.2016.10.011

APPENDIX

(A)

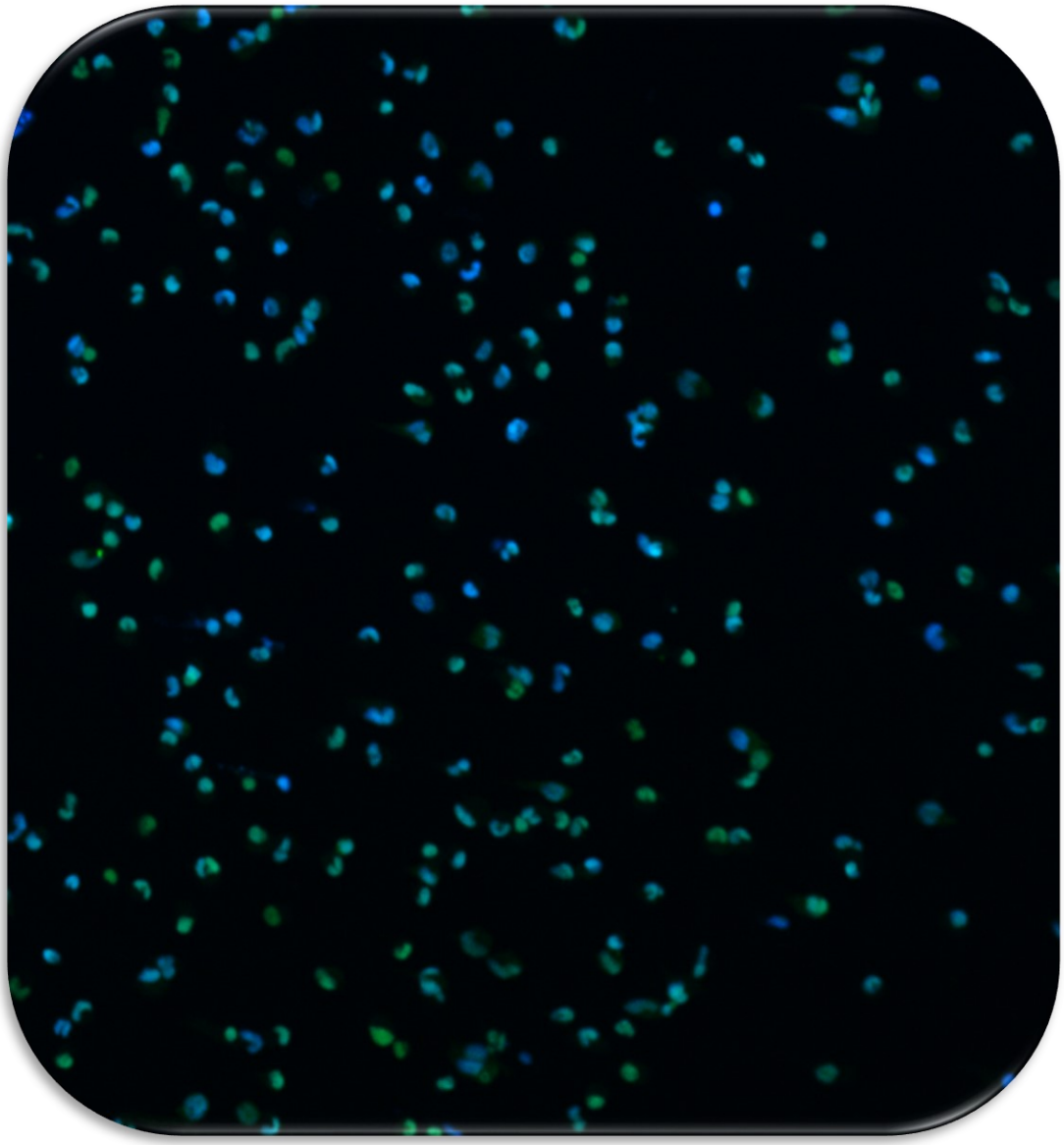

(B)

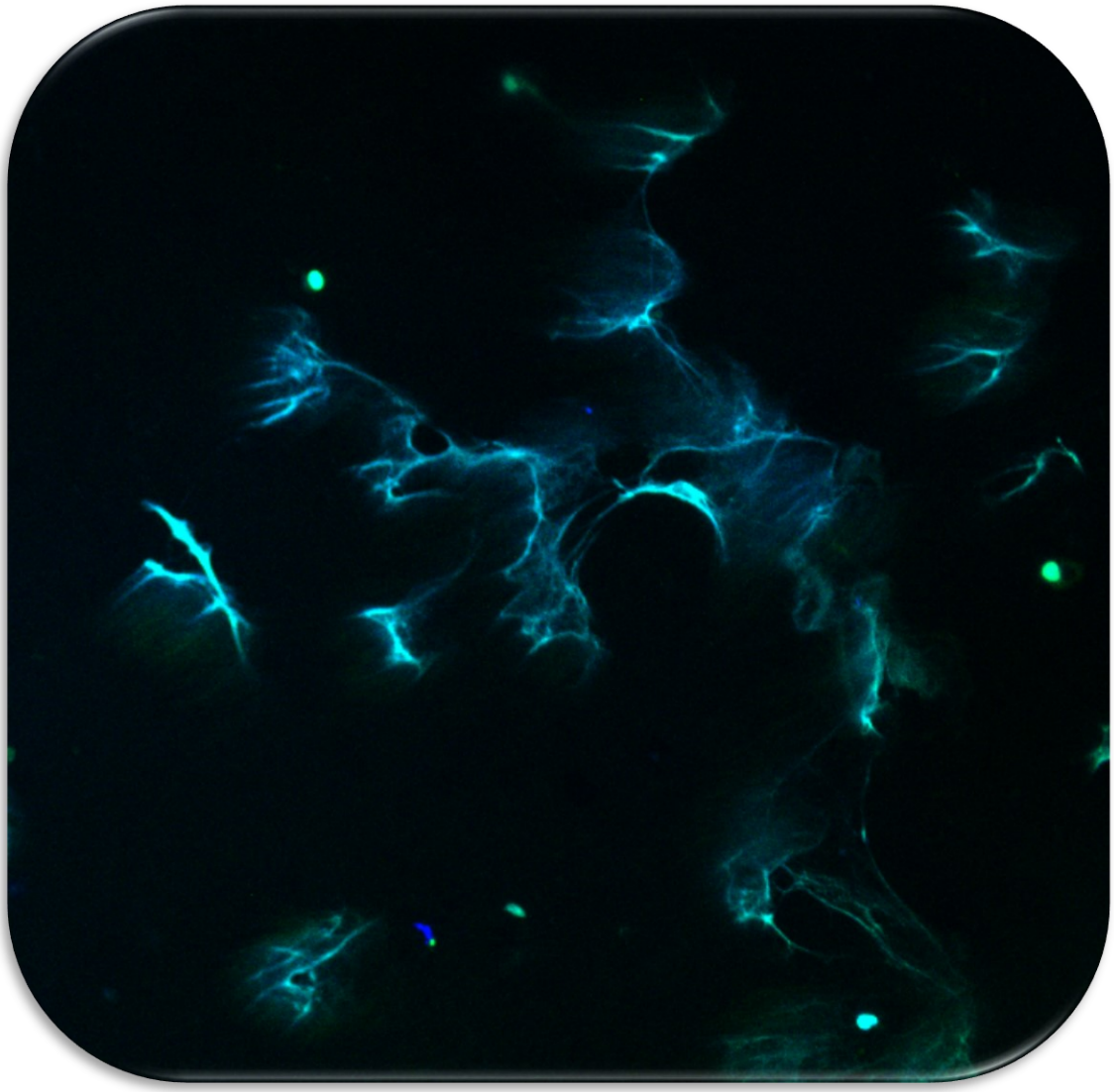

(C)

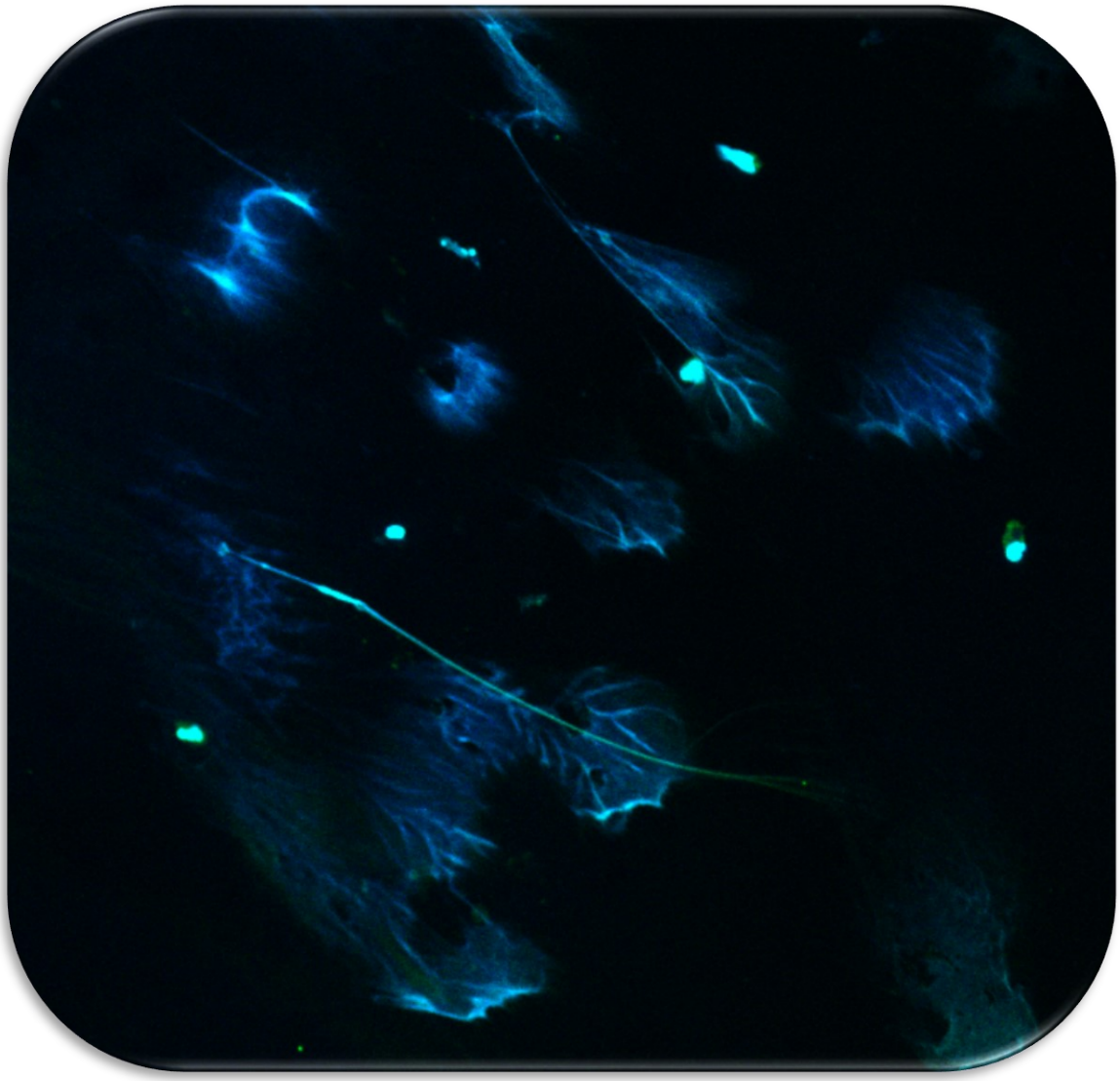

Appendix Figure 1. Goldfish PKNs release NETs 1 h post-stimulation with 5 µg/ml of calcium ionophore A23187. (A) Unstimulated goldfish PKNs. **(B-C)** PKN NETs. NETs/nuclei were stained by DAPI (blue) and SYTOX Green (green). PKNs pooled from four goldfish were seeded on poly-L-lysine-coated coverslips at RT for 1 h. Subsequently, the PKNs bathed in HBSS were stimulated with/without 5 µg/ml of calcium ionophore for 1 h. Afterward, three µl of SYTOX Green solution (0.5 mM) was added to each cell mixture (300 µl) for 3 min before washing with two rounds of HBSS. The coverslip was then mounted on a slide containing ProLong Gold Antifade Mountant with DAPI. These images were captured using an Olympus FLUOVIEW FV3000 Confocal Laser Scanning Microscope with a 40x objective lens.